UNIVERSIDAD COMPLUTENSE DE MADRID

FACULTAD DE FARMACIA

TESIS DOCTORAL

Identificación, expresión y caracterización de peroxidasas ligninolíticas de interés en genomas de basidiomicetos

MEMORIA PARA OPTAR AL GRADO DE DOCTORA

PRESENTADA POR

Elena Fernández Fueyo

Directores

Ángel Tomás Martínez Ferrer
Francisco Javier Ruiz Dueñas

Madrid, 2014

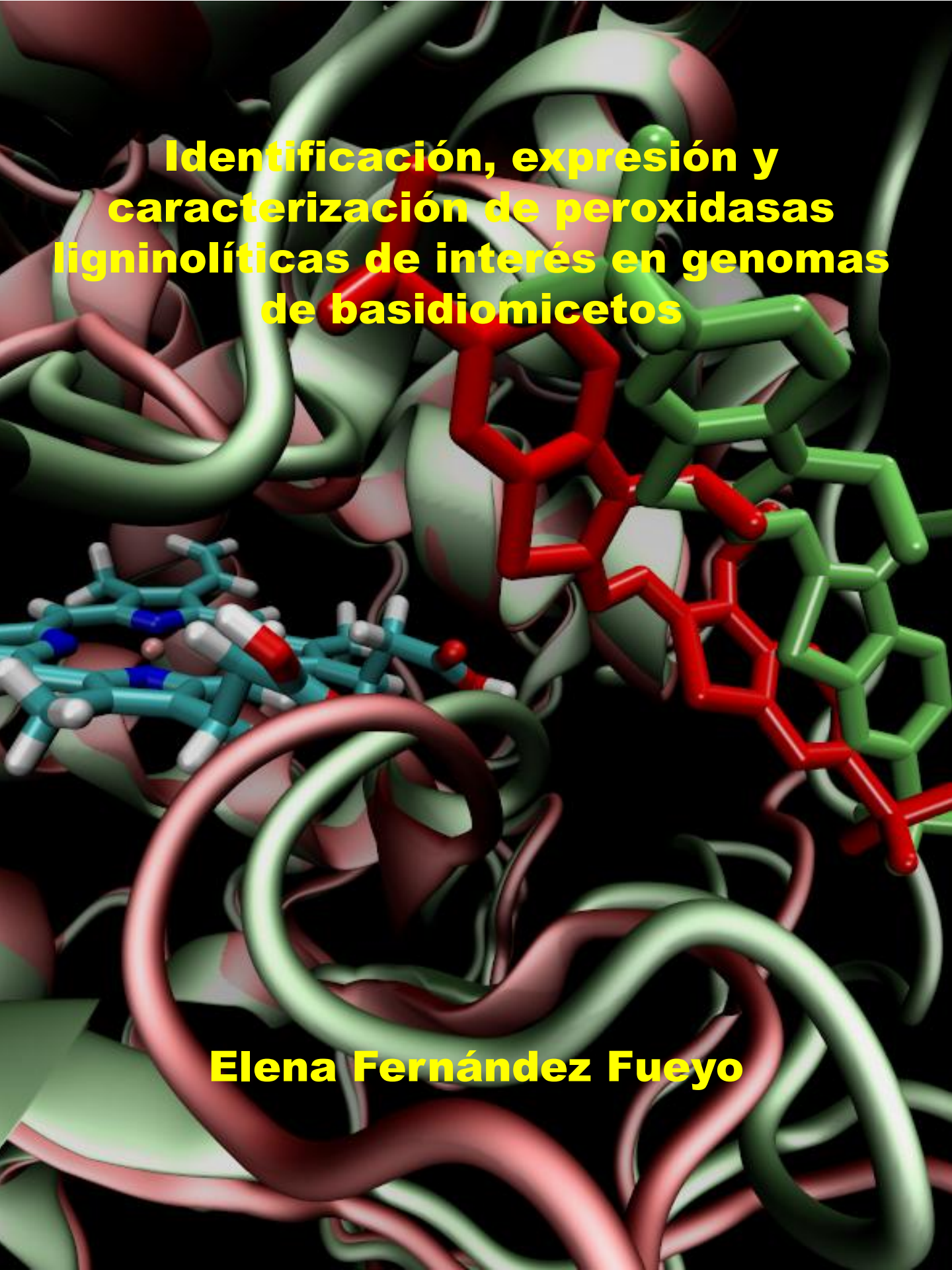

Identificación, expresión y caracterización de peroxidasas ligninolíticas de interés en genomas de basidiomicetos

Elena Fernández Fueyo

Identificación, expresión y caracterización de peroxidasas ligninolíticas de interés en genomas de basidiomicetos

Tesis doctoral

Elena Fernández Fueyo

Centro de Investigaciones Biológicas
CSIC
Universidad Complutense de Madrid
Facultad de Farmacia
Madrid, 2014

Identificación, expresión y caracterización de peroxidasas ligninolíticas de interés en genomas de basidiomicetos

Tesis doctoral para optar al grado de
Doctora por la Universidad Complutense de Madrid
presentada por:

Elena Fernández Fueyo

DIRECTORES:

Dr. Angel Tomás Martínez Ferrer
Profesor de Investigación, CSIC

Dr. Francisco Javier Ruíz Dueñas
Investigador, CSIC

A Isra

2v1a

Cuando llegues a la cima de una montaña
sigue subiendo

ESTRUCTURA DE LA TESIS

El presente trabajo, para obtener el Título de Doctor, se estructura en diez Capítulos que incluyen una Introducción (Cap. 1), cinco Artículos científicos ya publicados (Caps. 2-6), dos Artículos en proceso de revisión (Caps. 7 y 8), una Discusión general (Cap. 9), Conclusiones (Cap. 10) y un Anexo conteniendo Material suplementario (Cap. 11), tal como se detalla a continuación:

- **Capítulo 5: "Comparative genomics of *Ceriporiopisis subvermispora* and *Phanerochaete chrysosporium* provide insight into selective ligninolysis"**
  Fernández-Fueyo, E., F. J. Ruiz-Dueñas, P. Ferreira, D. Floudas, D. S. Hibbett, P. Canessa, L. Larrondo, T. Y. James, D. Seelenfreund, S. Lobos, R. Polanco, M. Tello, Y. Honda, T. Watanabe, T. Watanabe, J. S. Ryu, C. P. Kubicek, M. Schmoll, J. Gaskell, K. E. Hammel, F. J. St.John, A. Vanden Wymelenberg, G. Sabat, S. S. Bondurant, K. Syed, J. Yadav, H. Doddapaneni, V. Subramanian, J. L. Lavín, J. A. Oguiza, G. Perez, A. G. Pisabarro, L. Ramírez, F. Santoyo, E. Master, P. M. Coutinho, B. Henrissat, V. Lombard, J. K. Magnuson, U. Kües, C. Hori, K. Igarashi, M. Samejima, B. W. Held, K. Barry, K. LaButti, A. Lapidus, E. Lindquist, S. Lucas, R. Riley, A. Salamov, D. Hoffmeister, D. Schwenk, Y. Hadar, O. Yarden, R. P. de Vries, A. Wiebenga, J. Stenlid, D. C. Eastwood, I. V. Grigoriev, R. Berka, R. A. Blanchette, P. Kersten, A. T. Martínez, R. Vicuña, and D. Cullen.
  Proc. Natl. Acad. Sci. USA 109:5458-5463. 2012.

  Páginas 91-99

- **Capítulo 6: "Lignin-degrading peroxidases from genome of selective ligninolytic fungus *Ceriporiopsis subvermispora*"**
  Fernández-Fueyo, E., F. J. Ruiz-Dueñas, Y. Miki, M. J. Martínez, K. E. Hammel, and A. T. Martínez.
  J. Biol. Chem. 287:16903-16906. **2012**.

  Páginas 101-116

- **Capítulo 7: "Catalytic and stability properties of manganese peroxidase subfamilies: A study based on the *Ceriporiopsis subvermispora* genome"**
  Fernández-Fueyo, E., S Acebes. , F. J. Ruiz-Dueñas, , M. J. Martínez, A. Romero, F. J. M , V Guallar and A. T. Martínez
  (enviado).

  Páginas 117-133

- **Capítulo 8: "Engineering a lignin-degrading peroxidase acting at very acidic pH**
  Fernández-Fueyo, E., F. J. Ruiz-Dueñas and A. T. Martínez.
  (enviado).

  Páginas 135-150

- **Capítulo 9: Discusión**

  Páginas 151-159

- **Capítulo 10: Conclusiones**

  Páginas161-163

- **Capítulo 11: Anexo (con Material Suplementario)**

  Páginas 165-227

La secuenciación de los genomas de *Pleurotus ostreatus* y *Ceriporiopsis subvermispora* nos ha permitido investigar las propiedades bioquímicas, estructurales y operacionales de las diferentes hemoperoxidasas ligninolíticas presentes en dos hongos modelo de interés biotecnológico, por su capacidad para degradar preferentemente la lignina frente a la celulosa en diferentes sustratos lignocelulósicos.

Las constantes cinéticas de las diferentes peroxidasas de clase-II (de la superfamilia de peroxidasas vegetales-fúngicas-procariotas) del genoma de *P. ostreatus*, tras su expresión heteróloga en *Escherichia coli*, revelan un repertorio formado por tres peroxidasas versátiles (VPs) y seis manganeso peroxidasas (MnPs), confirmando la ausencia de lignina peroxidasa (LiP), a la que hasta ahora se ha asociado la capacidad para degradar la lignina, en los hongos ligninolíticos. Este estudio muestra por primera vez la presencia en una MnP del triptófano catalítico superficial conservado en todas las VPs y LiPs. Esta anomalía se explica por una mutación durante la evolución de estas peroxidasas que interrumpió la vía de transporte electrónico desde la superficie hasta el grupo hemo, como se demostró por mutagénesis dirigida reversa. Los estudios estructurales-funcionales de las seis MnPs de *P. ostreatus* revelan que éstas constituyen una nueva subfamilia, caracterizada por su actividad independiente de Mn sobre algunos sustratos y por la presencia de una cola en el extremo C-terminal más corta que en las típicas MnPs largas de *P. chrysosporium*. Se ha cristalizado un miembro de esta nueva subfamilia, siendo la primera MnP corta cristalizada. Además, usando dímeros modelo y lignina sintética marcados radioactivamente se ha mostrado por primera vez la capacidad de las VPs para degradar la lignina. Estos resultados confirman que la VP desempeña en *P. ostreatus* y en otras especies de agaricales el papel desempeñando por la LiP en *P. chrysosporium* y otras especies de poliporales.

En general las diferentes isoenzimas de MnP y de VP del genoma de *P. ostreatus* no presentan grandes diferencias en sus constantes catalíticas pero, sorprendentemente, si muestran grandes diferencias en su estabilidad a la temperatura (con valores de T_{50} de 43-63 ºC, tras 10 min a pH 5) y al pH (con actividades residuales de 0-96% a pH 3 y de 0-57% a pH 9, en ambos casos tras 4 h a 4 ºC). La isoenzima más estable al pH y la más estable a la temperatura de *P. ostreatus* se cristalizaron y su estructura fue resulta a 1.0-1.1 Å para intentar identificar las bases estructurales de estas propiedades. La mayor abundancia de residuos básicos, y de puentes de hidrogeno e interacciones salinas, en la superficie de la proteina se relaciona con la estabilidad de una de estas peroxidasas, como se ha confirmado en estudios posteriores de mutagénesis dirigida. Para investigar el significado biológico de la duplicación de genes y la existencia de múltiples MnPs y VPs, se diseñaron cebadores específicos para cada isoenzima y se analizaron por RT-qPCR las diferencias de expresión cuando se modifican las condiciones de temperatura y pH en cultivos de *P. ostreatus* sobre material lignocelulósico, en combinación con estudios proteómicos y medidas de actividad. No se encontró una correlación entre los resultados secretómicos y de transcripción de la isoenzima más expresada, debido a una secreción deficiente puesta de manifiesto mediante la comparación del secretoma y el proteoma intracelular. Sin embargo, los genes de algunas de las enzimas más estables mostraron niveles de transcripción relativa mayores en las condiciones más extremas de pH y temperatura ensayadas. Estos resultados muestran una regulación ambiental de la expresión de las isoenzimas, pero también ponen de manifiesto la necesidad de realizar estudios cuidadosos para establecer relaciones entre los datos transcriptómicos y la producción extracelular de enzimas por estos hongos.

Aunque *Phanerochaete chrysosporium* ha sido durante años el hongo ligninolítico modelo, su patrón de degradacion simultanea de la lignocelulosa, impide su uso en

aplicaciones biotecnológicas donde se busca el aprovechamiento de la celulosa. Por el contrario, *C. subvermispora* es un degradador selectivo de interés en la deslignificacion de la madera (como las especies de *Pleurotus* en la deslignificación de residuos agricolas) pero en sus cultivos nunca se habían identificado peroxidasas degradadoras de lignina, como LiP y VP. La secuenciación del genoma de *C. subvermipora* mostró un número inusualmente elevado de MnPs, junto con genes implicados en la síntesis de ácidos grasos insaturados, lo que sugirió su contribución en la degradación de la lignina a traves de los radicales derivados de la peroxidación de los lípidos. Sin embargo, en el genoma de *C. subvermispora* también se identificaron dos genes de una putativa LiP y una putativa VP. Estos genes se expresaron, las proteínas obtenidas se caracterizaron bioquímicamente y, al igual que en el caso de *P. ostreatus*, se determinó su capacidad de degradar directamente la lignina usando dímeros modelo y lignina sintética marcada radioactivamente. Estos estudios confirman que los dos nuevos genes identificados en el genoma de *C. subvermispora* corresponden a LiPs funcionales, que posiblemente representan formas de transición entre VP y LiP. Esta última conclusión se deduce de la incapacidad de oxidar Mn^{2+} y de las constantes cinéticas sobre sustratos aromáticos por parte de la enzima inicialmente identificada como VP. Esta enzima presenta un sitio hipotético de oxidación de Mn^{2+} (constituido por tres residuos ácidos junto al propionato interno del hemo) que resultó ser no-funcional por la presencia de un cuarto residuo ácido contiguo (ausente en VPs y MnPs) tal como se mostró mediante mutagénesis dirigida.

En los últimos estudios de los genomas de basidiomicetos se ha diferenciado una nueva subfamilia de MnPs, además de las MnP de tipo corto y largo mencionadas anteriormente, que se han denominado MnP extralargas. Estos tres tipos de MnPs comparten el sitio de unión del Mn, y se ha sugerido que presentarían propiedades catalíticas y de estabilidad diferentes. Los tres tipos de MnP están presentes en el genoma de *C. subvermispora*, lo que ha supuesto una oportunidad única para comparar las tres subfamilias propuestas, sin las interferencias derivadas de diferentes historias evolutivas (en diferentes hongos). Tras su expresión heteróloga, se caracterizaron bioquímica y estructuralmente y se realizaron estudios de mutagénesis dirigida en la cola C-terminal. Esta cola se localiza próxima al sitio de oxidación del Mn y su eliminación confiere a las MnPs largas y extralargas la actividad independiente de Mn que caracteriza a las MnPs cortas. Estos estudios permitieron concluir que las MnP de tipo corto constituyen una subfamilia verdadera, con diferentes propiedades catalíticas y de estabilidad debidas a la presencia de una cola de tipo corto, mientras que las MnPs llamadas largas y extralargas no muestran suficientes diferencias para considerarse dos subfamilias diferentes. Una MnP extralarga extremadamente estable (que mantiene la actividad a pH 2, que inactiva a otras peroxidasas ligninolíticas) fue cristalizada y su estructura resuelta a 1.2 Å, siendo la primera peroxidasa de este tipo de la que se obtiene la estructura molecular. Tras su caracterización estructural-funcional, esta MnP se usó como una base "robusta" para, mediante la introducción de un triptófano catalítico, construir una peroxidasa de interés biotecnológico. Ésta es capaz de actuar a pH extremadamente ácido, lo que incrementa el poder oxidante sobre compuestos aromáticos recalcitrantes pero inactiva a las LiPs y VPs naturales.

Los resultados obtenidos en la presente tesis han permitido establecer la existencia de enzimas de tipo LiP en *C. subvermispora* y confirmado su ausencia en *P. ostreatus*, donde estarían sustituidas por VPs. Por otro lado, aportan la primera caracterización estructural-funcional de las MnP cortas, y muestran que las descritas como MnPs largas y extralargas no presentan suficientes diferencias para establecer dos subfamilias.

The sequenced genomes of *P. ostreatus* and *C. subvermispora* allowed us to investigate the biochemical, structural and operational properties of the different ligninolytic hemeperoxidases present in two model fungi of biotechnological interest, due to their ability to degrade lignin preferentially when growing on lignocellulosic substrates.

The kinetic constants of the different class-II peroxidases (of the superfamily of plant-fungal-prokaryotic peroxidases) from the *P. ostreatus* genome, after their heterologous expression in *Escherichia coli*, revealed a repertoire formed by three VPs and six MnPs and confirmed the absence of LiP, which until now has been associated with the ability of white-rot fungi to degrade lignin. The study also showed for the first time the presence in a MnP of the conserved catalytic tryptophan that oxidizes the bulky lignin polymer at the surface of VPs and LiPs. This anomaly was explained by a natural mutation in peroxidase evolution that interrupts the electron transfer pathway from the surface to the activated heme cofactor, as shown by reversed mutagenesis. The structural-functional study of the six MnPs revealed that they correspond to a novel subfamily characterized by their Mn-independent activity on some substrates and the presence of a C-terminal tail shorter than in typical (long) MnPs from *Phanerochaete chrysosporium*. One member of this new subfamily has been crystallized, being the first short MnP crystallized to date. Moreover, studies using ^{14}C-labeled lignin and model dimers showed for the first time the lignin degrading ability of VPs. The above results confirm that VP plays in *P. ostreatus* and other species of Agaricales the role of LiP in *P. chrysosporium* and other species of the order Polyporales.

In general the different MnP and VP isoenzymes from *P. ostreatus* genome present slightly differences in their catalytic constants but, surprisingly, they show significant differences in their stability against temperature (with T_{50} values of 43-63 ºC, after 10 min at pH 5) and pH (with residual activities of 0-96% at pH 3 and 0-57 % at pH 9, after 4 h at 4 ºC). To take advantage from all the above findings, the two isoenzymes from the *P. ostreatus* genome with the highest thermal and pH stabilities were crystallized, with the aim of identifying the structural bases of the above properties. The high abundance of basic residues and salt-bridge/H-bond interactions at the surface of the protein was related to the high stability of one of these peroxidases, as confirmed by directed mutagenesis. To investigate the biological meaning of these differences, specific primers were designed for each isoenzyme and their differential transcription was analyzed by quantitative PCR, by varying the temperature and pH conditions of cultures grown in a lignocellulose medium, combined with secretomic and activity studies. Although the genes of some of the most stable isoenzymes showed higher relative transcription levels at the most extreme temperature and pH conditions assayed, no correlation between the transcriptomic and secretomic results was observed for the most expressed MnP gene. This was due to impaired secretion as shown by the abundance of this isoenzyme in the intracellular proteome. These results showed the environmental regulation of isoenzyme gene expression, but also evidenced the need for careful studies to establish correlations between transcriptomic data and production of extracellular enzymes by these fungi.

Although *P. chrysosporium* has been the model ligninolytic fungus for years, the simultaneous degradation of wood lignin and polysaccharides prevents its use in biotechnological applications, where the use of cellulose is intended. In contrast, *C. subvermispora* is a selective lignin degrader of interest in wood delignification (similar to *Pleurotus* species in delignification of agricultural wastes) but its production of lignin-degrading peroxidases (LiPs and VPs) remained unknown. The sequenced *C.*

subvermipora genome revealed an unusually high number of MnPs, together with genes implicated in the synthesis of unsaturated fatty acids, suggesting their contribution in lignin degradation via free radicals derived from lipid peroxidation. However, in the *C. subvermispora* genome two genes of one putative VP and one putative LiP were also found. These genes were heterologously expressed, the obtained proteins were biochemically characterized and, as in the case of *P. ostreatus* peroxidases, their ability to degrade lignin was demonstrated using a radiolabeled model dimer and synthetic lignin. These studies confirm that these two new identified genes in *C. subvermispora* genome correspond to functionally competent LiPs, which probably represent VP-to-LiP transitional forms. This conclusion was based on the kinetics constant on aromatic substrates and the inability to oxidize Mn^{2+} of the enzyme initially identified as a VP. This enzyme presents an hypothetical Mn^{2+}-oxidizing site (formed by three acidic residues close to the internal heme propionate) which was non-functional due to the presence of a neighbor forth acidic residue (absent in VPs and MnPs) as demonstrated by site directed mutagenesis.

In addition to the above mentioned short and long MnP subfamilies, a new subfamily of the so-called extralong MnPs has been distinguished in recent surveys of basidiomicete genomes. The three different MnP types share a Mn-binding site, but it has been suggested that they would differ in their catalytic and stability properties. Interestingly, the genome of *C. subvermispora* revealed the joint presence of short, long and extralong MnPs (in addition to the above mentioned LiPs) offering a unique opportunity to compare the three proposed subfamilies. After their heterologous expression, we performed a biochemical and structural characterization, together with directed mutagenesis studies of the C-terminal tail. This tail is located at the vicinity of the conserved Mn-oxidation site and its removal from extralong and long MnPs confers them the Mn-independent activity characteristic of short MnPs. It was concluded that the short forms represent a true MnP subfamily, whose different catalytic and stability properties are related to the presence of the tail, while the so-called long and extralong MnPs did not show enough differences to be classified as two separate subfamilies. A highly stable extralong MnP (maintaining its activity at pH 2, which inactivate other peroxidases) was crystallized and its structure was solved at 1.2 Å, being the first extralong MnP crystallized to date. After its structural-functional characterization, this MnP was used as a robust scaffold to obtain stable high redox-potential peroxidases of biotechnological interest, by introducing an exposed catalytic tryptophan. This enzyme was able to act at extremely acidic pH that increases its oxidizing power against recalcitrant aromatic compounds but inactivates wild-type LiPs and VPs.

The results obtained in this thesis have allowed to establish the existence of LiP type enzymes in *C. subvermispora* and confirm their absence in *P. ostreatus*, where they are substituted by VPs. On the other hand, the first structural-functional characterization of short-MnP has been performed and the results obtained for long and extralong MnPs show that they do not present enough differences to be classified as two different peroxidase subfamilies.

Capítulo 1

Introducción

1. Biorrefinerias

La biomasa lignocelulosica es la materia prima renovable más abundante en la tierra, con una producción anual de unos 200 billones de toneladas. La bioconversión de la biomasa lignocelulósica (residuos agrícolas, madera, cultivos para la producción energía y otros) en biocombustibles y otros productos de valor añadido, ofrece numerosas ventajas geopolíticas y ambientales, así como beneficios económicos (Ragauskas et al., 2006).

Del mismo modo que en las refinerías petrolíferas se producen diferentes combustibles y productos derivados del petróleo, las biorrefinerias lignocelulósicas buscan maximizar el valor de la biomasa vegetal como materia prima mediante la obtención de productos de valor añadido a partir de cada uno de sus diferentes componentes (**Figura 1**). Mediante diferentes conversiones tecnológicas se pueden obtener combustibles de segunda generación, productos químicos de valor añadido y piensos para la alimentación animal, simultáneamente con la electricidad necesaria para autoabastecerse. El aumento de la obtención de productos de valor añadido, la reducción de los costes energéticos y la disminución de la producción de residuos contaminantes permite avanzar hacia la sostenibilidad industrial.

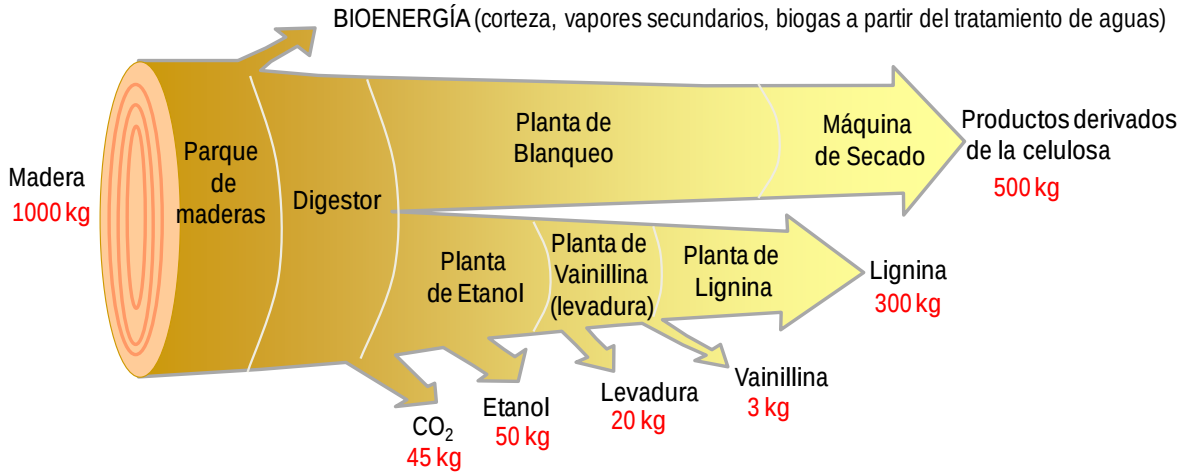

Figura 1. La biorrefineria lignocelulósica: concepto integrado de los productos químicos basados en la madera obtenidos por la empresa Borregaard en Noruega (adaptado de G. Rodsrud).

El proceso clave y limitante para el uso de esta biomasa lignocelulósica es la eliminación de la lignina. La eliminación industrial, a menudo implica el uso de tratamientos químicos agresivos y muy costosos, por lo que el uso de la biotecnología puede representar una alternativa más económica y respetuosa con el medio ambiente (Himmel et al., 2007; Martínez et al., 2009).

En los últimos años, la biotecnología “blanca” (biotecnología industrial) ha evolucionado mucho gracias a los avances en la biología molecular, la genómica y otras ramas de la biología y la ingeniería, y a los compromisos políticos para fomentar el uso de biocombustibles y la obtención de productos de interés a partir de la biomasa lignocelulósica.

El desarrollo de los bioprocesos es complejo, al estar dividido en diferentes etapas susceptibles de optimización, que incluyen la búsqueda de nuevos catalizadores, la caracterización, ingeniería, y aplicación de los nuevos biocatalizadores y el proceso de

recuperación de los productos obtenidos (**Figura 2**). Entre los últimos avances en la búsqueda de nuevos catalizadores, cabe destacar el esfuerzo del departamento de energía de Estados Unidos (DOE) secuenciado más de 80 genomas fúngicos de interés en las biorrefinerias de la lignocelulosa (www.jgi.doe.gov), entre los que se incluyen los genomas de *Ceriporiopsis subvermispora* y *Pleurorus ostreatus* en los que se ha basado esta tesis doctoral. Utilizando estos dos genomas, se han buscado biocatalizadores (de tipo peroxidasa) capaces de degradar la lignina, se han expresado y caracterizado tanto catalíticamente como estructuralmente y se ha determinado su estabilidad. Los biocatalizadores con propiedades interesantes para su aplicación biotecnológica, han sido sometidos a mutagénesis dirigida para mejorar sus propiedades.

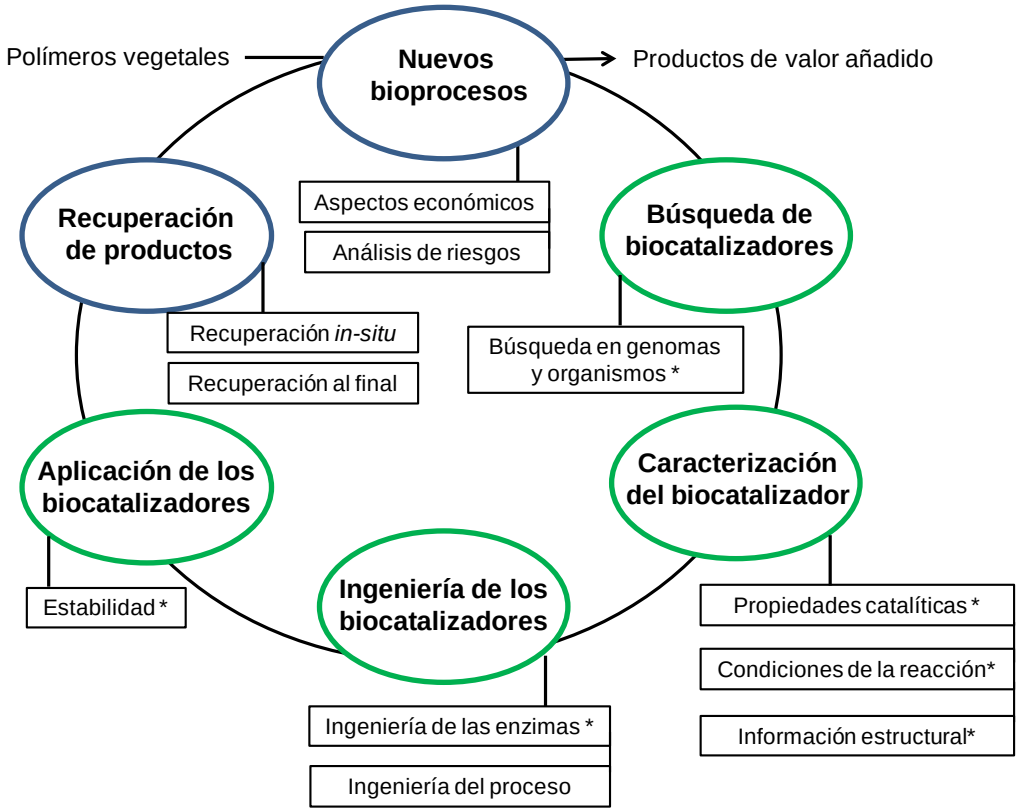

Figura 2. El ciclo de optimización de un bioproceso. Los procesos estudiados durante esta tesis doctoral están marcados con un asterisco. Adaptado de Schmid et al. (2001).

2. Composicion de la biomasa lignocelulósica

La mayor parte del carbono fijado por fotosíntesis se acumula en forma de biomasa vegetal, formada principalmente por celulosa (30-50%), hemicelulosa (15-35%) y lignina (10-25%), además de pequeñas cantidades de otros materiales como lípidos y otros compuestos extraíbles, ceniza, proteínas y pectina en diferentes proporciones (**Figura 3**) (Fengel and Wegener, 1984; Pettersen, 1984; Sánchez, 2009).

La celulosa, el componente mayoritario y la molécula orgánica más abundante en la tierra, es un polímero lineal y muy ordenado formado por moléculas de glucosa unidas por enlaces β-1,4-glicosídicos, mientras que la hemicelulosa es un polímero heterogéneo formado por la unión de pentosas, hexosas y otros azúcares en cadenas ramificadas. La composición de la hemicelulosa varía ampliamente entre las diferentes especies de plantas.

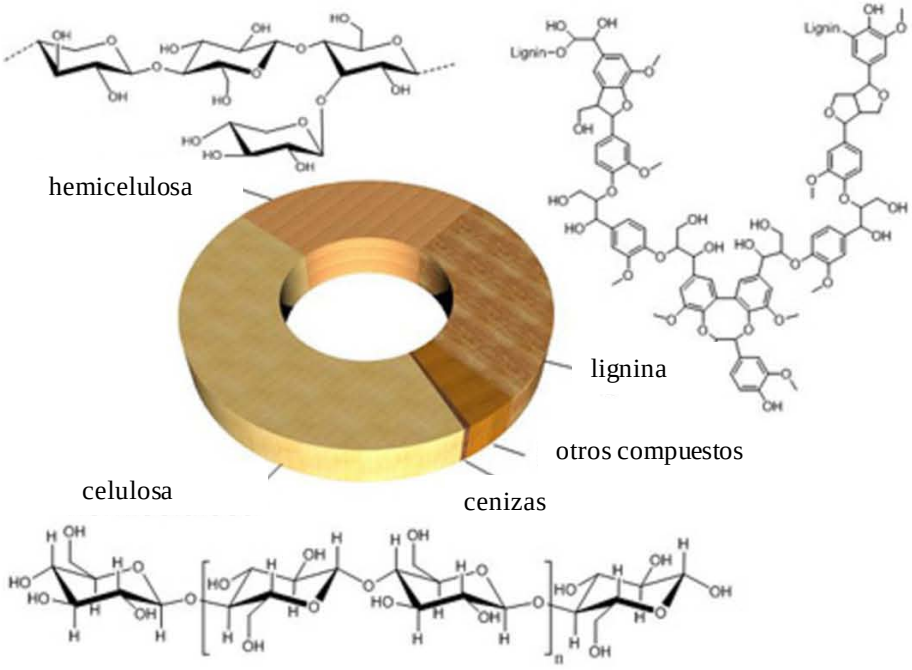

Figura 3. Componentes de la biomasa vegetal: celulosa, hemicelulosa, lignina, cenizas y otros compuestos.

La lignina es el segundo polímero más abundante en la tierra y la forma de carbono aromático más abundante. Al ser una macromolécula aromática muy compleja, es altamente recalcitrante. La lignina proporciona dureza y rigidez a la pared celular y a los tejidos vasculares de las plantas al actuar como un pegamento entre los filamentos de polisacáridos y las fibras de la madera. También está implicada en el transporte de agua en las plantas y constituye una barrera frente al ataque de los microorganismos, protegiendo a los polisacáridos. En la evolución de las plantas apareció hace 450 millones de años, permitiendo el desarrollo de las plantas vasculares (Weng and Chapple, 2010).

3. Estructura de la lignina

Desde un punto de vista químico, la lignina es un polímero tridimensional, ópticamente inactivo formado por la unión de unidades fenilpropanoides, formada aleatoriamente a partir de la polimerización de los radicales de los alcoholes precursores coniferílico (unidades G o guayacilo), p-cumarílico (unidades H o p-hidroxifenilo) y sinapílico (unidades S o siringilo) y sus formas acetiladas abundantes en plantas anuales (Sarkanen and Ludwig, 1971; Ralph et al., 2004; Gellerstedt and Henriksson, 2008; del Río et al., 2008) (**Figura 4**). Estas unidades están unidas por diferentes tipos de enlaces covalentes, dando lugar un polímero muy heterogéneo (**Figura 4**), que no puede ser descompuesto por enzimas hidrolíticas como la mayoría de los polímeros naturales (celulosa, almidón, proteínas, etc).

Su estructura y composición depende de cada tipo de planta, en gimnospermas (maderas blandas) está formada casi exclusivamente por unidades G y una cantidad minoritaria de unidades H (**Figura 4**), en las angiopermas leñosas (maderas duras) está formada tanto por unidades G como unidades S y en monocotiledoneas, los tres alcoholes se usan como precursores. El contenido en lignina también varía entre los diferentes tipos de plantas, en plantas leñosas constituye entre el 15-40% del peso total mientras que en herbáceas es menor del 15%.

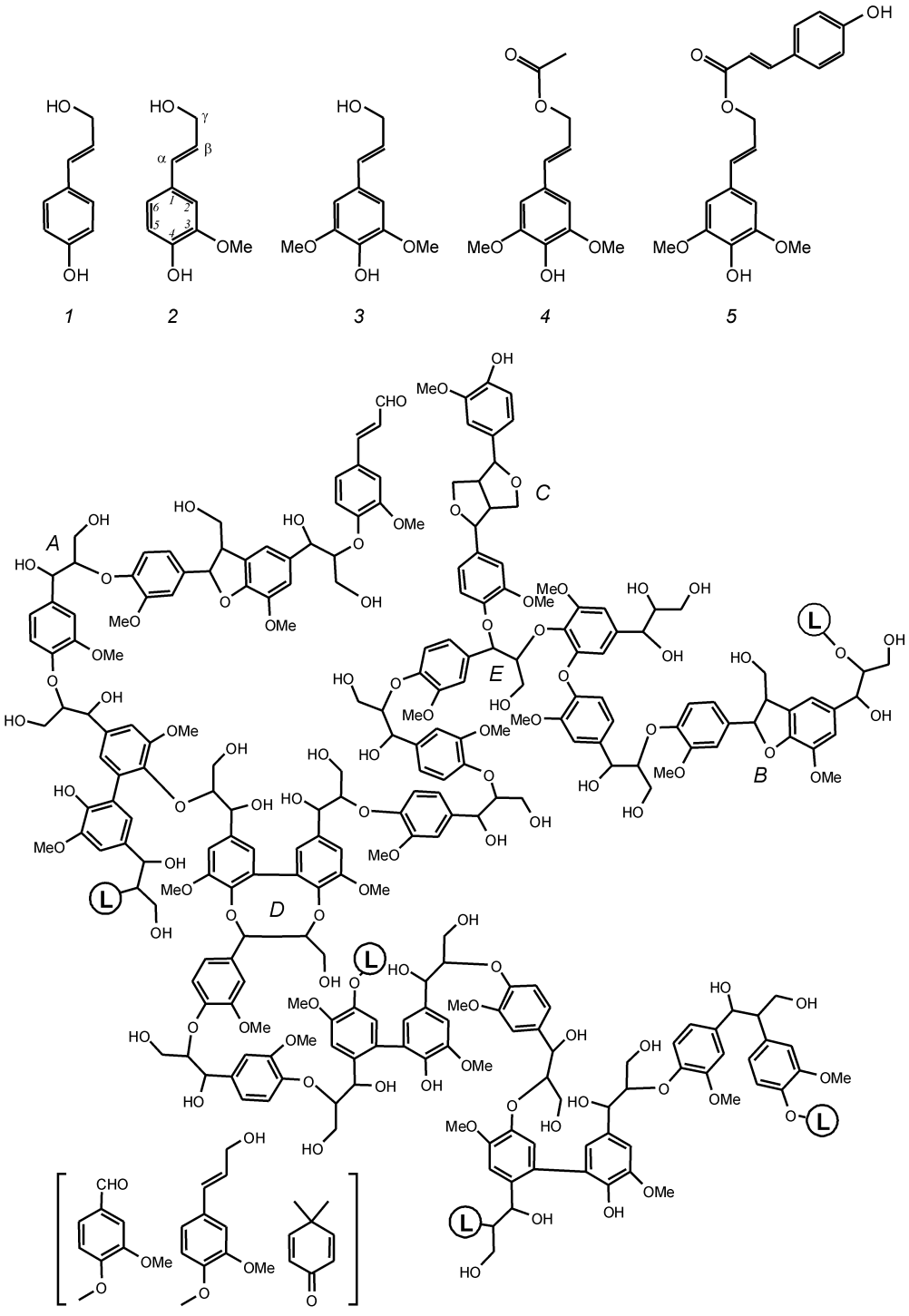

Figura 4. Monolignoles precursores de la lignina (arriba) y modelo estructural de la lignina de gimnospermas (abajo). Los clásicos: p-cumarílico (1), coniferílico (2) y sinapílico (3). Acetilados: derivados del alcohol sinapílico γ-esterificado con acético (4) y ácido p–cumárico (5). El tipo de lignina más simple es producido por las gimnospermas y está formado exclusivamente por unidades G, como se ve en la figura. Una variedad de enlaces éter y C-C se forman durante la polimerización de los monolignoles, resultando en subestructuras β-O-4´(**A**), fenilcumarano (**B**), pirroresinol (**C**), dibenzodioxocina (**D**) y otras como α-O-4´/β-O-4´ (**E**) (**L:** lignina). Las subestructuras minoritarias (entre corchetes) incluyen vainillina, alcohol coniferílico terminal y dimetilciclohexadienonas como las espirodienonas (Zhang et al., 2006). Tomado de Ruiz-Dueñas et al. (2009)

4. Organismos degradadores de lignina

La degradación de la lignina es un paso clave en el reciclado del carbono terrestre, al permitir la degradación de los polisacáridos vegetales. A lo largo de la evolución, sólo un grupo de basidiomicetes junto con algunos ascomicetes y bacterias, ha desarrollado la habilidad de degradar (o modificar) la lignina (Martínez et al., 2005). La aparición de estos basidiomicetes ligninolíticos se correlaciona con el descenso brusco de la acumulación de carbono orgánico en el suelo y la formación de carbón al final del Carbonífero (Floudas et al., 2012).

En función de los patrones de degradación, los hongos se dividen en cuatro grupos, hongos de la podredumbre blanca, hongos de la podredumbre parda, hongos de la podredumbre blanda y hongos que tiñen la madera (Liese, 1970; Blanchette, 1991; Schwarze et al., 2000; Martínez et al., 2005; 2011). Estos dos últimos grupos son ascomicetes que sólo son capaces de modificar la madera en condiciones ambientales especiales (podredumbre blanda) o colonizarla a través de los vasos o canales existentes (hongos que tiñen la madera).

Los hongos de la podredumbre parda son capaces de modificar la lignina, pero los productos resultantes de la reacción permanecen *in situ* como un residuo polimérico de color parduzco (Yelle et al., 2008; Martínez et al., 2011) (**Figura 5**). *Postia placenta* fue elegido como organismo modelo en el estudio del genoma, transcriptoma y secretoma de este tipo de hongos (Martinez et al., 2009).

Los hongos de la podredumbre blanca son los únicos organismos conocidos capaces de degradar completamente la lignina, transformándola en dióxido de carbono y agua (Kirk and Farrell, 1987), sin embargo no pueden utilizar la lignina como única fuente de carbono y energía. La degradación de la lignina, les permite el acceso a la celulosa y hemicelulosa, que son sus fuentes de carbono y energía (Leatham, 1986).

Figura 5. Patrones de degradación de la madera por los basidiomicetos. A la izquierda, patrón de degradación por un hongo de la podredumbre blanca que elimina la lignina dejando accesibles la celulosa, de color blanquecino, que excepcionalmente puede llegar a ser consumida por el ganado. A la derecha, patrón de degradación por un hongo de la podredumbre parda, donde los polisacáridos son consumidos y la lignina permanece *in situ* como un residuo polimérico de color parduzco. Tomado de Martínez et al. (Martínez et al., 2011).

Los hongos de la podredumbre blanca, se dividen a su vez en dos grupos que se caracterizan, bien por degradar tanto la lignina como los polisacáridos (degradación simultánea) como *P. chrysosporium*, o por una degradación preferencial de la lignina, donde la mayoría de los

polisacáridos quedan intactos (degradación selectiva) como en el caso de *C. subvermispora* (Blanchette et al., 1985; Blanchette et al., 1997; del Río et al., 2001).

Aunque *P. chrysosporium* ha sido el hongo modelo en estudios de biodegradación de lignina (Kersten and Cullen, 2007), su aplicación biotecnológica es limitada al degradar los polisacáridos simultáneamente con la lignina (Martínez et al., 2009). Por el contrario, *C. subvermispora* ha sido muy estudiado para el bio-pulpeo en la industria papelera, por ser un degradador selectivo (Scott et al., 1998; Ferraz et al., 2003) (**Figura 6**). Por otro lado, *Pleurotus eryngii* ha sido estudiado por su capacidad de degradar selectivamente la lignina de plantas anuales (Martínez et al., 1994) utilizando un sistema ligninolítico diferente al de *P. chrysosporium* (Ruiz-Dueñas et al., 2011).

Figura 6. *C. subvermispora* creciendo en la naturaleza y proceso de bio-pulpeo de 50 toneladas de madera tratado con este hongo. Biopulping realizado por Gary M. Scott en la Facultad de Papel e Ingeniería de Bioprocesos en Nueva York.

5. Sistema ligninolítico de los hongos de la podredumbre blanca

En 1987, se describió el proceso de degradación de la lignina como una "combustión enzimática" (Kirk and Farrell, 1987), es decir, una degradación oxidativa inespecífica catalizada por enzimas. El gran tamaño de la lignina junto con su estructura ramificada formando una red tridimensional, implica que los mecanismos de degradación sean extracelulares. La heterogeneidad de la lignina (**Figura 4**) requiere un proceso poco específico y su baja solubilidad en agua, que limita su biodisponibilidad, hace que su degradación sea un proceso lento.

Hoy sabemos, que el sistema ligninolítico de los hongos de la podredumbre blanca está formado por enzimas extracelulares de tipo fenoloxidasa, peroxidasa y oxidasa generadora de peróxido junto con compuestos de bajo peso molecular que actúan como intermediarios.

5.1. Enzimas implicadas

Las **lacasas** (EC 1.10.3.2) contienen átomos de cobre en su centro catalítico y pertenecen al grupo de las oxidasas multicobre (Baldrian, 2006). Catalizan la reducción del oxígeno a agua a través de la oxidación de fenoles substituidos o aminas aromáticas, entre otros (Thurston, 1994; Mayer and Staples, 2002). Son capaces de romper dímeros fenólicos de forma directa y de tipo no fenólico en presencia de intermediarios o mediadores redox (Cañas and Camarero, 2010), entre los que se incluyen metabolitos fúngicos y productos derivados de la lignina (Eggert et al., 1996; Johannes and Majcherczyk, 2000; Camarero et al., 2005).

Están presentes tanto en hongos de la podredumbre parda como de podredumbre blanca (Floudas et al., 2012), aunque en el caso de *P. chrysosporium* no se ha detectado en su genoma ninguna lacasa en sentido estricto (Martinez et al., 2004).

Las **peroxidasas ligninolíticas** son un grupo de hemoperoxidasas incluidas en la clase II de la superfamilia de peroxidasas vegetales-fúngicas-procariotas. Estas enzimas presentan un grupo hemo de tipo protoporfirina IX unido de forma no covalente y localizado en una cavidad interna conectada con el solvente a través de un canal principal, que permite el acceso tanto de peróxido de hidrógeno como de pequeños sustratos (Banci, 1997; Dunford, 1999). Catalizan la oxidación de gran variedad de compuestos orgánicos e inorgánicos a expensas de H_2O_2 (Dunford, 1999). Las peroxidasas ligninolíticas se dividen en tres familias - lignina peroxidasas (LiP), manganeso peroxidasas (MnP) y peroxidasas versátiles (VP) - y se caracterizan por su elevado potencial redox. Se ha demostrado la capacidad de la LiP de degradar la lignina *in vitro* (Hammel et al., 1993) y recientemente de la VP (como parte de esta tesis doctoral) (Fernández-Fueyo et al., 2014). La MnP puede degradar la lignina a través de la peroxidación de los lípidos (Bao et al., 1994), ya que su acción directa (Wariishi et al., 1991) está por confirmar. De acuerdo con el papel central de las peroxidasas en la degradación de la lignina, los hongos de la podredumbre blanca tienen entre 5 y 26 copias de genes que codifican para peroxidasas ligninolíticas (14 copias de media) (**Tabla 1**) y, como se ha mencionado anteriormente, no están presentes ni en hongos de la podredumbre parda ni en hongos patógenos, a diferencia de las lacasas (Floudas et al., 2012) .

El **H_2O_2** desempeña un papel central en el ataque a la madera por parte de los hongos. Es el sustrato oxidante de las peroxidasas ligninolíticas (Ruiz-Dueñas and Martínez, 2009). Además, en presencia de Fe^{2+}, puede atacar la pared celular a través del radical hidroxilo ($OH^{\bullet}$) procedente de la reacción de Fenton ($Fe^{2+} + H_2O_2 \rightarrow Fe^{3+} + H_2O + OH^{\bullet}$) en hongos de la podredumbre parda y blanca (Forney et al., 1982; Faison and Kirk, 1983; Guillén et al., 2000; Gómez-Toribio et al., 2009). En 1983, Faison y Kirk (1983) demostraron que el H_2O_2 se produce simultáneamente con el sistema ligninolítico, y que la adicción de catalasa a los cultivos fúngicos, disminuye la capacidad de degradar la lignina. Se han propuesto numerosas enzimas extracelulares que pueden estar implicadas en la producción de H_2O_2 extracelular en los hongos de la podredumbre blanca, como la glioxal-oxidasa (Kersten and Kirk, 1987), la aril-alcohol oxidasa (AAO) (Guillén et al., 1992a; Guillén et al., 1992b), la metanol oxidasa (Ozimek et al., 2005)y la piranosa oxidasa (Daniel et al., 1994). También existen enzimas intracelulares productoras de H_2O_2 (Greene and Gould, 1984; Eriksson et al., 1986), pero se desconoce la existencia de un sistema transportador para el H_2O_2 producido. Los sustratos de estas enzimas durante la degradación de la lignocelulosa incluyen tanto compuestos derivados de la lignina como metabolitos aromáticos producidos por los hongos, entre los que se incluyen aldehídos, ácidos aromáticos de tipo fenólico y aldehídos aromáticos derivados de las ruptura de enlaces Cα-Cβ o sintetizados de *novo* por el hongo (Kirk and Farrell, 1987; Shimada and Higuchi, 1991). La celobiosa deshidogenasa (CDH) podría estar implicada en la degradación de la lignocelulosa por su capacidad para reducir el Fe^{3+} a Fe^{2+} y formar H_2O_2 (reactivo de Fenton) (Henriksson et al., 2000)

La comparación de los genomas, trascriptomas y secretomas de los hongos modelo *P. placenta* (de podredumbre parda), *P. chrysosporium* (podredumbre blanda y degradación simultanea) y *C. subvermispora* (podredumbre blanda y degradación selectiva) reflejan las diferencias en los patrones de degradación lignocelulósica. La comparación de sus genomas (**Tabla 2**) indica que durante la evolución de los hongos de la podredumbre parda se concentraron o perdieron familias de genes que son importantes en los hongos de la podredumbre blanca como las peroxidasas ligninolíticas y la celobiosa deshidrogenasa. Las

diferencias entre los mecanismos de degradación simultánea o selectiva de los hongos de la podredumbre blanca, serán analizadas en detalle en el capítulo 5.

Tabla 1. Número de genes de peroxidasas de clase II presentes en los genomas de 20 Agaromicotina y otros once tipos de hongos. Especies: Ad, *Auricularia delicata*; Cp, *Coniophora puteana*; Da, *Dacryopinax sp*., Ds, *Dichomitus squalens*; Fm, *Fomitiporia mediterranea*; Fp, *Fomitopsis pinicola*; Gt, *Gloeophyllum trabeum*; Pu, *Punctularia strigosozonata*; Sh, *Stereum hirsutum*; Tm, *Tremella mesenterica*, Tv, *Trametes versicolor*; Wc, *Wolfiporia cocos*, An, *Aspergillus niger*; Bd, *Batrachochytrium dendrobatidis*; Cc, *Coprinopsis cinerea*; Cn, *Cryptococcus neoformans*; Cr, *Cryphonectria parasitica*; Ha, *Heterobasidion annosum*(ahora reclasificado como *H. irregulare*); Lb, *Laccaria bicolor*; Mg, *Malassezia globosa*; Ml, *Melampsora laricis-populina*; Pb, *Phycomyces blakesleeanus*; Pc, *P. chrysosporium*; Pp, *P. placenta*; Ps, *Pichia stipitis*; Sc, *Schizophyllum commune*; Sl, *S. lacrymans*; Sn, *Stagonospora nodorum*; Sr, *Sporobolomyces roseus*; Tr, *Trichoderma reesei*; Um, *Ustilago maydis*. Ecología: WR, podredumbre blanca; BR, podredumbre parda; ECM, micorriza; S, saprófito; MP, micoparasito; AP, patógeno/parasito animal; PP, patógeno de planta; Y, levadura. Basado en Floudas et al (2012).

	Taxonomía		Genoma	Ecología	Nº de PODs
Basidiomycota	Agaromycotina	Agaromycetes	Ha	WR	8
			Sh		6
			Pu		11
			Fm		17
			Ad		19
			Tv		26
			Ds		12
			Pc		16
			Pp	BR	1
			Wc		1
			Fp		1
			Gt		0
			Sl		0
			Cp		0
			Lb	ECM	1
			Sc	WR	0
			Cc	S	1
		Dac	Da	BR	0
		Trem	Tm	MP	0
			Cn	AP	0
	Ust		Mg	AP	0
			Um	PP	0
	Pucc		Ml	PP	0
			Sr	Y	0
Ascomycota	Pez		An	AP	0
			Cr	PP	1
			Tr	S	0
			Sn	PP	5
	Sc		Ps	Y	0
	Ch		Bd	AP	0
	Mu		Pb	S	0

Tabla 2. Comparación de los genes de enzimas potencialmente implicados en la degradación de la lignina encontrados en los genomas de los hongos modelo *P. placenta* (de podredumbre parda), *P. chrysosporium* (podredumbre blanda y degradación simultanea) y *C. subvermispora* (podredumbre blanda y degradación selectiva).

	Podredumbre parda	Podredumbre blanca	
	P. placenta	*P. chrysosporium* (degradación simultánea)	*C. subvermispora* (degradación selectiva)
Enzimas productoras de H_2O_2:			
Metanol (alcohol) oxidasa	1	2	4
AAO	3	3	5
Glucosa oxidasa	5	1	0
Glioxal oxidasa y otras oxidasas cobre-radical	3	7	4
Enzimas implicadas en modificación de lignina:			
LiP	0	10	2
MnP	0	5	13
VP	0	0	0
Peroxidasa genérica (GP)	1	0	1
Lacasas	3	0	7
Reductoras de Hierro:			
Quinona reductasa	1	4	1
Celobiosa deshidrogenasa	0	1	1

5.2. Intermediarios o mediadores redox

El gran tamaño de lignina y su posición en la pared vegetal, hacen que las enzimas ligninolíticas como MnP, LiP y VP y las lacasas necesiten mediadores para oxidarla (Flournoy et al., 1993). Se han identificado varios compuestos de bajo peso molecular que pueden desempeñar un papel clave dentro del sistema ligninolítico de los hongos de la podredumbre blanca (Lundquist and Kirk, 1978a; Wariishi et al., 1992; de Jong et al., 1994a; Mester and Field, 1997).

5.2.1. Manganeso

Es un componente natural de la madera, donde está presente en una concentración entre 10-100 mg/kg de madera seca (Fengel and Wegener, 1984). Favorece la ligninolisis en los hongos de la podredumbre blanca al estimular la producción de MnP aunque suele inhibir la producción de LiP (Bonnarme and Jeffries, 1990). También induce la manganeso superoxido dismutasa que contribuye a disminuir el estrés oxidativo (Rothschild et al., 1999).

La oxidaxión de Mn^{2+} a Mn^{3+} es realizado por las MnPs y VPs , mientras que las LiPs carecen del sitio de oxidación del Mn^{2+}. Se ha encontrado actividad MnP en la mayoría de los hongos de la podredumbre blanca y en los hongos del suelo (Orth et al., 1993; Hatakka, 1994). La oxidación del Mn^{2+} también puede producirse indirectamente a través del radical aniónico superóxido (Muñoz et al., 1997).

El Mn^{3+} es un oxidante fuerte ($E_0' = 1{,}54V$), pero es muy inestable en el medio acuoso, ya que puede reaccionar con sustratos reductores o dismutar dando lugar a Mn^{2+} y Mn^{4+}. Los hongos de la podredumbre blanca secretan ácidos orgánicos, principalmente ácido oxálico (Takao,

1965), que forman quelatos con el Mn^{3+} estabilizándolo con un potencial rédox algo menor (E_0´= 0,9-1,2V). Estos quelatos actúan como oxidantes estables difusibles de compuestos fenólicos, aminas aromáticas y ácidos carboxílicos (Paszczynski et al., 1986; Wariishi and Gold, 1989; Wariishi et al., 1991; Hammel et al., 1993). Estos quelatos también son capaces de oxidar ácidos grasos insaturados y sus derivados formando radicales lipídicos de tipo peroxilo (Kapich and Shishbina, 1995), que son altamente reactivos y pueden reaccionar con otras moléculas de lípidos insaturados para propagar la oxidación, produciendo un proceso de peroxidación lipídica en cadena.

Se ha descrito como la peroxidación de acidos grasos insaturados por parte de las MnP permite la ruptura oxidativa de fenantreno, hidrocarburos policíclicos aromáticos y de un dímero modelo no fenólico de lignina (Moen and Hammel, 1994; Bao et al., 1994). Este mecanismo parece estar implicado en la degradación de la lignina por algunos hongos basidiomicetos de la podredumbre blanca (Fernández-Fueyo et al., 2012a).

5.2.2. Alcohol veratrílico (VA)

Es un metabolito aromático de los basidiomicetos que se sintetiza de novo a partir de glucosa (Shimada and Takahashi, 1991). Es el sustrato típico de las LiPs aunque también es oxidado con menor eficiencia por VPs (Fernández-Fueyo et al., 2012b). Es secretado por algunos hongos como *P. chrysosporium* y *Bjerkandera adusta* durante la oxidación de la lignina (Lundquist and Kirk, 1978b; Shimada et al., 1981).

Existe cierta controversia sobre el papel del alcohol veratrílico en la degradación de la lignina. Se ha demostrado que su presencia permite a la LiP oxidar compuestos que no es capaz de oxidar por si sola, como el Reactive Black 5 o alcohol anisílico (Harvey et al., 1986). Algunos autores proponen que el radical cationico ($VA^{+\bullet}$) formado tras la oxidación del alcohol (por la sustracción de un electrón) es el que oxida estos compuestos, actuando como mediador rédox (Harvey et al., 1986; Paszczynski and Crawford, 1991; Tien and Ma, 1997), pudiendo actuar como mediador en la despolimerización de la lignina. Por otra parte, se ha descrito como el alcohol anisílico reduce el compuesto I de la LiP, pero no el compuesto II. Por lo tanto, el alcohol veratrílico podría actuar completando el ciclo de la enzima, al reaccionar con el compuesto II, permitiendo la regeneración de la enzima al estado de reposo y evitando la formación de compuesto III (Koduri and Tien, 1994). De acuerdo a esto, se ha propuesto que el alcohol veratrilico actuaría como un agente reductor previniendo la inactivación de la enzima por peróxido (Collins et al., 1997).

Aunque la VP no requiere de mediadores redox para la oxidación de colorantes de alto potencial redox como el Reactive Black 5 (Heinfling et al., 1998), la presencia del alcohol veratrílico es necesaria para la oxidación de la lignina *in vitro* (Fernández-Fueyo et al., 2014) al igual que en el caso de la LiP (Hammel et al., 1993).

5.2.3. Metabolitos clorados

Los hongos de podredumbre blanca producen una gran variedad de compuestos halogenados (de Jong et al., 1994c; de Jong and Field, 1997), siendo los más comunes los metabolitos anisílicos clorados y las hidroquinonas cloradas (de Jong et al., 1994c; Field et al., 1995). Los primeros pueden tener importancia en la degradación de la lignina en condiciones fisiológicas, al ser sustratos de la AAO, productora de H_2O_2 en hongos de la podredumbre blanca como *P. ostreatus* y *B. adusta* (de Jong et al., 1994b). Estos compuestos clorados tienen K_m extremadamente bajas para la AAO de los hongos que los producen en comparación con los equivalentes no clorados.

Estudios previos, han descrito que el 1,4 dimetoxibenceno puede remplazar al VA como mediador (Joshi and Gold, 1996). Mientras que este compuesto no es un metabolito de los hongos de la podredumbre blanca, el 2-cloro-1,4-dimetoxibenceno y 2,6-cloro-1,4-dimetoxibenceno, que están estructuralmente relacionados, han sido detectados en cultivos de *B. adusta*, (Spinnler et al., 1994). El 2-cloro-1,4-dimetoxybenceno es oxidado por la LiP de *P. chrysosporium* (Teunissen and Field, 1998b), produciendo su radical catiónico, que actúa como un mediador difusible oxidando sustratos que la LiP no es capaz de oxidar por si sola (Teunissen et al., 1998; Teunissen and Field, 1998a; 1998b). Solamente concentraciones catalíticas (10-50 µM) de este compuesto son necesarias para mediar en la oxidación de los sustratos, lo que sugiere la importancia de este metabolito fúngico en la degradación de la lignina.

5.2.4. Mediadores de las lacasas

Las lacasas tienen un potencial redox relativamente bajo (≤0.8 V), por lo que su acción quedaría restringida a la oxidación de las unidades fenólicas de lignina (Kawai et al., 1987). Sin embargo, en presencia de mediadores redox, la actividad catalítica de las lacasas puede ser expandida hacia sustratos no fenólicos más difícilmente oxidables, en lo que se denomina sistema lacasa-mediador.

Los mediadores, mediante mecanismos de oxidación no enzimáticos, oxidan compuestos que bien sea por su elevado tamaño molecular o por su alto potencial redox, en principio no son sustratos de las lacasas. Bourbonnais y Paice (1990) fueron los primeros en describir la oxidación de dímeros no fenólicos de lignina en presencia de lacasa y el mediador ABTS (2,2'-azino-bis(3-etilbenzotiazolin-6-sulfonato)).

Los mediadores sintéticos más eficaces son compuestos que portan un grupo NOH como el 1-hidroxibenzotriazol, el ácido violúrico o la N-hidroxiacetanilida (Böhmer et al., 1998; Johannes et al., 1998; Galli and Gentili, 2004). Entre los mediadores de origen natural, destacan el ácido 3-hidroxiantranílico y el ácido 4-hidroxibenzoico, que son metabolitos secundarios de *Pycnoporus cinnabarinus* y de *T. versicolor*, respectivamente (Eggert et al., 1996; Johannes and Majcherczyk, 2000). Recientemente, Camarero et al (2005) han descrito la capacidad de ciertos compuestos fenólicos liberados durante la biodegradación de la lignina, como la acetosiringona, el siringilaldehido, la vainillina y el ácido *p*-cumárico, para actuar como mediadores redox de lacasa.

6. Enzimas de tipo peroxidasa

6.1 Características generales

Las peroxidasas (EC 1.11.1) son un tipo de enzimas muy extendidas en toda la escala filogenética, que catalizan la oxidación de gran variedad de compuestos orgánicos e inorgánicos a expensas de H_2O_2 u otros hidroperóxidos (Dunford, 1999). Los análisis filogenéticos revelan que los genes que codifican para peroxidasas tiene un origen procariota muy antiguo, que probablemente se remonta a la aparición del oxígeno atmosférico.

Se pueden dividir en dos clases según su sitio activo: las hemoperoxidasas, que contienen un grupo hemo como cofactor, presentan una gran diversidad funcional y están presenten en la mayoría de los organismos; y las peroxidasas sin grupo hemo, entre las que se encuentran pequeñas familias de proteínas heterogéneas (algunas haloperoxidasas, alquil-

hidroperoxidasas, NADH peroxidasas, tiol peroxidasas, glutation peroxidasas, peroxirredoxinas y manganeso catalasas) (Passardi et al., 2007).

En función de sus diferencias bioquímicas y estructurales, las hemoperoxidasas se han clasificado tradicionalmente en dos superfamilias: la superfamilia de peroxidasas animales (Kimura and Ikeda-Saito, 1988) y la superfamilia de peroxidasas vegetales-fúngicas-procariotas (no animales) (Welinder, 1992). Recientemente se han añadido dos nuevas superfamilias: de hemotiolato peroxidasas y DyPs (Ruiz-Dueñas and Martínez, 2010; Hofrichter et al., 2010) abundantes en genomas de basidiomicetos (Floudas et al., 2012). Estas superfamilias surgieron independientemente, tal y como se deduce de sus diferencias de secuencia, plegamiento general, unión del grupo prostético y coordinación del hierro, entre otras características.

6.2 Superfamilia de peroxidasas vegetales-fúngicas-procariotas

Los miembros de la superfamilia vegetales-fúngicas-procariotas se caracterizan por presentar un grupo hemo de tipo b (ferriprotoporfirina IX) unido de forma no covalente a la proteína, que en estado de reposo presenta un ión férrico. Se localiza en una cavidad interna y está conectado con el solvente a través de uno o dos canales (**Figura 7**). Todas las peroxidasas presentan un canal principal de acceso al hemo, que permite al de H_2O_2 para activar la enzima así como la entrada de pequeños sustratos en las peroxidasas de plantas (Gajhede et al., 1997) o algunas fúngicas (CIP) (Tsukamoto et al., 1999). Algunos miembros de esta superfamilia, presentan un segundo pequeño canal, que también actúa como un sitio catalítico, que se extiende directamente sobre los propionatos del hemo, como en las ascorbato peroxidasas (Sharp et al., 2003), las MnPs (Sundaramoorthy et al., 2005) y en las VPs (Ruiz-Dueñas et al., 2007).

Esta superfamilia está dividida en tres clases: la clase I formada por las peroxidasas intracelulares bacterianas y de orgánulos de origen procariotico, entre las que se incluyen la citocromo c peroxidasa (CcP, EC 1.11.15) y las catalasas-peroxidasas. La clase II está formada por las peroxidasas fúngicas y la clase III que está formada por las peroxidasas de plantas, que participan en la formación de la lignina mediante la oxidación de los monolignoles. En la clase III se encuentra la peroxidasa de rábano, *Armoracia rusticana*, HRP (EC 1.11.1.7), que es la peroxidasa más estudiada de esta superfamilia.

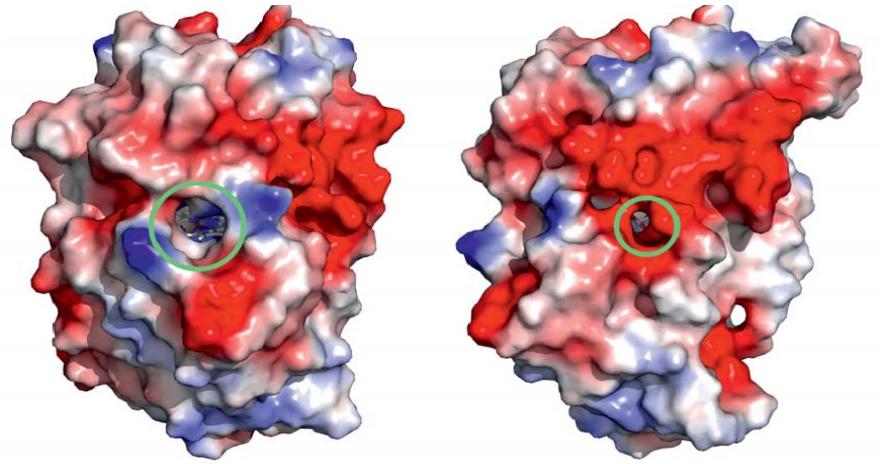

Figura 7. Superficie electrostática de la VP (PDB: 4BLK) de *P. ostreatus*. Se muestran dos orientaciones diferentes: en la derecha el canal principal de acceso al hemo y en la izquierda el canal del manganeso.

La peroxidasas de la clase II (PODs) se divididen en cuatro familias: GPs, LiPs, MnPs y VPs (Fernández-Fueyo et al., 2012b). Las tres últimas familias constituyen el grupo de las peroxidasas ligninolíticas por su implicación en la degradación de la lignina y como se ha mencionado anteriormente, son exclusivas de los hongos de la podredumbre blanca.

7. Peroxidasas ligninolíticas:

Las peroxidasas ligninolíticas son proteínas globulares de 30-40 kDa, y alrededor de 330 aminoácidos. Son extracelulares y presentan un péptido señal en el N-terminal que dirige la secreción a través del retículo endoplasmático. Su grado de glicosilación está en torno al 5%. Generalmente, el aminoácido tirosina está ausente en la secuencia, ya que sería susceptible de oxidación en las condiciones oxidativas que caracterizan a la degradación de la lignina. Sin embargo, en la LiP de *Trametopsis cervina* (Miki et al., 2011; 2013), una tirosina desempeña el mismo papel catalítico que el triptófano en otras LiPs y VPs.

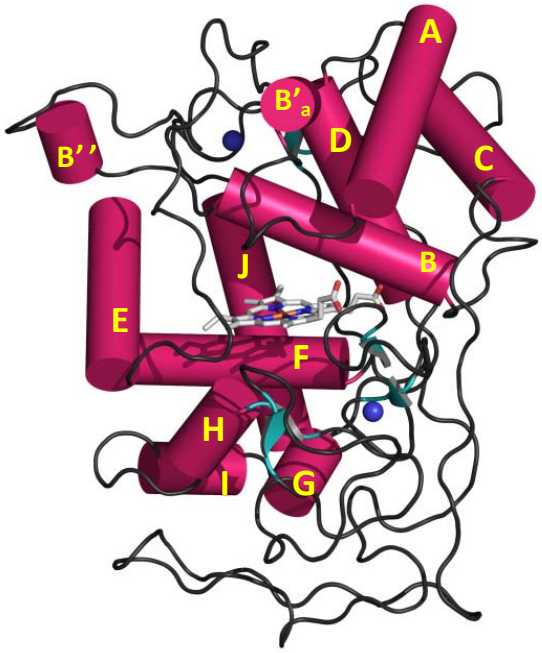

Figura 8. Estructura de la LiP-H8 de *P. chrysosporium* (PDB: 1LGA). Se muestran las 10 α hélices (de la A a la J). También se muestran los dos calcios estructurales y el grupo hemo.

7.1. Estructura de las peroxidasas ligninolíticas:

La primera peroxidasa ligninolítica cristalizada fue una LiP de *P. chrysosporium* en 1993 (Poulos et al., 1993; Edwards et al., 1993), con una estructura helicoidal muy similar a la de la CcP, cristalizada en 1984 (Finzel et al., 1984), lo que sugiere un plegamiento común entre las peroxidasas de la superfamilia de plantas, hongos y bacterias.

La estructura está formada por 10α -hélices, denominadas A-J, que constituyen alrededor del 50% de la molécula, junto con 5 estructuraβ (**Figura 8**). El grupo hemo se encuentra entre las hélices B y F, y divide a la peroxidasa en dos dominios. El dominio distal, está formado por las hélices A-D, y se localiza sobre el hemo, mientras que el dominio proximal está

formado por las hélices E-F, junto con la mayor parte de la estructura β. El nombre de estos dominios se deben a que albergan las denominadas histidinas proximal y distal, mencionadas más adelante. Presentan cuatro (VPs y MnP cortas) o cinco puentes disulfuro (MnPs largas y extralargas) que le confieren rigidez y dos iones calcios imprescindibles en el mantenimiento de la estructura.

7.2. Entorno del grupo hemo

Como se ha comentado anteriormente, las peroxidasas de clase II presentan un grupo hemo de tipo b unido de forma no covalente a la proteína. El átomo de hierro se encuentra pentacoordinado por los cuatro nitrógenos del macrociclo tetrapirrolico con la quinta posición ocupada por el Nε del anillo imidazolico de una histidina axial que recibe el nombre de histidina proximal, que se encuentra conservada en toda la superfamilia (**Figura 9A**). Además de la histidina proximal, existen otra serie de aminoácidos del entorno del hemo que se encuentran conservados, como una arginina y una histidina en la zona distal, y un aspártico en la zona proximal en las peroxidasas ligninoliticas (**Figura 9B)** (Martínez, 2002).

La histidina y la arginina distales están implicadas en la ruptura heterolítica del H_2O_2 durante la activación de la enzima en estado de reposo dando lugar al compuesto I, así como en la estabilización de los estados de oxidación de la enzima (Hiner et al., 2002).

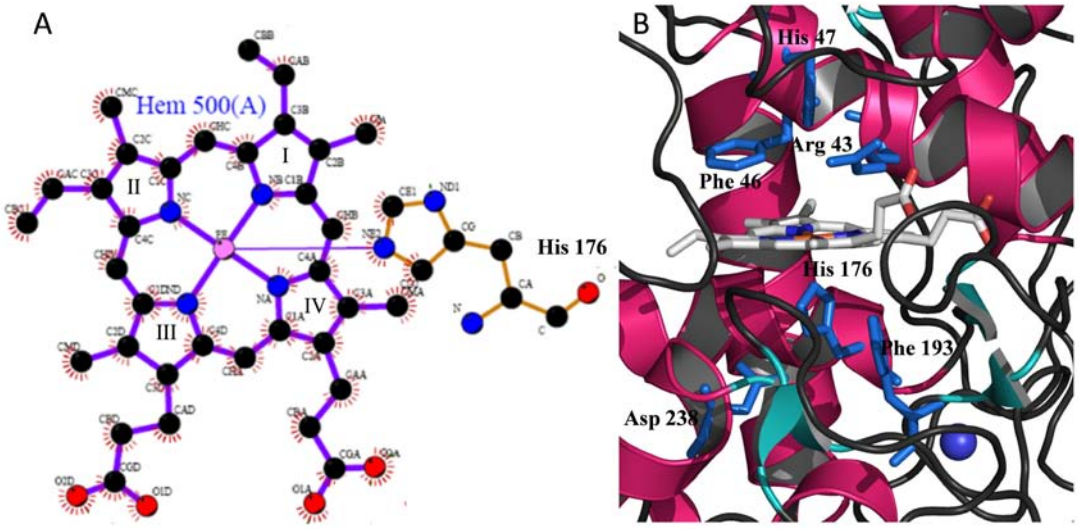

Figura 9. Estructura del grupo hemo de tipo b (ferriporfirina IX) unido a la His proximal y entorno del hemo en la LiP-H8 de *P. chrysosporium* (PDB: 1LGA). A) El grupo hemo está formado por un átomo de Fe^{3+} (rosa) coordinado por cuatro anillos pirrólicos (I, II, III y IV) unidos por puentes metileno. Tiene ocho cadenas laterales: cuatro grupos metilo, dos grupos vinilo y dos grupos propionato. B). Se muestran los aminoácidos del entorno del hemo R43, F46, H47, H176, F190 y D238, que se encuentran conservados en las peroxidasas ligninolíticas.

La histidina proximal está implicada en el potencial redox de la enzima. En la **Figura 10**, se muestra como se establece un puente de hidrógeno entre la cadena lateral de una serina (Ser177) de la hélice F y la de un aspártico (Asp201) de la hélice G, que arrastra la hélice F alejándola del hemo. Los estudios de resonancia magnética nuclear (NMR) en complejos de peroxidasas con cianuro, relacionan inversamente el valor del desplazamiento del protón Hε1 de la histidina proximal con el potencial redox de la enzima (Banci et al., 1992).

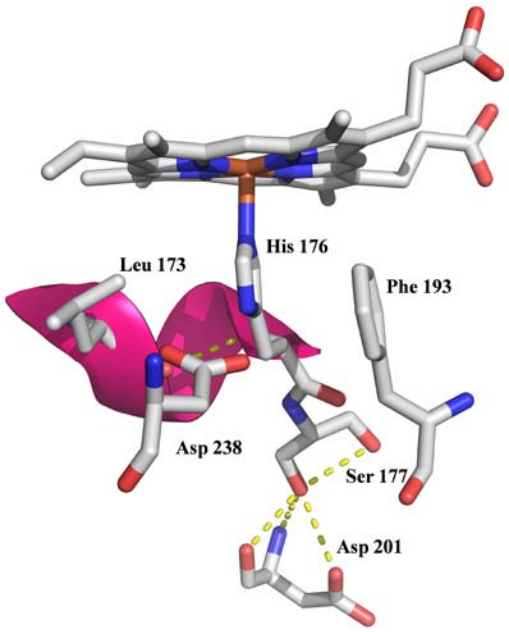

Figura 10. Residuos del lado proximal del entorno del hemo en la LiP-H8 de *P. chrysosporium* (PDB: 1LGA). Las líneas discontinuas representan puentes de hidrógeno.

7.3. Calcios estructurales

Las peroxidasas de clase II y III presentan dos iones de calcio, uno localizado en el dominio proximal y otro en el distal. De acuerdo con las estructuras cristalográficas, el sitio de unión de los calcios se encuentra altamente conservado entre las peroxidasas fúngicas y las de plantas. Estos iones calcio desempeñan un papel esencial en el mantenimiento de la integridad del sitio activo y por tanto en la actividad enzimática (Howes et al., 2001).

El calcio proximal está unido por ocho átomos de oxígenos del esqueleto y de las cadenas laterales de los residuos, en la LiP, Ser177, Asp194, Thr196, Iso199 y Asp201 (**Figura 11 A**). Estos residuos están conservados entre todas las peroxidasas fúngicas, mientras que en las peroxidasas de clase III el Asp194 se desplaza a la posición 193 (Welinder, 1992). Este ión calcio no está accesible al solvente. La Ser 177 es el residuo contiguo a la His proximal (His176), el calcio proximal está implicado en la posición relativa de la histidina proximal respecto al hemo, lo que afecta directamente al potencial redox de la enzima.

El calcio distal está unido por siete átomos de oxigeno del esqueleto y de las cadenas laterales de los residuos, Asp48, Gly66, Asp68 y Ser70 (en la LiP) y por dos moléculas de agua **(Figura 11 B)**. Este ión calcio se libera más fácilmente, ya que el sitio de unión está más cercano a la superficie y expuesto al solvente. El Asp48, es el residuo contiguo a la His distal (His47), el calcio distal fija la hélice donde se localiza la histidina distal y por tanto afecta directamente a la activación por peróxido y a la actividad catalítica de la enzima.

7.4. Ciclo catalítico

La oxidación por parte de las peroxidasas de diversos compuestos se produce a expensas de peróxido, generalmente H_2O_2. En la **Figura 12** se muestra el ciclo que implica tres pasos consecutivos, en los que se forman sucesivamente las dos especies catalíticas del ciclo, el compuesto I y el compuesto II (**Figura 13**).

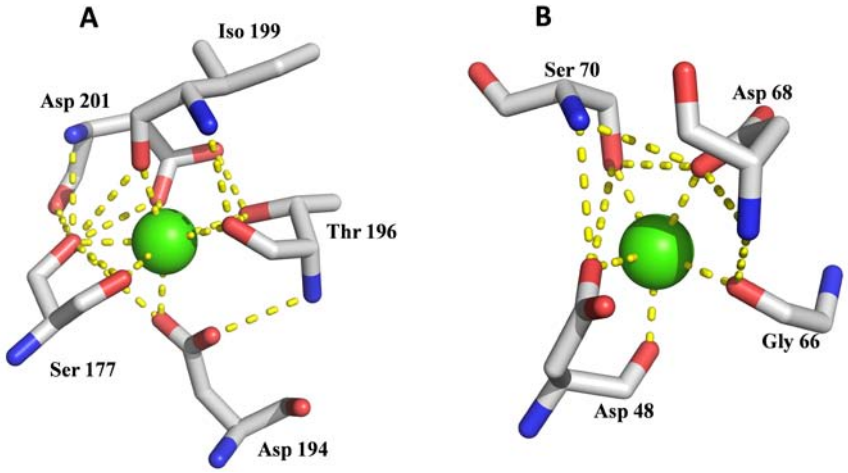

Figura 11. Residuos implicados en la unión del calcio proximal (A) y en la unión del calcio distal (B) en la LiP-H8 de *P. chrysosporium* (PDB: 1LGA). Las líneas discontinuas representan puentes de hidrógeno.

En el primer paso, la enzima en estado de reposo, con el Fe^{3+}, reacciona con un equivalente de H_2O_2 en una reacción de oxido-reducción de dos electrones para dar el compuesto I. En esta reacción, el H_2O_2 se reduce a H_2O y el compuestro I recibe los dos equivalentes de oxidación. Un electron es abstraído del atomo de hiero, que se oxida a Fe^{4+}. Además la proteína retiene un átomo de oxigeno porcedente del H_2O_2 en forma de intermediario oxiferrilo [Fe^{4+}=O]. El segundo electron es abstraído del macrociclo del hemo, formándose un radical cationico de la porfirina, que en la mayoria de la peroxidasas permanece como tal. En la VP y la LiP, el segundo electrón es posteriormente transferido desde la cadena lateral de un triptófano, donde queda centrado el radical.

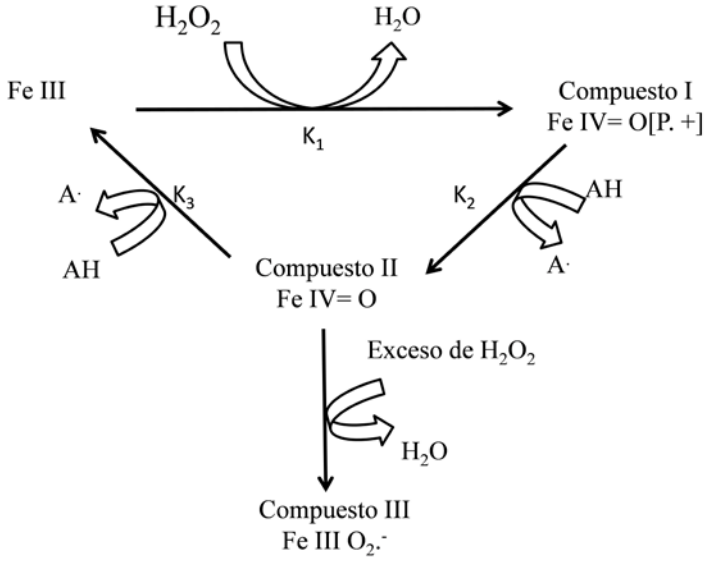

Figura 12. Ciclo catalítico de las peroxidasas ligninolitica. Adaptado de Gold (1989).

En un segundo paso, la enzima recupera un electron oxidando una molecula de sustrato (AH) al radical correspondiente (A•). La especie catalítica resultante es el compuesto II, que mantiene el centro [Fe^{4+}=O] oxidado, mientras que es el radical de la porfirina el primero que recupera su electrón.

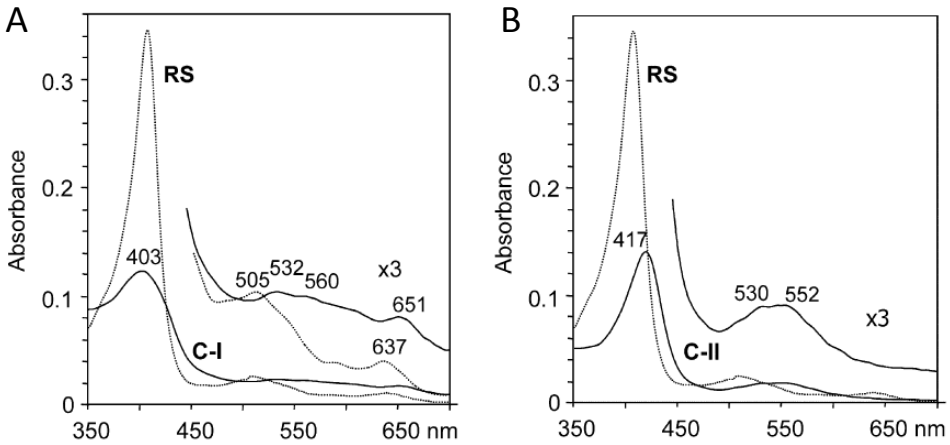

Figura 13. Propiedades espectroscopicas de las especies catalíticas de la VP de *P. eryngii* expresada en *E. coli.* A) Espectro de la enzima en estado de reposo (RS, línea punteada) y compuesto I (línea contínua), formado por la adición de un equivalente de H_2O_2. B) Espectro de la enzima en estado de reposo (RS) de la VP (línea punteada) y compuesto II (línea contínua), formado por la adición de dos equivalentes de H_2O_2. Un detalle de la región 450-700 nm está ampliado tres veces. Tomado de Pérez-Boada et al. (2005).

En el tercer paso, el compuesto II es reducido por una segunda molécula de sustrato, recuperando así el estado de reposo de la enzima, con el Fe^{3+}.

En ausencia de sustratos reductores, el H_2O_2 en exceso reacciona con el compuesto II para formar el compuesto III, en un complejo con el radical superóxido. Esta reacción produce primero la inactivación y posteriormente la perdida del grupo hemo, dando lugar al blanqueamiento de la enzima (Wariishi and Gold, 1990).

El ciclo catalitico básico es esencialmente el mismo para todas las peroxidasas, diferenciandose en la estructura electronica del compuesto I y en los sustratos que son capaces de oxidar.

7.5. Peroxidasas ligninolíticas

Las peroxidasas ligninolíticas se dividen en tres familias: LiP, MnP y VP. Esta división está basada en la presencia o ausencia de un sitio de oxidación del Mn^{2+} y en la presencia o ausencia de un triptófano catalítico, y por tanto en su capacidad de oxidar diferentes sustratos.

7.5.1. LiP (EC 1.11.1.14)

Fue la primera enzima ligninolítica descrita. Se descubrió en el medio extracelular de *P. chrysosporium* creciendo en condiciones limitantes de nitrógeno (Tien and Kirk, 1983). Fue la segunda peroxidasa cuya estructura fue resuelta (Scriban, 1985; Piontek et al., 1993) tras la CcP (Finzel et al., 1984).

Despolimeriza la lignina y oxida compuestos aromáticos de alto potencial rédox, como el alcohol veratrílico y dímeros de lignina de tipo no fenólico. Presenta un triptófano catalítico (W171) expuesto en la superficie de la enzima, implicado en la oxidación de la lignina y punto de inicio de una ruta de transporte electrónico de largo recorrido hasta el hemo. Su alto

potencial redox, se debe a que el hierro del anillo de porfirina es más deficiente en electrones que el de las peroxidasas clásicas.

Este triptófano catalítico esta conservado entre todas las LiPs, con la excepción de una LiP de *T. cervina*, que presenta un residuo de tirosina que desempeña el mismo papel, localizado en una posición diferente (Miki et al., 2003; 2011; 2013).

7.5.2. MnP (EC 1.11.1.13)

Se descubrió en 1984 en *P. chrysosporium* por Kuwahara et al. (1984) y fue la tercera peroxidasa cuya estructura cristalográfica fue resuelta (Sundaramoorthy et al., 1994). Su presencia entre los hongos de la podredumbre blanca está más extendida que la de la LiPs o las VPs

No presentan un triptófano catalítico, pero si un sitio de oxidación de manganeso, que consiste en un pequeño canal de acceso formado por tres residuos ácidos, situado directamente sobre el propionato interno del hemo (propionato del anillo pirrólico III) (**Figura 7**), oxidando Mn^{2+} a Mn^{3+}.

Gracias a la gran cantidad de genomas secuenciados en los últimos años, más de 200 secuencias de MnPs están disponibles, y de acuerdo a estos datos genómicos, esta familia ha sido dividida en tres subfamilias, cortas, largas y extralargas en función de la longitud del C-terminal. Las peroxidasas caracterizadas en *P. chrysosporium* son de tipo largo, oxidando solo Mn^{2+}, mientras que las peroxidasas de tipo corto, con mayor identidad de secuencia con las VP que con las MnPs largas y extralargas, son capaces de oxidar otros sustratos como el ABTS y el DMP. Estas nuevas subfamilias propuestas se analizan en detalle en el capítulo 7.

7.5.3. VP (EC 1.11.1.16)

Se describió en *P. eryngii* como una MnP con actividad independiente de Mn (Martínez et al., 1996) y tras su clonación se describió como una nueva enzima (Ruiz-Dueñas et al., 1999; Camarero et al., 1999). También se ha encontrado en *Bjerkandera spp*. (Mester and Field, 1998). Se caracteriza por combinar las propiedades catalíticas de la LiP y la MnP, al presentar tanto un triptófano catalítico, responsable de la oxidación de sustratos de alto potencial redox, como un sitio de oxidación del Mn^{2+}. A diferencia de las LiPs, oxida el alcohol VA con menor eficiencia, pero es capaz de oxidar el RB5 sin necesidad de ningún mediador.

7.6. Evolución de las peroxidasas ligninolíticas

Hasta hace poco los estudios filogenéticos de los hongos se basaban en el análisis de diferentes regiones del DNA ribosomal y un limitado número de genes (James et al., 2006). Sin embargo, el aumento en la secuenciación de genomas fúngicos ha permitido que los estudios evolutivos actuales utilicen genomas completos (Fitzpatrick et al., 2006).

Los estudios de Floudas et al (2012), en el que se analizan 31 genomas fúngicos, y el de Ruiz-Dueñas et al (2013) en el que se analizan 10 genomas de Polyporales, han reconstruido la historia evolutiva de las peroxidasas ligninolíticas. Los análisis de diversificación génica confirman que la tasa de duplicación de genes de PODs es más elevada en la línea de los hongos de la podredumbre blanca que en las otras líneas, de modo que a partir de una única copia de un gen de POD en el ancestro común de los Basidiomycota, ésta se expandiría dando lugar a 26 peroxidasas en *T. versicolor*, 16 en *P. chrysosporium* o 12 en *D. squalens*, entre otros ejemplos. Por el contrario, esta única copia se perdería o se mantendría, en las líneas que han dado lugar a los hongos micorrizógenos, de podredumbre parda y micoparásitos (**Figura 14 A**).

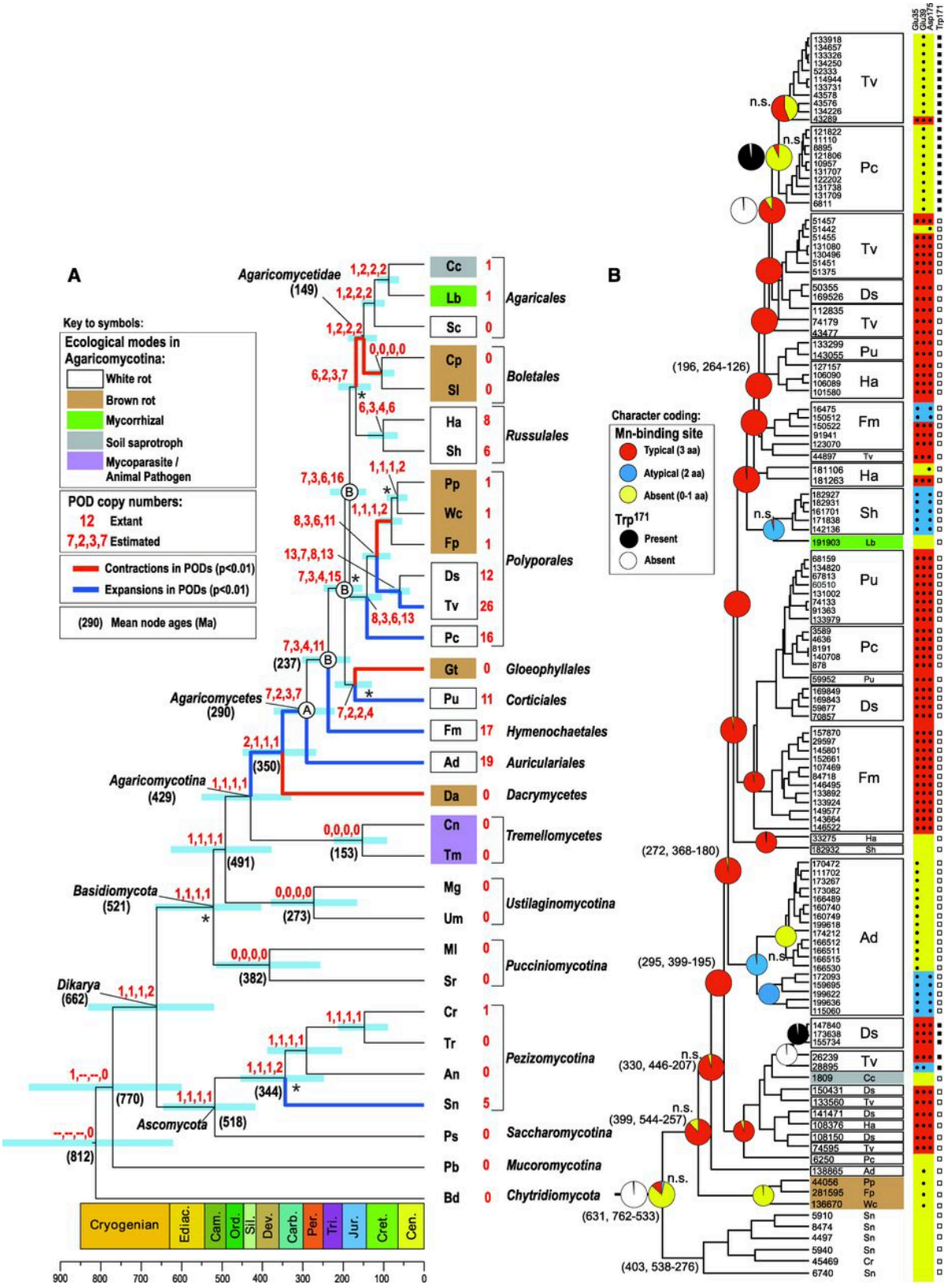

Figura 14. Leyenda en la página siguiente.

Estos estudios revelan que el ancestro de todas las peroxidasas de clase II carecía de sitio de unión al Mn^{2+} y de triptófano catalítico, es decir, sería una enzima no ligninolítica de tipo GP. Los mismos análisis muestran que la primera peroxidasa ligninolítica fue MnP derivada de una GP ancestral (**Figura 14 B**), hecho que concuerda con la presencia de MnP en todos los hongos de podredumbre blanca.

Las peroxidasas tipo VP habrían evolucionado a partir de una MnP ancestral que adquirió un triptófano catalítico. Durante la evolución posterior, alguna VP habría perdido uno de los aminoácidos del sitio de unión del Mn, dando lugar a las VPs atípicas (que sólo presentan dos de los tres aminoácidos implicados en la unión del Mn). Este proceso habría ido más lejos en alguna otra VP ancestral, que habría perdido la funcionalidad del sitio de oxidación del Mn dando lugar a las LiPs.

Lo anterior no excluye líneas de evolución secundaria, como alguna de las mostradas en la presente tesis.

Figura 14. Filogenia de 31 basidiomicetos y otros hongos a partir de sus genomas (A) e historia evolutiva de las peroxidasas ligninolíticas (LiP, MnP y VP) y GPs (B). A) La filogenia de los hongos (cronograma) fue obtenida con BEAST partir de 26 genes. Las barras azules son intervalos del 95% para las edades de los nodos, cuyo promedio (en millones de años) se indica en los paréntesis. Las ramas azules y rojas indican expansión y contracción, respectivamente, en el número de genes de PODs inferido utilizando CAFE. Los números rojos junto a la clave de las especies indican el número real de genes de cada una. Los números en rojo, separados por comas, son los números de copias de genes de PODs estimados con CAFE, Notung (usando dos umbrales diferentes) y DrML. El nodo A sería el antepasado de los Agaricomycetes; los nodos B corresponden a ancestros de otros grupos de Agaricomycetes. Los asteriscos indican los nodos que no reciben apoyo en todos los análisis. Véase la Tabla 1 para las abreviaturas de las especies. **B)** Filogenia de los genes de PODs estimada en BEAST con reconstrucciones del estado ancestral para el sitio de unión de manganeso (rojo, azul y amarillo) y el triptófano implicado en la degradación de la lignina (negro y blanco) estimados con BayesTraits. Las casillas de la derecha indican la presencia de residuos funcionales. Las edades medias de los nodos, entre paréntesis, están seguidas por sus intervalos de confianza del 95%. Tomado de Floudas et al (2012).

Referencias

Baldrian, P. 2006. Fungal laccases - occurrence and properties. FEMS Microbiol. Rev. 30:215-242.

Banci, L. 1997. Structural properties of peroxidases. J. Biotechnol. 53:253-263.

Banci, L., I. Bertini, E. A. Pease, M. Tien, and P. Turano. 1992. ^{1}H NMR investigation of manganese peroxidase from *Phanerochaete chrysosporium.* A comparison with other peroxidases. Biochemistry 31:10009-10017.

Bao, W. L., Y. Fukushima, K. A. Jensen, M. A. Moen, and K. E. Hammel. 1994. Oxidative degradation of non-phenolic lignin during lipid peroxidation by fungal manganese peroxidase. FEBS Lett. 354:297-300.

Blanchette, R. A. 1991. Delignification by wood-decay fungi. Annu. Rev. Phytopathol. 29:381-398.

Blanchette, R. A., E. W. Krueger, J. E. Haight, M. Akhtar, and D. E. Akin. 1997. Cell wall alterations in loblolly pine wood decayed by the white- rot fungus, *Ceriporiopsis subvermispora*. J. Biotechnol. 53:203-213.

Blanchette, R. A., L. Otjen, M. J. Effland, and W. E. Eslyn. 1985. Changes in structural and chemical components of wood delignified by fungi. Wood Sci. Technol. 19:35-46.

Böhmer, S., K. Messner, and E. Srebotnik. 1998. Oxidation of phenanthrene by a fungal laccase in the presence of 1-hydroxybenzotriazole and unsaturated lipids. Biochem. Biophys. Res. Commun. 244:233-238.

Bonnarme, P. and T. W. Jeffries. 1990. Mn(II) regulation of lignin peroxidases and manganese-dependent peroxidases from lignin-degrading white rot fungi. Appl. Environ. Microbiol. 56:210-217.

Bourbonnais, R. and M. G. Paice. 1990. Oxidation of non-phenolic substrates. An expanded role for laccase in lignin biodegradation. FEBS Lett. 267:99-102.

Camarero, S., D. Ibarra, M. J. Martínez, and A. T. Martínez. 2005. Lignin-derived compounds as efficient laccase mediators for decolorization of different types of recalcitrant dyes. Appl. Environ. Microbiol. 71:1775-1784.

Camarero, S., S. Sarkar, F. J. Ruiz-Dueñas, M. J. Martínez, and A. T. Martínez. 1999. Description of a versatile peroxidase involved in natural degradation of lignin that has both Mn-peroxidase and lignin-peroxidase substrate binding sites. J. Biol. Chem. 274:10324-10330.

Cañas, A. I. and S. Camarero. 2010. Laccases and their natural mediators: Biotechnological tools for sustainable eco-friendly processes. Biotechnol. Adv. 28:694-705.

Collins, P. J., J. A. Field, P. Teunissen, and A. D. W. Dobson. 1997. Stabilization of lignin peroxidases in white rot fungi by tryptophan. Appl. Environ. Microbiol. 63:2543-2548.

Daniel, G., J. Volc, and E. Kubátová. 1994. Pyranose oxidase, a major source of H_2O_2 during wood degradation by *Phanerochaete chrysosporium, Trametes versicolor*, and *Oudemansiella mucida*. Appl. Environ. Microbiol. 60:2524-2532.

de Jong, E., A. E. Cazemier, J. A. Field, and J. A. M. de Bont. 1994a. Physiological role of chlorinated aryl alcohols biosynthesized de novo by the white rot fungus *Bjerkandera* sp strain BOS55. Appl. Environ. Microbiol. 60:271-277.

de Jong, E. and J. A. Field. 1997. Sulfur tuft and turkey tail: Biosynthesis and biodegradation of organohalogens by basidiomycetes. Annu. Rev. Microbiol. 51:375-414:375-414.

de Jong, E., J. A. Field, and J. A. M. de Bont. 1994b. Aryl alcohols in the physiology of ligninolytic fungi. FEMS Microbiol. Rev. 13:153-188.

de Jong, E., J. A. Field, H. E. Spinnler, J. B. P. A. Wijnberg, and J. A. M. de Bont. 1994c. Significant biogenesis of chlorinated aromatics by fungi in natural environments. Appl. Environ. Microbiol. 60:264-270.

del Río, J. C., A. Gutiérrez, M. J. Martínez, and A. T. Martínez. 2001. Py-GC-MS study of *Eucalyptus globulus* wood treated with different fungi. J. Anal. Appl. Pyrolysis 58/59:441-453.

del Río, J. C., J. Rencoret, G. Marques, A. Gutiérrez, D. Ibarra, J. I. Santos, J. Jiménez-Barbero, and A. T. Martínez. 2008. Highly acylated (acetylated and/or *p*-coumaroylated) native lignins from diverse herbaceous plants. J. Agric. Food Chem. 56:9525-9534.

Dunford, H. B. 1999. Heme peroxidases. Wiley-VCH, New York.

Edwards, S. L., R. Raag, H. Wariishi, M. H. Gold, and T. L. Poulos. 1993. Crystal structure of lignin peroxidase. Proc. Natl. Acad. Sci. USA 90:750-754.

Eggert, C., U. Temp, J. F. D. Dean, and K.-E. L. Eriksson. 1996. A fungal metabolite mediates degradation of non-phenolic lignin structures and synthetic lignin by laccase. FEBS Lett. 391:144-148.

Eriksson, K.-E., B. Pettersson, J. Volc, and V. Musílek. 1986. Formation and partial characterization of glucose-2-oxidase, a H_2O_2 producing enzyme in *Phanerochaete chrysosporium*. Appl. Microbiol. Biotechnol. 23:257-262.

Faison, B. D. and T. K. Kirk. 1983. Relationship between lignin degradation and production of reduced oxygen species by *Phanerochaete chrysosporium*. Appl. Environ. Microbiol. 46:1140-1145.

Fengel, D. and G. Wegener. 1984. Wood: Chemistry, ultrastructure, reactions. De Gruyter, Berlin.

Fernández-Fueyo, E., F. J. Ruiz-Dueñas, P. Ferreira, D. Floudas, D. S. Hibbett, P. Canessa, L. Larrondo, T. Y. James, D. Seelenfreund, S. Lobos, R. Polanco, M. Tello, Y. Honda, T. Watanabe, T. Watanabe, J. S. Ryu, C. P. Kubicek, M. Schmoll, J. Gaskell, K. E. Hammel, F. J. St.John, A. Vanden Wymelenberg, G. Sabat, S. S. Bondurant, K. Syed, J. Yadav, H. Doddapaneni, V. Subramanian, J. L. Lavín, J. A. Oguiza, G. Perez, A. G. Pisabarro, L. Ramírez, F. Santoyo, E. Master, P. M. Coutinho, B. Henrissat, V. Lombard, J. K. Magnuson, U. Kües, C. Hori, K. Igarashi, M. Samejima, B. W. Held, K. Barry, K. LaButti, A. Lapidus, E. Lindquist, S. Lucas, R. Riley, A. Salamov, D. Hoffmeister, D. Schwenk, Y. Hadar, O. Yarden, R. P. de Vries, A. Wiebenga, J. Stenlid, D. C. Eastwood, I. V. Grigoriev, R. Berka, R. A. Blanchette, P. Kersten, A. T. Martínez, R. Vicuña, and D. Cullen. 2012a. Comparative genomics of *Ceriporiopisis subvermispora* and *Phanerochaete chrysosporium* provide insight into selective ligninolysis. Proc. Natl. Acad. Sci. USA 109:5458-5463.

Fernández-Fueyo, E., F. J. Ruiz-Dueñas, M. J. Martínez, A. Romero, K. E. Hammel, F. J. Medrano, and A. T. Martínez. 2014. Ligninolytic peroxidase genes in the oyster mushroom genome: Heterologous expression, molecular structure, catalytic and stability properties and lignin-degrading ability. Biotechnol. Biofuels 7:2.

Fernández-Fueyo, E., F. J. Ruiz-Dueñas, Y. Miki, M. J. Martínez, K. E. Hammel, and A. T. Martínez. 2012b. Lignin-degrading peroxidases from genome of selective ligninolytic fungus *Ceriporiopsis subvermispora*. J. Biol. Chem. 287:16903-16906.

Ferraz, A., A. M. Cordova, and A. Machuca. 2003. Wood biodegradation and enzyme production by *Ceriporiopsis subvermispora* during solid-state fermentation of *Eucalyptus grandis*. Enzyme Microb. Technol. 32:59-65.

Field, J. A., F. J. M. Verhagen, and E. de Jong. 1995. Natural organohalogen production by basidiomycetes. Trends Biotechnol. 13:451-456.

Finzel, B. C., T. L. Poulos, and J. Kraut. 1984. Crystal structure of yeast cytochrome *c* peroxidase refined at 1.7 Å resolution. J. Biol. Chem. 259:13027-13036.

Fitzpatrick, D. A., M. E. Logue, J. E. Stajich, and G. Butler. 2006. A fungal phylogeny based on 42 complete genomes derived from supertree and combined gene analysis. BMC Evolutionary Biology 6.

Floudas, D., M. Binder, R. Riley, K. Barry, R. A. Blanchette, B. Henrissat, A. T. Martínez, R. Otillar, J. W. Spatafora, J. S. Yadav, A. Aerts, I. Benoit, A. Boyd, A. Carlson, A. Copeland, P. M. Coutinho, R. P. de Vries, P. Ferreira, K. Findley, B. Foster, J. Gaskell, D. Glotzer, P. Górecki, J. Heitman, C. Hesse, C. Hori, K. Igarashi, J. A. Jurgens, N. Kallen, P. Kersten, A. Kohler, U. Kües, T. K. A. Kumar, A. Kuo, K. LaButti, L. F. Larrondo, E. Lindquist, A. Ling, V. Lombard, S. Lucas, T. Lundell, R. Martin, D. J. McLaughlin, I. Morgenstern, E. Morin, C. Murat, M. Nolan, R. A. Ohm, A. Patyshakuliyeva, A. Rokas, F. J. Ruiz-Dueñas, G. Sabat, A. Salamov, M. Samejima, J. Schmutz, J. C. Slot, F. St.John, J. Stenlid, H. Sun, S. Sun, K. Syed, A. Tsang, A. Wiebenga, D. Young, A. Pisabarro, D. C. Eastwood, F. Martin, D. Cullen, I. V. Grigoriev, and D. S. Hibbett. 2012. The Paleozoic origin of enzymatic lignin decomposition reconstructed from 31 fungal genomes. Science 336:1715-1719.

Flournoy, D. S., J. A. Paul, T. K. Kirk, and T. L. Highley. 1993. Changes in the size and volume of pores in sweetgum wood during simultaneous rot by *Phanerochaete chrysosporium* Burds. Holzforschung 47:297-301.

Forney, L. J., C. A. Reddy, M. Tien, and S. D. Aust. 1982. The involvement of hydroxyl radical derived from hydrogen peroxide in lignin degradation by the white rot fungus *Phanerochaete chrysosporium*. J. Biol. Chem. 257:11455-11462.

Gajhede, M., D. J. Schuller, A. Henriksen, A. T. Smith, and T. L. Poulos. 1997. Crystal structure of horseradish peroxidase C at 2.15 Å resolution. Nature Struct. Biology 4:1032-1038.

Galli, C. and P. Gentili. 2004. Chemical messengers: mediated oxidations with the enzyme laccase. J. Phys. Org. Chem. 17:973-977.

Gellerstedt, G. and G. Henriksson. 2008. Lignins: Major sources, structure and properties, p. 201-224. *In* M. Belgacem and A. Gandini (eds.), Monomers, polymers and composites from renewable resources. Elsevier, Amsterdam.

Gold, M. H., H. Wariishi, and K. Valli. 1989. Extracellular peroxidases involved in lignin degradation by the white-rot basidiomycetes *Phanerochaete chrysosporium*, p. 127-140. *In* J. R. Whitaker and P. E. Sonnet (eds.), Biocatalystists in Agricultural Biotechnology. ACS, Washington, DC.

Gómez-Toribio, V., A. B. García-Martín, M. J. Martínez, A. T. Martínez, and F. Guillén. 2009. Induction of extracellular hydroxyl radical production by white-rot fungi through quinone redox cycling. Appl. Environ. Microbiol. 75:3944-3953.

Greene, R. V. and J. M. Gould. 1984. Fatty acyl-coenzyme A oxidase activity and H2O2 production in *Phanerochaete chrysosporium* mycelia. Biochem. Biophys. Res. Commun. 118:437-443.

Guillén, F., V. Gómez-Toribio, M. J. Martínez, and A. T. Martínez. 2000. Production of hydroxyl radical by the synergistic action of fungal laccase and aryl alcohol oxidase. Arch. Biochem. Biophys. 383:142-147.

Guillén, F., A. T. Martínez, and M. J. Martínez. 1992a. Aryl-alcohol oxidase from *Pleurotus eryngii*: substrate specificity and H_2O_2-producing system, p. 371-376. *In* M. Kuwahara and M. Shimada (eds.), Biotechnology in pulp and paper industry. UNI Pub. Co., Ltd., Tokyo.

Guillén, F., A. T. Martínez, and M. J. Martínez. 1992b. Substrate specificity and properties of the aryl-alcohol oxidase from the ligninolytic fungus *Pleurotus eryngii*. Eur. J. Biochem. 209:603-611.

Hammel, K. E., K. A. Jensen, M. D. Mozuch, L. L. Landucci, M. Tien, and E. A. Pease. 1993. Ligninolysis by a purified lignin peroxidase. J. Biol. Chem. 268:12274-12281.

Harvey, P. J., H. E. Schoemaker, and J. M. Palmer. 1986. Veratryl alcohol as a mediator and the role of radical cations in lignin biodegradation by *Phanerochaete chrysosporium*. FEBS Lett. 195:242-246.

Hatakka, A. 1994. Lignin-modifying enzymes from selected white-rot fungi - Production and role in lignin degradation. FEMS Microbiol. Rev. 13:125-135.

Heinfling, A., F. J. Ruiz-Dueñas, M. J. Martínez, M. Bergbauer, U. Szewzyk, and A. T. Martínez. 1998. A study on reducing substrates of manganese-oxidizing peroxidases from *Pleurotus eryngii* and *Bjerkandera adusta*. FEBS Lett. 428:141-146.

Henriksson, G., G. Johansson, and G. Pettersson. 2000. A critical review of cellobiose dehydrogenases. J. Biotechnol. 78:93-113.

Himmel, M. E., S. Y. Ding, D. K. Johnson, W. S. Adney, M. R. Nimlos, J. W. Brady, and T. D. Foust. 2007. Biomass recalcitrance: Engineering plants and enzymes for biofuels production. Science 315:804-807.

Hiner, A. N. P., E. L. Raven, R. N. F. Thorneley, F. García-Canovas, and J. N. Rodríguez-López. 2002. Mechanisms of compound I formation in heme peroxidases. J. Inorg. Biochem. 91:27-34.

Hofrichter, M., R. Ullrich, M. J. Pecyna, C. Liers, and T. Lundell. 2010. New and classic families of secreted fungal heme peroxidases. Appl. Microbiol. Biotechnol. 87:871-897.

Howes, B. D., A. Feis, L. Raimondi, C. Indiani, and G. Smulevich. 2001. The critical role of the proximal calcium ion in the structural properties of horseradish peroxidase. J. Biol. Chem. 276:40704-40711.

James, T. Y., F. Kauff, C. L. Schoch, P. Matheny, V. Hofstetter, C. J. Cox, G. Celio, C. Gueidan, E. Fraker, J. Miadlikowska, H. Lumbsch, A. Rauhut, V. Reeb, A. Arnold, A. Amtoft, J. E. Stajich, K. Hosaka, G. H. Sung, D. Johnson, B. O'Rourke, M. Crockett, M. Binder, J. M. Curtis, J. C. Slot, Z. Wang, A. W. Wilson, A. Schuessler, J. E. Longcore, K. O'Donnell, S. Mozley-Standridge, D. Porter, P. M. Letcher, M. J. Powell, J. W. Taylor, M. M. White, G. W. Griffith, D. R. Davies, R. A. Humber, J. B. Morton, J. Sugiyama, A. Y. Rossman, J. D. Rogers, D. H. Pfister, D. Hewitt, K. Hansen, S. Hambleton, R. A. Shoemaker, J. Kohlmeyer, B. Volkmann-Kohlmeyer, R. A. Spotts, M. Serdani, P. W. Crous, K. W. Hughes, K. Matsuura, E. Langer, G. Langer, W. A. Untereiner, R. Lucking, B. Buedel, D. M. Geiser, A. Aptroot, P. Diederich, I. Schmitt, M. Schultz, R. Yahr, D. S. Hibbett, F. Lutzoni, D. J. McLaughlin, J. W. Spatafora, and R. Vilgalys. 2006. Reconstructing the early evolution of Fungi using a six-gene phylogeny. Nature 443:818-822.

Johannes, C. and A. Majcherczyk. 2000. Natural mediators in the oxidation of polycyclic aromatic hydrocarbons by laccase mediator systems. Appl. Environ. Microbiol. 66:524-528.

Johannes, C., A. Majcherczyk, and A. Hüttermann. 1998. Oxidation of acenaphthene and acenaphthylene by laccase of *Trametes versicolor* in a laccase-mediator system. J. Biotechnol. 61:151-156.

Joshi, D. K. and M. H. Gold. 1996. Oxidation of dimethoxylated aromatic compounds by lignin peroxidase from *Phanerochaete chrysosporium*. Eur. J. Biochem. 237:45-57.

Kapich, A. N. and L. N. Shishbina. 1995. Lipid peroxidation and its regulation in the mycelium of xylotrophic basidiomycetes. Microbiology-Engl. Tr. 64:266-271.

Kawai, S., T. Umezawa, M. Shimada, T. Higuchi, K. Koide, T. Nishida, N. Morohoshi, and T. Haraguchi. 1987. C_α-C_β cleavage of phenolic β-1 lignin substructure model compound by laccase of *Coriolus versicolor*. Mokuzai Gakkaishi 33:792-797.

Kersten, P. and D. Cullen. 2007. Extracellular oxidative systems of the lignin-degrading basidiomycete *Phanerochaete chrysosporium*. Fungal Genet. Biol. 44:77-87.
Kersten, P. J. and T. K. Kirk. 1987. Involvement of a new enzyme, glyoxal oxidase, in extracellular H_2O_2 production by *Phanerochaete chrysosporium*. J. Bacteriol. 169:2195-2201.
Kimura, S. and M. Ikeda-Saito. 1988. Human myeloperoxidase and thyroid peroxidase, two enzymes with separate and distinct physiological functions, are evolutionarily related members of the same gene family. Proteins 3:113-120.
Kirk, T. K. and R. L. Farrell. 1987. Enzymatic "combustion": The microbial degradation of lignin. Annu. Rev. Microbiol. 41:465-505.
Koduri, R. S. and M. Tien. 1994. Kinetic analysis of lignin peroxidase - Explanation for the mediation phenomenon by veratryl alcohol. Biochemistry 33:4225-4230.
Kuwahara, M., J. K. Glenn, M. A. Morgan, and M. H. Gold. 1984. Separation and characterization of two extracellular H_2O_2-dependent oxidases from ligninolytic cultures of *Phanerochaete chrysosporium*. FEBS Lett. 169:247-250.
Leatham, G. F. 1986. The ligninolytic activities of *Lentinus edodes* and *Phanerochaete chrysosporium*. Appl. Microbiol. Biotechnol. 24:51-58.
Liese, W. 1970. Ultrastructural aspects of woody tissue disintegration. Annu. Rev. Phytopathol. 8:231-258.
Lundquist, K. and Kirk, T. K. *De novo* synthesis and decomposition of veratryl alcohol by a lignin degrading basidiomicete. Phytochemistry 17, 1676. 1978a.
Ref Type: Generic
Lundquist, K. and T. K. Kirk. 1978b. *De novo* synthesis and decomposition of veratryl alcohol by a lignin degrading basidiomycete. Phytochemistry 17:1676.
Martínez, A. T. 2002. Molecular biology and structure-function of lignin-degrading heme peroxidases. Enzyme Microb. Technol. 30:425-444.
Martínez, A. T., S. Camarero, F. Guillén, A. Gutiérrez, C. Muñoz, E. Varela, M. J. Martínez, J. M. Barrasa, K. Ruel, and M. Pelayo. 1994. Progress in biopulping of non-woody materials: Chemical, enzymatic and ultrastructural aspects of wheat-straw delignification with ligninolytic fungi from the genus *Pleurotus*. FEMS Microbiol. Rev. 13:265-274.
Martínez, A. T., J. Rencoret, L. Nieto, J. Jiménez-Barbero, A. Gutiérrez, and J. C. del Río. 2011. Selective lignin and polysaccharide removal in natural fungal decay of wood as evidenced by *in situ* structural analyses. Environ. Microbiol. 13:96-107.
Martínez, A. T., F. J. Ruiz-Dueñas, M. J. Martínez, J. C. del Río, and A. Gutiérrez. 2009. Enzymatic delignification of plant cell wall: from nature to mill. Curr. Opin. Biotechnol. 20:348-357.
Martínez, A. T., M. Speranza, F. J. Ruiz-Dueñas, P. Ferreira, S. Camarero, F. Guillén, M. J. Martínez, A. Gutiérrez, and J. C. del Río. 2005. Biodegradation of lignocellulosics: Microbiological, chemical and enzymatic aspects of fungal attack to lignin. Int. Microbiol. 8:195-204.
Martinez, D., J. Challacombe, I. Morgenstern, D. S. Hibbett, M. Schmoll, C. P. Kubicek, P. Ferreira, F. J. Ruiz-Dueñas, A. T. Martínez, P. Kersten, K. E. Hammel, A. Vanden Wymelenberg, J. Gaskell, E. Lindquist, G. Sabat, S. S. Bondurant, L. F. Larrondo, P. Canessa, R. Vicuña, J. Yadav, H. Doddapaneni, V. Subramanian, A. G. Pisabarro, J. L. Lavín, J. A. Oguiza, E. Master, B. Henrissat, P. M. Coutinho, P. Harris, J. K. Magnuson, S. E. Baker, K. Bruno, W. Kenealy, P. J. Hoegger, U. Kues, P. Ramaiya, S. Lucas, A. Salamov, H. Shapiro, H. Tu, C. L. Chee, M. Misra, G. Xie, S. Teter, D. Yaver, T. James, M. Mokrejs, M. Pospisek, I. V. Grigoriev, T. Brettin, D. Rokhsar, R. Berka, and D. Cullen. 2009. Genome, transcriptome, and secretome analysis of wood decay fungus *Postia*

placenta supports unique mechanisms of lignocellulose conversion. Proc. Natl. Acad. Sci. USA 106:1954-1959.

Martinez, D., L. F. Larrondo, N. Putnam, M. D. Gelpke, K. Huang, J. Chapman, K. G. Helfenbein, P. Ramaiya, J. C. Detter, F. Larimer, P. M. Coutinho, B. Henrissat, R. Berka, D. Cullen, and D. Rokhsar. 2004. Genome sequence of the lignocellulose degrading fungus *Phanerochaete chrysosporium* strain RP78. Nat. Biotechnol. 22:695-700.

Martínez, M. J., F. J. Ruiz-Dueñas, F. Guillén, and A. T. Martínez. 1996. Purification and catalytic properties of two manganese-peroxidase isoenzymes from *Pleurotus eryngii*. Eur. J. Biochem. 237:424-432.

Mayer, A. M. and R. C. Staples. 2002. Laccase: new functions for an old enzyme. Phytochemistry 60:551-565.

Mester, T. and J. A. Field. 1997. Optimization of manganese peroxidase production by the white rot fungus *Bjerkandera* sp. strain BOS55. FEMS Microbiol. Lett. 155:161-168.

Mester, T. and J. A. Field. 1998. Characterization of a novel manganese peroxidase-lignin peroxidase hybrid isozyme produced by *Bjerkandera* species strain BOS55 in the absence of manganese. J. Biol. Chem. 273:15412-15417.

Miki, Y., F. R. Calviño, R. Pogni, S. Giansanti, F. J. Ruiz-Dueñas, M. J. Martínez, R. Basosi, A. Romero, and A. T. Martínez. 2011. Crystallographic, kinetic, and spectroscopic study of the first ligninolytic peroxidase presenting a catalytic tyrosine. J. Biol. Chem. 286:15525-15534.

Miki, Y., R. Pogni, S. Acebes, F. Lucas, E. Fernández-Fueyo, M. C. Baratto, M. I. Fernández, V. de los Ríos, F. J. Ruiz-Dueñas, A. Sinicropi, R. Basosi, K. E. Hammel, V. Guallar, and A. T. Martínez. 2013. Formation of a tyrosine adduct involved in lignin degradation by *Trametopsis cervina* lignin peroxidase: A novel peroxidase activation mechanism. Biochem. J. 452:575-584.

Miki, Y., H. Wariishi, and H. Tanaka. 2003. Lignin peroxidase from the white-rot basidiomycete *Trametes cervina*. Proc. 12th ISWPC, Madison, 9-12 June II:95.

Moen, M. A. and K. E. Hammel. 1994. Lipid peroxidation by the manganese peroxidase of *Phanerochaete chrysosporium* is the basis for phenanthrene oxidation by the intact fungus. Appl. Environ. Microbiol. 60:1956-1961.

Muñoz, C., F. Guillén, A. T. Martínez, and M. J. Martínez. 1997. Laccase isoenzymes of *Pleurotus eryngii:* Characterization, catalytic properties and participation in activation of molecular oxygen and Mn^{2+} oxidation. Appl. Environ. Microbiol. 63:2166-2174.

Orth, A. B., D. J. Royse, and M. Tien. 1993. Ubiquity of lignin-degrading peroxidases among various wood-degrading fungi. Appl. Environ. Microbiol. 59:4017-4023.

Ozimek, P., M. Veenhuis, and I. J. van der Klei. 2005. Alcohol oxidase: A complex peroxisomal, oligomeric flavoprotein. FEMS Yeast Res. 5:975-983.

Passardi, F., Theiler, G., Zamocky, M., Cosio, C., Rouhier, N., Teixera, F., Margis-Pinheiro, M., Ionnidis, V., Penel, C., Falquet, L., and Dunand, C. Peroxibase: The peroxidase database. Phytochemistry 68, 1605-1611. 2007.

Ref Type: Generic

Paszczynski, A. and R. L. Crawford. 1991. Degradation of azo compounds by ligninase from *Phanerochaete chrysosporium*: Involvement of veratryl alcohol. Biochem. Biophys. Res. Commun. 178:1056-1063.

Paszczynski, A., V.-B. Huynh, and R. Crawford. 1986. Comparison of ligninase-I and peroxidase-M2 from the white-rot fungus *Phanerochaete chrysosporium*. Arch. Biochem. Biophys. 244:750-765.

Pérez-Boada, M., F. J. Ruiz-Dueñas, R. Pogni, R. Basosi, T. Choinowski, M. J. Martínez, K. Piontek, and A. T. Martínez. 2005. Versatile peroxidase oxidation of high redox potential

aromatic compounds: Site-directed mutagenesis, spectroscopic and crystallographic investigations of three long-range electron transfer pathways. J. Mol. Biol. 354:385-402.
Pettersen, R. C. 1984. The chemical composition of wood, p. 57-126. *In* R. M. Powell (ed.), The Chemistry of Solid Wood. ACS.
Piontek, K., T. Glumoff, and K. Winterhalter. 1993. Low pH crystal structure of glycosylated lignin peroxidase from *Phanerochaete chrysosporium* at 2.5 Å resolution. FEBS Lett. 315:119-124.
Poulos, T. L., S. L. Edwards, H. Wariishi, and M. H. Gold. 1993. Crystallographic refinement of lignin peroxidase at 2 Å. J. Biol. Chem. 268:4429-4440.
Ragauskas, A. J., C. K. Williams, B. H. Davison, G. Britovsek, J. Cairney, C. A. Eckert, W. J. Frederick, J. P. Hallett, D. J. Leak, C. L. Liotta, J. R. Mielenz, R. Murphy, R. Templer, and T. Tschaplinski. 2006. The path forward for biofuels and biomaterials. Science 311:484-489.
Ralph, J., K. Lundquist, G. Brunow, F. Lu, H. Kim, P. F. Schatz, J. M. Marita, R. D. Hatfield, S. A. Ralph, J. H. Christensen, and W. Boerjan. 2004. Lignins: Natural polymers from oxidative coupling of 4-hydroxyphenylpropanoids. Phytochem. Rev. 3:29-60.
Rothschild, N., A. Levkowitz, Y. Hadar, and C. G. Dosoretz. 1999. Manganese deficiency can replace high oxygen levels needed for lignin peroxidase formation by *Phanerochaete chrysosporium*. Appl. Environ. Microbiol. 65:483-488.
Ruiz-Dueñas, F. J., E. Fernández, M. J. Martínez, and A. T. Martínez. 2011. *Pleurotus ostreatus* heme peroxidases: An *in silico* analysis from the genome sequence to the enzyme molecular structure. C. R. Biol. 334:795-805.
Ruiz-Dueñas, F. J., T. Lundell, D. Floudas, L. G. Nagy, J. M. Barrasa, D. S. Hibbett, and A. T. Martínez. 2013. Lignin-degrading peroxidases in Polyporales: An evolutionary survey based on ten sequenced genomes. Mycologia 105:1428-1444.
Ruiz-Dueñas, F. J. and A. T. Martínez. 2009. Microbial degradation of lignin: How a bulky recalcitrant polymer is efficiently recycled in nature and how we can take advantage of this. Microbial Biotechnol. 2:164-177.
Ruiz-Dueñas, F. J. and A. T. Martínez. 2010. Structural and functional features of peroxidases with a potential as industrial biocatalysts, p. 37-59. *In* E. Torres and M. Ayala (eds.), Biocatalysts based on heme peroxidases. Springer-Verlag, Berlin.
Ruiz-Dueñas, F. J., M. J. Martínez, and A. T. Martínez. 1999. Molecular characterization of a novel peroxidase isolated from the ligninolytic fungus *Pleurotus eryngii*. Mol. Microbiol. 31:223-236.
Ruiz-Dueñas, F. J., M. Morales, M. Pérez-Boada, T. Choinowski, M. J. Martínez, K. Piontek, and A. T. Martínez. 2007. Manganese oxidation site in *Pleurotus eryngii* versatile peroxidase: A site-directed mutagenesis, kinetic and crystallographic study. Biochemistry 46:66-77.
Sánchez, C. 2009. Lignocellulosic residues: biodegradation and bioconversion by fungi. Biotechnol. Adv. 27:185-194.
Sarkanen, K. V. and C. H. Ludwig. 1971. Lignins. Occurrence, formation, structure and reactions. Wiley-Interscience, New York.
Schmid, A., J. S. Dordick, B. Hauer, A. Kiener, M. Wubbolts, and B. Witholt. 2001. Industrial biocatalysis today and tomorrow. Nature 409:258-268.
Schwarze, F. W. M. R., J. Engels, and C. Mattheck. 2000. Fungal strategies of decay in trees. Springer, Berlin.
Scott, G. M., M. Akhtar, M. J. Lenz, and R. E. Swaney. 1998. Engineering, scale-up, and economic aspects of fungal pretreatment of wood chips, p. 341-384. *In* R. A. Young and

M. Akhtar (eds.), Environmentally friendly technologies for the pulp and paper industry. TAPPI Press, Atlanta.
Scriban, R. 1985. Biotecnologia. Editorial El Manual Moderno; Mexico.
Sharp, K. H., M. Mewies, P. C. Moody, and E. L. Raven. 2003. Crystal structure of the ascorbate peroxidase-ascorbate complex. Nat. Struct. Biol. 10:303-307.
Shimada, M. and T. Higuchi. 1991. Microbial, enzymatic and biomimetic degradation of lignin, p. 557-619. *In* D. N. S. Hon and N. Shiraishi (eds.), Wood and cellulosic chemistry. Marcel Dekker, N.Y.
Shimada, M., F. Nakatsubo, T. K. Kirk, and T. Higuchi. 1981. Biosynthesis of the secondary metabolite veratryl alcohol in relation to lignin degradation by *Phanerochaete chrysosporium*. Arch. Microbiol. 129:321-324.
Shimada, M. and M. Takahashi. 1991. Biodegradation of cellulosic materials, p. 621-663. *In* D. N. S. Hon and N. Shiraishi (eds.), Wood and cellulosic chemistry. Marcel Dekker, N.Y.
Spinnler, H. E., E. de Jong, G. Mauvais, E. Semon, and J.-L. Le Quéré. 1994. Production of halogenated compounds by *Bjerkandera adusta*. Appl. Microbiol. Biotechnol. 42:212-221.
Sundaramoorthy, M., K. Kishi, M. H. Gold, and T. L. Poulos. 1994. The crystal structure of manganese peroxidase from *Phanerochaete chrysosporium* at 2.06-Å resolution. J. Biol. Chem. 269:32759-32767.
Sundaramoorthy, M., H. L. Youngs, M. H. Gold, and T. L. Poulos. 2005. High-resolution crystal structure of manganese peroxidase: substrate and inhibitor complexes. Biochemistry 44:6463-6470.
Takao, S. 1965. Organic acid production by Basidiomycetes. I Screening of acid-producing strains. Arch. Microbiol. 13:732-737.
Teunissen, P. J. M. and J. A. Field. 1998a. 2-Chloro-1,4-dimethoxybenzene as a mediator of lignin peroxidase catalyzed oxidations. FEBS Lett. 439:219-223.
Teunissen, P. J. M. and J. A. Field. 1998b. 2-Chloro-1,4-dimethoxybenzene as a novel catalytic cofactor for oxidation of anisyl alcohol by lignin peroxidase. Appl. Environ. Microbiol. 64:830-835.
Teunissen, P. J. M., D. W. Sheng, G. V. B. Reddy, P. Moënne-Loccoz, J. A. Field, and M. H. Gold. 1998. 2-Chloro-1,4-dimethoxybenzene cation radical: Formation and role in the lignin peroxidase oxidation of anisyl alcohol. Arch. Biochem. Biophys. 360:233-238.
Thurston, C. F. 1994. The structure and function of fungal laccases. Microbiology 140:19-26.
Tien, M. and T. K. Kirk. 1983. Lignin-degrading enzyme from the hymenomycete *Phanerochaete chrysosporium* Burds. Science 221:661-663.
Tien, M. and D. Ma. 1997. Oxidation of 4-methoxymandelic acid by lignin peroxidase. Mediation by veratryl alcohol. J. Biol. Chem. 272:8912-8917.
Tsukamoto, K., H. Itakura, K. Sato, K. Fukuyama, S. Miura, S. Takahashi, H. Ikezawa, and T. Hosoya. 1999. Binding of salicylhydroxamic acid and several aromatic donor molecules to *Arthromyces ramosus* peroxidase, investigated by X-ray crystallography, optical difference spectroscopy, NMR relaxation, molecular dynamics, and kinetics. Biochemistry 38:12558-12568.
Wariishi, H. and M. H. Gold. 1989. Lignin peroxidase compound III: Formation, inactivation, and conversion to the native enzyme. FEBS Lett. 243:165-168.
Wariishi, H. and M. H. Gold. 1990. Lignin peroxidase compound III. Mechanism of formation and decomposition. J. Biol. Chem. 265:2070-2077.
Wariishi, H., K. Valli, and M. H. Gold. 1991. *In vitro* depolymerization of lignin by manganese peroxidase of *Phanerochaete chrysosporium*. Biochem. Biophys. Res. Commun. 176:269-275.

Wariishi, H., K. Valli, and M. H. Gold. 1992. Manganese(II) oxidation by manganese peroxidase from the basidiomycete *Phanerochaete chrysosporium*. Kinetic mechanism and role of chelators. J. Biol. Chem. 267:23688-23695.

Welinder, K. G. 1992. Superfamily of plant, fungal and bacterial peroxidases. Curr. Opin. Struct. Biol. 2:388-393.

Weng, J. K. and C. Chapple. 2010. The origin and evolution of lignin biosynthesis. New Phytol. 187:273-285.

Yelle, D. J., J. Ralph, F. Lu, and K. E. Hammel. 2008. Evidence for cleavage of lignin by a brown rot basidiomycete. Environ. Microbiol. 10:1844-1849.

Zhang, L. M., G. Gellerstedt, J. Ralph, and F. C. Lu. 2006. NMR studies on the occurrence of spirodienone structures in lignins. J. Wood Chem. Technol. 26:65-79.

Capítulo 2

"*Pleurotus ostreatus* heme peroxidases: An *in silico* analysis from the genome sequence to the enzyme molecular structure"

Ruiz-Dueñas, F. J**., E. Fernández**, M. J. Martínez, and A. T. Martínez.

C. R. Biol. 334:795-805. **2011.**

C. R. Biologies xxx (2011) xxx–xxx

Contents lists available at ScienceDirect

Comptes Rendus Biologies

www.sciencedirect.com

Review/Revue

Pleurotus ostreatus heme peroxidases: An *in silico* analysis from the genome sequence to the enzyme molecular structure

Francisco J. Ruiz-Dueñas *, Elena Fernández, María Jesús Martínez, Angel T. Martínez *

Centro de Investigaciones Biológicas, CSIC, Ramiro de Maeztu 9, 28040 Madrid, Spain

ARTICLE INFO

Keywords:
Pleurotus ostreatus
Genome sequence
In silico analysis
Heme peroxidases
Ligninolytic peroxidases
Heme-thiolate peroxidases
Dye-decolorizing peroxidases

ABSTRACT

An exhaustive screening of the *Pleurotus ostreatus* genome was performed to search for nucleotide sequences of heme peroxidases in this white-rot fungus, which could be useful for different biotechnological applications. After sequence identification and manual curation of the corresponding genes and cDNAs, the deduced amino acid sequences were converted into structural homology models. A comparative study of these sequences and their structural models with those of known fungal peroxidases revealed the complete inventory of heme peroxidases of this fungus. This consists of cytochrome *c* peroxidase and ligninolytic peroxidases, including manganese peroxidase and versatile peroxidase but not lignin peroxidase, as representative of the "classical" superfamily of plant, fungal, and bacterial peroxidases; and members of two relatively "new" peroxidase superfamilies, namely heme-thiolate peroxidases, here described for the first time in a fungus from the genus *Pleurotus*, and dye-decolorizing peroxidases, already known in *P. ostreatus* but still to be thoroughly explored and characterized.

1. Introduction

A series of basidiomycete genomes have been completed during last years corresponding to plant and animal pathogens, and soil and mycorrhizal species, together with wood-rotting fungi. The latter have raised much interest in the search for peroxidases with industrial interest in bulk and fine chemistry, food and other sectors. They include the genomes of *Phanerochaete chrysosporium* [1] (the first basidiomycete genome to be sequenced) and *Postia placenta* [2], the recently published genome of *Schizophyllum commune* [3], and many others that are in different phases of the sequencing process (up to 53 only at the Joint Genome Institute, JGI, of the US Department of Energy, DOE) including those of *Pleurotus ostreatus* and *Ceriporiopsis subvermispora* (both to be published soon), *Pycnoporus cinnabarinus* (to be released) and *Phlebiopsis gigantea*.

Among the above basidiomycetes, several white-rot fungi from the genus *Pleurotus* have been described as being able to degrade lignin selectively [4]. The limited attack to cellulose makes them very interesting in different biotechnological applications related to the use of plant biomass, including the integrated lignocellulose biorefineries for the future production of chemicals, materials and biofuels. This fact, together with the understanding of the regulation of the ligninolytic system constituted by heme peroxidases and other enzymes [5], as well as the increasing interest in *Pleurotus* as an edible mushroom (with a world production near that of *Agaricus bisporus* [6]) were the main reasons to include a representative of this genus among the organisms to be sequenced by the DOE, in a project coordinated by Dr A.G. Pisabarro from the Public University of Navarre (Spain).

Ligninolytic peroxidases from *P. ostreatus* and other white-rot fungi have been widely studied over the last years [7–9]. However, only in the case of *P. chrysosporium* a complete catalog of these enzymes can be obtained from its genome sequence. On the other hand, new superfamilies of heme peroxidases, namely heme-thiolate peroxidases and

* Corresponding authors.
E-mail addresses: fjruiz@cib.csic.es (F.J. Ruiz-Dueñas), atmartinez@cib.csic.es (A.T. Martínez).

1631-0691/$ – see front matter © 2011 Académie des sciences. Published by Elsevier Masson SAS. All rights reserved.
doi:10.1016/j.crvi.2011.06.004

dye-decolorizing peroxidases, exhibiting very interesting catalytic properties have been recently described in basidiomycetes [10]. Although their role in nature is still unknown, they have a very promising future as industrial biocatalysts due to the wide variety of aliphatic and aromatic compounds they are able to oxidize and oxygenate.

Herein we show the result of our participation in the search for genes encoding peroxidases in the genome of *P. ostreatus*. Different heme peroxidase genes models were identified, which could be grouped into different "classical" and "new" families and superfamilies of interest from a biotechnological point of view. At present, these heme peroxidases are being expressed in *Escherichia coli* and their stability and catalytic properties studied with the aim of determining their substrate specificity and real biotechnological potential.

2. Materials and methods

2.1. Fungal strains and P. ostreatus genome sequence

The JGI (DOE, http://www.jgi.doe.gov) has sequenced the genome of *P. ostreatus* (dikaryotic strain N001 deposited in the Spanish Type Culture Collection with the accession number CECT20600). The strategy followed consisted of sequencing the DNA of two monokaryons (PC9 and PC15 deposited in the aforementioned Type Culture Collection with the accession numbers CECT20311 and CECT20312, respectively) which had been previously obtained from the dikaryotic strain N001 [11]. The sequences of both monokaryons have been released to different collaborators after assembly by the Stanford Human Genome Center and subsequent annotation by JGI using custom analyses and the automated JGI Annotation Pipeline (genome assemblies v1.0 for PC9 and v1.0 and v2.0 for PC15). The 35.6 (PC9 v1.0) Mbp and 34.3 (PC15 v2.0) Mbp assemblies contain 572 and 12 nuclear scaffolds, and are predicted to have approximately 12206 and 12330 gene models, respectively. The significant differences in the number of scaffolds between both assemblies are a consequence of the sequencing method used for each monokaryon. The traditional Sanger sequencing technology was used for PC15, whereas a Sanger/454 pyrosequencing hybrid approach was used for PC9.

2.2. Screening and analysis of the heme peroxidase models

The search for heme peroxidase gene models in the genome sequence of both monokaryotic strains was performed at the Centro de Investigaciones Biológicas (CIB-CSIC). The process carried out to obtain the complete heme peroxidase inventory consisted of the following stages: (1) screening the automatically-annotated genome of *P. ostreatus*, monokaryons PC9 and PC15, using the Advanced Search option ("peroxidase" as search term) at the JGI web-site; (2) revising and manual curating (when necessary) the precise positions of introns, strongly affecting the deduced protein sequence and C-termini of the selected models; (3) comparing the amino acid sequence identities; and (4) confirming the presence of characteristic residues at the active center and substrate oxidation sites after homology modeling using crystal structures of reference proteins, deposited in the RCSB Protein Data Bank (PDB, http://www.pdb.org), as templates. The allelic variants of one dye-decolorizing peroxidase and three ligninolytic peroxidases genes previously cloned from *P. ostreatus* [12–15] were identified following this strategy, and used as references to validate the screening and analysis process. Programs used in this process were: BLAST (Basic Local Alignment Tool) at National Center for Biotechnology Information (NCBI) for searching nucleotide and protein databases; MEGA4 [16] for conducting automatic and manual sequence alignment during the heme peroxidase gene model search and curation process, and also for inferring phylogenetic trees; and SignalP 3.0 [17] for predicting the presence and location of signal peptides and cleavage sites. Theoretical molecular models of heme peroxidases were generated by using the programs implemented by the automated protein homology-modeling server SWISS-MODEL [18].

3. Results and discussion

3.1. Identification of heme peroxidase gene models in the P. ostreatus genome

Twenty-eight gene models were initially identified in the genome sequence of the *P. ostreatus* monokaryotic strain PC15 v1.0 (the first assembly released to collaborators) derived from the parental dikaryotic strain N001. However, eleven of these models were subsequently excluded by two main reasons: (i) seven of them (with identification numbers, ID#, 30148, 52526, 62301, 160045, 166150, 170674 and 173675) most probably do not correspond to heme protein genes, although they were automatically annotated as such due to the presence of short sequences reminiscent of heme protein conserved motifs; and (ii) four ones (IDs# 30776, 41714, 154272 and 170654) could correspond to heme proteins but they are not related to fungal peroxidase genes (the highest sequence identities were with oxygenases and cytochrome P450-type genes). The automatic annotation of the remaining seventeen heme peroxidase gene models was analyzed and subsequently their sequence manually improved in the PC9 v1.0 and PC15 v2.0 assemblies by modifying the intron positions and the deduced protein sequence and C-termini (affected by the intron changes) when errors were detected. Multiple nucleotide (DNA and cDNA) and amino acid sequence alignments with seventy basidiomycete and two ascomycete heme peroxidases were used for this task (protein sequence entries for the seventy peroxidases are given in the dendrogram of peroxidase evolutionary relationships present in Ruiz-Dueñas et al. [19]). The seventeen heme peroxidase gene models identified have the corresponding alleles in PC9 and PC15. All of them are summarized in Table 1, but only those corresponding to PC9 are hereafter cited in the text for simplifying the reading.

During the automatic annotation process, the programs used by JGI identified canonical GT-AG splice sites (GT-AG introns), and only one noncanonical GC-AG site (GC-AG introns) which was located in the sequence of the putative

Please cite this article in press as: F.J. Ruiz-Dueñas, et al., *Pleurotus ostreatus* heme peroxidases: An *in silico* analysis from the genome sequence to the enzyme molecular structure, C. R. Biologies (2011), doi:10.1016/j.crvi.2011.06.004

Table 1
Summary of heme peroxidase gene models in the genome of *P. ostreatus*. Reference (ID #), scaffold number (Sc.), and position of the manually curated/annotated sequences in monokaryons PC9 (v1.0) and PC15 (v2.0); and model analysis including: (i) amino acid sequence identity of PC9 and PC15 alleles (Ide-PC9/PC15, %); (ii) name of best hit protein (after species abbreviation) and whole protein identity (Ide-Best hit, %); (iii) presence of ligninolytic peroxidase catalytic residues (Wc, Ea, Eb and Dc); and (iv) peroxidase type based on structural-functional classification.

	PC9 (v1.0)			PC15 (v2.0)			Analysis of the heme peroxidase models							
	ID#	Sc.	Position	ID#	Sc.	Position	Ide-PC9-PC15	Best hit	Ide-Best hit	Wc	Ea	Eb	Dc	Type
1.	77045	3	583621-585384	1096819	5	734156-735921	99.7	CC-CCP	71	–	–	–	–	CCP
2.	114464	1	3116892-3118095	1110336	1	1483346-1484549	99.7	AB-CPO	55	–	–	–	–	CPO/APO
3.	123372	2	3213565-3214450	1111884	4	262016-262902	99.2	AB-CPO	27	–	–	–	–	CPO/APO
4.	127284	7	560895-561684	1108212	9	535259-536048	98.8	AB-CPO	33	–	–	–	–	CPO/APO
5.	87639§	7	191407-193574	62271§	9	213879-216064	98.6	PO-DyP	97	–	–	–	–	DyP
6.	115057	2	2850334-2852370	1092668	4	657069-659105	99.8	PO-DyP	64	–	–	–	–	DyP
7.	97865	6	2056440-2058411	52170	7	3196067-3198039	98.7	PO-DyP	62	–	–	–	–	DyP
8.	117204	12	215278-217337	1069077	11	2524348-2526415	98.2	BA-DyP	44	–	–	–	–	DyP
9.	137740§	3	1767677-1769279	1089546§	5	1981555-1983678	99.7	PO-MnP	99	–	+	+	+	MnP
10.	137765	3	1625766-1627664	199511	5	1840285-1842183	99.7	PSA-VPL	76	–	+	+	+	MnP
11.	137764	9	32682-34394	199510	2	1135915-1137627	100	TV-MRP	63	–	+	+	+	MnP
12.	51713	12	2544215-2545903	1041740	5	2768778-2770466	100	TV-MRP	64	–	+	+	+	MnP
13.	121638	1	2703196-2704913	1099081	1	1827850-1829567	100	TV-MRP	62	–	+	+	+	MnP
14.	137757	8	536529-538627	1089895	6	1701105-1704309	100	PSA-VPL	98	+	+	+	+	VPL
15.	137760§	2	3291830-3293748	1096331§	4	186162-188472	100	PO-MnP	99	+	+	+	+	VP
16.	123383	2	3246008-3247917	156336	4	212622-214530	99.7	PO-MnP	78	+	+	+	+	VP
17.	137766§	8	635476-637382	199491§	6	1618102-1620009	100	PO-MnP	99	+	+	+	+	VPS

Published genes: the previously published *P. ostreatus* peroxidase genes, ID # 87639/62271, 137740/1089546, 137760/1096331 and 137766/199491 (PC9/PC15) are marked with §; Peroxidase families: CCP: cytochrome *c* peroxidase; CPO/APO: heme-thiolate peroxidase; DyP: dye-decolorizing peroxidase; MnP: manganese peroxidase; VP: versatile peroxidase (VPL, liquid culture isoenzyme; VPS, solid culture isoenzyme) (MRP, so-called manganese-repressed peroxidase of *T. versicolor*). Species abbreviations: AB: *Agaricus bisporus*; BA: *Bjerkandera adusta*; CC: *Coprinopsis cinerea*; PO: *Pleurotus ostreatus*; PSA: *Pleurotus sapidus*; TV: *Trametes versicolor*; Catalytic residues (of ligninolytic peroxidases): Wc: catalytic tryptophan (as *Pleurotus eryngii* VPL W164); Ea, Eb and Dc: three acidic catalytic residues (2 glutamates and 1 aspartate) at the manganese oxidation-site (as *Pleurotus eryngii* VPL Glu36, Glu40 and Asp175).

dye-decolorizing peroxidase gene 87639 (see below for more details about this peroxidase superfamily). Additionally, two noncanonical GC-AG splice sites could be also manually predicted in the genomic sequence of both alleles of a putative manganese peroxidase (MnP) (137764) during the curation process after comparing the deduced cDNA sequences of all the heme peroxidase genes identified. This is not the first time this type of low frequent introns containing GC instead of GT at the 5' splice site is identified in fungal genes. Their existence have been previously reported for both ascomycete and basidiomycete genes [20,21], including those encoding two oxalate-degrading enzymes from the white-rot fungi *C. subvermispora* and *Dichomitus squalens* [22,23]. On the other hand, the presence of a high number of introns (among 10 and 15) and the small size of some exons, several of them encoding for only three amino acid residues, resulted in very significant differences after manual curation of six of the nine sequences corresponding to ligninolytic peroxidases (sequences 9 to 17 in Table 1) (see below for more details about these sequences) compared with those initially included by JGI in the automatically annotated *P. ostreatus* gene catalog.

Once the sequences were manually curated, subsequent functional classification of the heme peroxidases was based on: (i) the use of BLAST scores (best hit proteins and whole sequence identities are shown in Table 1); and (ii) the 3D-modeling results. In order to define the gene family these heme peroxidases belong to, a structural-functional analysis was conducted. Identification of the gene family was based on the presence of conserved (active site and substrate oxidation sites) residues in molecular models built by homology modeling of the curated protein sequences. The structural models used as templates during this process were selected in function of the crystal structure availability of related heme peroxidases (see next subsections for each particular heme peroxidase). This approach allowed us to make a more precise definition of some of the automatic models, such as shown in the last column of Table 1 (e.g. several enzymes initially identified as MnP according to the best Blast hit score are putative versatile peroxidases (VP) and, conversely, a VP is in fact a MnP). After manual curation and annotation, new protein identification numbers were automatically assigned to the gene models by JGI (Table 1).

The seventeen heme peroxidase models from each monokaryon could be classified into four different groups, corresponding to classical families and new recently described superfamilies [10], as follows: (i) cytochrome *c* peroxidase (CCP) (1 model); (ii) ligninolytic peroxidases (9 models), including five MnPs and four VPs; (iii) heme-thiolate peroxidases (CPO/APO-type) (3 models); and (iv) dye-decolorizing peroxidases (DyP) (4 models). A dendrogram showing sequence relationships between these enzymes, and structural-functional classification of the ligninolytic peroxidases according to the presence of different catalytic sites in their theoretical molecular structure is shown in Fig. 1. Finally, an important question related to the presence or absence of lignin peroxidase (LiP) genes in the *P. ostreatus* genome has been solved. Their absence is definitively confirmed, as expected according to previous expression/production studies [24]

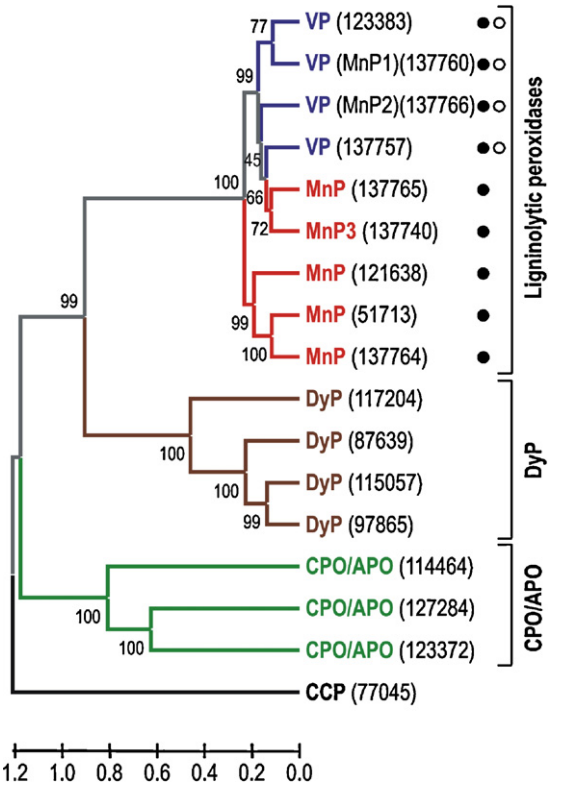

Fig. 1. Dendrogram of seventeen deduced heme peroxidase sequences (accession numbers in parentheses) from the *P. ostreatus* genome (monokaryon PC9, v1.0) showing sequence relationships and structural-functional classification of the ligninolytic peroxidases (filled circle, Mn^{2+}-oxidation site; and open circle, catalytic tryptophan). Sequence comparison as Poisson distances, and clustering using the UPGMA method and "pairwise deletion" option of MEGA4. The percentage of replicate trees in which the associated taxa clustered together in the bootstrap test (1000 replicates) are shown next to the branches. The corresponding allelic variants can be identified in the sequence of monokaryon PC15, v2.0 (Table 1).

and DNA hybridization analysis [25]. The heme peroxidase models identified in the *P. ostreatus* genome are described below considering the family they belong to, and some interesting aspects of these enzymes are discussed.

3.2. Cytochrome c peroxidase (CCP)

CCP is a Class I low redox-potential enzyme of the superfamily of prokaryotic, fungal and plant peroxidases [26] with a His residue acting as the fith ligand of the heme iron. The only model of this family identified in *P. ostreatus* (77045) (Table 1) shows the highest amino acid sequence identity (71% of whole protein sequence) with the recently reported *Coprinopsis cinerea* CCP (NCBI XP_001830809) [27]. However, the theoretical structural model for this mitochondrial enzyme was obtained using the *Saccharomyces cerevisiae* CCP crystal structure (PDB entry 1CCP) as template, since this is the enzyme of this family exhibiting the highest amino-acid sequence identity (41%) whose crystal structure is available. Homology and crystal models of *P. ostreatus* and *S. cerevisiae* were superimposed and the rms distance between Cα measured. The low value obtained (0.26 Å, 256 residues computed) evidenced a high structural

Please cite this article in press as: F.J. Ruiz-Dueñas, et al., *Pleurotus ostreatus* heme peroxidases: An *in silico* analysis from the genome sequence to the enzyme molecular structure, C. R. Biologies (2011), doi:10.1016/j.crvi.2011.06.004

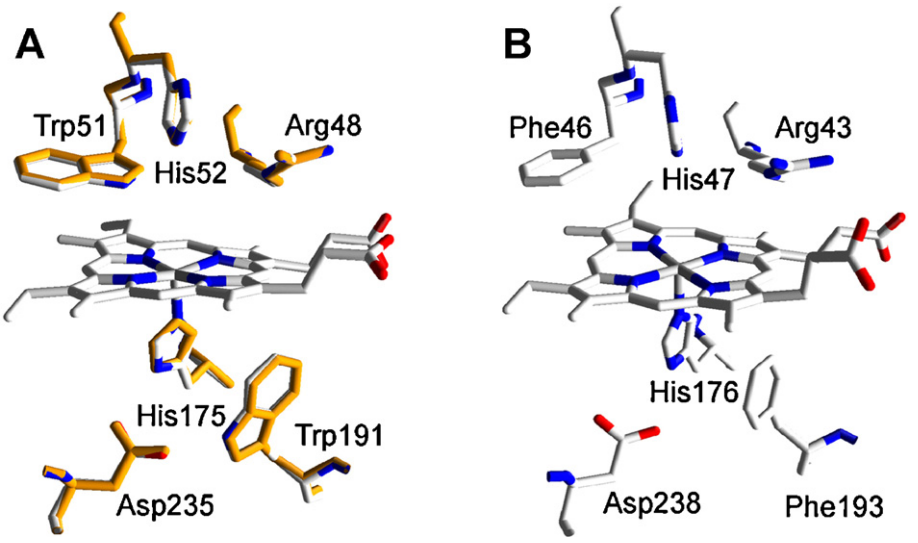

Fig. 2. Heme environment in the homology model of *P. ostreatus* CCP obtained using *S. cerevisiae* CCP crystal structure (PDB entry 1CCP) as template: **A**. Structural alignment of the model obtained (orange, 77045) and 1CCP (CPK colors) (numbers refer to the amino acid residues in 1CCP). **B**. Equivalent residues in *P. chrysosporium* LiP (PDB entry 1LLP), as a model ligninolytic enzyme (MnP and VP present the same residues, here shown, in their molecular structure).

similarity between both proteins. Structurally, CCP is characterized, among others, by the heme distal and proximal residues (located above and below of the heme plane, respectively) similar to those found in ligninolytic peroxidases but showing two tryptophan, instead of phenylalanine, residues at both sides of the heme (see Fig. 2 for a comparison between CCP and ligninolytic peroxidases heme environments). As observed in Fig. 2A, the heme environment is completely conserved in the *P. ostreatus* CCP homology model. This fact strongly suggests a CCP-type activity for this enzyme. Among the different conserved amino acids, the proximal tryptophan has been described as a catalytically relevant residue in CCP. One of the two oxidizing equivalents of CCP compound I (generated after H_2O_2 enzyme activation) is stored in an intermediate protein radical centered on this amino acid residue [28] which would be involved in the electron transfer between the natural substrate cytochrome *c* and the enzyme [29].

3.3. Ligninolytic peroxidases

Ligninolytic peroxidases are Class II high redox-potential enzymes of the above-mentioned superfamily of prokaryotic, fungal and plant peroxidases. They are secretion enzymes able to oxidize, directly or through mediators, the different units forming the lignin aromatic polymer as well as other aromatic compounds (such as polycyclic aromatic hydrocarbons, pesticides and dyes) [5,30]. Members of the three families of ligninolytic peroxidases (LiP, MnP, and VP) share an almost identical heme environment (Fig. 2B), responsible among others for their high redox potential [31,32], but differ in the substrates they can oxidize as consequence of the presence of different catalytic sites in their molecular structures. So, LiP oxidizes non-phenolic lignin model compounds in direct contact with a tryptophan radical exposed to the solvent [33,34], whereas MnP is very specific oxidizing Mn^{2+} in a small channel formed by three acidic residues and located directly on the heme internal propionate [35]. VP shares catalytic and structural properties with LiP and MnP. Furthermore, it is able to directly oxidize low redox potential substrates, including phenols, as well as high redox potential dyes that are oxidized by LiP only in the presence of some mediators [9].

Most changes with respect to the best gene model offered by the automatic annotation of the *P. ostreatus* genome by JGI corresponded to the nine ligninolytic peroxidase (five MnPs and four VPs, Table 1) models identified due, among other reasons, to the abundant information available on structure-function and molecular biology of these peroxidases of biotechnological interest [5,7–9,36,37]. Analyzing in detail the MnP models, it was observed that all of them correspond to the subfamily of "short" MnPs, recently described for the first time in *Phlebia radiata* [38], in comparison to the typical "long" MnPs (including an extra C-terminal extension in their amino acid sequence) from the model ligninolytic fungus *P. chrysosporium*. "Long" MnPs are specific for Mn^{2+}, whereas "short" MnPs are also able to oxidize phenols, amines and ABTS in the absence of Mn^{2+}. This fact suggests relative wide substrate specificity for the five MnPs identified in the *P. ostreatus* genome. Among these, three models (137764, 51713 and 121638) show the highest amino acid sequence identity (62–64% of the whole protein) with the so-called manganese-repressed peroxidase from *Trametes versicolor* (GenBank AAB63460) and are grouped together in the dendrogram of Fig. 1. By contrast, the other two MnP models (137740 and 137765) are clustered with VP models. One of them (137740) seems to be an allelic variant (differing in only two amino acid residues, one of them in the signal peptide) of the already described and cloned *P. ostreatus* MnP3 (GenBank BAA33449) [14], whereas the other one (137765) has the highest amino acid sequence identity (76% of the whole protein) with the unpublished VP (putative VPL isoenzyme) of *Pleurotus*

Please cite this article in press as: F.J. Ruiz-Dueñas, et al., *Pleurotus ostreatus* heme peroxidases: An *in silico* analysis from the genome sequence to the enzyme molecular structure, C. R. Biologies (2011), doi:10.1016/j.crvi.2011.06.004

sapidus (GenBank CAJ01576) although the catalytic tryptophan is absent and, therefore, it is classified as MnP.

Regarding VP, two models (137760 and 137766) seem to be allelic variants (differing in only 1-2 amino acids of the whole sequence) of the previously cloned and described *P. ostreatus* MnP1 (GenBank AAA84396) [12] and MnP2 (GenBank CAB51617) [13], respectively. The first one is a putative VP due to the presence of the catalytic tryptophan, whereas the second one has already been demonstrated to be a VP by its ability to act on Mn^{2+}, and directly oxidize 3,4-dimethoxybenzyl (veratryl) alcohol and polymeric azo dyes at an exposed tryptophan [39]. A third model (123383) shows the highest amino acid sequence identity (78% of the whole protein sequence) with *P. ostreatus* MnP1 (the putative VP mentioned above), whereas the fourth model (137757) has high identity (98% of the whole protein sequence) with the aforementioned unpublished VP of *P. sapidus*. The allelic variant of this model in PC15 v2.0 (1089895) presents a stop codon in the middle of the sequence, suggesting it is a putative VP pseudogene. A sequencing mistake should be ruled out considering this codon appears in the two PC15 assemblies (v1.0 and v2.0). The amino acid sequence analysis of the above four sequences in PC9, three in PC15 due to the putative pseudogen, revealed the presence of both residues forming the manganese binding site and the catalytic tryptophan, typical from VP [9].

The subsequent analysis of the theoretical structural models of *P. ostreatus* MnP and VP isoenzymes, built using the wild type *P. chrysosporium* MnP and *P. eryngii* VP crystal structures (PDB entries 1YYD and 3FJW, respectively) as templates, revealed that these peroxidases maintain a well conserved tertiary structure. The homology models not only confirmed the typical predominant α-helical structure of the superfamily of plant, fungal, and bacterial peroxidases, but also the location of key amino acid residues. So, MnP isoenzymes exhibit the characteristic Mn^{2+} binding site formed by one aspartic and two glutamic acids (Fig. 3A), responsible for Mn^{2+} oxidation, whereas VP theoretical models include both the Mn^{2+} binding site and the tryptophan residue exposed to the solvent at the same position of that involved in oxidation of high redox potential substrates by *P. eryngii* VP (Fig. 3B) [9].

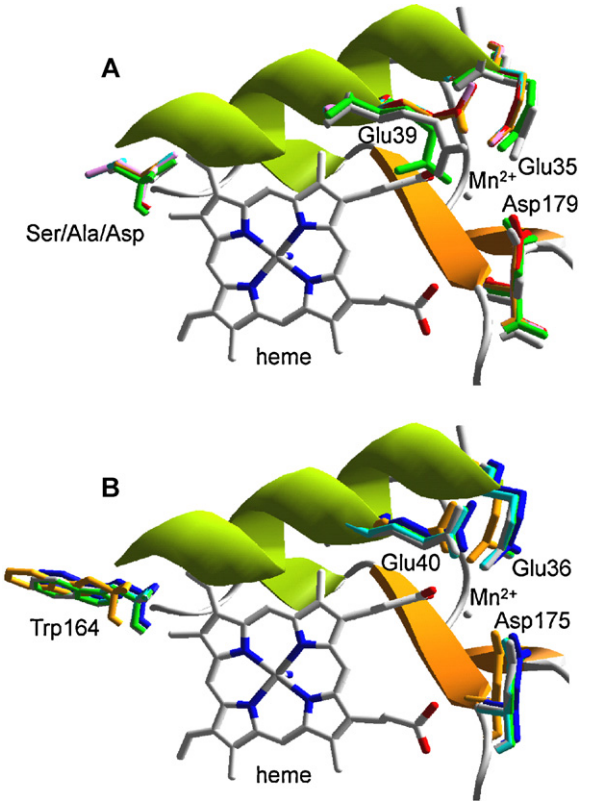

Fig. 3. Axial view of the heme region in nine *P. ostreatus* ligninolytic peroxidase homology models obtained using *P. eryngii* VP and *P. chrysosporium* MnP crystal structures (PDB entries 3FJW and 1YYD, respectively) as templates: **A**. MnP-type models including a putative Mn^{2+}-oxidation site (right) formed by two glutamic and one aspartic acidic residues (grey, 1YYD, E35/E39/D179; pink, 137764, E36/E40/D181; light blue, 51713, E36/E40/D181; red, 121638, E36/E40/D181; orange, 137765, E36/E40/D175; and green, 137740, E36/E40/D175). **B**. VP-type models including an exposed tryptophan (oxidizing high redox-potential substrates) in addition to the Mn^{2+}-oxidation site described in **A** (grey, 3FJW, W164/E36/E40/D175; dark blue, 137766, W170/E36/E40/D181; light blue, 123383, W164/E36/E40/D175; green, 137760, W165/E36/E40/D176; and orange, 137757, W164/E36/E40/D175). The amino acid numbering showed above refers to putative mature sequences.

3.4. Heme-thiolate peroxidases (CPO/APO-type)

Heme-thiolate peroxidases have been described as secretion enzymes characterized by the presence of a cysteine residue acting as the proximal axial ligand of heme. CPO from the ascomycete *Leptoxyphium fumago* has been the only heme-thiolate peroxidase known, and exhaustively characterized, since its discovery in 1961 [40] until recently. Lately a large amount of sequences for putative heme-thiolate chloroperoxidases have been accumulated from the analysis of ascomycete and basidiomycete genome sequences, many of them being included in PeroxiBase (http://peroxibase.toulouse.inra.fr) [41]. Recently, a second heme-thiolate peroxidase described as an aromatic peroxygenase (APO) has been reported in agaric basidiomycetes, the APO from *Agrocybe aegerita* being the best characterized [42,43]. The CPO and APO wide substrate specificity, catalyzing halogenation reactions and sharing catalytic properties with peroxidases, catalases and cytochrome P450 monooxygenases (APO even oxygenating aromatic substrates), make these enzymes very interesting from a biotechnological point of view [44]. Amino acid sequence, catalytic activity and structure of these two heme-thiolate peroxidases differ from those of classical heme peroxidases, and they have been lately considered as members of the new heme-thiolate peroxidase superfamily [10].

Three heme-thiolate peroxidase gene models were identified in the *P. ostreatus* genome (sequences 2 to 4 in Table 1), being the first time this type of heme peroxidases is described in a fungus from the genus *Pleurotus*. All of them show the highest amino acid sequence identity with the unpublished putative CPO of *A. bisporus* (GenBank CAC03461). The identity values range from 55% of model 114464 (290 amino acids long) to 27–33% of models 123372 (255 amino acids long) and 127284 (242 amino acids long)

Please cite this article in press as: F.J. Ruiz-Dueñas, et al., *Pleurotus ostreatus* heme peroxidases: An *in silico* analysis from the genome sequence to the enzyme molecular structure, C. R. Biologies (2011), doi:10.1016/j.crvi.2011.06.004

for the whole protein sequence. Unlike the intron-less CPO gene of *L. fumago*, the three *P. ostreatus* gene models contain introns (3, 2 and 1 introns, respectively), as also observed for the sixteen genes encoding putative CPOs (fifteen genes containing four introns and one gene containing only one intron) in the recently sequenced genome of *A. bisporus* var *bisporus* (H97) v2.0 (JGI, DOE) and the *apo1* gene (five introns) encoding the *A. aegerita* peroxygenase [45]. Surprisingly, only one (123372) of the three models identified in *P. ostreatus* seems to be clearly a secretory protein (signal peptide probability 0.987 for the allelic variant 1111884 in PC15) with a putative 23 amino acid signal peptide and the corresponding cleavage site, according to the scores reported by SignalP 3.0. The probability of the presence of a signal sequence in model 114464 is very low (0.334) and zero for model 127284. These data suggest a different cellular localization or secretion pathway for these three *P. ostreatus* heme-thiolate peroxidases, which would be also independent of a C-terminal propeptide (absent in their amino acid sequences), unlike what happen with *L. fumago* CPO, where a 21 amino acid N-terminal signal peptide and a 52 amino acid C-terminal propeptide, the latter probably having a chaperone-like function, have been identified [46].

Although the amino acid sequence identities with two model enzymes of this new superfamily, *A. aegerita* APO [45] and *L. fumago* CPO [47], were very low (only around 20% in both cases), theoretical molecular models for the three putative *P. ostreatus* heme-thiolate peroxidases were obtained using the crystal structure of the last one (PDB entry 1CPO) as template. This was because CPO of *L. fumago* is the only heme-thiolate peroxidase whose molecular structure has been experimentally solved [48] and it is available in PDB. Crystallization of *A. aegerita* APO has been recently reported [49] but its structure has not been yet published nor deposited in the PDB. Molecular models built for heme-thiolate peroxidases 123372 and 127284 fitted quite well with the whole crystal model of *L. fumago* CPO, and only the 10-11 N-terminal and 15-26 C-terminal amino acids, respectively, were not included in the final theoretical models. Both homology models were superimposed on the crystal model of *L. fumago* CPO. The rms distances between Cα were 0.37 Å with 123372 (194 amino acid residues computed of a total of 232 corresponding to the predicted mature protein) and 0.35 Å with 127284 (195 residues computed of a total of 242). This indicates high structural affinity taking into account, for example, that the rms distance between LiP isoenzymes H2 and H8 of *P. chrysosporium* is 1.1 Å [50]. By contrast, the structural homology model obtained for 114464 excluded not only the first 39 amino acid residues of the sequence but also the C-terminal 145 residues representing more than half of the amino acid sequence of the whole protein. These amino acid residues could not be automatically modeled and they were not considered in the final model. The modeled sequence of the remaining 102 amino acids fitted well with the equivalent region of *L. fumago* CPO, the rms distances between Cα being 0.32 Å. This region contains both the most relevant residues of the proximal side of the heme group, including the cysteine residue acting as the fifth ligand of the heme iron, as well as ligands for a Mn^{2+} ion described in the *L. fumago* CPO crystal structure. These data suggest that a structural "core" containing the heme active site is conserved in the three *P. ostreatus* heme-thiolate peroxidases and *L. fumago* CPO, even though the low percentage of amino acid sequence identity presented.

A detail of the heme environment in the three *P. ostreatus* heme-thiolate peroxidase homology models and the crystallographic model of CPO from *L. fumago* is shown in Fig. 4. Cysteine serving as axial heme ligand and surrounding residues stabilizing the cysteine-ligand loop by hydrogen-bonding are conserved at the proximal side. The only significant difference among them is the presence of an Ala and a Cys residues contiguous to the axial Cys in 114464, which could be reinforcing the hydrogen-bonds structure at this site. On the other hand, the theoretical models show the same three amino acid residues (Glu, Ser and His) responsible for cation coordination in CPO, and also include those present at the distal heme pocket. Differences at this region between the three models, and also with CPO, suggest different catalytic properties (activation rate and mechanism, substrate specificity, etc.) for these *P. ostreatus* hemo-thiolate peroxidases, since residues at this side in CPO have been involved in both enzyme activation by H_2O_2 (Glu183 acting as acid-base catalyst in the peroxide O-O bond cleavage mechanism, assisted by His105 and Asp106) and substrate binding (including, among others, Phe103, Phe186 and Asn74) [48,51,52]. Although catalytic differences can be suggested from this *in silico* analysis, these are only speculations. Homologous or heterologous expression of these *P. ostreatus* heme-thiolate peroxidases is necessary to determine their final catalytic properties, and definitively identify the heme-thiolate peroxidase family (CPO or APO) they belong to.

3.5. Dye-decolorizing peroxidases (DyPs)

DyP-type peroxidases constitute a new superfamily of heme peroxidases widespread in fungi and bacteria [53]. The first peroxidase giving name to this superfamilly was purified and characterized from cultures of the white-rot basidiomycete *Bjerkandera adusta* [54], although it appears in the bibliography as *Thanatephorus cucumeris* Dec 1 DyP due to a molecular misidentification.[1] As previously

[1] This strain was first described as *Geotrichum candidum* [55] and reidentified as *Thanathephorus cucumeris* (the sexual state of *Rhizoctonia solanii*) based on ITS-5.8S rDNA sequence identity with GenBank AF455461 (Y. Sugano, personal communication). The latter corresponds to a medical strain that had been identified by ITS sequence identity with AJ000198 (W. Buzina, personal communication). GenBank AJ000198 was at the origin of the above and other misidentifications (over 20 rDNA GenBank entries) of *B. adusta* strains as *T. cucumeris* (or *R. solanii*). It corresponds to a fungus that had been misidentified as *R. solanii* by classical methods and, although the comparison of rDNA sequences showed that it did not cluster with *R. solanii* and related species [56], its rDNA sequence was deposited in GenBank with the erroneous name. However, this fungus, as well as the above Dec 1 and medical strains, show high rDNA sequence identity with authentic *B. adusta* cultures (such as GenBank Y089741) indicating that the DyP-producing fungus, initially described as *T. cuccumeris*, must be referred in the future as *B. adusta*.

Please cite this article in press as: F.J. Ruiz-Dueñas, et al., *Pleurotus ostreatus* heme peroxidases: An *in silico* analysis from the genome sequence to the enzyme molecular structure, C. R. Biologies (2011), doi:10.1016/j.crvi.2011.06.004

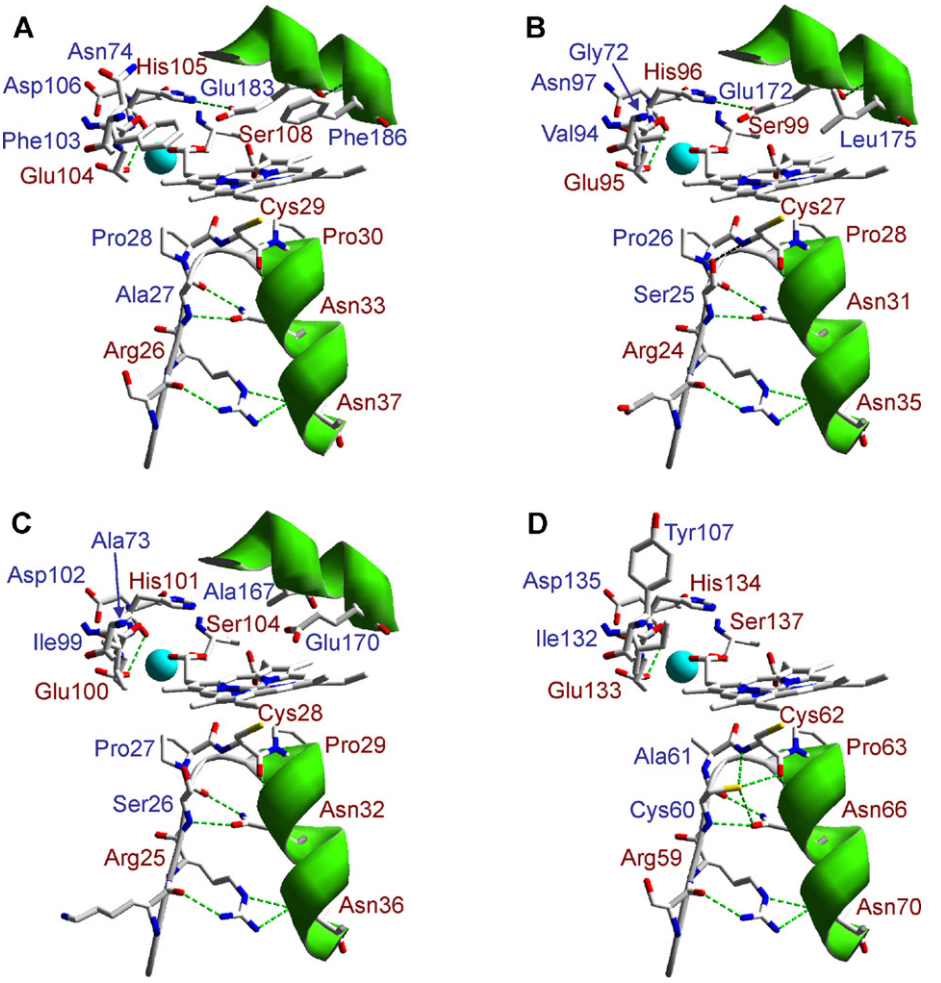

Fig. 4. Lateral view of the heme region in three *P. ostreatus* heme-thiolate (CPO/APO) peroxidase homology models obtained using *L. fumago* CPO crystal structure (PDB entry 1CPO) as template. Conserved amino acid residues in the crystal and homology models at the heme proximal and distal sides, including those involved in the cation (Mn^{2+}) (light blue sphere) binding, are shown in red color (**A**: 1CPO; **B**: 123372; **C**: 127284; and **D**: 114464). The amino acid numbering refers to putative mature sequences.

described for ligninolytic and heme-thiolate peroxidases, fungal DyPs are enzymes with a high biotechnological interest. They exhibit a significant catalytic versatility due to its ability to bleach different dyes, including high redox potential anthraquinone derivatives not oxidized by other peroxidases, oxidize phenols and cleave carotenoids [53,57,58]. Additionally, DyPs have demonstrated to be very robust enzymes. So, isoform AjPI of *Auricularia auricula-judae* maintains 100% activity at pH 2.5 for 4 h [59] and MsP1 of *Marasmius scorodonius* is able to withstand high temperatures (up to 70 °C, with the optimum between 55 and 60 °C) and works at high pressure, even better than at atmospheric pressure (2-fold activity increase at 500 bar) [60]. Although the role of these enzymes in nature is still unknown, it has been suggested that some DyPs, e.g. those from *A. auricula-judae*, could be involved in lignin biodegradation according to their ability to oxidize methoxylated aromatics and lignin model compounds, as veratryl alcohol and a β-O-4 nonphenolic dimer representative of the most frequent substructure present in the lignin polymer [59]. The same authors have suggested that DyPs may supplement or replace the classical high-redox potential ligninolytic peroxidases (LiP and VP). In favour of the idea of peroxidase complementarity, Sugano et al. [61] have reported complete decolourization of an anthraquinone dye as result of a concerted action of DyP and VP from the above *B. adusta* strain (that they misidentified as *T. cucumeris*).

Up to four different models of this superfamily were identified in the genome sequence of *P. ostreatus* (Table 1). Model 87639 from PC9 v1.0 and the corresponding 62271 from PC15 v2.0 seem to be alleles (98.4% and 98.6% nucleotide sequence identities, respectively) of the already cloned and described DyP from *P. ostreatus* (GenBank CAK55151) [15]. The amino acid sequences of these three allelic variants are highly similar, that of 62271 differing in only one residue (located in the signal peptide) from the previously published sequence. Two more models (115057 and 97865) have the highest amino acid sequence identity (67–69% for the whole protein) with model 87639 mentioned above, all of them containing nine introns. By contrast, model 117204 has the highest identity (only 38%

Please cite this article in press as: F.J. Ruiz-Dueñas, et al., *Pleurotus ostreatus* heme peroxidases: An *in silico* analysis from the genome sequence to the enzyme molecular structure, C. R. Biologies (2011), doi:10.1016/j.crvi.2011.06.004

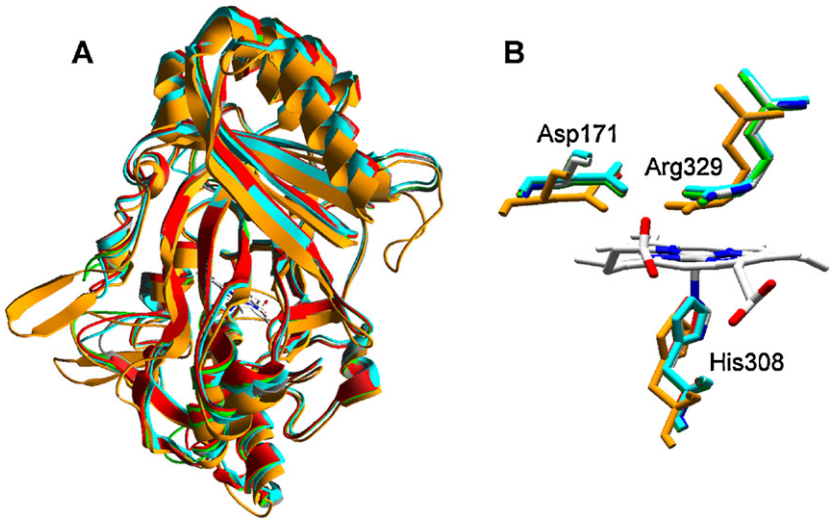

Fig. 5. Homology models of four *P. ostreatus* DyP-type peroxidases obtained with *B. adusta* DyP (reported as *T. cucumeris* DyP) crystal structure (PDB entry 2D3Q) as template: **A**. Superimposition of ribbon-type molecular models (grey, 2D3Q; green, 87639; red, 115057; light blue, 97865; and orange, 117204) with the central heme as CPK bars. **B**. Detail of the heme region (lateral view from the propionate side) showing conserved histidine (heme axial ligand at the proximal side) and aspartic acid and arginine residues at the heme distal side (colors as in **A** but 2D3Q in CPK colors). The numbers of the conserved histidine, aspartic acid and arginine residues in 2D3Q (shown in figure) and the putative mature sequences of the different *P. ostreatus* models (2D3Q/87639/115057/97865/117204) are the following: H308/H356/H351/H343/H334, D171/D213/D208/D200/D196, and R329/R377/R372/R364/R360.

of the whole protein sequence) with DyP (GenBank BAA77283) cloned from a *B. adusta* strain (formerly misidentified as *T. cucumeris*), and differs significantly from the others from *P. ostreatus* in intron number (only seven compared with the nine introns observed in the other three DyP models) and position. Surprisingly, models 97865 and 117204 do not contain signal sequences guiding these peroxidases in their transit through endoplasmic reticulum and Golgi apparatus suggesting, as in the case of the heme-thiolate peroxidases mentioned above, different cellular locations or secretion pathways for these peroxidases.

Homology models for DyPs of *P. ostreatus* were built using the *B. adusta* DyP (reported as *T. cucumeris* DyP) crystal structure (PDB entry 2D3Q) as template. The rms distance between Cα of the crystal model and the four homology models (ranging from 0.34 to 0.44 Å and covering from 83 to 90% of the amino acid sequences) revealed a high structural similarity among them, as in the case of the other peroxidases previously analyzed. The theoretical models present characteristic β-barrel tertiary structure (Fig. 5A) and heme environment (Fig. 5B). This includes proximal histidine acting as the fifth heme iron ligand, and conserved arginine and aspartate residues involved in enzyme activation by H_2O_2 at the distal side of heme, instead of typical histidine and arginine residues present in classical fungal heme peroxidases (Fig. 2). Unfortunately, not much more about structure-function relationships of these peroxidases is known.

4. Conclusion

As a result of the present work, a complete inventory of ligninolytic peroxidase, including VP and MnP, genes is provided and the absence of *lip* genes in the genome of *P. ostreatus* is definitively demonstrated. Heme-thiolate peroxidase genes initially represented by the *L. fumago* CPO and related enzymes, but also including APO recently described in several agaric basidiomycetes with very interesting catalytic properties (e.g. aromatic oxygenation), are described for the first time in *Pleurotus*. Moreover, one already identified DyP-type peroxidase is confirmed and more genes of this family are reported. On the other hand, the analysis of the amino acid sequences and structural homology models obtained for these enzymes reveal certain differences, not only among the members of different peroxidase super/families, but also among the members of the same super/family. In this sense, cellular localization and secretion pathways seem to be different among CPO/APO-type peroxidases and also among DyP-type peroxidases. Moreover, small sequence and structural details could determine differences in the catalytic properties of these heme peroxidases. A good example of this refers to the ligninolytic peroxidases, since it is possible to distinguish among LiP, MnP and VP on the basis of the presence or absence of only one or a few amino acid residues. After publishing the APO crystal structure it will be possible to determine differences between this and CPO, and then determine whether the *P. ostreatus* heme-thiolate peroxidases correspond to the CPO or APO type enzymes.

Disclosure of interest

The authors declare that they have no conflicts of interest concerning this article.

Acknowledgements

This study has been supported by the EU projects BIORENEW (NMP2-CT-2006-026456) and PEROXICATS

Please cite this article in press as: F.J. Ruiz-Dueñas, et al., *Pleurotus ostreatus* heme peroxidases: An *in silico* analysis from the genome sequence to the enzyme molecular structure, C. R. Biologies (2011), doi:10.1016/j.crvi.2011.06.004

(KBBE-2010-4-265397) and the Spanish project BIO2008-01533. The work conducted by the US Department of Energy Joint Genome Institute is supported by the Office of Science of the US Department of Energy under Contract No. DE-AC02-05CH11231. Antonio G. Pisabarro (Public University of Navarre) is acknowledged for coordinating the *P. ostreatus* genome project, and Yasushi Sugano (Tokyo Institute of Technology) and Walter Buzina (Medical University of Graz) for their collaboration in the reappraisal of the molecular identification of the DyP-producing *B. adusta* strain (formerly reported as *T. cucumeris* Dec 1). E.F. thanks CSIC for a JAE fellowship and F.J.R.-D. thanks the Spanish MICINN for a *Ramón y Cajal* contract.

References

[1] D. Martínez, L.F. Larrondo, N. Putnam, M.D. Gelpke, K. Huang, J. Chapman, K.G. Helfenbein, P. Ramaiya, J.C. Detter, F. Larimer, P.M. Coutinho, B. Henrissat, R. Berka, D. Cullen, D. Rokhsar, Genome sequence of the lignocellulose degrading fungus *Phanerochaete chrysosporium* strain RP78, Nat. Biotechnol. 22 (2004) 695–700.

[2] D. Martínez, J. Challacombe, I. Morgenstern, D.S. Hibbett, M. Schmoll, C.P. Kubicek, P. Ferreira, F.J. Ruiz-Dueñas, A.T. Martínez, P. Kersten, K.E. Hammel, A. Vanden Wymelenberg, J. Gaskell, E. Lindquist, G. Sabat, S.S. Bondurant, L.F. Larrondo, P. Canessa, R. Vicuña, J. Yadav, H. Doddapaneni, V. Subramanian, A.G. Pisabarro, J.L. Lavín, J.A. Oguiza, E. Master, B. Henrissat, P.M. Coutinho, P. Harris, J.K. Magnuson, S.E. Baker, K. Bruno, W. Kenealy, P.J. Hoegger, U. Kues, P. Ramaiya, S. Lucas, A. Salamov, H. Shapiro, H. Tu, C.L. Chee, M. Misra, G. Xie, S. Teter, D. Yaver, T. James, M. Mokrejs, M. Pospisek, I.V. Grigoriev, T. Brettin, D. Rokhsar, R. Berka, D. Cullen, Genome, transcriptome, and secretome analysis of wood decay fungus *Postia placenta* supports unique mechanisms of lignocellulose conversion, Proc. Natl. Acad. Sci. U. S. A. 106 (2009) 1954–1959.

[3] R.A. Ohm, J.F. de Jong, L.G. Lugones, A. Aerts, E. Kothe, J.E. Stajich, R.P. de Vries, E. Record, A. Levasseur, S.E. Baker, K.A. Bartholomew, P.M. Coutinho, S. Erdmann, T.J. Fowler, A.C. Gathman, V. Lombard, B. Henrissat, N. Knabe, U. Kues, W.W. Lilly, E. Lindquist, S. Lucas, J.K. Magnuson, F. Piumi, M. Raudaskoski, A. Salamov, J. Schmutz, F.W.M.R. Schwarze, P.A. vanKuyk, J.S. Horton, I.V. Grigoriev, H.A.B. Wosten, Genome sequence of the model mushroom *Schizophyllum commune*, Nat. Biotechnol. 28 (2010) 957–1010.

[4] A.T. Martínez, S. Camarero, F. Guillén, A. Gutiérrez, C. Muñoz, E. Varela, M.J. Martínez, J.M. Barrasa, K. Ruel, M. Pelayo, Progress in biopulping of non-woody materials: chemical, enzymatic and ultrastructural aspects of wheat-straw delignification with ligninolytic fungi from the genus *Pleurotus*, FEMS Microbiol. Rev. 13 (1994) 265–274.

[5] F.J. Ruiz-Dueñas, A.T. Martínez, Microbial degradation of lignin: how a bulky recalcitrant polymer is efficiently recycled in nature and how we can take advantage of this, Microbial. Biotechnol. 2 (2009) 164–177.

[6] C. Sánchez, Cultivation of *Pleurotus ostreatus* and other edible mushrooms, Appl. Microbiol. Biotechnol. 85 (2010) 1321–1337.

[7] K.E. Hammel, D. Cullen, Role of fungal peroxidases in biological ligninolysis, Curr. Opin. Plant Biol. 11 (2008) 349–355.

[8] A.T. Martínez, Molecular biology and structure-function of lignin-degrading heme peroxidases, Enzyme Microb. Technol. 30 (2002) 425–444.

[9] F.J. Ruiz-Dueñas, M. Morales, E. García, Y. Miki, M.J. Martínez, A.T. Martínez, Substrate oxidation sites in versatile peroxidase and other basidiomycete peroxidases, J. Exp. Bot. 60 (2009) 441–452.

[10] M. Hofrichter, R. Ullrich, M.J. Pecyna, C. Liers, T. Lundell, New and classic families of secreted fungal heme peroxidases, Appl. Microbiol. Biotechnol. 87 (2010) 871–897.

[11] L.M. Larraya, G. Pérez, M.M. Peñas, J.J.P. Baars, T.S.P. Mikosch, A.G. Pisabarro, L. Ramírez, Molecular karyotype of the white rot fungus *Pleurotus ostreatus*, Appl. Environ. Microbiol. 65 (1999) 3413–3417.

[12] Y. Asada, A. Watanabe, T. Irie, T. Nakayama, M. Kuwahara, Structures of genomic and complementary DNAs coding for *Pleurotus ostreatus* manganese (II) peroxidase, Biochim. Biophys. Acta 1251 (1995) 205–209.

[13] P. Giardina, G. Palmieri, B. Fontanella, V. Rivieccio, G. Sannia, Manganese peroxidase isoenzymes produced by *Pleurotus ostreatus* grown on wood sawdust, Arch. Biochem. Biophys. 376 (2000) 171–179.

[14] T. Irie, Y. Honda, H.-C. Ha, T. Watanabe, M. Kuwahara, Isolation of cDNA and genomic fragments encoding the major manganese peroxidase isoenzyme from the white rot basidiomycete *Pleurotus ostreatus*, J. Wood Sci. 46 (2000) 230–233.

[15] V. Faraco, A. Piscitelli, G. Sannia, P. Giardina, Identification of a new member of the dye-decolorizing peroxidase family from *Pleurotus ostreatus*, World J. Microbiol. Biotechnol. 23 (2007) 889–893.

[16] K. Tamura, J. Dudley, M. Nei, S. Kumar, MEGA4: molecular evolutionary genetics analysis (MEGA) software version 4.0, Mol. Biol. Evol. 24 (2007) 1596–1599.

[17] J.D. Bendtsen, H. Nielsen, G. von Heijne, S. Brunak, Improved prediction of signal peptides: SignalP 3.0, J. Mol. Biol. 340 (2004) 783–795.

[18] L. Bordoli, F. Kiefer, K. Arnold, P. Benkert, J. Battey, T. Schwede, Protein structure homology modeling using SWISS-MODEL workspace, Nat. Protoc. 4 (2009) 1–13.

[19] F.J. Ruiz-Dueñas, A.T. Martínez, Structural and functional features of peroxidases with a potential as industrial biocatalysts, in: E. Torres, M. Ayala (Eds.), Biocatalysts based on heme peroxidases, Springer-Verlag, Berlin, 2010, pp. 37–59.

[20] D.M. Kupfer, S.D. Drabenstot, K.L. Buchanan, H.S. Lai, H. Zhu, D.W. Dyer, B.A. Roe, J.W. Murphy, Introns and splicing elements of five diverse fungi, Eukaryot. Cell 3 (2004) 1088–1100.

[21] M. Rep, R.G.E. Duyvesteijn, L. Gale, T. Usgaard, B.J.C. Cornelissen, L.J. Ma, T.J. Ward, The presence of GC-AG introns in *Neurospora crassa* and other euascomycetes determined from analyses of complete genomes: Implications for automated gene prediction, Genomics 87 (2006) 338–347.

[22] M.R. Makela, K. Hilden, A. Hatakka, T.K. Lundell, Oxalate decarboxylase of the white-rot fungus *Dichomitus squalens* demonstrates a novel enzyme primary structure and non-induced expression on wood and in liquid cultures, Microbiol. Sgm 155 (2009) 2726–2738.

[23] M.R. Escutia, L. Bowater, A. Edwards, A.R. Bottrill, M.R. Burrell, R. Polanco, R. Vicuña, S. Bornemann, Cloning and Sequencing of two *Ceriporiopsis subvermispora* bicupin oxalate oxidase allelic isoforms: implications for the reaction specificity of oxalate oxidases and decarboxylases, Appl. Environ. Microbiol. 71 (2005) 3608–3616.

[24] F. Peláez, M.J. Martínez, A.T. Martínez, Screening of 68 species of basidiomycetes for enzymes involved in lignin degradation, Mycol. Res. 99 (1995) 37–42.

[25] E. Varela, A.T. Martínez, M.J. Martínez, Southern blot screening for lignin peroxidase and aryl-alcohol oxidase genes in 30 fungal species, J. Biotechnol. 83 (2000) 245–251.

[26] K.G. Welinder, Superfamily of plant, fungal and bacterial peroxidases, Curr. Opin. Struct. Biol. 2 (1992) 388–393.

[27] J.E. Stajich, S.K. Wilke, D. Ahren, C.H. Au, B.W. Birren, M. Borodovsky, C. Burns, B. Canback, L.A. Casselton, C.K. Cheng, J.X. Deng, F.S. Dietrich, D.C. Fargo, M.L. Farman, A.C. Gathman, J. Goldberg, R. Guigo, P.J. Hoegger, J.B. Hooker, A. Huggins, T.Y. James, T. Kamada, S. Kilaru, C. Kodira, U. Kues, D. Kupfert, H.S. Kwan, A. Lomsadze, W.X. Li, W.W. Lilly, L.J. Ma, A.J. Mackey, G. Manning, F. Martin, H. Muraguchi, D.O. Natvig, H. Palmerini, M.A. Ramesh, C.J. Rehmeyer, B.A. Roe, N. Shenoy, M. Stanke, V. Ter Hovhannisyan, A. Tunlid, R. Velagapudi, T.J. Vision, Q.D. Zeng, M.E. Zolan, P.J. Pukkila, Insights into evolution of multicellular fungi from the assembled chromosomes of the mushroom *Coprinopsis cinerea* (*Coprinus cinereus*), Proc. Natl. Acad. Sci. U. S. A. 107 (2010) 11889–11894.

[28] M. Sivaraja, D.B. Goodin, M. Smith, B.M. Hoffman, Identification by ENDOR of Trp191 as the free-radical site in cytochrome-*c* peroxidase compound ES, Science 245 (1989) 738.

[29] H. Pelletier, J. Kraut, Crystal structure of a complex between electron transfer partners, cytochrome *c* peroxidase and cytochrome *c*, Science 258 (1992) 1748–1755.

[30] Q. Husain, M. Husain, Y. Kulshrestha, Remediation and treatment of organopollutants mediated by peroxidases: a review, Crit. Rev. Biotechnol. 29 (2009) 94–119.

[31] L. Banci, I. Bertini, P. Turano, M. Tien, T.K. Kirk, Proton NMR investigation into the basis for the relatively high redox potential of lignin peroxidase, Proc. Natl. Acad. Sci. U. S. A. 88 (1991) 6956–6960.

[32] L. Banci, S. Camarero, A.T. Martínez, M.J. Martínez, M. Pérez-Boada, R. Pierattelli, F.J. Ruiz-Dueñas, NMR study of Mn(II) binding by the new versatile peroxidase from the white-rot fungus *Pleurotus eryngii*, J. Biol. Inorg. Chem. 8 (2003) 751–760.

[33] T. Mester, K. Ambert-Balay, S. Ciofi-Baffoni, L. Banci, A.D. Jones, M. Tien, Oxidation of a tetrameric nonphenolic lignin model compound by lignin peroxidase, J. Biol. Chem. 276 (2001) 22985–22990.

[34] A.T. Smith, W.A. Doyle, P. Dorlet, A. Ivancich, Spectroscopic evidence for an engineered, catalytically active Trp radical that creates the unique reactivity of lignin peroxidase, Proc. Natl. Acad. Sci. U. S. A. 106 (2009) 16084–16089.

[35] M. Sundaramoorthy, M.H. Gold, T.L. Poulos, Ultrahigh (0.93 angstrom) resolution structure of manganese peroxidase from *Phanerochaete chrysosporium*: Implications for the catalytic mechanism, J. Inorg. Biochem. 104 (2010) 683–690.

Please cite this article in press as: F.J. Ruiz-Dueñas, et al., *Pleurotus ostreatus* heme peroxidases: An *in silico* analysis from the genome sequence to the enzyme molecular structure, C. R. Biologies (2011), doi:10.1016/j.crvi.2011.06.004

[36] D. Cullen, P.J. Kersten, Enzymology and molecular biology of lignin degradation, in: R. Brambl, G.A. Marzluf (Eds.), Mycota III: biochemistry and molecular biology, Springer, Berlin, 2004, pp. 249–273.
[37] M.H. Gold, H.L. Youngs, M.D. Gelpke, Manganese peroxidase, Met. Ions Biol. Syst. 37 (2000) 559–586.
[38] K. Hildén, A.T. Martínez, A. Hatakka, T. Lundell, The two manganese peroxidases Pr-MnP2 and Pr-MnP3 of *Phlebia radiata*, a lignin-degrading basidiomycete, are phylogenetically and structurally divergent, Fungal Genet. Biol. 42 (2005) 403–419.
[39] T. Tsukihara, Y. Honda, R. Sakai, T. Watanabe, T. Watanabe, Mechanism for oxidation of high-molecular-weight substrates by a fungal versatile peroxidase, MnP2, Appl. Environ. Microbiol. 74 (2008) 2873–2881.
[40] P.D. Shaw, L.P. Hager, Biological chlorination. 6. Chloroperoxidase - Component of beta-ketoadipate chlorinase system, J. Biol. Chem. 236 (1961) 1626.
[41] D. Koua, L. Cerutti, L. Falquet, C.J.A. Sigrist, G. Theiler, N. Hulo, C. Dunand, PeroxiBase: a database with new tools for peroxidase family classification, Nucleic Acids Res. 37 (2009) D261–D266.
[42] R. Ullrich, J. Nuske, K. Scheibner, J. Spantzel, M. Hofrichter, Novel haloperoxidase from the agaric basidiomycete *Agrocybe aegerita* oxidizes aryl alcohols and aldehydes, Appl. Environ. Microbiol. 70 (2004) 4575–4581.
[43] D.H. Anh, R. Ullrich, D. Benndorf, A. Svatos, A. Muck, M. Hofrichter, The coprophilous mushroom *Coprinus radians* secretes a haloperoxidase that catalyzes aromatic peroxygenation, Appl. Environ. Microbiol. 73 (2007) 5477–5485.
[44] M. Hofrichter, R. Ullrich, Heme-thiolate haloperoxidases: versatile biocatalysts with biotechnological and environmental significance, Appl. Microbiol. Biotechnol. 71 (2006) 276–288.
[45] M.J. Pecyna, R. Ullrich, B. Bittner, A. Clemens, K. Scheibner, R. Schubert, M. Hofrichter, Molecular characterization of aromatic peroxygenase from *Agrocybe aegerita*, Appl. Microbiol. Biotechnol. 84 (2009) 885–897.
[46] A. Conesa, G. Weelink, C.A.M.J. van den Hondel, P.J. Punt, C-terminal propeptide of the *Caldariomyces fumago* chloroperoxidase: an intramolecular chaperone? FEBS Lett. 503 (2001) 117–120.
[47] M.J. Nuell, G.H. Fang, M.J. Axley, P. Kenigsberg, L.P. Hager, Isolation and nucleotide sequence of the chloroperoxidase gene from *Caldariomyces fumago*, J. Bacteriol. 170 (1988) 1007–1011.
[48] M. Sundaramoorthy, J. Terner, T.L. Poulos, The crystal structure of chloroperoxidase: a heme peroxidase-cytochrome P450 functional hybrid, Structure 3 (1995) 1367–1377.
[49] K. Piontek, R. Ullrich, C. Liers, K. Diederichs, D.A. Plattner, M. Hofrichter, Crystallization of a 45 kDa peroxygenase/peroxidase from the mushroom *Agrocybe aegerita* and structure determination by SAD utilizing only the haem iron, Acta Crystallogr. F 66 (2010) 693–698.
[50] F.J. Ruiz-Dueñas, M.J. Martínez, A.T. Martínez, Molecular characterization of a novel peroxidase isolated from the ligninolytic fungus *Pleurotus eryngii*, Mol. Microbiol. 31 (1999) 223–236.
[51] M. Sundaramoorthy, J. Terner, T.L. Poulos, Stereochemistry of the chloroperoxidase active site: crystallographic and molecular-modeling studies, Chem. Biol. 5 (1998) 461–473.
[52] K. Kühnel, W. Blankenfeldt, J. Terner, I. Schlichting, Crystal structures of chloroperoxidase with its bound substrates and complexed with formate, acetate, and nitrate, J. Biol. Chem. 281 (2006) 23990–23998.
[53] Y. Sugano, DyP-type peroxidases comprise a novel heme peroxidase family, Cell Mol. Life Sci. 66 (2009) 1387–1403.
[54] S.J. Kim, M. Shoda, Purification and characterization of a novel peroxidase from *Geotrichum candidum* Dec 1 involved in decolorization of dyes, Appl. Environ. Microbiol. 65 (1999) 1029–1035.
[55] Y. Sugano, K. Sasaki, M. Shoda, cDNA cloning and genetic analysis of a novel decolorizing enzyme, peroxidase gene *dyp* from *Geotrichum candidum* Dec 1, J. Biosci. Bioeng. 87 (1999) 411–417.
[56] A. Johanson, H.C. Turner, G.J. Mckay, A.E. Brown, A PCR-based method to distinguish fungi of the rice sheath-blight complex, *Rhizoctonia solani*, *R-oryzae* and *R-oryzae-sativae*, FEMS Microbiol. Lett. 162 (1998) 289–294.
[57] Y. Sugano, Y. Matsushima, K. Tsuchiya, H. Aoki, M. Hirai, M. Shoda, Degradation pathway of an anthraquinone dye catalyzed by a unique peroxidase DyP from *Thanatephorus cucumeris* Dec 1, Biodegradation 20 (2009) 433–440.
[58] K. Zelena, B. Hardebusch, B. Hulsdau, R.G. Berger, H. Zorn, Generation of norisoprenoid flavors from carotenoids by fungal peroxidases, J. Agric. Food Chem. 57 (2009) 9951–9955.
[59] C. Liers, C. Bobeth, M. Pecyna, R. Ullrich, M. Hofrichter, DyP-like peroxidases of the jelly fungus *Auricularia auricula-judae* oxidize nonphenolic lignin model compounds and high-redox potential dyes, Appl. Microbiol. Biotechnol. 85 (2010) 1869–1879.
[60] M. Puhse, R.T. Szweda, Y.Y. Ma, C. Jeworrek, R. Winter, H. Zorn, *Marasmius scorodonius* extracellular dimeric peroxidase - Exploring its temperature and pressure stability, BBA Proteins Proteomics 1794 (2009) 1091–1098.
[61] Y. Sugano, Y. Matsushima, M. Shoda, Complete decolorization of the anthraquinone dye Reactive blue 5 by the concerted action of two peroxidases from *Thanatephorus cucumeris* Dec 1, Appl. Microbiol. Biotechnol. 73 (2006) 862–871.

Please cite this article in press as: F.J. Ruiz-Dueñas, et al., *Pleurotus ostreatus* heme peroxidases: An *in silico* analysis from the genome sequence to the enzyme molecular structure, C. R. Biologies (2011), doi:10.1016/j.crvi.2011.06.004

Capítulo 3

"**Ligninolytic peroxidase genes in the oyster mushroom genome: Heterologous expression, molecular structure, catalytic and stability properties and lignin-degrading ability"**
Fernández-Fueyo, E., F. J. Ruiz-Dueñas, M. J. Martínez, A. Romero, K. E. Hammel, F. J. Medrano, and A. T. Martínez.
Biotechnol. Biofuels 7:2. 2014.

Biotechnology for Biofuels

RESEARCH Open Access

Ligninolytic peroxidase genes in the oyster mushroom genome: heterologous expression, molecular structure, catalytic and stability properties, and lignin-degrading ability

Elena Fernández-Fueyo[1], Francisco J Ruiz-Dueñas[1], María Jesús Martínez[1], Antonio Romero[1], Kenneth E Hammel[2*], Francisco Javier Medrano[1*] and Angel T Martínez[1*]

Abstract

Background: The genome of *Pleurotus ostreatus*, an important edible mushroom and a model ligninolytic organism of interest in lignocellulose biorefineries due to its ability to delignify agricultural wastes, was sequenced with the purpose of identifying and characterizing the enzymes responsible for lignin degradation.

Results: Heterologous expression of the class II peroxidase genes, followed by kinetic studies, enabled their functional classification. The resulting inventory revealed the absence of lignin peroxidases (LiPs) and the presence of three versatile peroxidases (VPs) and six manganese peroxidases (MnPs), the crystal structures of two of them (VP1 and MnP4) were solved at 1.0 to 1.1 Å showing significant structural differences. Gene expansion supports the importance of both peroxidase types in the white-rot lifestyle of this fungus. Using a lignin model dimer and synthetic lignin, we showed that VP is able to degrade lignin. Moreover, the dual Mn-mediated and Mn-independent activity of *P. ostreatus* MnPs justifies their inclusion in a new peroxidase subfamily. The availability of the whole POD repertoire enabled investigation, at a biochemical level, of the existence of duplicated genes. Differences between isoenzymes are not limited to their kinetic constants. Surprising differences in their activity T_{50} and residual activity at both acidic and alkaline pH were observed. Directed mutagenesis and spectroscopic/structural information were combined to explain the catalytic and stability properties of the most interesting isoenzymes, and their evolutionary history was analyzed in the context of over 200 basidiomycete peroxidase sequences.

Conclusions: The analysis of the *P. ostreatus* genome shows a lignin-degrading system where the role generally played by LiP has been assumed by VP. Moreover, it enabled the first characterization of the complete set of peroxidase isoenzymes in a basidiomycete, revealing strong differences in stability properties and providing enzymes of biotechnological interest.

Keywords: Genome, *Pleurotus ostreatus*, Ligninolytic peroxidase genes, Heterologous expression, Crystal structure, Catalytic properties, Thermal stability, pH stability, Gene duplication, Peroxidase evolution

Background

Pleurotus ostreatus, the oyster mushroom, is the second most consumed edible mushroom worldwide, just after *Agaricus bisporus*, with a current production accounting for over 25% of mushroom world production (that is, around 3 million metric tons/year, with a market value of several thousand million euros per year) [1]. In addition to their food properties, *Pleurotus* species also have medicinal properties due to their production of anticholesterolemic statins [2] and antitumor polysaccharides [3], among other bioactive molecules. China is the main producer of *P. ostreatus* and related species. Sawdust and cereal straw are the usual substrates for *Pleurotus* production, together with other agricultural, forest, and/or industrial lignocellulosic wastes.

From an ecophysiological point of view, *Pleurotus* species belong to the group of fungi causing a so-called

* Correspondence: kehammel@facstaff.wisc.edu; fjmedrano@cib.csic.es; atmartinez@cib.csic.es
[2]US Forest Products Laboratory, One Gifford Pinchot Drive, Madison, WI 53726, USA
[1]Centro de Investigaciones Biológicas, Consejo Superior de Investigaciones Científicas (CSIC), Ramiro de Maeztu 9, E-28040 Madrid, Spain

white rot of wood and other lignocellulosic materials, due to their ability to degrade the recalcitrant lignin polymer that protects polysaccharides in vascular plants [4]. Among these fungi, *Pleurotus* species are of particular biotechnological interest because they degrade lignin selectively (that is, with limited attack on cellulose) when growing on cereal straw and related materials [5]. Biological delignification with these lignin-degrading fungi saves energy and chemicals in the manufacture of cellulose pulp from woody [6] and non-woody [7] plant feedstocks. Moreover, it also results in an increased digestibility of lignocellulose [8,9], which is of interest in lignocellulose biorefineries for the production of second generation bioethanol and other cellulose-based chemicals [10,11].

From 2004, when the first basidiomycete genome (from the model white-rot fungus *Phanerochaete chrysosporium*) was sequenced at the Joint Genome Institute (JGI; Walnut Creek, CA, USA) [12], the US Department of Energy (DOE) has funded genome sequencing of ascomycetes and basidiomycetes that are potentially applicable in lignocellulose biorefineries. The latter fungi include the brown-rot basidiomycetes *Rhodonia placenta* (synonym: *Postia placenta*) and *Serpula lacrymans* (which are able to use wood cellulose without the prior removal of lignin) [13,14] and the selective degrader of wood lignin *Gelatoporia subvermispora* (synonym: *Ceriporiopsis subvermispora*) [15], among others. More recently, over 30 fungal genomes were comparatively analyzed to obtain an overview of the enzymatic machinery involved in the two main types of wood decay (white rot and brown rot), and to establish the evolutionary history of ligninolytic peroxidases belonging to class II of the superfamily of non-animal (plant-fungal-prokaryotic) heme peroxidases (hereinafter PODs) [16].

Most of the basidiomycete genomes currently available are from wood decay fungi (from the order Polyporales), but agricultural wastes and crops are the preferred feedstocks in lignocellulose biorefineries for the production of fuels and chemicals. In this context, the genome of *P. ostreatus* was sequenced at JGI as a representative white-rot fungus that can delignify non-woody lignocellulosic materials. This fact, together with the taxonomic position of *Pleurotus* as a member of the order Agaricales, suggested that different enzymatic machinery might be revealed by genome sequencing. Our preliminary *in silico* analysis of the *P. ostreatus* genome [17] showed the genes encoding manganese peroxidases (MnPs) and versatile peroxidases (VPs) but not lignin peroxidases (LiPs), which are involved in lignin degradation by the model fungus *P. chrysosporium* and many other wood-rotting species [18]. With the purpose of furthering our understanding of the enzymatic mechanism for lignin degradation by *Pleurotus* species, the above peroxidase genes from the *P. ostreatus* genome have now been heterologously expressed, structurally characterized using crystallographic and site-directed mutagenesis methods, and evaluated for their activity on lignin and related substrates. In addition, the stability and catalytic properties of the various isoenzymes detected have been analyzed with a view towards future biotechnological applications.

Results

Peroxidase genes in the genome of *P. ostreatus*

Seventeen putative peroxidase genes were identified in the genomes of each of the two *P. ostreatus* monokaryons (PC9 and PC15) sequenced at JGI. Their structural-functional classification was based on homology modeling of the curated deduced sequences [17]. The presence of proximal and distal histidines at both sides of the heme cofactor is a characteristic of the superfamily of plant-fungal-prokaryotic peroxidases. One of them is substituted by one aspartate/glutamate in the superfamily of dye-decolorizing peroxidases (DyPs), while one cysteine and one glutamate occupy their positions in the heme-thiolate peroxidase (HTP) superfamily [19,20]. The final peroxidase inventory yielded nine class II peroxidases (PODs) and one class I peroxidase genes, both in the superfamily of plant-fungal-prokaryotic peroxidases, as well as four and three genes from the DyP and HTP superfamilies, respectively (for JGI references in the two monokaryons and evolutionary relationships, see Additional file 1: Figure S1). The present study focused on the nine PODs since lignin-degrading peroxidases belong in this group.

The *P. ostreatus* PODs were initially classified as five MnPs and four VPs according to the presence in the homology models of: i) a putative Mn^{2+} oxidation site; and ii) both Mn^{2+} and lignin oxidation putative sites, respectively (but one putative VP was reclassified as MnP1 in the course of the present study). The first site comprises three acidic residues that bind Mn^{2+} cations, whereas the second contains an exposed tryptophan involved in electron transfer from lignin-related donor substrates. The position of the above and other residues of interest on the deduced amino acid sequences of the nine PODs from the *P. ostreatus* genome is indicated in Figure 1. The sequence length of the nine mature proteins varies slightly (331 to 339 residues), and there is some variation in amino acid composition (Additional file 1: Figure S2). Interestingly, the number of prolines varies from 25 to 26 (in MnP2 and MnP4) to 30 to 31 (in VP1, VP3, and MnP5) and they are not evenly distributed along the sequences, with the C-terminal region having by far the highest concentration (21 to 38% residues after the last cysteine, positions 307/314 to 331/339, are prolines) as compared with the whole protein (7 to 9% proline residues). However, the most important difference in

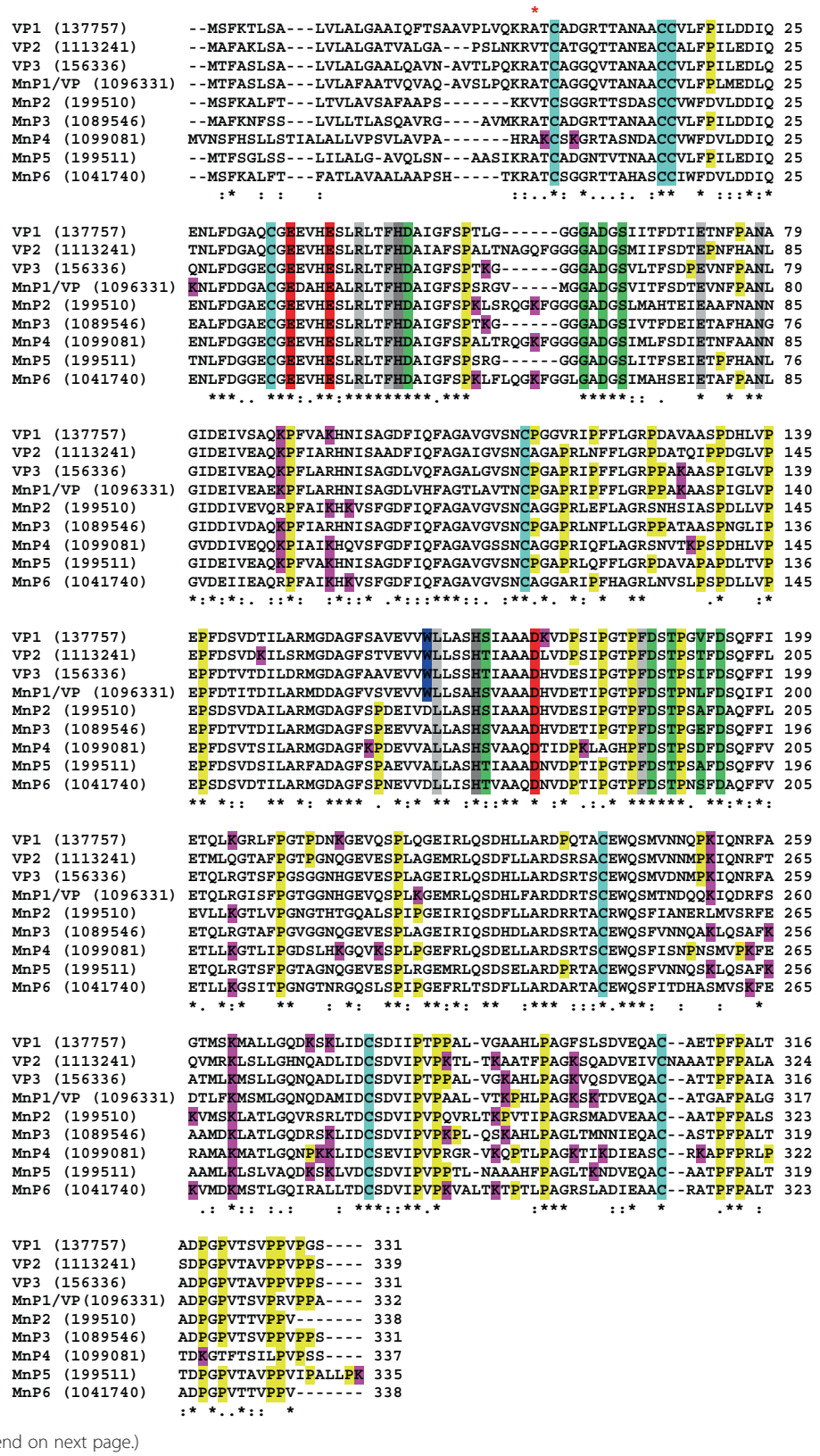

Figure 1 (See legend on next page.)

(See figure on previous page.)
Figure 1 Multiple alignment of amino acid sequences of the nine PODs from the *P. ostreatus* genome (current JGI references, after manual annotation, included). Conserved catalytic and other relevant residues are indicated with different colors including: eight cysteines (cyan) forming four disulfide bridges; nine ligands (green) of two structural Ca^{2+} ions; two active site histidines (dark gray); three acidic residues (orange) forming the Mn^{2+} oxidation site; one tryptophan (blue) responsible for aromatic substrate oxidation by VPs (also present in MnP1, initially classified as a VP); several active site conserved residues (light gray); and several lysine (purple) and proline (yellow) residues being particularly frequent in some of the sequences. Alignment was prepared using ClustalW2 (European Bioinformatics Institute, Hinxton, UK). Amino acid numbering starts at the first residue of the mature protein (red asterisk on the alignment). Symbols below indicate full conservation of the same (*) or equivalent residues (:) and partial residue conservation (.). JGI, Joint Genome Institute; MnP, manganese peroxidase; POD, class II peroxidase from the superfamily of non-animal (plant-fungal-prokaryotic) peroxidases; VP, versatile peroxidase.

the amino acid composition of the different PODs concerns the number of lysine residues, which in MnP4 (20 lysines) is almost the double of those observed in the other PODs (seven to ten lysines).

Heterologous expression and catalytic properties

To confirm the above POD classification, characterize the two families present in *P. ostreatus*, and investigate differences between the VP and MnP isoenzymes, the coding DNA sequences of the nine PODs (mature proteins) from PC15 (except 1089895, which includes a premature termination codon and was substituted by the PC9 allele 137757) were overexpressed in *Escherichia coli* (Additional file 1: Figure S3A). At optimized induction times, peroxidase proteins were recovered from inclusion bodies (Additional file 1: Figure S3B), activated *in vitro* for heme and structural Ca^{2+} incorporation and disulfide bridge formation, purified, and characterized. The purification yield was always over 95% of the refolded protein although it only represented 3 to 28% of the total protein recovered from the inclusion bodies, with all the purified enzymes showing typical spectra with Reinheitszahl (Rz; A_{410}/A_{280} ratio) values ≥3.8 (Additional file 2: Table S1).

Comparison of the catalytic properties of the nine *P. ostreatus* PODs included estimation of the steady-state kinetic constants for the reducing substrates veratryl alcohol (VA), Reactive Black 5 (RB5), 2,2′-azino-bis(3-ethylbenzothiazoline-6-sulfonate (ABTS), 2,6-dimethoxyphenol (DMP), and Mn^{2+}, and for the oxidizing substrate H_2O_2 (Table 1). Surprisingly, peroxidase 1096331, which had been classified as a VP due to the presence of the putative catalytic tryptophan, was unable to oxidize the high redox potential substrates VA and RB5 and was therefore renamed as MnP1 (and re-annotated at the JGI portal).

The three functional VPs oxidized all the substrates assayed, although with different catalytic efficiencies (k_{cat}/K_m). In general, Mn^{2+} was their best substrate (1,900 to 4,510 $s^{-1}.mM^{-1}$) but VP1 also oxidized ABTS and RB5 efficiently (the other isoenzymes oxidized ABTS with five- to ninefold lower efficiencies). DMP, and particularly VA, are poor VP substrates, although the catalytic efficiencies were higher (two- to eightfold) for VP1. The bimodal kinetic curves yielding two sets of kinetic constants for ABTS and DMP oxidation in VPs indicate that these substrates are oxidized at a second low catalytic efficiency site, in addition to the high efficiency site that could be the same involved in VA and RB5 oxidation. The six MnPs were unable to oxidize VA and RB5, and their efficiencies on Mn^{2+} were in the range 1,200 to 1,930 $s^{-1}.mM^{-1}$. Interestingly, the *P. ostreatus* MnPs could also oxidize ABTS (and some of them DMP). However, their low (ABTS) or very low (DMP) efficiency on these substrates distinguish them from the VPs. The nine PODs showed high catalytic efficiencies in their reaction with H_2O_2, with all but one of the MnPs (the exception was the anomalous MnP1) having higher values (3,000 to 3,700 $s^{-1}.mM^{-1}$) than VPs (1,700 to 2,500 $s^{-1}.mM^{-1}$).

pH stability of the *P. ostreatus* PODs

The nine PODs were incubated in the pH 2 to 9 range (at 4°C) for five time periods and the residual activities determined. A comparison of normalized activities after 4 hours of incubation (at five pH values) is shown in Figure 2A (and the complete set of residual activities of the nine PODs after 1 minute, 1, 4, 24, and 120 hours at the eight pH values is included as Additional file 1: Figure S4). All the enzymes were nearly inactivated at pH 2 after the shortest incubation times, and only MnP4 and VP3 retained significant activity at pH 9 when incubation was extended (Additional file 1: Figure S4G and C, respectively). Interestingly, MnP4 appears as the most stable POD at both acidic and moderately alkaline pH, and VP2 was stable at pH 3 but unstable at pH 9 (Additional file 1: Figure S4B). On the other hand, MnP2 and MnP3 were the most unstable PODs under both acidic and alkaline conditions (Additional file 1: Figure S4E and F, respectively). For comparison with spectroscopic analyses, pH stability was also evaluated at 25°C, resulting in lower residual activities (Additional file 1: Figure S5).

The effects of pH on the heme environment and protein structure were investigated by UV-visible absorption and far-UV circular dichroism (CD) spectroscopy. MnP3 and MnP4 were used as model unstable and stable PODs, respectively, and spectral changes were followed

Table 1 Kinetic constants (K_m, μM; k_{cat}, s^{-1}; and k_{cat}/K_m, $s^{-1}.mM^{-1}$) for the nine PODs from the *P. ostreatus* genome[a]

Substrate	Kinetic constants	VP1	VP2	VP3	MnP1[b]	MnP2	MnP3	MnP4	MnP5	MnP6
VA	K_m	5,500 ± 46	10,400 ± 133	5,500 ± 100	-[c]	-	-	-	-	-
	k_{cat}	12.7 ± 0.5	4.4 ± 0.2	1.7 ± 0.1	0	0	0	0	0	0
	k_{cat}/K_m	2.3 ± 0.2	0.4 ± 0	0.3 ± 0	0	0	0	0	0	0
RB5	K_m	5.4 ± 0.2	9.6 ± 1.8	1.2 ± 0.2	-	-	-	-	-	-
	k_{cat}	12.9 ± 0.3	20.3 ± 2	1.2 ± 0.1	0	0	0	0	0	0
	k_{cat}/K_m	2,380 ± 50	2,120 ± 175	990 ± 150	0	0	0	0	0	0
ABTS[e]	K_m	605 ± 81 (4.0 ± 0.4)	3,260 ± 363 (12 ± 1.6)	726 ± 30 (ns[d])	111 ± 18	1,150 ± 38	778 ± 103	1,560 ± 76	455 ± 69	1,020 ± 80
	k_{cat}	126 ± 5 (14.4 ± 0.4)	209 ± 12 (8.7 ± 0.4)	328 ± 17 (ns)	90 ± 8	175 ± 3	222 ± 15	128 ± 3	53 ± 3	115 ± 5
	k_{cat}/K_m	209 ± 21 (3,600 ± 20)	64 ± 4 (725 ± 36)	452 ± 10 (407 ± 12)	803 ± 7	152 ± 3	285 ± 19	82 ± 3	110 ± 10	112 ± 4
DMP[e]	K_m	45,100 ± 3,600 (54 ± 4)	18,900 ± 2,070 (607 ± 57)	108,000 ± 13,000 (51 ± 14)	-	63,300 ± 12,800	59,100 ± 6,800	ns	ns	117,000 ± 18,000
	k_{cat}	98 ± 4 (6.6 ± 0.1)	92 ± 5 (17 ± 0.6)	311 ± 0.4 (2.9 ± 0.2)	0	109 ± 14	101 ± 7.2	ns	ns	56 ± 6
	k_{cat}/K_m	2.2 ± 0.1 (122 ± 7)	4.9 ± 0 (28 ± 1)	2.9 ± 0.1 (57 ± 2)	0	1.7 ± 0.1	1.7 ± 0	0.4 ± 0	0.4 ± 0	0.5 ± 0
Mn^{2+}	K_m	98 ± 5.6	18 ± 2	45 ± 3	7 ± 1	92 ± 5	101 ± 12	88 ± 4	22 ± 2	73 ± 9
	k_{cat}	185 ± 2.6	79 ± 2	172 ± 2	9 ± 0	159 ± 3	163 ± 5	125 ± 2	41 ± 1	109 ± 3
	k_{cat}/K_m	1,900 ± 90	4,510 ± 412	3,930 ± 210	1,200 ± 80	1,730 ± 71	1,610 ± 170	1,410 ± 60	1,930 ± 170	1,500 ± 100
H_2O_2	K_m	64.6 ± 6.7	42.5 ± 1.4	220 ± 16	530 ± 92	66.7 ± 11.7	136 ± 7.5	85.6 ± 7.6	27.6 ± 1.2	22.8 ± 4.4
	k_{cat}/K_m	1,750 ± 150	1,880 ± 40	2,410 ± 140	372 ± 54	3,680 ± 470	3,070 ± 130	3,040 ± 210	3,130 ± 110	3,280 ± 490

[a]Means and 95% confidence limits are shown; [b]described as MnP [21], changed to VP because of the putative catalytic tryptophan [17], and renamed now as MnP1 because of its inability to oxidize high redox potential substrates; [c]dashes correspond to undetermined K_m values when no activity was detected (k_{cat} 0); [d]ns, K_m, and k_{cat} not determined because of non-saturation (but k_{cat}/K_m determined from slope of observed activity versus concentration); [e]ABTS and DMP oxidation by VPs showed biphasic kinetics providing a second set of constants (parenthesis) characterized by lower K_m values (see Materials and methods section of Kinetic constants on selected substrates). ABTS, 2,2′-azino-bis(3-ethylbenzothiazoline-6-sulfonate; DMP, 2,6-dimethoxyphenol; MnP, manganese peroxidase; POD, class II peroxidase from the superfamily of non-animal (plant-fungal-prokaryotic) peroxidases; RB5, Reactive Black 5; VA, veratryl alcohol; VP, versatile peroxidase.

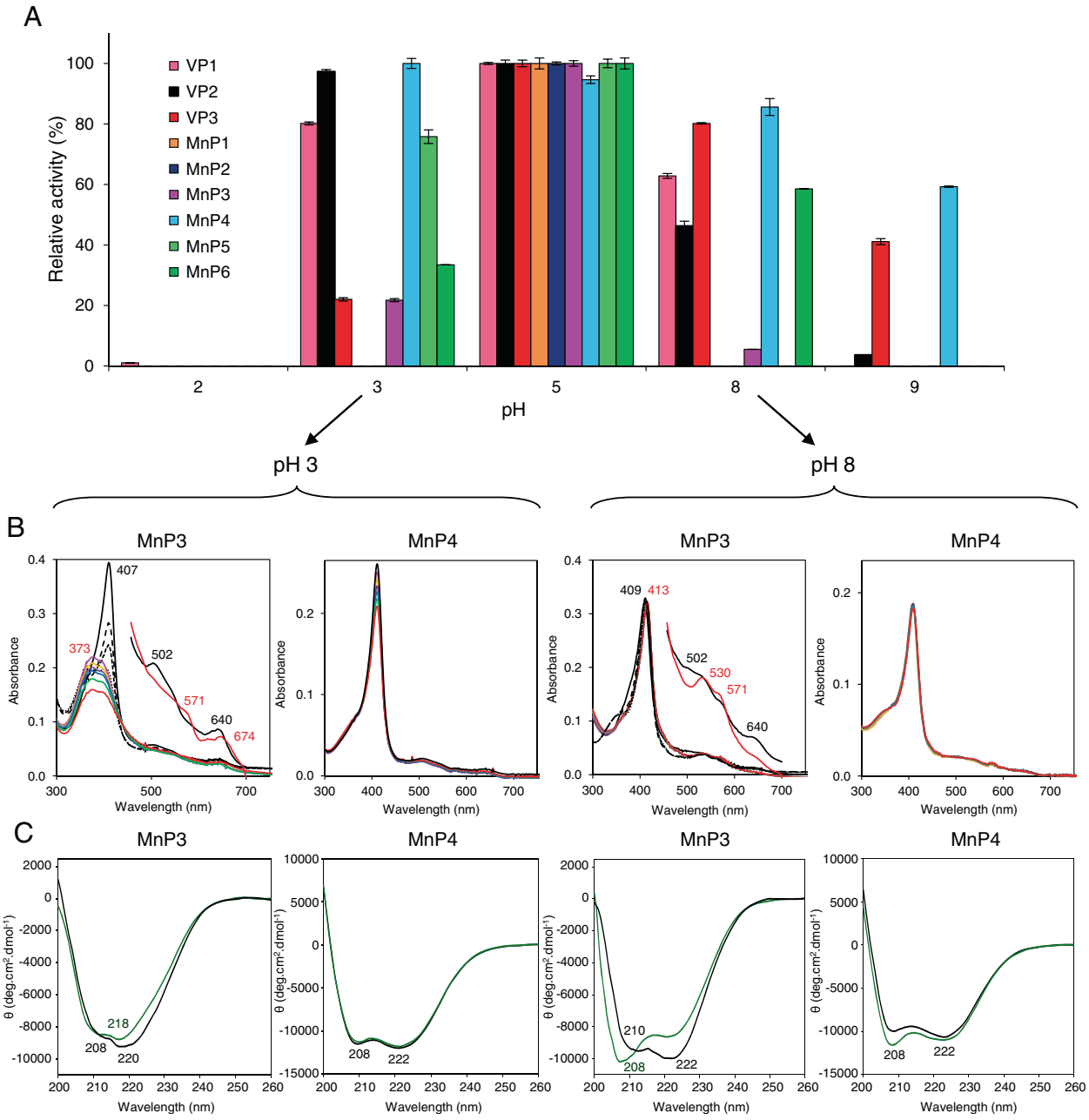

Figure 2 pH stabilities of the nine PODs from the *P. ostreatus* genome. (A) Residual activities after 4 hours of incubation at five selected pH values in the pH 2 to 9 range. Residual activities of the *E. coli*-expressed and *in vitro*-activated three VP and six MnP isoenzymes were determined (by 5 mM ABTS oxidation in 0.1 M tartrate, pH 3.5, except for MnP1 and MnP6, for which 2 mM ABTS was used) after incubation (at 4°C) in 100 mM B&R buffer of pH 2 to 9 (Additional file 1: Figure S4 shows data at eight pH values after 1 minute, 1, 4, 24, and 120 hours of incubation, and Figure S5 shows comparison of pH stability at 4°C and 25°C). Means and 95% confidence limits. **(B)** UV-visible spectra of unstable MnP3 and stable MnP4 isoenzymes after 0 (black), 30 (magenta), 60 (yellow), 90 (purple), 120 (blue), 180 (green), and 240 minutes (red) of incubation at pH 3 and 8. Three additional scans at 30 (large dashes), 60 (short dashes), and 90 seconds (dots) of incubation, and amplified (x 5 absorbance) 450 to 700 nm region are shown for MnP3 initial and final spectra. Main maxima are indicated. **(C)** Far-UV CD spectra of unstable MnP3 and stable MnP4 isoenzymes after 1 minute (black) and 1 hour (green) of incubation at pH 3 and 5. Results are shown as molar ellipticities (θ) and main minima are indicated. All spectra were recorded at 25°C. ABTS, 2,2′-azino-bis(3-ethylbenzothiazoline-6-sulfonate); B&R, Britton-Robinson; CD, circular dichroism; MnP, manganese peroxidase; POD, class II peroxidase from the superfamily of non-animal (plant-fungal-prokaryotic) peroxidases; VP, versatile peroxidase.

for 4 hours at three pH values. Both the UV-visible spectrum (with the Soret band at 407 nm and the small maxima at 502 and 640 nm) and CD spectrum (with the 208 and 222 nm ellipticity minima) were basically unchanged during incubation at pH 5 (spectra not shown). However, acidic/alkaline conditions caused strong modifications of the MnP3 spectra, and only slight changes in those of MnP4. The latter showed a very slight decrease of the Soret band at pH 3 (Figure 2B) but an appreciable modification of the CD spectrum at pH 8 (Figure 2C), in agreement with the partial decrease of activity at alkaline pH. However, a pH 3 incubation of MnP3 immediately resulted in the loss of the Soret band, the appearance of a broad band at 373 nm (that decreased with time), and the displacement of the visible maxima to 571 and 674 nm (Figure 2B). Surprisingly, although MnP3 inactivation was more drastic at pH 8, the UV-visible spectral changes were less evident, consisting of a slight displacement of the Soret band to 413 nm and the appearance of new maxima at 530 and 571 nm (Figure 2B). However, the MnP3 CD spectrum was significantly modified during pH 8 incubation with displacement of the main minimum from 222 to 208 nm, while the spectral changes were less intense at pH 3 (Figure 2C).

Temperature stability of the *P. ostreatus* PODs

The thermal stability of the nine PODs was investigated by measuring the residual activity after 10 minutes (Figure 3A) and 4 hours (Figure 3B) of incubation in the 25 to 70°C range (at pH 5). The activity T_{50} values averaged 54°C and 44°C after 10 minutes and 4 hours of incubation, respectively (the individual values are included in Additional file 2: Table S2). VP1 is the most stable POD retaining over 80% activity after 10 minutes up to 60°C, followed by MnP4, VP3, MnP1, and VP2 (although

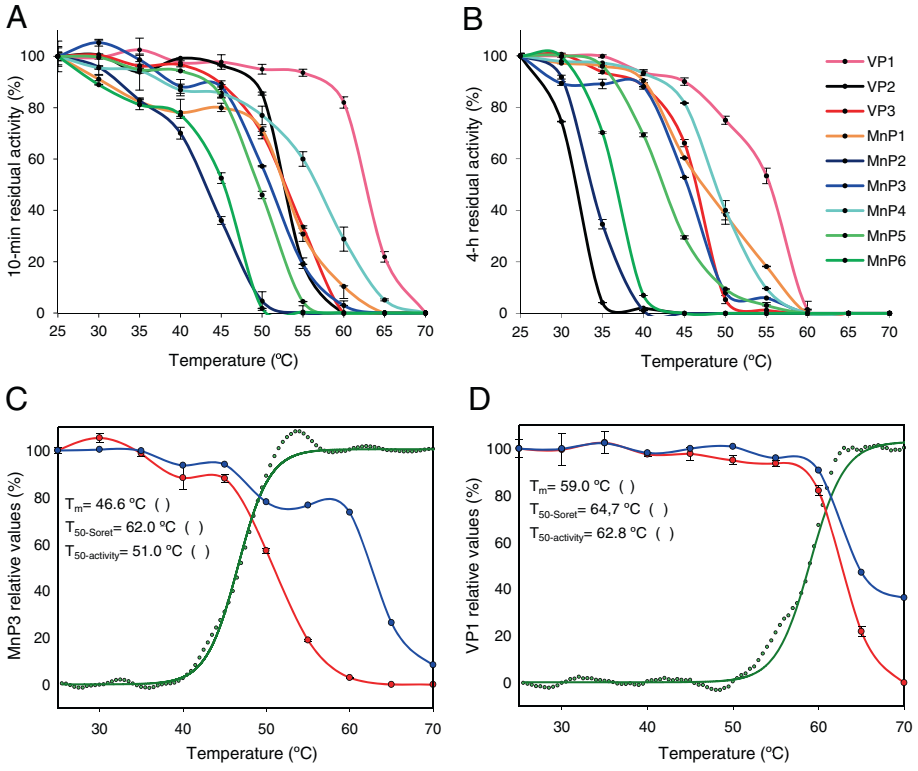

Figure 3 Thermal stabilities of the nine PODs from the *P. ostreatus* genome. (A, B) Residual activities after 10 minutes and 4 hours of incubation, respectively, in the range of 25 to 70°C. Residual activities were determined as described in Figure 2 after 10 minutes and 4 hours of incubation in 10 mM tartrate (pH 5) at ten temperatures (5°C intervals). Means and 95% confidence limits. From the above curves, the 10-minute and 4-hour $T_{50\text{-activity}}$ values were obtained (Additional file 2: Table S2). **(C, D)** Denaturation of temperature-unstable MnP3 and stable VP1, respectively, as shown by UV-visible (blue) and CD (green) spectroscopy, compared with activity lost (red). The effect of temperature (25 to 70°C) is shown by the θ increase at 222 nm in CD spectra acquired each 0.5°C, the absorbance decrease at the Soret maximum (at 407 nm) in the UV-visible spectra acquired each 5°C, and the decrease of enzyme residual activity after 10 minutes of incubation, estimated as described in Figure 2. All measurements were performed in 10 mM tartrate (pH 5). T_{50} values corresponding to those temperatures where 50% protein denaturation (main melting transition) is shown by CD spectra (T_m), 50% decrease of heme Soret band is shown by UV-visible spectra ($T_{50\text{-Soret}}$), and 50% decrease of enzymatic activity is produced ($T_{50\text{-activity}}$; means and 95% confidence limits) are included. CD, circular dichroism; MnP, manganese peroxidase; POD, class II peroxidase from the superfamily of non-animal (plant-fungal-prokaryotic) peroxidases; VP, versatile peroxidase.

the VP2 stability sharply decreased with incubation time). In general, the VPs were more stable than the MnPs at both 10 minutes (average $T_{50\text{-activity}}$ values of 56°C and 46°C, respectively) and 4 hours of incubation (average $T_{50\text{-activity}}$ values of 46°C and 43°C, respectively).

In the thermally-stable VP1 the Soret and visible maxima and the CD spectrum were only slightly modified in the 25 to 60°C range, but stronger changes were produced in the temperature-unstable MnP3. At higher temperatures MnP3 yielded a flat UV-visible spectrum, whereas a broad peak around 400 nm was still observed in VP1 at 70°C, and the VP1 CD spectrum lost the 222 nm minimum (as already found for MnP3 at lower temperature). The different temperature courses of the above changes in the MnP3 and VP1 spectra are illustrated in Figure 3C and D, respectively, which presents the loss of secondary (helix) structure (as shown by the ellipticity changes at the 222 nm CD minimum) and the modification of the heme environment (as shown by the decrease of the Soret band) together with the loss of catalytic activity. The differences between MnP3 and VP1 were more important for the loss of protein structure (with T_m for the main transition of 47°C and 59°C, respectively), which parallels the inactivation profiles (with $T_{50\text{-activity}}$ of 51°C and 63°C, respectively), than for the loss of the heme cofactor (with more similar $T_{50\text{-Soret}}$ values of 62°C and 65°C, respectively).

Molecular structures of VP1 and MnP4

P. ostreatus VP and MnP were crystallized and their whole structures are comparatively described for the first time (data collection and refinement statistics are provided in Additional file 2: Table S3). The two solved structures correspond to the isoenzymes most stable to temperature (VP1) and pH (MnP4) extremes, among the nine *P. ostreatus* PODs (Protein Data Bank, PDB, entries [PDB:4BLK] and [PDB:4BM1], respectively).

Main differences in the general molecular architecture

The overall structure of VP1 and MnP4 showed a heme group dividing the protein into a distal largely helical domain (formed by four main helices and two to three small ones) with one structural calcium ion, and a proximal domain composed by another six helices and a non-ordered region stabilized by a second calcium ion. Besides the overall similarity between the two PODs, several differences could be seen, the most significant ones being depicted (in darker colors) in Figure 4A.

The first difference was in the upper domain, close to the calcium ion (Figure 4A, left). At this site, the P56 to G59 loop of VP1 presents a six-residue insertion in MnP4 forming a small extra helix that protrudes into the solvent. Also, residues A130 and V131 in this VP1 region adopted a different conformation with respect to V135 and T136 in MnP4 (Figure 5A and Additional file 1: Figure S6A). These changes allow the F62 hydrophobic side chain of MnP4 to interact with K137 and, due to this interaction, the hydroxyl group of T136 interacts with one of the waters coordinating the distal calcium ion. The above extra helix is also predicted in the homology models of VP2, MnP2, and MnP6.

Significant differences were also found at the main heme access channel. They include four changes at the upper mouth of this channel (P76 to A82, A79 to N85, K176 to T182, and V177 to I183 in VP1 and MnP4, respectively) (Figure 4C and Additional file 1: Figure S6B). The result is that the channel is wider, and the heme is more accessible in VP1 than in MnP4 (larger circles in Figure 4B). Another difference is located at the lower lip of the channel (Figure 5C). The first change was N214 (VP1) to H220 (MnP4), since the histidine occupies a larger volume that leads to a shift of the D184 to K186 region. The above change also affects D217, which is shifted towards the outside in MnP4 with respect to T211 in VP1. Another change affects I214 in MnP4 (F208 in VP1), whose smaller side chain allows L219 to be oriented towards the surface, while in VP1 the big phenylalanine side chain forces D213 to be exposed to the solvent. The last change in this region concerns S180 in VP1, which is occupied by K186 in MnP4, thus affecting both the surface shape and charge. The lower lip in VP1 presents a clear negative charge and the shape of a wide reservoir, while in MnP4 it displays a less charged surface with a narrow groove (circles in Figure 5C). The above differences might affect substrate oxidation at the heme access channel.

Another difference between VP1 and MnP4 is located at the back of the protein (Figure 4A, right), with respect to the heme access channel. It affects two sequence stretches (V248 to P252 and P286 to H293 in VP1, and I254 to S259 and R292 to P298 in MnP4) with different conformational arrangements (Figure 5B and Additional file 1: Figure S6C and D). The first sequence is close to the VP1 catalytic tryptophan (W164) and the second close to the proximal calcium-binding site. The largest difference in the first stretch is the change of Q251 in VP1 to P257 in MnP4, but the changes in the second stretch are more pronounced. Most of them involve the change of small hydrophobic side chains in VP1 for large hydrophilic side chains, such as the substitution of G290 in VP1 by K296 in MnP4. This lysine has interactions with D198 and D200, which are directly involved in the coordination of the proximal calcium.

Differences in surface charge affect not only the main heme channel environment. When the MnP4 crystal structure was solved, a striking observation was the high number of solvent-exposed lysines (a total of 20) and other basic residues (up to a total of 34) (Figure 4B). By

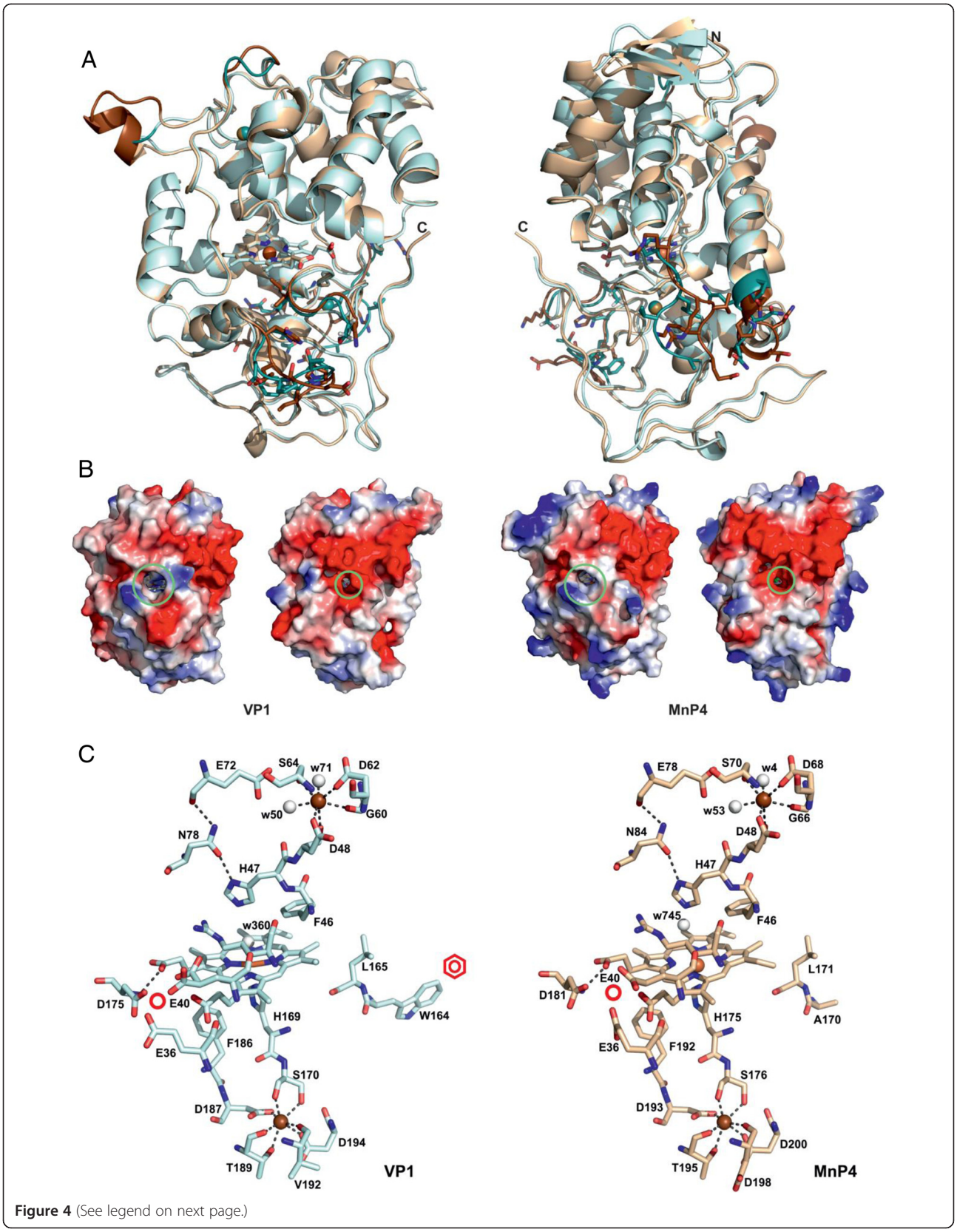

Figure 4 (See legend on next page.)

(See figure on previous page.)
Figure 4 Crystal structures of the most interesting VP/MnP isoenzymes from the *P. ostreatus* genome (1.05 to 1.10 Å). (A) Superposition of the overall structures of VP1 (light blue) and MnP4 (light brown) from two different orientations. The significant differences between the structures are shown in darker color with some side chains of these regions as sticks. **(B)** Electrostatic surface of VP1 and MnP4 from two different orientations showing the main heme access channel (larger circle) and the narrower Mn^{2+} access channel (smaller circle) as well as the more basic MnP4 surface with a high number of exposed lysine residues. **(C)** Detail of the VP1 and MnP4 heme and neighbor regions showing: proximal histidine (H169 and H175, respectively); distal histidine (H47) and neighbor arginine (R43); two conserved phenylalanines at the proximal histidine side (F186 and F182, respectively) and the distal histidine side (F46) of the heme; two conserved asparagines (N78 and N84, respectively) and glutamate residues (E72 and E78, respectively) forming a H-bond network from the distal histidine; two structural Ca^{2+} ions (brown spheres) with their four/five conserved ligands; one site for oxidation of Mn^{2+} (whose predicted position is marked with a red circle) near the internal propionate of heme, formed by two glutamates (E36 and E40) and one aspartate (D175 and D181, respectively); one tryptophan residue (W164) constituting the site (marked with a red benzenic ring) of VP1 oxidation of aromatic substrates by LRET via a contiguous leucine residue (L165); and several water molecules (white spheres) near the distal histidine and Ca^{2+} ion. From entries [PDB:4BLK] (VP1) and [PDB:4BM1] (MnP4). LRET, long-range electron transfer; MnP, manganese peroxidase; PDB, Protein Data Bank; VP, versatile peroxidase.

contrast, VP1 has only nine lysines and a total of 21 surface basic residues. The number of exposed basic residues in the nine *P. ostreatus* PODs varies in the 18 to 35 range, while that of exposed acidic residues scarcely varies (29 to 37 range). The above differences correlate to protein pI, which is at least one unit higher in MnP4 (Additional file 2: Table S2). On the other hand, when the interactions between residues occupying the molecular surface were analyzed, a higher number of H-bonds and salt bridges were observed in MnP4 than in VP1, which stabilize loops (E92 to S75 H-bond) and connect helices and loops (R245 connected with T152 and D243, and E238 with R233).

Heme environment and Ca^{2+}-binding sites

A total of 28 residues make up the heme pocket of the two crystallized proteins (Additional file 1: Figure S7), most of them being conserved except four (I171, A174, K176, and V177 in VP1, being V177, Q180, T182, and I183 in MnP4, respectively). The first change, I171 to V177, was located far from the entrance to the heme access channel, while the other three changes are located close to or at the heme access channel and modify the accessibility to the cofactor. Among the above changes, V177 in VP1 to I183 in MnP4 removes one of the heme-apoenzyme H-bonds. The above differences in heme pocket residues are accompanied by the change of I226 in VP1 to F232 in MnP4, in close contact to A174 and Q180, respectively. The larger volume of these two residues in MnP4 pushes outwards the loop that forms the lower lip of the heme access channel (Figure 5C).

The heme environment in VP1 and MnP4 (Figure 4C) includes a proximal histidine (H169 and H175, respectively) acting as the fifth ligand of the heme iron, and a distal histidine (H47 in both enzymes) establishing H-bonds with several heme pocket residues and water molecules. The water located between the iron and the distal histidine showed elongated density in both structures (Additional file 1: Figure S7B and D), which might indicate multiple conformations for this molecule (which also binds conserved R43). The residues contiguous to proximal and distal histidines in VP1 (S170 and D48, respectively) and MnP4 (S176 and D48, respectively) participate in coordination of the two Ca^{2+} ions present in the structure, together with four other residues at the proximal side, and three residues plus two water molecules at the distal side (all of them at 2.4 to 2.5 Å distance) (Figure 4C). The calcium ligands are conserved except for VP1 V192, which in MnP4 is D198. Both the proximal histidine of VP1 and MnP4 and the contiguous Ca^{2+}-binding serine are in the same helix, whereas another Ca^{2+} ligand (D194 and D200, respectively) is contiguous to the next helix. Therefore, this Ca^{2+} ion stabilizes the position of the proximal histidine. In a similar way, the second Ca^{2+} ion would fix the helix where the distal histidine is located. The Ca^{2+}-binding residues are also conserved in the other seven *P. ostreatus* PODs, excepting only those homologous to VP1 Ser170 and Val192 (but note that in these two cases the backbone carbonyls are the ligands to Ca^{2+}) (Figure 1 and Additional file 2: Table S2).

Substrate oxidation sites

Both VPs and MnPs are able to oxidize Mn^{2+} (Table 1). The site where this takes place is conserved and comprises three acidic residues (E36/E40/D175 in VP1 and E36/E40/D181 in MnP4) located near the heme propionate occupying the most internal position with respect to the main access channel (Figure 4C). This propionate is accessible to the solvent by a narrow second access channel (smaller circles in Figure 4B) that opens at a negatively-charged region, at approximately 15 Å from the main access channel. The Mn^{2+} oxidation site is conserved in all the *P. ostreatus* MnPs and VPs, as shown by the homology models (Additional file 1: Figure S2).

In addition to the Mn^{2+} oxidation site, VPs also present a lignin oxidation site, whose presence was detected using VA and RB5 as substrates (Table 1). This

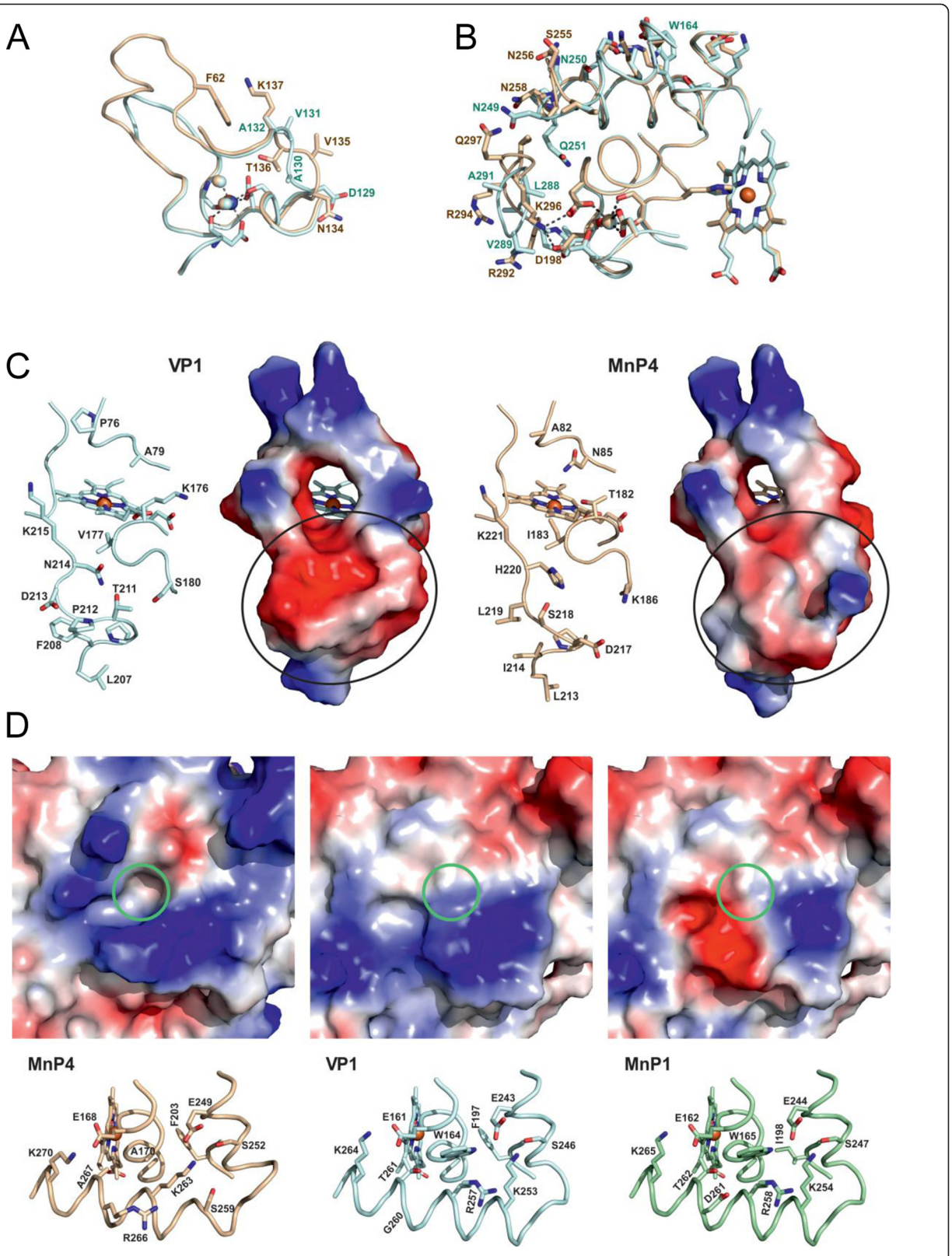

Figure 5 (See legend on next page.)

(See figure on previous page.)
Figure 5 Comparison of three regions in the VP1 (blue) and MnP4 (brown) crystal structures; and catalytic tryptophan environment in VP1 and homologous regions in MnP4 and MnP1. (A) Loop close to the distal calcium and its ligands including two water molecules (light spheres) and differences in the VP1/MnP4 D129 to A132/N134 to K137 region including MnP4 K137 interacting with the F62 side chain. **(B)** Two sequence stretches (V248 to P252 and P286 to H293 in VP1, and I254 to S259 and R292 to P298 in MnP4) at the back of the protein with indication of those residues differing in the two peroxidases (the heme cofactor, proximal Ca^{2+}, spheres, and its ligands, and VP1 W164 are also visible). **(C)** Selected residues and solvent access surface in the VP1 and MnP4 heme access channel and surrounding area (differences in surface electronegativity below the channel entrance are indicated with circles). **(D)** Structure (bottom) and electrostatic surface (top) showing the catalytic tryptophan and surrounding residues of VP1 (including G260 and F197, among others) compared with the same region in MnP1 (including D261 and I198) and MnP4 (including R266 and F203) (the green circles represent the position of the conserved tryptophan in VP1 and MnP1, or the corresponding alanine in MnP4). From entries [PDB:4BM1] (MnP4) and [PDB:4BLK] (VP1), and MnP1 homology model based on [PDB:4BLK]. MnP, manganese peroxidase; PDB, Protein Data Bank; VP, versatile peroxidase.

site in VP1 would consist of W164, connected to the heme group via a long-range electron transfer (LRET) (Figure 4C). The indolic side chain of W164 in VP1 is largely exposed (Figure 5D, center) allowing the collection of electrons from the bulky lignin molecule. The oxidation of lignin-related substrates was not detected in MnP4, where the active tryptophan is substituted by an alanine (Figure 5D, left). The same substitution occurs in MnP3 and MnP5, while an aspartic acid occupies this position in MnP2 and MnP6 (Additional file 1: Figure S2). However, the VP1 W164 is conserved in the two other VPs (as VP2 W170 and VP3 W164). Moreover, a putative lignin oxidation site (at W165) exists in MnP1, but the enzyme was unable to oxidize VA and RB5.

Directed mutagenesis of *P. ostreatus* PODs

The putative Mn^{2+} and lignin oxidation sites identified in the crystal structures were confirmed by site-directed mutagenesis of the three acidic residues near the internal heme propionate and of the exposed tryptophan (Additional file 2: Tables S4 and S5). The ability to oxidize Mn^{2+} completely disappeared after the simple E36A, E40A, or D179A mutations in MnP4, and also after the double E35A/E39A mutation in VP1 (the simple E35A, E39A, and D175A VP1 variants lost over 99.8% of their catalytic efficiency but retained detectable activity on Mn^{2+}). In a similar way, the W164S mutation in VP1 resulted in a complete loss of activity on VA and RB5 (used as two simple lignin model compounds). By contrast, the VP1 E35A, E39A, and E175A (as well as the double E35A/E39A) variants maintained unchanged kinetic constants for VA and RB5 oxidation, and those of W164A on Mn^{2+} were only slightly modified.

One special case was isoenzyme MnP1. This protein presents the exposed tryptophan characteristic of VPs (MnP1 W165) but has no activity on VA or RB5. A MnP1 molecular model showed that most of the exposed residues surrounding the conserved tryptophan (W164 in VP1 and W165 in MnP1) were conserved, but the small G260 in VP1 was substituted by an aspartate (D261) in MnP1 (Figure 5D, right). This influenced the surface shape and charge of the tryptophan environment, and therefore might influence substrate binding (Figure 5D, top). Other differences affect residues located between W165 and the heme cofactor (Figure 5D, bottom). Among them, the substitution of F197 in VP1 by I198 in MnP1 seems especially relevant since this residue is conserved in all the other *P. ostreatus* PODs (Figure 1). Therefore, the MnP1 D261G and I198F single and double mutations were incorporated, and the kinetic constants compared with those of native MnP1 and VP1 (Additional file 2: Table S6). A *Pleurotus pulmonarius* POD, which had been classified as VP but has a conserved tryptophan environment similar to *P. ostreatus* MnP1, was also included in the comparison. As suspected, the *P. pulmonarius* enzyme was unable to oxidize VA and RB5 and must be, therefore, reclassified as a MnP. Concerning MnP1, the D261G mutation did not modify the catalytic properties, indicating that impaired substrate binding is not the reason for the lack of activity. However, the I198F mutation, although it was not enough to confer the ability to oxidize VA, provided to MnP1 the ability to oxidize the second high redox potential VP substrate, RB5 (with K_m 2.3 ± 0.4 μM, k_{cat} 10.0 ± 0.8 s^{-1}, and k_{cat}/K_m 4270 ± 410 $s^{-1}.mM^{-1}$) and the same result was obtained with the double (I198F/D261G) mutation.

Lignin model degradation by *P. ostreatus* VP

The POD repertoire in *P. ostreatus* includes functional VPs and MnPs, but lacks lignin-degrading LiPs even though the fungus is ligninolytic. To look for an explanation of this discrepancy, we treated a nonphenolic β-O-4' lignin model dimer (labeled with ^{14}C to facilitate product detection) with *P. ostreatus* VP1 in the presence of limiting H_2O_2 to prevent enzyme inactivation. The results showed that oxidative degradation of the model compound occurred (Figure 6A). Both C_α-C_β bond cleavage releasing 4-ethoxy-3-methoxybenzaldehyde (peak 2) and C_α oxidation resulting in the corresponding dimeric ketone (peak 3) were obtained. Minor amounts of the phenylglycerol product from C_β-O-C_4' ether bond cleavage (peak 5) and the corresponding C_α-ketone (peak 4) were also obtained. The experiment was performed on

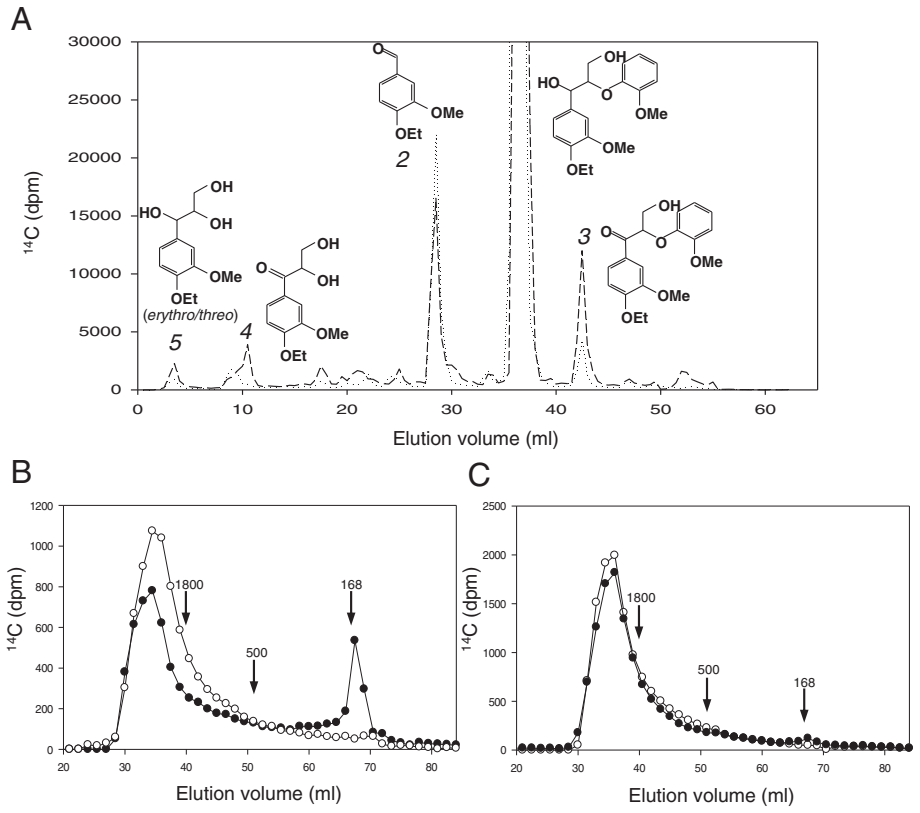

Figure 6 Demonstration of lignin-degrading ability of *P. ostreatus* VP. (A) Oxidative degradation of a nonphenolic lignin model dimer by VP1. The erythro (dotted line) and threo (dashed line) isomers of ^{14}C-labeled 4-ethoxy-3-methoxyphenylglycerol-β-guaiacyl ether (peak 1) were treated with VP1, and the completed reactions were analyzed by HPLC. The main products were 4-ethoxy-3-methoxybenzaldehyde (peak 2) and 1-(4-ethoxy-3-methoxyphenyl)-3-hydroxy-2-(2-methoxyphenoxy)-propan-1-one (peak 3). The minor peaks 4 and 5 correspond to 1-(4-ethoxy-3-methoxyphenyl)-2, 3-dihydroxypropan-1-one and 1-(4-ethoxy-3-methoxyphenyl)glycerol, respectively. **(B, C)** Lignin depolymerization by VP1.^{14}C-labeled synthetic lignin (DHP) was treated with VP1 from the *P. ostreatus* genome in the presence **(B)** and absence **(C)** of VA. Black symbols indicate reactions with enzyme and open symbols indicate controls without enzyme. Total recoveries of initially added ^{14}C from complete reactions before GPC analysis were 62% for reaction B and 92% for reaction C. Recoveries from control reactions were somewhat higher as reported earlier [22]. The arrows indicate elution volumes of two polystyrene molecular mass standards (1,800 and 500 Da) and VA (168 Da). DHP, dehydrogenation polymer; GPC, gel permeation chromatography; HPLC, high performance liquid chromatography; VA, veratryl alcohol; VP, versatile peroxidase.

the two stereoisomers of the model dimer, and VP1 oxidation resulted in relatively higher C_α-C_β bond cleavage of the erythro form (dotted line) and higher C_α oxidation of the threo form (dashed line).

Most important, when a β-^{14}C-labeled synthetic lignin (dehydrogenation polymer, DHP) was treated with VP1 in the presence of VA and then analyzed by gel permeation chromatography (GPC) (Figure 6B), significant depolymerization of the lignin was observed (black symbols), as shown by the production of low molecular mass products (near the position of the 168 Da marker). Depolymerization did not occur in the control experiment without enzyme (white symbols). In contrast with the results obtained with the model dimer (Figure 6A) lignin depolymerization by VP1 required the presence of VA, since no significant changes were observed when the DHP was treated in the absence of this mediator compound (Figure 6C).

Discussion

VP and MnP characterization from *P. ostreatus* genome

In spite of the interest in *P. ostreatus* and related species as both edible mushrooms and selective lignin-degrading fungi of interest in lignocellulose biorefineries, only three *P. ostreatus* POD genes (encoding the MnP1, VP2, and MnP3 isoenzymes) were available to date (as [GenBank:AAA84396], [GenBank:AJ243977], and [GenBank: BAA33449], respectively). MnP1 was the first *P. ostreatus* POD to be cloned by Asada *et al.* [21]. MnP3 and VP2 were cloned and both reported as MnPs [23,24], and VA oxidation by VP2, which established that it is in fact a VP, was reported later [25]. VP1 had been purified from *P. ostreatus* cultures [26], and cloned from related *P. eryngii* (VPL) [27] together with *P. eryngii* VPS1, homologous to *P. ostreatus* VP2 [28], but not from *P. ostreatus*. The heterologous expression of the POD genes from the *P. ostreatus* genome, and subsequent

kinetic studies, reveal a peroxidase array consisting of three VPs and six MnPs. In all but one (isoenzyme MnP1) the catalytic properties of the purified enzymes agree with the presence in the homology models of a putative Mn^{2+} oxidation site, and for the VPs they agree with the presence in the models of an exposed tryptophan likely responsible for oxidation of high redox potential substrates and lignin [29,30].

The *P. ostreatus* VPs are highly efficient at oxidizing Mn^{2+} and RB5, and their lower catalytic efficiency on VA is related to the low apparent affinity for this substrate. The low redox potential substrate ABTS is also oxidized with high efficiency, but this is not the case for DMP. The kinetic constants obtained are similar to those reported for *P. eryngii* and *Bjerkandera adusta* VP on the same substrates [31]. The *P. ostreatus* VPs not only show wider substrate specificity than MnPs, but their catalytic efficiencies on Mn^{2+} are also higher, which has not been previously reported. The Mn^{2+}-independent activity of VP on phenols and dyes can be related to the existence of two more catalytic sites in addition to the Mn^{2+} oxidation site. The first site, characterized by its high catalytic efficiency, corresponds to the same exposed tryptophan involved in VA/RB5 oxidation as shown by directed mutagenesis, while the second site has been assigned to the main heme channel [32]. In contrast with the best known MnPs from *P. chrysosporium*, whose activity is always mediated by Mn^{3+} [33], the *P. ostreatus* MnPs also have Mn-independent activity on ABTS and (except MnP1) on DMP. This activity has already been reported for *P. ostreatus* MnP3 [23] and for *Agrocybe praecox* MnP [34], and is expected to be present in many other hypothetical MnPs reported from genomes as members of a new subfamily of short MnPs [16], which would also include all the *P. ostreatus* MnPs.

Concerning MnP1, previously classified as a VP [17], some differences in the environment of the nonfunctional tryptophan (W165) are responsible for its inability to oxidize high redox potential substrates, as shown by the I198F variant being able to oxidize RB5. This mutation introduced a phenylalanine residue that could be important for correct positioning of the neighboring proximal histidine (which modulates the redox potential of the enzyme) and/or for LRET from W165 to the heme cofactor [18]. In addition to the presence of W165, MnP1 also has a close evolutionary relationship (Additional file 1: Figure S1) and the highest sequence identity (70%) with VP3 (for sequence identity between different PODs, see Additional file 2: Table S7). It has been recently shown that MnPs represent an ancestral peroxidase type in Agaricomycetes from which VPs and LiPs originated [16]. Our results on *P. ostreatus* MnP1 (and the above *P. pulmonarius* MnP) suggest a more complicated picture of POD evolution, where some MnP-type peroxidases might derive secondarily from an ancestral VP-type enzyme.

VP and short MnP crystal structures

The VP1 and MnP4 crystal structures were solved as representative for the two POD families present in the *P. ostreatus* genome. Several aspects of the crystal structure of *P. eryngii* VP were discussed when studying the catalytic sites of this enzyme [29,32,35], although a comparative description of the whole VP structure was not reported. On the other hand, the molecular structure of long MnP from *P. chrysosporium* has been reported at different resolutions [36-38], but no crystal structure for a short MnP was available before the present study.

As already described for *P. eryngii* VPL [29], the main structural feature of the *P. ostreatus* VP1 crystal structure is the combination of the Mn oxidation site of MnPs [36] and the high redox potential substrate oxidation site of LiPs [39]. Differences in the side chain position of the Mn-binding E36 (in VP1 and MnP4) would be related to the mobility of this residue at the oxidation site entrance. On the other hand, the catalytic W164 environment in VP1 is less acidic than the corresponding region in *P. chrysosporium* LiP, the latter probably contributing to stabilize the VA cation radical [40]. A characteristic of ligninolytic peroxidases is their narrow heme access channel, which has been related to the need to protect the enzyme from inactivation by substrate radicals generated at the heme pocket [18,29]. However, one of the main characteristics of the VP1 structure, when compared with MnP4, is the broader main heme access channel (whose lower lip has the shape of a wide reservoir), which could be related to the reported existence of a third substrate oxidation site in VP [32]. The fact that only low redox potential substrates (and not VA) are oxidized at the main heme access channel could explain the lack of enzyme inactivation in these VP reactions.

Concerning short MnP, whose crystal structure is now solved for the first time (from *P. ostreatus* MnP4), its main structural difference from *P. chrysosporium* long MnP concerns the existence of a more exposed Mn oxidation site, due to the absence of the C-terminal extension that in *P. chrysosporium* MnP (with a total of 357 residues) is partially fixed by a fifth disulfide bridge. Whether this difference, which is used to define the new subfamily of short MnPs from genomes [16], underlies the low but significant Mn-independent activity (on ABTS) exhibited by these and other short MnPs remains to be confirmed. Other characteristics of the MnP4 structure, such as the high number of exposed basic residues and H-bonds/salt-bridges, and the differences in the environment of the two structural Ca^{2+} ions, are discussed below in connection with the PODs' pH stability.

Catalytic properties of POD isoenzymes

The existence of multiple isoforms (isoenzymes) is a well-known phenomenon among degradative enzymes secreted by fungi, including peroxidases. LiP isoenzymes were first isolated from *P. chrysosporium* cultures [41,42]. DNA cloning showed that some of them were encoded by different genes [43], but post-translational modifications are at the origin of other isoforms [44]. The number of POD 'true isoenzymes' increased when more LiP and MnP genes were cloned from other Polyporales. Studies in Agaricales reported cloning of three POD isoenzymes from *P. ostreatus* [21,23,24]. However, a correlation between cloned genes and purified isoenzymes was not clearly established, and characterization of the different isoenzymes was lacking with a few exceptions [41,42,45]. Therefore, the number and characteristics of the POD isoenzymes produced by white-rot fungi remained an open matter to date.

The availability of genomes provides evidence on the large and widespread duplication of POD genes in white-rot basidiomycetes [12,15,17,46]. This availability, together with the possibility to optimize the *in vitro* activation of *E. coli*-expressed PODs [47], enabled us to obtain the complete set of POD isoenzymes encoded by the *P. ostreatus* genome for biochemical comparisons, an important complement to differential expression studies [48]. Substrate specificity was used for functional classification into the VP and MnP families. Moreover, kinetic constants revealed some quantitative differences between the members (isoenzymes) from each family including: i) the higher efficiency of VP1 oxidizing aromatics and dyes, and also its lower efficiency relative to VP2 and VP3 at oxidizing Mn^{2+}; ii) the non-saturation kinetics exhibited by MnP3 and MnP4 in DMP oxidation, as compared with MnP3 to MnP6 (MnP1 had no activity); and iii) the unusual properties of MnP1, including its higher ABTS oxidation efficiency (in the range of VP isoenzymes), low H_2O_2 reaction efficiency, and inability to oxidize DMP. The unique properties of isoenzyme MnP1 can be related to its separate evolutionary origin, whereas the structural/evolutionary basis of other differences in catalytic properties are still to be determined. However, the most interesting differences between the *P. ostreatus* VP and MnP isoenzymes concern the temperature and pH stability properties discussed below.

Different stabilities of the POD isoenzymes

P. ostreatus is not a thermophilic fungus [49]. However, a comparison of the temperature stabilities of the nine *P. ostreatus* PODs reveals some thermostable isoenzymes, as shown by $T_{50\text{-activity}}$ values that, after 10 minutes of incubation, ranged from 53°C (VP2 and VP3) to 63°C (VP1) in the case of VPs; and from 43°C (MnP6) to 57°C (MnP4) in the case of MnPs. These thermostabilities are significant in high redox potential peroxidases, which are generally isolated from wood-rotting mesophilic basidiomycetes. Among peroxidases, the most temperature- and pH-stable forms have been isolated from palm species [50] but plant peroxidases lack the structural adaptations enabling oxidation of recalcitrant aromatics. Moreover, the above VP and MnP $T_{50\text{-activity}}$ ranges (10°C and 14°C, respectively) are notable for isoenzymes from the same organism (and attain 23°C and 16°C, respectively, after 4 hours of incubation). Some information on the mechanisms of thermal stability/inactivation was provided by CD and UV-visible spectroscopy. A rough correlation between activity loss, structure melting (shown by CD spectroscopy), and partial loss of heme (shown by visible spectroscopy of the Soret band) was observed during inactivation of the most stable isoenzyme VP1, whereas the unstable MnP3 was fully inactivated in parallel with structure melting, and the loss of the heme cofactor was delayed. This indicates that POD thermal inactivation is due to an unspecific effect of temperature on the protein structure, and the cofactor loss appears as a secondary phenomenon.

Wood lignin degradation takes place at acidic pH due to secretion of organic acids by white-rot basidiomycetes [18]. The redox potential of heme peroxidases increases at low pH, providing LiP and VP the capability to oxidize the recalcitrant lignin polymer, which optimally takes place around pH 3. Although partial stability under acidic conditions is therefore requisite for these enzymes, inactivation inexorably takes place below the above pH value [51]. Moreover, PODs are inherently unstable to slightly alkaline pH due to loss of the structural Ca^{2+} ions [52,53]. This does not represent a problem in natural biodegradation of lignin but can be a drawback for industrial applications. The *P. ostreatus* VPs and MnPs are quickly inactivated at pH ≤2 and pH ≥9, but the residual activities of the different isoenzymes strongly varied after incubation at both pH 3 (20 to 95% for VPs, and 0 to 95% for MnPs, after 4 hours at 4°C) and pH 8 (45 to 80% for VPs, and 0 to 80% for MnPs). Among the enzymes investigated, isoenzyme MnP4 is especially resistant to alkaline inactivation, maintaining significant activity after 1 hour at pH 9 (over 75%), pH 10 (over 50%), and even pH 11 (over 30%). The acidic pH effect on the CD and UV-visible spectra of *P. ostreatus* PODs is reminiscent of that observed during thermal inactivation. By contrast, at alkaline pH the heme cofactor remains quantitatively linked to the protein, even when complete inactivation and structure loss was produced (as found for MnP3). The displacements of the Soret band (from 407 to 413 nm) and other visible maxima (with a marked peak appearing at 530 nm) agree with formation of a bis-histidyl heme iron complex [52].

Several structural features, potentially involved in POD thermal and acidic/alkaline inactivation, were examined first on the homology models of the nine isoenzymes, and then on the VP1 and MnP4 crystal structures. For example, we tried to correlate the POD thermal stability to the proline number and position in β-turns [54] and to the effect of heme-apoenzyme bonds [55]. This approach agreed with the fact that VP1 has 12 β-turn prolines (compared with a POD average of nine) and one more heme-apoenzyme bond (than MnP4) but could not be extended to other thermostable *P. ostreatus* PODs. Concerning the effect of pH, acidic inactivation seemed related to general structural stability, as in the case of temperature inactivation. However, alkaline inactivation suggests a specific mechanism involving

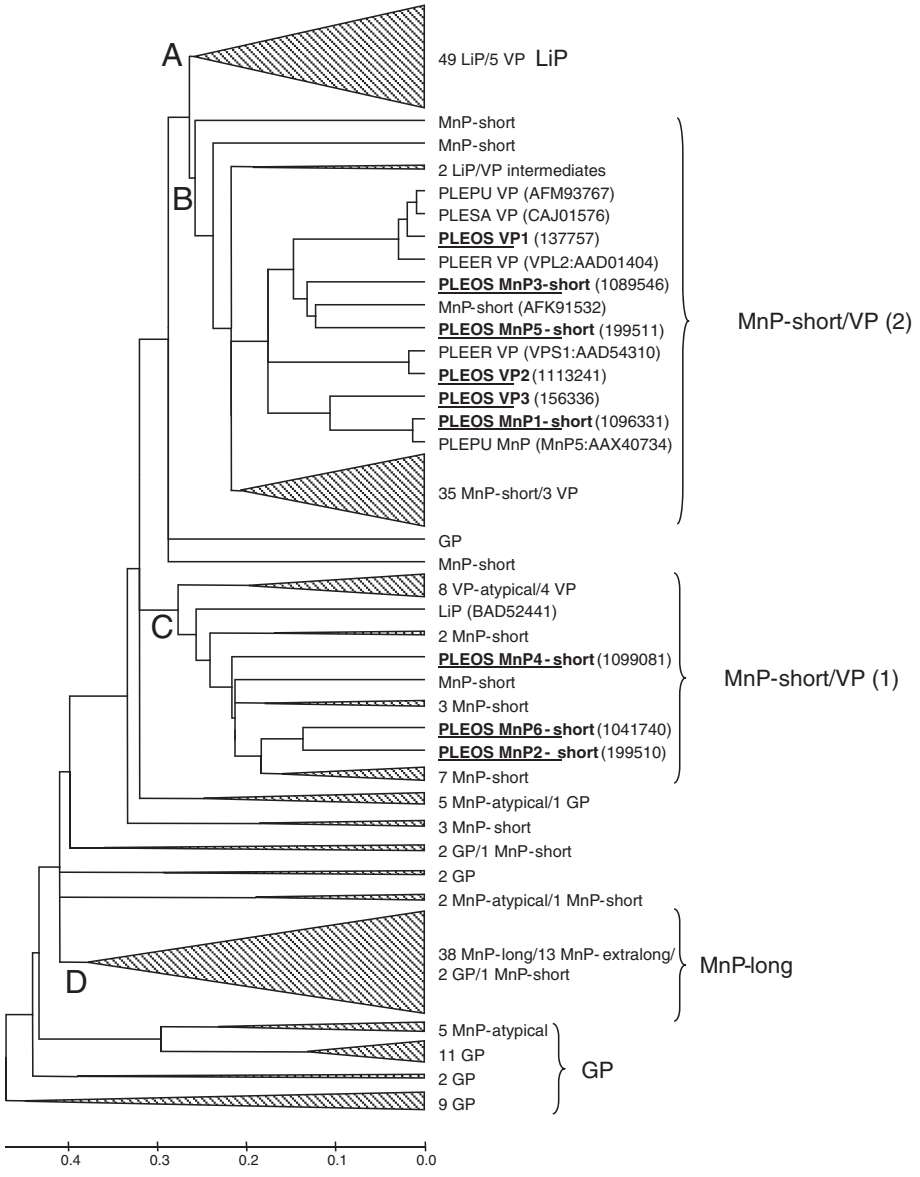

Figure 7 Phylogram of 237 sequences of basidiomycete PODs including the nine sequences from *P. ostreatus* genome (underlined). POD sequences from 21 genomes (and GenBank) were analyzed. Four main clusters were identified corresponding to LiP **(A)**, MnP-short/VP clusters 1 and 2 **(B, C)**, and MnP-long **(D)**, together with the most ancestral group of GPs and unclustered sequences. Those clusters/subclusters where *Pleurotus* (PLEOS, *P. ostreatus*; PLEER, *P. eryngii*; PLEPU, *P. pulmonarius*; and PLESA, *P. sapidus*) sequences are not included were collapsed, with indication of the number and type of sequences included. Two LiP-type enzymes from *G. subvermispora* representing LiP/VP transition stages [47] are indicated, as well as a *Cerrena unicolor* MnP (AFK91532) related to *P. ostreatus* short MnPs, and the unique *Trametes cervina* LiP (BAD52441). MnP-atypical corresponds to a MnP type with only two acidic residues at the oxidation site [16]. Protein model numbers are provided for the nine *P. ostreatus* genome sequences, and GenBank references for other six POD sequences. See Ruiz-Dueñas and Martínez [19] for references of other basidiomycete PODs. GP, generic peroxidase; LiP, lignin peroxidase; MnP, manganese peroxidase; POD, class II peroxidase from the superfamily of non-animal (plant-fungal-prokaryotic) peroxidases; VP, versatile peroxidase.

formation of a bis-histidyl heme iron complex due to loss of structural Ca^{2+} ions [53]. In this context, two of the main differences in the crystal structure of the pH-stable MnP4, compared with VP1, affect regions neighbor to the Ca^{2+}-binding sites, such as the loop containing the MnP4 extra helix in the upper domain and the two different sequence stretches at the lower domain. In both cases, MnP4 has an extra interaction in the second coordination sphere of the Ca^{2+} ions (due to presence of T136 and K296) that could increase its alkaline stability. The highest stability of MnP4 could be also due to some interactions lacking in VP1 that stabilize loops and connect helices and loops at the molecular surface. Another noteworthy characteristic of MnP4 is the high number of surface-exposed lysines (up to a total of 20) and other alkaline residues (up to a total of 35) compared with the other *P. ostreatus* PODs, which would result in a higher net positive charge of the protein and increased stability at acidic pH. Involvement of the above surface interactions and alkaline residues in MnP4 pH stability is being confirmed by site-directed mutagenesis studies in course (unpublished data).

Evolutionary relationships of basidiomycete PODs

The evolutionary relationships of *P. ostreatus* and other basidiomycete PODs are shown in Figure 7. The most basal sequences correspond to generic peroxidases (GPs), which gave rise to MnPs by progressive incorporation of the three residues forming the Mn oxidation site [16]. Long (and extra long) MnPs from *P. chrysosporium* and other fungi form cluster D, separated from the rest of PODs. A few more GPs and atypical MnPs are unclustered (between clusters C and D) and the rest of the sequences are intermixed, except for the well-defined cluster A that includes all the LiPs, and a few VPs related to the common VP-type ancestor of both families [16].

The *P. ostreatus* PODs are in the two other clusters, both containing short MnP and VP sequences, in agreement with higher sequence identity of short MnPs with VPs than with long MnPs from *P. chrysosporium* and other fungi (see Additional file 2: Table S7). Cluster C includes *P. ostreatus* MnP2, MnP4, and MnP6, together with other short MnPs and a group of VPs. Cluster B is constituted by: i) a *Pleurotus* group formed by the other six genome PODs and five more sequences from GenBank; ii) a second group of short MnPs/VPs; and iii) unclustered short MnPs and two LiP/VP intermediates [47]. Inside the *Pleurotus* group, *P. ostreatus* VP1 is closely related to *P. eryngii* VPL, the best characterized VP [29,35] (97% identity), and to the only *Pleurotus sapidus* and *P. pulmonarius* VPs, suggesting that the four sequences correspond to the same isoenzyme in four related species. Moreover, *P. ostreatus* VP2 clusters with *P. eryngii* VPS1, the second cloned VP [28] (98% identity), revealing that both are also the same isoenzyme, and the same is true of *P. ostreatus* MnP1 and a *P. pulmonarius* MnP (96% sequence identity). As discussed, the structural characteristics of the two latter MnPs suggest a secondary origin from an ancestral VP-type enzyme that, according to the phylogram, could be related to *P. ostreatus* VP3.

P. ostreatus PODs: demonstration of ligninolysis

POD involvement in fungal ligninolysis is supported by the presence of LiP, VP, and/or MnP encoding genes in all the currently available genomes of lignin-degrading basidiomycetes (white-rot fungi) and their absence from all the genomes of basidiomycetes that degrade cellulose without removing lignin significantly (brown-rot fungi) [16]. Oxidation of a non-phenolic lignin model dimer by DyP has been reported [56], although in other cases its direct action seems restricted to the minor phenolic units [57] as in the case of laccases [4]. Some HTPs can also degrade non-phenolic lignin model dimers [58] but they seem unable to act on polymeric lignin [59]. Moreover, the genes of these two peroxidase superfamilies (and laccases) are not restricted to the genomes of white-rot fungi, as in the case of PODs [16].

In *P. chrysosporium*, LiP is the enzyme principally responsible for cleavage of the predominant and most recalcitrant nonphenolic structures in lignin [60], whereas classical MnPs contribute Mn^{3+} that can act as a diffusible oxidant of minor phenolic lignin moieties [61]. VP was described as a fourth POD family combining some of the catalytic properties of LiPs, MnPs, and fungal GPs (which act on the same substrates that plant peroxidases oxidize) [27,28]. The chimeric nature of VPs raised questions about their role in ligninolysis, and no studies on their lignin-degrading ability have been available until now.

The present genomic study establishes the absence of LiP in a ligninolytic white-rot fungus, *P. ostreatus*, in accordance with the *in silico* analysis of its genome, which indicated the presence of only VP and MnP genes. Moreover, we demonstrate for the first time the ligninolytic capabilities of one of these VPs, showing that it is able to: i) cleave the most frequent interunit linkages in lignin (β-O-4' ether structures); and ii) depolymerize lignin. These capabilities are similar to those reported for *P. chrysosporium* LiP in terms of reactions and products obtained [22]. Concerning MnPs, we also provide evidence on the dual Mn-mediated and Mn-independent activity of the so-called short MnPs found in *P. ostreatus*, whose presence had been reported in several fungal genomes [16] without the corresponding catalytic studies.

We show the existence, in *P. ostreatus*, of a POD repertoire constituted by VPs and MnPs, with the former peroxidases assuming the role played by LiPs in *P.*

chrysosporium (and most other white-rot fungi). This different enzymatic machinery is most probably related to the different phylogenetic position of the two fungi, which are in the orders Agaricales and Polyporales, respectively. It seems that the POD evolutionary history in the Agaricales did not include the final transition from VP to LiP enzymes via loss of the Mn^{2+} oxidation site, as occurred in the Polyporales [46].

Conclusions

As a result of the current genomic screening we were able to: i) show the presence in the model agaric *P. ostreatus* of a peroxidase repertoire in which VPs play the role that LiPs do in white-rot polypores; ii) describe the catalytic properties of *P. ostreatus* MnPs, as representatives of a new peroxidase subfamily; iii) establish the evolutionary relationships of the above enzymes with the other basidiomycete PODs; iv) describe the first crystal structure of a short MnP, which was compared with the solved VP structure; and v) demonstrate the existence of strongly divergent thermal and pH stabilities among a wide array of POD isoenzymes encoded by duplicated genes.

Materials and methods

Fungal strains and genome sequencing

Monokaryons PC9 (CECT20311) and PC15 (CECT20312) were isolated from *P. ostreatus* N001 (CECT20600), and their genomic DNA sequences obtained at JGI in a project coordinated by AG Pisabarro (Public University of Navarre, Pamplona, Spain). The 35.6 Mbp (PC9 v1.0) and 34.3 Mbp (PC15 v2.0) assemblies are predicted to include 12,206 and 12,330 gene models, respectively (the results are available for searching at http://genome.jgi.doe.gov/PleosPC15_2/PleosPC15_2.home.html and http://genome.jgi.doe.gov/PleosPC9_1/PleosPC9_1.home.html).

Genome screening and analysis of peroxidase models

The final inventory of heme peroxidase genes in the *P. ostreatus* genome was obtained by: i) screening the automatically annotated genomes; ii) revising and manually curating the positions of introns, and the N and C termini, using SignalP 3.0 (Center for Biological Sequence Analysis, Kongens Lyngby, Denmark) for predicting signal peptides; iii) comparing the predicted amino acid sequences with related peroxidases, after multiple alignment with MEGA5 (Center for Evolutionary Medicine and Informatics, Tempe, AZ, USA); and iv) confirming the presence of characteristic residues at the heme pocket and substrate oxidation sites, after homology modeling at the Swiss-Model server (Protein Structure Bioinformatics Group, Swiss Institute of Bioinformatics and the Biozentrum of the University of Basel, Basel, Switzerland) using the crystal structures of *P. eryngii* VPL ([PDB:3FJW]) and *P. ostreatus* MnP4 (this study) as templates. Finally, the revised POD sequences from the sequenced genome were compared with all the basidiomycete POD sequences available (up to a total of 237 sequences from 21 genomes and GenBank) and phylograms were constructed with MEGA5, using Poisson-corrected distances and an unweighted pair group method with arithmetic mean (UPGMA) clustering (bootstrap consensus trees were inferred from 1,000 replicates).

Gene synthesis

The revised mature protein-coding sequences of the nine POD genes (models 156336, 199510, 199511, 1041740, 1089546, 1096331, 1099081, and 1113241 from PC15, and model 137757 from PC9) were synthesized by ATG:biosynthetics (Merzhausen, Germany) after verifying that all the codons had previously been used for expressing other genes in the same *E. coli* strains (and substituting them when required). A MnP-encoding gene from *P. pulmonarius* ([GenBank:AAX40734]) was also synthesized for comparison.

Directed mutagenesis

I198F and D261G mutations were introduced in the *P. ostreatus* MnP1 (109633) gene by PCR using the expression plasmid pFLAG1-109633 (see below) as template, and the QuikChange kit from Stratagene (La Jolla, CA, USA). The 5′- CG CCA AAC CTT TTC GAT TCA CAA *TTC* TTC ATC GAG ACG C –3′ (I198F) and 5′- C CGC TTC TCC *GGA* ACG CTG TTC AAG ATG TCG –3′ (D261G) direct primers (mutated codons in italics), and the reverse primers bearing the complementary sequences were synthesized. The PCR reaction (50 μl volume) was carried out in an Eppendorf (Hamburg, Germany) Mastercycler pro S thermal cycler using 20 ng of template DNA, 500 μM each dNTP, 125 ng direct and reverse primers, 2.5 units of *Pfu*Turbo polymerase (Stratagene), and the manufacturer's buffer. Reaction conditions included: i) a start cycle of 1 minute at 95°C; ii) 18 cycles of 50 seconds at 95°C, 50 seconds at 55°C, and 10 minutes at 68°C; and iii) a final cycle of 10 minutes at 68°C. The mutated gene was expressed in *E. coli* and purified as were the wild type genes.

E. coli expression

The nine *P. ostreatus* genome coding sequences and the only *P. pulmonarius* mature POD coding sequences, together with the two *P. ostreatus* MnP1 (10963331) mutated sequences, were cloned in the expression vectors pFLAG1 (International Biotechnologies Inc, Kodak, CT, USA) or pET23a (+) (Novagen, Darmstadt, Germany) and the resulting plasmids (pET23a-156336, pET23a-1099081, pET23a-1041740, pFLAG1-137757,

pFLAG1-199511, pFLAG1-199510, pFLAG1-1089546, pFLAG1-1113241, pFLAG1-1096331, and pFLAG1-AAX40734) were used for expression.

Peroxidases were produced in *E. coli* W3110 (pFLAG1 plasmids) and BL21(DE3)pLysS (pET23a plasmids). Cells were grown for 3 hours in Terrific Broth, induced with 1 mM isopropyl-β-D-thiogalactopyranoside (IPTG), and grown further for 4 hours. The apoenzyme accumulated in inclusion bodies, as observed by SDS-PAGE, and was solubilized with 8 M urea. *In vitro* refolding was performed using 0.16 M urea, 5 mM Ca^{2+}, 20 μM hemin, 0.5 mM oxidized glutathione, 0.1 mM dithiothreitol, and 0.1 mg/ml protein, at pH 9.5 [62]. For *P. ostreatus* MnP6 (1041740) refolding was obtained using 0.1 M urea, 5 mM Ca^{2+}, 20 μM hemin, 1.5 mM oxidized glutathione, 0.1 mM dithiothreitol, and 0.1 mg/ml protein, at pH 8. Enzymes were purified by Resource Q chromatography using a 0 to 300 mM NaCl gradient (2 $ml.min^{-1}$, 20 minutes) in 10 mM sodium tartrate (pH 5.5) containing 1 mM $CaCl_2$ (except for MnP4-1099081, for which pH 6 was used).

Crystallization, data collection, and refinement

Crystallization trials were carried out by the sitting drop vapor diffusion method, in 96-well plates using Wizard screens I to III (Emerald Bio, Bainbridge Island, WA, USA) and JBScreen Kits 1-10 (Jena Biosciences, Jena, Germany) at 22°C. Drops consisted of 0.2 μl of protein solution (10 mg/ml in 10 mM sodium tartrate, pH 5.0) and 0.2 μl of reservoir solution. Crystals of VP1 belonged to three crystal forms in two space groups. Form I belonged to the $P4_3$ group and was obtained in the five following conditions: i) 0.1 M sodium acetate (pH 4.6) containing 8% PEG 4000; ii) 20% PEG 3350 and 0.2 M ammonium chloride; iii) 20% PEG 3350 and 0.2 M ammonium formate; iv) 0.1 M sodium HEPES buffer (pH 7.5) containing 1.6 M ammonium sulfate and 2% PEG 1000; and v) 0.1 M sodium HEPES buffer (pH 7.5) containing 0.2 M sodium acetate and 20% PEG 3000. Form II also belonged to the $P4_3$ group and was obtained in 0.1 M imidazole (pH 8.0) containing 1.0 M K/Na tartrate and 0.2 M NaCl. Form III belonged to the $P2_1$ group and was obtained in 0.1 M sodium acetate (pH 4.5) containing 20% PEG 1000 and 0.2 M zinc acetate. Four different conditions gave two different MnP4 crystal forms. Form I belonged to the P1 group and was obtained in 0.1 M sodium citrate (pH 5.5) containing 2.0 M ammonium sulfate. Finally, form II belonged to the C2 group and was obtained in: i) 0.1 M sodium acetate (pH 4.6) containing 2.0 M ammonium sulfate; ii) 0.1 M Tris-HCl buffer (pH 7.0) containing 2.0 M ammonium sulfate and 0.2 M lithium sulfate; and iii) 0.1 M sodium CAPS buffer (pH 10.5) containing 1.2 M NaH_2PO_4/0.8 M K_2HPO_4 and 0.2 M lithium sulfate. Crystals were mounted in nylon loops and flash-frozen in liquid N_2 in the mother liquor containing various cryoprotectants.

X-ray diffraction data were collected at 100 K at the X06DA and X06SA beam lines at the Swiss Light Source (Villigen, Switzerland) using a wavelength of 1.0000 Å, and Pilatus 2 M and 6 M detectors, respectively. Diffraction data were indexed, integrated, merged, and scaled using XDS and XSCALE. Only the highest resolution structure for each POD (crystal form I) is presented (their data collection statistics are shown in Additional file 2: Table S3).

The structures of VP1 and MnP4 were solved by molecular replacement using the crystal structure of *P. eryngii* VPL (3FMU) as the search model and the program AutoMR of the PHENIX package (Lawrence Berkeley Laboratory, Berkeley, CA, USA). The final models were obtained by successive refinement rounds followed by manual building with Coot using σ_A weighted 2Fo-Fc and Fo-Fc electron density maps. Solvent molecules were introduced in the refinement, as implemented in the PHENIX package, and visually inspected. A total of 5% of reflections was used to calculate the R_{free} value throughout the refinement process. The VP1 final model contained all but the last residue of the sequence (S331) (which did not present any electron density), one heme cofactor, two Ca^{2+} ions, and 452 water molecules; and the MnP4 final model contained all the 337 residues of the sequence, one heme cofactor, two Ca^{2+} ions, and 1,212 water molecules (representative details of the VP1 and MnP4 electron density maps, corresponding to the heme pocket, are shown in Additional file 1: Figure S7). The structures were validated with MolProbity (The Richardson Laboratory, Duke University, Durham, NC, USA). Refinement and final model statistics are shown in Additional file 2: Table S3. Figures were produced with PyMOL (Schrödinger, Portland, OR, USA). The coordinates and structure factors have been deposited with the PDB accession codes [PDB:4BLK] and [PDB:4BM1].

Kinetic constants on selected substrates

Absorbance changes during substrate oxidation in 0.1 M tartrate (at various pH values) were recorded at 25°C in a Biomate5 spectrophotometer (Thermo Scientific, Waltham, MA, USA) using approximately 0.01 μM enzyme concentration, estimated from the ε_{406} of each isoenzyme (Additional file 2: Table S1). The reactions were initiated by H_2O_2 (0.1 mM) addition. Oxidation of Mn^{2+} was followed at pH 5 by monitoring Mn^{3+}.tartrate complex (ε_{238} 6.5 $mM^{-1}.cm^{-1}$) formation. VA oxidation was followed at pH 3 for veratraldehyde (ε_{310} 9.3 $mM^{-1}.cm^{-1}$) formation. RB5, ABTS, and DMP oxidation were assayed at pH 3.5, and monitored for RB5 disappearance (ε_{598} 30 $mM^{-1}.cm^{-1}$) and formation of ABTS cation radical (ε_{436} 29.3 $mM^{-1}.cm^{-1}$) and dimeric coerulignone (ε_{469} 55 $mM^{-1}.cm^{-1}$), respectively. ABTS and DMP oxidation

by VP showed double kinetics, with sigmoidal activity curves at increasing substrate concentration (Additional file 2: Figure S8), that enabled calculation of two sets of kinetic constants. Kinetic constants for enzyme activation by H_2O_2 were determined using 5 mM ABTS (except for MnP1 and MnP6, for which 2 mM was used). Means and standard errors for Michaelis constant (K_m) and enzyme turnover (k_{cat}) values were obtained by nonlinear least-squares fitting to the Michaelis–Menten model. Fitting of these constants to the normalized equation $v = (k_{cat}/K_m)[S]/(1 + [S]/K_m)$ yielded the catalytic efficiency values (k_{cat}/K_m) with their corresponding standard errors.

pH inactivation studies

To study the effect of preincubation at different pH values on activity, the nine PODs were dissolved (0.05 μM) in Britton-Robinson (B&R) buffer with a pH range from 2 to 9, and kept at 4°C for different time periods. Activity was determined by oxidation of a saturating concentration of ABTS (5 mM, except for MnP1-1096331 and MnP6-1041740, for which 2 mM was used) in 0.1 M tartrate (pH 3.5) under the conditions described above. Residual activities were measured after 1 minute (to evaluate the initial survival of the enzyme at each pH value), and 1, 4, 24, and 120 hours of incubation. The highest activity after 1 minute (at any pH) was taken as 100% activity, and the percentage of residual activity at the different times and pH conditions was calculated according to this maximal value. The same experiment was repeated with the more stable (MnP4) and the less stable enzyme (MnP3) by keeping them at 25°C instead of at 4°C.

Thermal inactivation studies

To study the effect of enzyme preincubation at different temperatures on the activity, the nine PODs (0.05 μM) in 10 mM tartrate (pH 5) were incubated at 5°C for 10 minutes or 4 hours in the temperature range of 25 to 70°C. Residual activity was determined at 25°C, as described above, and that obtained after 25°C preincubation was taken as 100%. Temperature stability was presented as 10-minute and 4-hour $T_{50\text{-activity}}$ values, that is, the temperature at which 50% of the activity was lost after incubation for the above time periods.

CD and UV-visible absorption spectroscopy

The effect of pH and temperature on the structure and cofactor binding of different PODs was followed by CD and UV-visible absorption spectroscopies. Far-UV (190 to 250 nm) CD measurements were carried out on a J-720 spectropolarimeter (Jasco, Oklahoma City, OK, USA) equipped with a peltier temperature controller and a thermostated cell holder using a 0.01 cm path length quartz cell. The effect of three pHs (3, 5, and 8) on the CD spectra was estimated at different incubation times (1 minute, 1 hour, and 4 hours) at a protein concentration of approximately 50 μM in 0.1 mM B&R buffer, at 25°C. The spectra from five averaged scans were corrected for the baseline contribution of the buffer and the observed ellipticities were converted into mean residue ellipticities (θ). The effect of temperature on CD spectra was analyzed at a protein concentration of approximately 5 μM in 0.01 mM phosphate (pH 6). Thermal denaturation was estimated by increasing the temperature from 20 to 70°C at 20°C.h^{-1}, and recording the CD signal at 222 nm. T_m represents the temperature at the midpoint of the unfolding transition. UV-visible (300 to 800 nm) absorption spectra of the two proteins after incubation at different pHs and temperatures were obtained on an 8453E diode-array spectrophotometer (Agilent, Santa Clara, CA, USA), using a 1 cm path length quartz cell. The effect of three pHs (3, 5, and 8) after different incubation times (0, 30, 60, 90, 120, 180, and 240 minutes) was estimated at a protein concentration of approximately 3.5 μM in 0.1 mM B&R buffer, at 25°C. The UV-visible spectra of different PODs were also collected in the range of 25 to 70°C, after 10 minutes of incubation at 5°C intervals, using a protein concentration of approximately 2 μM in 10 mM tartrate (pH 5). $T_{50\text{-Soret}}$ represents the temperature at the midpoint of the heme-loss transition, as estimated by the Soret band intensity at 407 nm.

Oxidative degradation of a lignin model dimer

Ring-^{14}C-labeled (1.0 mCi.mmol^{-1}) 4-ethoxy-3-methoxyphenylglycerol-β-guaiacyl ether was prepared, and its erythro and threo isomers were chromatographically separated, as described earlier [63]. The radiolabeled erythro or threo dimer was treated with VP1 (137757) from *P. ostreatus* in 10 mM sodium acetate (pH 3.0) at 25°C for 1 hour. The products formed were analyzed by reversed-phase HPLC using a Gilson (Middleton, WI, USA) system equipped with a C-18 column (Luna C18 (2), Phenomenex, Macclesfield, UK; 150 by 4.6 mm, 5 μm particle size), and methanol:water as mobile phase (35:65 for 15 minutes, followed by 50:50) at a flow rate of 1 ml.min^{-1}. Elution was monitored at 255 nm, and the ^{14}C-content in collected fractions (0.5 ml) was measured in a liquid scintillation counter. HPLC in conjunction with gas chromatography–mass spectrometry (GC-MS) was used in parallel analyses with unlabeled dimers to confirm the identity of the products obtained.

Enzymatic depolymerization of synthetic lignin

A radiolabeled syringyl-guaiacyl DHP (with a syringyl/guaiacyl ratio of approximately 4:1) was prepared by copolymerization of β-[^{14}C]-sinapyl alcohol (0.01 mCi.mmol^{-1}) and unlabeled coniferyl alcohol using horseradish

peroxidase and fractionated on a 1.8 × 30 cm column of Sephadex LH-20 in *N,N*-dimethylformamide. The high molecular mass fractions excluded from the column (>1 kDa) were pooled for use in depolymerization experiments [64].

Enzymatic depolymerization by the same peroxidase used in the dimer degradation assays was investigated in 10 mM Na acetate (pH 4.5) containing 0.25% Tween 20, 1.5×10^4 dpm (188 μg) DHP, and 0.01 μM enzyme in a final volume of 40 ml, in the presence or absence of 10 mM VA. Reactions were conducted at 25°C by adding H_2O_2 (7.5 mM in experiments with VA, and 0.3 mM in experiments without VA) over 24 hours with a syringe pump [22]. Control reactions without enzyme were run for comparison. The reaction mixtures were then concentrated by rotary vacuum evaporation, redissolved in *N,N*-dimethylformamide containing 0.1 M LiCl, and centrifuged as described earlier [22]. Molecular mass distributions of the supernatant fractions were assessed by GPC on a 1.8 × 30 cm column of Sephadex LH20, using *N,N´*-dimethylformamide containing 0.1 M LiCl as the mobile phase. Fractions (2 ml) were collected and assayed for ^{14}C in a liquid scintillation counter.

Additional files

Additional file 1: Sequence comparison, amino acid composition, heterologous expression, pH stability (4°C and 25°C), molecular structure (VP1 and MnP4 differences and heme pockets), and ABTS sigmoidal kinetics (VP1) for different PODs from the *P. ostreatus* genome. Figure S1. Phylogram of heme peroxidase sequences from the genomes of two *P. ostreatus* monokaryons. **Figure S2.** Amino acid composition of the PODs from the *P. ostreatus* genome (predicted mature proteins). **Figure S3.** *E. coli* expression of *P. ostreatus* genome peroxidases (SDS-PAGE). **Figure S4.** pH 2 to 9 stability of the nine PODs from the *P. ostreatus* genome at different incubation times. **Figure S5.** Influence of temperature on the pH stability of PODs from the *P. ostreatus* genome. **Figure S6.** Stereo views of some of the main differences between VP1 and MnP4 crystal structures. **Figure S7.** Partial 2Fo-Fc electron density map, contoured at the 1.1 σ level, of heme cofactor, neighbor residues and several water molecules, and position of surrounding heme pocket residues, in the VP1 and MnP4 crystals. **Figure S8.** Sigmoidal curve for ABTS oxidation by VP (isoenzyme VP1) enabling calculation of two sets of kinetic constants.

Additional file 2: Gene inventory, isoenzyme structural properties, crystallographic data, kinetic constants (native VP1, MnP4 and MnP1, and mutated variants), and sequence identities for different PODs from the *P. ostreatus* genome. Table S1. Inventory of peroxidase genes in the genomes of *P. ostreatus* monokaryons PC9 and PC15 and some characteristics of the purified PODs from *E. coli* expression. **Table S2.** Structural properties potentially related to temperature/pH stability in the nine PODs from the *P. ostreatus* genome, together with experimentally-determined thermal stability ($T_{50\text{-activity}}$) and pH stability range. **Table S3.** Crystallographic data collection and refinement statistics of *P. ostreatus* VP1 and MnP4. **Table S4.** Kinetic constants of W165, E35A, E39A, D175A, and E35A/E39A variants of *P. ostreatus* VP1 oxidizing VA, RB5, and Mn^{2+}, compared with native VP1. **Table S5.** Kinetic constants of E36A, E40A, D179A, and E36A/E40A variants of *P. ostreatus* MnP4 oxidizing Mn^{2+}, compared with native MnP4. **Table S6.** Kinetic constants of two variants in the environment of Trp165 of *P. ostreatus* MnP1, compared with the native MnP1, and a related MnP from *P. pulmonarius* oxidizing VA, RB5, ABTS, DMP, and Mn^{2+}. **Table S7.** Amino acid sequence identities between the nine PODs from the *P. ostreatus* genome, *P. chrysosporium* LiP and MnP, and two *P. eryngii* VPs.

Abbreviations

ABTS: 2,2'-azino-bis(3-ethylbenzothiazoline-6-sulfonate); B&R: Britton-Robinson; CAPS: N-cyclohexyl-3-aminopropanesulfonic acid; CD: Circular dichroism; DHP: Dehydrogenation polymer (lignin); DMP: 2,6-dimethoxyphenol; dNTP: Deoxyribonucleotide triphosphates; DOE: Department of Energy; DyP: Dye-decolorizing peroxidase; GC-MS: Gas chromatography–mass spectrometry; GP: Generic peroxidase; GPC: Gel permeation chromatography; HEPES: 4-(2-hydroxyethyl)-1-piperazineethanesulfonic acid; HPLC: High performance liquid chromatography; HTP: Heme-thiolate peroxidase; IPTG: Isopropyl-β-D-thiogalactopyranoside; JGI: Joint Genome Institute; k_{cat}: Catalytic constant; K_m: Michaelis constant; LiP: Lignin peroxidase; LRET: Long-range electron transfer; MnP: Manganese peroxidase; PCR: Polymerase chain reaction; PDB: Protein Data Bank; PEG: Polyethylene glycol; POD: Class II peroxidase from the superfamily of non-animal (plant-fungal-prokaryotic) peroxidases; RB5: Reactive Black 5; Rz: Reinheitszahl; UPGMA: Unweighted pair group method with arithmetic mean; VA: Veratryl alcohol; VP: Versatile peroxidase.

Competing interests

The authors declare that they have no competing interests.

Authors' contributions

ATM and FJR-D conceived and designed the experiments. FJM carried out the crystallographic study. EF-F, FJR-D, and FJM performed the experiments. EF-F, FJR-D, FJM, AR, MJM, KEH, and ATM analyzed the data. ATM, FJM, and KEH wrote the paper. All authors read and approved the final manuscript.

Acknowledgements

This work was supported by the PEROXICATS (KBBE-2010-4-265397) and INDOX (KBBE-2013-7-613549) grants of the European Union (to ATM), by grants BIO2011-26694 (to FJR-D) and BFU2011-24615 (to AR) of the Spanish Ministry of Economy and Competitiveness (MINECO), and by US DOE grant DE-AI02-07ER64480 (to KEH). The work conducted by the US DOE JGI is supported by the Office of Science of the US DOE under contract number DE-AC02-05CH11231. AG Pisabarro (Public University of Navarre, Pamplona, Spain) is acknowledged for coordinating the *P. ostreatus* genome project. We thank Michael D Mozuch for assistance with the lignin depolymerization studies. EF-F acknowledges a Junta de Ampliación de Estudios fellowship of the CSIC, co-funded by the European Social Fund, and FJR-D acknowledges a MINECO Ramón y Cajal contract.

Received: 26 September 2013 Accepted: 16 December 2013
Published: 3 January 2014

References

1. Sánchez C: **Cultivation of *Pleurotus ostreatus* and other edible mushrooms.** *Appl Microbiol Biotechnol* 2010, **85:**1321–1337.
2. Gunde-Cimerman N, Cimerman A: ***Pleurotus* fruiting bodies contain the inhibitor of 3-hydroxy-3-methylglutaryl-coenzyme-A reductase-lovastatin.** *Exp Mycol* 1995, **19:**1–6.
3. Lavi I, Levinson D, Peri I, Tekoah Y, Hadar Y, Schwartz B: **Chemical characterization, antiproliferative and antiadhesive properties of polysaccharides extracted from Pleurotus pulmonarius mycelium and fruiting bodies.** *Appl Microbiol Biotechnol* 2010, **85:**1977–1990.
4. Ruiz-Dueñas FJ, Martínez AT: **Microbial degradation of lignin: how a bulky recalcitrant polymer is efficiently recycled in nature and how we can take advantage of this.** *Microbial Biotechnol* 2009, **2:**164–177.
5. Martínez AT, Camarero S, Guillén F, Gutiérrez A, Muñoz C, Varela E, Martínez MJ, Barrasa JM, Ruel K, Pelayo M: **Progress in biopulping of non-woody materials: chemical, enzymatic and ultrastructural aspects of wheat-straw delignification with ligninolytic fungi from the genus *Pleurotus*.** *FEMS Microbiol Rev* 1994, **13:**265–274.
6. Young RA, Akhtar M: *Environmentally Friendly Technologies for the Pulp and Paper Industry.* New York: John Wiley and Sons; 1998.
7. Camarero S, Barrasa JM, Pelayo M, Martínez AT: **Evaluation of *Pleurotus* species for wheat-straw biopulping.** *J Pulp Paper Sci* 1998, **24:**197–203.
8. Valmaseda M, Almendros G, Martínez AT: **Chemical transformation of wheat straw constituents after solid-state fermentation with selected lignocellulose-degrading fungi.** *Biomass and Bioenergy* 1991, **1:**261–266.
9. Salvachúa D, Prieto A, Lopez-Abelairas M, Lú-Chau T, Martínez AT, Martínez MJ: **Fungal pretreatment: an alternative in second-generation ethanol from wheat straw.** *Bioresource Technol* 2011, **102:**7500–7506.

10. Ragauskas AJ, Williams CK, Davison BH, Britovsek G, Cairney J, Eckert CA, Frederick WJ, Hallett JP, Leak DJ, Liotta CL, Mielenz JR, Murphy R, Templer R, Tschaplinski T: **The path forward for biofuels and biomaterials.** *Science* 2006, **311:**484–489.
11. Martínez AT, Ruiz-Dueñas FJ, Martínez MJ, del Río JC, Gutiérrez A: **Enzymatic delignification of plant cell wall: from nature to mill.** *Curr Opin Biotechnol* 2009, **20:**348–357.
12. Martinez D, Larrondo LF, Putnam N, Gelpke MD, Huang K, Chapman J, Helfenbein KG, Ramaiya P, Detter JC, Larimer F, Coutinho PM, Henrissat B, Berka R, Cullen D, Rokhsar D: **Genome sequence of the lignocellulose degrading fungus *Phanerochaete chrysosporium* strain RP78.** *Nat Biotechnol* 2004, **22:**695–700.
13. Martinez D, Challacombe J, Morgenstern I, Hibbett D, Schmoll M, Kubicek CP, Ferreira P, Ruiz-Duenas FJ, Martinez AT, Kersten P, Hammel KE, Vanden Wymelenberg A, Gaskell J, Lindquist E, Sabat G, Bondurant SS, Larrondo LF, Canessa P, Vicuna R, Yadav J, Doddapaneni H, Subramanian V, Pisabarro AG, Lavín JL, Oguiza JA, Master E, Henrissat B, Coutinho PM, Harris P, Magnuson JK, *et al*: **Genome, transcriptome, and secretome analysis of wood decay fungus *Postia placenta* supports unique mechanisms of lignocellulose conversion.** *Proc Natl Acad Sci U S A* 2009, **106:**1954–1959.
14. Eastwood DC, Floudas D, Binder M, Majcherczyk A, Schneider P, Aerts A, Asiegbu FO, Baker SE, Barry K, Bendiksby M, Blumentritt M, Coutinho PM, Cullen D, de Vries RP, Gathman A, Goodell B, Henrissat B, Ihrmark K, Kauserud H, Kohler A, LaButti K, Lapidus A, Lavin JL, Lee YH, Lindquist E, Lilly W, Lucas S, Morin E, Murat C, Oguiza JA, *et al*: **The plant cell wall-decomposing machinery underlies the functional diversity of forest fungi.** *Science* 2011, **333:**762–765.
15. Fernandez-Fueyo E, Ruiz-Dueñas FJ, Ferreira P, Floudas D, Hibbett DS, Canessa P, Larrondo LF, James TY, Seelenfreund D, Lobos S, Polanco R, Tello M, Honda Y, Watanabe T, Watanabe T, Ryu JS, Kubicek CP, Schmoll M, Gaskell J, Hammel KE, St John FJ, Vanden Wymelenberg A, Sabat G, Splinter BonDurant S, Syed K, Yadav JS, Doddapaneni H, Subramanian V, Lavín JL, Oguiza JA, *et al*: **Comparative genomics of *Ceriporiopisis subvermispora* and *Phanerochaete chrysosporium* provide insight into selective ligninolysis.** *Proc Natl Acad Sci U S A* 2012, **109:**5458–5463.
16. Floudas D, Binder M, Riley R, Barry K, Blanchette RA, Henrissat B, Martínez AT, Otillar R, Spatafora JW, Yadav JS, Aerts A, Benoit I, Boyd A, Carlson A, Copeland A, Coutinho PM, de Vries RP, Ferreira P, Findley K, Foster B, Gaskell J, Glotzer D, Górecki P, Heitman J, Hesse C, Hori C, Igarashi K, Jurgens JA, Kallen N, Kersten P, *et al*: **The Paleozoic origin of enzymatic lignin decomposition reconstructed from 31 fungal genomes.** *Science* 2012, **336:**1715–1719.
17. Ruiz-Dueñas FJ, Fernández E, Martínez MJ, Martínez AT: ***Pleurotus ostreatus* heme peroxidases: an *in silico* analysis from the genome sequence to the enzyme molecular structure.** *C R Biol* 2011, **334:**795–805.
18. Martínez AT: **Molecular biology and structure-function of lignin-degrading heme peroxidases.** *Enzyme Microb Technol* 2002, **30:**425–444.
19. Ruiz-Dueñas FJ, Martínez AT: **Structural and functional features of peroxidases with a potential as industrial biocatalysts**. In *Biocatalysts Based on Heme Peroxidases*. Edited by Torres E, Ayala M. Berlin: Springer; 2010:37–59.
20. Sugano Y, Muramatsu R, Ichiyanagi A, Sato T, Shoda M: **DyP, a unique dye-decolorizing peroxidase, represents a novel heme peroxidase family.** *J Biol Chem* 2007, **282:**36652–36658.
21. Asada Y, Watanabe A, Irie T, Nakayama T, Kuwahara M: **Structures of genomic and complementary DNAs coding for *Pleurotus ostreatus* manganese (II) peroxidase.** *Biochim Biophys Acta* 1995, **1251:**205–209.
22. Hammel KE, Jensen KA, Mozuch MD, Landucci LL, Tien M, Pease EA: **Ligninolysis by a purified lignin peroxidase.** *J Biol Chem* 1993, **268:**12274–12281.
23. Giardina P, Palmieri G, Fontanella B, Rivieccio V, Sannia G: **Manganese peroxidase isoenzymes produced by *Pleurotus ostreatus* grown on wood sawdust.** *Arch Biochem Biophys* 2000, **376:**171–179.
24. Irie T, Honda Y, Ha H-C, Watanabe T, Kuwahara M: **Isolation of cDNA and genomic fragments encoding the major manganese peroxidase isoenzyme from the white rot basidiomycete *Pleurotus ostreatus*.** *J Wood Sci* 2000, **46:**230–233.
25. Kamitsuji H, Honda Y, Watanabe T, Kuwahara M: **Production and induction of manganese peroxidase isozymes in a white-rot fungus *Pleurotus ostreatus*.** *Appl Microbiol Biotechnol* 2004, **65:**287–294.
26. Sarkar S, Martínez AT, Martínez MJ: **Biochemical and molecular characterization of a manganese peroxidase isoenzyme from *Pleurotus ostreatus*.** *Biochim Biophys Acta* 1997, **1339:**23–30.
27. Ruiz-Dueñas FJ, Martínez MJ, Martínez AT: **Molecular characterization of a novel peroxidase isolated from the ligninolytic fungus *Pleurotus eryngii*.** *Mol Microbiol* 1999, **31:**223–236.
28. Camarero S, Sarkar S, Ruiz-Dueñas FJ, Martínez MJ, Martínez AT: **Description of a versatile peroxidase involved in natural degradation of lignin that has both Mn-peroxidase and lignin-peroxidase substrate binding sites.** *J Biol Chem* 1999, **274:**10324–10330.
29. Ruiz-Dueñas FJ, Morales M, García E, Miki Y, Martínez MJ, Martínez AT: **Substrate oxidation sites in versatile peroxidase and other basidiomycete peroxidases.** *J Exp Bot* 2009, **60:**441–452.
30. Mester T, Ambert-Balay K, Ciofi-Baffoni S, Banci L, Jones AD, Tien M: **Oxidation of a tetrameric nonphenolic lignin model compound by lignin peroxidase.** *J Biol Chem* 2001, **276:**22985–22990.
31. Heinfling A, Ruiz-Dueñas FJ, Martínez MJ, Bergbauer M, Szewzyk U, Martínez AT: **A study on reducing substrates of manganese-oxidizing peroxidases from *Pleurotus eryngii* and *Bjerkandera adusta*.** *FEBS Lett* 1998, **428:**141–146.
32. Morales M, Mate MJ, Romero A, Martínez MJ, Martínez AT, Ruiz-Dueñas FJ: **Two oxidation sites for low redox-potential substrates: a directed mutagenesis, kinetic and crystallographic study on *Pleurotus eryngii* versatile peroxidase.** *J Biol Chem* 2012, **287:**41053–41067.
33. Palma C, Martínez AT, Lema J, Martínez MJ: **Different fungal manganese-oxidizing peroxidases: a comparison between *Bjerkandera* sp. and *Phanerochaete chrysosporium*.** *J Biotechnol* 2000, **77:**235–245.
34. Steffen KT, Hofrichter M, Hatakka A: **Purification and characterization of manganese peroxidases from the litter-decomposing basidiomycetes *Agrocybe praecox* and *Stropharia coronilla*.** *Enzyme Microb Technol* 2002, **30:**550–555.
35. Ruiz-Dueñas FJ, Pogni R, Morales M, Giansanti S, Mate MJ, Romero A, Martínez MJ, Basosi R, Martínez AT: **Protein radicals in fungal versatile peroxidase: catalytic tryptophan radical in both compound I and compound II and studies on W164Y, W164H and W164S variants.** *J Biol Chem* 2009, **284:**7986–7994.
36. Sundaramoorthy M, Kishi K, Gold MH, Poulos TL: **The crystal structure of manganese peroxidase from *Phanerochaete chrysosporium* at 2.06-Å resolution.** *J Biol Chem* 1994, **269:**32759–32767.
37. Sundaramoorthy M, Youngs HL, Gold MH, Poulos TL: **High-resolution crystal structure of manganese peroxidase: substrate and inhibitor complexes.** *Biochemistry* 2005, **44:**6463–6470.
38. Sundaramoorthy M, Gold MH, Poulos TL: **Ultrahigh (0.93 angstrom) resolution structure of manganese peroxidase from *Phanerochaete chrysosporium*: Implications for the catalytic mechanism.** *J Inorg Biochem* 2010, **104:**683–690.
39. Poulos TL, Edwards SL, Wariishi H, Gold MH: **Crystallographic refinement of lignin peroxidase at 2 Å.** *J Biol Chem* 1993, **268:**4429–4440.
40. Khindaria A, Yamazaki I, Aust SD: **Stabilization of the veratryl alcohol cation radical by lignin peroxidase.** *Biochemistry* 1996, **35:**6418–6424.
41. Glumoff T, Harvey PJ, Molinari S, Goble M, Frank G, Palmer JM, Smit JDG, Leisola MSA: **Lignin peroxidase from *Phanerochaete chrysosporium*. Molecular and kinetic characterization of isozymes.** *Eur J Biochem* 1990, **187:**515–520.
42. Farrell RL, Murtagh KE, Tien M, Mozuch MD, Kirk KT: **Physical and enzymatic properties of lignin peroxidase isoenzimes from *Phanerochaete chrysosporium*.** *Enzyme Microb Technol* 1989, **11:**322–328.
43. Cullen D: **Recent advances on the molecular genetics of ligninolytic fungi.** *J Biotechnol* 1997, **53:**273–289.
44. Rothschild N, Hadar Y, Dosoretz CG: **Lignin peroxidase isozymes from *Phanerochaete chrysosporium* can be enzymatically dephosphorylated.** *Appl Environ Microbiol* 1997, **63:**857–861.
45. Johansson T, Welinder KG, Nyman PO: **Isozymes of lignin peroxidase and manganese(II) peroxidase from the white-rot basidiomycete *Trametes versicolor*. II. Partial sequences, peptide maps, and amino acid and carbohydrate compositions.** *Arch Biochem Biophys* 1993, **300:**57–62.
46. Ruiz-Dueñas FJ, Lundell T, Floudas D, Nagy LG, Barrasa JM, Hibbett DS, Martínez AT: **Lignin-degrading peroxidases in Polyporales: an evolutionary survey based on ten sequenced genomes.** *Mycologia* 2013, **105:**1428–1444.
47. Fernández-Fueyo E, Ruiz-Dueñas FJ, Miki Y, Martínez MJ, Hammel KE, Martínez AT: **Lignin-degrading peroxidases from genome of selective ligninolytic fungus *Ceriporiopsis subvermispora*.** *J Biol Chem* 2012, **287:**16903–16906.
48. Salame TM, Knop D, Levinson D, Yarden O, Hadar Y: **Redundancy among manganese peroxidases in *Pleurotus ostreatus*.** *Appl Environ Microbiol* 2013, **79:**2405–2415.

49. Zervakis G, Philippoussis A, Ioannidou S, Diamantopoulou P: **Mycelium growth kinetics and optimal temperature conditions for the cultivation of edible mushroom species on lignocellulosic substrates.** *Folia Microbiol Prague* 2001, **46:**231–234.
50. Sakharov IY: **Palm tree peroxidases.** *Biochemistry Engl Tr* 2004, **69:**823–829.
51. Tuisel H, Sinclair R, Bumpus JA, Ashbaugh W, Brock BJ, Aust SD: **Lignin peroxidase H2 from *Phanerochaete chrysosporium*: purification, characterization and stability to temperature and pH.** *Arch Biochem Biophys* 1990, **279:**158–166.
52. Youngs HL, Moënne-Loccoz P, Loehr TM, Gold MH: **Formation of a bis (histidyl) heme iron complex in manganese peroxidase at high pH and restoration of the native enzyme structure by calcium.** *Biochemistry* 2000, **39:**9994–10000.
53. George SJ, Kvaratskhelia M, Dilworth MJ, Thorneley RNF: **Reversible alkaline inactivation of lignin peroxidase involves the release of both the distal and proximal site calcium ions and bishistidine co-ordination of the haem.** *Biochem J* 1999, **344:**237–244.
54. Fu HL, Grimsley GR, Razvi A, Scholtz JM, Pace CN: **Increasing protein stability by improving b-turns.** *Proteins* 2009, **77:**491–498.
55. Zakharova GS, Uporov IV, Tishkov VI: **Horseradish peroxidase: modulation of properties by chemical modification of protein and heme.** *Biochemistry (Mosc)* 2011, **76:**1391–1401.
56. Liers C, Bobeth C, Pecyna M, Ullrich R, Hofrichter M: **DyP-like peroxidases of the jelly fungus *Auricularia auricula-judae* oxidize nonphenolic lignin model compounds and high-redox potential dyes.** *Appl Microbiol Biotechnol* 2010, **85:**1869–1879.
57. Ahmad M, Roberts JN, Hardiman EM, Singh R, Eltis LD, Bugg TDH: **Identification of DypB from *Rhodococcus jostii* RHA1 as a lignin peroxidase.** *Biochemistry* 2011, **50:**5096–5107.
58. Kinne M, Poraj-Kobielska M, Ullrich R, Nousiainen P, Sipila J, Scheibner K, Hammel KE, Hofrichter M: **Oxidative cleavage of non-phenolic beta-O-4 lignin model dimers by an extracellular aromatic peroxygenase.** *Holzforschung* 2011, **65:**673–679.
59. Hofrichter M, Ullrich R, Pecyna MJ, Liers C, Lundell T: **New and classic families of secreted fungal heme peroxidases.** *Appl Microbiol Biotechnol* 2010, **87:**871–897.
60. Tien M, Kirk TK: **Lignin-degrading enzyme from the hymenomycete *Phanerochaete chrysosporium* Burds.** *Science* 1983, **221:**661–663.
61. Wariishi H, Valli K, Gold MH: **Manganese(II) oxidation by manganese peroxidase from the basidiomycete *Phanerochaete chrysosporium*. Kinetic mechanism and role of chelators.** *J Biol Chem* 1992, **267:**23688–23695.
62. Pérez-Boada M, Doyle WA, Ruiz-Dueñas FJ, Martínez MJ, Martínez AT, Smith AT: **Expression of *Pleurotus eryngii* versatile peroxidase in *Escherichia coli* and optimisation of *in vitro* folding.** *Enzyme Microb Technol* 2002, **30:**518–524.
63. Srebotnik E, Jensen KA, Hammel KE: **Fungal degradation of recalcitrant nonphenolic lignin structures without lignin peroxidase.** *Proc Natl Acad Sci U S A* 1994, **91:**12794–12797.
64. Shary S, Ralph SA, Hammel KE: **New insights into the ligninolytic capability of a wood decay ascomycete.** *Appl Environ Microbiol* 2007, **73:**6691–6694.

doi:10.1186/1754-6834-7-2
Cite this article as: Fernández-Fueyo *et al.*: Ligninolytic peroxidase genes in the oyster mushroom genome: heterologous expression, molecular structure, catalytic and stability properties, and lignin-degrading ability. *Biotechnology for Biofuels* 2014 **7**:2.

Capítulo 4

"**Ligninolytic peroxidase gene expression by *Pleurotus ostreatus*: Differential regulation in lignocellulose medium and effect of temperature and pH"**
Fernández-Fueyo, E., R. Castanera, F. J. Ruiz-Dueñas, M. F. López-Lucendo, L. Ramírez, A. G. Pisabarro, and A. T. Martínez.
Fungal Genet. Biol. 2014.

Fungal Genetics and Biology xxx (2014) xxx–xxx

Contents lists available at ScienceDirect

Fungal Genetics and Biology

journal homepage: www.elsevier.com/locate/yfgbi

Ligninolytic peroxidase gene expression by *Pleurotus ostreatus*: Differential regulation in lignocellulose medium and effect of temperature and pH

Elena Fernández-Fueyo [a], Raul Castanera [b], Francisco J. Ruiz-Dueñas [a], María F. López-Lucendo [a], Lucía Ramírez [b], Antonio G. Pisabarro [b], Angel T. Martínez [a,*]

[a] Centro de Investigaciones Biológicas, CSIC, Ramiro de Maeztu 9, E-28006 Madrid, Spain
[b] Department of Agrarian Production, Universidad Pública de Navarra, E-31006 Pamplona, Spain

ARTICLE INFO

Article history:
Available online xxxx

Keywords:
Pleurotus ostreatus
Manganese peroxidases
Versatile peroxidases
Secretome analysis
Quantitative PCR
Differential expression

ABSTRACT

Pleurotus ostreatus is an important edible mushroom and a model lignin degrading organism, whose genome contains nine genes of ligninolytic peroxidases, characteristic of white-rot fungi. These genes encode six manganese peroxidase (MnP) and three versatile peroxidase (VP) isoenzymes. Using liquid chromatography coupled to tandem mass spectrometry, secretion of four of these peroxidase isoenzymes (VP1, VP2, MnP2 and MnP6) was confirmed when *P. ostreatus* grows in a lignocellulose medium at 25 °C (three more isoenzymes were identified by only one unique peptide). Then, the effect of environmental parameters on the expression of the above nine genes was studied by reverse transcription-quantitative PCR by changing the incubation temperature and medium pH of *P. ostreatus* cultures pre-grown under the above conditions (using specific primers and two reference genes for result normalization). The cultures maintained at 25 °C (without pH adjustment) provided the highest levels of peroxidase transcripts and the highest total activity on Mn^{2+} (a substrate of both MnP and VP) and Reactive Black 5 (a VP specific substrate). The global analysis of the expression patterns divides peroxidase genes into three main groups according to the level of expression at optimal conditions (*vp1/mnp3* > *vp2/vp3/mnp1/mnp2/mnp6* > *mnp4/mnp5*). Decreasing or increasing the incubation temperature (to 10 °C or 37 °C) and adjusting the culture pH to acidic or alkaline conditions (pH 3 and 8) generally led to downregulation of most of the peroxidase genes (and decrease of the enzymatic activity), as shown when the transcription levels were referred to those found in the cultures maintained at the initial conditions. Temperature modification produced less dramatic effects than pH modification, with most genes being downregulated during the whole 10 °C treatment, while many of them were alternatively upregulated (often 6 h after the thermal shock) and downregulated (12 h) at 37 °C. Interestingly, *mnp4* and *mnp5* were the only peroxidase genes upregulated under alkaline pH conditions. The differences in the transcription levels of the peroxidase genes when the culture temperature and pH parameters were changed suggest an adaptive expression according to environmental conditions. Finally, the intracellular proteome was analyzed, under the same conditions used in the secretomic analysis, and the protein product of the highly-transcribed gene *mnp3* was detected. Therefore, it was concluded that the absence of MnP3 from the secretome of the *P. ostreatus* lignocellulose cultures was related to impaired secretion.

1. Introduction

Pleurotus ostreatus, the oyster mushroom, is the second in importance edible fungus worldwide (Sánchez, 2010). From an ecophysiological point of view, *Pleurotus* species belong to the group of fungi causing the so-called white rot of wood and other lignocellulosic materials, due to their ability to degrade the recalcitrant lignin polymer that protects polysaccharides in vascular plants (Ruiz-Dueñas and Martínez, 2009). Among these fungi, *Pleurotus* species are of biotechnological interest because some of them degrade lignin selectively (i.e., with a limited attack on cellulose) when growing on cereal straw and related materials (Martínez et al., 1994). Biological delignification with lignin-degrading fungi saves energy and chemicals in the manufacture of cellulose pulp from woody (Young and Akhtar, 1998) and non-woody (Camarero

* Corresponding author.
E-mail address: ATMartinez@cib.csic.es (A.T. Martínez).

http://dx.doi.org/10.1016/j.fgb.2014.02.003
1087-1845/

et al., 1998) plant feedstocks, and can be also of interest in the production of second generation bioethanol (Salvachúa et al., 2011).

Since the sequencing of white-rot *Phanerochaete chrysosporium* genome in 2004 (Martinez et al., 2004), many other basidiomycete genomes have been sequenced, up to a total of 90 by the JGI (http://www.jgi.doe.gov), as those of *Postia placenta* (first brown-rot fungal genome) (Martinez et al., 2009), *Ceriporiopsis subvermispora* (first selective white-rot fungal genome) (Fernández-Fueyo et al., 2012) and *P. ostreatus*. According to the genomic data, ligninolytic peroxidases – including lignin peroxidase (LiP), manganese peroxidase (MnP) and versatile peroxidase (VP) – are exclusive of lignin-degrading white-rot basidiomycetes, being absent from polysaccharide-degrading brown-rot basidiomycetes (Floudas et al., 2012). The above distribution of ligninolytic peroxidase genes in basidiomycete genomes confirms its central role in lignin biodegradation. *In vitro* degradation of lignin was first reported for LiP (Tien and Kirk, 1983; Hammel et al., 1993) and recently for VP (Fernández-Fueyo et al., 2014), being ligninolytic enzymes largely investigated because of their biotechnological interest (Martínez et al., 2009).

The existence of multiple isoforms (isoenzymes) is a well-known phenomenon among degradative enzymes secreted by fungi, already described years ago for ligninolytic peroxidases (Farrell et al., 1989; Glumoff et al., 1990). However, the biochemical and operational differences between isoenzymes remain largely unknown. The availability of genomes provides evidence on the large and widespread duplication of peroxidase genes in white-rot basidiomycetes (Martinez et al., 2004; Floudas et al., 2012; Fernández-Fueyo et al., 2012; Ruiz-Dueñas et al., 2013). Our preliminary *in silico* analysis of the *P. ostreatus* genome (Ruiz-Dueñas et al., 2011) indicated the presence of nine genes encoding five MnP and four VP isoenzymes, and the absence of genes encoding LiP and generic peroxidases (a fourth non-ligninolytic peroxidase family at the class II of the superfamily of plant-fungal-prokaryotic peroxidases) (Ruiz-Dueñas and Martínez, 2010). The heterologous expression of these nine genes showed the existence of three VPs and six MnPs in *P. ostreatus* (including an unusual MnP that had been *in silico* classified as a VP) with significant differences in their pH and temperature stabilities suggesting environmental regulation (Fernández-Fueyo et al., 2014).

Media composition and fungal growth conditions strongly affect the production of ligninolytic enzymes and the extent of lignin degradation, e.g. no ligninolytic peroxidase activity is produced by *Pleurotus* species in the synthetic medium used to produce these enzymes in *P. chrysosporium*, while activity was found in peptone and lignocellulose cultures (Martínez et al., 1996). Transcriptional regulation of *vp* and *mnp* genes has been investigated in *Pleurotus* species (Ruiz-Dueñas et al., 1999; Cohen et al., 2001). Differential expression is also characteristic among the members of a gene family, including ligninolytic peroxidase isoenzymes (Salame et al., 2010; MacDonald et al., 2011; Wymelenberg et al., 2011). Recently, the effect of natural (lignocellulosic) vs. simple (glucose) C sources has been addressed in different transcriptomic studies on sequenced wood-rotting basidiomycetes (Martinez et al., 2009; Sato et al., 2009; Wymelenberg et al., 2011; Fernández-Fueyo et al., 2012). Reverse transcription followed by quantitative PCR (RT-qPCR) represents the most powerful technology to quantitatively amplify trace amounts of mRNA (Heid et al., 1996; Pfaffl, 2004). Moreover, RT-qPCR is considered the gold standard for measuring gene expression (Qin et al., 2006) because of its high sensitivity and specificity, robust reproducibility, and wide dynamic range (Pfaffl and Hageleit, 2001). However, this technique requires the careful selection and validation of reference genes (internal standards), which are processed in parallel with the target gene (Ling and Salvaterra, 2011). Moreover, it is critical to determine the amplification efficiency (Pfaffl, 2001; Ramakers et al., 2003), which is used in mathematical models for the accurate estimation of the expression levels.

In the present study, we analyze the ligninolytic peroxidases secreted by *P. ostreatus* when grown in a culture medium with lignocellulose as the sole carbon (and nitrogen) source, by activity estimation and isoenzyme identification by nanoflow liquid chromatography coupled to tandem mass spectrometry (nLC-MS/MS) of a whole secretome hydrolyzate. Then, we designed specific primers for each of the corresponding transcripts, and used RT-qPCR to quantify the differential expression of the nine peroxidase genes when the cultures were transferred to extreme pH (3 and 8) and temperature (10 °C and 37 °C), compared with those maintained at optimal conditions (25 °C and pH 5.5), using two reference genes that were validated for the present qPCR experiments. Finally, an intracellular proteomic study was performed to explain some differences between the results from the previous transcriptomic and secretomic analyses.

2. Material and methods

2.1. P. ostreatus strain and genome

Monokaryotic *P. ostreatus* PC9 (CECT-20311) was used in this study. This strain is a protoclone obtained by dedikaryotization from the commercial dikaryon N001 (CECT-20600) (Larraya et al., 1999). The fungus was maintained in 2% malt extract agar.

The genomic sequence of *P. ostreatus* PC9 is available at the JGI website (http://genome.jgi-psf.org/PleosPC9_1), together with that of the second monokaryon PC15, after sequencing in a project coordinated by A.G. Pisabarro. The manual annotation of nine ligninolytic peroxidase gene models in the PC9 genome, including intron positions and N/C termini, has been already described (Ruiz-Dueñas et al., 2011).

In addition, 1 kb promoter fragment from each of the nine *P. ostreatus* (PC9) ligninolytic peroxidase genes was manually analyzed looking for the presence of conserved regulatory and other promoter elements (Janusz et al., 2013) (see Supplemental Information Section S1, for the specific sequences searched).

2.2. Fungal growth in lignocellulose medium

Lignocellulose cultures were carried out at 25 °C on 5 g of a mixture of milled wheat straw and small poplar chips (particle size <4 mm, ratio 1:1) soaked with 35 mL of distilled water (unadjusted pH 5.5) in glass flasks at a surface to volume ratio of 1 cm^{-1} (hereinafter referred as standard conditions). Inocula consisted of 15 mL of homogenized actively growing mycelium from liquid cultures grown at 200 rpm in the dark in M7GY medium, comprising (per liter) 2 g ammonium tartrate, 0.5 g $MgSO_4{\cdot}7\ H_20$, 1 g KH_2PO_4, 0.5 g KCl, 10 g glucose, and 1 ml element's trace solution (0.1 g $Na_2B_4O_7{\cdot}H_2O$, 0.07 g $ZnSO_4$, 0.01 g $CuSO_4{\cdot}5\ H_2O$, 0.01 g $MnSO_4{\cdot}4\ H_2O$, 0.05 g $FeSO_4{\cdot}7\ H_2O$, 0.01 g $(NH_4)_6Mo_7O_2{\cdot}4\ H_2O$ per liter) (Castanera et al., 2012).

To study the expression of the nine ligninolytic peroxidase genes when temperature turned to be nearly limiting for fungal growth, twenty-four 7-day-old flask cultures were transferred to 10 °C or 37 °C (twelve flasks per condition) and incubated for additional 24 h to study the effect of temperature change on the transcript levels along the time (twelve additional flasks were maintained at 25 °C and used as reference). In a similar way, other twenty-four 7-day-old cultures were adjusted to pH 3 or 8 (twelve flasks per condition) by adding 0.2 M Brighton&Robin buffer pH 2 or 9, respectively, and incubated for 24 h to study the effect of extreme pH on the transcription levels (the twelve flasks

Please cite this article in press as: Fernández-Fueyo, E., et al. Ligninolytic peroxidase gene expression by *Pleurotus ostreatus*: Differential regulation in lignocellulose medium and effect of temperature and pH. Fungal Genet. Biol. (2014), http://dx.doi.org/10.1016/j.fgb.2014.02.003

maintained at 25 °C, without pH adjustment, were used as reference). In both cases, three replicate flasks were sampled after 1, 6, 12 and 24 h, combined and analyzed as described below.

2.3. Enzymatic activities

For enzymatic activity measurements, three technical replicates (1 mL each) were collected from each biological replicate and centrifuged at 15,000 rpm for 5 min at 4 °C to remove debris. Peroxidase activity was determined using a Biomate5 (Thermo Scientific) spectrophotometer for following the oxidation of 3 mM Mn^{2+}, 10 μM Reactive Black 5 (RB5) and 5 mM 2,2′-azino-bis(3-ethylbenzothiazoline-6-sulfonic acid) (ABTS) in 0.1 M sodium tartrate, at different pH values, in the presence/absence of 0.1 mM H_2O_2. Mn^{2+} oxidation was followed at pH 5 for the formation of Mn^{3+} tartrate complex (ε_{238} 6.5 mM^{-1} cm^{-1}). RB5 and ABTS oxidation were assayed at pH 3.5 by monitoring RB5 disappearance (ε_{598} 30 mM^{-1} cm^{-1}) and formation of ABTS cation radical (ε_{436} 29.3 mM^{-1} cm^{-1}), respectively. Reactions were at 25 °C being initiated by the addition of H_2O_2. One enzymatic activity unit was defined as the amount of enzyme that oxidizes 1 μmol of substrate in 1 min.

2.4. Analysis of P. ostreatus extracellular and intracellular proteomes

For secretomic analysis, total extracellular proteins in the filtrate of a *P. ostreatus* culture grown in lignocellulose medium for seven days under standard conditions were concentrated, dialyzed against 10 mM sodium acetate (pH 4.3), and centrifuged. The soluble proteins were concentrated and impurities removed by a short polyacrylamide gel electrophoresis (PAGE) run, followed by Colloidal Blue Kit (Invitrogen) staining. The total protein band was cut and destained using 50 mM ammonium bicarbonate in 50% acetonitrile (ACN), reduced with 10 mM dithiothreitol for 30 min at 56 °C, alkylated with 55 mM iodoacetamide in obscurity for 30 min (24 °C) and digested with 12.5 ng μl^{-1} trypsin in 50 mm ammonium bicarbonate, overnight at 30 °C. Peptides were extracted at 37 °C using 100% ACN and them 0.5% trifluoroacetic acid, dried, cleaned using ZipTip with 0.6 μl C18 resin (Millipore), and reconstituted in 5 μl of 0.1% formic acid in 2% ACN.

The tryptic peptides were analyzed in an LTQ-Orbitrap Velos mass spectrometer (Thermo Scientific) coupled to a nanoEasy high-performance liquid chromatography (HPLC) equipment (Proxeon). Peptides were first trapped onto a C18-A1 ASY-Column 2 cm precolumn (Thermo Scientific), and then eluted onto a Biosphere C18 column (75 μm inner diameter, 15 cm long and 3 μm particle size) (NanoSeparations) using a 130 min gradient from 0 to 45% buffer-B (buffer-A: 0.1% formic acid in 2% ACN; buffer B: 0.1% formic acid in pure ACN) at a flow rate of 250 nl min^{-1}. Mass spectra were acquired in the positive ion mode and data dependent manner selecting the 20 most intense ions for fragmentation using CID (collision induced dissociation). Full scan MS spectra (*m/z* 300–1600) were acquired in the Orbitrap with a target value of 1,000,000 at a resolution of 30,000 (at *m/z* 400) and MS2 spectra were acquired in the linear ion trap with a target value of 10,000 and normalized collision energy of 35%. Precursor ion charge state screening and monoisotopic precursor selection were enabled. Singly charged ions and unassigned charge states were rejected. Dynamic exclusion was enabled with a repeat count of 1 and exclusion duration of 30 s.

Acquired spectra were searched against the *P. ostreatus* PC9 genomic database from JGI (PleosPC9_1_GeneModels_Filtered-models2_aa) using Sequest search engine through Proteome Discoverer (version 1.4). As for the search parameters, precursor and fragment mass tolerance were set to 10 ppm and 0.8 Da, respectively. Carbamidomethylation of cysteines was set as a fixed modification and oxidation of methionines was set as a dynamic modification. Two missed cleavages were allowed. Identified peptides were validated using Percolator algorithm with a *q*-value threshold of 0.01.

The intracellular proteome from the *P. ostreatus* lignocellulose culture under standard conditions was also analyzed. With this purpose, the mycelium was harvested, ground in a sterile mortar with liquid N_2, and resuspended in 0.1 M TRIS, pH 7.0. The suspension was homogenized for 10 min and centrifuged at 15,000 rpm for 15 min. The supernatant was processed as described above for the extracellular secretome.

2.5. Nucleic acid extraction, reverse transcription, primer design and real-time qPCR

The mycelia from 7-day-old *P. ostreatus* lignocellulose cultures, maintained at standard (25 °C, pH 5.5) and extreme temperature (10 °C and 37 °C) and pH (pH 3 and pH 8) conditions for 1, 6, 12 or 24 h, were harvested, frozen and ground in a sterile mortar with liquid N_2. Total RNA was extracted from ~200 mg of deep frozen tissue using Fungal RNA E.Z.N.A Kit (Omega Bio-Tek, Norcross, GA) and its integrity estimated by denaturing electrophoresis on 1% (w/v) agarose gels. Nucleic acid concentrations were measured using a Nanodrop™ 2000 (Thermo Scientific, Wilmington, DE), and the purity of the total RNA was estimated by the 260/280 nm absorbance ratio. Samples were DNAse treated using 1 U of RQ1 DNase (Promega, Madison, WI) per μg of RNA.

One μg of total RNA was reverse-transcribed into cDNA in a 20 μl volume using the iScript cDNA Synthesis kit (Bio-Rad, Alcobendas, Spain). A set of specific primers was designed for amplification of the transcripts from the nine ligninolytic peroxidase genes identified in the genome (Table 1). Primers corresponding to the reference gene panel were designed using the filtered model transcripts sequences of PC9 (http://www.jgi.doe.gov) and the PrimerQuest℠ tool (Integrated DNA Technologies, Madrid, Spain). PCR products were purified and sequenced to confirm primer specificity.

RT-qPCR experiments were performed using a CFX96 (Bio-Rad) thermal cycler. SYBR green fluorescent dye was used to detect product amplification. Each reaction was set to a final volume of 20 μl and contained 1X IQ SYBR green Supermix from Bio-Rad, 300 nM forward and reverse primers, and 1 μl of 1:25 dilution of RT product in nuclease-free water. The amplification program was the following: 5 min at 95 °C, 40 cycles of 15 s at 95 °C and 30 s at 63 °C, followed by 1 min at 95 °C, and a final melting curve with increments of 0.5 °C every 5 s in a linear gradient of 78–95 °C. High temperature fluorescence acquisition (78 °C) was performed to eliminate the impact of PCR artifacts in cDNA quantification, whose absence was confirmed by melting-curve analysis. Baseline correction and crossing-point (*Cp*) acquisition were performed using the Bio-Rad CFXManager. The reactions were performed in triplicate in 96-well microtiter plates, and no-template controls were included for each master mix (one for each primer set). The amplification efficiencies were sample-estimated by linear regression from a Window-of-Linearity set in the exponential phase of the fluorescence history, which was plotted in log scale using the LinReg tool (Ramakers et al., 2003).

2.6. Selection of reference genes, quantification of RT-qPCR data, and statistical analyses

Taking advantage from previous studies (Castanera et al., 2012, 2013) ten genes of different functional classes were selected as reference candidates on the basis of their expression stability in *P. ostreatus*. The expression of the ten genes was evaluated in five samples corresponding to our experimental conditions. GeNorm (Vandesompele et al., 2002) and NormFinder

Please cite this article in press as: Fernández-Fueyo, E., et al. Ligninolytic peroxidase gene expression by *Pleurotus ostreatus*: Differential regulation in lignocellulose medium and effect of temperature and pH. Fungal Genet. Biol. (2014), http://dx.doi.org/10.1016/j.fgb.2014.02.003

Table 1
Transcript identification (gene, monokaryon and chromosome), PCR primers used (type – forward or reverse – and sequences) and amplification length and efficiency for the *P. ostreatus* ligninolytic peroxidase genes and the selected references genes.

Transcript identification				Primer used		Amplification	
Gene	PC15	PC9	Chr[a]	Type[b]	Sequence	Length (bp)	Efficiency
Peroxidase genes							
mnp1	1096331	137760	IV	Fw	CTACAGAAGAACTTGTTCGACGAC	165	1.76
				Rv	GGCAGGGAAGTTAACCTCAGTAT		
mnp2	199510	137764	II	Fw	TGCTTCTCAAAGGAACGCTTGTGC	174	1.89
				Rv	CGAATCGCGAAACCATGAGCCTTT		
mnp3	1089546	137740	V	Fw	ATGGACAAGTTGGCTACACTCGGT	139	1.70
				Rv	CACACGCTTGCTCGATGTTGTTCA		
mnp4	1099081	121638	I	Fw	TCGGACAGAACCCAAAGAAGCTGA	127	1.85
				Rv	GCTTTGCGGCAGGATGCTTCAATA		
mnp5	199511	137765	V	Fw	GCCGCGATGTTGAAACTGTCTTTGG	171	1.85
				Rv	AGTCAAAGCGGGGAAAGGAGTAGC		
mnp6	1041740	51713	V	Fw	GCTATTGGATTCTCCCCTAAGCTCTT	81	1.86
				Rv	AGAGTGGGCCATGATGGAACCATC		
vp1	1089895	137757	VI	Fw	CTCCTGACAACAAGGGAGAAGTCC	198	1.89
				Rv	CAATCAGTTTGCTCTTGTCCTGG		
vp2	1113241	137766	VI	Fw	TATCGCTCGTCACAACATCAGT	146	1.86
				Rv	CTGGGACAAGACCATCAGGTGGA		
vp3	156336	123383	IV	Fw	TGGATTCTCTCCCACCAAAG	195	1.84
				Rv	GGGCAGTTGGAAACACCTAA		
Reference genes							
Actin1	1087906	114148	I	Fw	AGTCGGTGCCTTGGTTAT	129	1.83
				Rv	ATACCGACCATCACACCT		
Pep	1092697	115017	IV	Fw	TGATTCCAGAGGACAAGGACGCAA	148	1.70
				Rv	AAATCTTCCGCGATACGGGTCACT		

[a] Ch, chromosomes I–VI.
[b] Fw and Rv, forward and reverse primer types.

(Andersen et al., 2004) algorithms were applied to rank the ten candidates according to their expression stability, and a reference index consisting of the geometric mean of the best-performing candidates was used for RT-qPCR data normalization.

Then, the transcription level of each peroxidase gene was expressed using two approaches: (i) Relative quantities (RQ) in comparison to a stable reference index, and (ii) Expression relative to a paired calibrator sample. Data pre-processing was performed using Genex software (MultiD Analyses, Göteborg, Sweden; http://www.multid.se) and included, among others, efficiency calibration, reference gene normalization, calculation of RQs, and calculation of the level of expression of a sample relative to its paired calibrator condition (e.g. gene expression after 1 h at 10 °C vs. 1 h at 25 °C) using the delta–delta Ct method of Livak and Schmittgen (2001) (Eqs. (1)–(4), respectively).

$$Cp_E = Cp_U \frac{\log(1+E)}{\log 2} \quad (1)$$

$$\Delta Cp_E = Cp_{GOI} - \frac{1}{n}\sum_{i=1}^{n} Cp_{RGi} \quad (2)$$

$$RQ = 2^{-\Delta Cp_E} \quad (3)$$

$$Expression = 2^{-(\Delta\Delta Cp_E)} \quad (4)$$

In the above equations, Cp_E represents the efficiency corrected Cp. Cp_U is the uncorrected Cp, and E is the amplification efficiency; ΔCp_E is the level of expression of a gene in comparison to the reference index (arbitrary units); Cp_{GOI} is the efficiency-corrected Cp of the gene of interest (peroxidases) and Cp_{RGi} is the efficiency-corrected Cp of each reference gene. RQ is the equivalent linear form of ΔCp_E.

For multivariate analysis, heatmap and hierarchical clustering was performed using the Wards algorithm and Euclidean distance available in Genex software. For this purpose, RQs were log2 transformed and autoscaled to classify genes according to their expression profiles without taking into account the amplitude of the changes (Stahlberg et al., 2008; Bergkvist et al., 2010). Finally, the REST random pairwise reallocation test was used to reveal statistical differences between the expression of each peroxidase gene under the different temperature and pH treatments in comparison to its paired control sample (corresponding to 1, 6, 12 or 24 h under standard conditions).

2.7. VP1. purification from lignocellulose cultures and comparison with recombinant VP1

The supernatants of standard lignocellulose cultures were concentrated (Amicon 10-kDa-cut-off) and dialysed against 20 mM sodium acetate, pH 4.3, with 1 mM $CaCl_2$. Insoluble material was eliminated (15,000 rpm for 30 min) and the solution further dialysed (10 mM sodium tartrate, pH 5.5, with 1 mM $CaCl_2$). The most abundant peroxidase was purified using an ÄKTA HPLC system (GE Healthcare), in three consecutive steps. The first separation was performed on a HiTrap Q Fast Flow 5-mL cartridge at a flow rate of 1 mL min^{-1}. After 12 mL, the retained proteins were eluted with a 0–35% NaCl gradient in 50 mL, followed by 50–100% gradient in 10 mL and 100% NaCl in 15 mL. Peroxidase activity was followed by Mn^{2+}, RB5 and ABTS oxidation in the presence of H_2O_2, as described above, and the appropriate fractions were pooled, concentrated and dialyzed against 10 mM sodium tartrate (pH 5). Then, size-exclusion chromatography in a Superdex-75 HR 10/30 column with 10 mM sodium tartrate (pH 5), containing 100 mM NaCl, at 0.2 mL min^{-1}, was performed. Appropriate fractions were processed as described above, and loaded into a Mono-Q high-resolution 5/5 column at a flow rate of 0.8 mL min^{-1}, using a 0–30% NaCl gradient in 40 mL, followed by 100% NaCl in 10 mL. The purified peroxidase was dialyzed as above, and its homogeneity confirmed by sodium dodecyl sulfate (SDS)–PAGE in 12% gels stained with Coomassie brilliant blue R-250 (Sigma). The N-terminal sequence was analyzed by sequential Edman degradation in a Procise 494 protein sequencer (PerkinElmer).

For comparison with the enzyme purified from lignocellulosic cultures, the gene encoding VP1 from the *P. ostreatus* (PC9) genome (model 137757) was synthesized (by ATG Biosynthetic), cloned in

Please cite this article in press as: Fernández-Fueyo, E., et al. Ligninolytic peroxidase gene expression by *Pleurotus ostreatus*: Differential regulation in lignocellulose medium and effect of temperature and pH. Fungal Genet. Biol. (2014), http://dx.doi.org/10.1016/j.fgb.2014.02.003

pET23a (Novagen) and expressed in *E. coli* BL21 (DE3) pLysS. Cells were grown for 3 h in Terrific Broth, induced with 1 mM isopropyl-β-D-thiogalactopyranoside and grown for 4 h. The apoenzyme accumulated in inclusion bodies and was solubilized using 8 M urea. *In vitro* refolding was performed using 0.16 M urea, 5 mM Ca^{2+}, 20 μM hemin, 0.5 mM oxidized glutathione, 0.1 mM dithiothreitol, and 0.1 mg mL protein, at pH 9.5 (Pérez-Boada et al., 2002). Active enzyme was purified by Resource-Q chromatography using a 0–300 mM NaCl gradient (2 mL min^{-1}, 20 min) in 10 mM sodium tartrate, pH 5.5, containing 1 mM $CaCl_2$.

Oxidation of Mn^{2+}, RB5 and ABTS by the purified VP1 from *P. ostreatus* lignocelulose cultures, and the recombinant VP1 expressed in *E. coli*, was investigated as described in Section 2.3 (using ~0.01 μM enzyme). Ten mM veratryl alcohol (VA) and 2.5 mM 2,6-dimethoxyphenol (DMP) oxidation were followed under the same conditions, but using pH 3 tartrate for veratraldehyde (ε_{310} 9.3 mM^{-1} cm^{-1}) formation, and pH 3.5 tartrate for dimeric coerulignone (ε_{469} 55 mM^{-1} cm^{-1}) formation, respectively.

3. Results

3.1. Analysis of secreted ligninolytic peroxidase isoenzymes by nLC-MS/MS

The secretome of *P. ostreatus* grown in lignocellulose medium under standard conditions was analyzed by nLC-MS/MS of total tryptic peptides to identify the ligninolytic peroxidase isoenzymes produced and secreted. The VP and MnP isoenzymes identified from the presence of unique peptides (at least 2 per protein and sample), corresponding to the isoenzyme sequences in the available genome, are shown in Table 2 (and Supplemental Table S1). In this way, VP1, VP2, MnP2 and MnP6 were identified, with VP1 appearing as the most abundant isoenzyme in the lignocellulose medium (highest PSM number). No MnP1 and MnP4 peptides were detected, and one MnP3, MnP5 and VP3 peptide was found, but the presence of the three latter isoenzymes could not be confirmed by a second unique peptide.

3.2. Analysis of the promoter region of the nine P. ostreatus ligninolytic peroxidase genes

The 5́-upstream sequence of the ligninolytic peroxidase genes in the *P. ostreatus* (PC9) genome contains different responsive elements such as SP-1, AP-1, AP-2 and GATA, together with putative heat-shock elements (HSE), metal-response elements (MRE), xenobiotic-response elements (XRE) and cAMP response elements (CRE), which may be implicated in regulation of their expression by environmental conditions (a detailed description of the promoter region in the nine peroxidase genes is included in a Supplemental section, and summarized in Table S2). Regarding HSEs, they are the most extended elements, being present in seven of the nine promoters (HSEs absent in *vp3* and *mnp1*). Concerning MREs, *mnp6, vp1,* and *vp3* present only one, while *vp2* contains two elements. Finally, the presence of XREs is limited to *vp2* and *mnp3*.

3.3. Identification and validation of reference genes for qPCR analysis

The GeNorm algorithm identified *Actin1* and *Pep* as the most stable genes along all the conditions assayed, displaying an expression stability value (*M*-value) of 0.45. NormFinder ranked *Actin1* as the most stable gene, showing a standard deviation of 0.23 cycles. The accumulated standard deviations of increasing number of reference genes were analyzed to determine the optimal number of genes to be used (Supplemental Figs. S1 and S2). As a consequence of this analysis, *Actin1* and *Pep* were selected as reference index for data normalization, displaying an accumulated standard deviation of 0.21 cycles (Fig. S2).

A dramatic co-downregulation in the expression of every reference gene was observed in the pH 3 samples (Fig. S1). This fact entailed the following implications: (i) due to the unstable expression of the reference index at this condition, the RQ approach (Eq. (3)) could not be quantitatively compared with the others, although the classification of genes according to their relative expression changes was unaffected by this issue; and (ii) the expression of pH 3 samples was normalized using total RNA as internal standard, instead of reference genes, to avoid this limitation in the delta–delta Ct approach (Eq. (4)).

3.4. Differential transcription of peroxidase genes: Exploratory analysis of the expression profiles

For analyzing the transcriptional regulation of ligninolytic peroxidase genes by temperature and pH, *P. ostreatus* was first grown in lignocellulose medium under standard conditions. Then, we monitored by RT-q-PCR using specific primers (Table 1) the time-course (1–24 h) of transcriptional changes of the nine peroxidase

Table 2
Ligninolytic peroxidases in the extracellular and intracellular proteomes of *P. ostreatus* (monokaryon PC9) grown in lignocellulose medium (25 °C).

	nLC-MS/MS					Protein properties		
Enzyme	Score	Coverage (%)	Unique Peptides	Total Peptides	PSMs	AAs	MW [kDa]	Calculated pI
Extracellular								
VP1	715.87	33.84	6	7	165	331	34.6	4.63
VP2	242.93	16.81	3	4	96	339	35.8	4.56
MnP2	228.61	15.09	4	5	94	338	35.7	4.97
MnP6	77.11	22.78	7	7	30	338	35.7	4.88
VP3	35.97	9.67	1	2	12	331	34.6	4.63
MnP3	8.84	2.72	1	1	4	331	34.5	4.60
MnP5	8.33	5.67	1	1	2	335	35.0	4.59
Intracellular								
VP1	46.06	20.78	3	4	13	331	34.6	4.63
VP2	18.58	16.48	3	4	6	339	35.8	4.56
MnP2	16.47	12.85	2	4	6	338	35.7	4.97
VP3	14.52	14.72	2	3	5	331	34.6	4.63
MnP3	11.20	15.13	3	3	3	331	34.6	4.63
MnP6	10.63	8.61	2	3	4	335	35.0	4.59

Score, statistic reliability of protein identification; Coverage, percentage of tryptic peptides identified; PSM, number of scans where the isoenzyme was identified; AAs, amino-acid number

Please cite this article in press as: Fernández-Fueyo, E., et al. Ligninolytic peroxidase gene expression by *Pleurotus ostreatus*: Differential regulation in lignocellulose medium and effect of temperature and pH. Fungal Genet. Biol. (2014), http://dx.doi.org/10.1016/j.fgb.2014.02.003

genes after modifying the temperature (from 25 °C to 10 °C and 37 °C) and pH (from pH 5.5 to pH 3 and pH 8). Two approaches were used for this purpose: (i) an exploratory analysis using multivariate methods to uncover similar expression trends among genes and samples; and (ii) a classical expression analysis using the delta–delta Ct method under a paired experimental design (treatment vs. control) where controls are the different sampling times of *P. ostreatus* growing under the standard conditions.

The transcription of peroxidase genes was firstly analyzed under standard conditions in four sampling times along 24 h. The aim was to obtain an expression map of *P. ostreatus* ligninolytic peroxidase genes under lignin degradation conditions. The analysis resulted in an expression heatmap associated with a dendrogram of hierarchical clusters (Fig. 1A) classifying genes and samples according to their similar profiles. Three groups of genes were clearly differentiated in that sense, displaying high (group I: *mnp3* and *vp1*), medium (group II: *mnp2, vp2, mnp6*, *vp3* and *mnp1*) or low expression (group III: *mnp4* and *mnp5*) in the lignocellulose medium. The expression trends of group II genes fluctuated along the 24 h, making the alternate sampling times cluster together.

3.5. Effect of temperature and pH conditions on the expression of ligninolytic peroxidase genes

A similar analysis to that performed for the standard growth conditions, was performed in all samples after the temperature and pH modifications to uncover a putative coregulation of the ligninolytic peroxidase genes. The hierarchical clustering dendrogram obtained from the averaged expression during the 24 h period shows the gene expression trends under the modified temperature and pH conditions (Fig. 1B, bottom). Interestingly, the expression groups obtained under standard conditions (Fig. 1A) were maintained with the only exception of *vp1*, which was re-classified as member of group II (Fig. 1B, bottom). The expression profiles along the 24-h sampling period (Fig. 1B, top) allowed us to understand the rationale of the above gene classification. *mnp3* expression (group I) was higher than the reference (mean expression of the two reference genes) after every treatment. Genes of group II displayed a relative expression greater than the reference in pH 3 treatment (and for *vp1* and *mnp2* at 25 °C). Nevertheless, the expression in pH 8 and temperature treatments remained lower than the reference, and displayed similar trends among the members of the two sub-groups. Finally, *mnp4* and *mnp5* (group III) displayed lower expression than the reference after every treatment, although it was higher after pH treatment in comparison to temperature treatment.

Then, the individual effect of the different environmental conditions and times on the ligninolytic peroxidase expression were analyzed by referring the transcriptional levels observed at different times (1–24 h) after changing the culture temperature (from 25 °C to 10 °C and 37 °C) and pH (from pH 5.5 to pH 3 and pH 8) to those obtained under the standard conditions (Fig. 2). Changing the temperature and pH led to a transcriptional downregulation of most ligninolytic peroxidase genes, with a few significant exceptions discussed below.

Concerning temperature effects, in those cultures placed at 10 °C (Fig. 2A) the expression decreased gradually along the time, becoming statistically significant in every peroxidase gene after 24 h. The expression change was more patent for the three *vp* genes, which attained −5.3 to −5.9-fold decreases (with respect to the 25 °C control). By contrast, the expression of *mnp3* was the less altered, fluctuating between a slight upregulation during the first 12 h and a final downregulation of −1.7-fold after 24 h. Cultures exposed to 37 °C (Fig. 2B) showed an interesting transcriptional profile, as they displayed wide and alternate up/down regulations along the four sampling times in genes of groups II and III. Again, *mnp3* showed a different profile, its expression being

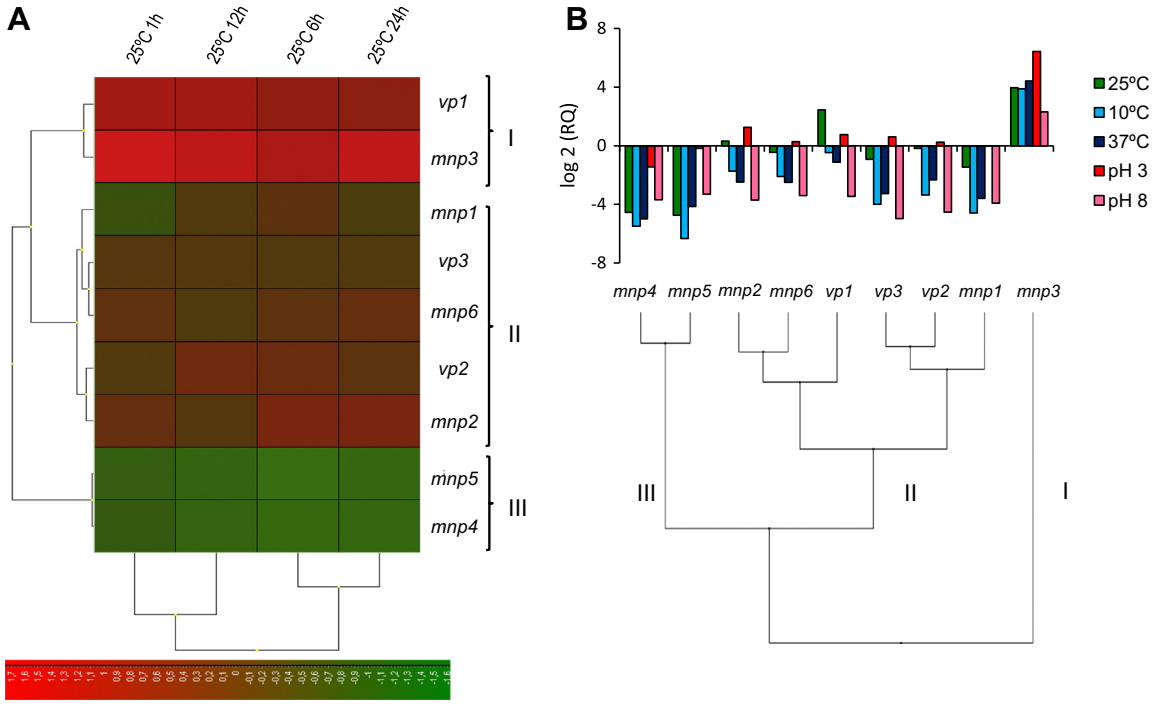

Fig. 1. Exploratory analysis of gene expression of the nine *P. ostreatus* ligninolytic peroxidases. (A) Heatmap combined with dendrograms representing gene expression and sample (1, 6, 12 and 24 h) clustering under standard conditions (25 °C and unadjusted pH 5.5) after seven days of culture. (B) Averaged expression of RQs along 24 h, combined with hierarchical clustering dendrogram summarizing the gene expression trends under modified temperature and pH conditions. The pH 3 expression values were normalized with the total RNA, while the reference genes were used for normalization in the other cases.

Please cite this article in press as: Fernández-Fueyo, E., et al. Ligninolytic peroxidase gene expression by *Pleurotus ostreatus*: Differential regulation in lignocellulose medium and effect of temperature and pH. Fungal Genet. Biol. (2014), http://dx.doi.org/10.1016/j.fgb.2014.02.003

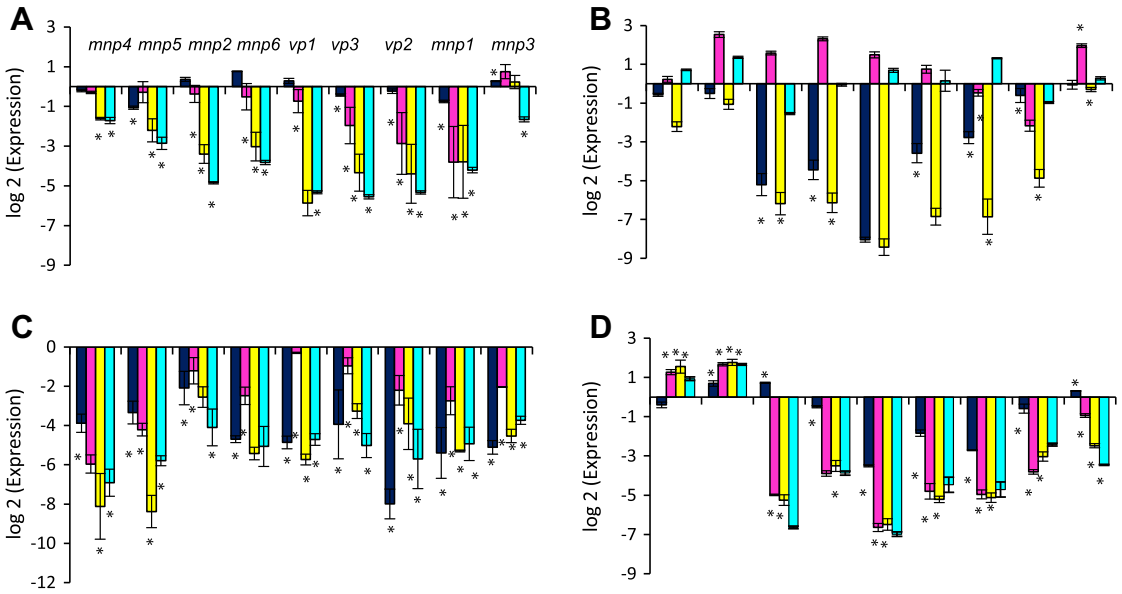

Fig. 2. Effect of changes in temperature and pH conditions on the expression levels of the nine *P. ostreatus* ligninolytic peroxidase genes. (A) 10 °C. (B) 37 °C. (C) pH 3. (D) pH 8. The increased or decreased expression values at 1 h (black), 6 h (magenta), 12 h (yellow) and 24 h (blue) after changing the temperature and pH conditions were referred to those obtained under the standard conditions (25 °C and unadjusted pH 5.5). Error bars represent the standard deviations of the means of three independent amplifications of pooled samples, and asterisks mean that the changes referred to the control (standard conditions) are statistically significant at $p < 0.05$. (For interpretation of the references to color in this figure legend, the reader is referred to the web version of this article.)

similar (at 1, 12 and 24 h) or greater than the control (2.0-fold increase after 6 h).

The pH 3 treatment (Fig. 2C) led to a general downregulation of the ligninolytic peroxidase genes. This fact could be observed just 1 h after the pH modification (reaching −11.4-fold decrease) and was maintained over the 24-h period (up to −10.9-fold decreases). Regarding pH 8 (Fig. 2D), most genes showed a similar downregulation, which increased with time. However, *mnp4* and *mnp5* expression (group III) was significantly upregulated by pH 8. Group II genes displayed a strong repression from the 6 h period, with the highest alkaline downregulation corresponding to genes *mnp2* (−6.6-fold) and *vp1* (−7.0-fold). Finally, *mnp3* (group I) showed a gradual repression along the time, reaching a −3.5-fold decrease after 24 h at pH 8.

3.6. Contribution of each isoenzyme to the global peroxidase expression

Changes in the expression of the nine *P. ostreatus* ligninolytic peroxidase genes under the different temperature and pH conditions were further analyzed by considering the percentual contribution of each of them to the total peroxidase gene expression (as averaged values for a 24-h period) under each condition (Fig. 3). The predominant expression of gene *mnp3* over the eight other peroxidase genes, was already noticed when analyzing the peroxidase transcriptional levels under standard conditions. However, its contribution was even higher in the cultures grown under more extreme conditions: pH 3 (25 °C) > pH 8 (25 °C) > 10 °C (pH 5.5) > 37 °C (pH 5.5) > 25 °C (pH 5.5) (Fig. 3A). Under the three last conditions, which correspond to the lowest *mnp3* relative transcription levels, gene *vp1* was significantly transcribed with around 20% contribution to the total peroxidase expression, while the transcription levels of the other seven peroxidase genes were low (<5% of the total).

To better analyze the contribution of the latter genes, their transcription levels were also shown as percentages of total expression without gene *mnp3* (Fig. 3B). In this way, two different expression profiles could be identified under the modified temperature and

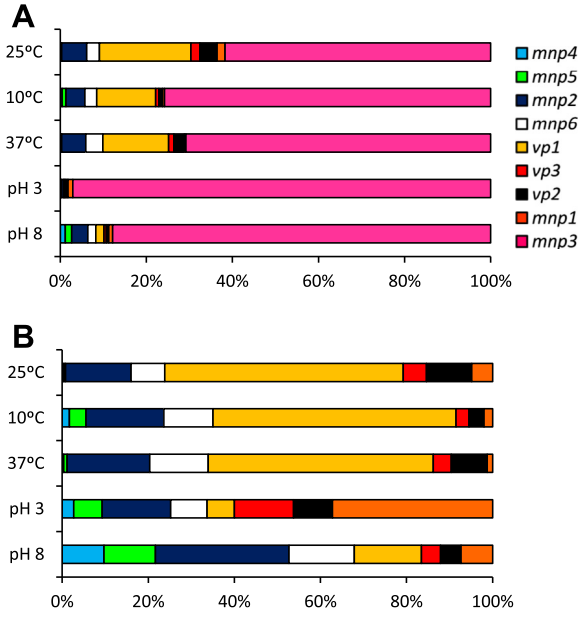

Fig. 3. Relative expression of the ligninolytic peroxidase genes when temperature and pH conditions were changed. (A) Relative expression of each peroxidase gene, as percentage of the total expression of the nine genes (in RQs), under the extreme temperature (10 °C and 37 °C) and pH (3 and 8) conditions assayed, compared with the 25 °C (and unadjusted pH 5.5) standard conditions. (B) Relative expressions after excluding the predominantly-expressed gene *mnp3*. Averaged values for the 24-h sampling period are shown (as means from the 1, 6, 12 and 24 h samples; see Figs. S3 and S4 for the whole set of relative transcriptional values for each gene and treatment time with and without gene *mnp3*, respectively).

pH conditions. On the one hand, at the standard and temperature modified conditions, *vp* genes represented the majority of the total ligninolytic peroxidase expression (*mnp3* excluded): 72% at 25 °C (with *vp1* representing 52% of the total transcription), 65% at 37 °C and 63% at 10 °C. On the other hand, changes in the pH led to a predominant expression of the *mnp* genes, representing 71%

Please cite this article in press as: Fernández-Fueyo, E., et al. Ligninolytic peroxidase gene expression by *Pleurotus ostreatus*: Differential regulation in lignocellulose medium and effect of temperature and pH. Fungal Genet. Biol. (2014), http://dx.doi.org/10.1016/j.fgb.2014.02.003

and 75% of the total ligninolytic peroxidase transcripts at pH 3 and pH 8, respectively (*mnp3* excluded).

For easier identification of the relative expression patterns, the above comparisons were performed on the averaged data for the 24-h sampling period after changing the temperature and pH conditions. However, additional information on the time-course of each gene expression was obtained when the four sampling times were analyzed separately. Gene *mnp3* remained as the most expressed gene at the four sampling times under each condition (Supplemental Fig. S3), although the relative transcriptional levels at 10 °C progressively increased from 1 h to 24 h, and those at 37 °C attained the highest value at 1 h and 12 h. Concerning the other eight ligninolytic peroxidase genes (Supplemental Fig. S4), their relative transcriptional patterns showed significant differences with time. For example, the initial transcription (1 h) of gene *mnp2* was high at both pH 8 and pH 3 but it decreased later, being accompanied by the increased expression of genes *mnp1* (pH 3) and *mnp4*/*mnp5* (pH 8) that finally (12/24 h) represented over 50% of the total expression of the eight genes analyzed here.

3.7. Effect of temperature and pH on the peroxidase activity in the lignocellulose cultures

In lignocellulose cultures of *P. ostreatus*, the highest extracellular ligninolytic peroxidase activities, measured with Mn^{2+}, ABTS or RB5 in the presence of H_2O_2 (by subtracting the ABTS oxidation observed in the absence of H_2O_2) were generally observed under the standard conditions (Fig. 4 bars 1–4) in agreement with the transcriptomic results. RB5 oxidation was the most affected by the temperature and pH modification. In the 10 °C treatments, a sharp decrease of Mn^{2+} and RB5 oxidation activity was observed after 1 h incubation (and after 6 h incubation in the case of ABTS). Mn-oxidation was the most affected activity, with a 2.6-fold reduction. There was a slightly recovery in RB5 and ABTS oxidation after 6 and 24 h, respectively (although the activities were still 2.3 and 1.5-fold lower, respectively). In the 37 °C treatments, no strong changes of the ABTS and Mn^{2+} oxidation activities were initially produced, being similar or even higher (ABTS, 1 h) than found at 25 °C. However, a decrease of ABTS and RB5 oxidation was produced after 12 h, while Mn^{2+} oxidation was less affected.

pH 3 turned out to be a too severe condition resulting in a complete lack of peroxidase activity. Finally, at pH 8 the ligninolytic peroxidase activities were less affected than at pH 3 but strong decreases were detected, especially immediately after the pH adjustment (8-fold reduction for Mn^{2+}, 4-fold decrease for ABTS and 11-fold reduction for RB5 oxidation, in the 1 h sample). Then, some recovery of Mn^{2+} and ABTS oxidation activities were produced (attaining 4 and 2-fold lower levels, respectively, than found at 25 °C) but the RB5 oxidation activity maintained similar low levels during the whole 24-h period.

3.8. Analysis of intracellular ligninolytic peroxidases isoenzymes by nLC-MS/MS

As already described, MnP3 could not be confirmed in the *P. ostreatus* secretome due to detection of a single unique peptide (Table 2). However, *mnp3* was the most transcribed gene in the *P. ostreatus* cultures (Fig. 1B). To explain this apparent contradiction, mycelium of *P. ostreatus* grown on the lignocellulose medium for seven days at 25 °C was harvested, homogenized, and the supernatant analyzed by nLC-MS/MS to identify intracellular ligninolytic peroxidase isoenzymes.

As in the secretomic analysis, the identification of intracellular proteins was based on the detection of at least two unique peptides in each sample (Tables 2 and S1). VP1, VP2, MnP2, VP3, MnP6 and MnP3 were identified in decreasing order of importance (according to PSM values). VP1 was found to be the most abundant intracellular ligninolytic peroxidase isoenzyme, as in the case of the extracellular analysis, while MnP1, MnP4 and MnP5 were not detected. More importantly, translation of the *mnp3* transcripts and intracellular presence of the MnP3 isoenzyme was confirmed.

3.9. VP1. purification

The transcriptomic, enzymatic activity, and extracellular/intracellular proteomic studies were completed by purification of the main peroxidase isoenzyme present in the *P. ostreatus* lignocellulose cultures (after 7-day growth under standard conditions). The purification process included three chromatographic steps, and concluded with Mono Q chromatography (Fig. 5) yielding an electrophoretically homogeneous protein, as shown by SDS–PAGE chromatography (Fig. 5 inset). The visible spectrum of the purified enzyme showed the main Soret band (at 406 nm) and the small heme bands at 502 and 640 nm, confirming that it had properly incorporated the cofactor.

The peroxidase purified from lignocellulose cultures had activity on ABTS, DMP, Mn^{2+}, VA and RB5 (Table 3) revealing that it corresponds to one of the three *P. ostreatus* VPs. With the aim of identifying the isoenzyme purified, the following N-terminal sequence was determined: ATXADGRTTANAXXVLFPILDDIQ (X correspond to three conserved cysteine residues). A comparison with the predicted mature N-terminal sequences of the nine ligninolytic peroxidases from the *P. ostreatus* genome (Table S3) showed 100% sequence identity with both VP1 and MnP3. However, its ability to oxidize VA and RB5 excluded the MnP isoenzyme, and revealed that the main ligninolytic peroxidase produced in lignocellulose cultures is isoenzyme VP1.

Finally, gene *vp1* was expressed in *E. coli*, and the catalytic activities of the recombinant enzyme compared with those of the wild enzyme from the fungal culture (Table 3). Differences in oxidation of substrates other than Mn^{2+}, being 2–3-fold lower for the recombinant VP1, suggest some involvement of the glycosidic moiety in VP activity. However, the similar substrate specificity range, including Mn^{2+} and high and low redox-potential aromatic compounds as substrates, confirmed the identification of the main peroxidase present in lignocellulose cultures as *P. ostreatus* isoenzyme VP1.

4. Discussion

4.1. Ligninolytic peroxidases in P. ostreatus

P. ostreatus has nine ligninolytic peroxidase genes as shown by its sequenced genome (Ruiz-Dueñas et al., 2011). According to their catalytic properties after heterologous expression, they have been classified as six MnPs and three VPs, and a definitive isoenzyme numbering has been assigned (Fernández-Fueyo et al., 2014) in agreement with that shown at the JGI portal after manual annotation (http://genome.jgi-psf.org/PleosPC9_1).

These peroxidases play an active role in lignin degradation by *Pleurotus* species as shown in different studies (Camarero et al., 1998; Salame et al., 2013). Recently, Fernández-Fueyo et al. (2014) demonstrated that *P. ostreatus* VP degrades non-phenolic lignin model dimers and depolymerizes synthetic lignin as previously reported for *P. chrysosporium* LiP (Hammel et al., 1993), and suggested that VP in some Agaricales plays the same role of LiP in many Polyporales. The same authors (Fernández-Fueyo et al., 2014) have shown that *P. ostreatus* MnPs represent a subfamily of short MnPs different from those found in *P. chrysosporium* (long MnP subfamily) characterized by broader

Please cite this article in press as: Fernández-Fueyo, E., et al. Ligninolytic peroxidase gene expression by *Pleurotus ostreatus*: Differential regulation in lignocellulose medium and effect of temperature and pH. Fungal Genet. Biol. (2014), http://dx.doi.org/10.1016/j.fgb.2014.02.003

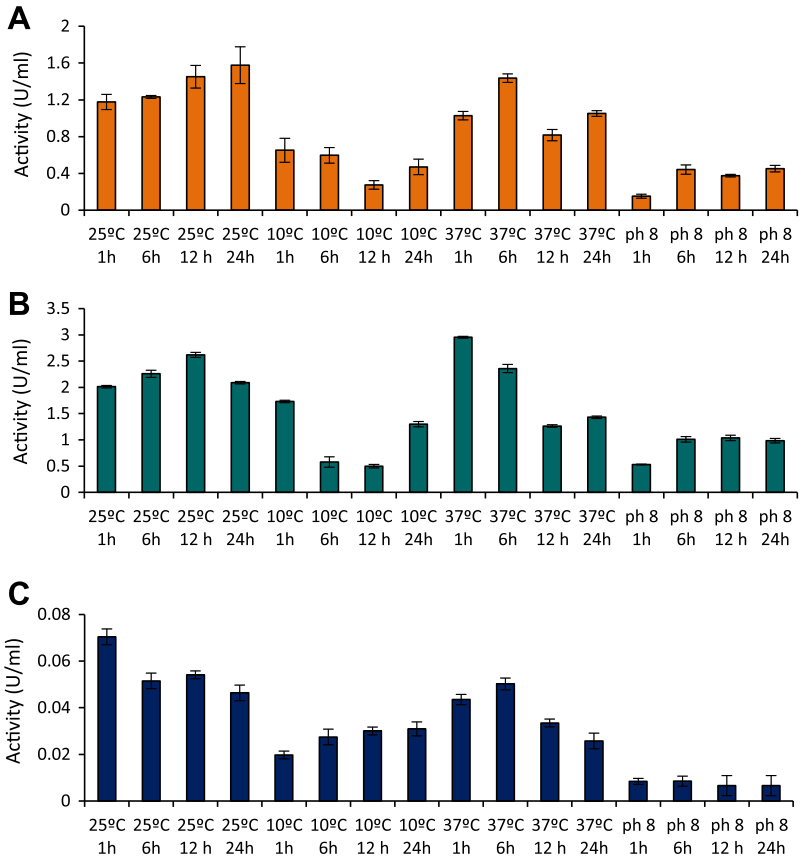

Fig. 4. Change of extracellular peroxidase activity determined using Mn^{2+} (A), ABTS (B) and RB5 (C) as substrates. Effect of change in temperature and pH conditions and incubation times (after conditions change). Error bars represent the standard deviations of the means of three independent measurements of the same pooled samples.

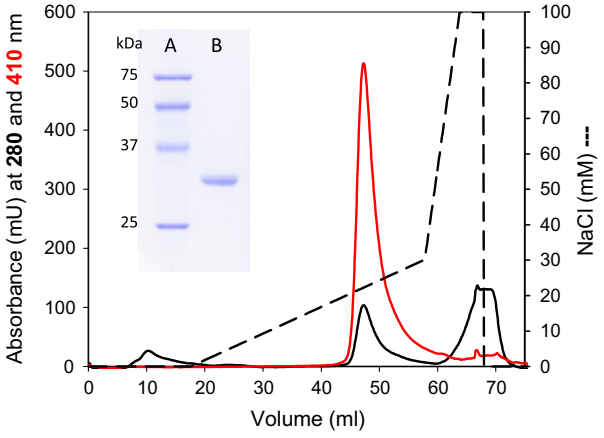

Fig. 5. Purification of the major ligninolytic peroxidase present in the *P. ostreatus* cultures after 7-d growth in lignocellulose medium: Mono Q chromatography showing 280 nm (continuous black line) and 410 nm (continuous red line) absorbance and NaCl (dashed line) profiles, and SDS–PAGE (inset) of the purified enzyme (lane B) compared with different molecular mass standards (lane A). (For interpretation of the references to colour in this figure legend, the reader is referred to the web version of this article.)

substrate specificity including Mn-independent oxidation of phenols and other compounds, which would enable direct oxidation of lignin-related compounds.

The high number of genes encoding VP and MnP isoenzymes in the *P. ostreatus* genome points to the potential redundancy and/or diversity in their properties, and suggest differential regulation as discussed below.

Table 3
Activity (U mg^{-1}) of main ligninolytic peroxidase found in lignocellulose cultures (wild VP1), and the same isoenzyme after *E. coli* expression (recombinant VP1).

	Wild VP1	Recombinant VP1
Mn^{2+}	289 ± 12	259 ± 9
ABTS	574 ± 24	198 ± 13
DMP	300 ± 15	83 ± 2
VA	54 ± 4	18 ± 1
RB5	35 ± 3	12 ± 1

4.2. Differential expression of ligninolytic peroxidase isoenzymes in lignocellulose medium

Differential expression of some peroxidase genes depending of environmental and nutritional conditions had already been described in *Pleurotus* cultures grown on different media (Ruiz-Dueñas et al., 1999; Cohen et al., 2002a; Salame et al., 2010). To study the differential expression (and environmental regulation) of the whole array of ligninolytic peroxidase genes identified in the *P. ostreatus* genome we decided to use a lignocellulose medium. Sawdust and cereal straw are the usual substrates for the commercial production of *P. ostreatus* (Sánchez, 2010), a fungus that naturally grows on deciduous trees (Phillips, 2006). Therefore, in the present study we used a combination of milled wheat straw and poplar wood chips as the only growth substrate in stationary cultures (containing a small water volume). These conditions are more similar to the fungal natural growth conditions than shaken synthetic liquid media.

To study the expression of the nine peroxidase genes in the lignocellulose medium, we determined the relative abundance of

Please cite this article in press as: Fernández-Fueyo, E., et al. Ligninolytic peroxidase gene expression by *Pleurotus ostreatus*: Differential regulation in lignocellulose medium and effect of temperature and pH. Fungal Genet. Biol. (2014), http://dx.doi.org/10.1016/j.fgb.2014.02.003

the corresponding transcripts by RT-qPCR using selected reference genes. In terms of studying the effect of different factors on transcript level, RT-qPCR has been shown to be 10^3–10^4 more sensitive than Northern blotting (Sooknanan et al., 1993). According to the pattern of expression (abundance of transcripts) at the standard growth conditions, the ligninolytic peroxidase genes of *P. ostreatus* were divided into three different groups, being *mnp3* and *vp1* the most expressed genes. This agrees with previous studies using other culture media (such as glucose-peptone medium amended with Mn^{2+}). Among them, Irie et al. (2000) described MnP3 as the major MnP isoenzyme in *P. ostreatus*, and Salame et al. (2012, 2013) described *vp1* (*mnp4* for these authors) and *mnp3,* together with *mnp2* (*mnp9* for these authors), as the most transcribed *P. ostreatus* PC9 genes. On the other hand, *mnp4* and *mnp5* appeared as the least expressed genes at the standard conditions used in the present study.

4.3. Environmental regulation of ligninolytic peroxidase isoenzymes by temperature and pH

Two extreme temperature and pH conditions were selected to study the environmental regulation of the nine ligninolytic peroxidase genes in *P. ostreatus*, in connection with previous studies (Fernández-Fueyo et al., 2014). Previous observations had shown that 10 °C and 37 °C are the most extreme temperatures, in which this fungus continues growing. On the other hand, although the highest fungal ligninolysis and activity of ligninolytic enzymes (LiP and VP) is often produced at acidic conditions (Ruiz-Dueñas and Martínez, 2009), pH 3 always results in progressive peroxidase inactivation, as shown for most of the *P. ostreatus* isoenzymes (Fernández-Fueyo et al., 2014). The same study also showed that pH 8 inactivates these peroxidases, except the most stable isoenzymes, due to loss of structural Ca^{2+} ions and formation of bis(histidyl) heme iron complexes. Therefore, to study environmental regulation, *P. ostreatus* cultures pregrown under standard conditions were transferred to 10 °C and 37 °C or the medium pH adjusted to pH 3 and pH 8, and the peroxidase transcriptional levels (during the subsequent 24 h) referred to those of cultures maintained under unchanged conditions.

Modifications of temperature and pH led to a downregulation of most ligninolytic peroxidase genes, although the individual genes were differentially affected. In general, the pH modifications produced more severe effects than the temperature modifications, and *vp* genes were more affected than *mnp* genes. Among the latter, *mnp3* appears as the most transcribed ligninolytic peroxidase gene in all the conditions, and the least downregulated by temperature modification. pH 3 seems to be a too stressful condition for the fungus, with a downregulation of more than 10 folds in all genes after only 1 h incubation. On the other hand, while all *vp* genes were dramatically downregulated at pH 8, *mnp4* and *mnp5* were upregulated under these conditions. Interestingly, MnP4 has been reported as the most stable *P. ostreatus* peroxidase isoenzyme under alkaline conditions (Fernández-Fueyo et al., 2014).

Concerning temperature, all genes except *mnp3* were downregulated at 10 °C. Conversely, at 37 °C most of the genes were upregulated after 24 h, with the exception of *mnp2*, *mnp6* and *mnp1*. This general upregulation at 37 °C could be related to HSEs, which are present in all the *P. ostreatus* peroxidase promoters except in those of *mnp1* and *vp3*. The existence of HSEs has been reported in the promoters of other ligninolytic peroxidase genes, such as *P. chrysosporium mnp* (Godfrey et al., 1994; Mayfield et al., 1994). No correlation between the thermal stability of the different isoenzymes (Fernández-Fueyo et al., 2014) and the expression levels of the nine ligninolytic peroxidase genes was observed under the present experimental conditions.

4.4. Activity levels, proteomes, and enzyme purification from lignocellulose cultures

In the *P. ostreatus* lignocellulose cultures under standard conditions, the maximal peroxidase activity coincided with the highest expression of ligninolytic peroxidase genes. In most of the cases, there was also a correlation between the expression and activity levels in the modified temperature and pH conditions. Regarding pH, no activity was detected for any substrate at pH 3, where the fungus could not survive and the peroxidase expression sharply decreases. On the other hand, RB5 oxidation (a specific VP reaction) was the most affected activity at pH 8, in agreement with the higher decrease of *vp* than *mnp* transcripts. In the case of temperature, the lack of activity in the cultures transferred at 10 °C, a temperature at which these peroxidases are fully stable (Fernández-Fueyo et al., 2014) correlates with the strong decrease of all transcript levels. Thus, it seems that a constant production of the enzyme is necessary to maintain the activity. At 37 °C, while no strong changes in Mn^{2+} oxidation were produced, there was a decrease in ABTS and RB5 oxidation activities (after 12 h) which coincided with the stronger reduction in *vp* expression.

In previous studies, only VP1 (Sarkar et al., 1997; Kamitsuji et al., 2004), VP2 (Kamitsuji et al., 2004) and MnP3 (Cohen et al., 2001, 2002b) had been purified from *P. ostreatus* cultures, suggesting that they are the most abundant ligninolytic peroxidases in the different culture conditions assayed. In our case, only VP1 was purified from lignocellulose fungal cultures, highlighting the role of VPs in lignin degradation by this fungus (Fernández-Fueyo et al., 2014). By nLC-MS/MS, a highly sensitive technique, VP2, MnP2 and MnP6 were also detected, and a single unique peptide was found for MnP3, MnP5 and VP3 (while MnP4 and MnP1 were not detected). In a similar study on *P. ostreatus* secretome (from Mn^{2+}-amended glucose-peptone medium) only MnP3, VP1 and MnP2 were detected by Salame et al. (2013) (the two latter isoenzymes respectively called VP4 and MnP9 by these authors).

The secretome results mostly agree with the transcript levels at 25 °C except for gene *mnp3* that showed the highest transcription level, but whose protein product could not be confirmed by a second unique peptide. However, the intracellular presence of MnP3 was shown by the nLC-MS/MS analysis of the corresponding proteome, revealing a limited secretion of this isoenzyme. A similar case was reported for a *P. ostreatus* laccase (POXA1b) that shows the highest transcription levels in copper-supplemented cultures, but it is not a major extracellular protein due to inefficient secretion (it appears in the cellular extract) and the action of specific proteases (Palmieri et al., 2000).

Although all the ligninolytic peroxidase genes are transcribed in the *P. ostreatus* lignocellulose cultures, those peroxidases being absent from both the intracellular/extracellular secretomes (MnP4 and MnP1) correspond to the less transcribed genes at the standard growth conditions (together with gene *mnp5*). Another possible reason for the absence of these two peroxidases from the proteomes is that MnP4 has the highest number of lysine residues (20) followed by MnP1, a fact that would difficult nLC-MS/MS identification due to the high number and small size of tryptic peptides. Moreover, Salame et al. (2013) proposed that MnP4 (called MnP7 in this study) could be anchored to the membrane, according to the prediction of a transmembrane domain that would limit its secretion.

5. Conclusions

The main ligninolytic peroxidase genes expressed in *P. ostreatus* cultures with lignocellulose as the sole carbon (and nitrogen) source were investigated by transcriptomic, secretomic and enzyme purification studies. Genes *mnp3* and *vp1* showed the

Please cite this article in press as: Fernández-Fueyo, E., et al. Ligninolytic peroxidase gene expression by *Pleurotus ostreatus*: Differential regulation in lignocellulose medium and effect of temperature and pH. Fungal Genet. Biol. (2014), http://dx.doi.org/10.1016/j.fgb.2014.02.003

highest transcription levels, but the presence of isoenzyme MnP3 in the cultures seems affected by a limited secretion (as shown by comparison of the intracellular and extracellular proteomes). However, the product of gene *vp1* was the most abundant protein in the secretome and the only peroxidase purified from the *P. ostreatus* lignocellulose cultures. For the rest of genes there was also a general correlation between the level of transcripts and the secretome abundance. Expression of the *P. ostreatus* six *mnp* and the three *vp* genes was differentially affected by changes in the culture temperature and pH. Although an increase of temperature (to 37 °C) caused a transient increase of gene expression with respect to 25 °C (6 h sample), a general downregulation was observed after 24 h at 37 °C, as well as in nearly all the samples from the 10 °C treatments. Concerning the effect of pH, all the ligninolytic peroxidase genes were downregulated at pH 3 with respect to the standard conditions (pH 5.5). Finally, pH 8 downregulated all the genes but *mnp4* and *mnp5*, whose upregulation by alkaline pH constitutes an intriguing finding since most ligninolytic peroxidases are inactivated over pH 7. However, it agrees with previous studies that described the unusual alkaline stability of the MnP4 isoenzyme from the *P. ostreatus* genome.

Acknowledgments

This work was supported by the PEROXICATS (KBBE-2010-4-265397; www.peroxicats.org) and INDOX (KBBE-2013-7-613549; www.indoxproject.eu) EU projects, and by the BIO2011-26694 and AGL2011-30495 projects of the Spanish Ministry of Economy and Competitiveness (MINECO). EF-F acknowledges a Junta de Ampliación de Estudios fellowship of the CSIC, co-funded by the European Social Fund, and FJR-D acknowledges a MINECO Ramón y Cajal contract.

Appendix A. Supplementary material

Supplemental Information concerns gene promoters, secretome peptides, N-terminus of purified peroxidase, crossing point and stability of reference genes, and expression of ligninolytic peroxidase genes at different times, including a section on the promoter region of the ligninolytic peroxidase genes, the peroxidase peptide sequences identified in the secretome of *P. ostreatus* (Table S1), a list of putative regulatory elements in the different promoters (Table S2), the N-terminal sequence identity of the peroxidase purified from lignocellulose cultures (Table S3), the crossing point distribution of ten candidate reference genes at different temperature and pH conditions (Fig. S1), the expression stability of these ten genes using GeNorm and Normfinder (Fig. S2), the relative expression of the nine ligninolytic peroxidase genes at different times after changing the incubation conditions (Fig. S3) and the same information excluding *mnp3* (Fig. S4). Supplementary data associated with this article can be found, in the online version, at http://dx.doi.org/10.1016/j.fgb.2014.02.003.

References

Andersen, C.L., Jensen, J.L., Orntoft, T.F., 2004. Normalization of real-time quantitative reverse transcription-PCR data: a model-based variance estimation approach to identify genes suited for normalization, applied to bladder and colon cancer data sets. Cancer Res. 64, 5245–5250.

Bergkvist, A., Rusnakova, V., Sindelka, R., Garda, J.M.A., Sjogreen, B., Lindh, D., Forootan, A., Kubista, M., 2010. Gene expression profiling – clusters of possibilities. Methods 50, 323–335.

Camarero, S., Barrasa, J.M., Pelayo, M., Martínez, A.T., 1998. Evaluation of *Pleurotus* species for wheat–straw biopulping. J. Pulp Paper Sci. 24, 197–203.

Castanera, R., Pérez, G., Omarini, A., Alfaro, M., Pisabarro, A.G., Faraco, V., Amore, A., Ramírez, L., 2012. Transcriptional and enzymatic profiling of *Pleurotus ostreatus* laccase genes in submerged and solid-state fermentation cultures. Appl. Environ. Microbiol. 78, 4037–4045.

Castanera, R., Omarini, A., Santoyo, F., Pérez, G., Pisabarro, A.G., Ramírez, L., 2013. Non-additive transcriptional profiles underlie dikaryotic superiority in *Pleurotus ostreatus* laccase activity. PLoS ONE 8, 9.

Cohen, R., Hadar, Y., Yarden, O., 2001. Transcript and activity levels of different *Pleurotus ostreatus* peroxidases are differentially affected by $Mn2^{+}$. Environ. Microbiol. 3, 312–322.

Cohen, R., Persky, L., Hadar, Y., 2002a. Biotechnological applications and potential of wood-degrading mushrooms of the genus *Pleurotus*. Appl. Microbiol. Biotechnol. 58, 582–594.

Cohen, R., Persky, L., Hazan-Eitan, Z., Yarden, C., Hadar, Y., 2002b. Mn^{2+} alters peroxidase profiles and lignin degradation by the white-rot fungus *Pleurotus ostreatus* under different nutritional and growth conditions. Appl. Biochem. Biotechnol. 102, 415–429.

Farrell, R.L., Murtagh, K.E., Tien, M., Mozuch, M.D., Kirk, K.T., 1989. Physical and enzymatic properties of lignin peroxidase isoenzymes from *Phanerochaete chrysosporium*. Enzyme Microb. Technol. 11, 322–328.

Fernández-Fueyo, E., Ruiz-Dueñas, F.J., Ferreira, P., Floudas, D., Hibbett, D.S., Canessa, P., Larrondo, L., James, T.Y., Seelenfreund, D., Lobos, S., Polanco, R., Tello, M., Honda, Y., Watanabe, T., Watanabe, T., Ryu, J.S., Kubicek, C.P., Schmoll, M., Gaskell, J., Hammel, K.E., St. John, F.J., Vanden Wymelenberg, A., Sabat, G., Bondurant, S.S., Syed, K., Yadav, J., Doddapaneni, H., Subramanian, V., Lavín, J.L., Oguiza, J.A., Perez, G., Pisabarro, A.G., Ramírez, L., Santoyo, F., Master, E., Coutinho, P.M., Henrissat, B., Lombard, V., Magnuson, J.K., Kües, U., Hori, C., Igarashi, K., Samejima, M., Held, B.W., Barry, K., LaButti, K., Lapidus, A., Lindquist, E., Lucas, S., Riley, R., Salamov, A., Hoffmeister, D., Schwenk, D., Hadar, Y., Yarden, O., de Vries, R.P., Wiebenga, A., Stenlid, J., Eastwood, D.C., Grigoriev, I.V., Berka, R., Blanchette, R.A., Kersten, P., Martínez, A.T., Vicuña, R., Cullen, D., 2012. Comparative genomics of *Ceriporiopisis subvermispora* and *Phanerochaete chrysosporium* provide insight into selective ligninolysis. Proc. Natl. Acad. Sci. USA 109, 5458–5463.

Fernández-Fueyo, E., Ruiz-Dueñas, F.J., Martínez, M.J., Romero, A., Hammel, K.E., Medrano, F.J., Martínez, A.T., 2014. Ligninolytic peroxidase genes in the oyster mushroom genome: heterologous expression, molecular structure, catalytic and stability properties and lignin-degrading ability. Biotechnol. Biofuels 7, 2.

Floudas, D., Binder, M., Riley, R., Barry, K., Blanchette, R.A., Henrissat, B., Martínez, A.T., Otillar, R., Spatafora, J.W., Yadav, J.S., Aerts, A., Benoit, I., Boyd, A., Carlson, A., Copeland, A., Coutinho, P.M., de Vries, R.P., Ferreira, P., Findley, K., Foster, B., Gaskell, J., Glotzer, D., Górecki, P., Heitman, J., Hesse, C., Hori, C., Igarashi, K., Jurgens, J.A., Kallen, N., Kersten, P., Kohler, A., Kües, U., Kumar, T.K.A., Kuo, A., LaButti, K., Larrondo, L.F., Lindquist, E., Ling, A., Lombard, V., Lucas, S., Lundell, T., Martin, R., McLaughlin, D.J., Morgenstern, I., Morin, E., Murat, C., Nolan, M., Ohm, R.A., Patyshakuliyeva, A., Rokas, A., Ruiz-Dueñas, F.J., Sabat, G., Salamov, A., Samejima, M., Schmutz, J., Slot, J.C., St John, F., Stenlid, J., Sun, H., Sun, S., Syed, K., Tsang, A., Wiebenga, A., Young, D., Pisabarro, A., Eastwood, D.C., Martin, F., Cullen, D., Grigoriev, I.V., Hibbett, D.S., 2012. The Paleozoic origin of enzymatic lignin decomposition reconstructed from 31 fungal genomes. Science 336, 1715–1719.

Glumoff, T., Harvey, P.J., Molinari, S., Goble, M., Frank, G., Palmer, J.M., Smit, J.D.G., Leisola, M.S.A., 1990. Lignin peroxidase from *Phanerochaete chrysosporium* – molecular and kinetic characterization of isozymes. Eur. J. Biochem. 187, 515–520.

Godfrey, B.J., Akileswaran, L., Gold, M.H., 1994. A reporter gene construct for studying the regulation of manganese peroxidase gene expression. Appl. Environ. Microbiol. 60, 1353–1358.

Hammel, K.E., Jensen, K.A., Mozuch, M.D., Landucci, L.L., Tien, M., Pease, E.A., 1993. Ligninolysis by a purified lignin peroxidase. J. Biol. Chem. 268, 12274–12281.

Heid, C.A., Stevens, J., Livak, K.J., Williams, P.M., 1996. Real time quantitative PCR. Genome Res. 6, 986–994.

Irie, T., Honda, Y., Ha, H.-C., Watanabe, T., Kuwahara, M., 2000. Isolation of cDNA and genomic fragments encoding the major manganese peroxidase isoenzyme from the white rot basidiomycete *Pleurotus ostreatus*. J. Wood Sci. 46, 230–233.

Janusz, G., Kucharzyk, K.H., Pawlik, A., Staszczak, M., Paszczynski, A.J., 2013. Fungal laccase, manganese peroxidase and lignin peroxidase: gene expression and regulation. Enzyme Microb. Technol. 52, 1–12.

Kamitsuji, H., Honda, Y., Watanabe, T., Kuwahara, M., 2004. Production and induction of manganese peroxidase isozymes in a white-rot fungus *Pleurotus ostreatus*. Appl. Microbiol. Biotechnol. 65, 287–294.

Larraya, L.M., Pérez, G., Peñas, M.M., Baars, J.J.P., Mikosch, T.S.P., Pisabarro, A.G., Ramírez, L., 1999. Molecular karyotype of the white rot fungus *Pleurotus ostreatus*. Appl. Environ. Microbiol. 65, 3413–3417.

Ling, D.J., Salvaterra, P.M., 2011. Robust RT-qPCR data normalization: validation and selection of internal reference genes during post-experimental data analysis. PLoS ONE 6, 3.

Livak, K.J., Schmittgen, T.D., 2001. Analysis of relative gene expression data using real-time quantitative PCR and the 2(T)(-Delta Delta C) method. Methods 25, 402–408.

MacDonald, J., Doering, M., Canam, T., Gong, Y.C., Guttman, D.S., Campbell, M.M., Master, E.R., 2011. Transcriptomic responses of the softwood-degrading white-rot fungus *Phanerochaete carnosa* during growth on coniferous and deciduous wood. Appl. Environ. Microbiol. 77, 3211–3218.

Martínez, A.T., Camarero, S., Guillén, F., Gutiérrez, A., Muñoz, C., Varela, E., Martínez, M.J., Barrasa, J.M., Ruel, K., Pelayo, M., 1994. Progress in biopulping of non-woody materials: Chemical, enzymatic and ultrastructural aspects of wheat–straw delignification with ligninolytic fungi from the genus *Pleurotus*. FEMS Microbiol. Rev. 13, 265–274.

Please cite this article in press as: Fernández-Fueyo, E., et al. Ligninolytic peroxidase gene expression by *Pleurotus ostreatus*: Differential regulation in lignocellulose medium and effect of temperature and pH. Fungal Genet. Biol. (2014), http://dx.doi.org/10.1016/j.fgb.2014.02.003

Martínez, M.J., Böckle, B., Camarero, S., Guillén, F., Martínez, A.T., 1996. MnP isoenzymes produced by two Pleurotus species in liquid culture and during wheat straw solid-state fermentation. In: Jeffries, T.W., Viikari, L. (Eds.), Enzymes for Pulp and Paper Processing ACS, Washington, pp. 183–196.

Martinez, D., Larrondo, L.F., Putnam, N., Gelpke, M.D., Huang, K., Chapman, J., Helfenbein, K.G., Ramaiya, P., Detter, J.C., Larimer, F., Coutinho, P.M., Henrissat, B., Berka, R., Cullen, D., Rokhsar, D., 2004. Genome sequence of the lignocellulose degrading fungus *Phanerochaete chrysosporium* strain RP78. Nat. Biotechnol. 22, 695–700.

Martínez, A.T., Ruiz-Dueñas, F.J., Martínez, M.J., del Río, J.C., Gutiérrez, A., 2009. Enzymatic delignification of plant cell wall: from nature to mill. Curr. Opin. Biotechnol. 20, 348–357.

Martinez, D., Challacombe, J., Morgenstern, I., Hibbett, D.S., Schmoll, M., Kubicek, C.P., Ferreira, P., Ruiz-Dueñas, F.J., Martínez, A.T., Kersten, P., Hammel, K.E., Vanden Wymelenberg, A., Gaskell, J., Lindquist, E., Sabat, G., Bondurant, S.S., Larrondo, L.F., Canessa, P., Vicuña, R., Yadav, J., Doddapaneni, H., Subramanian, V., Pisabarro, A.G., Lavín, J.L., Oguiza, J.A., Master, E., Henrissat, B., Coutinho, P.M., Harris, P., Magnuson, J.K., Baker, S.E., Bruno, K., Kenealy, W., Hoegger, P.J., Kues, U., Ramaiya, P., Lucas, S., Salamov, A., Shapiro, H., Tu, H., Chee, C.L., Misra, M., Xie, G., Teter, S., Yaver, D., James, T., Mokrejs, M., Pospisek, M., Grigoriev, I.V., Brettin, T., Rokhsar, D., Berka, R., Cullen, D., 2009. Genome, transcriptome, and secretome analysis of wood decay fungus *Postia placenta* supports unique mechanisms of lignocellulose conversion. Proc. Natl. Acad. Sci. USA 106, 1954–1959.

Mayfield, M.B., Godfrey, B.J., Gold, M.H., 1994. Characterization of the *mnp2* gene encoding manganese peroxidase isozyme 2 from the basidiomycete *Phanerochaete chrysosporium*. Gene 142, 231–235.

Palmieri, G., Giardina, P., Bianco, C., Fontanella, B., Sannia, G., 2000. Copper induction of laccase isoenzymes in the ligninolytic fungus *Pleurotus ostreatus*. Appl. Environ. Microbiol. 66, 920–924.

Pérez-Boada, M., Doyle, W.A., Ruiz-Dueñas, F.J., Martínez, M.J., Martínez, A.T., Smith, A.T., 2002. Expression of *Pleurotus eryngii* versatile peroxidase in *Escherichia coli* and optimisation of *in vitro* folding. Enzyme Microb. Technol. 30, 518–524.

Pfaffl, M.W., Hageleit, M., 2001. Validities of mRNA quantification using recombinant RNA and recombinant DNA external calibration curves in real-time RT-PCR. Biotechnol. Lett. 23, 275–282.

Pfaffl, M.W., 2001. A new mathematical model for relative quantification in real-time RT-PCR. Nucleic Acids Res. 29, 9.

Pfaffl, M.W., 2004. Quantification strategies in real-time PCR. In: Bustin, S.A. (Ed.), A–Z of Quantitative PCR International University Line. La Jolla, CA, pp. 87–120.

Phillips, R., 2006. Mushrooms. McMilan.

Qin, L.X., Beyer, R.P., Hudson, F.N., Linford, N.J., Morris, D.E., Kerr, K.F., 2006. Evaluation of methods for oligonucleotide array data via quantitative real-time PCR. BMC Bioinformatics 7.

Ramakers, C., Ruijter, J.M., Deprez, R.H.L., Moorman, A.F.M., 2003. Assumption-free analysis of quantitative real-time polymerase chain reaction (PCR) data. Neurosci. Lett. 339, 62–66.

Ruiz-Dueñas, F.J., Martínez, A.T., 2009. Microbial degradation of lignin: how a bulky recalcitrant polymer is efficiently recycled in nature and how we can take advantage of this. Microbial Biotechnol. 2, 164–177.

Ruiz-Dueñas, F.J., Martínez, A.T., 2010. Structural and functional features of peroxidases with a potential as industrial biocatalysts. In: Torres, E., Ayala, M. (Eds.), Biocatalysts based on Heme Peroxidases, Springer-Verlag, Berlin, pp. 37–59.

Ruiz-Dueñas, F.J., Guillén, F., Camarero, S., Pérez-Boada, M., Martínez, M.J., Martínez, A.T., 1999. Regulation of peroxidase transcript levels in liquid cultures of the ligninolytic fungus *Pleurotus eryngii*. Appl. Environ. Microbiol. 65, 4458–4463.

Ruiz-Dueñas, F.J., Fernández, E., Martínez, M.J., Martínez, A.T., 2011. *Pleurotus ostreatus* heme peroxidases: an *in silico* analysis from the genome sequence to the enzyme molecular structure. C. R. Biol. 334, 795–805.

Ruiz-Dueñas, F.J., Lundell, T., Floudas, D., Nagy, L.G., Barrasa, J.M., Hibbett, D.S., Martínez, A.T., 2013. Lignin-degrading peroxidases in Polyporales: an evolutionary survey based on ten sequenced genomes. Mycologia 105, 1428–1444.

Salame, T.M., Yarden, O., Hadar, Y., 2010. *Pleurotus ostreatus* manganese-dependent peroxidase silencing impairs decolourization of Orange II. Microbial Biotechnol. 3, 93–106.

Salame, T.M., Knop, D., Levinson, D., Mabjeesh, S.J., Yarden, O., Hadar, Y., 2012. Release of *Pleurotus ostreatus* versatile-peroxidase from Mn2+ repression enhances anthropogenic and natural substrate degradation. PLoS ONE 7, 12.

Salame, T.M., Knop, D., Levinson, D., Yarden, O., Hadar, Y., 2013. Redundancy among manganese peroxidases in *Pleurotus ostreatus*. Appl. Environ. Microbiol. 79, 2405–2415.

Salvachúa, D., Prieto, A., Lopez-Abelairas, M., Lú-Chau, T., Martínez, A.T., Martínez, M.J., 2011. Fungal pretreatment: an alternative in second-generation ethanol from wheat straw. Bioresource Technol. 102, 7500–7506.

Sánchez, C., 2010. Cultivation of *Pleurotus ostreatus* and other edible mushrooms. Appl. Microbiol. Biotechnol. 85, 1321–1337.

Sarkar, S., Martínez, A.T., Martínez, M.J., 1997. Biochemical and molecular characterization of a manganese peroxidase isoenzyme from *Pleurotus ostreatus*. Biochim. Biophys. Acta 1339, 23–30.

Sato, S., Feltus, F.A., Iyer, P., Tien, M., 2009. The first genome-level transcriptome of the wood-degrading fungus *Phanerochaete chrysosporium* grown on red oak. Curr. Genetics 55, 273–286.

Sooknanan, R., Malek, L., Wang, X.H., Siebert, T., Keating, A., 1993. Detection and direct-sequence identification of BCR-ABL messenger-RNA in Ph(+) chronic myeloid-leukemia. Exp. Hematol. 21, 1719–1724.

Stahlberg, A., Elbing, K., Andrade-Garda, J.M., Sjogreen, B., Forootan, A., Kubista, M., 2008. Multiway real-time PCR gene expression profiling in yeast *Saccharomyces cerevisiae* reveals altered transcriptional response of ADH-genes to glucose stimuli. BMC Genomics 9, 170.

Tien, M., Kirk, T.K., 1983. Lignin-degrading enzyme from the hymenomycete *Phanerochaete chrysosporium* Burds. Science 221, 661–663.

Vandesompele, J., De Preter, K., Pattyn, F., Poppe, B., Van Roy, N., De Paepe, A., Speleman, F., 2002. Accurate normalization of real-time quantitative RT-PCR data by geometric averaging of multiple internal control genes. Genome Biol. 3, 7.

Wymelenberg, A.V., Gaskell, J., Mozuch, M., Bondurant, S.S., Sabat, G., Ralph, J., Skyba, O., Mansfield, S.D., Blanchette, R.A., Grigoriev, I.V., Kersten, P.J., Cullen, D., 2011. Significant alteration of gene expression in wood decay fungi *Postia placenta* and *Phanerochaete chrysosporium* by plant species. Appl. Environ. Microbiol. 77, 4499–4507.

Young, R.A., Akhtar, M., 1998. Environmentally-Friendly Technologies for the Pulp and Paper Industry. John Wiley and Sons, New York.

Please cite this article in press as: Fernández-Fueyo, E., et al. Ligninolytic peroxidase gene expression by *Pleurotus ostreatus*: Differential regulation in lignocellulose medium and effect of temperature and pH. Fungal Genet. Biol. (2014), http://dx.doi.org/10.1016/j.fgb.2014.02.003

Capítulo 5

"Comparative genomics of *Ceriporiopisis subvermispora* and *Phanerochaete chrysosporium* provide insight into selective ligninolysis"

Fernández-Fueyo, E., F. J. Ruiz-Dueñas, P. Ferreira, D. Floudas, D. S. Hibbett, P. Canessa, L. Larrondo, T. Y. James, D. Seelenfreund, S. Lobos, R. Polanco, M. Tello, Y. Honda, T. Watanabe, T. Watanabe, J. S. Ryu, C. P. Kubicek, M. Schmoll, J. Gaskell, K. E. Hammel, F. J. St.John, A. Vanden Wymelenberg, G. Sabat, S. S. Bondurant, K. Syed, J. Yadav, H. Doddapaneni, V. Subramanian, J. L. Lavín, J. A. Oguiza, G. Perez, A. G. Pisabarro, L. Ramírez, F. Santoyo, E. Master, P. M. Coutinho, B. Henrissat, V. Lombard, J. K. Magnuson, U. Kües, C. Hori, K. Igarashi, M. Samejima, B. W. Held, K. Barry, K. LaButti, A. Lapidus, E. Lindquist, S. Lucas, R. Riley, A. Salamov, D. Hoffmeister, D. Schwenk, Y. Hadar, O. Yarden, R. P. de Vries, A. Wiebenga, J. Stenlid, D. C. Eastwood, I. V. Grigoriev, R. Berka, R. A. Blanchette, P. Kersten, A. T. Martínez, R. Vicuña, and D. Cullen.

Proc. Natl. Acad. Sci. USA 109:5458-5463. 2012.

Comparative genomics of *Ceriporiopsis subvermispora* and *Phanerochaete chrysosporium* provide insight into selective ligninolysis

Elena Fernandez-Fueyo[a], Francisco J. Ruiz-Dueñas[a], Patricia Ferreira[b], Dimitrios Floudas[c], David S. Hibbett[c], Paulo Canessa[d], Luis F. Larrondo[d], Tim Y. James[e], Daniela Seelenfreund[f], Sergio Lobos[f], Rubén Polanco[g], Mario Tello[h], Yoichi Honda[i], Takahito Watanabe[i], Takashi Watanabe[i], Jae San Ryu[j], Christian P. Kubicek[k,l], Monika Schmoll[k], Jill Gaskell[m], Kenneth E. Hammel[m], Franz J. St. John[m], Amber Vanden Wymelenberg[n], Grzegorz Sabat[o], Sandra Splinter BonDurant[o], Khajamohiddin Syed[p], Jagjit S. Yadav[p], Harshavardhan Doddapaneni[q], Venkataramanan Subramanian[r], José L. Lavín[s], José A. Oguiza[s], Gumer Perez[s], Antonio G. Pisabarro[s], Lucia Ramirez[s], Francisco Santoyo[s], Emma Master[t], Pedro M. Coutinho[u], Bernard Henrissat[u], Vincent Lombard[u], Jon Karl Magnuson[v], Ursula Kües[w], Chiaki Hori[x], Kiyohiko Igarashi[x], Masahiro Samejima[x], Benjamin W. Held[y], Kerrie W. Barry[z], Kurt M. LaButti[z], Alla Lapidus[z], Erika A. Lindquist[z], Susan M. Lucas[z], Robert Riley[z], Asaf A. Salamov[z], Dirk Hoffmeister[aa], Daniel Schwenk[aa], Yitzhak Hadar[bb], Oded Yarden[bb], Ronald P. de Vries[cc], Ad Wiebenga[cc], Jan Stenlid[dd], Daniel Eastwood[ee], Igor V. Grigoriev[z], Randy M. Berka[ff], Robert A. Blanchette[y], Phil Kersten[m], Angel T. Martinez[a], Rafael Vicuna[d], and Dan Cullen[m,1]

[a]Centro de Investigaciones Biológicas, Consejo Superior de Investigaciones Cientificas, E-28040 Madrid, Spain; [b]Department of Biochemistry and Molecular and Cellular Biology and Institute of Biocomputation and Physics of Complex Systems, University of Zaragoza, 50018 Zaragoza, Spain; [c]Biology Department, Clark University, Worcester, MA 01610; [d]Department of Molecular Genetics and Microbiology, Faculty of Biological Sciences, Pontificia Universidad Católica de Chile and Millennium Institute for Fundamental and Applied Biology, 7780344 Santiago, Chile; [e]Department of Ecology and Evolution, University of Michigan, Ann Arbor, MI 48109; [f]Department of Biochemistry and Molecular Biology, Faculty of Chemical Sciences and Pharmaceuticals, Universidad de Chile, Santiago, Chile; [g]Department of Biological Sciences, Faculty of Biological Sciences, Universidad Andrés Bello, Santiago, Chile; [h]Aquatic Biotechnology Center, Department of Biology, Faculty of Chemistry and Biology, Universidad de Santiago de Chile, Santiago, Chile; [i]Laboratory of Biomass Conversion, Research Institute for Sustainable Humanosphere, Kyoto University, Uji 611-0011, Japan; [j]Department of Ecofriendliness Research, Gyeongnam Agricultural Research and Extension Services, Gyeongnam 621-802, Korea; [k]Research Area of Biotechnology and Microbiology, Institute of Chemical Engineering, Technische Universität Wien, A-1060 Vienna, Austria; [l]Institute of Chemical Engineering, Austrian Center of Industrial Biotechnology, Technische Universitat Wien, A-1060 Vienna, Austria; [m]Forest Service, Forest Products Laboratory, US Department of Agriculture, Madison, WI 53726; [n]Department of Bacteriology, University of Wisconsin, Madison, WI 53706; [o]University of Wisconsin Biotechnology Center, Madison, WI 53706; [p]Department of Environmental Health, University of Cincinnati, Cincinnati, OH 45267; [q]Department of Biology, University of Iowa, Iowa City, IA 52242, [r]National Renewable Energy Laboratory and Colorado School of Mines, Golden, CO 80401; [s]Genetics and Microbiology Research Group, Public University of Navarre, 31006 Pamplona, Spain; [t]Department of Chemical Engineering, University of Toronto, Toronto, ON, Canada M5S 3E5; [u]Architecture et Fonction des Macromolécules Biologiques, Aix-Marseille Université, Centre National de la Recherche Scientifique, Unité Mixte de Recherche 7257, 13288 Marseille, France; [v]Pacific Northwest National Laboratory, Richland, WA 99352; [w]Molecular Wood Biotechnology and Technical Mycology, Büsgen-Institute, Georg-August-University Göttingen, Büsgenweg2, 37077 Göttingen, Germany; [x]Department of Biomaterial Sciences, University of Tokyo, Japan; [y]Department of Plant Pathology, University of Minnesota, St. Paul, MN 55108; [z]US Department of Energy Joint Genome Institute, Walnut Creek, CA 94598; [aa]Department of Pharmaceutical Biology, Friedrich-Schiller-University, 07745 Jena, Germany; [bb]Department of Plant Pathology and Microbiology, Hebrew University of Jerusalem, Rehovot 91120, Israel; [cc]Fungal Biodiversity Centre, Centraalbureau voor Schimmelcultures, Royal Netherlands Academy of Arts and Sciences, 3584 CT Utrecht, The Netherlands; [dd]Department of Forest Mycology and Pathology, Swedish University of Agricultural Sciences, 75007 Uppsala, Sweden; [ee]Department of Biosciences, Swansea University, Swansea SA2 8PP, United Kingdom; and [ff]Novozymes, Davis, CA 95618

Edited by Richard A. Dixon, The Samuel Roberts Noble Foundation, Ardmore, OK, and approved February 22, 2012 (received for review December 6, 2011)

Efficient lignin depolymerization is unique to the wood decay basidiomycetes, collectively referred to as white rot fungi. *Phanerochaete chrysosporium* simultaneously degrades lignin and cellulose, whereas the closely related species, *Ceriporiopsis subvermispora,* also depolymerizes lignin but may do so with relatively little cellulose degradation. To investigate the basis for selective ligninolysis, we conducted comparative genome analysis of *C. subvermispora* and *P. chrysosporium*. Genes encoding manganese peroxidase numbered 13 and five in *C. subvermispora* and *P. chrysosporium*, respectively. In addition, the *C. subvermispora* genome contains at least seven genes predicted to encode laccases, whereas the *P. chrysosporium* genome contains none. We also observed expansion of the number of *C. subvermispora* desaturase-encoding genes putatively involved in lipid metabolism. Microarray-based transcriptome analysis showed substantial upregulation of several desaturase and MnP genes in wood-containing medium. MS identified MnP proteins in *C. subvermispora* culture filtrates, but none in *P. chrysosporium* cultures. These results support the importance of MnP and a lignin degradation mechanism whereby cleavage of the dominant nonphenolic structures is mediated by lipid peroxidation products. Two *C. subvermispora* genes were predicted to encode peroxidases structurally similar to *P. chrysosporium* lignin peroxidase and, following heterologous expression in *Escherichia coli*, the enzymes were shown to oxidize high redox potential substrates, but not Mn^{2+}. Apart from oxidative lignin degradation, we also examined cellulolytic and hemicellulolytic systems in both fungi. In summary, the *C. subvermispora* genetic inventory and expression patterns exhibit increased oxidoreductase potential and diminished cellulolytic capability relative to *P. chrysosporium*.

Author contributions: S.S.B., K.W.B., E.A.L., S.M.L., I.V.G., R.M.B., R.A.B., P.K., A.T.M., R.V., and D.C. designed research; E.F.-F., J.G., A.V.W., G.S., B.W.H., K.M.L., A.L., R.R., A.A.S., and A.W. performed research; E.F.-F., F.J.R.-D., P.F., D.F., D.S.H., P.C., L.F.L., T.Y.J., D. Seelenfreund, S.L., R.P., M.T., Y. Honda, Takahito Watanabe, Takashi Watanabe, J.S.R., C.P.K., M. Schmoll, J.G., F.J.S.J., A.V.W., G.S., S.S.B., K.S., J.S.Y., H.D., V.S., J.L.L., J.A.O., G.P., A.G.P., L.R., F.S., E.M., P.M.C., B.H., V.L., J.K.M., U.K., C.H., K.I., M. Samejima, B.W.H., K.W.B., K.M.L., A.L., E.A.L., S.M.L., R.R., A.A.S., D.H., D. Schwenk, Y. Hadar, O.Y., R.P.d.V., A.W., J.S., D.E., I.V.G., R.M.B., R.A.B., P.K., A.T.M., R.V., and D.C. analyzed data; and E.F.-F., F.J.R.-D., P.F., D.F., D.S.H., P.C., L.F.L., T.Y.J., D. Seelenfreund, S.L., R.P., M.T., Y. Honda, Takahito Watanabe, Takashi Watanabe, J.S.R., C.P.K., M. Schmoll, J.G., K.E.H., F.J.S.J., G.S., S.S.B., K.S., J.S.Y., H.D., V.S., J.L.L., J.A.O., G.P., A.G.P., L.R., F.S., E.M., P.M.C., B.H., V.L., J.K.M., U.K., C.H., K.I., M. Samejima, B.W.H., K.W.B., K.M.L., A.L., E.A.L., S.M.L., R.R., A.A.S., D.H., D. Schwenk, Y. Hadar, O.Y., R.P.d.V., A.W., J.S., D.E., I.V.G., R.M.B., R.A.B., P.K., A.T.M., R.V., and D.C. wrote the paper.

The authors declare no conflict of interest.

This article is a PNAS Direct Submission.

Data deposition: The annotated genome is available on an interactive web portal, http://jgi.doe.gov/Ceriporiopsis and at DNA Data Base in Japan/European Molecular Biology Laboratory (DDBJ/EMBL)/GenBank (project accession no. AEOV00000000). The data reported in this paper have been deposited in the Gene Expression Omnibus (GEO) database, www.ncbi.nlm.nih.gov/geo (accession no. GSE34636).

[1]To whom correspondence should be addressed. E-mail: dcullen@wisc.edu.

This article contains supporting information online at www.pnas.org/lookup/suppl/doi:10.1073/pnas.1119912109/-/DCSupplemental.

The most abundant source of photosynthetically fixed carbon in land ecosystems is plant biomass, composed primarily of cellulose, hemicellulose, and lignin. Many microorganisms are capable of using cellulose and hemicellulose as carbon and energy sources, but a much smaller group of filamentous fungi in the phylum Basidiomycota has also evolved with the unique ability to efficiently depolymerize and mineralize lignin, the most recalcitrant component of plant cell walls. Collectively known as white rot fungi, they remove lignin to gain access to cell wall carbohydrates for carbon and energy sources. These wood-decay fungi are common inhabitants of fallen trees and forest litter. As such, white rot fungi play a pivotal role in the carbon cycle. Their unique metabolic capabilities are of considerable recent interest in bioenergy-related processes (1).

White rot basidiomycetes differ in their gross morphological patterns of decay (ref. 2 and refs. therein). *Phanerochaete chrysosporium* simultaneously degrades cellulose, hemicellulose, and lignin, whereas a few others such as the closely related polypore species, *Ceriporiopsis subvermispora*, have the ability to remove lignin in advance of cellulose. The mechanistic basis of this selectivity is unknown.

The roles of *P. chrysosporium* lignin peroxidase [LiP; Enzyme Commission (EC) 1.11.1.14] and manganese peroxidase (EC 1.11.1.13) have been intensively studied (3). Reactions catalyzed by LiP include C_α-C_β cleavage of propyl side chains in lignin and lignin models, hydroxylation of benzylic methylene groups, oxidation of benzyl alcohols to the corresponding aldehydes or ketones, phenol oxidation, and aromatic ring cleavage in nonphenolic lignin model compounds. In addition to *P. chrysosporium*, multiple ligninolytic peroxidase isozymes and their corresponding genes have been identified in several efficient lignin-degrading fungi (4). In some white rot fungi, such as the oyster mushroom *Pleurotus ostreatus* and related species, LiP is absent, but a third ligninolytic peroxidase type that combines LiP and MnP catalytic properties, versatile peroxidase (VP; EC 1.11.1.16), has been characterized (4, 5) and identified by genome analysis (6). Repeated and systematic attempts have failed to identify LiP (or VP) activity in *C. subvermispora* cultures, but substantial evidence implicates MnP in ligninolysis (e.g., refs 7, 8). First discovered in *P. chrysosporium* cultures, this enzyme oxidizes Mn^{2+} to Mn^{3+}, using H_2O_2 as an oxidant (9, 10). MnP cannot directly cleave the dominant nonphenolic structures within lignin, but it has been suggested that oxidation may be mediated by lipid peroxidation mechanisms that are promoted by Mn^{3+} (3).

In addition to peroxidases, laccases (EC 1.10.3.2) have been implicated in lignin degradation. Several have been characterized from *C. subvermispora* cultures (11), whereas no genes encoding laccase, in the strict sense, are present in the *P. chrysosporium* genome (12). The mechanism by which laccases might degrade lignin remains unclear, as the enzyme lacks sufficient oxidation potential to cleave nonphenolic linkages within the polymer. However, various mediators have been proposed (13).

Other components commonly ascribed to ligninolytic systems include extracellular enzymes capable of generating hydrogen peroxide. Glucose–methanol–choline oxidoreductases such as aryl-alcohol oxidase, methanol oxidase and pyranose oxidase, together with copper radical oxidases such as glyoxal oxidase, have been characterized in *P. chrysosporium* (14), but none of these activities have been reported in *C. subvermispora* cultures.

Conceivably, selective lignin degradation patterns may involve modulation of the hydrolytic enzymes commonly associated with cellulose and hemicellulose degradation. These systems are well characterized in *P. chrysosporium*, whereas little is known about *C. subvermispora* glycoside hydrolases (GHs) (15).

To further our understanding of selective ligninolysis, we report here initial analysis of the *C. subvermispora* genome. Comparison with the genome, transcriptome, and secretome of *P. chrysosporium* reveal substantial differences among the genes that are likely to be involved in lignocellulose degradation, providing insight into diversification of the white rot mechanism.

Results

General Features of *C. subvermispora* Genome. The 39-Mb haploid genome of *C. subvermispora* monokaryotic strain B (16) (*SI Appendix*, Fig. S1) is predicted to encode 12,125 proteins (*SI Appendix* provides detailed assembly and annotation information). For comparison, the latest release of the related polypore white rot fungus *P. chrysosporium* features 35.1 Mb of nonredundant sequence and 10,048 gene models (12, 17). The overall relatedness of these polypore fungi was clearly evident from the syntenic regions between their largest scaffolds and large number of similar (BLAST E-values $<10^{-5}$) protein sequences, i.e., 74% (n = 9,007) of *C. subvermispora* models aligned with *P. chrysosporium* and 82% (n = 8,258) of *P. chrysosporium* models aligned with *C. subvermispora*. Most (n = 5,443) of these pairs were also reciprocal "best hits" and are thus likely to represent orthologues. Significant expansions compared with *P. chrysosporium* and/or other sequenced Agaricomycetes were observed in transporters, various oxidoreductases including peroxidases, cytochrome p450s, and other gene families discussed here.

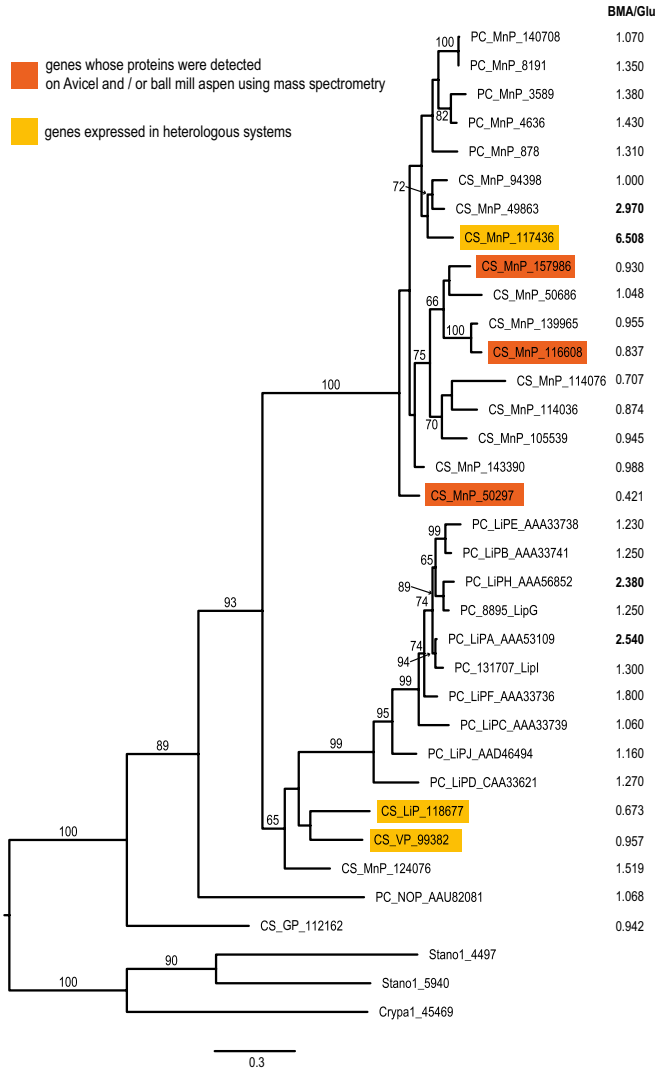

Fig. 1. Phylogenetic analysis of selected peroxidases from *C. subvermispora* and *P. chrysosporium*. The analysis was performed in RAxML Blackbox under the model GTRGAMMA, using the substitution matrix WAG with 100 rapid bootstrap replicates. The ascomycete sequences of class II peroxidases were used to root the tree (http://phylobench.vital-it.ch/raxml-bb/) (32). Ball-milled aspen versus glucose transcript ratios (BMA/Glu) are indicated, and complete data are available under Gene Expression Omnibus accession nos. GSE1473 and GSE34636 for *P. chrysosporium* and *C. subvermispora*, respectively.

MICROBIOLOGY

Peroxidases. Twenty-six *C. subvermispora* gene models are predicted to encode heme peroxidases. Fifteen were classified as probable ligninolytic peroxidases, which included 13 MnPs, a VP, and an LiP. These classifications were based on homology modeling (18) with particular attention to conserved Mn^{2+} oxidation and catalytic tryptophan sites (19, 20). Those classified as MnPs include seven typical "long" MnPs specific for Mn^{2+}, and a "short" MnP also able to oxidize phenols and 2,2′-azino-bis(3-ethylbenzothiazoline-6-sulfonate) in the absence of Mn^{2+}, as previously reported in the *P. ostreatus* genome (6). The remaining five could be classified as "extra long" MnPs in view of their long C-termini, as reported for the first time in *Dichomitus squalens* MnPs (21). Only four full-length MnP-encoding genes were previously identified in *C. subvermispora* (GenBank accession nos. AAB03480, AAB92247, AAO61784, and AF161585). Additional class II peroxidases have long been suspected (22, 23), but no LiP/VP-like transcripts or activities have been identified. Thus, the repertoire of *C. subvermispora* peroxidases differs from *P. chrysosporium*, which features 10 LiP and five MnP genes (Fig. 1). Extending comparative analysis to 90 basidiomycete peroxidases (*SI Appendix*, Fig. S3) suggested that the *C. subvermispora* VP and LiP represent divergent proteins, an observation consistent with their catalytic properties (as detailed later).

By using a previously developed *Escherichia coli* expression system including in vitro activation (24, 25), the *C. subvermispora* putative LiP (Cesubv118677) and VP (Cesubv99382) were evaluated for their oxidation of three representative substrates, namely Mn^{2+}, the high redox-potential veratryl alcohol (VA), and Reactive Black 5 (RB5) (Table 1). The corresponding steady-state kinetic constants were compared with those of *Pleurotus eryngii* VP (isozyme VPL; AF007244), a *P. chrysosporium* LiP (isozyme H8; GenBank accession no. Y00262), and a conventional *C. subvermispora* MnP (Cesubv117436; Fig. 1) also produced in *E. coli*. The putative *C. subvermispora* LiP (protein model Cesubv118677) was unable to oxidize Mn^{2+}, as expected given the absence of a typical manganese oxidation site in its theoretical molecular structure (*SI Appendix*, Fig. S2). A conventional *C. subvermispora* MnP protein (Cesubv117436), also predicted based on structure, and the VP from *P. eryngii* showed Mn^{2+} oxidation. Surprisingly, the *C. subvermispora* protein designated Cesubv99382, which we tentatively classified as a VP, was not able to oxidize Mn^{2+}, irrespective of the presence of a putative manganese oxidation site in its structural model (*SI Appendix*, Fig. S2). The catalytic behaviors of Cesubv99382 and Cesubv118677 are very similar. Both enzymes oxidize VA, the typical LiP (and VP) substrate, and also RB5, a characteristic substrate of VP (that LiP is unable to oxidize in the absence of mediators), with similar K_m, k_{cat}, and k_{cat}/K_m values (Table 1).

Peroxidase expression patterns differed significantly between *C. subvermispora* and *P. chrysosporium*. In medium containing ball-milled *Populus grandidentata* (aspen) as sole carbon source, transcript levels of two *C. subvermispora* MnPs were significantly up-regulated relative to glucose medium. Liquid chromatography/tandem MS (LC-MS/MS) analysis of culture filtrates identified peptides corresponding to three *C. subvermispora* MnP genes (Fig. 1). In identical media, none of the *P. chrysosporium* MnP genes were up-regulated, but significant accumulation of two LiP gene transcripts was observed relative to glucose (Fig. 1). No peroxidases were identified by LC-MS/MS analysis of *P. chrysosporium* culture filtrates.

Multicopper Oxidases. Nine multicopper (MCO)-encoding *C. subvermispora* genes may be relevant to lignin degradation. Multiple alignments emphasizing signature regions (26, 27) revealed the presence of seven laccases, in the strictest sense, one of which was previously known (28). This observation is in distinct contrast to the *P. chrysosporium* genome, which contains no laccases (12) (Fig. 2). Consistent with a role in lignocellulose modification, transcript levels corresponding to *C. subvermispora* laccase was significantly up-regulated (more than threefold; $P < 0.01$) in media containing ball-milled *P. grandidentata* wood (aspen) relative to glucose medium (Fig. 2).

In addition to the laccases, *C. subvermispora* MCO-encoding genes included a canonical ferroxidase (Fet3). Involved in high-affinity iron uptake, the Fet3 genes of *C. subvermispora* (Cesubv67172) and *Postia placenta* (Pospl129808) show significant up-regulation on aspen-containing medium, whereas the *P. chrysosporium* orthologue (Phchr26890) is sharply down-regulated under identical conditions (Fig. 2). This strongly suggests that iron homeostasis is achieved by different mechanisms in these fungi.

Other Enzymes Potentially Involved in Extracellular Redox Processes. Peroxide and free radical generation are considered key components of ligninolysis, and analysis of the *C. subvermispora* genome, transcriptome, and secretome revealed a diverse array of relevant proteins. These included four copper radical oxidases, cellobiose dehydrogenase, various other glucose–methanol–choline oxidoreductases, and several putative transporters. Possibly related to selectivity of ligninolysis, expression patterns exhibited by certain genes, e.g., methanol oxidase, differed significantly between *P. chrysosporium* and *C. subvermispora*. (*SI Appendix* and *SI Appendix*, Table S1, include detailed listings of all annotated genes, transcript levels, and LC-MS/MS identification of extracellular proteins.)

Of particular relevance to lignin degradation by MnP, we observed a significant expansion of the genes putatively involved in fatty acid metabolism (Table 2). Relative to the single gene in *P. chrysosporium* (encoding Phchr125220) the Δ-12 fatty acid desaturase gene family was particularly expanded (five paralogues) in *C. subvermispora*. The *P. chrysosporium* and *C. subvermispora*

Table 1. Steady-state kinetic constants of three peroxidases from *C. subvermispora* genome vs. *P. chrysosporium* LiP and *P. eryngii* VP

	C. subvermispora			*P. chrysosporium*	*P. eryngii*
Constant	99382 ("VP")	118677 (LiP)	117436 (MnP)	Y00262 (LiPH8)	AF007244 (VPL)
Mn^{2+}					
K_m, μM	ND [b]	ND	58.5 ± 8.5	ND	181 ± 10
k_{cat}, s^{-1}	0	0	331 ± 20	0	275 ± 4
k_{cat}/K_m, $mM^{-1}·s^{-1}$	0	0	5,600 ± 500	0	1,520 ± 70
VA					
K_m, μM	3,120 ± 526	1,620 ± 290	ND	190 ± 17	4,130 ± 320
k_{cat}, s^{-1}	8.6 ± 0.7	8.7 ± 0.6	0	17.5 ± 0.5	9.5 ± 0.2
k_{cat}/K_m, $mM^{-1}·s^{-1}$	2.8 ± 0.3	5.4 ± 0.7	0	92.0 ± 6.0	2.3 ± 0.1
RB5					
K_m, μM	3.97 ± 0.65	4.48 ± 0.64	ND	ND	3.4 ± 0.3
k_{cat}, s^{-1}	9.8 ± 0.9	7.3 ± 0.5	0	0	5.5 ± 0.3
k_{cat}/K_m, $mM^{-1}·s^{-1}$	2,460 ± 185	1,620 ± 138	0	0	1,310 ± 90

Reactions were at 25 °C in 0.1 M tartrate (pH 3 for VA, pH 3.5 for RB5, and pH 5 for Mn^{2+}). ND, not determined because of lack of activity. Means and 95% SEM are provided.

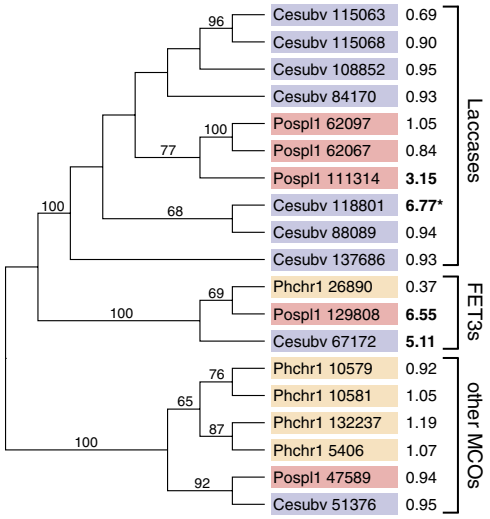

Fig. 2. Phylogenetic analysis of all MCO oxidases from *C. subvermispora*, *P. chrysosporium*, and the related polypore *P. placenta*. Analysis was performed by using RAxML with the WAG substitution matrix, γ-distributed rates among sites, a proportion of invariant sites and empirical amino acid frequencies (i.e., m = PROTGAMMAIWAGF). Shown is the maximum-likelihood tree found by using 1,000 heuristic searches, with bootstrap support shown for nodes with values greater than 50%. As in Fig. 1, transcript level ratios are adjacent to protein identification numbers. Complete *P. placenta* microarray data are available under Gene Expression Omnibus accession no. GSE12540 (33).

genes were previously designated *Pcfad2* and *Csfad2* (29, 30), respectively. Transcript levels of *P. chrysosporium Pcfad2* were significantly reduced (0.25-fold; $P < 0.01$) in media with aspen relative to glucose, whereas a *C. subvermispora* Δ-12 fatty acid desaturase (Cesubv124119) was up-regulated (2.9-fold; $P < 0.01$). With regard to Δ-9 fatty acid desaturases, only two *P. chrysosporium* genes were detected and, as in the case of Δ-12 fatty acid synthetases, both were down-regulated more than twofold ($P < 0.01$). Modest transcript accumulation (1.48-fold; $P = 0.03$) was observed for one of the four *C. subvermispora* Δ-9 fatty acid desaturases (Cesubv117066) in aspen wood media relative to glucose media. Increased numbers of MnP and lipid metabolism genes, viewed together with their expression patterns, are consistent with an important role for peroxyl radical attack on nonphenolic substructures of lignin.

Carbohydrate Active Enzymes. Overall, the number of GHs encoded by the *C. subvermispora* genome is slightly lower than that of other plant cell wall degrading basidiomycetes whose genomes have been sequenced (Dataset S1 and *SI Appendix*, Table S1). The number of GHs in *C. subvermispora* ($n = 171$) is close to that in *P. chrysosporium* ($n = 177$), and noticeably different in total number and in family distribution compared with the phylogenetically related brown rot fungus *P. placenta* ($n = 145$; Fig. 3). Differences between *C. subvermispora* and *P. chrysosporium* are limited to a few families, but these distinctions might have consequences for degradation of plant cell wall polysaccharides. For example, *C. subvermispora* contained only three predicted proteins belonging to family GH7, an important group typically featuring "exo" cellobiohydrolases. In contrast, at least six GH7 protein models were identified in the *P. chrysosporium* genome. Family GH3, containing β-glucosidases involved in the hydrolysis of cellobiose, was represented by only six gene models in the *C. subvermispora* genome, unlike the 11 GH3 models found in *P. chrysosporium*. In addition, the *C. subvermispora* genome revealed only 16 cellulose binding modules (CBM1s), compared with 31 CBM1-containing protein models found in the *P. chrysosporium* genome.

In contrast to the oxidative systems, transcriptome and secretome analysis of GHs generally showed lower expression in *C. subvermispora* relative to *P. chrysosporium* (Table 3 and *SI Appendix*, Table S1). Transcripts corresponding to 30 *C. subvermispora* GH-encoding genes accumulated more than twofold ($P < 0.05$) in aspen wood- vs. glucose-containing media. In contrast, 52 *P. chrysosporium* GH-encoding genes were up-regulated (more than twofold; $P < 0.05$). MS unambiguously identified 60 and 121 proteins in filtrates from aspen wood media of *P. chrysosporium* and *C. subvermispora* cultures, respectively, among which 18 and three, respectively, corresponded to GHs.

Genes encoding likely cellulases showed only modest transcript levels in *C. subvermispora* (Table 3). *C. subvermispora* transcripts corresponding to single copies of a CBM1-containing cellobiohydrolase (GH7), a CBM1-containing endo-β-1,4-glucanase (GH5), and a GH12 endoglucanase, all canonical cellulases, were significantly up-regulated (more than twofold; $P < 0.01$) in aspen wood relative to glucose media. Under identical conditions, accumulating *P. chrysosporium* transcripts included four GH7 cellobiohydrolases, two GH5 endo-β-1,4-glucanases, and two GH12 endoglucanases (Table 3).

The foregoing analysis is limited to expression patterns of genes with putative function inferred from sequence comparisons. However, many of the predicted proteins that show no significant sequence similarity to known proteins could be important in selective ligninolysis. Specifically, we identified 139 "hypothetical" *C. subvermispora* proteins whose sequences show

Table 2. Number, overall relatedness, and transcript levels of genes putatively involved in lipid metabolism

C. subvermispora						*P. chrysosporium*						
Protein ID	Glc	BMA	B/G	*P* value	Comment	Protein ID	E-value	ID, %	Glc	BMA	B/G	*P* value
Δ-12 fatty acid desaturase (COG 3239)												
124119	11.01	12.54	2.90*	< 0.01	—	125220	1.00×10^{-67}	72	12.76	10.77	0.25*	<0.01
58880	10.36	10.29	0.96	0.729	—	125220	3.00×10^{-70}	72	12.76	10.77	0.25*	<0.01
109092	10.58	10.23	0.78	0.0149	—	125220	5.00×10^{-59}	72	12.76	10.77	0.25*	<0.01
155708	10.67	10.11	0.68	< 0.01	—	125220	2.00×10^{-77}	72	12.76	10.77	0.25*	<0.01
112068	12.74	12.66	0.94	0.653	*Csfad2* (29); *Pcfad2* (30)	125220	0.00	72	12.76	10.77	0.25*	<0.01
Δ-9 fatty acid desaturase (COG 1398)												
117066	11.78	12.35	1.48	0.0298	*CsOle1* & *PcOle1* (29)	128650	0.00	81	13.82	12.48	0.40*	<0.01
87875	8.93	8.94	1.01	0.88	—	121154	2.00×10^{-68}	33	13.49	12.38	0.46*	0.017
117063	8.95	8.91	0.97	0.527	5′ needs editing	121154	2.00×10^{-62}	33	13.49	12.38	0.46*	0.017
121693	9.64	9.51	0.92	0.179	—	121154	1.00×10^{-154}	33	13.49	12.38	0.46*	0.017

Normalized microarray data are presented as $\log_2$ signal strength average of fully replicated experiments. Significant accumulation (B/G ratio) of transcripts in BMA relative to glucose-grown (Glc) cultures was determined using the Moderated *t* test and associated FDR. See Gene Expression Omnibus accession no. GSE14736 (33) for *P. chrysosporium* data. Both gene families are expanded in *C. subvermispora* relative to *P. chrysosporium*. BMA, ball-milled aspen; COG, clusters of orthologous groups; FDR, false detection rate.
*Significant ratio (<0.5-fold to >2-fold).

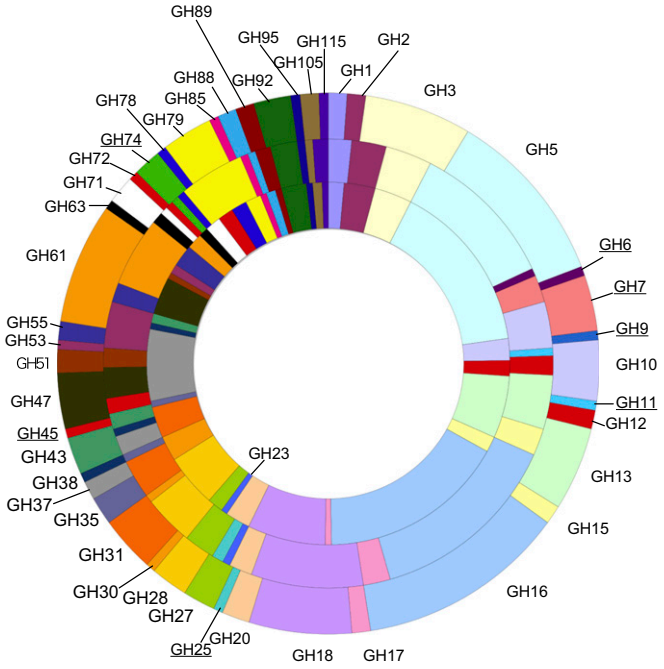

Fig. 3. Distribution of GHs in *P. placenta* (inner ring), *C. subvermispora* (middle ring), and *P. chrysosporium* (outer ring). Families absent from at least one species are underlined. Detailed listings of gene numbers within these and other species appear in Dataset S1, and expression patterns (transcript and protein) are presented in *SI Appendix*, Table S1.

no significant similarity to *P. chrysosporium* models but were otherwise highly expressed, i.e., transcript levels more than two SDs above the genome-wide mean (n = 12084, X = 10.56) or more than twofold transcript accumulation in aspen wood media vs. glucose or unambiguously identified via MS (at least two unique peptide sequences).

Discussion

C. subvermispora and *P. chrysosporium* are both members of the order Polyporales, but they differ sharply in their ability to selectively degrade lignin. The genetics and physiology of *P. chrysosporium* have been intensively studied for decades. Largely because of its efficient degradation of plant cell walls, including the recalcitrant lignin, *P. chrysosporium* was selected as the first sequenced basidiomycete (12). In contrast, *C. subvermispora* has received less attention, although its selective lignin degradation is well known (2). Overall, our comparisons of *C. subvermispora* and *P. chrysosporium* gene repertoires, together with expression patterns on a complex lignocellulose substrate, suggest divergent strategies of plant cell wall degradation and provide clues about mechanisms of selective delignification.

Generally accepted as important components of lignin degradation systems, class II peroxidases were skewed toward expansion of the number of MnPs and accompanied by a putative LiP (Cesubv118677) and a VP (Cesubv99382). To confirm these predictions, both peroxidases were obtained by *E. coli* expression, and their steady-state kinetic constants for oxidation of selected peroxidase substrates were compared with those of a typical MnP from the *C. subvermispora* genome (Cesubv117436), a well characterized VP from *P. eryngii* (GenBank AF007244), and the well studied *P. chrysosporium* LiP isozyme H8 (all expressed in *E. coli*). Cesubv118677 and Cesubv99382 are able to directly oxidize VA and RB5, a unique characteristic of VP, exhibiting similar catalytic efficiency values to those observed for typical VPs. Moreover, both peroxidases are unable to oxidize Mn^{2+}, despite the presence in Cesubv99382 of a putative oxidation site for this cation. Thus, considering their sequences (Fig. 1 and *SI Appendix*) and catalytic activities (Table 1), these two peroxidases seem to represent an intermediate evolutionary state between LiP and VP.

In addition to the distinct repertoire of class II peroxidases, selective ligninolysis of *C. subvermispora* may be related, in part, to the expansion and coexpression of the genes putatively involved in lipid metabolism. Substantial evidence implicates MnP involvement (7, 8) in lignin degradation, but this enzyme cannot directly cleave the dominant nonphenolic structures within lignin. Nevertheless, several studies support mechanisms involving peroxidation of lipids (3). The expansion of *C. subvermispora* desaturase and MnP gene families, together with their high ex-

Table 3. Expression of *C. subvermispora* and *P. chrysosporium* cellulases

	C. subvermispora							*P. chrysosporium*						
		LC-MS/MS (unique peptides)†		Microarrays* Signal (log_2)					LC-MS/MS (unique peptides)†		Microarrays* Signal (log_2)			
Putative activity/family	ID no.	Glc	BMA	Glc	BMA	B/G ratio	*P* value	ID no.	Glu	BMA	Glu	BMA	B/G ratio	*P* value
CBH1/GH7	136606	—	—	11.0	12.6	3.02‡	<0.01	126964	—	—	10.6	10.7	1.08	0.45
CBH1/GH7	89943	—	1	8.84	8.96	1.09	0.09	137042	—	—	10.1	10.3	1.13	0.18
CBH1/GH7	109983	—	—	9.09	9.03	0.96	0.32	127029	—	3‡	10.3	12.1	3.53‡	<0.01
CBH1/GH7	—	—	—	—	—	—	—	137372	—	5‡	9.6	12.8	9.18‡	<0.01
CBH1/GH7	—	—	—	—	—	—	—	129072	—	—	10.4	12.2	3.40‡	<0.01
CBH1/GH7	—	—	—	—	—	—	—	137216	—	—	10.2	14.5	19.6‡	<0.01
CBH2/GH6§	72777	—	2‡	—	—	—	—	133052	—	2‡	11.8	15.3	11.5‡	<0.01
EG/GH5	79557	—	—	10.2	14.0	13.9‡	<0.01	6458	—	—	12.1	14.8	6.46‡	<0.01
EG/GH5	117046	—	—	9.8	10.8	1.99	0.02	4361	—	2‡	10.5	14.1	12.2‡	<0.01
EG/GH12	34428	—	—	8.95	10.9	3.81‡	<0.01	8466	—	2‡	11.4	14.0	5.94‡	<0.01
EG/GH12	111819	—	—	9.75	10.0	1.20	0.07	7048	—	3‡	12.1	15.1	8.16‡	<0.01

BMA, ball-milled aspen; FDR, false detection rate; Glc, glucose.

*As in Table 2, normalized microarray data are presented as log_2 signal strength average of three fully replicated experiments. Significant accumulation (B/G ratio) of transcripts in BMA relative to glucose grown cultures was determined using the moderated *t* test and associated FDR.

†Number of unique peptides detected by LC-MS/MS after 5 d growth on BMA or glucose medium. Complete microarray and LC-MS/MS results are listed in *SI Appendix*, Table S1. For detailed *P. chrysosporium* microarray and LC-MS/MS data, see refs. 33 and 31, respectively.

‡Significant ratio and/or peptide score.

§Initial microarrays did not feature probes for the *C. subvermispora* gene encoding GH6 (protein model Cesubv72777), but multiple ESTs and the presence of detectable peptides show the gene is expressed, and likely at substantial levels.

pression levels relative to *P. chrysosporium* (Table 2 and Fig. 1), are consistent with a role in lignin degradation.

Overall numbers and family distributions of GH-encoding genes were similar between *C. subvermispora* and *P. chrysosporium* (Fig. 3), but subtle differences in number and expression were noted. Among the cellulases, cellobiohydrolases (*cel7s*) and endoglucanases (*cel5s* and *cel12s*) were particularly notable in their transcript and protein accumulation in *P. chrysosporium* cultures (Table 3). In contrast, expression of the *C. subvermispora* cellulolytic system was substantially lower than *P. chrysosporium*, whereas the converse was observed for enzymes important in extracellular oxidative systems (Figs. 1 and 2, Table 2, and *SI Appendix*, Table S1).

These observations provide functional models that may explain the shift toward selective ligninolysis by *C. subvermispora*. Definitive mechanisms remain uncertain, but our investigations identify a subset of potentially important genes, including those encoding hypothetical proteins. More detailed functional analysis is complicated by the insoluble nature of lignocellulose substrates and by the slow, asynchronous hyphal growth of lignin degrading fungi. Direct and persuasive proof of gene function would be aided by development of experimental tools such as gene disruption/suppression or isozyme-specific immunolocalization of secreted proteins.

Methods

Genome Sequencing, Assembly, and Annotation. A whole genome shotgun approach was used to sequence *C. subvermispora* monokaryotic strain B (16) (US Department of Agriculture Forest Mycology Center, Madison, WI). Assembly and annotations are available through interactive visualization and analysis tools from the Joint Genome Institute genome portal (http://www.jgi.doe.gov/Ceriporiopsis) and at DNA Data Base in Japan/European Molecular Biology Laboratory/GenBank under project accession no. AEOV00000000. Details regarding the assembly, repetitive elements (Dataset S2), ESTs annotation, and specific gene sets are provided separately (*SI Appendix*, Figs. S1–S6).

MS. Soluble extracellular proteins were concentrated from *C. subvermispora* cultures containing ball-milled aspen as previously described for *P. chrysosporium* (31) This medium allows rapid growth on a lignocellulose substrate more relevant than glucose- or cellulose-containing media. However, the milling process pulverizes wood cell walls and the culture conditions may not replicate "natural" decay processes. Sample preparation and nano-LC-MS/MS analyses were performed as described in *SI Appendix*. Peptides were identified by using a Mascot search engine (Matrix Science) against protein sequences of 12,125 predicted gene models described earlier. Complete listings of carbohydrate active enzymes and oxidative enzymes, including peptide sequences and scores, are provided in *SI Appendix*, Table S1.

Expression Microarrays. NimbleGen arrays (Roche) were designed to assess expression of 12,084 genes during growth on ball-milled aspen (*P. grandidentata*) or on glucose as sole carbon sources. Methods are detailed in *SI Appendix*, and all data deposited under Gene Expression Omnibus accession no. GSE34636.

ACKNOWLEDGMENTS. We thank Sally Ralph (Forest Products Laboratory) for preparation of ball-milled wood. The major portions of this work were performed under US Department of Agriculture Cooperative State, Research, Education, and Extension Service Grant 2007-35504-18257 (to D.C. and R.A.B.). The US Department of Energy Joint Genome Institute is supported by the Office of Science of the US Department of Energy under Contract DE-AC02-05CH11231. This work was supported by Spanish Projects BIO2008-01533 and BIO2011-26694, European Project Peroxidases as Biocatalysts KBBE-2010-4-265397 (to F.J.R.-D. and A.T.M.), the Chilean National Fund for Scientific and Technological Development Grant 1090513 (to L.F.L.), and a "Ramon y Cajal" contract (to F.J.R.-D.).

1. United States Department of Energy (2006) *Breaking the Biological Barriers to Cellulosic Ethanol: A Joint Research Agenda. Report from the December 2005 Workshop, DOE/SC-0095* (US Department of Energy Office of Science, Washington, DC).
2. Blanchette R, Krueger E, Haight J, Akhtar M, Akin D (1997) Cell wall alterations in loblolly pine wood decayed by the white-rot fungus, *Ceriporiopsis subvermispora*. *J Biotechnol* 53:203–213.
3. Hammel KE, Cullen D (2008) Role of fungal peroxidases in biological ligninolysis. *Curr Opin Plant Biol* 11:349–355.
4. Martinez AT (2002) Molecular biology and structure-function of lignin-degrading heme peroxidases. *Enzyme Microb Technol* 30:425–444.
5. Tsukihara T, Honda Y, Sakai R, Watanabe T, Watanabe T (2008) Mechanism for oxidation of high-molecular-weight substrates by a fungal versatile peroxidase, MnP2. *Appl Environ Microbiol* 74:2873–2881.
6. Ruiz-Dueñas FJ, Fernández E, Martínez MJ, Martínez AT (2011) *Pleurotus ostreatus* heme peroxidases: An *in silico* analysis from the genome sequence to the enzyme molecular structure. *C R Biol* 334:795–805.
7. Urzúa U, Fernando Larrondo L, Lobos S, Larraín J, Vicuña R (1995) Oxidation reactions catalyzed by manganese peroxidase isoenzymes from *Ceriporiopsis subvermispora*. *FEBS Lett* 371:132–136.
8. Jensen KA, Bao W, Kawai S, Srebotnik E, Hammel KE (1996) Manganese-dependent cleavage of nonphenolic lignin structures by *Ceriporiopsis subvermispora* in the absence of lignin peroxidase. *Appl Environ Microbiol* 62:3679–3686.
9. Paszczynski A, Huynh V-B, Crawford RL (1985) Enzymatic activities of an extracellular, manganese-dependent peroxidase from *Phanerochaete chrysosporium*. *FEMS Microbiol Lett* 29:37–41.
10. Gold MH, Kuwahara M, Chiu AA, Glenn JK (1984) Purification and characterization of an extracellular H_2O_2-requiring diarylpropane oxygenase from the white rot basidiomycete, *Phanerochaete chrysosporium*. *Arch Biochem Biophys* 234:353–362.
11. Larrondo LF, Avila M, Salas L, Cullen D, Vicuña R (2003) Heterologous expression of laccase cDNA from *Ceriporiopsis subvermispora* yields copper-activated apoprotein and complex isoform patterns. *Microbiology* 149:1177–1182.
12. Martinez D, et al. (2004) Genome sequence of the lignocellulose degrading fungus *Phanerochaete chrysosporium* strain RP78. *Nat Biotechnol* 22:695–700.
13. Camarero S, Ibarra D, Martínez MJ, Martínez AT (2005) Lignin-derived compounds as efficient laccase mediators for decolorization of different types of recalcitrant dyes. *Appl Environ Microbiol* 71:1775–1784.
14. Kersten P, Cullen D (2007) Extracellular oxidative systems of the lignin-degrading basidiomycete Phanerochaete chrysosporium. *Fungal Genet Biol* 44:77–87.
15. Baldrian P, Valásková V (2008) Degradation of cellulose by basidiomycetous fungi. *FEMS Microbiol Rev* 32:501–521.
16. Tello M, et al. (2001) Isolation and characterization of homokaryotic strains from the ligninolytic basidiomycete *Ceriporiopsis subvermispora*. *FEMS Microbiol Lett* 199:91–96.
17. Vanden Wymelenberg A, et al. (2006) Computational analysis of the Phanerochaete chrysosporium v2.0 genome database and mass spectrometry identification of peptides in ligninolytic cultures reveal complex mixtures of secreted proteins. *Fungal Genet Biol* 43:343–356.
18. Bordoli L, et al. (2009) Protein structure homology modeling using SWISS-MODEL workspace. *Nat Protoc* 4:1–13.
19. Ruiz-Dueñas FJ, et al. (2009) Substrate oxidation sites in versatile peroxidase and other basidiomycete peroxidases. *J Exp Bot* 60:441–452.
20. Ruiz-Duenas FJ, Martinez AT (2010) Structural and functional features of peroxidases with a potential as industrial biocatalysts. *Biocatalysts Based on Heme Peroxidase*, eds Torres E, Ayala M (Springer, Berlin), pp 37–59.
21. Li D, Li N, Ma B, Mayfield MB, Gold MH (1999) Characterization of genes encoding two manganese peroxidases from the lignin-degrading fungus Dichomitus squalens (1). *Biochim Biophys Acta* 1434:356–364.
22. Rajakumar S, et al. (1996) Lip-like genes in *Phanerochaete sordida* and *Ceriporiopsis subvermispora*, white rot fungi with no detectable lignin peroxidase activity. *Appl Environ Microbiol* 62:2660–2663.
23. Ruttimann C, Schwember E, Salas L, Cullen D, Vicuna R (1992) Ligninolytic enzymes of the white rot basidiomycetes *Phlebia brevispora* and *Ceriporiopsis subvermispora*. *Biotechnol Appl Biochem* 16:64–76.
24. Doyle WA, Smith AT (1996) Expression of lignin peroxidase H8 in *Escherichia coli*: Folding and activation of the recombinant enzyme with Ca^{2+} and haem. *Biochem J* 315:15–19.
25. Perez-Boada JM, et al. (2002) Expression of *Pleurotus eryngii* versatile peroxidase in *Escherichia coli* and optimization of *in vitro* folding. *Enzyme Microb Technol* 30:518–524.
26. Hoegger PJ, Kilaru S, James TY, Thacker JR, Kües U (2006) Phylogenetic comparison and classification of laccase and related multicopper oxidase protein sequences. *FEBS J* 273:2308–2326.
27. Kumar SV, Phale PS, Durani S, Wangikar PP (2003) Combined sequence and structure analysis of the fungal laccase family. *Biotechnol Bioeng* 83:386–394.
28. Karahanian E, Corsini G, Lobos S, Vicuña R (1998) Structure and expression of a laccase gene from the ligninolytic basidiomycete *Ceriporiopsis subvermispora*. *Biochim Biophys Acta* 1443:65–74.
29. Watanabe T, Tsuda S, Nishimura H, Honda Y, Watanabe T (2010) Characterization of a Delta12-fatty acid desaturase gene from *Ceriporiopsis subvermispora*, a selective lignin-degrading fungus. *Appl Microbiol Biotechnol* 87:215–224.
30. Minto RE, Blacklock BJ, Younus H, Pratt AC (2009) Atypical biosynthetic properties of a Delta 12/nu+3 desaturase from the model basidiomycete *Phanerochaete chrysosporium*. *Appl Environ Microbiol* 75:1156–1164.
31. Vanden Wymelenberg A, et al. (2011) Significant alteration of gene expression in wood decay fungi *Postia placenta* and *Phanerochaete chrysosporium* by plant species. *Appl Environ Microbiol* 77:4499–4507.
32. Stamatakis A, Hoover P, Rougemont J (2008) A rapid bootstrap algorithm for the RAxML Web servers. *Syst Biol* 57:758–771.
33. Vanden Wymelenberg A, et al. (2010) Comparative transcriptome and secretome analysis of wood decay fungi *Postia placenta* and *Phanerochaete chrysosporium*. *Appl Environ Microbiol* 76:3599–3610.

Corrections

MICROBIOLOGY

Correction for "Comparative genomics of *Ceriporiopsis subvermispora* and *Phanerochaete chrysosporium* provide insight into selective ligninolysis," by Elena Fernandez-Fueyo, Francisco J. Ruiz-Dueñas, Patricia Ferreira, Dimitrios Floudas, David S. Hibbett, Paulo Canessa, Luis F. Larrondo, Tim Y. James, Daniela Seelenfreund, Sergio Lobos, Rubén Polanco, Mario Tello, Yoichi Honda, Takahito Watanabe, Takashi Watanabe, Ryu Jae San, Christian P. Kubicek, Monika Schmoll, Jill Gaskell, Kenneth E. Hammel, Franz J. St. John, Amber Vanden Wymelenberg, Grzegorz Sabat, Sandra Splinter BonDurant, Khajamohiddin Syed, Jagjit S. Yadav, Harshavardhan Doddapaneni, Venkataramanan Subramanian, José L. Lavín, José A. Oguiza, Gumer Perez, Antonio G. Pisabarro, Lucia Ramirez, Francisco Santoyo, Emma Master, Pedro M. Coutinho, Bernard Henrissat, Vincent Lombard, Jon Karl Magnuson, Ursula Kües, Chiaki Hori, Kiyohiko Igarashi, Masahiro Samejima, Benjamin W. Held, Kerrie W. Barry, Kurt M. LaButti, Alla Lapidus, Erika A. Lindquist, Susan M. Lucas, Robert Riley, Asaf A. Salamov, Dirk Hoffmeister, Daniel Schwenk, Yitzhak Hadar, Oded Yarden, Ronald P. de Vries, Ad Wiebenga, Jan Stenlid, Daniel Eastwood, Igor V. Grigoriev, Randy M. Berka, Robert A. Blanchette, Phil Kersten, Angel T. Martinez, Rafael Vicuna, and Dan Cullen, which appeared in issue 14, April 3, 2012, of *Proc Natl Acad Sci USA* (109:5458–5463; first published March 20, 2012; 10.1073/pnas.1119912109).

The authors note that the author name Ryu Jae San should instead appear as Jae San Ryu. The corrected author line appears below. The online version has been corrected.

Elena Ferandez-Fueyo, Francisco J. Ruiz-Dueñas, Patricia Ferreira, Dimitrios Floudas, David S. Hibbett, Paulo Canessa, Luis F. Larrondo, Tim Y. James, Daniela Seelenfreund, Sergio Lobos, Reuben Polanco, Mario Tello, Yoichi Honda, Takahito Watanabe, Takashi Watanabe, Jae San Ryu, Christian P. Kubicek, Monika Schmoll, Jill Gaskell, Kenneth E. Hammel, Franz J. St. John, Amber Vanden Wymelenberg, Grzegorz Sabat, Sandra Splinter BonDurant, Khajamohiddin Syed, Jagjit S. Yadav, Harshavardhan Doddapaneni, Venkataramanan Subramanian, José L. Lavín, José A. Oguiza, Gumer Perez, Antonio G. Pisabarro, Lucia Ramirez, Francisco Santoyo, Emma Master, Pedro M. Coutinho, Bernard Henrissat, Vincent Lombard, Jon Karl Magnuson, Ursula Kües, Chiaki Hori, Kiyohiko Igarashi, Masahiro Samejima, Benjamin W. Held, Kerrie W. Barry, Kurt M. LaButti, Alla Lapidus, Erika A. Lindquist, Susan M. Lucas, Robert Riley, Asaf A. Salamov, Dirk Hoffmeister, Daniel Schwenk, Yitzhak Hadar, Oded Yarden, Ronald P. de Vries, Ad Wiebenga, Jan Stenlid, Daniel Eastwood, Igor V. Grigoriev, Randy M. Berka, Robert A. Blanchette, Phil Kersten, Angel T. Martinez, Rafael Vicuna, and Dan Cullen

www.pnas.org/cgi/doi/10.1073/pnas.1206295109

EDITORIAL

Correction for "Uncensored exchange of scientific results," by Journal Editors and Authors Group, which appeared in issue 4, February 18, 2003, of *Proc Natl Acad Sci USA* (100:1464; first published February 15, 2003; 10.1073/pnas.0630491100).

Due to a printer's error, the author name "Steven Salzburg" should instead appear as "Steven Salzberg." Additionally, the affiliation for Steven Salzberg should instead appear as "The Institute for Genomic Research." The corrected group author footnote appears below. The online version has been corrected.

*Group members: Ronald Atlas, President, ASM, and Editor, *CRC Critical Reviews in Microbiology*; Philip Campbell, Editor, *Nature*; Nicholas R. Cozzarelli, Editor, PNAS; Greg Curfman, Deputy Editor, *New England Journal of Medicine*; Lynn Enquist, Editor, *Journal of Virology*; Gerald Fink, Massachusetts Institute of Technology; Annette Flanagin, Managing Senior Editor, *Journal of the American Medical Association*, and President, Council of Science Editors; Jacqueline Fletcher, President, American Phytopathological Society; Elizabeth George, Program Manager, National Nuclear Security Administration, Department of Energy; Gordon Hammes, Editor, *Biochemistry*; David Heyman, Senior Fellow and Director of Science and Security Initiatives, Center for Strategic and International Studies; Thomas Inglesby, Editor, *Biosecurity and Bioterrorism*; Samuel Kaplan, Chair, ASM Publications Board; Donald Kennedy, Editor, *Science*; Judith Krug, Director, Office for Intellectual Freedom, American Library Association; Rachel E. Levinson, Assistant Director for Life Sciences, Office of Science and Technology Policy; Emilie Marcus, Editor, *Neuron*; Henry Metzger, National Institute of Arthritis and Musculoskeletal and Skin Diseases, National Institutes of Health; Stephen S. Morse, Columbia University; Alison O'Brien, Editor, *Infection and Immunity*; Andrew Onderdonk, Editor, *Journal of Clinical Microbiology*; George Poste, Chief Executive Officer, Health Technology Networks; Beatrice Renault, Editor, *Nature Medicine*; Robert Rich, Editor, *Journal of Immunology*; Ariella Rosengard, University of Pennsylvania; Steven Salzberg, The Institute for Genomic Research; Mary Scanlan, Director, Publishing Operations, American Chemical Society; Thomas Shenk, President Elect, ASM, and Past Editor, *Journal of Virology*; Herbert Tabor, Editor, *Journal of Biological Chemistry*; Harold Varmus, Memorial Sloan–Kettering Cancer Center; Eckard Wimmer, State University of New York at Stony Brook; Keith Yamamoto, Editor, *Molecular Biology of the Cell*.

www.pnas.org/cgi/doi/10.1073/pnas.1206993109

CELL BIOLOGY

Correction for "ATM signals to TSC2 in the cytoplasm to regulate mTORC1 in response to ROS," by Angela Alexander, Sheng-Li Cai, Jinhee Kim, Adrian Nanez, Mustafa Sahin, Kirsteen H. MacLean, Ken Inoki, Kun-Liang Guan, Jianjun Shen, Maria D. Person, Donna Kusewitt, Gordon B. Mills, Michael B. Kastan, and Cheryl Lyn Walker, which appeared in issue 9, March 2, 2010, of *Proc Natl Acad Sci USA* (107:4153–4158; first published February 16, 2010; 10.1073/pnas.0913860107).

The authors note that in Fig. 2*A*, the error bars represent SEM (mean ± SEM). In Figs. 3*D* and 4*B*, the error bars represent standard deviation (mean ± SD). These corrections do not affect the conclusions of the article.

www.pnas.org/cgi/doi/10.1073/pnas.1206201109

Capítulo 6

"**Lignin-degrading peroxidases from genome of selective ligninolytic fungus *Ceriporiopsis subvermispora*"**
Fernández-Fueyo, E., F. J. Ruiz-Dueñas, Y. Miki, M. J. Martínez, K. E. Hammel, and A. T. Martínez.
J. Biol. Chem. 287:16903-16906. 2012.

THE JOURNAL OF BIOLOGICAL CHEMISTRY VOL. 287, NO. 20, pp. 16903–16916, May 11, 2012
Published in the U.S.A.

Lignin-degrading Peroxidases from Genome of Selective Ligninolytic Fungus *Ceriporiopsis subvermispora*[*S]

Received for publication, February 25, 2012, and in revised form, March 19, 2012 Published, JBC Papers in Press, March 21, 2012, DOI 10.1074/jbc.M112.356378

Elena Fernández-Fueyo[‡1], Francisco J. Ruiz-Dueñas[‡2], Yuta Miki[‡], María Jesús Martínez[‡], Kenneth E. Hammel[§3], and Angel T. Martínez[‡4]

From the [‡]Centro de Investigaciones Biológicas, Consejo Superior de Investigaciones Científicas, Ramiro de Maeztu 9, E-28040 Madrid, Spain and the [§]Forest Products Laboratory, United States Department of Agriculture, Madison, Wisconsin 53726

Background: The first genome of a selective lignin degrader is available.
Results: Its screening shows 26 peroxidase genes, and 5 genes were heterologously expressed and the catalytic properties investigated.
Conclusion: Two new peroxidases oxidize simple and dimeric lignin models and efficiently depolymerize lignin.
Significance: Although lignin peroxidase and versatile peroxidase had not been reported in *C. subvermispora*, the genomic screening suggests the presence of related lignin-degrading enzymes.

The white-rot fungus *Ceriporiopsis subvermispora* delignifies lignocellulose with high selectivity, but until now it has appeared to lack the specialized peroxidases, termed lignin peroxidases (LiPs) and versatile peroxidases (VPs), that are generally thought important for ligninolysis. We screened the recently sequenced *C. subvermispora* genome for genes that encode peroxidases with a potential ligninolytic role. A total of 26 peroxidase genes was apparent after a structural-functional classification based on homology modeling and a search for diagnostic catalytic amino acid residues. In addition to revealing the presence of nine heme-thiolate peroxidase superfamily members and the unexpected absence of the dye-decolorizing peroxidase superfamily, the search showed that the *C. subvermispora* genome encodes 16 class II enzymes in the plant-fungal-bacterial peroxidase superfamily, where LiPs and VPs are classified. The 16 encoded enzymes include 13 putative manganese peroxidases and one generic peroxidase but most notably two peroxidases containing the catalytic tryptophan characteristic of LiPs and VPs. We expressed these two enzymes in *Escherichia coli* and determined their substrate specificities on typical LiP/VP substrates, including nonphenolic lignin model monomers and dimers, as well as synthetic lignin. The results show that the two newly discovered *C. subvermispora* peroxidases are functionally competent LiPs and also suggest that they are phylogenetically and catalytically intermediate between classical LiPs and VPs. These results offer new insight into selective lignin degradation by *C. subvermispora*.

Most of the carbon fixed by land photosynthesis is stored in the plant polymers cellulose, hemicellulose, and lignin. Lignin is an aromatic macromolecule (1) that protects the other two polysaccharidic polymers against biodegradation. After plant death, only certain specialized filamentous fungi, especially the highly active basidiomycetes termed white-rot fungi (2), are able to degrade lignin via oxidative mechanisms. Lignin biodegradation is a key step in terrestrial carbon recycling, enabling subsequent degradation of plant polysaccharides by complex microbial communities. Its removal is also a central issue for the current industrial use of lignocellulosic biomass (*e.g.* in cellulose production for paper) as well as in lignocellulose biorefineries for the sustainable production of fuels, chemicals, and materials from plant feedstocks (3). Industrial removal of lignin often involves harsh chemical treatments, but lignin-degrading fungi and their enzymes may present environmentally friendly alternatives (4).

Two decay patterns are produced by white-rot fungi, being characterized by degradation of both lignin and polysaccharides (simultaneous decay) and by a preferential removal of lignin leaving most of the polysaccharides unaffected (selective decay) (5). Among selective decay basidiomycetes, *Ceriporiopsis* (*Gelatoporia*) *subvermispora* has been selected for delignification of different types of wood (6–8) in paper pulp manufacture (9). More recently, it has also been assayed for delignification in bioethanol production (10). The usual model fungus in lignin biodegradation studies, *Phanerochaete chrysosporium* (11), is of limited interest for such applications because it generally causes a simultaneous decay pattern (2). From the first pilot scale trials on wood biopulping with *C. subvermispora*, a high interest in its lignocellulolytic enzymatic machinery has been sustained, with the double purpose of enhancing enzyme production and discovering new or more efficient enzymes of interest as industrial biocatalysts.

* This work was supported by the RAPERO Grant BIO2008-01533 and HIPOP Grant BIO2011-26694 from the Spanish Ministry of Economy and Competitiveness (to A. T. M. and F. J. R.-D., respectively), by PEROXICATS European Project Grant KBBE-2010-4-265397 (to A. T. M.), and by United States Department of Energy Grant DE-AI02-07ER64480 (to K. E. H.).
[S] This article contains supplemental Figs. S1 and S2 and Table S1.
[1] Supported by a Junta para Ampliación de Estudios fellowship of the Consejo Superior de Investigaciones Científicas, co-funded by the European Social Fund.
[2] Supported by a Ministry of Economy and Competitiveness (MINECO) Ramón y Cajal contract.
[3] To whom correspondence may be addressed. Tel.: 608-231-9528; Fax: 608-231-9262; E-mail: kehammel@wisc.edu.
[4] To whom correspondence may be addressed. Tel.: 34-918373112; Fax: 34-915360432; E-mail: ATMartinez@cib.csic.es.

White-rot fungi secrete multiple isoenzymes of three heme peroxidases with proposed roles in oxidative ligninolysis as follows: lignin peroxidases (LiPs),[5] manganese peroxidases (MnPs), and hybrid enzymes known as versatile peroxidases (VPs) that combine the structural-functional properties of LiPs and MnPs. In addition, these fungi secrete various oxidases to produce the H_2O_2 required by peroxidases, and most of them also secrete laccases (12). LiPs and VPs are able to oxidize and cleave the recalcitrant nonphenolic structures that compose the bulk of lignin, as shown by studies with dimeric lignin model compounds (13, 14), and also by depolymerization experiments with synthetic lignins in the case of LiPs (15). MnPs and VPs oxidize Mn^{2+} to Mn^{3+}, which can oxidize only the minor phenolic units in lignin (16). Likewise, laccases are directly able to oxidize only the phenolic units in lignin (17).

Because the cleavage of nonphenolic lignin structures is central to efficient ligninolysis, it might be expected that LiPs and/or VPs are essential participants in the process. However, among the above oxidoreductases, only laccase and MnP isoenzymes have been found in *C. subvermispora* cultures (18, 19), although DNA hybridization/amplification with LiP sequences was reported in initial studies (20, 21), and some manganese-independent peroxidase activity has been detected (22). The unexpected lack of LiPs or VPs in this selective delignifier has led to various alternative hypotheses. One is that lipid peroxidation reactions catalyzed by MnP might generate fatty acid-derived oxyradicals that cleave lignin (23). There is some experimental support for this mechanism, as it can depolymerize nonphenolic synthetic lignin *in vitro*, but the reaction is slow and inefficient (23–25). Alternatively, the ability of laccases to oxidize nonphenolic lignin structures in the presence of various low molecular weight naturally occurring redox mediators has been demonstrated (26). This might lead to ligninolysis if the fungus produces such mediators as extracellular metabolites or lignin degradation products, but so far this has not been demonstrated.

The recent sequencing of the *C. subvermispora* genome at the Joint Genome Institute, Department of Energy, allows a new look at this longstanding problem. This project supplements the first white-rot (27) and brown-rot (28) fungal genome sequences to be obtained and reflects strong current interest in lignocellulose decay mechanisms that may inspire new biotechnological applications. In this study, an inventory of all the peroxidase genes, with special emphasis on class II heme peroxidases (29), was obtained with manual curation. Then a structural-functional annotation of the predicted proteins was produced, as recently reported for the *Pleurotus ostreatus* genome (30), and their evolutionary history was established by comparison with all the basidiomycete peroxidase sequences currently available. Surprisingly, this annotation revealed the presence in *C. subvermispora* of two genes that encode putative LiP/VP enzymes. To assess the significance of this finding, we have expressed these two peroxidases heterologously (together with other *C. subvermispora* and reference class II peroxidases) and have estimated their kinetic constants using high and low redox potential substrates. Furthermore, we have assessed the ligninolytic capability of these two peroxidases in experiments with a nonphenolic lignin model dimer and with synthetic lignin.

MATERIALS AND METHODS

Fungal Strain and Genome Sequencing—The genome of monokaryotic *C. subvermispora* strain B (31) was sequenced at the Joint Genome Institute using a shotgun approach (39.0 Mb total) in a project coordinated by Daniel Cullen (United States Department of Agriculture Forest Products Laboratory, Madison, WI) and Rafael Vicuña (Pontificia Universidad Católica de Chile, Santiago, Chile). The results from gene prediction and annotation are available for searching at the Joint Genome Institute genome portal.

Genome Screening and Analysis of Peroxidase Models—The process to obtain the complete inventory of *C. subvermispora* heme peroxidase genes consisted of the following steps: (i) screening the automatically annotated genome at the Joint Genome Institute genome portal; (ii) revising and manually curating (when necessary) the positions of introns, and the N and C termini of the selected models; (iii) comparing the amino acid sequence identities with related proteins; and (iv) confirming the presence of characteristic residues at the heme pocket and substrate oxidation sites, after homology modeling using crystal structures of related proteins from the RCSB Protein Data Bank as templates.

Three MnP genes previously cloned from *C. subvermispora* (GenBank™ accession numbers AAB03480, AAD45725, and AAO61784 and described as MnP1, MnP3, and MnP4, respectively) (32, 33) were identified (as models 116608, 139965, and 94398, respectively, showing 98–100% identities with the corresponding GenBank™ sequences). *C. subvermispora* MnP2 (GenBank™ entries AAB92247 and AAD43581 with 99% sequence identity) was not localized in the genome but could be an allelic variant of gene 50297 (94% identity). The deduced amino acid sequences of the *C. subvermispora* heme peroxidase gene models were compared with all the basidiomycete heme peroxidase sequences (from GenBank™ and genomes) available to date (a total of 376 sequences, prokaryotic class I peroxidases excluded), and phylogenetic trees were constructed using Poisson-corrected distances and unweighted pair group method with arithmetic mean clustering (bootstrap consensus trees were inferred from 1000 replicates).

The programs used in the above analyses include the following: (i) BLAST (Basic Local Alignment Tool) at the National Center for Biotechnology Information for searching nucleotide and protein databases; (ii) MEGA5 (34) for conducting automatic and manual sequence alignment during the heme peroxidase gene search and curation, and for inferring evolutionary trees; and (iii) SignalP 3.0 (35) for predicting the presence and location of signal peptides and cleavage sites. The latter predictions were validated by multiple alignment (from MEGA5) of the 196 class II sequences available, including proteins whose N termini have been sequenced. Theoretical molecular models

[5] The abbreviations used are: LiP, lignin peroxidase; DHP, dehydrogenation (lignin) polymer; GPC, gel permeation chromatography; HTP, heme-thiolate peroxidase; MnP, manganese peroxidase; VP, versatile peroxidase; ABTS, 2,2′-azinobis(3-ethylbenzothiazoline-6-sulfonate).

were generated at the Swiss-Model automated protein homology-modeling server (36).

Gene Synthesis and Directed Mutagenesis—The mature protein-coding sequences of five selected *C. subvermispora* peroxidase genes (49863, 99382, 112162, 118677, and 117436 models) after the above manual curation, two VP genes from *Pleurotus eryngii* (GenBank™ AF007244) and *Pleurotus ostreatus* (genome 137757), and a *P. chrysosporium* LiP gene (GenBank™ Y00262) were synthesized by ATG:biosynthetics (Merzhausen, Germany) after verifying that all the codons had been previously used for expressing other genes in the same *Escherichia coli* strains (and substituting them when required).

The E183K mutation was introduced in *C. subvermispora* gene 99382 by PCR using the expression plasmid pFLAG1-99382 (see below) as template, and the QuikChange kit from Stratagene. The 5′-CGCGGCTGCCGACAAGGTCGATCCTACCATCCCG-3′ direct (mutated triplet underlined) and reverse primers were synthesized. The PCR (50-μl volume) was carried out in a PerkinElmer Life Sciences GeneAmp PCR System 240 using 20 ng of template DNA, 500 μM each dNTP, 125 ng of each primer, 2.5 units of *Pfu*Turbo DNA polymerase (Stratagene), and the manufacturer's buffer. Reaction conditions were as follows: (i) a "hot start" at 95 °C for 1 min; (ii) 18 cycles at 95 °C for 50 s, 55 °C for 50 s, and 68 °C for 10 min; and (iii) a final cycle at 68 °C for 10 min.

E. coli Expression of Heme Peroxidase Genes—The five *C. subvermispora* peroxidases, the *P. eryngii* and *P. ostreatus* VPs, and the *P. chrysosporium* LiP mature protein-codifying sequences were cloned in the expression vectors pFLAG1 (International Biotechnologies Inc.) or pET23a(+) (Novagen). The resulting plasmids pET23a-49863, pFLAG1-99382, pET23a-112162, pFLAG1-118677, pET23a-117436, pFLAG1-AF007244, pFLAG1-137757, and pFLAG1-Y00262 were directly used for expression, and for the above-described directed mutagenesis (pFLAG1-99382). *E. coli* DH5α was used for plasmid propagation.

The different peroxidases (and the 99382 E183K variant) were produced in *E. coli* W3110 (pFLAG1-derived plasmids) and BL21(DE3)pLysS (pET23a-derived plasmids). Cells were grown for 3 h in Terrific Broth (37), induced with 1 mM isopropyl β-D-thiogalactopyranoside, and grown further for 4 h. The apoenzyme accumulated in inclusion bodies, as observed by SDS-PAGE, and was solubilized using 8 M urea. Subsequent *in vitro* refolding of *C. subvermispora* peroxidases and *Pleurotus* VPs was performed using 0.16 M urea, 5 mM Ca^{2+}, 20 μM hemin, 0.5 mM oxidized glutathione, 0.1 mM dithiothreitol, and 0.1 mg/ml protein, at pH 9.5 (38). *C. subvermispora* peroxidase 112162 was refolded using 1 M urea, 5 mM Ca^{2+}, 10 μM hemin, 0.5 mM oxidized glutathione, 0.1 mM dithiothreitol, and 0.1 mg/ml protein, at pH 9. Refolding of *P. chrysosporium* LiP was performed using 2.1 M urea, 5 mM Ca^{2+}, 10 μM hemin, 0.7 mM oxidized glutathione, 0.1 mM dithiothreitol, and 0.2 mg/ml protein, at pH 8 (39). Active enzyme was purified by Resource-Q chromatography using a 0–300 mM NaCl gradient (2 ml·min^{-1}, 20 min) in 10 mM sodium tartrate (pH 5.5) containing 1 mM $CaCl_2$.

Kinetic Constants on Selected Substrates—Absorbance changes during substrate oxidation in 0.1 M tartrate (at various pH values) by the above *E. coli*-expressed peroxidases were recorded in a Thermo Scientific Biomate5 spectrophotometer (using ~0.01 μM enzyme). Oxidation of Mn^{2+} was followed at pH 5 for the formation of the Mn^{3+}·tartrate complex (ϵ_{238} 6.5 $mM^{-1}·cm^{-1}$). Veratryl alcohol oxidation was followed at pH 3 for veratraldehyde (ϵ_{310} 9.3 $mM^{-1}·cm^{-1}$) formation. Reactive Black 5, 2,2′-azinobis(3-ethylbenzothiazoline-6-sulfonate) (ABTS), and 2,6-dimethoxyphenol oxidation were all assayed at pH 3.5. These reactions were monitored for Reactive Black 5 disappearance (ϵ_{598} 30 $mM^{-1}·cm^{-1}$), for ABTS cation radical formation (ϵ_{436} 29.3 $mM^{-1}·cm^{-1}$), and for dimeric coerulignone formation (ϵ_{469} 5.5 mM^{-1} cm^{-1}), respectively. All reactions were at 25 °C and were initiated by addition of 0.1 mM H_2O_2. ABTS and 2,6-dimethoxyphenol oxidation by some *C. subvermipora* peroxidases shows double kinetics with sigmoidal activity curves (at increasing substrate concentrations) that enable calculation of two sets of kinetic constants (for high and low efficiency oxidation sites), as reported previously for VP (40, 41).

Means and standard errors for affinity constant (K_m) and enzyme turnover (k_{cat}) values were obtained by nonlinear least squares fitting of the experimental measurements to the Michaelis-Menten model. Fitting of these constants to the normalized equation $v = (k_{cat}/K_m)[S]/(1 + [S]/K_m)$ yielded the catalytic efficiency values (k_{cat}/K_m) with their corresponding standard errors.

p-Dimethoxybenzene and Ferrocytochrome c Oxidation—Spectral changes during oxidation of *p*-dimethoxybenzene (0.2 mM) and ferrocytochrome *c* (15 μM) by the above peroxidases (~0.1 μM) at 25 °C in the presence of 0.1 mM H_2O_2 were recorded with an Agilent 8453 diode-array spectrophotometer, showing the formation of *p*-benzoquinone and ferricytochrome *c*, respectively. Ferrocytochrome *c* was prepared before use by reducing ferricytochrome *c* with sodium dithionite, followed by removal of excess dithionite on a Sephadex G-25 column. *p*-Benzoquinone formation was followed at 245 nm in 20 mM sodium succinate (pH 3.5). Decrease of ferrocytochrome *c* concentration was followed at 550 nm in 20 mM sodium succinate (pH 4). Controls without enzyme and without H_2O_2 were included.

Oxidative Degradation of a Lignin Model Dimer—Unlabeled and *ring*-^{14}C-labeled (1.0 mCi $mmol^{-1}$) 4-ethoxy-3-methoxyphenylglycerol-β-guaiacyl ether were prepared, and their *erythro* and *threo* isomers were chromatographically separated, as described earlier (42).

For reactions involving product analysis, the radiolabeled *erythro* or *threo* dimer was treated either with one of the two *C. subvermispora* LiP-like peroxidases (from genes 118677 and 99382) or with *P. chrysosporium* LiPH8 in 10 mM sodium acetate (pH 3.0) at 25 °C for 1 h. The products formed were analyzed by reversed phase high performance liquid chromatography (HPLC) using a Gilson system equipped with a C-18 column (Phenomenex Luna C18(2); 150 by 4.6 mm, 5-μm particle size), and methanol/water as mobile phase (35:65 for 15 min, followed by 50:50) at a flow rate of 1 ml·min^{-1}. Elution was monitored at 255 nm, and the ^{14}C content in collected fractions (0.5 ml) was measured in a liquid scintillation counter. HPLC in conjunction with gas chromatography/mass spectrometry was

used in parallel analyses with unlabeled dimers to confirm the identity of the products obtained.

For experiments to determine reaction kinetics, unlabeled *erythro* or *threo* dimer was treated with *C. subvermispora* peroxidase at 25 °C in the same buffer. Approximate turnover numbers (s^{-1}) at various dimer concentrations were obtained from the increase in absorbance at 310 nm due to benzylic carbonyl formation, *i.e.* production of 4-ethoxy-3-methoxybenzaldehyde, 1-(4-ethoxy-3-methoxyphenyl)-3-hydroxy-2-(2-methoxyphenoxy)-propan-1-one, and 1-(4-ethoxy-3-methoxyphenyl)-2,3-dihydroxypropan-1-one (ϵ_{310} 9 $mM^{-1}\cdot cm^{-1}$). Kinetic constants were then calculated as described above.

Enzymatic Depolymerization of Synthetic Lignin—A radiolabeled syringyl/guaiacyl dehydrogenation polymer (DHP) with a syringyl/guaiacyl ratio of ~4:1 was prepared by enzymatic copolymerization of β-[^{14}C]sinapyl alcohol (0.01 mCi $mmol^{-1}$) and unlabeled coniferyl alcohol using horseradish peroxidase as described previously (43). The synthetic lignin was then fractionated on a column of Sephadex LH-20 as described (43), and the high molecular mass fractions (approximately ≥21 kDa) were pooled for use in depolymerization experiments.

Enzymatic depolymerization of the DHP by the same peroxidases used in the dimer degradation assays was investigated in 10 mM sodium acetate (pH 4.5) containing 0.25% Tween 20, 1.5×10^4 dpm (188 μg) DHP, and 0.01 μM enzyme in a final volume of 40 ml, in the presence or absence of 10 mM veratryl alcohol. Reactions were conducted at 25 °C by adding H_2O_2 (7.5 mM final concentration in experiments with veratryl alcohol and 0.3 mM in experiments without veratryl alcohol) continuously over 24 h with a syringe pump (15). Control reactions without enzyme were run for comparison. The reaction mixtures were then concentrated by rotary vacuum evaporation, redissolved in *N,N′*-dimethylformamide containing 0.1 M LiCl, and centrifuged as described earlier (15). Molecular mass distributions of the supernatant fractions were assessed by gel permeation chromatography (GPC) on a 1.8 × 30-cm column of Sephadex LH20, using *N,N′*-dimethylformamide containing 0.1 M LiCl as the mobile phase. Fractions (2 ml) were collected and assayed for ^{14}C in a liquid scintillation counter (15).

Chemicals—*p*-Dimethoxybenzene, *N,N′*-dimethylformamide, dithiothreitol, 2,6-dimethoxyphenol, ferricytochrome *c*, hemin, isopropyl β-D-thiogalactopyranoside, lithium chloride, manganese sulfate, methanol, oxidized glutathione, Reactive Black 5, sodium dithionite, sodium tartrate, Tween 20, veratryl alcohol, and other unlabeled chemicals were purchased from Sigma, with the exception of H_2O_2 that was from Merck, and ABTS that was from Roche Applied Science.

RESULTS

Inventory of Heme Peroxidase Genes in the C. subvermispora Genome—Among the 12,125 gene models identified in the *C. subvermispora* genome distributed in 740 main scaffolds, 26 models were found to encode heme peroxidases after manual revision of the possible candidates from automatic annotation (supplemental Table S1 provides the reference, scaffold, position, best hit, amino acid sequence identity, and peroxidase types encoded by these genes).

For the class II peroxidases we found (numbers 1–16 supplemental Table S1), the classification was based on the presence/absence in the molecular models (obtained using crystal structures of related enzymes as templates) of the following: (i) an exposed tryptophan (two models) putatively involved in oxidation of veratryl alcohol and other high redox potential aromatics (Wc, homologous to Trp-171 in *P. chrysosporium* LiP isoenzyme-H8 and to Trp-164 in *P. eryngii* VP isoenzyme-VPL) (Fig. 1, *A* and *B*); and/or (ii) a putative Mn^{2+} oxidation site (14 models) formed by three acidic residues near the most internal heme propionate (Ea, Eb, and Ec, homologous to *P. chrysosporium* MnP1 Glu-35, Glu-39, and Asp-179, and to *P. eryngii* VPL Glu-36, Glu-40 and Asp-175, respectively) (Fig. 1, *B* and *D*).

The only *C. subvermispora* peroxidase showing both of the above two catalytic sites (gene 99382) was initially classified as a putative VP (Fig. 1*B*). The 13 models showing only the Mn^{2+} oxidation site (genes 1–13 in supplemental Table S1) were classified as likely MnPs (Fig. 1*D*). The single peroxidase containing only the catalytic tryptophan (gene 118677) was classified as a putative LiP (Fig. 1*A*). Finally, the model lacking both oxidation sites (gene 112162) was classified as a generic peroxidase (Fig. 1*C*), related to the *Coprinopsis cinerea* peroxidase (44).

Among the MnPs, two types were identified (see supplemental Table S1). (i) MnP-long, represented by 12 gene models in the *C. subvermispora* genome, resembles typical MnPs described in *P. chrysosporium*, whose amino acid sequence is longer than those of LiPs and VPs and includes an additional disulfide bridge. (ii) MnP-short, represented by only one gene model (gene 124076), resembles some *Phlebia radiata* MnPs. MnP-long includes five "extra long" MnPs, whose differential catalytic properties are still to be reported.

An additional single model (supplemental Table S1, gene 83438) has predicted protein folding and heme pocket architecture similar to that of the above class II peroxidases. However, it is a class I (of prokaryotic origin but in the same superfamily) cytochrome *c* peroxidase and is therefore not included in the subsequent comparisons.

The other nine models (numbers 18–26 in supplemental Table S1) correspond to putative peroxidases from the HTP superfamily and are most probably related to the *Agrocybe aegerita* peroxygenase (GenBank™ entries CAV28568 and CAV28569) (45). This superfamily is characterized by the presence in the molecular structures (that of gene 80799 is shown in Fig. 2*A*) of a cysteine residue acting as the fifth heme ligand, instead of the histidine residue present in the above peroxidases, among other structural details (Fig. 2*B*).

Catalytic Properties of Peroxidases Expressed in E. coli—Among the 15 class II genes in the *C. subvermispora* genome, including genes putatively encoding ligninolytic peroxidases, we selected 118677, 99382, 117436, 49863, and 112162 for heterologous expression, as representative for the main families identified. Our first goal was to investigate their catalytic properties on selected peroxidase substrates and in this way to confirm or modify their putative structural/functional classifications. Additionally, we aimed to evaluate their ability to degrade lignin using a simple dimeric model compound and a polymeric synthetic lignin (DHP).

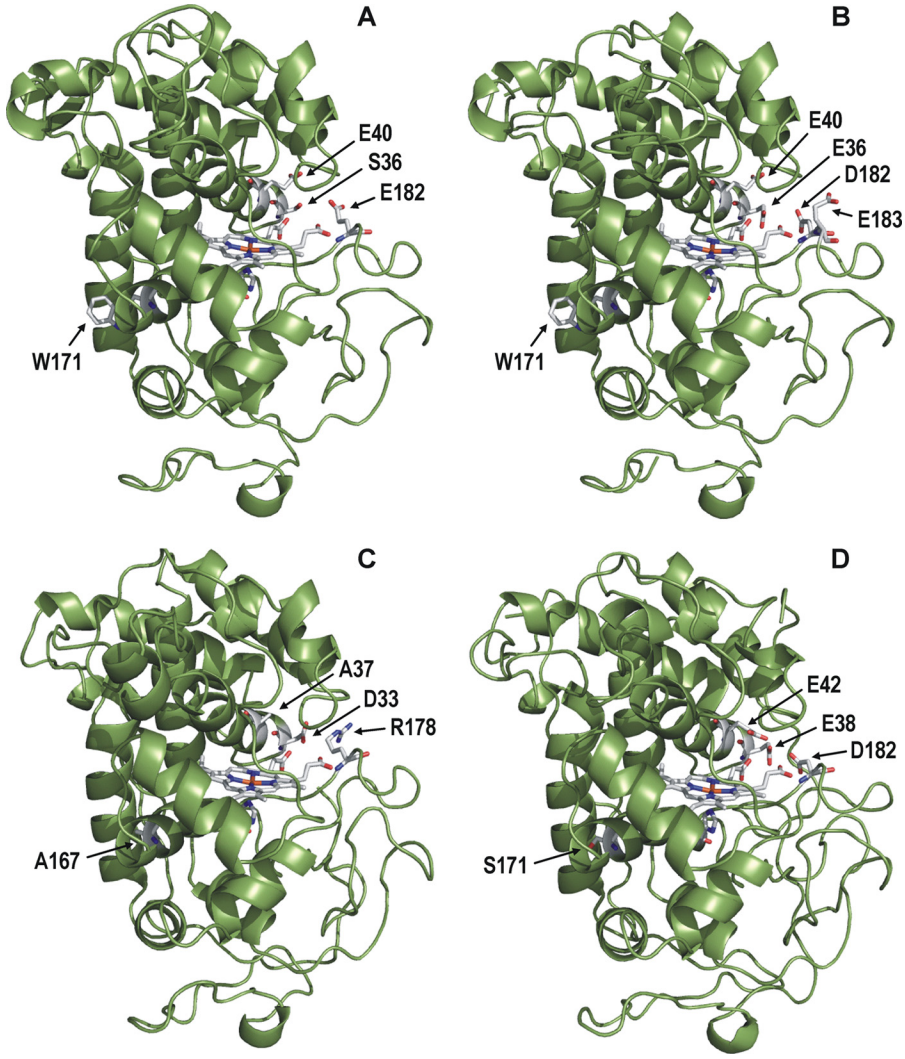

FIGURE 1. **Homology models for the molecular structures of four hypothetical members of class II (fungal peroxidases) from the *C. subvermispora* genome.** *A*, 118677 peroxidase; *B*, 99382 peroxidase; *C*, 112162 peroxidase; and *D*, 117436 peroxidase. The general folding is shown, together with details of the heme cofactor and residues forming the substrate oxidation sites of MnP/VP (two glutamates and one aspartate, *B* and *D*) and LiP/VP (exposed tryptophan, *A* and *B*)-type enzymes, as well as the homologous residues in the other proteins (residues and cofactor as Corey-Pauling-Koltun (CPK), *colored sticks*). The crystal structures of *P. eryngii* VP (Protein Data Bank code 2BOQ) and *P. chrysosporium* MnP (Protein Data Bank code 3M5Q) were used as templates. The amino acid numbering refers to putative mature sequences, after manual curation of their signal peptide sequences.

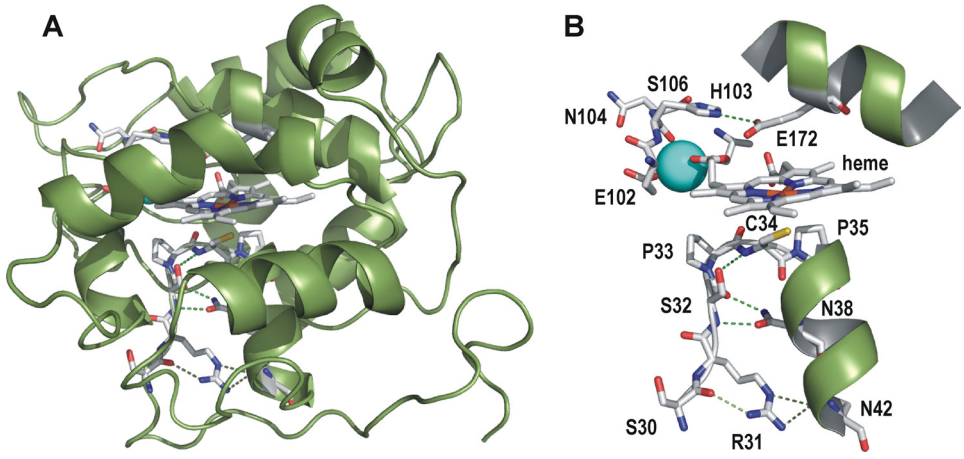

FIGURE 2. **Homology model for the molecular structure of a member of the HTP superfamily from the *C. subvermispora* genome.** The general folding of a putative *C. subvermispora* HTP (model 80799) is shown (*A*) together with details of its heme region (*B*, residues and cofactor as CPK-*colored sticks*, and metal ion as a *blue* van der Waals sphere). The crystal structure of *L. fumago* chloroperoxidase (Protein Data Bank code 1CPO) was used as a template. The amino acid numbering refers to putative mature sequence after manual curation of signal peptide sequences.

After manual curation, which entailed revision of predicted introns and N and C termini, we used the codifying DNA sequences to express the mature proteins in *E. coli* (see supplemental Fig. S1, *A–D* for sequences). We used this expression system because, although it requires heme insertion and protein refolding *in vitro*, the yields are high (~200 mg of protein per 5 liters of culture). Moreover, the lack of host-dependent protein glycosylation in this prokaryotic expression system facilitated comparisons of catalytic properties in our subsequent investigations. We purified the resulting active peroxidases to electrophoretic homogeneity in one chromatographic step using a Resource-Q column (Fig. 3). The average yield of the refolding process was ~6 mg of pure active protein per each 200 mg of protein recovered from the inclusion bodies. The molecular masses estimated by SDS-PAGE (Fig. 3, *inset*) coincided with the values obtained from the mature protein sequences, and electronic absorption spectra revealed the presence of Soret (406 nm) and other typical bands of resting state peroxidases, thus confirming correct incorporation of the heme cofactor (see the electronic absorption spectra in supplemental Fig. S2). Moreover, the A_{410}/A_{280} ratio was similar for all the refolded enzymes, with an average value of 4.

Next, we characterized the substrate specificity of our heterologously expressed peroxidases, including for comparison several well characterized enzymes as follows: *P. eryngii* VP, a closely homologous *P. ostreatus* VP, and *P. chrysosporium* LiPH8. For this experiment we used the following: (i) two simple high redox potential substrates (veratryl alcohol and Reactive Black 5), which can be oxidized only at the LiP or VP catalytic tryptophan; (ii) two low redox-potential substrates (ABTS and 2,6-dimethoxyphenol), which are oxidized at the above catalytic tryptophan with high efficiency but are also oxidized at a second site by VPs and generic peroxidases; and (iii) Mn^{2+}, which is oxidized only at the MnP or VP Mn^{2+} oxidation site (Table 1). In this way, we were able to check each enzyme's putative peroxidase classification as an LiP, VP, MnP, or generic peroxidase. The abovementioned existence of two oxidation sites for some phenols and dyes has been reported for VP (40, 41), although the second one is still to be fully characterized.

As shown by the kinetic constants obtained (Table 1), the putative MnP classification for model 117436 was confirmed by its very high catalytic efficiency for Mn^{2+} oxidation (>5000 $s^{-1}\cdot mM^{-1}$), its negligible efficiency (nonsaturation of the enzyme prevented estimation of other kinetic constants) for 2,6-dimethoxyphenol oxidation at a low efficiency site (<0.05 $s^{-1}\cdot mM^{-1}$), and its complete lack of activity in all the other reactions investigated (and very similar results were obtained for the 49863 peroxidase). The classification of peroxidase 112161 as a generic (nonligninolytic) peroxidase was also confirmed by its inability to oxidize veratryl alcohol and Mn^{2+}, as well as Reactive Black 5, although it oxidizes ABTS and 2,6-dimethoxyphenol (Table 1).

Likewise, the putative LiP classification for model 118677 appears appropriate, as it exhibited no activity toward Mn^{2+} but was able to oxidize the standard LiP substrate veratryl alcohol (Table 1). Although the catalytic efficiency of peroxidase 118677 is considerably lower than that of *P. chrysosporium*

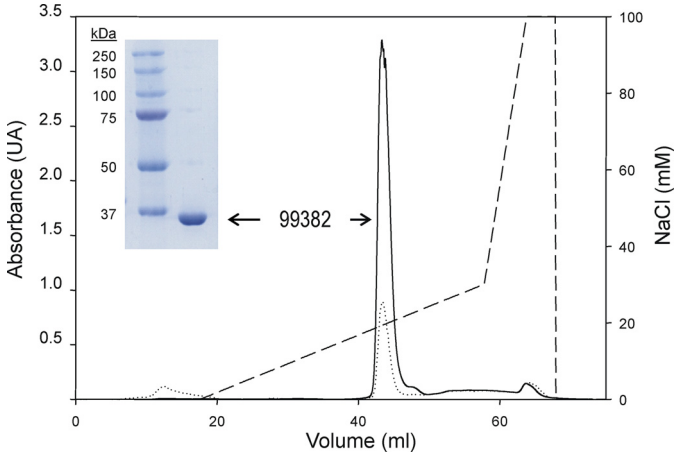

FIGURE 3. **Purification of the enzyme product of the putative *C. subvermispora* VP gene (99382) after *E. coli* expression and *in vitro* activation.** The gene (optimized manually curated codifying sequence) was synthesized, cloned in pFLAG1, expressed in *E. coli* W3110, refolded *in vitro*, and purified (38). The VP peak obtained using a Resource-Q column and a 0–300 mM NaCl gradient is shown. The elution profiles at 280 nm (total protein) and 410 nm (heme proteins) are shown by *dotted* and *continuous lines*, respectively (the actual NaCl gradient, from conductivity measurement, is shown by the *dashed line*). The electrophoretic homogeneity of the enzyme was confirmed by SDS-PAGE, as shown in the *inset* (*right lane*), and a molecular mass of ~35 kDa was estimated.

LiPH8 (~5 $s^{-1}\cdot mM^{-1}$ *versus* ~90 $s^{-1}\cdot mM^{-1}$), it is clearly a LiP-like enzyme.

The putative VP classification for model 99382 was not confirmed, as it was unable to oxidize Mn^{2+} (Table 1) despite having the three acidic residues that form the typical Mn^{2+} oxidation site in MnPs and VPs (Fig. 1*B*). This finding, together with our observation that peroxidase 99382 oxidized veratryl alcohol (Table 1), suggested that it, like peroxidase 118677, is an LiP-like enzyme with a low catalytic efficiency on veratryl alcohol (~3 $s^{-1}\cdot mM^{-1}$). In agreement, the catalytic efficiencies of enzyme 99382 for ABTS and 2,6-dimethoxyphenol oxidation at high and low efficiency sites (Table 1) were similar to those we found for the LiP-like peroxidase 118677, and its substrate specificity resembles that of *P. chrysosporium* LiPs (although typical LiPs lack the low efficiency site).

One peculiarity of the two *C. subvermispora* LiP-like enzymes, as compared with *P. chrysosporium* LiPs, is their ability to directly oxidize Reactive Black 5 (Table 1), a typical VP substrate that LiP cannot oxidize in the absence of veratryl alcohol as a mediator. Moreover, as noted above, the catalytic efficiencies of the two *C. subvermispora* LiP-like enzymes on veratryl alcohol are low relative to values for typical LiPs. Instead, they are similar to values found for typical VPs (~2 $s^{-1}\cdot mM^{-1}$). Accordingly, we surmise that *C. subvermispora* peroxidases 99382 and 118677 are VP-type enzymes that have lost the ability to oxidize Mn^{2+} and therefore must be formally classified as LiPs. They appear as such in Tables 1 and supplemental Table S1 and in Fig. 7.

The lack of Mn^{2+} oxidation activity in the 118677 peroxidase is explained by its having a serine in place of one of the three acidic (glutamate or aspartate) residues required for Mn^{2+} oxidation (Fig. 1, *A* and *D*). However, the lack of Mn^{2+} oxidation activity by the 99382 peroxidase is more difficult to explain because it has the three necessary acidic residues (Fig. 1*B*) that

TABLE 1

Kinetic constants (K_m (μM), k_{cat} (s^{-1}), and k_{cat}/K_m ($s^{-1}\cdot mM^{-1}$)) for *C. subvermispora* class II peroxidases (and the 99382 E183K variant) on the simple substrates veratryl alcohol (VA), Reactive Black 5 (RB5), ABTS, 2,6-dimethoxyphenol (DMP), and Mn^{2+}, compared with typical LiP and VP

Kinetic constants were estimated at 25 °C in 0.1 M tartrate (pH 3) for veratryl alcohol, pH 3.5 for Reactive Black 5, 2,6-dimethoxyphenol and ABTS, and pH 5 for Mn^{2+}. GP is generic peroxidase. Means and 95% confidence limits are shown. Dashes correspond to efficiency values (*i.e.* k_{cat}/k_m ratios) where both k_{cat} and k_m are 0.

		C. subvermispora genome						
		99382 (LiP1[a])	118677 (LiP2[a])	99382 (E183K)	117436 (MnP10)	112162 (GP)	LiP[b]	VP[c]
VA	K_m	3120 ± 526	1620 ± 290	2860 ± 179	0	0	190 ± 17	4130 ± 320
	k_{cat}	8.6 ± 0.7	8.7 ± 0.6	8.40 ± 0.37	0	0	17.5 ± 0.5	9.5 ± 0.2
	k_{cat}/K_m	2.8 ± 0.3	5.4 ± 0.7	2.9 ± 0.4	-	-	92.0 ± 6.0	2.3 ± 0.1
RB5	K_m	4.0 ± 0.7	4.5 ± 0.6	4.6 ± 0.6	0	0	0	3.4 ± 0.3
	k_{cat}	9.8 ± 0.9	7.3 ± 0.5	7.2 ± 0.4	0	0	0	5.5 ± 0.3
	k_{cat}/K_m	2460 ± 185	1620 ± 138	1560 ± 120	-	-	-	1310 ± 90
ABTS[d]	K_m	4.0 ± 0.4 (4250 ± 508)	7.2 ± 1.0 (NS)[e]	4.2 ± 0.3 (4110 ± 468)	0	40.5 ± 5	23.0 ± 1.6	3.0 ± 0.2 (1090 ± 42)
	k_{cat}	9.3 ± 0.2 (56 ± 2)	11.3 ± 0.5 (NS)	9.5 ± 0.4 (61 ± 3)	0	39.6 ± 2.6	13.0 ± 0.2	8.1 ± 0.2 (186 ± 3)
	k_{cat}/K_m	2300 ± 200 (13 ± 1)	1600 ± 200 (3 ± 0.1)	2260 ± 236 (15 ± 1)	-	976 ± 16	563 ± 36	2700 ± 140 (200 ± 3)
DMP[d]	K_m	29 ± 2 (NS)	37 ± 4 (NS)	30 ± 2 (NS)	NS	185 ± 28	6 ± 1	78 ± 8 (10500 ± 400)
	k_{cat}	6.4 ± 0.1 (NS)	6.1 ± 0.1 (NS)	6.9 ± 0.1 (NS)	NS	33.7 ± 2	10.0 ± 0.1	56 ± 1 (30 ± 0)
	k_{cat}/K_m	222 ± 13 (0.1 ± 0)	167 ± 17 (0.1 ± 0)	235 ± 15 (0.1 ± 0)	<0.1	181 ± 13	1720 ± 153	71 ± 6 (2.8 ± 0.1)
Mn^{2+}	K_m	0	0	9720 ± 1530	59 ± 9	0	0	181 ± 10
	k_{cat}	0	0	135 ± 8	331 ± 20	0	0	275 ± 4
	k_{cat}/K_m	-	-	14 ± 0	5600 ± 500	-	-	1520 ± 70

[a] LiP-VP transition enzymes.
[b] Data are from GenBank™ accession number Y00262 LiPH8.
[c] Data are from GenBank™ accession number AF007244 VPL.
[d] ABTS and DMP showed biphasic kinetics when oxidized by some VP-type and LiP-type enzymes enabling determination of two sets of constants (the second one, characterized by a low catalytic efficiency, is shown in parentheses).
[e] NS, K_m and k_{cat} values were not determined because of nonsaturation of the enzyme, but catalytic efficiencies were estimated from slope of observed activity *versus* substrate concentration.

are conserved in the Mn-oxidizing enzymes (Fig. 1*D*). The explanation may lie in the presence of a fourth acidic residue (Glu-183 contiguous to conserved Asp-182) (Fig. 1*B*), which constitutes a difference with respect to typical MnPs and VPs. In support, the E183K variant of the 99382 peroxidase is able to oxidize Mn^{2+}, as shown in Table 1, albeit with lower catalytic efficiency than typical MnPs and VPs, whereas its other catalytic properties are not significantly modified.

Oxidation of Recalcitrant Substrates by C. subvermispora Peroxidases—LiPs and VPs, unlike other peroxidases, are able to oxidize aromatics that lack strongly electron-donating –OH or $–NH_2$ substituents. This ability stems from their high redox potential and is central to their degradative activity on lignin. In addition, the ligninolytic activity of LiPs and VPs is likely promoted by their ability to oxidize bulky molecules due to the presence on their surface of an exposed tryptophan, which serves to receive electrons from the solvent region and transfer them to the heme cofactor.

To assess the reactivity of our heterologously expressed enzymes on recalcitrant substrates, we began by performing oxidations of two electron donors classically used to show the above properties, *p*-dimethoxybenzene and ferrocytochrome *c*. As shown in Fig. 4, where the same concentration of each enzyme (0.1 μM) was used, the *C. subvermispora* MnP (model 117436) was unable to oxidize either substrate, in agreement with the lack of a catalytic tryptophan. *P. chrysosporium* LiP catalyzed the fastest oxidation of *p*-dimethoxybenzene to *p*-benzoquinone, followed by the two *C. subvermispora* peroxidases (models 99382 and 118677) and the *Pleurotus* VP, which all exhibited similar oxidation rates (Fig. 4*A*). However, the *P. chrysosporium* LiP did not catalyze the fastest oxidation of ferrocytochrome *c*, as slightly higher rates were observed for one of the *C. subvermispora* peroxidases (model 118677) and the *Pleurotus* VP (Fig. 4*B*).

Next, we assayed the ability of the heterologously expressed *C. subvermispora* LiPs to cleave two nonphenolic lignin model dimers, the *erythro* and *threo* isomers of 4-ethoxy-3-methoxyphenylglycerol-β-guaiacyl ether, which represent the principal β-*O*-4 interunit linkage in lignin (1). The substrates were ^{14}C-labeled to facilitate detection and quantification of oxidized products by HPLC. The results (Fig. 5*A*) revealed that *C. subvermispora* LiP 118677 oxidized the dimer (peak 1) to yield 4-ethoxy-3-methoxybenzaldehyde (peak 2), the uncleaved ketone with an oxo group at Cα (peak 3), and 1-(4-ethoxy-3-methoxyphenyl)-2,3-dihydroxypropan-1-one (peak 4), together with small amounts of 1-(4-ethoxy-3-methoxyphenyl)glycerol (peak 5). Similar reaction products were produced by the 99382 peroxidase (data not shown). The *threo* isomer was oxidized with a higher k_{cat} than the *erythro* isomer but was not cleaved more rapidly, as virtually all of the additional oxidized product consisted of the uncleaved ketone 3 (Fig. 5, *A* and *B*).

Finally, we assessed the ability of the heterologously expressed *C. subvermispora* LiPs to depolymerize a radiolabeled synthetic lignin (DHP). Fig. 6, *A* and *B,* shows the results of GPC analyses of lignin treated with *C. subvermispora* peroxidase 118677 in the presence and absence of veratryl alcohol, respectively, together with controls without enzyme. Similar GPC profiles were obtained for the 99382 peroxidase (data not shown). These results show that the two *C. subvermispora* LiPs partially depolymerized polymeric lignin, provided veratryl alcohol was present. For comparison, we show here the result obtained in this work using *P. chrysosporium* LiPH8 in the presence of veratryl alcohol (Fig. 6*C*). We conclude that *C. subvermispora* peroxidases 99382 and 118677 are fully competent

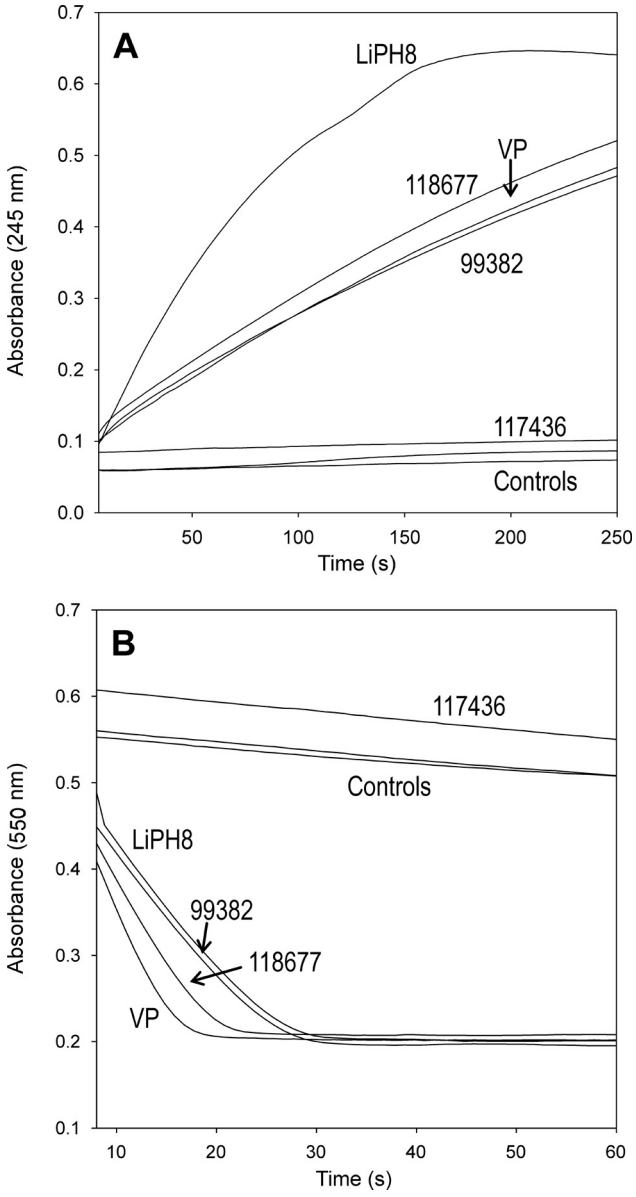

FIGURE 4. **Oxidation of *p*-dimethoxybenzene (*A*) and ferrocytochrome *c* (*B*) by three class II peroxidases from the *C. subvermispora* genome compared with oxidation by VP and LiP.** *p*-Dimethoxybenzene oxidation to *p*-benzoquinone by *E. coli*-expressed *C. subvermispora* 99382 (LiP), 118677 (LiP), and 117436 (MnP), *P. ostreatus* VP (genome 137757) and *P. chrysosporium* LiPH8 (GenBank™ Y00262) was followed at 245 nm in the presence of H_2O_2 (*A*). Ferrocytochrome *c* oxidation to ferricytochrome *c* was followed at 550 nm (*B*). Controls without enzyme and without H_2O_2 were included in both cases.

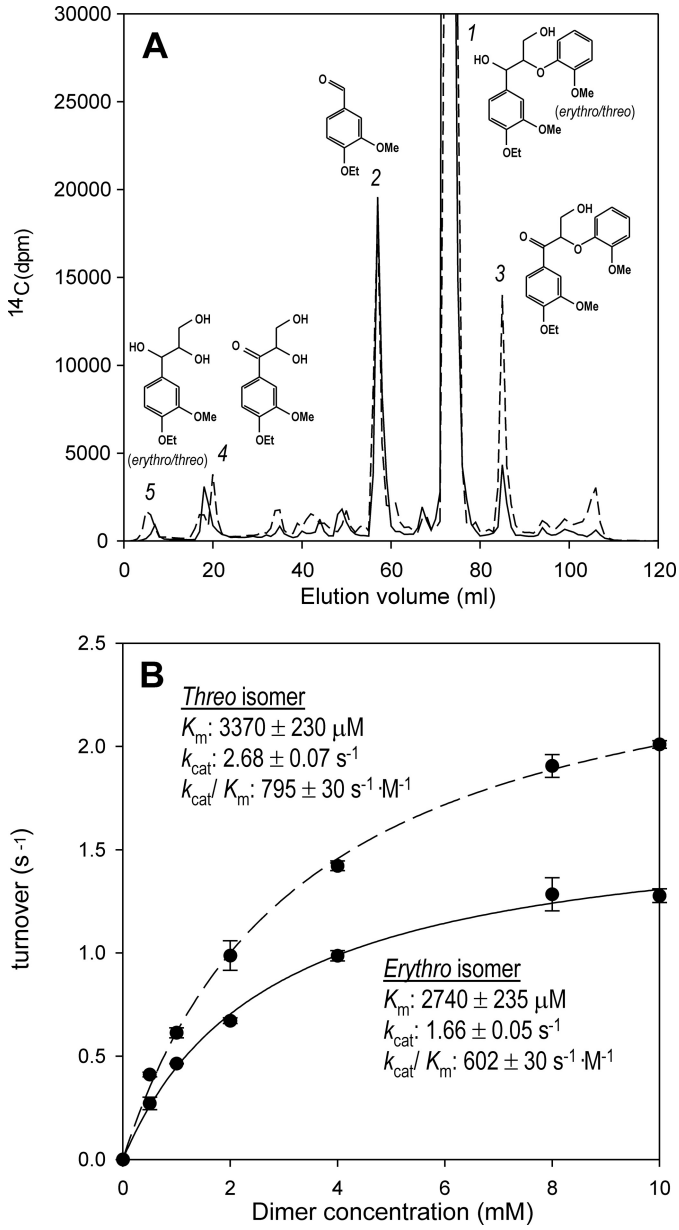

FIGURE 5. **Oxidative degradation of a nonphenolic lignin model dimer and estimation of the corresponding kinetic constants.** *A, erythro* (*continuous line*) and *threo* (*dashed line*) isomers of ^{14}C-labeled 4-ethoxy-3-methoxyphenylglycerol-β-guaiacyl ether (*peak 1*) were treated with *E. coli*-expressed *C. subvermispora* LiP (gene 118677), and the completed reactions were analyzed by HPLC. The main products were 4-ethoxy-3-methoxybenzaldehyde (*peak 2*), 1-(4-ethoxy-3-methoxyphenyl)-3-hydroxy-2-(2-methoxyphenoxy)-propan-1-one (*peak 3*), and 1-(4-ethoxy-3-methoxyphenyl)-2,3-dihydroxy-propan-1-one (*peak 4*). The minor *peak 5* corresponds to small amounts of *erythro* and *threo* 1-(4-ethoxy-3-methoxyphenyl)glycerol formed from the *erythro* and *threo* dimers, respectively. *B,* different concentrations of the *erythro* (*continuous line*) and *threo* (*dashed line*) isomers of the lignin model dimer were treated with *C. subvermispora* LiP 118677. Turnover numbers (s^{-1}) were obtained at different dimer concentrations by spectrophotometric estimation of the main products formed, and the kinetic constants were then calculated.

LiPs, despite their relatively low catalytic efficiency with the standard LiP substrate veratryl alcohol.

Evolutionary Relationships of C. subvermispora and Other Basidiomycete Peroxidases—Over 400 sequences of basidiomycete heme peroxidases are available to date (from GenBank™ and genomes). To establish the evolutionary relationships of *C. subvermispora* peroxidases, a comparison of their deduced protein sequences with the other peroxidases from basidiomycetes was performed with MEGA5 (44 class I sequences were excluded). In the dendrogram obtained (Fig. 7), all branches that do not include at least one *C. subvermispora* sequence are collapsed for simplicity. This is the case for the branch, including all members (47 sequences), of the dye-decolorizing peroxidase superfamily (group D). As for the HTPs (a total of 133 sequences), the nine *C. subvermispora* sequences are distributed in three of the four main clusters defined in this superfamily (Fig. 7, *E, G,* and *H*) with sequences 122198, 81391, and 114787 forming a homogeneous subcluster in cluster *E*.

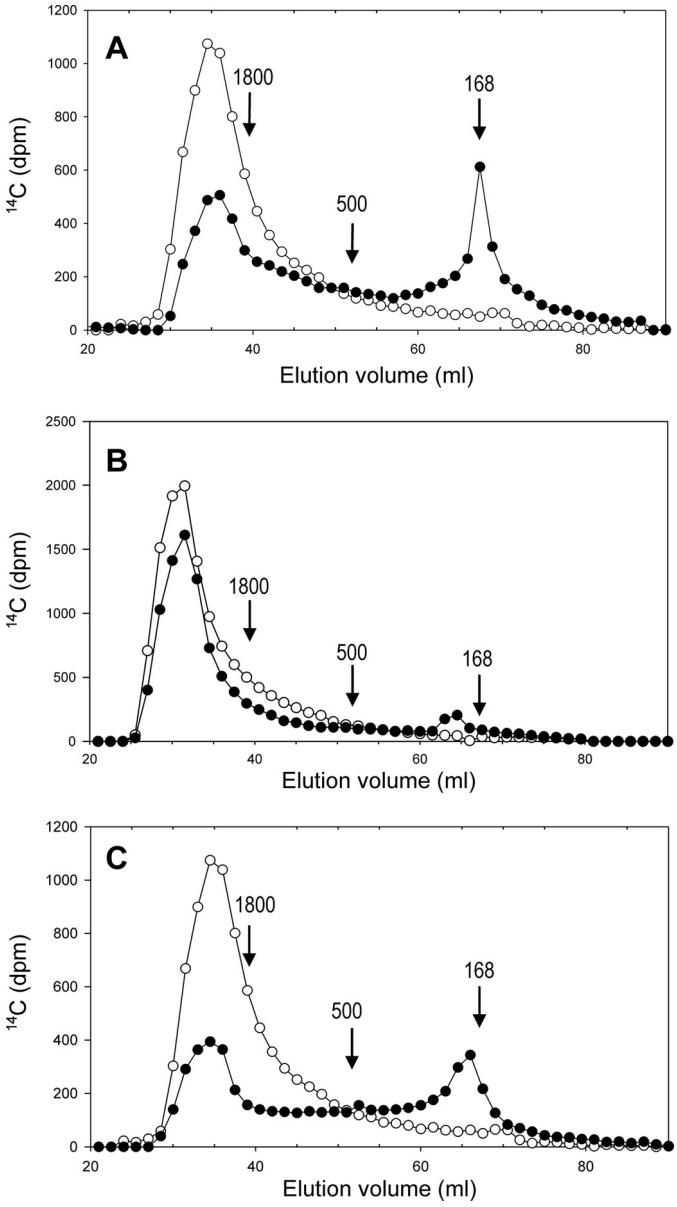

FIGURE 6. **Lignin depolymerization by *C. subvermispora* LiP as compared with depolymerization by *P. chrysosporium* LiP.** ^{14}C-Labeled synthetic lignin was treated with *E. coli*-expressed *C. subvermispora* LiP (gene 118677) in the presence (*A*) and absence (*B*) of veratryl alcohol and with *P. chrysosporium* LiPH8 (GenBank™ Y00262) in the presence of veratryl alcohol (*C*). *Black symbols* indicate reactions with enzymes, and *open symbols* indicate controls without enzymes. Total recoveries of initially added ^{14}C from complete reactions before GPC analysis were 72% for reaction *A*, 81% for reaction *B*, and 68% for reaction *C*. Recoveries from control reactions were somewhat higher as reported earlier (15). The *arrows* indicate elution volumes of two polystyrene molecular mass standards (1800 and 500) and of veratryl alcohol (168).

The most interesting information for our purposes was obtained for the class II peroxidases (a total of 196 sequences) in the plant-fungal-bacterial peroxidase superfamily. Most of the *C. subvermispora* sequences in this group correspond to long and extra long MnPs (12 sequences) in cluster B, together with all the related enzymes from *P. chrysosporium* and *Dichomitus squalens*, among other basidiomycetes. However, the unique MnP-short sequence and the two LiP-type sequences (from genes 118677 and 99382) are included in cluster A, where intermixed MnP-short and VP subclusters, as well as LiP/VP subclusters (including the 10 *P. chrysosporium* LiP genes) are included, together with additional VP and LiP sequences from other fungi. The position of these two *C. subvermispora* peroxidases (118677 and 99382), grouping together in cluster A, agrees with their LiP-like catalytic and lignin-degrading properties as described above, and thus with their description as new lignin-degrading peroxidases occupying an intermediate position between typical LiPs and VPs.

DISCUSSION

Overview—One of the most important pieces of evidence on the central role of ligninolytic peroxidases in lignin degradation comes from the comparison of the first white-rot (*P. chrysosporium*) (27) and brown-rot (*Postia placenta*) (28) genomes to be sequenced. Up to 15 ligninolytic peroxidase genes (10 *lip*s and 5 *mnp*s) were identified in the *P. chrysosporium* genome. By contrast, no such peroxidases are encoded in the genome of *P. placenta*, a related species that degrades polysaccharides while removing little of the lignin (4). These findings confirm earlier genetic and biochemical studies with the two fungi and point to a central role for LiPs and MnPs in efficient biological ligninolysis (47, 48). VP genes substitute for LiP genes in some genomes, such as that of *P. ostreatus* (30).

In light of these results, the apparent paucity of ligninolytic peroxidases in *C. subvermispora*, a white rot fungus closely related to *P. chrysosporium*, has been a perplexing research problem. When the *C. subvermispora* genome project was initiated, four MnP isoforms were the only peroxidases previously isolated (and/or cloned) from this organism (19, 32, 33, 49–51). The genomic screening results we report here now expand this number to include 26 heme peroxidase genes belonging to the plant-fungal-bacterial peroxidase superfamily (17 genes) and the HTP superfamily (nine genes) (29, 52). Surprisingly, no members of the growing dye-decolorizing peroxidase superfamily were identified, although they seem widespread among white-rot fungi (47 basidiomycete sequences available to date) and can oxidize nonphenolic lignin model compounds (53). The absence of related genes in *C. subvermispora* rules out their involvement in lignin degradation by this fungus.

HTPs—The chloroperoxidase from the ascomycete *Leptoxyphium fumago* was the only known fungal HTP for years, but the number of similar genes now apparent in basidiomycetes has increased greatly after the sequencing of the *A. aegerita* peroxygenase gene (45). Basidiomycete HTPs are among the most versatile peroxidase types, able to catalyze a wide variety of oxygenation and oxidation reactions on aromatic and aliphatic compounds (52, 54). However, the *A. aegerita* peroxygenase fails to cleave synthetic lignin, although it can oxidize nonphenolic lignin model dimers (55). It is also unable to oxidize chloride efficiently, although it has bromoperoxidase activity (56), and for this reason it is unlikely to cleave lignin through the agency of hypochlorous acid as the *L. fumago* chloroperoxidase has been shown to do (57). Accordingly, a role for *C. subvermispora* HTPs in ligninolysis appears unlikely.

Plant-Fungal-Bacterial Peroxidases—The *C. subvermispora* genome encodes a single class I cytochrome *c* peroxidase, a mitochondrial enzyme of prokaryotic origin. It encodes numer-

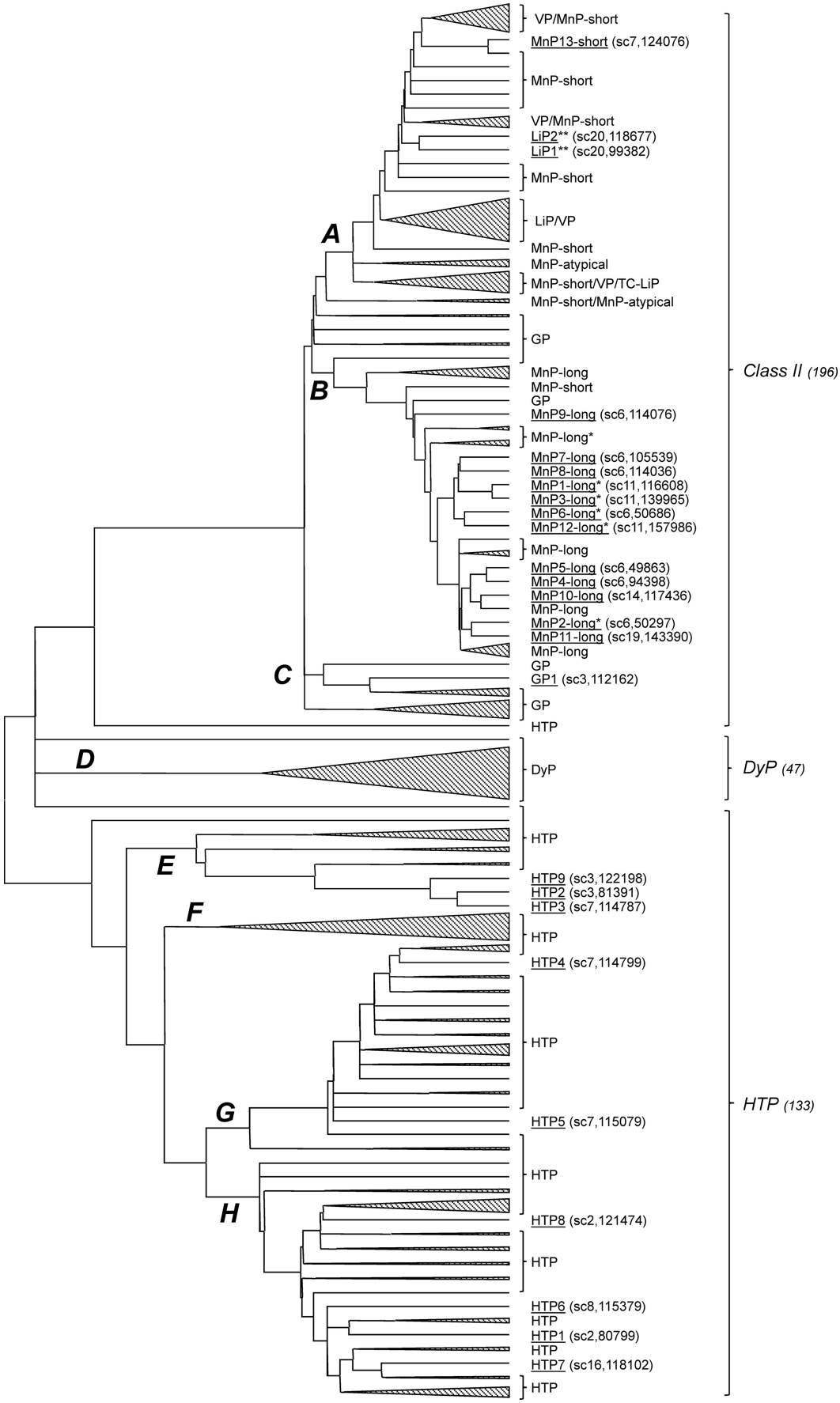

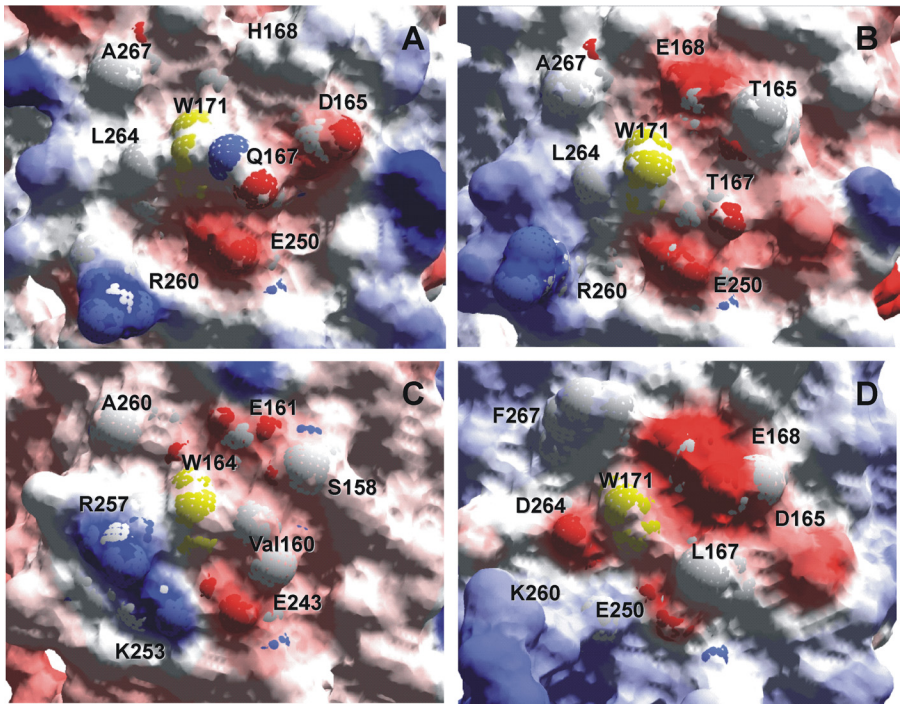

FIGURE 8. **Detail of the catalytic tryptophan surface environment (7 residues) in two *C. subvermispora* peroxidases (*top*) compared with typical VP and LiP (*bottom*).** *A, C. subvermispora* 118677 peroxidase (homology model) solvent access surface (showing the Asp-165, Gln-167, His-168, Trp-171, Glu-250, Arg-260, Leu-264, and Ala-267). *B*, *C. subvermispora* 99382 peroxidase (homology model) solvent access surface (showing Thr-165, Thr-167, Glu-168, Trp-171, Glu-250, Arg-260, Leu-264, and Ala-267). *C, P. eryngii* VPL crystal structure (Protein Data Bank code 2BOQ) solvent access surface (showing Ser-158, Val-160, Glu-161, Trp-164, Glu-243, Lys-253, Arg-257, and Ala-260). *D, P. chrysosporium* LiPH8 crystal structure (Protein Data Bank code 1LGA) solvent access surface (showing Asp-165, Leu-167, Glu-168, Trp-171, Lys-260, Asp-264, and Phe-267). Semitransparent solvent access surfaces colored by electrostatic potential (*red,* acidic residues; *blue,* basic residues) are shown. Amino acids are depicted as *white* or *yellow* (catalytic tryptophan) van der Waals spheres. The *C. subvermispora* peroxidase homology models correspond to those shown in Fig. 1, *A* and *B*. The amino acid numbering refers to putative mature sequences after manual curation of their signal peptide sequences.

ous class II peroxidases, compared with the other basidiomycete genomes available. Interestingly, all the class II peroxidase genes in the *C. subvermispora* genome appear to be functional, because transcripts for all have been detected in fungal cultures (transcriptomic data recently available under GEO accession GSE34636). This class II expansion is particularly true for the MnP models, which include a total of 13 genes, a greater number than in any sequenced basidiomycete genome except that of *Fomitiporia mediterranea* (58).

These *C. subvermispora* MnPs can be classified as short or long MnPs based on structural and catalytic properties. The latter corresponds to typical MnPs, first described in *P. chrysosporium*, and the former appears similar to some *P. radiata* MnPs that are able to oxidize certain phenols and dyes directly without the involvement of Mn^{2+} (59). The long *C. subvermispora* MnPs include five extra long MnPs similar to a thermostable MnP found in *D. squalens* (60), but their catalytic properties remain to be defined.

In addition and most interesting is the presence in the *C. subvermispora* genome of two LiP/VP-type genes that had never been detected in this fungus at the gene or protein level despite intensive efforts in past work. Our initial structural-functional classification of these peroxidases was based on whether they contain a conserved exposed tryptophan residue that could participate in electron transfer reactions or contain formal oxidation sites for Mn^{2+} (61). This analysis suggested that one gene encoded a VP (gene 99382) and the other encoded an LiP (gene 118677). However, heterologous expression showed that neither oxidized Mn^{2+}, although both oxidized veratryl alcohol, and therefore we classify both as LiPs.

Nevertheless, the relatively low catalytic efficiencies of the *C. subvermispora* LiPs on veratryl alcohol and 1,4-dimethoxybenzene, as compared with *P. chrysosporium* LiP, are reminiscent of a typical *Pleurotus* VP. This property could be related to the environment near the catalytic tryptophan (Fig. 8), which in the two *C. subvermispora* peroxidases (118677 and 99382) is closer

FIGURE 7. **Dendrogram of 376 sequences of basidiomycete heme peroxidases (from GenBank™ and different genomes) showing the position of 25 sequences from the *C. subvermispora* genome (*underlined*).** The evolutionary analysis was performed with MEGA5 (34) using Poisson distances and unweighted pair group method with arithmetic mean clustering. Those clusters where *C. subvermispora* sequences are not included were collapsed, and prokaryotic origin class I heme peroxidases, including the putative cytochrome *c* peroxidase from *C. subvermispora* genome (model 83438), are not included for simplicity. The three main peroxidase groups (class II in the plant, fungal, and prokaryotic peroxidase superfamily; dye-decolorizing peroxidase (*DyP*) superfamily; and HTP superfamily) and the number of sequences in each of them (*parentheses*) are indicated (*right*), together with their eight subclusters (*A–H*), and the scaffold and model numbers of the different *C. subvermispora* gene models (*parentheses*). Peroxidase (see supplemental Table S1 for details) include five MnP-long enzymes (*) that could be classified as extra long MnPs (60) and two LiP-type enzymes (**) representing LiP/VP transition stages. Additionally, MnP-atypical corresponds to a MnP type with only two acidic residues at the oxidation site (as found in the *Stereum hirsutum* genome), TC-LiP corresponds to the unique LiP from *Trametes cervina* (46), and *GP* corresponds to generic peroxidases. See Ruiz-Dueñas and Martínez (29) for references of class II basidiomycete peroxidases (from GenBank™ and genomes).

to that of *P. eryngii* VPL than to *P. chrysosporium* LiPH8 in terms of electrostatic charge distribution. A typical LiP, with four acidic residues, provides a significantly more electronegative environment than do the three other peroxidases with only two acidic residues.

Likewise, the ability of the *C. subvermispora* LiPs to directly oxidize the dye Reactive Black 5 is a typical property of VPs but not of LiPs. This property may be due to the absence in the *C. subvermispora* peroxidases of bulky residues near the catalytic tryptophan that could interfere with the binding of Reactive Black 5; LiPH8 has Phe-267 near Trp-171, whereas the two *C. subvermispora* LiPs and *P. eryngii* VPL have much smaller alanines at analogous positions. The differences in catalytic tryptophan environments of typical VPs and LiPs, as well as their possible implications in catalysis, have already been discussed (62).

The above catalytic properties, together with sequence-based phylogenetic analyses that group the *C. subvermispora* LiPs with VPs and short MnPs from other fungi, suggest that the two new *C. subvermispora* peroxidases represent VP-LiP transition stages. The discrepancy between the initial structural-functional classification of the 99382 peroxidase (as a VP-type enzyme) and the lack of Mn^{2+} oxidation activity after heterologous expression can be explained by conservation, near its hypothetical Mn^{2+} oxidation site, of a glutamate residue present in LiPs, which could disturb productive Mn^{2+} oxidation due to an excess of negative charge in this region of the protein. The Mn^{2+} oxidation activity of our 99382 E183K variant confirms this hypothesis.

Relevance of C. subvermispora LiPs to Ligninolysis—One diagnostic property of LiPs and VPs is their ability to cleave nonphenolic lignin model dimers by the one-electron abstraction mechanism reported earlier (2, 63). Our results show that the two *C. subvermispora* LiPs cleaved a dimer based on the principal nonphenolic *β-O*-4-linked lignin structure, giving product distributions very similar to those produced by *P. chrysosporium* LiPs. Even the well documented higher rate of LiPs on the *threo* isomer of this lignin structure is reproduced by the *C. subvermispora* enzymes. However, as with the monomeric substrate veratryl alcohol, the catalytic efficiency of LiPs 99382 and 118677 on dimeric lignin models is lower than that reported for *P. chrysosporium* LiPH8 (64–67).

The most stringent test available for whether a peroxidase should be classified as a LiP is to determine whether it partially depolymerizes a dispersion of synthetic lignin *in vitro* (15). Our results show that the two *C. subvermispora* LiPs were as effective as *P. chrysosporium* LiPH8 in this reaction, despite their lower catalytic efficiencies on monomeric and dimeric lignin models. As found also with other LiPs, veratryl alcohol was required for depolymerization.

The reason for the veratryl alcohol requirement remains unclear despite extensive research (68). One possibility is that veratryl alcohol is oxidized to its aryl cation radical by the LiP, and this radical then acts as a mediator to abstract an electron from insoluble lignin that cannot make sufficiently close contact with the enzyme's catalytic tryptophan. If this hypothesis turns out to be correct, it will be necessary to address the question of why veratryl alcohol, a natural metabolite of *P. chrysosporium*, has not so far been found in *C. subvermispora*.

Alternatively, because veratryl alcohol has been shown to stabilize LiPs against oxidative inactivation by H_2O_2 (68), and assays using synthetic lignins employ large quantities of this oxidant, the veratryl alcohol requirement may be an artifact of *in vitro* reaction conditions. If this second possibility, rather than the mediator hypothesis, proves to be correct, LiPs probably cleave lignin by making direct contact with it. Previous work showing that LiP can bind to lignin favors this second view (69). Moreover, our observation that the *C. subvermispora* LiPs are as effective as *P. chrysosporium* LiPH8 at oxidizing the bulky substrate ferrocytochrome *c* (46, 70) is consistent with our finding that these enzymes all exhibit similar activities on synthetic lignin.

Acknowledgments—We thank Dr. Daniel Cullen (United States Department of Agriculture, Forest Products Laboratory, Madison, WI) and Dr. Rafael Vicuña (Pontificia Universidad Católica de Chile, Santiago, Chile) for the invitation to participate in the C. subvermispora genome sequencing project. We thank Michael D. Mozuch for technical assistance with the DHP depolymerization reactions. Sequencing of the C. subvermispora genome by the Joint Genome Institute was supported by the Office of Science of the United States Department of Energy under Contract DE-AC02-05CH11231.

Note added in proof—While this article was being published, a description of the whole *C. subvermispora* genome was published online (71).

REFERENCES

1. Ralph, J., Lundquist, K., Brunow, G., Lu, F., Kim, H., Schatz, P. F., Marita, J. M., Hatfield, R. D., Ralph, S. A., Christensen, J. H., and Boerjan, W. (2004) Lignins. Natural polymers from oxidative coupling of 4-hydroxyphenylpropanoids. *Phytochem. Rev.* **3,** 29–60
2. Martínez, A. T., Speranza, M., Ruiz-Dueñas, F. J., Ferreira, P., Camarero, S., Guillén, F., Martínez, M. J., Gutiérrez, A., and del Río, J. C. (2005) Biodegradation of lignocellulosics. Microbial, chemical, and enzymatic aspects of the fungal attack of lignin. *Int. Microbiol.* **8,** 195–204
3. Ragauskas, A. J., Williams, C. K., Davison, B. H., Britovsek, G., Cairney, J., Eckert, C. A., Frederick, W. J., Jr., Hallett, J. P., Leak, D. J., Liotta, C. L., Mielenz, J. R., Murphy, R., Templer, R., and Tschaplinski, T. (2006) The path forward for biofuels and biomaterials. *Science* **311,** 484–489
4. Martínez, A. T., Ruiz-Dueñas, F. J., Martínez, M. J., Del Río, J. C., and Gutiérrez, A. (2009) Enzymatic delignification of plant cell wall: from nature to mill. *Curr. Opin. Biotechnol.* **20,** 348–357
5. Blanchette, R. A., Otjen, L., Effland, M. J., and Eslyn, W. E. (1985) Changes in structural and chemical components of wood delignified by fungi. *Wood Sci. Technol.* **19,** 35–46
6. Akhtar, M., Attridge, M. C., Myers, G. C., and Blanchette, R. A. (1993) Biomechanical pulping of loblolly pine chips with selected white-rot fungi. *Holzforschung* **47,** 36–40
7. Akhtar, M. (1994) Biomechanical pulping of aspen wood chips with three strains of *Ceriporiopsis subvermispora*. *Holzforschung* **48,** 199–202
8. Vicentim, M. P., Faria, R. D., and Ferraz, A. (2009) High yield kraft pulping of *Eucalyptus grandis* Hill ex Maiden biotreated by *Ceriporiopsis subvermispora* under two different culture conditions. *Holzforschung* **63,** 408–413
9. Scott, G. M., Akhtar, M., Lenz, M. J., and Swaney, R. E. (1998) in *Environmentally Friendly Technologies for the Pulp and Paper Industry* (Young, R. A., and Akhtar, M., eds) pp. 341–384, TAPPI Press, Atlanta
10. Salvachúa, D., Prieto, A., López-Abelairas, M., Lu-Chau, T., Martínez, A. T., and Martínez, M. J. (2011) Fungal pretreatment. An alternative in

second-generation ethanol from wheat straw. *Bioresour. Technol.* **102,** 7500–7506
11. Kersten, P., and Cullen, D. (2007) Extracellular oxidative systems of the lignin-degrading Basidiomycete *Phanerochaete chrysosporium*. *Fungal Genet. Biol.* **44,** 77–87
12. Ruiz-Dueñas, F. J., and Martínez, A. T. (2009) Microbial degradation of lignin. How a bulky recalcitrant polymer is efficiently recycled in nature and how we can take advantage of this. *Microbiol. Biotechnol.* **2,** 164–177
13. Tien, M., and Kirk, T. K. (1983) Lignin-degrading enzyme from the Hymenomycete *Phanerochaete chrysosporium* Burds. *Science* **221,** 661–663
14. Caramelo, L., Martinez, M. J., and Martinez, A. T. (1999) A search for ligninolytic peroxidases in the fungus *Pleurotus eryngii* involving α-keto-γ-thiomethylbutyric acid and lignin model dimers. *Appl. Environ. Microbiol.* **65,** 916–922
15. Hammel, K. E., Jensen, K. A., Jr., Mozuch, M. D., Landucci, L. L., Tien, M., and Pease, E. A. (1993) Ligninolysis by a purified lignin peroxidase. *J. Biol. Chem.* **268,** 12274–12281
16. Gold, M. H., Youngs, H. L., and Gelpke, M. D. (2000) Manganese peroxidase. *Met. Ions Biol. Syst.* **37,** 559–586
17. Camarero, S., Galletti, G. C., and Martínez, A. T. (1994) Preferential degradation of phenolic lignin units by two white rot fungi. *Appl. Environ. Microbiol.* **60,** 4509–4516
18. Salas, C., Lobos, S., Larraín, J., Salas, L., Cullen, D., and Vicuña, R. (1995) Properties of laccase isoenzymes produced by the basidiomycete *Ceriporiopsis subvermispora*. *Biotechnol. Appl. Biochem.* **21,** 323–333
19. Lobos, S., Larraín, J., Salas, L., Cullen, D., and Vicuña, R. (1994) Isoenzymes of manganese-dependent peroxidase and laccase produced by the lignin-degrading basidiomycete *Ceriporiopsis subvermispora*. *Microbiology* **140,** 2691–2698
20. Rüttimann, C., Schwember, E., Salas, L., Cullen, D., and Vicuña, R. (1992) Ligninolytic enzymes of the white rot basidiomycetes *Phlebia brevispora* and *Ceriporiopsis subvermispora*. *Biotechnol. Appl. Biochem.* **16,** 64–76
21. Rajakumar, S., Gaskell, J., Cullen, D., Lobos, S., Karahanian, E., and Vicuna, R. (1996) Lip-like genes in *Phanerochaete sordida* and *Ceriporiopsis subvermispora*, white rot fungi with no detectable lignin peroxidase activity. *Appl. Environ. Microbiol.* **62,** 2660–2663
22. Tanaka, H., Koike, K., Itakura, S., and Enoki, A. (2009) Degradation of wood and enzyme production by *Ceriporiopsis subvermispora*. *Enzyme Microb. Technol.* **45,** 384–390
23. Jensen, K. A., Bao, W., Kawai, S., Srebotnik, E., and Hammel, K. E. (1996) Manganese-dependent cleavage of nonphenolic lignin structures by *Ceriporiopsis subvermispora* in the absence of lignin peroxidase. *Appl. Environ. Microbiol.* **62,** 3679–3686
24. Srebotnik, E., Jensen, K. A., Kawai, S., and Hammel, K. E. (1997) Evidence that *Ceriporiopsis subvermispora* degrades nonphenolic lignin structures by a one-electron oxidation mechanism. *Appl. Environ. Microbiol.* **63,** 4435–4440
25. Moen, M. A., and Hammel, K. E. (1994) Lipid peroxidation by the manganese peroxidase of *Phanerochaete chrysosporium* is the basis for phenanthrene oxidation by the intact fungus. *Appl. Environ. Microbiol.* **60,** 1956–1961
26. Cañas, A. I., and Camarero, S. (2010) Laccases and their natural mediators. Biotechnological tools for sustainable eco-friendly processes. *Biotechnol. Adv.* **28,** 694–705
27. Martinez, D., Larrondo, L. F., Putnam, N., Gelpke, M. D., Huang, K., Chapman, J., Helfenbein, K. G., Ramaiya, P., Detter, J. C., Larimer, F., Coutinho, P. M., Henrissat, B., Berka, R., Cullen, D., and Rokhsar, D. (2004) Genome sequence of the lignocellulose degrading fungus *Phanerochaete chrysosporium* strain RP78. *Nat. Biotechnol.* **22,** 695–700
28. Martinez, D., Challacombe, J., Morgenstern, I., Hibbett, D., Schmoll, M., Kubicek, C. P., Ferreira, P., Ruiz-Duenas, F. J., Martinez, A. T., Kersten, P., Hammel, K. E., Vanden Wymelenberg, A., Gaskell, J., Lindquist, E., Sabat, G., Bondurant, S. S., Larrondo, L. F., Canessa, P., Vicuna, R., Yadav, J., Doddapaneni, H., Subramanian, V., Pisabarro, A. G., Lavín, J. L., Oguiza, J. A., Master, E., Henrissat, B., Coutinho, P. M., Harris, P., Magnuson, J. K., Baker, S. E., Bruno, K., Kenealy, W., Hoegger, P. J., Kües, U., Ramaiya, P., Lucas, S., Salamov, A., Shapiro, H., Tu, H., Chee, C. L., Misra, M., Xie, G., Teter, S., Yaver, D., James, T., Mokrejs, M., Pospisek, M., Grigoriev, I. V., Brettin, T., Rokhsar, D., Berka, R., and Cullen, D. (2009) Genome, transcriptome, and secretome analysis of wood decay fungus *Postia placenta* supports unique mechanisms of lignocellulose conversion. *Proc. Natl. Acad. Sci. U.S.A.* **106,** 1954–1959
29. Ruiz-Dueñas, F. J., and Martínez, A. T. (2010) in *Biocatalysts Based on Heme Peroxidases* (Torres, E., and Ayala, M., eds) pp. 37–59, Springer-Verlag, Berlin
30. Ruiz-Dueñas, F. J., Fernández, E., Martínez, M. J., and Martínez, A. T. (2011) *Pleurotus ostreatus* heme peroxidases. An *in silico* analysis from the genome sequence to the enzyme molecular structure. *C. R. Biol.* **334,** 795–805
31. Tello, M., Seelenfreund, D., Lobos, S., Gaskell, J., Cullen, D., and Vicuña, R. (2001) Isolation and characterization of homokaryotic strains from the ligninolytic basidiomycete *Ceriporiopsis subvermispora*. *FEMS Microbiol. Lett.* **199,** 91–96
32. Lobos, S., Larrondo, L., Salas, L., Karahanian, E., and Vicuña, R. (1998) Cloning and molecular analysis of a cDNA and the Cs-*mnp1* gene encoding a manganese peroxidase isoenzyme from the lignin-degrading basidiomycete *Ceriporiopsis subvermispora*. *Gene* **206,** 185–193
33. Tello, M., Corsini, G., Larrondo, L. F., Salas, L., Lobos, S., and Vicuña, R. (2000) Characterization of three new manganese peroxidase genes from the ligninolytic basidiomycete *Ceriporiopsis subvermispora*. *Biochim. Biophys. Acta* **1490,** 137–144
34. Tamura, K., Peterson, D., Peterson, N., Stecher, G., Nei, M., and Kumar, S. (2011) MEGA5. Molecular evolutionary genetics analysis using maximum likelihood, evolutionary distance, and maximum parsimony methods. *Mol. Biol. Evol.* **28,** 2731–2739
35. Bendtsen, J. D., Nielsen, H., von Heijne, G., and Brunak, S. (2004) Improved prediction of signal peptides. SignalP 3.0. *J. Mol. Biol.* **340,** 783–795
36. Bordoli, L., Kiefer, F., Arnold, K., Benkert, P., Battey, J., and Schwede, T. (2009) Protein structure homology modeling using SWISS-MODEL workspace. *Nat. Protoc.* **4,** 1–13
37. Sambrook, J., and Russell, D. W. (2001) *Molecular Cloning*, 3rd Ed., Cold Spring Harbor Laboratory Press, Cold Spring Harbor, NY
38. Pérez-Boada, M., Doyle, W. A., Ruiz-Dueñas, F. J., Martínez, M. J., Martínez, A. T., and Smith, A. T. (2002) Expression of *Pleurotus eryngii* versatile peroxidase in *Escherichia coli* and optimization of *in vitro* folding. *Enzyme Microb. Technol.* **30,** 518–524
39. Doyle, W. A., and Smith, A. T. (1996) Expression of lignin peroxidase H8 in *Escherichia coli*. Folding and activation of the recombinant enzyme with Ca^{2+} and heme. *Biochem. J.* **315,** 15–19
40. Heinfling, A., Ruiz-Dueñas, F. J., Martínez, M. J., Bergbauer, M., Szewzyk, U., and Martínez, A. T. (1998) A study on reducing substrates of manganese-oxidizing peroxidases from *Pleurotus eryngii* and *Bjerkandera adusta*. *FEBS Lett.* **428,** 141–146
41. Ruiz-Dueñas, F. J., Camarero, S., Pérez-Boada, M., Martínez, M. J., and Martínez, A. T. (2001) A new versatile peroxidase from *Pleurotus*. *Biochem. Soc. Trans.* **29,** 116–122
42. Srebotnik, E., Jensen, K. A., Jr., and Hammel, K. E. (1994) Fungal degradation of recalcitrant nonphenolic lignin structures without lignin peroxidase. *Proc. Natl. Acad. Sci. U.S.A.* **91,** 12794–12797
43. Shary, S., Ralph, S. A., and Hammel, K. E. (2007) New insights into the ligninolytic capability of a wood decay ascomycete. *Appl. Environ. Microbiol.* **73,** 6691–6694
44. Morita, Y., Yamashita, H., Mikami, B., Iwamoto, H., Aibara, S., Terada, M., and Minami, J. (1988) Purification, crystallization, and characterization of peroxidase from *Coprinus cinereus*. *J. Biochem.* **103,** 693–699
45. Pecyna, M. J., Ullrich, R., Bittner, B., Clemens, A., Scheibner, K., Schubert, R., and Hofrichter, M. (2009) Molecular characterization of aromatic peroxygenase from *Agrocybe aegerita*. *Appl. Microbiol. Biotechnol.* **84,** 885–897
46. Miki, Y., Calviño, F. R., Pogni, R., Giansanti, S., Ruiz-Dueñas, F. J., Martínez, M. J., Basosi, R., Romero, A., and Martínez, A. T. (2011) Crystallographic, kinetic, and spectroscopic study of the first ligninolytic peroxidase presenting a catalytic tyrosine. *J. Biol. Chem.* **286,** 15525–15534
47. Martínez, A. T. (2002) Molecular biology and structure-function of lignin-degrading heme peroxidases. *Enzyme Microb. Technol.* **30,** 425–444

48. Cullen, D. (1997) Recent advances on the molecular genetics of ligninolytic fungi. *J. Biotechnol.* **53,** 273–289
49. Alvarez, J. M., Canessa, P., Mancilla, R. A., Polanco, R., Santibáñez, P. A., and Vicuña, R. (2009) Expression of genes encoding laccase and manganese-dependent peroxidase in the fungus *Ceriporiopsis subvermispora* is mediated by an ACE1-like copper-fist transcription factor. *Fungal Genet. Biol.* **46,** 104–111
50. Larrondo, L. F., Lobos, S., Stewart, P., Cullen, D., and Vicuña, R. (2001) Isoenzyme multiplicity and characterization of recombinant manganese peroxidases from *Ceriporiopsis subvermispora* and *Phanerochaete chrysosporium*. *Appl. Environ. Microbiol.* **67,** 2070–2075
51. de Souza-Cruz, P. B., Freer, J., Siikaaho, M., and Ferraz, A. (2004) Extraction and determination of enzymes produced by *Ceriporiopsis subvermispora* during biopulping of *Pinus taeda* wood chips. *Enzyme Microb. Technol.* **34,** 228–234
52. Hofrichter, M., Ullrich, R., Pecyna, M. J., Liers, C., and Lundell, T. (2010) New and classic families of secreted fungal heme peroxidases. *Appl. Microbiol. Biotechnol.* **87,** 871–897
53. Liers, C., Bobeth, C., Pecyna, M., Ullrich, R., and Hofrichter, M. (2010) DyP-like peroxidases of the jelly fungus *Auricularia auricula-judae* oxidize nonphenolic lignin model compounds and high redox potential dyes. *Appl. Microbiol. Biotechnol.* **85,** 1869–1879
54. Gutiérrez, A., Babot, E. D., Ullrich, R., Hofrichter, M., Martínez, A. T., and del Río, J. C. (2011) Regioselective oxygenation of fatty acids, fatty alcohols, and other aliphatic compounds by a basidiomycete heme-thiolate peroxidase. *Arch. Biochem. Biophys.* **514,** 33–43
55. Kinne, M., Poraj-Kobielska, M., Ullrich, R., Nousiainen, P., Sipila, J., Scheibner, K., Hammel, K. E., and Hofrichter, M. (2011) Oxidative cleavage of nonphenolic β-*O*-4 lignin model dimers by an extracellular aromatic peroxygenase. *Holzforschung* **65,** 673–679
56. Hofrichter, M., and Ullrich, R. (2006) Heme-thiolate haloperoxidases. Versatile biocatalysts with biotechnological and environmental significance. *Appl. Microbiol. Biotechnol.* **71,** 276–288
57. Ortiz-Bermúdez, P., Srebotnik, E., and Hammel, K. E. (2003) Chlorination and cleavage of lignin structures by fungal chloroperoxidases. *Appl. Environ. Microbiol.* **69,** 5015–5018
58. Morgenstern, I., Robertson, D. L., and Hibbett, D. S. (2010) Characterization of three *mnp* genes of *Fomitiporia mediterranea* and report of additional class II peroxidases in the order Hymenochaetales. *Appl. Environ. Microbiol.* **76,** 6431–6440
59. Hildén, K., Martinez, A. T., Hatakka, A., and Lundell, T. (2005) The two manganese peroxidases Pr-MnP2 and Pr-MnP3 of *Phlebia radiata*, a lignin-degrading basidiomycete, are phylogenetically and structurally divergent. *Fungal Genet. Biol.* **42,** 403–419
60. Li, D., Li, N., Ma, B., Mayfield, M. B., and Gold, M. H. (1999) Characterization of genes encoding two manganese peroxidases from the lignin-degrading fungus *Dichomitus squalens*(1). *Biochim. Biophys. Acta* **1434,** 356–364
61. Ruiz-Dueñas, F. J., Morales, M., García, E., Miki, Y., Martínez, M. J., and Martínez, A. T. (2009) Substrate oxidation sites in versatile peroxidase and other basidiomycete peroxidases. *J. Exp. Bot.* **60,** 441–452
62. Ruiz-Dueñas, F. J., Morales, M., Mate, M. J., Romero, A., Martínez, M. J., Smith, A. T., and Martínez, A. T. (2008) Site-directed mutagenesis of the catalytic tryptophan environment in *Pleurotus eryngii* versatile peroxidase. *Biochemistry* **47,** 1685–1695
63. Kirk, T. K., and Farrell, R. L. (1987) Enzymatic "combustion." The microbial degradation of lignin. *Annu. Rev. Microbiol.* **41,** 465–505
64. Bohlin, C., Persson, P., Gorton, L., Lundquist, K., and Jonsson, L. F. (2005) Product profiles in enzymic and nonenzymic oxidations of the lignin model compound erythro-1-(3,4-dimethoxyphenyl)2-(2-methoxyphenoxy)-1,3-propanediol. *J. Mol. Catal. B-Enzym.* **35,** 100–107
65. Bohlin, C., Lundquist, K., and Jonsson, L. J. (2008) Diastereomer selectivity in the degradation of a lignin model compound of the arylglycerol β-aryl ether type by white-rot fungi. *Enzyme Microb. Technol.* **43,** 199–204
66. Jönsson, L., Karlsson, O., Lundquist, K., and Nyman, P. O. (1990) Stereospecificity in enzymic and nonenzymic oxidation of β-*O*-4 lignin model compounds. *FEBS Lett.* **276,** 45–48
67. Cho, D. W., Parthasarathi, R., Pimentel, A. S., Maestas, G. D., Park, H. J., Yoon, U. C., Dunaway-Mariano, D., Gnanakaran, S., Langan, P., and Mariano, P. S. (2010) Nature and kinetic analysis of carbon-carbon bond fragmentation reactions of cation radicals derived from SET-oxidation of lignin model compounds. *J. Org. Chem.* **75,** 6549–6562
68. Hammel, K. E., and Cullen, D. (2008) Role of fungal peroxidases in biological ligninolysis. *Curr. Opin. Plant Biol.* **11,** 349–355
69. Johjima, T., Itoh, N., Kabuto, M., Tokimura, F., Nakagawa, T., Wariishi, H., and Tanaka, H. (1999) Direct interaction of lignin and lignin peroxidase from *Phanerochaete chrysosporium*. *Proc. Natl. Acad. Sci. U.S.A.* **96,** 1989–1994
70. Wariishi, H., Sheng, D., and Gold, M. H. (1994) Oxidation of ferrocytochrome *c* by lignin peroxidase. *Biochemistry* **33,** 5545–5552
71. Fernandez-Fueyo, E., Ruiz-Dueñas, F. J., Ferreira, P., Floudas, D., Hibbett, D. S., Canessa, P., Larrondo, L. F., James, T. Y., Seelenfreund, D., Lobos, S. *et al.* (2012) Comparative genomics of *Ceriporiopsis subvermispora* and *Phanerochaete chrysosporium* provide insight into selective ligninolysis. *Proc. Natl. Acad. Sci. U.S.A.* **109,** 5458–5463

Capítulo 7

"Catalytic and stability properties of manganese peroxidase subfamilies: A study based on the *Ceriporiopsis subvermispora* genome"
Fernández-Fueyo, E., S. Acebes, F. J. Ruiz-Dueñas, , M. J. Martínez, A. Romero, F. J. Medrano, V Guallar and A. T. Martínez.
(enviado)

Catalytic and stability properties of manganese peroxidase subfamilies: A study based on the *Ceriporiopsis subvermispora* genome

Elena Fernández-Fueyo[a], Sandra Acebes[b], Francisco J. Ruiz-Dueñas[a], María Jesús Martínez[a], Antonio Romero[a], Francisco Javier Medrano[a], Victor Guallar[b,c,1], and Angel T. Martínez[a,1]

[a]Centro de Investigaciones Biológicas, CSIC, Ramiro de Maeztu 9, E-28040 Madrid, Spain; [b]Barcelona Supercomputing Center, Jordi Girona 29, E-08034 Barcelona, Spain; and [c]ICREA, Passeig Lluís Companys 23, E-08010 Barcelona, Spain

The genome of *Ceriporiopsis subvermispora* includes thirteen manganese peroxidase (MnP) genes, which were classified into three subfamilies according to the length of the C-terminal tail (Fernández-Fueyo et al. *PNAS* 109:5458, 2012). These putative subfamilies are widespread in ligninolytic basidiomycetes as shown by recent genome screening (Floudas et al. *Science* 336:1715, 2012). To confirm the differences between them, two long MnPs, two extralong MnPs and the only short MnP from the above genome were heterologous expressed and characterized, together with two "short" variants with partially-removed C-termini. It was found that the tail contributes to Mn^{2+} oxidation, with K_m values decreasing when its length increases. By contrast, long tails prevent oxidation of 2,2'-azino-bis(3-ethylbenzothiazoline-6-sulfonate) (ABTS), which is only oxidized by the short MnP and the two short-variants prepared. Moreover, the C-terminal extensions seem to contribute to pH stability, long/extralong MnPs maintaining over 60% activity after 24 h at pH 2, while the short tail MnPs were inactivated. Divalent cations increased MnP thermal stability, as shown for extralong MnP6 (12-14 ºC T_{50} increase by Cd^{2+} and Mn^{2+}) and its less-stable short-variant. To explain the above results, the first crystal structure of an extralong MnP was obtained (*C. subvermispora* MnP6) and compared with long and short MnP structures from related fungi. Inhibition studies showed that Cd^{2+} binds at the Mn^{2+}-oxidation site, as confirmed by MnP6-Mn^{2+}/Cd^{2+} crystal structures suggesting that the stabilizing effect is due to heme fixation, and it also inhibits ABTS oxidation (always at pH 4.5). More importantly, blocking the heme propionate channel with a double mutation (G82L/D85L) removed the activity on ABTS and Mn^{2+}. This agrees with ligand diffusion (by PELE) that positioned ABTS at electron-transfer distance from the heme propionates of a short-tail variant, while it remained far from the heme in the extralong MnP, in agreement with one order of magnitude different electron-coupling values. Interestingly, optimal Mn^{2+} and ABTS oxidation by the short-variants is produced at pH 4-5 and 3.5, respectively, the latter being favored by carboxylate protonation lowering the ABTS electrostatic repulsion. This agrees with more efficient ABTS oxidation when Mn^{2+}-binding residues (Glu35 and Glu39) are removed. Finally, it is possible to conclude that only small functional and structural differences exist between long and extralong MnPs. In contrast, short MnP appears as a distinct subfamily differing in both stability and catalytic properties. The latter are related to a shorter C-tail enabling the access of other substrates, in addition to Mn^{2+}, to the heme-propionate oxidation site.

Keywords: manganese peroxidase | *Ceriporiopsis subvermispora* | genome | Mn-independent activity | structural-functional relationships |
Running Title: Structural-functional comparison of MnP subfamilies
Classification: Biological Sciences (Microbiology)

Degradation of recalcitrant lignin, a key step for carbon recycling in land ecosystems, has been described as an "enzymatic combustion" (1), where high redox-potential peroxidases secreted by some basidiomycetes (the so-called white-rot fungi) play a central role (2). Among these oxidoreductases **(i)** lignin peroxidases (LiPs) have evolved a mechanism for oxidizing lignin at the enzyme surface based on an exposed protein

Author contributions: E.F.-F., F.J.R.-D. and A.T.M. designed research; E.F.-F., S.A., F.J.R.-D., and F.J.M. performed research; E.F.-F., S.A., F.J.R.-D., F.J.M., A.R., M.J.M., V.G. and A.T.M. analyzed data; and E.F.-F., V.G. and A.T.M. wrote the paper.
The authors declare no conflict of interest
This article is a Direct Submission.
Data deposition: The *Ceriporiopsis subvermispora* annotated genome is available on an interactive web portal, http://jgi.doe.gov/Ceriporiopsis. The atomic coordinates and structure factors reported in this paper have been deposited in the Protein data Bank, www.pdb.org (PDB ID codes XXX, XXX and XXX).
[1] To whom correspondence may be addressed. E-mails: ATMartinez@cib.csic.es and guallarv@gmail.com;
This article contains supporting information on line at www.pnas.org/xxxx

radical that abstracts electrons from the polymer; **(ii)** manganese peroxidases (MnPs) present a site for binding and oxidation of Mn^{2+} at one of the heme propionates, the resulting Mn^{3+} acting as an oxidizer on phenolic lignin units, and as a starter of peroxidation reactions degrading nonphenolic lignin; and **(iii)** versatile peroxidases (VPs) combine the catalytic properties of LiP and MnP due a hybrid molecular architecture (3). From an evolutionary point of view, MnPs evolved from fungal generic peroxidases (GPs) that oxidize the same substrates of plant peroxidases (4), and gave rise to VPs by incorporation of the catalytic protein radical, and finally to LiPs by loss of the VP Mn-oxidation site (5). Due to its ancestral origin, MnPs had been reported from many white-rot fungal species in the orders Polyporales, where most wood-rotting fungi are included, and Agaricales (6, 7), a distribution that is being enlarged by recent genomic studies.

After sequencing the first basidiomycete genome (8) of the model lignin-degrading fungus *Phanerochaete chrysosporium*, a large number of genomes of other wood decaying basidiomycetes have been sequenced at the Joint Genome Institute (JGI) of the US Department of Energy and other institutions, in the search for biotechnological tools for the sustainable production of biofuels, chemicals and different materials in lignocellulose biorefineries (9). In these transformations, lignin modification or removal is a prerequisite for the production of cellulose, fermentable sugars and other products. Therefore, lignin-degrading organisms (and enzymes) are the biocatalysts of choice for the initial processing of plant materials in biomass routes to substitute the current petrochemical routes (10).

A recent comparative analysis of over 30 fungal genomes has provided evidence on the involvement of the above peroxidases in lignin degradation, since the corresponding genes are present in all the white-rot fungal genomes and absent from all the genomes of brown-rot fungi (that depolymerize cellulose without a previous degradation of lignin), and recognized the existence of three MnP gene subfamilies that were defined for the length of the predicted C-terminal tail (5). The first described MnP from *P. chrysosporium* has been largely characterized including its dependence of Mn^{2+} to close the catalytic cycle (11) and would be representative for the long MnP subfamily (357 residues protein). It was the third peroxidase whose crystal structure was solved (12) and several high-resolution structures are currently available (13, 14). Extralong MnP was described from *Dichomitus squalens* as having a longer C-terminal tail (366 residues protein) and higher thermostability (15) but no additional reports nor crystal structure are available. Finally, short MnPs have been isolated from several Polyporales, such as *Trametes versicolor* (16), and also Agaricales, such as *Pleurotus ostreatus* (17), and some Mn-independent activity has been reported in two of them (18, 19). The first crystal structure of a short MnP (337 residues *P. ostreatus* MnP4) has been only recently solved (20).

The genome of *Ceriporiopsis subvermispora* was sequenced as a selective lignin-degrader of interest for industrial delignification of wood (21). In addition to some genes encoding LiP-type enzymes not previously described in this fungus (22), high expansion of MnP gene number (up to a total of thirteen) was observed (23). This number is higher than found in any other fungal genome, and suggests an important role in the lifestyle of this wood-rotting fungus. Interestingly for the purpose of the present study, the *C. subvermispora* genome includes representatives for the three MnP subfamilies proposed in genomic surveys (5), a fact that has not been reported for other genomes. This enabled us to compare the characteristics of the above subfamilies without "interferences" from the species evolutionary history. With this purpose, two extralong, two long and the only short MnP *C. subvermispora* genes were heterologously expressed and the kinetic and stability properties of the enzymes were investigated. At the same time the crystal structure of *C. subvermispora* MnP6 was solved providing the first structure of an extralong MnP. MnP crystal structures were used in ligand diffusion, molecular dynamics (MD) and quantum mechanics/molecular mechanics (QM/MM) calculations to investigate the catalytic site for the Mn-independent activity of some of them. Finally, several directed variants of an extralong MnP were built at the C-terminal tail (which was reduced in length) and then at the heme-propionate channel (which was blocked with bulkier residues) and they were analyzed for both Mn oxidation and Mn-independent activities. The final aim was to obtain an experimental validation of the MnP subfamilies proposed, in terms of catalytic and/or stability properties, and to identify the structural bases for these differences.

Results

Short, long and extralong MnPs from the *C. subvermispora* genome. Among the thirteen MnP genes annotated in the *C. subvermispora* genome (22), the following five were selected for heterologous expression, as representatives for the three MnP subfamilies proposed: extralong MnP6 (JGI model 50686) and MnP12 (157986), long MnP5 (49863) and MnP10 (117436), and short MnP13 (124076). The mature protein coding DNA sequences were synthesized, overexpressed in *E. coli* as inclusion bodies, *in vitro* activated, and purified to electrophoretic homogeneity in a single chromatographic step. The molecular

masses estimated by SDS-PAGE coincided with the values obtained from the predicted protein sequences, and the electronic absorption spectra showed the Soret (406 nm) and other typical bands of peroxidase resting state, confirming the correct incorporation of the cofactor.

Main structural differences between the MnP subfamilies. The crystal structure of the *E. coli* expressed *C. subvermispora* MnP6 was solved, and compared with those of long MnP (1YYB from *P. chrysosporium*; and *C. subvermispora* MnP10 homology model) and short MnP (4BM1 from *P. ostreatus*; and *C. subvermispora* MnP13 homology model). The most important difference between the three *C. subvermispora* MnPs concerns the C-terminal tail that in long and extralong MnPs includes fourteen and eighteen extra amino-acid residues, respectively (in red in **Fig. 1A-C**). When other MnPs are considered (Supporting **Fig. S1**) the length of the short and long C-terminal tails is generally conserved (with 14-residue difference) while some variation exists in the extralong tails (with 21 extra residues in *C. subvermispora* MnP12, and 23 extra residues in *D. squalens* and *P. radiata* MnPs).

The extralong and long MnPs from *C. subvermispora* (**Fig. 1D** and **E**) and other fungi show a fifth disulfide bond at the C-tail (Cys345-Cys352 and Cys341-Cys348, respectively) being absent from all short MnPs, which is partially responsible for forcing the tail away from the main body of the protein, while in short MnP the tail ends in front of the Mn-oxidation site formed by three acidic residues (in italics in **Fig. 1E**). Then, the tail extends to the upper domain of the protein, with tight contacts (discussed below) with helices C and A (24), and in long MnP ends over the heme propionate access channel (green circle in **Fig. 1B**, and region-a in **Fig. 1D**). The solved crystal structure reveals that in extralong MnP the final C-tail turns, and ends between the heme-propionate and the main heme access channels, reinforcing their separation (green circle and yellow ellipse, respectively, in **Fig. 1A**).

The difference in the numbering of cysteines forming the fifth disulfide bond in long and extralong MnP is related to a four residue insertion in the *C. subvermispora* extralong MnP (Thr231-G234) with respect to the long MnP, which attains eleven residues (extralong MnP Leu228-Thr238) when compared with the short MnPs (**Fig. S1**), and affects an exposed loop being longer in this protein (region-b in **Fig. 1D**). On the other hand, the short MnP has four extra residues in the upper domain (Gly33 and Pro55-Leu57) when compared with the long and extralong MnPs, which conserved in MnPs from other fungi (**Fig. S1**) and is located in a second loop that protrudes into the solvent including a short helix (region-c in **Fig. 1D**). This helix (located between helices B and C) represents the only significant difference in the secondary structure of the three MnPs, since the helical content of this loop is low in extralong MnP and even lower in long MnP.

Finally, the three MnPs share several characteristics of the MnP family (and other fungal peroxidases) such as the heme proximal and distal histidines and neighbor residues, the two structural Ca^{2+} ions and their ligands, and the Mn-oxidation site (**Fig. 1E**) together with the general helical topology (**Fig. S2**).

Catalytic properties of short/long/extralong MnPs and their shortened tail variants. The kinetic constants of the different *C. subvermispora* MnPs were investigated using Mn^{2+} and 2,2'-azino-bis(3-ethylbenzothiazoline-6-sulfonate) (ABTS), a low redox-potential dye oxidized by different peroxidases, as substrates. As shown in **Table 1**, all the wild-type recombinant (hereinafter native) MnPs are able to oxidize Mn^{2+}, but the long and extralong types showed much higher catalytic efficiency (k_{cat}/K_m>5000 $s^{-1}\cdot mM^{-1}$) than the short MnP (k_{cat}/K_m~750 $s^{-1}\cdot mM^{-1}$). The above differences agreed with increasing MnP apparent affinity for Mn^{2+} when the C-tail length increases, attaining one order of magnitude higher K_m values for the short MnP than for the extralong MnPs. The Mn^{3+} generated is able to oxidize ABTS, 2,6-dimethoxyphenol (DMP) and other dyes and phenolic substrates. However, in addition to the above Mn-mediated activity, the *C. subvermispora* short MnP also exhibits Mn-independent activity on ABTS (**Table 1**). The catalytic efficiency for direct oxidation of ABTS was much lower than for Mn^{2+} oxidation, due to a more than 20-fold higher K_m value. Such Mn-independent activity was absent from both long and extralong MnPs.

To investigate a possible connection between the C-tail length and the kinetic differences observed, two variants of extralong MnP6 with 4 and 18 residues shortened C-tail (hereinafter called MnP6 long-variant and short-variant, respectively) and one MnP10 variant with 14 residues shortened C-tail (called MnP10 short-variant) were designed and characterized. As shown in **Table 1**, all the shortened-tail variants incorporated the ability to oxidize ABTS, which was absent from the native enzymes. This was especially noteworthy for the MnP6 short-variant, whose catalytic efficiency was 7-fold higher that found for the native short MnP13, mainly due to a strong increase of ABTS apparent efficiency (over 20 fold lower K_m value). On the other hand, the enzyme efficiency oxidizing Mn^{2+} decreased (37-70%) when the C-tail of long and extralong MnPs was reduced, in agreement with the result obtained for the short MnP13. Both a reduction of k_{cat} and an increase of K_m were responsible for this decrease.

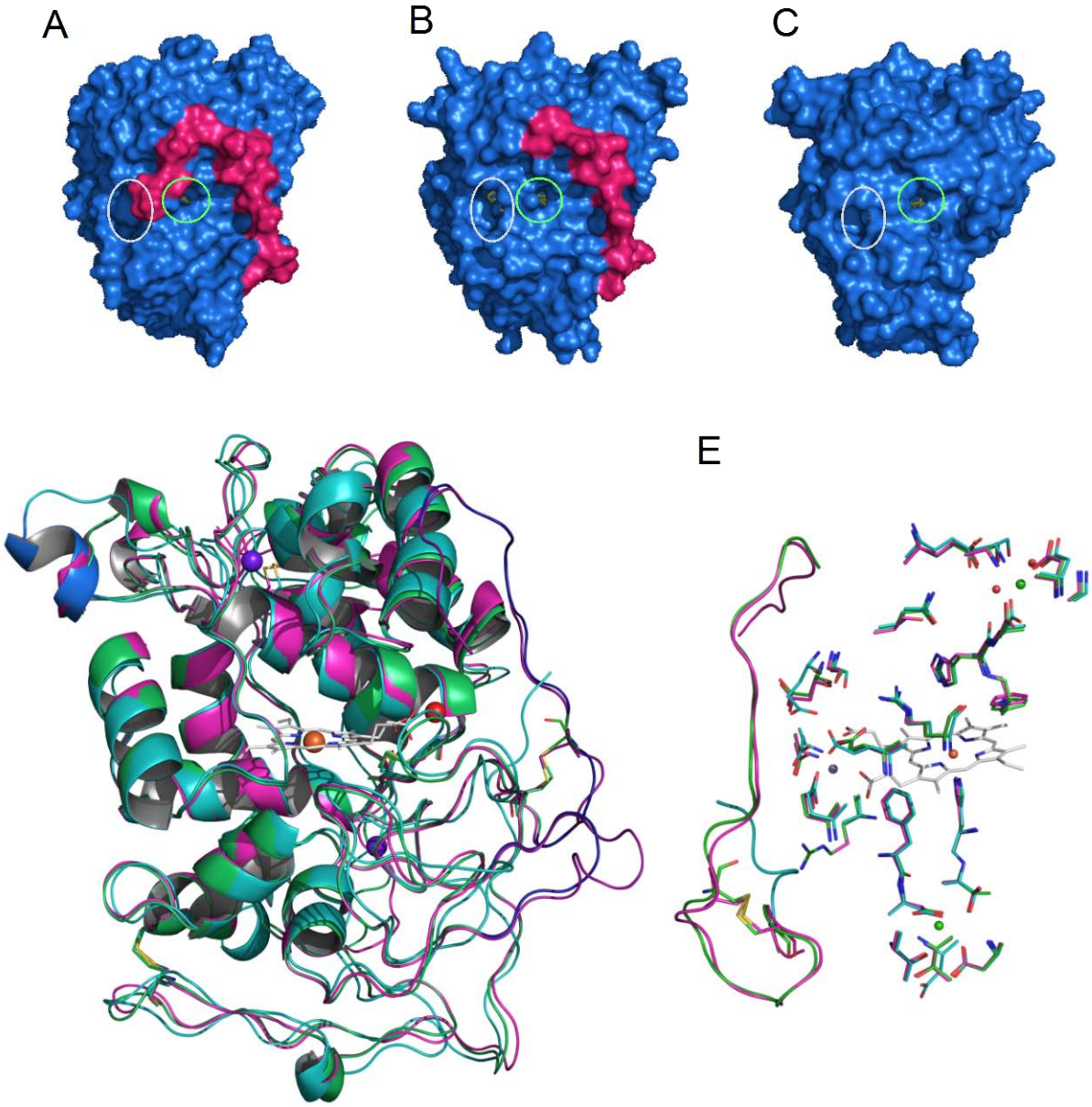

Fig. 1. Extralong (MnP6), long (MnP10) and short (MnP13) MnPs from the *C. subvermispora* genome. (**A-C**) Solvent access surfaces showing the C-tail disposition (magenta) surrounding the heme-propionate channel (green circles) neighbor to the main heme-access channel (white ellipses) of MnP6 (**C**), MnP10 (**D**) and MnP13 (**E**). (**D** and **E**) Superimposition of the general molecular structures (ribbons) with main differences in regions ***a-c***, also showing the iron (orange sphere) containing heme cofactor (sticks), 4-5 disulfide bonds (CPK sticks), two Ca^{2+} (magenta spheres) and one Mn^{2+} (red sphere) ions (**A**), and detail of the heme environment including Mn^{2+}-oxidation site (residue names in italics), Ca^{2+}-coordinating and other conserved residues at both sides of the cofactor (CPK colored sticks), together with the C-terminal tail (ribbon) (**B**) of MnP6 (magenta), MnP10 (cyan) and MnP13 (green). Residue numbering correspond to MnP6, the homologous residues in MnP6/MnP10/MnP13 being E35/E35/E37, E39/E39/E41, F45/F45/F47, H46/H46/H48, D47/D47/D49, G62/G62/G67, D64/D64/D69, S66/S66/S71, E74/E70/E79, S80/N80/N85, G82/G82/G87, D85/D85/E90, H173/H173/H176, T174/T174/S177, R177/R177/A180, D179/D179/D182, F190/F190/F193, D191/D191/D194, T193/T193/T196, T196/T196/D199 and D198/D198/D201 (five differences are underlined). Helices (A to J) are numbered following the nomenclature initially used for cytochrome *c* peroxidase (24). From MnP6 crystal structure (PDB XXX), and MnP10 and MnP13 homology models based on long and short MnP crystal structures (PDB entries 1YYD and 4BM1, respectively)

The optimal pH for oxidation of the above substrates was estimated for the native MnPs and the above variants. Optimal oxidation of Mn^{2+} is produced at pH 4-4.5, with the only exception of the short MnP13 that has the optimum at pH 5. The differences were more important for ABTS oxidation, with MnP13 showing

the optimum at pH 4, while the long and extralong MnPs had no detectable activity at this pH value, and the C-tail variants showed maximal ABTS oxidation at pH 3.5. However, the extralong MnP6 had some ABTS-oxidizing activity at pH 2.5, an unusually acidic pH for oxidation of this dye (with K_m 625±170 μM; k_{cat} 13±2 s^{-1}; and k_{cat}/K_m 22±0 $s^{-1}\cdot mM^{-1}$).

Table 1. Kinetic constants for Mn^{2+} and ABTS oxidation (at pH 5 and 3.5, respectively) by: i) short MnP13, long MnP5, long MnP10, extralong MnP6 and extralong MnP12 from the *C. subvermispora* genome; and ii) three variants at the C-tail of the long MnP10 and extralong MnP6.

	Mn^{2+}			ABTS		
	K_m (μM)	k_{cat} (s^{-1})	k_{cat}/K_m ($s^{-1}\cdot mM^{-1}$)	K_m (μM)	k_{cat} (s^{-1})	k_{cat}/K_m ($s^{-1}\cdot mM^{-1}$)
Native (wild-type)						
MnP13-short	116 ± 12	88 ± 2	756 ± 65	2440 ± 200	93 ± 3	38 ± 2
MnP5-long	50 ± 7	327 ± 15	6600 ± 700	0	0	-[1]
MnP10-long	59 ± 9	331 ± 20	5600 ± 500	0	0	-
MnP6-extralong	9 ± 2	83 ± 5	9540 ± 653	0	0	-
MnP12-extralong	11 ± 1	61 ± 0.8	5560 ± 325	0	0	-
C-tail variants[2]						
MnP10 short-variant	34 ± 3	118 ± 4	3500 ± 360	3430 ± 370	20 ± 1	5.8 ± 0.4
MnP6 long-variant	15 ± 2	63 ± 2	4140 ± 360	363 ± 46	41 ± 1	112 ± 12
MnP6 short-variant	16 ± 2	50 ± 1	3030 ± 390	116 ± 6	29 ± 1	251 ± 11

[1] -, no estimation because of lack of activity; [2]The C-tail of these three variants was adjusted to the length found in short and long MnPs by removing the 18 and 4 terminal residues, respectively

pH and thermal stability of short/long/extralong MnPs and their shortened tail variants. The pH and thermal stabilities of the five *C subvermispora* MnPs and the three C-tail variants described above, were investigated by monitoring the activity remaining after incubating the enzymes at different pHs (pH 2-9 range) and temperatures (25-70 ºC range).

In general, all the *C. subvermispora* MnPs are relatively stable at acidic pH maintaining more than 80% of the initial activity after 24 h at pH 3 (**Fig. 2A**). However, at pH 2 some differences appeared, with long and extralong MnPs maintaining over 60% and 80% of the initial activity, respectively, while the short MnP was very quickly (1 min) inactivated. On the other side, all the MnPs maintained over 70% of the initial activity at pH 7, but significantly different stabilities were observed at pH 8 with MnP10 and MnP12 showing the highest (near 60%) stabilities (**Fig. 2A**). Extralong MnP12, was by far the most stable at pH 9, with ~40% residual activity (data not shown). As found for the catalytic properties, shortening of the C-terminal tail also affected the pH stability of the MnPs. The most evident effect was at pH 2, where the three long/short-variants lost the stability shown by the native forms.

In the case of temperature, a rough inverse correlation was found between the length of the C-tail and the thermal stability of the native forms (**Fig. 2B)**. The most thermostable enzyme (with T_{50} ~55 ºC) was the short MnP, although it has only four disulfide bonds compared with the five bonds present in long and extralong MnPs (T_{50} ~40-45 ºC). However, shortening the C-tail resulted in a decrease of thermostability, with the long- and short-variants showing T_{50} values 4-7 ºC lower than the corresponding native enzymes.

Cation binding and effect on MnP stability. All the MnPs present a putative Mn^{2+}-binding site where this cation would be oxidized by the most internal (with respect to the main heme access channel) heme propionate (**Fig. 1E**). To confirm Mn^{2+}-binding at this site, and investigate the eventual binding of other divalent cations, the MnP6 crystal structure was also solved after soaking in Mn^{2+} and Cd^{2+} solutions, and anomalous difference electron density maps were obtained that unambiguously identified the two metal cations. The extralong MnP6 binds two Mn^{2+} ions, one at the predicted Mn-oxidation site - coordinated by Glu35, Glu39, Asp179 (whose involvement in Mn^{2+} oxidation was confirmed by directed mutagenesis as discussed below), the internal propionate of heme and two water molecules - and the second at a neighbor position in front of the heme propionates (6.7 Å from the external one), coordinated by Asp85 and four water molecules (**Fig. 3A**). Cd^{2+} binding was observed at the same two positions where Mn^{2+} binds, plus at a more distant third position also located at the upper side of the heme (10.7 Å from the external propionate), where it is coordinated by Asp363 and only two water molecules (**Fig. 3B**). As already mentioned, the MnP

molecular structure also includes two Ca^{2+} ions contributing to maintain the structure at the two enzyme domains.

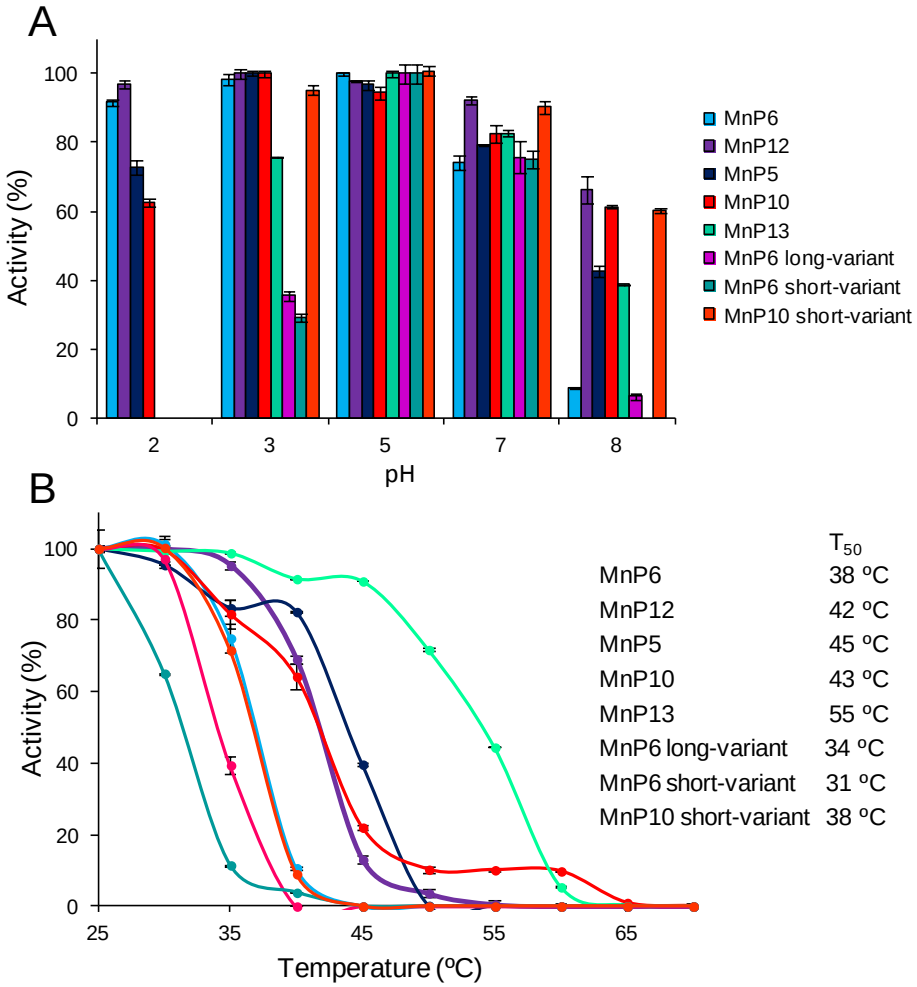

Fig. 2. Comparing pH and temperature stabilities of the extralong (MnP6 and MnP12), long (MnP5 and MnP10) and short (MnP13) MnPs, together with the MnP10 short-variant and the MnP6 long-variant and short-variant obtained by partial removal of the C-terminal tail: **(A)** pH stability (after 24 h at 4 ºC); and **(B)** Thermal stability (after 10 min incubation in pH 5 buffer) and corresponding T_{50} values.

The ability to bind different ions can increase protein stability. Therefore, the effect of the observed Mn^{2+} and Cd^{2+} (at 1 mM cation concentration) on the pH and thermal stability was studied using the same extralong MnP6 (**Fig. 3C** and **D**) and its short-variant (**Fig. 3E** and **F**), which include two Ca^{2+} ions per molecule, incorporated during *in vitro* folding, but has never been in contact with Mn^{2+} and Cd^{2+} ions. At acidic pH, only Ca^{2+} addition increases the enzyme stability as shown for: **i)** native MnP6 at pH 2, where the residual activity increased from ~60% to ~80%; and **ii)** its more instable short-variant at pH 3, where Ca^{2+} addition resulted in nearly three-fold higher stability. However, the three cations strongly increased the alkaline stability as shown for the native MnP6 and, especially, for the short-variant (that was completely inactivated at pH 8 in the absence of cations). In contrast with that observed for pH inactivation, the addition of Ca^{2+} did not improve the thermal stability of native MnP, while over 10 ºC increase of T_{50} was obtained after Mn^{2+} or Cd^{2+} addition. The same tendency was observed for the instable short-variant but, in this case, some stabilization was produced also by Ca^{2+}. In the above experiments Mn^{2+} and Cd^{2+} always caused similar stabilization effect. Moreover, no correlation between the presence of the extra C-tail and the stability enhancement by cations was observed.

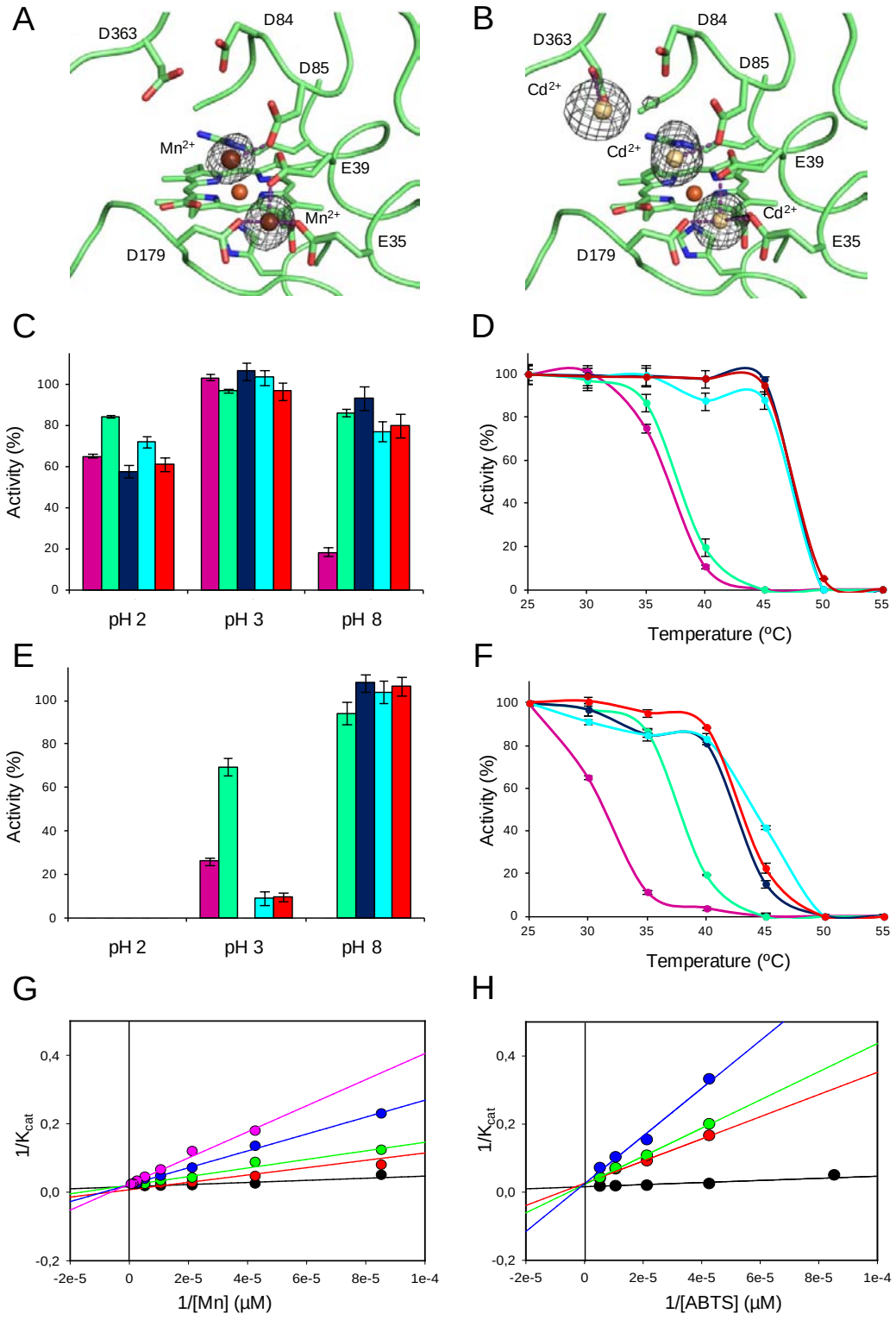

Fig. 3. Cation binding and effect on stability and enzymatic activity (inhibition) of extralong MnP6 and its short-variant. (**A** and **B**) Anomalous difference electron density map showing two Mn^{2+} (**A**) and three Cd^{2+} (**B**) ions at the proximity of heme (and six acidic residues) in the crystal structures of MnP6-metal complexes (PDB entries XXX and XXX, respectively). (**C** and **D**) Effect of 1 mM Ca^{2+} (green), Mn^{2+} (blue) or Cd^{2+} (cyan) and 0.5 mM Mn^{2+} + 0.5 mM Cd^{2+} (brown), compared with a control without the above cations (magenta), on the stability of MnP6 after incubation in the pH 2-8 range, for 24 h at 4 ºC (**C**), and in the 25-55 ºC range, for 10 min at pH 5 (**D**). (**E** and **F**) Effect of cations on the pH (**E**) and thermal (**F**) stability of the MnP6 short-variant assayed as described for **C** and **D**. (**G** and **H**) Inverse plots of MnP6 short-variant oxidation of Mn^{2+} at pH 5.0 in the presence of 0 (black), 0.1 (red), 0.25 (green), 0.5 (blue) and 1 mM Cd^{2+} (magenta) (**G**), and ABTS at pH 4.5 in the presence of 0 (black), 5.5 (red), 15 (green) and 30 mM Cd^{2+} (blue) (**H**).

ABTS oxidation site by short-tail MnPs: Inhibition and directed mutagenesis studies. Long and extralong MnPs only oxidize Mn^{2+}, but the ability to oxidize ABTS is introduced when their C-tails are shortened. Inhibition studies were on the effect of Cd^{2+} on the oxidation of two above substrates by the MnP6 short-variant. Mn^{2+}oxidation is clearly affected by the presence of Cd^{2+}. The inverse plots at various $CdSO_4$ concentrations showed a common ordinate-intercept, indicating that Cd^{2+} is a competitive inhibitor of both Mn^{2+} (**Fig. 3G**) and ABTS oxidation (**Fig 3H**). To confirm the above results, a battery of mutants was prepared at the heme propionate channel of the MnP6 short-variant to investigate the effect of: **i)** limiting the access of ABTS by introducing bulkier residues; and **ii)** charge inversion by removing acidic residues.

The mutated residues were Glu35, Glu39 and Asp179, involved in Mn^{2+}-binding; Gly82, whose substitution significantly reduced the size of the heme propionate channel; and Asp85, a neighbor fourth acidic residue. They were substituted by leucine or valine residues, in single and multiple variants, whose kinetic constants and optimal pH values are shown in **Table 2**. Substitution of the Mn^{2+}-binding residues, in single (E35L, E39L or D179V), double (E35L/E39L), triple (E35L/E39L/D179V) or "mixed" mutations (with Gly82 and/or Asp85) always resulted in the complete loss of the Mn^{2+}-oxidation activity. The same happened with the G82L/D85L variant, although the Mn^{2+}-binding site remained unchanged, and the corresponding single variants (G82L and D85L) maintained some activity (5 and 17 fold reduced catalytic efficiency, respectively). Interestingly, the above single and double mutations at the Mn^{2+}-binding site did not reduced, but increased, the ability of the enzyme oxidizing ABTS, up to double catalytic efficiency in the case of the E35L variant. Only the triple variant (E35L/E39L/D179V) reduced the catalytic efficiency (over 15 fold). In both cases, the higher/lower efficiencies are due to an increase/decrease of the turnover number (k_{cat}), respectively.

Table 2. Kinetic constants for Mn^{2+} and ABTS oxidation (at pH 5 and 3.5, respectively) by nine variants at the heme-propionate channel of the MnP6 ahort-variant.[1]

	Mn^{2+}			ABTS		
	K_m (μM)	k_{cat} (s^{-1})	k_{cat}/K_m ($s^{-1}\cdot mM^{-1}$)	K_m (μM)	k_{cat} (s^{-1})	k_{cat}/K_m ($s^{-1}\cdot mM^{-1}$)
MnP6 short-variant	16±2	50 ± 1	3030 ± 390	116 ± 6	29 ± 1	251 ± 11
E35L	0	0	- [2]	118 ± 13	64 ± 2	546 ± 51
E39L	0	0	-	250 ± 12	30 ± 1	120 ± 16
G82L	46 ± 5	30 ± 1	651 ± 46	1290 ± 150	100 ± 4	77 ± 5
D85L	107 ± 14	19 ± 1	179 ± 18	45 ± 8	4 ± 0	91 ± 15
D179V	0	0	-	288 ± 12	76 ± 1	263 ± 13
E35L/E39L	0	0	-	80 ± 9	34 ± 1	417 ± 38
G82L/D85L	0	0	-	0	0	-
D85L/D179V	0	0	-	35 ± 3	35 ± 1	977 ± 60
E35L/E39L/G82L	0	0	-	844 ± 121	98 ± 5	116 ± 12
E35L/E39L/D85L	0	0	-	243 ± 17	14 ± 3	59 ± 3
E35L/E39L/D179V	0	0	-	146 ± 17	2.2 ± 0.1	15 ± 1
E35L/E39L/G82L/D85L	0	0	-	0	0	-
E35L/E39L/D85L/D179V	0	0	-	0	0	-

[1]After C-tail shortening yielding the MnP6 short-variant (**Table 1**) additional single/multiple mutations were introduced at its heme-propionate channel; [2] -, no estimation because of lack of activity.

However, the most interesting mutations are those included in the G82L/D85L variant, whose combination would block the heme-propionate channel (as shown in **Fig. S4**). The individual variants (G82L and D85L) already showed a (3 fold) decrease of the ABTS oxidation efficiency, but their combination in the double variant resulted in complete inactivation of the enzyme oxidizing both ABTS and Mn^{2+} (and the same was observed for the E35L/E39L/G82L/D85L variant). The E35L/E39L/D85L/D179V quadruple variant was also unable to oxidize ABTS (and Mn^{2+}) although separate variants with the same mutations (namely E35L/E39L/D179V and D85L) maintained some Mn-independent activity, as mentioned above. Finally, near 4-fold increase of the ABTS oxidation efficiency, higher than obtained with the other single/double mutations mentioned above, was produced when the D85L and D179V mutations were combined in a double variant (that lacked Mn^{2+}-oxidation activity due to Asp179 removal).

Estimation of the optimal pH values for the above variants showed that optimal Mn^{2+} oxidation is always produced at pH 4-4.5. However, the optimum for ABTS oxidation varied between pH 3.5 as found for the

MnP6 short-variant and several of its propionate channel variants, and pH 4.5, as found for other of its propionate channel variants (such as D179V, E35L/E39L and D85L/D179V) (**Fig. S5**). Finally, under (non-physiological) pH 2.5 conditions, even the extralong MnP6 exhibited some activity on ABTS, although it disappeared when the pH was increased at the usual values.

Molecular simulation of ABTS access to the heme cofactor in short and (extra)long MnPs. No crystal structures of native short MnPs (or short-variants) including an ABTS molecule could be obtained to confirm its oxidation at the heme propionate channel, suggested by directed mutagenesis and other results. However, confirmatory evidence was provided by dynamic ligand diffusion using PELE (Protein Energy Landscape Exploration) software and other molecular simulation tools, using the structure of extralong MnP6 and its short-tail form. An initial 100 ns MD simulation, following protonation at pH 3.0, was performed to equilibrate the system. In both proteins, we observed that Glh35, Glh39 and Ash179 (protonated under these pH conditions) adopt different conformational states resulting in the opening/closing of the channel connecting the surface with the heme group at the propionate level. These MD simulations also showed a high number of stable H-bonds between the tail extension and the protein body (**Table S1**), probably contributing to MnP6 stability in spite of its extralong C-tail.

A first exploration on ABTS diffusion with PELE was performed on the whole enzyme, to identify the exposed regions were the ligand would bind preferentially (**Fig. S3**). In this way three binding energy minima were identified, the main one situating ABTS at 6.2 Å from the heme at the entrance of the propionate channel. To obtain an atomic detailed mechanism of ABTS's induced fit, and of its dependency with the C-terminal size, we performed a second ligand exploration with PELE focused on the heme propionate region of both the extralong MnP6 and its short-tail form. This time, the ligand was allowed to freely explore within a 20 Å distance from the CHA heme atom. **Fig. 4A** shows the relative ligand's interaction energy with respect to the distance between the heme group (carbon CHA) and the mass center of the ABTS molecule. In the case of the short-tail form (red dots) the structures with best interaction energy have the ABTS closer to the active site, adopting a favorable position for oxidation (**Fig. 4D**). In contrast, ABTS diffusion on the extralong MnP6 (blue dots) failed to identify and adequate structure with a good interaction energy and, in the best of the cases, the ABTS occupied a much farther position than in the short-tail form (**Fig. 4C**).

As shown in **Fig. 4E**, the presence (and the dynamics) of the C-terminal tail hinders the entrance of the ligand into the active site channel. Moreover, the tail also limits the above mentioned mobility of the residues situated at the entrance of the channel in the extralong enzyme. This is shown in **Fig. 4B** presenting the PELE binding energy in the extralong MnP6 and its short-tail form *vs* the distance between Glh35 and Ash179, located at both sides of the propionate channel. As already shown in **Fig. 4A**, ABTS has better binding energies in the short-tail form (red dots) than in the extralong MnP (blue dots) and this is accompanied by larger Glh35-Ash179 distances resulting in much higher frequency of "open gate" conformations enabling the approach of the ligand in the short-tail form. This is shown in **Figs. 4C** showing ABTS approaching to the internal propionate of heme (4.0 Å) at the same time that Asph179 (and Glh35) are displaced widening the channel entrance in the short-tail form. In contrast, Ash179 and Glh35 still maintain a close position in the best ligand position on extralong MnP6 (**Fig. 4D**) blocking the access of ABTS to the heme.

Finally, electron coupling energies were calculated to analyze ABTS oxidation by the extralong and the short-tail MnPs at the best positions predicted by PELE. The energies were one order of magnitude higher for the second MnP (**Fig. 4A**) in agreement with the experimental results showing that extralong MnP6 is unable to oxidize ABTS, but this ability can be introduced by shortening the C-tail in the short-variant.

Discussion

The most recent peroxidase inventories from basidiomycete genomes and other sources includes progressively growing numbers of genes of short (up to sixty-eight), long (up to forty) and extralong (up to thirteen) MnPs (5, 20, 25, 26). In current annotation of genomes, the three subfamilies are identified by the different extension of the C-terminal tail, but the evidence for biochemical and other differences between them is fragmentary and, more important, the structural bases for such differences remain largely unknown. The structural and functional comparison of *C. subvermispora* short, long and extralong MnPs, including their kinetic and stability properties, together with computational calculations on substrate diffusion and oxidation in the presence and the absence of the C-terminal tail, provide relevant answers to some of the above questions.

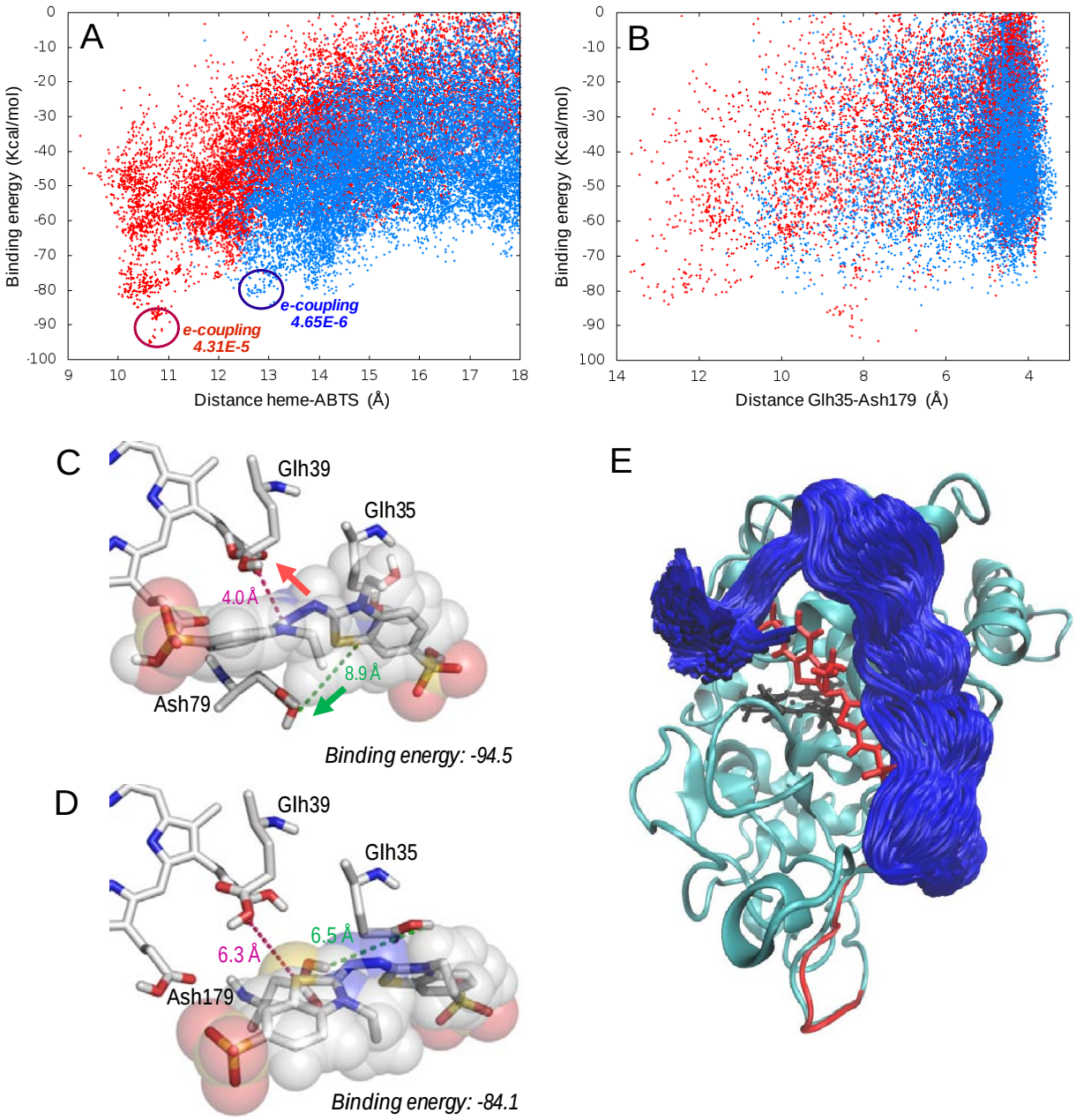

Fig. 4. Diffusion of ABTS on extralong MnP6 and its short-variant using PELE (28). (**A** and **B**) Binding energy (Kcal/mol) *vs* distance between heme (CHA) and ABTS (mass center) (**A**) and between protonated Glh35 (CG) and Ash179 (CD) (**B**) during substrate diffusion at the vicinity of the heme-propionate channel (a cutoff distance of a 20 Å between the heme CHA and the ABTS center of mass was fixed) of the extralong MnP6 (blue) and its short-variant (red), with indication of the heme-ABTS electron coupling energies at the most favorable positions in **A**. (**C** and **D)** Detail of the ABTS location and position of Glu35, Glu39 and Asp179 at two positions extracted from the PELE diffusion of ligand on the extralong MnP6 (**C**) and short-variant structures (**D**) with indication of the closest ABTS-heme and Glu35-Asp179 distances, the former being shorter in **D** and the latter in **C** (CPK sticks, and ABTS also as partially transparent spheres). (**E**) Superimposition of extralong MnP6 (blue ribbon, and heme) and one ABTS position (red sticks) selected from the PELE diffusion on the short-variant, showing collision with the extralong MnP6 tail whose PELE mobility is indicated in dark blue (the end of the short-variant tail is also shown in red). Based on MnP6 crystal structure (PDB XXX) and short-variant model.

Variability of MnP catalytic properties

The long and extralong MnPs from *C. subvermispora* only oxidize Mn^{2+}, as described for the best known long MnP of *P. chrysosporium* (27). Their catalytic efficiency oxidizing Mn^{2+} is one order of magnitude higher than estimated for the short MnP, but the latter is able to oxidize ABTS in the absence of Mn^{2+} as shown for the six short MnPs from the *P. ostreatus* genome (20). One of them was crystallized, and the comparison with the first crystal structure of an extralong MnP, obtained here, show that the extra residues at

the C-terminal tail adopt a characteristic disposition surrounding the entrance of the heme-propionate channel. Such disposition could limit bulky substrates (such as ABTS) access through this channel, as revealed by ligand diffusion calculations with PELE (28). Indeed, removal of the tail from extralong MnP6 decreases the heme-ligand distance from 6.3 Å to 4.0 Å, with a 20 Kcal/mol better binding energy. Experimental confirmation for the above prediction was obtained by reducing the C-tail extension in both extralong MnP6 and long MnP10 by directed mutagenesis, which resulted in the introduction of the ability to oxidize ABTS into two peroxidases that initially lacked this activity.

The above results, together with **(i)** ligand diffusions by PELE on the whole MnP surface showing the lowest binding energy at the heme-propionate channel and **(ii)** observed competitive inhibition by Cd^{2+} of both Mn^{2+} and ABTS oxidation, strongly pointed to ABTS oxidation at the heme-propionate channel of natural (MnP13) and engineered MnPs (MnP6 and MnP10 variants with a shortened tail). However, an effect of the C-tail on oxidation of ABTS at the main heme access channel, where oxidation of ABTS and other dyes and phenols has been shown in *P. eryngii* VP (29), could not be discarded. Therefore, additional mutations at the heme-propionate channel were performed on the (ABTS-oxidizing) MnP6 short-variant, and the simultaneous loss of both ABTS and Mn^{2+} oxidation activities was obtained by a double mutation (G82L/D85L) that blocked the heme-propionate channel, demonstrating that the two substrates are oxidized at the same site in short-tail MnPs. Conversely, improved ABTS oxidation was obtained by mutations reducing the negative charge at the heme-propionate channel due to reduced electrostatic repulsion with the anionic ABTS substrate. The activity on Mn^{2+} was lost when any of the three Mn-binding acidic residues was mutated. An easier oxidation of ABTS by the short-tail MnPs was also predicted by electron coupling calculations after ligand diffusion on the MnP6 structure before and after shortening the C-tail, the latter yielding one order of magnitude higher values. Interestingly, oxidation of a substrate other than Mn^{2+} (ascorbate) at the heme-propionate channel had been described in ascorbate peroxidase (30). While Mn^{2+} oxidation by MnPs (13) and VPs (31) imply the closure and opening of the heme-propionate channel (mainly by reorientation of the ion binding side-chains) for proper positioning of Mn^{2+} near the heme propionate and release of the Mn^{3+} formed, respectively, ABTS oxidation by the short MnPs would require more significant reorganizations enabling the approach and oxidation of this bulky substrate, as shown by the PELE simulations.

Variability of MnP stability properties

The *C. subvermispora* long and, especially, the extralong MnPs are exceptionally stable at pH 2 (over 60% and 90% residual activity, respectively, after 24 h at 4 ºC) while the short MnP was fully inactivated under the same conditions, in agreement with results obtained for the six short MnPs of *P. ostreatus* (20). However, the similar or even lower thermal stability of the extralong MnPs compared with the long MnPs contrasted with the previous assumption about their high thermostability, based on the initially described extralong MnPs from *Dichomitus squalens* (15). In fact, the highest thermal stability was shown for the short MnP, with a T_{50} value (55 ºC) in the range (43-57 ºC) found for the *P. ostreatus* short MnPs (20). However, the removal of the C-tail from long and extralong MnPs by directed mutagenesis did not result in improved thermostability (on the contrary a 5-7 ºC decrease of T_{50} was observed) revealing that the presence of the tail is not necessarily an instability factor, most probably because of the numerous and stable H-bond contacts with the protein body shown by MD calculations. In fact, the C-tail seems involved in the acidic stability of the *C. subvermispora* extralong MnPs as shown by their rapid inactivation at pH 2 when the tail is shortened by directed mutagenesis. Although the structural basis for the unique acidic stability of these MnPs is to be determined, the isoenzyme MnP6 from *C. subvermispora* has been used as a robust scaffold to build a lignin-degrading peroxidase of biotechnological interest acting at very acidic pH values (32).

Two manganese and three cadmium ions were identifying in the anomalous difference electron density maps of the extralong MnP6 in complex with Mn^{2+} and Cd^{2+}, respectively. One of them occupied the Mn-oxidation site and the others were located in neighbor positions. A similar situation has been described for the *P. chrysosporium* MnP (14), although the third site found in the extralong MnP does not exist due to the shorter C-tail. Those ions at the Mn-oxidation site would be responsible for the similar improvement of the MnP thermal and alkaline stability by Mn^{2+} and Cd^{2+} contributing to cofactor fixation on the protein, although a lower effect of the second Mn^{2+} and the two other Cd^{2+} ions fixing the protein structure cannot be discarded. An effect of Mn^{2+} and Cd^{2+} ions increasing the enzyme stability has been reported for long/extralong MnPs (33, 34). On the other hand, Ca^{2+} causes a general stabilizing effect on plant and fungal peroxidases (from the superfamily of plant-fungal-prokaryotic peroxidase) by reverting unfolding due to the loss of the two conserved structural Ca^{2+} ions (35, 36).

Evolutionary relationships of MnP subfamilies

The evolutionary relationships between the *C. subvermispora* heme peroxidases (a total of twenty-six including one cytochrome *c* peroxidase) and those isolated from other basidiomycetes, up to a total of 376 sequences, were analyzed by Fernández-Fueyo et al. (22). The phylogram obtained (see **Fig. S6**) revealed a large cluster for the superfamily of plant-fungal-prokaryotic peroxidases (196 members), together with two other clusters of the superfamilies of dye-decolorizing peroxidases (absent from *C. subvermispora)* and heme-thiolate peroxidases (nine in *C. subvermispora*). In the first cluster, three groups corresponding to **(i)** short-MnPs (only one in *C. subvermispora*), VPs (absent from *C. subvermispora*) and LiPs (two in *C. subvermispora*), **(ii)** long and extralong MnPs (up to a total of twelve in *C. subvermispora*), and **(iii)** generic peroxidases (only one in *C. subvermispora*) are defined, together with several unclustered sequences.

The separate clustering of short MnPs in the first group, and the intermixed presence of long and extralong MnPs in the second group (with high sequence identities among them, as shown in **Table S2**) suggest a separate origin for the short MnP subfamily, while the proposed long and extralong MnP types would not constitute two separate groups from a phylogenetic point of view. This fact, together with the significantly different catalytic and stability properties of the short MnPs (including Mn-independent activity, lower Mn^{2+} oxidizing efficiency and acidic stability, and higher thermal stability than the long and extralong MnPs) and the presence of a 14-22 residues shorter C-tail, strongly support their classification as a different MnP subfamily. In contrast, the so-called long and extralong MnPs cluster together in the peroxidase phylogram, their catalytic and stability properties only show gradual differences (such as the ~5-fold lower K_m and k_{cat} values for Mn^{2+} oxidation and the ~40% higher stability at pH 2 of the *C. subvermispora* extralong MnPs compared to the long MnPs) and variable C-tail lengths were observed. These modest differences do not justify maintaining long and extralong MnPs as two separate subfamilies.

Conclusions

From comparison of the different *C. subvermispora* MnPs and a collection of site-directed variants, together with the results from related enzymes available in the literature, we conclude that short MnPs would constitute a separate subfamily characterized by their ability to directly oxidize both Mn^{2+} and other substrates (such as ABTS) at the same heme access channel, located in front of the heme propionates. The access to this site in long and extralong MnPs would be limited by the C-tail that surrounds the channel preventing the approach of bulky substrates (such as ABTS) although the access of Mn^{2+} is not negatively affected (in fact the presence of the tail seems to improve the oxidation of Mn^{2+}). Another remarkable characteristic of the long and, especially, extralong MnPs (of C. *subvermispora*) is their stability at highly acidic pH, whose structural bases remain to be identified. In contrast with that found for the short MnPs, only gradual differences were observed between the two other MnPs that do not justify their classification in two different subfamilies.

Materials and Methods

Genome sequencing and inventory of MnP genes. The genome of *C. subvermispora* was sequenced at the JGI in a project coordinated by Daniel Cullen (USDA Forest Products Laboratory, Madison, USA) and Rafael Vicuña (Pontificia Universidad Católica, Santiago, Chile). The results from gene annotation (a total of 12 125 models) are available at the JGI portal (http://genome.jgi.doe.gov/Cersu1/Cersu1.home.html). The complete inventory of *C. subvermispora* heme peroxidase genes was obtained as described by Fernandez-Fueyo et al. (22). The manual annotation process included, among other steps, confirmation of the presence of characteristic residues at the heme pocket and substrate oxidation sites by homology modeling of the predicted sequences, using crystal structures of related proteins as templates (37). The homology models for the different MnP isoenzymes were also used in the subsequent structural-functional studies.

Gene synthesis and heterologous expression. The coding sequences of the *C. subvermispora* gene models encoding isoenzymes MnP5 (49863), MnP6 (50686), MnP10 (117436), MnP12 (157986) and MnP13 (124076) were designed with *E. coli* preferred codon usage (confirmed for other genes expressed in the BL21 strain), and synthesized by ATG:biosynthetics. The five genes were cloned in the expression vector pET23a (+) (Novagen). The resulting plasmids – pET23a-49863, pET23a-50686, pET23a-117436, pET23a-157986 and pET23a-124076 were used for expression and directed mutagenesis when required. *E. coli* DH5α was used for plasmid propagation, and the different peroxidases were produced in *E. coli* BL21 (DE3) pLys, in vitro folded and purified as previously described (22).

Directed mutagenesis. Stop mutations were introduced in the MnP6 (T362stop and G348stop) and MnP10 (G344stop) encoding genes by polymerase chain reaction (PCR) (22) using the expression plasmid pET23a-50686 and pET23a-117436 (see above) as template. The 5'- CC GTC CAA TTC TCG GGC CCC GCC TAA GAC TCC CC -3', 5'- CC CTC ATT CCT CAC TGC TCC GAC TAA CTC GAG AAC TGC -3' and 5'- CCC CAT TGC AAC TAA GGC CAA GAC TGC CC -3' direct primer (and the reverse primer bearing the complementary sequence) were used, respectively. Thirteen additional variants (E35L, E39L, G82L, D85L, D179V, E35LE39L G82LD85L, D85LD179V, E35LE39LG82, E35LE39LD85L, E35LE39LD179V E35LE39LG82LD85L and E35LE39LG82LD85LD179V) were obtained by mutating the following residues (located around the heme-propionate channel) on the previously obtained MnP6 short-variant (with

the G348stop mutation): E35L (GAA for CTA), E39L (GAG for CTG), G82L (GGT for CTT), D85L (GAC for CTC), and D179V (GAC for GTC).

Kinetics of Mn^{2+} and ABTS oxidation and inhibition by Cd^{2+}. Absorbance changes during substrate oxidation in 0.1 M tartrate (of different pH values) by the five *C. subvermispora* MnPs and the sixteen directed variants, whose *E. coli* expression is described above, were recorded in a UV-160 spectrophotometer (Shimadzu). Oxidation of Mn^{2+} was followed at pH 5 for the formation of Mn^{3+}·tartrate complex (ε_{238} 6.5 mM^{-1}·cm^{-1}). ABTS oxidation was followed (at pH 3.5) from ABTS cation radical (ε_{436} 29.3 mM^{-1}·cm^{-1}) formation. All reactions were carried out at 25 °C (using ~0.01 μM enzyme) and initiated by addition of 0.1 mM H_2O_2.

Means and standard errors for apparent affinity constant (K_m) and enzyme turnover (k_{cat}) were obtained by nonlinear least-squares fitting to the Michaelis-Menten model. Fitting of these constants to the normalized equation $v = (k_{cat}/K_m)[S]/(1+[S]/K_m)$, where v is the reaction rate and S is the substrate concentration, yielded the catalytic efficiency values (k_{cat}/K_m) with their corresponding standard errors.

Kinetic constants of MnP6 short-variant oxidation of Mn^{2+}, at pH 5.0 in the presence of 0-1 mM Cd^{2+}, and ABTS, at pH 4.5 in the presence of 0-30 mM Cd^{2+}, were determined as above, to investigate possible inhibitory effects. Inhibition constants (K_i) were obtained from inverse plots.

pH/temperature stability and optimal pH. To study the effect of pH on the stability of the five *C subvermispora* MnPs and the three short/long variants (after partial removal of the C-tail), the *E. coli*-expressed enzymes were dissolved in Britton-Robinson (B&R) buffer with a pH range from 2 to 9, and kept at 4 ºC. Activity was estimated by oxidation of a saturating concentration of Mn^{2+} (1.5 mM) in 0.1 M tartrate (pH 5) at 25 ºC. The reaction was initiated by addition of 0.1 mM H_2O_2, as described above. Residual activities were measured after 24-h incubation. The highest activity immediately after mixing (at any pH) was taken as 100% activity, and the percentage of residual activity at the different pH conditions was referred to this maximal value.

To study the effect of temperature on enzyme stability, the five *C subvermispora* MnPs and the three short/long variants in 10 mM tartrate, pH 5, were incubated at 5 ºC intervals in the temperature range of 25-70 ºC. Residual activity was estimated as described above. Activity immediately after mixing at 25 ºC was considered as 100%, and the percentage of residual activity was estimated according to this value. Temperature stability was presented as 10-min T_{50}, i.e. that temperature at which 50% of the activity was lost after 10 min incubation.

The same experiments were performed in presence of 1 mM $CaCl_2$, 1 mM $MnSO_4$, 1 mM $CdSO_4$, and 0,5 mM $MnSO_4$ + 0,5 mM $CdSO_4$, using the extralong MnP6 and its short-variant, to evaluate the effect of these cations on the pH and thermal stabilities.

The optimal pH values for substrate oxidation by the five *C subvermispora* MnPs and the different directed variants were determined by measuring the oxidation of saturating concentrations of Mn^{2+} (1.5 mM) and ABTS (5 mM) in 0.1 M B&R buffer of pH 2-6, as described above.

Crystal structure of extralong MnP6 and its Mn^{2+}/Cd^{2+} complexes. Crystallization trials were carried out by the sitting drop vapor diffusion method, using 96-well MRC2 plates with 50 µl reservoir solution and the commercially available screenings from Emerald (Wizard classic crystallization screens I, II and III) and Jena Biosciences (JBScreen Classic Kits 1-10). Drops consisted of 0.2 µl of protein solution (10 mg/ml in 10 mM sodium tartrate buffer at pH 5.0) and 0.2 µl of reservoir solution. Crystallization was carried out at 22°C. Crystals suitable for X-ray data collection were obtained from these initial trials using 0.1 M sodium acetate (pH 4.6) with 18% PEG 4000, and 20% glycerol (as cryoprotectant). Mn^{2+} and Cd^{2+}-containing crystals were obtained by including 5 mM $MnCl_2$ and $CdCl_2$ in the above solution.

For data collection, crystals were mounted in nylon loops and flash-frozen in liquid nitrogen in the mother liquor containing the cryoprotectant indicated above. All diffraction data were obtained at 100 K. X-ray diffraction intensities were collected at the X06DA beam line at the Swiss Light Source (Villigen, Switzerland) using a wavelength of 1.0000 Å and a Pilatus 2M detector. Diffraction data were indexed, integrated, merged and scaled using the programs XDS and XSCALE. Anomalous difference electron density maps for each dataset were calculated using SCALA from the CCP4 suite. Only the higher resolution structure for each crystal form is presented. Data collection statistics are shown in **Table S3**.

The structure of one crystal form from both proteins was solved by molecular replacement using the crystal structure of *P. chrysosporium* MnP (PDB entry 3M5Q) as the search model and the program AUTOMR implemented in the PHENIX package (M2). These first models were used to solve the structure of the other crystal forms. The final models were obtained by consecutive rounds of refinement, performed with the PHENIX package (PHENIX.REFINE); followed by manual model building, performed with Coot (38) using σ_A weighted 2Fo-Fc and Fo-Fc electron density maps. Solvent molecules were introduced in the structure automatically in the refinement as implemented in the PHENIX package and visually inspected. A total of 5 % of reflections was used to calculate the R_{free} value throughout the refinement process. The structures were validated using MolProbity (39). Refinement and final model statistics are summarized in **Table S3**. Figures were produced with PyMOL (Schrödinger, Portland, OR, USA). The coordinates and structure factors have been deposited with the Protein Data Bank with accession codes XXX, XXX and XXX.

Computational simulations. The coordinates for *C. subvermispora* extralong MnP6 were taken from the Protein Data Bank (PDB) entry XXX. A terminal proline residue (not visible in the crystal structure) was added. A truncated MnP6 structure was obtained by removing the last 18 residues. The protonated states were assigned assuming systems at pH 3.0 (which corresponds with the optimum environment to oxidize the ligand) with the protein preparation wizard from Schrödinger. Therefore, the heme propionates and some residues in its access channel (Glh35, Glu39 and Ash179) were protonated. Partial charges for the heme moiety were obtained by QM/MM calculations at the B3LYP(lacvp*)/OPLS2005 level of theory with Qsite. Likewise, the ligand ABTS was optimized at DFT level, B3LYP(6-31g**) with Jaguar.

100 ns MD simulation was carried out with Desmond using the AMBER force field for both extralong MnP6 and its short-variant. Proteins were placed in an orthorhombic box of water with an ionic strength of 0.15M. A time step of 2.0 fs

was used throughout the simulations in combination with the SHAKE algorithm to constrain bond lengths involving hydrogen atoms. Non-bonded interactions were explicitly evaluated for distances below 9 Å. The particle mesh Ewald method was employed to treat long-range electrostatic interactions. Constant pressure and temperature (NPT ensemble) were maintained by weakly coupling the system to an external bath at 1 bar and 300 K, using the Martyna-Tobias Klein barostat and the Nose-Hoover thermostat, respectively.

PELE software was used to study ABTS diffusion. This software uses a Monte Carlo scheme to describe the protein-ligand conformational dynamics. It is capable of reproducing their induced fit, including ligand migration and cavity search in a computational efficient manner (typically requiring no more than 24 hours). At each iteration the algorithm performs: 1) translation and rotation of the ligand, 2) protein perturbation following a combination of normal modes, 3) side chain prediction, and 4) overall minimization. Subsequently, the final structure is accepted or rejected based on a Metropolis criteria (for more details see, for example, https://pele.bsc.es) In this study, the ligand first explored the whole protein surface, and then was forced to explore the area close to the heme's propionates, by using a cutoff distance of a 20 Å between the heme carbon CHA and the ABTS center of mass.

Chemicals. All chemicals were from Sigma-Aldrich, with the exception of H_2O_2 that was from Merck, and ABTS that was from Roche.

ACKNOWLEDGEMENTS. This work was supported by the HIPOP (BIO2011-26694; to F.J.R.-D.) project of the Spanish Ministry of Economy and Competitiveness (MINECO) and by the PEROXICATS (KBBE-2010-4-265397; to A.T.M.) and INDOX (KBBE-2013-3-613549; to A.T.M. and V.G.) European projects. Sequencing of the *Ceriporiopsis subvermispora* genome by the Joint Genome Institute was supported by the Office of Science of the U.S, Department of Energy under Contract No. DE-AC02-05CH11231. E.F.F. acknowledges a JAE Fellowship of the Spanish CSIC, and F.J.R.D. acknowledges a Ramón y Cajal contract of the Spanish MINECO.

1. Kirk, T. K. & Farrell, R. L. (1987) Enzymatic "combustion": The microbial degradation of lignin. *Annu. Rev. Microbiol.* 41: 465-505.
2. Ruiz-Dueñas, F. J. & Martínez, A. T. (2009) Microbial degradation of lignin: How a bulky recalcitrant polymer is efficiently recycled in nature and how we can take advantage of this. *Microbial Biotechnol.* 2: 164-177.
3. Ruiz-Dueñas, F. J., Morales, M., García, E., Miki, Y., Martínez, M. J., & Martínez, A. T. (2009) Substrate oxidation sites in versatile peroxidase and other basidiomycete peroxidases. *J. Exp. Bot.* 60: 441-452.
4. Ruiz-Dueñas, F. J. & Martínez, A. T. (2010) Structural and functional features of peroxidases with a potential as industrial biocatalysts in *Biocatalysts based on heme peroxidases*, eds. Torres, E. & Ayala, M. (Springer-Verlag, Berlin), pp. 37-59.
5. Floudas, D., Binder, M., Riley, R., Barry, K., Blanchette, R. A., Henrissat, B., Martínez, A. T., Otillar, R., Spatafora, J. W., Yadav, J. S. *et al.* (2012) The Paleozoic origin of enzymatic lignin decomposition reconstructed from 31 fungal genomes. *Science* 336: 1715-1719.
6. Peláez, F., Martínez, M. J., & Martínez, A. T. (1995) Screening of 68 species of basidiomycetes for enzymes involved in lignin degradation. *Mycol. Res.* 99: 37-42.
7. Hatakka, A. (1994) Lignin-modifying enzymes from selected white-rot fungi - Production and role in lignin degradation. *FEMS Microbiol. Rev.* 13: 125-135.
8. Martinez, D., Larrondo, L. F., Putnam, N., Gelpke, M. D., Huang, K., Chapman, J., Helfenbein, K. G., Ramaiya, P., Detter, J. C., Larimer, F. *et al.* (2004) Genome sequence of the lignocellulose degrading fungus *Phanerochaete chrysosporium* strain RP78. *Nat. Biotechnol.* 22: 695-700.
9. Ragauskas, A. J., Williams, C. K., Davison, B. H., Britovsek, G., Cairney, J., Eckert, C. A., Frederick, W. J., Hallett, J. P., Leak, D. J., Liotta, C. L. *et al.* (2006) The path forward for biofuels and biomaterials. *Science* 311: 484-489.
10. Martínez, A. T., Ruiz-Dueñas, F. J., Martínez, M. J., del Río, J. C., & Gutiérrez, A. (2009) Enzymatic delignification of plant cell wall: from nature to mill. *Curr. Opin. Biotechnol.* 20: 348-357.
11. Gold, M. H., Youngs, H. L., & Gelpke, M. D. (2000) Manganese peroxidase. *Met. Ions Biol. Syst.* 37: 559-586.
12. Sundaramoorthy, M., Kishi, K., Gold, M. H., & Poulos, T. L. (1994) The crystal structure of manganese peroxidase from *Phanerochaete chrysosporium* at 2.06-Å resolution. *J. Biol. Chem.* 269: 32759-32767.
13. Sundaramoorthy, M., Gold, M. H., & Poulos, T. L. (2010) Ultrahigh (0.93 angstrom) resolution structure of manganese peroxidase from *Phanerochaete chrysosporium*: Implications for the catalytic mechanism. *J. Inorg. Biochem.* 104: 683-690.
14. Sundaramoorthy, M., Youngs, H. L., Gold, M. H., & Poulos, T. L. (2005) High-resolution crystal structure of manganese peroxidase: substrate and inhibitor complexes. *Biochemistry* 44: 6463-6470.
15. Li, D. M., Youngs, H. L., & Gold, M. H. (2001) Heterologous expression of a thermostable manganese peroxidase from *Dichomitus squalens* in *Phanerochaete chrysosporium*. *Arch. Biochem. Biophys.* 385: 348-356.
16. Johansson, T. & Nyman, P. O. (1996) A cluster of genes encoding major isozymes of lignin peroxidase and manganese peroxidase from the white-rot fungus *Trametes versicolor*. *Gene* 170: 31-38.
17. Asada, Y., Watanabe, A., Irie, T., Nakayama, T., & Kuwahara, M. (1995) Structures of genomic and complementary DNAs coding for *Pleurotus ostreatus* manganese (II) peroxidase. *Biochim. Biophys. Acta* 1251: 205-209.
18. Giardina, P., Palmieri, G., Fontanella, B., Rivieccio, V., & Sannia, G. (2000) Manganese peroxidase isoenzymes produced by *Pleurotus ostreatus* grown on wood sawdust. *Arch. Biochem. Biophys.* 376: 171-179.
19. Steffen, K. T., Hofrichter, M., & Hatakka, A. (2002) Purification and characterization of manganese peroxidases from the litter-decomposing basidiomycetes *Agrocybe praecox* and *Stropharia coronilla*. *Enzyme Microb. Technol.* 30: 550-555.
20. Fernández-Fueyo, E., Ruiz-Dueñas, F. J., Martínez, M. J., Romero, A., Hammel, K. E., Medrano, F. J., & Martínez, A. T. (2014) Ligninolytic peroxidase genes in the oyster mushroom genome: Heterologous expression, molecular structure, catalytic and stability properties and lignin-degrading ability. *Biotechnol. Biofuels* 7:2.

21. Scott, G. M., Akhtar, M., Lenz, M. J., & Swaney, R. E. (1998) Engineering, scale-up, and economic aspects of fungal pretreatment of wood chips in *Environmentally friendly technologies for the pulp and paper industry*, eds. Young, R. A. & Akhtar, M. (TAPPI Press, Atlanta), pp. 341-384.
22. Fernández-Fueyo, E., Ruiz-Dueñas, F. J., Miki, Y., Martínez, M. J., Hammel, K. E., & Martínez, A. T. (2012) Lignin-degrading peroxidases from genome of selective ligninolytic fungus *Ceriporiopsis subvermispora*. *J. Biol. Chem.* 287: 16903-16906.
23. Fernández-Fueyo, E., Ruiz-Dueñas, F. J., Ferreira, P., Floudas, D., Hibbett, D. S., Canessa, P., Larrondo, L., James, T. Y., Seelenfreund, D., Lobos, S. *et al.* (2012) Comparative genomics of *Ceriporiopisis subvermispora* and *Phanerochaete chrysosporium* provide insight into selective ligninolysis. *Proc. Natl. Acad. Sci. USA* 109: 5458-5463.
24. Poulos, T. L., Freer, S. T., Alden, R. A., Edwards, S. L., Skogland, U., Takio, K., Eriksson, B., Xuong, N., Yonetani, T., & Kraut, J. (1980) The crystal structure of cytochrome *c* peroxidase. *J. Biol. Chem.* 255: 575-580.
25. Ruiz-Dueñas, F. J., Lundell, T., Floudas, D., Nagy, L. G., Barrasa, J. M., Hibbett, D. S., & Martínez, A. T. (2013) Lignin-degrading peroxidases in Polyporales: An evolutionary survey based on ten sequenced genomes. *Mycologia* 105: 1428-1444.
26. Levasseur, A., Lomascolo, A., Chabrol, O., Ruiz-Dueñas, F. J., Uzan, E., Piumi, F., Kues, U., Ram, A. F. J., Murat, C., Haon, M. *et al.* (2014) The genome of the white-rot fungus *Pycnoporus cinnabarinus*: a new basidiomycete model with a versatile arsenal for lignin deconstruction. *Genome Biol.* (in press).
27. Wariishi, H., Akileswaran, L., & Gold, M. H. (1988) Manganese peroxidase from the basidiomycete *Phanerochaete chrysosporium*: Spectral characterization of the oxidized states and the catalytic cycle. *Biochemistry* 27: 5365-5370.
28. Borrelli, K. W., Vitalis, A., Alcantara, R., & Guallar, V. (2005) PELE: Protein energy landscape exploration. A novel Monte Carlo based technique. *J. Chem. Theory Comput.* 1: 1304-1311.
29. Morales, M., Mate, M. J., Romero, A., Martínez, M. J., Martínez, A. T., & Ruiz-Dueñas, F. J. (2012) Two oxidation sites for low redox-potential substrates: A directed mutagenesis, kinetic and crystallographic study on *Pleurotus eryngii* versatile peroxidase. *J. Biol. Chem.* 287: 41053-41067.
30. Mandelman, D., Jamal, J., & Poulos, T. L. (1998) Identification of two electron-transfer sites in ascorbate peroxidase using chemical modification, enzyme kinetics, and crystallography. *Biochemistry* 37: 17610-17617.
31. Ruiz-Dueñas, F. J., Morales, M., Pérez-Boada, M., Choinowski, T., Martínez, M. J., Piontek, K., & Martínez, A. T. (2007) Manganese oxidation site in *Pleurotus eryngii* versatile peroxidase: A site-directed mutagenesis, kinetic and crystallographic study. *Biochemistry* 46: 66-77.
32. Fernández-Fueyo, E., Ruiz-Dueñas, F. J., & Martínez, A. T. (2014) Engineering a lignin-degrading peroxidase acting at very acidic. *(submitted)*.
33. Youngs, H. L., Sundaramoorthy, M., & Gold, M. H. (2000) Effects of cadmium on manganese peroxidase - Competitive inhibition of Mn-II oxidation and thermal stabilization of the enzyme. *Eur. J. Biochem.* 267: 1761-1769.
34. Mauk, M. R., Kishi, K., Gold, M. H., & Mauk, A. G. (1998) pH-linked binding of Mn(II) to manganese peroxidase. *Biochemistry* 37: 6767-6771.
35. Youngs, H. L., Moënne-Loccoz, P., Loehr, T. M., & Gold, M. H. (2000) Formation of a bis(histidyl) heme iron complex in manganese peroxidase at high pH and restoration of the native enzyme structure by calcium. *Biochemistry* 39: 9994-10000.
36. George, S. J., Kvaratskhelia, M., Dilworth, M. J., & Thorneley, R. N. F. (1999) Reversible alkaline inactivation of lignin peroxidase involves the release of both the distal and proximal site calcium ions and bishistidine co-ordination of the haem. *Biochem. J.* 344: 237-244.
37. Bordoli, L., Kiefer, F., Arnold, K., Benkert, P., Battey, J., & Schwede, T. (2009) Protein structure homology modeling using SWISS-MODEL workspace. *Nat. Protoc.* 4: 1-13.
38. Emsley, P. & Cowtan, K. (2004) Coot: model-building tools for molecular graphics. *Acta Crystallogr. D. Biol. Crystallogr.* 60: 2132.
39. Davis, I. W., Leaver-Fay, A., Chen, V. B., Block, J. N., Kapral, G. J., Wang, X., Murray, L. W., Arendall III, W. B., Snoeyink, J., Richardson, J. S. *et al.* (2007) MolProbity: all-atom contacts and structure validation for proteins and nucleic acids. *Nucleic Acids Res.* 35: W375-W385.

Capítulo 8

Engineering a lignin-degrading peroxidase acting at very acidic pH
Fernández-Fueyo, E., F. J. Ruiz-Dueñas and A. T. Martínez.
(enviado)

Engineering a lignin-degrading peroxidase acting at very acidic pH

Elena FERNÁNDEZ-FUEYO, Francisco J. RUIZ-DUEÑAS and Angel T. MARTÍNEZ[1]

Centro de Investigaciones Biológicas, CSIC, Ramiro de Maeztu 9, E-28040 Madrid, Spain

Short title: Engineering a versatile peroxidase acting at acidic pH

Ligninolytic peroxidases are divided into three families, manganese peroxidases (MnPs), lignin peroxidases (LiPs)and versatile peroxidases (VPs). The two latter are able to degrade nonphenolic lignin model compounds, with VP oxidizing the widest range of aromatic substrates and dyes. One of the limiting issues for the industrial use of these two enzymes is their progressive inactivation under acidic pH conditions, where they exhibit the highest activities. In the screening of peroxidases from basidiomycete genomes, one MnP from *Ceriporiopsis subvermispora* was found to have a remarkable acidic stability. The crystal structure of this enzyme is available and, after comparison with VP and LiP structures, it was used as a robust scaffold to engineer a stable VP by introducing an exposed catalytic tryptophan, with different protein environments. The variants obtained maintained the acidic stability and strong Mn^{2+}-oxidizing activity, and the abilities to oxidize veratryl alcohol and Reactive Black 5 (two simple VP substrates) were introduced. The different peroxidase activities were discussed in the light of the molecular structures available. The engineered peroxidases present more acidic optimal pH than the best VP from *Pleurotus ostreatus* enabling higher catalytic efficiency oxidizing lignin, by lowering the reaction pH, as shown using a nonphenolic model dimer.

Key words: acidic pH stability, catalytic tryptophan, lignin model dimer, manganese peroxidase, versatile peroxidase, white-rot basidiomycete

INTRODUCTION

Lignin removal is a key step for recycling the carbon fixed by land photosynthesis and a limiting issue for the use of lignocellulosic biomass by the pulp and paper industry and in the sustainable production of biofuels and other chemicals. Only a group of basidiomycetes, the so-called white-rot fungi, are efficient lignin degraders in nature [1]. According to genomic data, ligninolytic peroxidases - the so-called lignin peroxidase (LiP, EC1.11.1.14), manganese peroxidase (MnP, EC1.11.1.13) and versatile peroxidase (VP, EC 1.11.1.16) - are exclusive of white-rot basidiomycetes and would play a central role in lignin degradation [2]. Due to their high redox-potential, these peroxidases are enzymes of industrial interest in lignocellulose biorefineries for plant cell-wall delignification and production of cellulose, ethanol and other chemicals, functionalization of fibers, production of lignin adhesives, and modification of aromatic compounds in a variety of green chemistry and bioremediation reactions of industrial interest [3-5].

LiP and MnP were described 30-years ago in the model white-rot basidiomycete *Phanerochaete chrysosporium* [6;7]. VP, the third family of ligninolytic peroxidases, was described later in *Pleurotus eryngii* [8;9] and is also found in *Bjerkandera* sp [10]. LiP possess a tryptophan residue in the surface of the enzyme corresponding to Trp^{171} in *P. chrysosporium* LiP (isoenzyme H8) that enables direct oxidation of lignin via long-range electron transfer to heme [11;12]. MnP possess three residues located in an anionic pocket (Glu^{35}, Glu^{39} and Asp^{179} in *P. chrysosporium* MnP, isoenzyme 1) forming a Mn-binding site [13] in which Mn^{2+} is oxidized to Mn^{3+}. VP possess both the catalytic tryptophan (Trp^{164} in *P. eryngii* VP isoenzyme VPL) and the manganese binding site

Abbreviations used: DHP, dehydrogenation (lignin) polymer; DMP, 2,6-dimethoxyphenol; LiP, lignin peroxidase; MnP, manganese peroxidase; RB5, Reactive Black 5; SDS-PAGE, sodium dodecyl sulfate-polyacrylamide gel electrophoresis; VA, veratryl alcohol; VP, versatile peroxidase.

[1] To whom correspondence should be addressed (email ATMartinez@cib.csic.es)

(VPL Glu^{36}, Glu^{40} and Asp^{175}) [14;15]. Moreover, a low-efficiency site involved in oxidation of phenols is operating at the entrance of the heme distal pocket of VP [16]. On the other hand, the oxidation of phenols and dyes in the absence of manganese has been described in *Pleurotus ostreatus* MnPs [17] and related enzymes belonging to the subfamily of short MnPs, defined in fungal genomic screenings together with the so-called long and extralong MnP subfamilies [2;18]. In addition to its ability to oxidize Mn^{2+} to Mn^{3+}, VP presents wider substrate specificity than LiP oxidizing high redox-potential aromatics and dyes, as Reactive Black 5 (RB5), that LiP oxidizes only in the presence of redox mediators [19;20]. This wider VP activity would be related to differences in the residues surrounding the exposed catalytic tryptophan which are not conserved between LiP and VP.

Wild peroxidases are not well-suited for industrial use that generally requires particular substrate specificities and application conditions (including pH, temperature, and reaction media) in addition to high expression levels. Therefore, protein engineering is often required to obtain highly expressed and efficient biocatalysts [4]. In nature, wood lignin degradation takes place at acidic pH due to secretion of organic acids by white-rot basidiomycetes [21], in agreement with the highest LiP and VP activities on aromatic compounds, which optimally takes place around pH 3 [21]. Although partial stability under acidic conditions is therefore requisite for these enzymes, inactivation inexorably takes place at acidic pH. The lack of stability under acidic pH limits the potential industrial use of these enzymes due to the necessity of carrying out reactions at pH values in which the enzymes are less active, to protect them from inactivation.

In this study, we performed a screening of ligninolytic peroxidases from the genomes of the white-rot fungi *P. ostreatus* and *Ceriporiopsis subvermispora* (up to a total of fourteen genes) for stability at acidic pH. Among them, *C. subvermispora* MnP6 showed a remarkable acidic stability being the most acidic stable ligninolytic peroxidases described to date. Therefore, this peroxidase isoenzyme was used as a robust protein scaffold to obtain a VP-type peroxidase by introducing an exposed catalytic tryptophan, in two different protein environments, using directed mutagenesis. The engineered peroxidase would be of interest as industrial biocatalyst, because of the combination of promiscuity oxidizing different aromatic compounds and dyes and high stability at acidic pH.

MATERIAL AND METHODS

Peroxidase coding sequences

The mature protein-coding sequences of nine peroxidase (VP1 to VP3 and MnP1 to MnP6) genes from the *P. ostreatus* genomes (models 137757 from the homokaryon PC9 genome and 1113241, 156336, 1096331, 199510, 1089546, 1099081, 199511 and 1041740 from the homokaryon PC15 genome, respectively), five MnP (MnP5, MnP6, MnP10, MnP12 and MnP13) genes from the *C. subvermispora* genome (models 49683, 50686, 117436, 157986 and 124076, respectively) and the LiP-H8 coding sequence from the *P. chrysosporium* genome (model 131707), together with the S168W-environment variant from *C. subvermispora* MnP6, which contains the T162S, S168W, F258E, F262M, F268K, Q271N, S272R and S275G mutations, were synthesized by ATG:biosynthetics (Merzhausen, Germany) after verifying that all the codons had previously been used for expressing other genes in the same *E. coli* strains, and substituting them when required (the VP1 model 1089895 from the *P. ostreatus* PC15 monokaryon was discarded because of the presence of a premature termination codon).

Directed mutagenesis

The S168W variant was obtained by site-directed mutagenesis of the *C. subvermispora* MnP6 encoding gene by polymerase chain reaction (PCR) using the expression plasmid pET23a-50686 (see below) as template, and the QuikChange™ kit from Stratagene. The 5'- G CCC CAG GAC AAT GTC ACA TGG ATC CTG GAG CGC- 3' direct primer (mutated codon underlined) and the reverse primer bearing the complementary sequences were synthesized. The PCR reaction (50 µl volume) was carried out in an Mastercycler proS thermal cycler (Eppendorf) using 20 ng of template DNA, 500 µM each dNTP, 125 ng direct and reverse primers, 2.5 units of *Pfu*Turbo

polymerase (Stratagene), and the manufacturer buffer. Reaction conditions included: **i)** a first cycle at 95 ºC (1 min); **ii)** 18 cycles at 95 ºC (50 s), 55 ºC (50 s) and 68 ºC (10 min); and **iii)** a final cycle at 68 ºC (10 min).

Heterologous expression

The nine *P. ostreatus*, the five *C. subvermispora* and the only *P. chrysosporium* peroxidase sequences, together with the two *C. subvermispora* MnP6 mutated sequences (S168W and S168W-environment), were cloned in the expression vectors pFLAG1 (International Biotechnologies Inc.) or pET23a (+) (Novagen) and the resulting plasmids (pET23a-137757, pFLAG1-1113241, pET23a-156336, pFLAG1-1096331, pFLAG1-199510, pFLAG1-1089546, pET23a-1099081, pFLAG1-199511, pET23a-1041740, pET23a-49683, pET23a-50686, pET23a-50686/S168W, pET23a-50686/S168W-environment, pET23a-117436, pET23a-157986, pET23a-124076 and pFLAG1-131707) were used for expression.

The peroxidases were produced in *E. coli* BL21(DE3)pLysS. Cells were grown for 3 h in Terrific Broth, induced with 1 mM isopropyl-β-D-thiogalactopyranoside, and grown further for 4 h. The apoenzymes, which accumulated in inclusion bodies, as shown by sodium dodecyl sulfate-polyacrylamide gel electrophoresis (SDS-PAGE), were solubilized in 8 M urea. Subsequent *in vitro* folding was performed using 0.16 M urea, 5 mM Ca^{2+}, 20 μM hemin, 0.5 mM oxidized glutathione, 0.1 mM dithiothreitol and 0.1 mg/ml protein, at pH 9.5 [17;22]. Refolding of *P. chrysosporium* LiP-H8 was performed as previously described [23]. Active enzymes were purified by Resource-Q chromatography using a 0-300 mM NaCl gradient (2 ml·min^{-1}, 20 min) in 10 mM sodium tartrate, pH 5.5, containing 1 mM $CaCl_2$.

Kinetic constants

Steady-state kinetic constants for oxidation of representative substrates were estimated for purified native (wild-type) MnP6 from *C. subvermispora*, its S168W and S168W-environment variants, *P. chrysosporium* LiP-H8 and *P. ostreatus* VP1. Absorbance changes during substrate oxidation in 0.1 M tartrate (at various pH values) were recorded at 25 ºC in a Biomate5 (Thermo) spectrophotometer (using ~0.01 μM enzyme) being initiated by H_2O_2 (0.1 mM) addition. Oxidation of Mn^{2+} was followed at pH 5 by monitoring Mn^{3+}·tartrate complex (ε_{238} 6.5 mM^{-1}·cm^{-1}) formation. Veratryl alcohol (VA) oxidation and 4-*O*-methylsyringylglycerol-β-guaiacyl ether (nonphenolic lignin model dimer) oxidative cleavage were followed at pH 3 for veratraldehyde (ε_{310} 9.3 mM^{-1}.cm^{-1}) and 3,4,5-trimethoxybenzaldehyde (ε_{310} 6.3 mM^{-1}.cm^{-1}) formation, respectively. RB5, 2,2'-azino-bis(3-ethylbenzothiazoline-6-sulfonate) (ABTS) and 2,6-dimethoxyphenol (DMP) oxidation were assayed at pH 3.5, and monitored for RB5 disappearance (ε_{598} 30 mM^{-1}.cm^{-1}) and formation of ABTS cation radical (ε_{436} 29.3 mM^{-1}.cm^{-1}) and dimeric coerulignone (ε_{469} 55 mM^{-1}. cm^{-1}), respectively. Means and standard errors for apparent affinity constant (K_m) and enzyme turnover (k_{cat}) values were obtained by nonlinear least-squares fitting to the Michaelis-Menten model. Fitting of these constants to the normalized equation $v = (k_{cat}/K_m)[S]/(1+[S]/K_m)$ yielded the catalytic efficiency values (k_{cat}/K_m) with their corresponding standard errors.

pH stability and optimal pH estimation

pH stability was estimated by preincubating the purified native enzymes and variants (~0.05 μM) in Britton-Robinson buffer (B&R) at different pH values (pH 2-8) for 4 or 24 hours (at 4 ºC). Residual activities were estimated by oxidation of saturating concentrations of ABTS (5 mM) or Mn^{2+} (1.5 mM) in 0.1 M tartrate (pH 3.5 or 5, respectively), under the standard conditions described above, immediately after mixing and after 4 h and 24-h incubation at 4ºC. For each enzyme, the highest activity after mixing (at any pH) was taken as 100% activity, and the percentage of residual activity at the different times and pH conditions was calculated according to this maximal value.

The optimal pH values for substrate oxidation by the two *C. subvermispora* MnP6 variants, and the native *P. ostreatus* VP1, were determined by measuring the oxidation of saturating

concentrations of RB5 (15 μM) and VA (6 mM) in 0.1 M B&R buffer of pH 1.6-5, as described above.

RESULTS

Screening for acidic pH stable peroxidases

Fourteen peroxidases from the genomes of *P. ostreatus* (nine VP or MnP encoding genes) and *C. subvermispora* (five MnP encoding genes) were obtained by *E. coli* over-expression of the mature protein codifying sequences, followed by *in vitro* activation (for cofactor and Ca^{2+} incorporation, and disulfide bond formation), and purified to electrophoretic homogeneity in a single chromatographic step. The molecular masses from SDS-PAGE coincided with the values obtained from the predicted protein sequences, and the electronic absorption spectra showed the Soret (406 nm) and other typical bands of the peroxidase resting state, confirming the heme cofactor was correctly incorporated.

The stability of the different enzymes was estimated as the residual activity after 24-h incubation, at 4ºC, and the results obtained in the range of pH 2-5 are shown in **Figure 1**. The fourteen peroxidases are fully stable at pH 5 (80-100% of the maximal residual activity generally obtained at pH 6), however, they present huge differences in their stability towards acidic pH. Several of them started to be inactivated at pH 4, half of the total were near completely inactivated at pH 3, and only four maintained their activity after incubation at pH 2. These results showed the remarkable acidic stability of the long and extralong MnPs from *C. subvermispora* that maintained over 60% and 80% of the initial activity at pH 2, respectively, the extralong MnP6 being the most stable isoenzyme (arrow in **Figure 1**). On the other hand, none of the *P. ostreatus* peroxidases (VPs and short MnPs) were stable at pH 2.

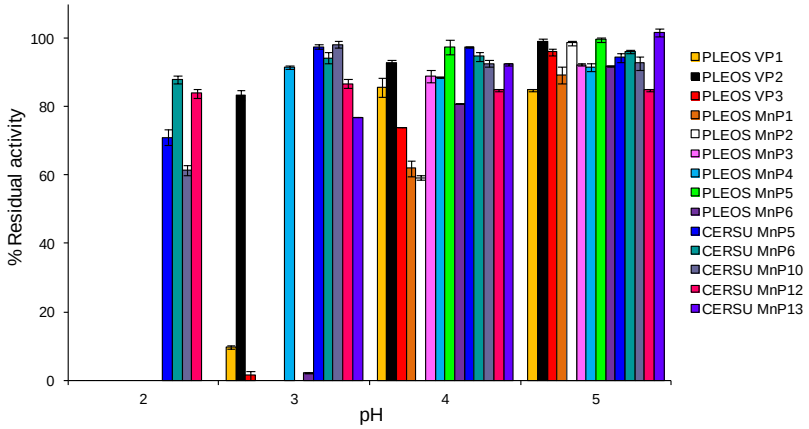

Figure 1 Acidic pH stabilities of fourteen ligninolytic peroxidases from the *P. ostreatus* and *C. subvermispora* genomes. Residual activities of *P. ostreatus* (PLEOS) VP1 (PC9 genome model 137757), VP2 (PC15 genome model 1113241), VP3 (PC15 genome model 156336), MnP1 (PC15 genome model 1096331), MnP2 (PC15 genome model 199510), MnP3 (PC15 genome model 1089546), MnP4 (PC15 genome model 1099081), MnP5 (PC15 genome model 199511) and MnP6 (PC15 genome model 1041740) and *C. subvermispora* (CERSU) MnP5 (genome model 49683), MnP6 (genome model 50686), MnP10 (genome model 117436), MnP12 (genome model 157986) and MnP13 (genome model 124076) peroxidases, after 24-h incubated, at 4 ºC, in 100 mM B&R buffer of pH 2-5. Means and 95% confidence limits.

Engineering a catalytic tryptophan on an acidic pH stable extralong MnP

The crystal structures of the *E. coli*-expressed *P. ostreatus* VP1 and *C. subvermispora* MnP6 were recently solved, the latter being the first extralong MnP whose crystal structure is available. The *C. subvermispora* MnP6 presents a serine (**Figure 2A** Ser^{168}) at the position equivalent to VP1 catalytic tryptophan (**Figure 2B**), and two approaches were followed to confer VP-type activity on aromatic substrates and dyes to this enzyme by directed mutagenesis. The first strategy consisted in

entering only the tryptophan residue (**Figure 2C**) to obtain the S168W variant, while the second approach included modeling a tryptophan environment similar to that of Trp^{164} in *P. ostreatus* VP1 resulting in the S168W-environment variant (**Figure 2D**). For designing the second MnP6 variant, we compared the catalytic tryptophan surface environments in the *P. ostreatus* VP1 and *P. chrysosporium* LiP-H8 crystal structures (**Figure S1A** and **B**), and the corresponding region in the *C. subvermispora* MnP6 structure (**Figure S1D**). In this way, we selected those residues that could contribute to the higher promiscuity of VP oxidizing aromatic substrates and dyes for their introduction in *C. subvermispora* MnP6. The environment of VP1 Trp^{164} is less electronegative including only the acidic Glu^{161} and Glu^{243}, while the LiP-H8 Trp^{171} is surrounded by Asp^{165}, Glu^{166}, Glu^{168}, Glu^{250} and Asp^{264}. Moreover, there are the basic Lys^{253} and Arg^{257} in the VP tryptophan environment, while only Lys^{260} is present in the LiP tryptophan environment. On the other hand, the VP tryptophan is surrounded by small residues, such as Gly^{260} and Val^{160}, instead of the bulky Leu^{167} and Phe^{267} in LiP. Finally, Asn^{257} and Met^{247} are conserved among VPs, forming hydrogen bonds with Arg^{247} and Glu^{243}, respectively, but they are absent from LiP. According with the above analysis, the following mutations were performed in MnP6 to introduce the exposed catalytic tryptophan and provide it with a VP-type environment (S168W-environment variant): T162S, S168W, F258E, F262M, F268K, Q271N, S272R and S275G (**Figure 2C**). The two variants were successfully over-expressed in *E. coli*, *in vitro* activated, and purified.

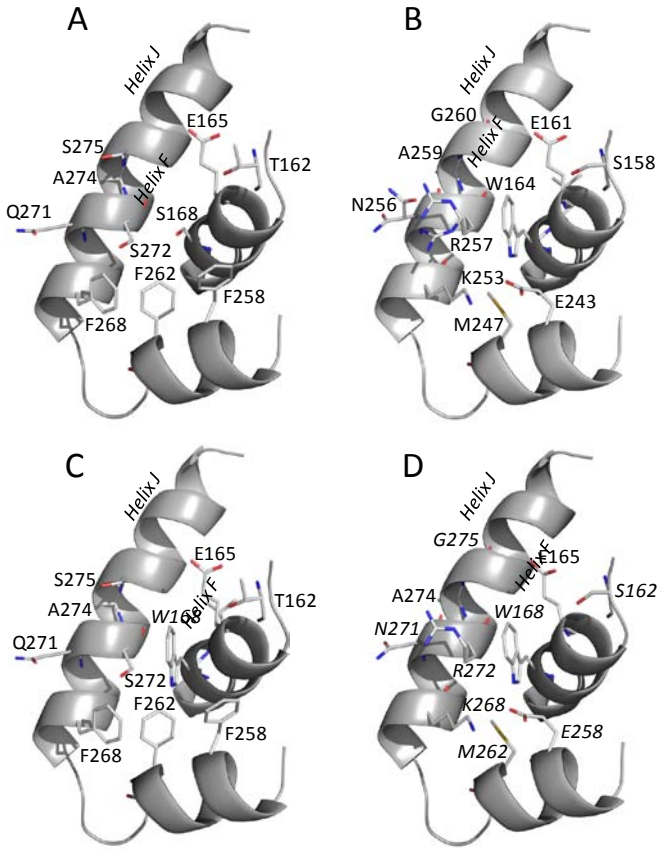

Figure 2 Engineering the acidic-pH stable MnP6 from *C. subvermispora* by introducing a catalytic tryptophan (S168W variant) and changing the tryptophan environment (S168W-environment variant). The two variants were built by substituting Ser^{168} of *C. subvermispora* MnP6 (A) by a catalytic tryptophan to obtain the S168W variant (C) and engineering its environment as found in *P. ostreatus* VP1 (B) to obtain the S168W-environment variant (D). The mutated residues in C (Trp^{168}) and D (Ser^{162}, Trp^{168}, Glu^{258}, Met^{262}, Lys^{268}, Asn^{271}, Arg^{272} and Gly^{275}) are in italics. Based on MnP6 crystal structure (PDB xxx) and homology models of the S168W and S168W-environment variants.

Catalytic properties of the *C. subvermispora* MnP variants with a putative catalytic tryptophan

After obtaining the S168W and S168W-environment variants of the acidic-pH stable *C. subvermispora* MnP6, we investigated their catalytic properties to know the effect of the mutations included. **Table 1** shows their kinetic constants, compared with those of the native *C. subvermispora* MnP6, the *P. ostreatus* VP1 and the *P. chrysosporium* LiP-H8, which had also been expressed in *E. coli*. For this comparison we used **(i)** Mn^{2+}, which is oxidized at the MnP and VP Mn-oxidation site, **(ii)** high redox-potential VA and RB5, which are oxidized at the LiP and VP catalytic tryptophan, and **(iii)** low redox-potential ABTS and DMP, which are oxidized by VPs at the catalytic tryptophan (with high efficiency) but also at a second (low-efficiency) site. The two variants conserve the high affinity for Mn^{2+} of extralong MnP6, with a K_m value approximately ten folds lower than VP1, demonstrating that the mutations introduced did not affect the Mn^{2+} oxidation ability. More importantly, the kinetic constants showed that the two strategies for introducing a functional catalytic tryptophan were successful, since both variants incorporated the ability to oxidize VA, as well as RB5.

Table 1

Kinetic constants for oxidation of five substrates (at fixed pH for each substrate) by the *C. subvermispora* MnP6 and its S168W and S168W-environment variants compared with *P. ostreatus* VP1 and *P. chrysosporium* LiP-H8

Means and 95% confidence limits from reactions of the *C. subvermispora* MnP6, its S168W and S168W-environment variants (the latter combining T162S, S168W, F258E, F262M, F268K, Q271N, S272R and S275G mutations), *P. ostreatus* VP1 (JGI genome model 137757) and *P. chrysosporium* LiP-H8 (JGI genome model 131707) at 25 °C in 0.1 M tartrate, pH 5 for Mn^{2+}, pH 3 for VA, and pH 3.5 for RB5, DMP and ABTS oxidation. ABTS and DMP oxidation by VP1 shows biphasic kinetics enabling calculation of a second low-efficiency set of constants (not shown).

		MnP6	S168W	S168W-environment	LiP-H8	VP1
Mn^{2+}	K_m (μM)	8.7 ± 1.6	8.5 ± 1.2	11.0 ± 1.8	-	98.0 ± 5.6
	k_{cat} (s^{-1})	83.0 ± 5.0	60.5 ± 5.0	66.9 ± 6.0	0	185.0 ± 2.6
	k_{cat}/K_m ($s^{-1}.mM^{-1}$)	9540 ± 650	7110 ± 650	6060 ± 650	0	1900 ± 90
VA	K_m (μM)	0	2740 ± 560	21600 ± 200	190 ± 17	5500 ± 46
	k_{cat} (s^{-1})	0	0.54 ± 0.04	1.69 ± 0.04	17.5 ± 0.5	12.7 ± 0.5
	k_{cat}/K_m ($s^{-1}.mM^{-1}$)	-	0.197 ± 0	0.078 ± 0	92.0 ± 6.0	2.3 ± 0.2
RB5	K_m (μM)	0	12.6 ± 3	5.4 ± 3	0	5.4 ± 0.2
	k_{cat} (s^{-1})	0	7.8 ± 1.1	7.0 ± 1.1	0	12.9 ± 0.3
	k_{cat}/K_m ($s^{-1}.mM^{-1}$)	-	619 ± 27	1310 ± 100	-	2380 ± 50
ABTS	K_m (μM)	0	60.2 ± 13.4	0	23.0 ± 1.6	4.0 ± 0.4
	k_{cat} (s^{-1})	0	1.4 ± 0.1	0	13.0 ± 0.2	14.4 ± 0.4
	k_{cat}/K_m ($s^{-1}.mM^{-1}$)	-	23 ± 3	-	563 ± 36	3600 ± 20
DMP	K_m (μM)	0	0	0	5.8 ± 0.5	54 ± 4
	k_{cat} (s^{-1})	0	0	0	10.0 ± 0.1	6.6 ± 0.1
	k_{cat}/K_m ($s^{-1}.mM^{-1}$)	-	-	-	1720 ± 153	122 ± 7

Although the catalytic efficiency of the variants oxidizing VA was very low compared with *P. chrysosporium* LiP-H8, they were more similar to those of *P. ostreatus* VP1. The above differences are mainly due to the very different K_m values, which for LiP-H8 were in the micromolar range (K_m 190 ± 17 μM) while they were in the millimolar range for the other peroxidases attaining the highest value for the S168W-environment variant (K_m 21.6 ± 0.2 mM). Interestingly, the S168W variant

had higher affinity for VA (K_m 2.74 ± 0.56 mM) than VP1 (K_m 5.50 ± 0.05 mM) and this resulted in a higher catalytic efficiency on this substrate than the S168W-environment variant.

Concerning RB5 oxidation, the two variants behave as VPs being able to oxidize this recalcitrant dye, which was not oxidized by LiP-H8. When compared with *P. ostreatus* VP1, they present much lower differences in the catalytic efficiency than found for VA oxidation, and the highest RB5 catalytic efficiency corresponded to the S168W-environment variant. Since both variants showed similar activities on RB5 (k_{cat} 7-8 ± 1 s^{-1}), the latter difference was due to the higher affinity of the S168W-environment variant on the dye, which was similar to that found for VP1 (K_m 5.4 μM).

Neither the extralong MnP6 nor the two mutated variants were able to oxidize DMP, as both VP1 and LiP-H8 did, suggesting that the engineered sites were unable to properly bind this phenolic substrate. In a similar way, only the S168W variant (not the S168-environment variant) oxidized ABTS, although with lower efficiency than VP1 and LiP-H8. While a second set of kinetic constants could be determined for ABTS oxidation by VP1 (corresponding to a second low-efficiency oxidation site), this was not the case for the S168W variant revealing that ABTS oxidation by this variant is being produced at the catalytic tryptophan.

Acidic stability of the VP-type variants of the *C. subvermispora* extralong MnP

After confirming that the two MnP6 variants (S168W and S168-environment) presented VP-type catalytic properties, their pH stabilities were investigated to know if they retain the acidic-pH stability of the parent enzyme. With this purpose residual activities were estimated after incubating them, together with *C. subvermispora* MnP6 and *P. ostreatus* VP1, in the range of pH 2-8, at 4 ºC, and normalized as described above. The residual activities in the acidic-pH range of interest, after 4-h and 24-h incubation, are shown in **Figure 3A** and **3B**, respectively.

At pH 4 and 5, the S168W and S168W-environment variants and native *C. subvermispora* MnP6 showed 90-100% residual activities after both 4 and 24 h of incubation, while VP1 showed ~80% activity. However, at pH 3 a strong difference between *C. subvermispora* MnP6, its directed variants and the *P. ostreatus* VP1 was observed. This was especially noticeable after 24-h incubation, where VP1 lost over 90% activity, while the three other peroxidases retained ~90% residual activity. Finally, at pH 2 VP1 was fully inactivated after only 4 h, while a significant inactivation of the MnP enzymes was only produced after 24-h incubation (always with residual activities >50%). Although under the latter conditions the native *C. subvermispora* MnP6 was more stable (~70% residual activity) than its S168W and S168W-environment variants (50-55% residual activity), the results obtained demonstrated that these variants successfully retained most of the acidic-pH stability of the parent enzyme, resulting in VP-type enzymes with much higher pH stability than natural VPs (such as *P. ostreatus* VP1).

Effect of pH on activity and kinetic constants of a VP-type variant of *C. subvermispora* MnP

Due to the high stability of the *C. subvermispora* MnP6 variants at acidic pH, compared to VP, we investigated if the optimal pH for the oxidation of VA and RB5 by these variants would be lower than normally used for VA and RB5 (pH 3-3.5) oxidation by VP and LiP (e.g. in **Table 1**). To estimate the optimal pH for oxidation of these two substrates by the S168W variant (the S168W-environment variant was produced in too low yield to be used in these assays) we used saturating concentrations of VA and RB5 in B&R buffer of pH 1.6-5.

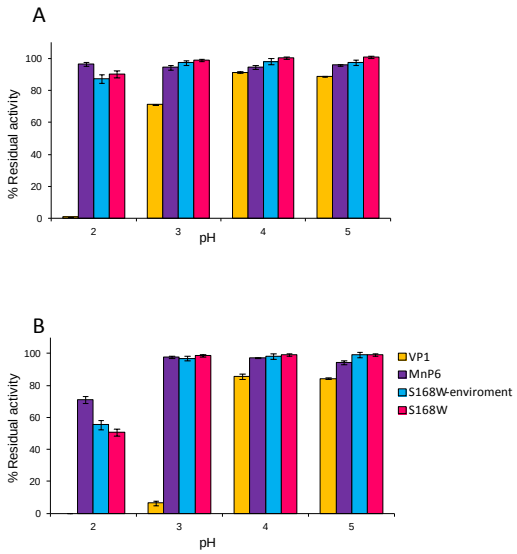

Figure 3 pH stabilities of the S168W and S168W-environment variants of *C. subvermispora* MnP6 compared to the native MnP6 and the *P. ostreatus* VP1. Residual activities after 4-h (A) and 24-h incubation (B) at pH 2-5 of VP1 from *P. ostreatus*, MnP6 from *C. subvermispora*, and its S168W and S168W-environment variants were determined (by 1.5 mM Mn^{2+} oxidation in 0.1 M tartrate, pH 5) after incubation (at 4 ºC) in 100 mM B&R buffer. Means and 95% confidence limits.

The optimal VA oxidation by the variant took place at the most acidic conditions assayed, that is at pH 1.6 (**Figure 4A**) (where the variants still maintained 50% residual activity after 24-h incubation at 4ºC). With respect to pH 3 we found activity increases over 4 fold, 6 fold and 8 fold when the reaction was measured at pH 2.5, 2 and 1.6 respectively. On the other hand, the optimal RB5 oxidation was at pH 2.5 (**Figure 4B**), the activity being 1.7 fold higher than at pH 3.5 (used in the standard assay) and over 28 fold higher than at the optimal pH for VA oxidation (pH 1.6). When the optimal pH values were compared with those of *P. ostreatus* VP1, a clear displacement to more acidic pH optima was observed for both VA and RB5 oxidation by the MnP6 variant (**Figure 4C** and **D**, respectively).

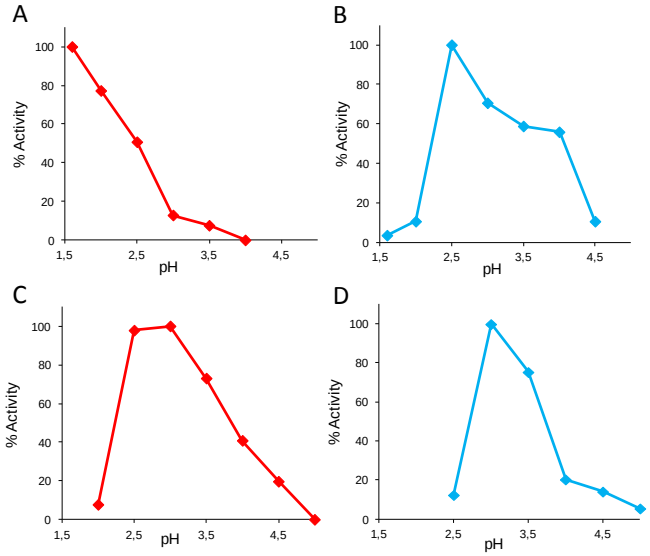

Figure 4 Optimal pH for VA (left) and RB5 (right) oxidation by S168W variant of *C. subvermispora* MnP6 (A and B) and native *P. ostreatus* VP1 (C and D). Activities for 6 mM VA (A and C) and 15 µM RB5 (B and D) oxidation by the S168W variant of *C. subvermispora* MnP6 (A and B) and the native *P. ostreatus* VP1 (C and D) were estimated in 100 mM B&R buffer of pH 1.6 -5.0.

To obtain more information about the effect of pH on the oxidation of VA and RB5 by the MnP6 variant, its kinetic constants were estimated at different pH values. Over 10-fold increase of the catalytic efficiency for VA oxidation was found when the reaction was performed at pH 1.6, instead of pH 3.0 (**Table 2**, top). Interestingly, this increase was due to improvements in both the enzyme affinity (K_m passing from 2.7 ± 0.6 mM to 0.7 ± 0.1 mM) and turnover (k_{cat} passing from 0.5 ± 0.0 s^{-1} to 1.4 ± 0.1 s^{-1}) at the most acidic pH. Under these conditions, the catalytic efficiency of the variant (2.1 ± 0.2 $s^{-1}.mM^{-1}$) was similar to that of *P. ostreatus* VP1 (2.3 ± 0.2 $s^{-1}.mM^{-1}$) (see **Table 1**) although kinetic differences exist between the two enzymes. Likewise, when RB5 oxidation by the MnP6 variant was analyzed at lower pH, there was an increase of the catalytic efficiency being 14-fold higher at pH 2.5 than at the usual pH 3.5 (**Table 2**, bottom). In this case, the main improvement was related to the increased enzyme affinity, as shown by the 9-fold decrease of K_m. More interestingly, when kinetics at optimal pH were compared, the S168W variant of *C. subvermispora* MnP6 is over 3-fold more efficient that the *P. ostreatus* VP1 oxidizing RB5 (see **Table 1**) due to its apparent higher affinity (the two k_{cat} values being identical).

Table 2

Kinetic constants for VA and RB5 oxidation by the S164W variant of *C. subvermispora* MnP6 at acidic pH values

Means and 95% confidence limits from VA and RB5 oxidation by the S168W variant of *C. subvermispora* MnP6 at 25 °C in 100 mM B&R buffer of different pH values.

		pH 1.6	pH 2.0	pH 3.0
VA	K_m (μM)	650 ± 97	913 ± 52	2740 ± 560
	k_{cat} (s^{-1})	1.35 ± 0.06	1.08 ± 0.01	0.54 ± 0.04
	k_{cat}/K_m ($s^{-1}.mM^{-1}$)	2.08 ± 0.24	1.08 ± 0.06	0.197 ± 0
		pH 2.5		pH 3.5
RB5	K_m (μM)	1.4 ± 0.2		12.6 ± 3
	k_{cat} (s^{-1})	12.9 ± 0.7		7.8 ± 1.1
	k_{cat}/K_m ($s^{-1}.mM^{-1}$)	9050 ± 930		619 ± 27

Lignin model dimer degradation (by the S168W variant) and effect of pH

VA is the simple nonphenolic substrate used to estimate both LiP and VP activities in white-rot fungi. Therefore, the VA oxidation by the S168W and S168W-environment variants already suggested the lignin-degrading ability of these enzymes. To confirm this ability a nonphenolic β-*O*-4' lignin model dimer (4-*O*-methylsyringilglycerol-β-guaiacyl ether) was treated (at pH 3) with the S168W variant, which showed the highest efficiency oxidizing VA. Oxidative degradation of the model compound occurred being the variant able to cleave the C_α-C_β bond releasing 3,4,5-trimethoxybenzaldehyde.

The kinetic constants for the oxidative degradation of the dimer were estimated at pH 3.0 and pH 1.6 (**Table 3**), and compared with those obtained for *P. ostreatus* VP1 at pH 3 (this enzyme is quickly inactivated at more acidic pH values, as shown in **Figure 1**). As in the case of VA oxidation, the oxidation significantly increased at the more acidic pH value. In this way, the catalytic efficiency of the S168W variant oxidizing the dimer was 7-fold higher at pH 1.6 than at pH 3.0. Although a small increase in turnover was observed when the reaction pH was lowered, the increased efficiency was mainly related to a lower K_m value (passing from 4.9 ± 1.3 μM to only 1.1 ± 0.2 μM). The latter K_m value was 1.5-fold lower than found for dimer oxidation by the *P. ostreatus* VP1 (**Table 3**) and, due to this difference, the VP-type engineered variant was expected to

be 1.5 fold more efficient degrading lignin than natural VP, if the reaction is performed at the optimal pH for each enzyme.

DISCUSSION

Catalytic promiscuity and acidic stability of lignin-degrading peroxidases

Among ligninolytic peroxidases produced by white-rot fungi, VP is arousing great interest because of its reaction promiscuity as a result of combination of the catalytic properties of well-known LiP and MnP [24], together with the presence of a low-efficiency site involved in oxidation of phenols and dyes similar to that found in plant and fungal generic peroxidases [16]. Recently, Fernández-Fueyo et al. [17] demonstrated that *P. ostreatus* VP degrades a nonphenolic lignin model dimer and depolymerizes synthetic lignin as previously reported for *P. chrysosporium* LiP [6;25], and suggested that VP in some Agaricales would play the same role played by LiP in many Polyporales. Indeed, VPs can directly oxidize high redox-potential compounds, such as polycyclic aromatic hydrocarbons, different types of dyes (RB5 included) and many other recalcitrant molecules, that LiP only oxidizes in the presence of VA [19;20].

Table 3

Kinetic constants for degradation of a lignin model dimer by the S168W variant of *C. subvermispora* MnP6 and VP1, at their optimal pH 1.6 and pH 3.0 (S168W oxidation at pH 3.0 also shown)

Means and 95% confidence limits from nonphenolic lignin model dimer (4-*O*-methyl-syringylglycerol-β-guaiacyl ether) degradation by the S168W variant of *C. subvermispora* MnP6 and the *P. ostreatus* VP1 (JGI genome model 137757) at 25 °C in 100 mM B&R buffer of pH 1.6 (only S168W) and 3.0.

		S168W pH 1.6	S168W pH 3.0	VP1 pH 3.0
Model dimer	K_m (μM)	1.1 ± 0.2	4.9 ± 1.3	1.7 ± 0.1
	k_{cat} (s^{-1})	0.47 ± 0.0	0.36 ± 0.1	0.49 ± 0.0
	k_{cat}/K_m ($s^{-1}.mM^{-1}$)	0.42 ± 0.0	0.07 ± 0.0	0.28 ± 0.0

Due to the relatively low acidic stability of the above peroxidases, lignin depolymerization and other reactions are often carried out at less acidic pH conditions in which the enzymes do not present the maximal activity but are fully active in time [17]. With the aim of avoiding such reduction in enzyme activity, in favor of maintaining the enzyme stability, we evaluated fourteen white-rot fungal peroxidases towards acidic pH stability, and the so-called extralong and long MnPs [2;18] were found to be significantly more stable than the short MnPs and VPs. Among them, one extralong MnP from the *C. subvermispora* genome (isoenzyme MnP6) maintained over 80% of the initial activity after 24-h incubation at pH 2, representing the highest acidic stability reported to date for a fungal member of the classical superfamily of non-animal peroxidases [17]. The presence of an extra disulfide bond in long and extralong peroxidases could contribute to this enhanced pH stability, since the acidic pH stability of *C. subvermispora* MnP6 was lost when the extra C-terminal tail was removed, including the fifth disulfide bond [26].

Engineering a VP-type peroxidase stable at highly acidic pH

Due to the above stability characteristics, the *C. subvermispora* extralong MnP6 was taken as protein scaffold to engineer an acidic-pH stable VP-type peroxidase. Two previous studies described the introduction of the ability to oxidize VA in a MnP from *P. chrysosporium* [27] and in a generic peroxidase from *Coprinopsis cinerea* (synonym: *Coprinus cinereus*) [28]. Going further

in this direction, we aimed to engineer a peroxidase with wide (VP-type) substrate specificity on aromatic and dyes, and high acidic stability, two properties of interest for its use in enzymatic biocatalysis.

To expand the substrate specificity of the extralong MnP6 maintaining its stability, two variants were prepared after comparing its recently reported crystal structure [29] with those of *P. ostreatus* VP1 [17] and *P. chrysosporium* LiP-H8 [30]. The S168W variant incorporated a putative catalytic tryptophan substituting the homologous Ser^{168}, and maintained the original environment of this residue. In the S168W-environment variant, the environment of the new tryptophan was engineered to mimic the environment of the catalytic tryptophan in VPs, by introducing seven additional mutations resulting, among other changes, in the substitution of three bulky phenylalanine residues located at the protein surface near the engineered Trp^{168}.

The two variants incorporated to different extents the capabilities to oxidize both VA and RB5 characteristic of VPs [24]. In the best case, the efficiency oxidizing VA was 10% of that found for *P. ostreatus* VP1, while the RB5 oxidation efficiency attained 55% of that estimated for VP1 (when activities were estimated at the standard pH 3.0-3.5). The comparison confirmed that LiP is more efficient oxidizing VA, but has no activity on RB5. Interestingly, a comparison of the two variants revealed that the peroxidase with the VP-type environment of Trp^{168} has the highest efficiency oxidizing RB5, while the opposite happens for VA oxidation. On the other hand, the introduction of Trp^{168} did not significantly affect the kinetics for Mn^{2+} oxidation, and the good affinity and extremely high efficiency of extralong MnPs oxidizing the cation [29] was largely maintained in the two VP-type variants (over 6000 $s^{-1} \cdot mM^{-1}$).

Influence of the catalytic tryptophan environment

Residues surrounding the catalytic tryptophan would play a role modulating the substrate specificity and the efficiency of the reactions catalyzed, and could explain differences between LiP and VP reactions. LiP presents a more acidic tryptophan environment that would stabilize the VA cation radical [31], but could interfere oxidation of the anionic substrate RB5. Ruiz-Dueñas et al. [32] demonstrate that the introduction of extra acidic residues in the tryptophan environment of VP from *P. eryngii*, emulating the LiP environment, results in the lack of direct RB5 oxidation, although a VA-mediated oxidation was possible, as found for LiP-H8.

The S168W variant would present a tryptophan environment inherited from the parent *C. subvermispora* MnP6 (**Figure S1C**) with only one exposed acidic residue (Glu^{165} equivalent to Glu^{161} and Glu^{168} in VP and LiP, respectively) and none of the basic residues present in the VP. The lack of additional acidic residues in the Trp^{168} surface environment could explain its low efficiency oxidizing VA, and favor oxidation of RB5. The R257D mutation in VP from *P. eryngii*, removes RB5 oxidation, whereas the R257A mutation does not affect this ability [32]. In agreement with this finding, the ability of the S168W variant to oxidize RB5 could be related to the absence of an acidic residue at this position, which in *C. subvermispora* MnP6 is occupied by Ser^{272}. In the case of the S168W-environment variant, the RB5 catalytic constants were even closer to those of VP (with an identical K_m of 5.4 μM). This could be due to the introduction of two basic residues at the Trp^{168} environment (Lys^{268} and Arg^{272}) similar to those found in VP1 (Lys^{253} and Arg^{257}) (**Figure S1A** and **C**). Conversely, the presence of a more basic tryptophan environment in this variant would decrease the VA oxidation activity that, as reported for LiP [31], is improved by the presence of neighbor acidic residues stabilizing the aromatic cation radical.

Improved activity and enzymatic ligninolysis at acidic pH

It is known that the oxidative activity of heme peroxidases increases at acidic pH. Gazarian et al. [33] described a tobacco peroxidase that oxidizes VA at pH 1.8, although it maintained the activity only for 15 minutes, and similar activities for shorter time periods have been reported for other plant peroxidases [34]. Some of these enzymes present a conserved tryptophan but its eventual involvement in catalysis is to be demonstrated [35]. On the other hand, some palm peroxidases are extremely resistant enzymes [36] with acidic-pH stabilities comparable to those of the *C.*

subvermispora extralong MnPs, but oxidation of high redox-potential substrates (such as VA) has not been reported.

The S168W variant of *C. subvermispora* MnP6 was highly stable at pH 2 (and maintained 50% activity after 24-h at pH 1.6) and the same is expected for the S168W-environment variant. Moreover, the optimal pH values for oxidation of VA (pH 1.6) and RB5 (pH 2.5) are lower than found for *P. ostreatus* VP1 (pH 3). Whereas the VA activity progressively increases as the pH decreases, the RB5 maximal activity is at pH 2.5, suggesting that RB5 must be deprotonated for optimal binding. In this way, the catalytic efficiency oxidizing VA and RB5 strongly increased (10-15 fold) when the kinetic constants were estimated at the optimal pH values. Under these conditions, the S168W variant is as efficient as the *P. ostreatus* VP1 oxidizing VA and, surprisingly, 4-fold more efficient oxidizing RB5.

The ability of LiP and VP to degrade lignin has been shown using nonphenolic lignin model dimers, in the absence of mediators [17;25]. On the other hand, MnP can oxidize nonphenolic dimers only in the presence of mediating compounds [37]. The introduction of the catalytic tryptophan in the extralong MnP from *C. subvermispora* confers the enzyme ability to oxidize a nonphenolic dimer by itself, i.e. in the absence of mediators, confirming the tryptophan functionality in enzymatic ligninolysis. Moreover, the potential of the variant for lignin degradation is significantly enhanced by its acidic pH stability enabling to perform the reaction under more acidic conditions. In this way, a 7-fold improvement in catalytic efficiency oxidizing the nonphenolic dimer was obtained when the reaction pH was lowered from pH 3 to pH 1.6, attaining efficiency values that were higher than found for *P. ostreatus* VP1.

Conclusion

A single mutation (S168W) added the ability to oxidize VA to an acidic-pH stable extralong MnP without significantly affecting its high Mn^{2+} peroxidase activity and acidic-pH stability. Due to the high intrinsic stability and the shift of the optimal pH, the new variant behaves as a remarkably acidic-pH stable VP showing higher catalytic efficiency oxidizing a non phenolic lignin model dimer (VA and Mn^{2+}) than the best native VP from the *P. ostreatus* genome. Moreover, the aromatic substrate promiscuity of this variant could be improved when the environment of the catalytic tryptophan was engineered by seven additional mutations resulting in a second variant, whose activity on RB5 (a recalcitrant dye that cannot be oxidized by LiP) was several fold higher than found for the best VP, when the reactions were performed at the optimal pH values.

Author contributions

E. Fernández-Fueyo performed most of the experimental work. F. J. Ruiz-Dueñas contributed to the genomic screening and biochemical characterization. All authors participated in the interpretation and discussion of results. E. Fernández-Fueyo and A. T. Martínez wrote the paper.

Acknowledgments

Authors thank Paula Nousiainen and Jussi Sipilä (University of Helsinki) for synthesizing the 4-*O*-methylsyringylglycerol-β-guaiacyl ether model dimer, in the frame of the BIORENEW EU-project. E.F.-F. acknowledges a Junta de Ampliación de Estudios fellowship of CSIC, co-funded by the European Social Fund, and F.J.R.-D. acknowledges a Ramón y Cajal contract of the Spanish Ministry of Economy and Competitiveness.

Funding

This work was supported by the Spanish project BIO2011-26694 and the European projects PEROXICATS (KBBE-2010-4-265397) and INDOX (KBBE-2013-7-613549).

REFERENCES

1 Martínez, A. T., Speranza, M., Ruiz-Dueñas, F. J., Ferreira, P., Camarero, S., Guillén, F., Martínez, M. J., Gutiérrez, A. and del Río, J. C. (2005) Biodegradation of lignocellulosics: Microbiological, chemical and enzymatic aspects of fungal attack to lignin. Int.Microbiol., 8, 195-204

2 Floudas, D., Binder, M., Riley, R., Barry, K., Blanchette, R. A., Henrissat, B., Martínez, A. T., Otillar, R., Spatafora, J. W., Yadav, J. S., Aerts, A., Benoit, I., Boyd, A., Carlson, A., Copeland, A., Coutinho, P. M., de Vries, R. P., Ferreira, P., Findley, K., Foster, B., Gaskell, J., Glotzer, D., Górecki, P., Heitman, J., Hesse, C., Hori, C., Igarashi, K., Jurgens, J. A., Kallen, N., Kersten, P., Kohler, A., Kües, U., Kumar, T. K. A., Kuo, A., LaButti, K., Larrondo, L. F., Lindquist, E., Ling, A., Lombard, V., Lucas, S., Lundell, T., Martin, R., McLaughlin, D. J., Morgenstern, I., Morin, E., Murat, C., Nolan, M., Ohm, R. A., Patyshakuliyeva, A., Rokas, A., Ruiz-Dueñas, F. J., Sabat, G., Salamov, A., Samejima, M., Schmutz, J., Slot, J. C., St.John, F., Stenlid, J., Sun, H., Sun, S., Syed, K., Tsang, A., Wiebenga, A., Young, D., Pisabarro, A., Eastwood, D. C., Martin, F., Cullen, D., Grigoriev, I. V. and Hibbett, D. S. (2012) The Paleozoic origin of enzymatic lignin decomposition reconstructed from 31 fungal genomes. Science, **336**, 1715-1719

3 Martínez, A. T., Ruiz-Dueñas, F. J., Martínez, M. J., del Río, J. C. and Gutiérrez, A. (2009) Enzymatic delignification of plant cell wall: from nature to mill. Curr.Opin.Biotechnol., **20**, 348-357

4 Ayala, M., Pickard, M. A. and Vázquez-Duhalt, R. (2008) Fungal enzymes for environmental purposes, a molecular biology challenge. J.Mol.Microbiol.Biotechnol., **15**, 172-180

5 Martínez, A. T. (2007) High redox potential peroxidases. In Industrial Enzymes: Structure, Function and Applications (Polaina,J. and MacCabe,A.P. Eds.), pp. 475-486. Springer, Berlin

6 Tien, M. and Kirk, T. K. (1983) Lignin-degrading enzyme from the hymenomycete *Phanerochaete chrysosporium* Burds. Science, **221**, 661-663

7 Kuwahara, M., Glenn, J. K., Morgan, M. A. and Gold, M. H. (1984) Separation and characterization of two extracellular H_2O_2-dependent oxidases from ligninolytic cultures of *Phanerochaete chrysosporium*. FEBS Lett., **169**, 247-250

8 Martínez, M. J., Ruiz-Dueñas, F. J., Guillén, F. and Martínez, A. T. (1996) Purification and catalytic properties of two manganese-peroxidase isoenzymes from *Pleurotus eryngii*. Eur.J.Biochem., **237**, 424-432

9 Ruiz-Dueñas, F. J., Martínez, M. J. and Martínez, A. T. (1999) Molecular characterization of a novel peroxidase isolated from the ligninolytic fungus *Pleurotus eryngii*. Mol.Microbiol., **31**, 223-236

10 Mester, T. and Field, J. A. (1998) Characterization of a novel manganese peroxidase-lignin peroxidase hybrid isozyme produced by *Bjerkandera* species strain BOS55 in the absence of manganese. J.Biol.Chem., **273**, 15412-15417

11 Doyle, W. A., Blodig, W., Veitch, N. C., Piontek, K. and Smith, A. T. (1998) Two substrate interaction sites in lignin peroxidase revealed by site-directed mutagenesis. Biochemistry, **37**, 15097-15105

12 Mester, T., Ambert-Balay, K., Ciofi-Baffoni, S., Banci, L., Jones, A. D. and Tien, M. (2001) Oxidation of a tetrameric nonphenolic lignin model compound by lignin peroxidase. J.Biol.Chem., **276**, 22985-22990

13 Kishi, K., Kusters-van Someren, M., Mayfield, M. B., Sun, J., Loehr, T. M. and Gold, M. H. (1996) Characterization of manganese(II) binding site mutants of manganese peroxidase. Biochemistry, **35**, 8986-8994

14 Pérez-Boada, M., Ruiz-Dueñas, F. J., Pogni, R., Basosi, R., Choinowski, T., Martínez, M. J., Piontek, K. and Martínez, A. T. (2005) Versatile peroxidase oxidation of high redox potential aromatic compounds: Site-directed mutagenesis, spectroscopic and crystallographic investigations of three long-range electron transfer pathways. J.Mol.Biol., **354**, 385-402

15 Ruiz-Dueñas, F. J., Morales, M., Pérez-Boada, M., Choinowski, T., Martínez, M. J., Piontek, K. and Martínez, A. T. (2007) Manganese oxidation site in *Pleurotus eryngii* versatile peroxidase: A site-directed mutagenesis, kinetic and crystallographic study. Biochemistry, **46**, 66-77

16 Morales, M., Mate, M. J., Romero, A., Martínez, M. J., Martínez, A. T. and Ruiz-Dueñas, F. J. (2012) Two oxidation sites for low redox-potential substrates: A directed mutagenesis, kinetic and crystallographic study on *Pleurotus eryngii* versatile peroxidase. J.Biol.Chem., **287**, 41053-41067

17 Fernández-Fueyo, E., Ruiz-Dueñas, F. J., Martínez, M. J., Romero, A., Hammel, K. E., Medrano, F. J. and Martínez, A. T. (2014) Ligninolytic peroxidase genes in the oyster mushroom genome: Heterologous expression, molecular structure, catalytic and stability properties and lignin-degrading ability. Biotechnol.Biofuels, **7:2**,

18 Ruiz-Dueñas, F. J., Lundell, T., Floudas, D., Nagy, L. G., Barrasa, J. M., Hibbett, D. S. and Martínez, A. T. (2013) Lignin-degrading peroxidases in Polyporales: An evolutionary survey based on ten sequenced genomes. Mycologia, **105**, 1428-1444

19 Heinfling, A., Ruiz-Dueñas, F. J., Martínez, M. J., Bergbauer, M., Szewzyk, U. and Martínez, A. T. (1998) A study on reducing substrates of manganese-oxidizing peroxidases from *Pleurotus eryngii* and *Bjerkandera adusta*. FEBS Lett., **428**, 141-146

20 Kamitsuji, H., Watanabe, T., Honda, Y. and Kuwahara, M. (2005) Direct oxidation of polymeric substrates by multifunctional manganese peroxidase isozyme from *Pleurotus ostreatus* without redox mediators. Biochem.J., **386**, 387-393

21 Martínez, A. T. (2002) Molecular biology and structure-function of lignin-degrading heme peroxidases. Enzyme Microb.Technol., **30**, 425-444

22 Pérez-Boada, M., Doyle, W. A., Ruiz-Dueñas, F. J., Martínez, M. J., Martínez, A. T. and Smith, A. T. (2002) Expression of *Pleurotus eryngii* versatile peroxidase in *Escherichia coli* and optimisation of *in vitro* folding. Enzyme Microb.Technol., **30**, 518-524
23 Doyle, W. A. and Smith, A. T. (1996) Expression of lignin peroxidase H8 in *Escherichia coli*: Folding and activation of the recombinant enzyme with Ca^{2+} and haem. Biochem.J., **315**, 15-19
24 Ruiz-Dueñas, F. J., Morales, M., García, E., Miki, Y., Martínez, M. J. and Martínez, A. T. (2009) Substrate oxidation sites in versatile peroxidase and other basidiomycete peroxidases. J.Exp.Bot., **60**, 441-452
25 Hammel, K. E., Jensen, K. A., Mozuch, M. D., Landucci, L. L., Tien, M. and Pease, E. A. (1993) Ligninolysis by a purified lignin peroxidase. J.Biol.Chem., **268**, 12274-12281
26 Fernández-Fueyo, E., Acebes, S., Ruiz-Dueñas, F. J., Martínez, M. J., Romero, A., Medrano, F. J., Guallar, V. and Martínez, A. T. (2014) Catalytic and stability properties of manganese peroxidase subfamilies: A study based on the *Ceriporiopsis subvermispora* genome. (submitted),
27 Timofeevski, S. L., Nie, G., Reading, N. S. and Aust, S. D. (1999) Addition of veratryl alcohol oxidase activity to manganese peroxidase by site-directed mutagenesis. Biochem.Biophys.Res.Commun., **256**, 500-504
28 Smith, A. T. and Doyle, W. A. (2006) Engineered peroxidases with veratryl alcohol oxidase activity. Patent (International), WO/2006-114616
29 Fernández-Fueyo, E., Acebes, S., Ruiz-Dueñas, F. J., Martínez, M. J., Romero, A., Medrano, F. J., Guallar, V. and Martínez, A. T. (2014) Catalytic and stability properties of manganese peroxidase subfamilies: A structural-functional study based on the *Ceriporiopsis subvermispora* genome. Proc.Natl.Acad.Sci.USA, (submitted)
30 Poulos, T. L., Edwards, S. L., Wariishi, H. and Gold, M. H. (1993) Crystallographic refinement of lignin peroxidase at 2 Å. J.Biol.Chem., **268**, 4429-4440
31 Khindaria, A., Yamazaki, I. and Aust, S. D. (1996) Stabilization of the veratryl alcohol cation radical by lignin peroxidase. Biochemistry, **35**, 6418-6424
32 Ruiz-Dueñas, F. J., Morales, M., Mate, M. J., Romero, A., Martínez, M. J., Smith, A. T. and Martínez, A. T. (2008) Site-directed mutagenesis of the catalytic tryptophan environment in *Pleurotus eryngii* versatile peroxidase. Biochemistry, **47**, 1685-1695
33 Gazarian, I. G., Lagrimini, M., George, S. J. and Thorneley, R. N. F. (1996) Anionic tobacco peroxidase is active at extremely low pH: Veratryl alcohol oxidation with a pH optimum of 1.8. Biochem.J., **320**, 369-372
34 McEldoon, J. P., Pokora, A. R. and Dordick, J. S. (1995) Lignin peroxidase-type activity of soybean peroxidase. Enzyme Microb.Technol., **17**, 359-365
35 Gazaryan, I. G., Chubar, T. A., Ignatenko, O. V., Mareeva, E. A., Orlova, M. A., Kapeliuch, Y. L., Savitsky, P. A., Rojkova, A. M. and Tishkov, V. I. (1999) Tryptophanless recombinant horseradish peroxidase: stability and catalytic properties. Biochem.Biophys.Res.Commun., **262**, 297-301
36 Sakharov, I. Y. and Sakharova, T. V. (2002) Extremely high stability of African oil palm tree peroxidase. BBA Proteins Proteomics, **1598**, 108-114
37 Kapich, A. N., Korneichik, T. V., Hatakka, A. and Hammel, K. E. (2010) Oxidizability of unsaturated fatty acids and of a non-phenolic lignin structure in the manganese peroxidase-dependent lipid peroxidation system. Enzyme Microb.Technol., **46**, 136-140

Capítulo 9

Discusión

Diversidad de peroxidasas tras el análisis genómico de basidiomicetos

Como se ha comentado en la Introducción, las peroxidasas ligninolíticas, características de los basidiomicetos de podredumbre blanca (que degradan la lignina) y ausentes de los de podredumbre parda (que degradan los polisacáridos), se dividen en tres familias en función de sus propiedades catalíticas. La LiP y la MnP se describieron hace unos 30 años en *P. chrysosporium* (Tien and Kirk, 1983; Kuwahara et al., 1984), mientras que la VP se describió en *Pleurotus enryngii*, primero como una MnP "con actividad sobre alcohol veratrílico" (Martínez et al., 1996) y posteriormente como una nueva peroxidasa caracterizada por su versatilidad catalítica (Ruiz-Dueñas et al., 1999; Camarero et al., 1999), y más tarde se encontró también en *Bjerkandera* sp (Mester and Field, 1998).

P. chrysosporium ha sido el hongo modelo utilizado en muchos estudios bioquímicos, enzimáticos y moleculares de degradación de la lignina, por esta razón fue el primer basidiomiceto cuyo genoma fue secuenciado (Martinez et al., 2004). En diferentes estudios se ha demostrado la capacidad que tiene la LiP de este hongo para degradar dímeros modelo no-fenólicos y lignina polimérica (Tien and Kirk, 1983; Hammel et al., 1985). Debido a esto, y a estudios posteriores con LiPs de otros basidiomicetos, la presencia de LiPs se ha asociado con la capacidad de degradar la lignina natural (un polímero de escaso contenido fenólico). Sin embargo, en varios hongos con demostrada capacidad ligninolítica no había sido posible demostrar la existencia de enzimas de tipo LiP. Entre ellos se encontraban *C. subvermispora* y *P. ostreatus*, dos especies de interés biotecnológico por su capacidad para degradar selectivamente la lignina (de madera y residuos agrícolas, respectivamente), que han sido objeto de estudio en la presente Tesis.

En *C. subvermispora* sólo se habían detectado enzimas de tipo lacasa y MnP, a pesar de haberse realizado considerables esfuerzos para aislar enzimas de tipo LiP de los cultivos, o para clonar los correspondientes genes. La ausencia de LiPs, que en aquel momento eran las únicas enzimas con capacidad reconocida para degradar la lignina no-fenólica, llevaron a sugerir que en este hongo la degradación tendría lugar por un mecanismo alternativo, en el que estarían implicadas las MnPs (Jensen et al., 1996). La secuenciación del genoma de *C. subvermipora* mostró un número inusualmente elevado de MnPs, junto con genes implicados en la síntesis de ácidos grasos insaturados, lo que nos hizo sugerir que la degradación de la lignina por este hongo ocurriría a traves de los radicales libres derivados de la peroxidación de los lípidos (Fernández-Fueyo et al., 2012a). La capacidad de estos radicales para degradar la lignina no-fenólica había sido descrito anteriormente (Bao et al., 1994). Sin embargo, poco después se produjo el descubrimiento más sorprendente en el genoma de *C. subvermispora* al identificarse dos genes cuyas secuencias codificaban peroxidasas con el triptófano catalítico conservado en VPs y LiPs, que no habían sido previamente descritas en este hongo. Estos dos genes se clasificaron inicialmente como una putativa LiP y una putativa VP. Sin embargo su caracterización bioquímica, tras expresión heteróloga, demostró que se trataba de dos LiPs funcionales, capaces de degradar lignina sintética y un dímero modelo no-fenólico. Como consecuencia, podrían ser responsables de la degradación natural de la lignina por este hongo. Por otro lado, las peculiares constantes cinéticas de las dos nuevas enzimas, y su posición en el árbol filogenético de las peroxidasas, nos permitieron sugerir que muy posiblemente representan formas de transición entre VP y LiP (Fernández-Fueyo et al., 2012b).

En *P. ostreatus* y especies relacionadas se habían encontrado MnPs y lacasas, como en *C. subvermispora*. Además, en estos hongos se había descrito por vez primera la VP, como una nueva familia de peroxidasas combinando las propiedades catalíticas y estructurales de LiPs y MnPs. Sin embargo, se mantenía la incógnita de si, como en el caso de *C. subvermispora*, pudieran también producir enzimas de tipo LiP implicadas en la degradación de la lignina. La secuenciación del genoma de *P. ostreatus* ha proporcionado respuesta a esta pregunta al mostrar la existencia de genes de MnPs y VPs y la ausencia de genes de LiP en este hongo (Ruiz-Dueñas et al., 2011). Mas importante, tras la expresión heteróloga de todos ellos, se encontró que la VP de *P. ostreatus* es capaz de oxidar dímeros modelo no-fenólicos y degradar la lignina con una eficiencia similar a la de la LiP mas estudiada (isoenzima H8) de *P. chrysosporium*. Estos resultados nos han permitido postular que la VP desempeñaría en *P. ostreatus* y probablemente en otras especies del orden Agaricales, en cuyos cultivos y genomas no se han encontrado nunca evidencias de presencia de LiP (Floudas et al., 2012), el papel desempeñando por las LiPs en *P. chrysosporium* y otras especies de Poliporales (Fernández-Fueyo et al., 2014d).

La clasificación de los genes de peroxidasas ligninolíticas en el creciente número de genomas de basidiomicetos disponibles (Floudas et al., 2012), se basa en la presencia o ausencia del sitio de oxidación del Mn^{2+} (formado por tres residuos ácidos junto al propionato interno del hemo) y/o del triptófano catalítico en las proteínas predichas. En la mayoría de los casos, los residuos conservados son funcionales tras expresión heteróloga, y la clasificación inicial - estructural y teórica - coincide con la clasificación funcional. Sin embargo, en la presente tesis hemos encontrado dos excepciones significativas correspondientes a una MnP y una VP cuya clasificación inicial tuvo que modificarse tras la determinación experimental de sus propiedades catalíticas. Así, en el genoma de *P. ostreatus* se encontró una MnP con un triptófano superficial homólogo al de las LiPs/VPs, por lo que el gen había sido inicialmente clasificado como un gen de LiP, pero dicho residuo resultó posteriormente no ser funcional. Esta anomalía se explica por una mutación durante la evolución de estas peroxidasas que interrumpió la ruta de transporte electrónico desde la superficie hasta el grupo hemo, como se demostró por mutagénesis dirigida reversa (Fernández-Fueyo et al., 2014d). Esta misma mutación natural pudo también localizarse en otra MnP de la especie relacionada *P. pulmonarius*. Por otra parte, en el genoma de *C. subvermipora* hubo que reclasificar, como gen de LiP, uno que la clasificación teórica había considerado codificaba una VP. Dicha reclasificación se debió a la incapacidad de la enzima para oxidar Mn^{2+} a pesar de presentar los tres residuos conservados que forman el sitio de unión del Mn en todas las VPs y MnPs. En este caso, la falta de actividad era debida a la presencia de un cuarto residuo ácido contiguo, como se mostró al aparecer la actividad sobre el Mn^{2+} cuando el residuo se eliminó por mutagénesis dirigida (Fernández-Fueyo et al., 2012b).

Estudios recientes han mostrado que la historia evolutiva general de las peroxidasas ligninolíticas se inició con una MnP primitiva que adquirió el triptófano catalítico para dar lugar a la primera VP y que, posteriormente, una VP perdió el sitio de oxidación del Mn para dar lugar a la primera LiP (esta última transición únicamente en Poliporales) (Floudas et al., 2012; Ruiz-Dueñas et al., 2013). Sin embargo, los resultados anteriores muestran la existencia más que probable de líneas evolutivas secundarias en las que, por ejemplo, una VP pudo dar lugar a una MnP, como en el caso de *P. ostreatus*, al mismo tiempo que nos revelan formas intermedias que explican las diferentes transiciones.

Existencia y significado de múltiples isoformas de peroxidasas

Una característica en la evolución de las enzimas que componen el sistema oxidativo de los hongos, incluyendo las peroxidasas ligninolíticas, es la existencia de duplicaciones recientes codificando diferentes isoformas. Dichas isoenzimas difieren escasamente en su secuencia y, a pesar de que existen pocos datos al respecto, deben poseer características diferentes de forma que su expresión confiera al hongo una ventaja evolutiva en determinados hábitats o sustratos. Desde hace tiempo se conoce la existencia de un número limitado de isoenzimas de LiP, MnP y VP. Sin embargo, hasta muy recientemente, no ha sido posible conocer la gran magnitud de este fenómeno de duplicación génica al disponerse de un número considerable de genomas, en los que se han realizado inventarios detallados de los diferentes tipos de genes (Floudas et al., 2012; Ruiz-Dueñas et al., 2013).

De esta forma, hasta la secuenciación del genoma de *C. subvermispora* solamente habían sido descritos cuatro genes de MnPs en este hongo, mientras que en su genoma hemos podido identificar quince genes de peroxidasas ligninolíticas clasificados inicialmente como trece MnPs, una LiP y una VP (Fernández-Fueyo et al., 2012a), esta última reclasificada como una LiP tras su caracterización bioquímica (Fernández-Fueyo et al., 2012b), tal como se ha discutido anteriormente. De igual forma, en *P. ostreatus* sólo se habían sido descrito tres genes de peroxidasas ligninolíticas, sin embargo en su genoma encontramos nueve, que inicialmente se clasificaron en cuatro genes de VP y cinco de MnP (Ruiz-Dueñas et al., 2011). Gracias a la disponibilidad de los genomas y a la activación *in vitro* de las peroxidasas expresadas en *E. coli*, hemos caracterizado bioquímicamente el inventario completo de las peroxidasas ligninolíticas presentes en *P. ostreatus* describiendo de esta forma seis nuevas peroxidasas ligninolíticas. Tras la caracterización funcional de todas ellas, el inventario final en *P. ostreatus* está formado por seis MnPs y tres VPs, ya que una de las inicialmente clasificadas como VP resultó ser una MnP funcional (Fernández-Fueyo et al., 2014d), tal como se ha discutido anteriormente.

La caracterización bioquímica de las seis isoenzimas de MnP y las tres de VP de *P. ostreatus* sólo mostró ligeras diferencias en sus constantes catalíticas frente a cinco sustratos representativos, lo que coincide con un estudio de Salame et al. (2013) donde describen la redundancia funcional entre las peroxidasas ligninolíticas de *P. ostreatus* mediante el silenciamiento génico de algunas de ellas. Sin embargo, sorprendentemente, la caracterización bioquímica de las nueve isoenzimas de *P. ostreatus* mostró grandes diferencias en su estabilidad a la temperatura (con valores de T_{50} de 43-63 ºC, tras 10 min a pH 5) y al pH (con actividades residuales de 0-96% a pH 3 y de 0-57% a pH 9, en ambos casos tras 4 h a 4 ºC). Para intentar identificar las bases estructurales de las mayores estabilidades, la isoenzima más estable al pH y la más estable a la temperatura se cristalizaron y su estructura fue resulta a 1.0-1.1 Å (Fernández-Fueyo et al., 2014d). Se ha demostrado que la mayor abundancia de residuos básicos, y de puentes de hidrogeno e interacciones salinas, en la superficie de la proteina se relaciona con la estabilidad de una de estas peroxidasas (Sáez-Jiménez et al., 2013).

Para investigar el significado biológico de la duplicación de genes de peroxidasas ligninolíticas, que da lugar a múltiples isoenzimas con diferencias significativas en su estabilidad, se analizó por RT-qPCR la expresión de estos genes cuando se modifican las condiciones de temperatura y pH en cultivos de *P. ostreatus* creciendo sobre material lignocelulósico, en combinación con estudios proteómicos y medidas de

actividad (Fernández-Fueyo et al., 2014b). Las condiciones óptimas de cultivo coinciden con el máximo de actividad y con el mayor nivel de expresión de los genes. Aunque todos los genes se transcriben en todas las condiciones, el estudio muestra que en condiciones óptimas se expresan dos genes principalmente, MnP3 seguida de VP1, coincidiendo con estudios previos (Irie et al., 2000; Salame et al., 2012; 2013). Al no encontrarse una correlación entre los resultados secretómicos y de transcripción de la isoenzima más expresada, se analizó el proteoma intracelular detectándose la presencia de esta proteína y demostrándose que su baja secreción era el factor limitante. Sin embargo, sí se observó que la proteína codificada por el segundo gen que más se transcribía era la más abundante en el secretoma, pudiendo ser purificada y caracterizada a partir de los cultivos. También se observó que la expresión de los genes de estas peroxidasas se ve más afectada por los cambios de pH que por los cambios de temperatura, dentro de los márgenes investigados, y que para la mayoría de las condiciones analizadas existe una correlación entre el nivel de expresión y la actividad peroxidasa detectada en los cultivos. El conjunto de los resultados muestra que algunas de las enzimas más estables presentan niveles de transcripción relativa mayores en las condiciones más extremas de pH y temperatura, lo que sugiere una regulación ambiental de la expresión de las isoenzimas relacionada con la estabilidad de las mismas. De esta forma, los resultados obtenidos aportan nuevas evidencias sobre el significado biológico de la diversidad de isoenzimas de peroxidasas ligninolíticas en *P. ostreatus* y probablemente en otros hongos ligninolíticos.

Estudio y posible validación de nuevas subfamilias de peroxidasas

La primera MnP se describió en 1984 en *P. chrysosporium* (Kuwahara et al., 1984). Actualmente hay disponibles más de 200 secuencias y esto ha llevado a dividirlas en tres subfamilias - extralargas, largas y cortas - en función de las diferencias estructurales basadas en la longitud del extremo C-terminal. Cuando se analiza la identidad de secuencia protéica, se ve que, mientras que las MnPs largas y extralargas presentran entre sí identidades superiores al 75%, las MnP de tipo corto presentan mayores identidades con las VP que con las MnPs largas y extralargas, siendo estas últimas a menudo inferiores al 50%. Los tres tipos de MnPs comparten el sitio de unión del Mn pero se ha sugerido que presentarían propiedades catalíticas y de estabilidad diferentes. De esta forma, las MnP de tipo largo de *P. chrysosporium* no presentan actividad independiente de Mn (Palma et al., 2000), mientras que las MnP de tipo corto presentes en *P. ostreatus* son capaces de oxidar ABTS y DMP en ausencia de Mn^{2+} (Fernández-Fueyo et al., 2014d).

En el genoma de *C. subvermispora* se encontraron genes para los tres tipos de MnPs, lo que ha permitido comparar las tres subfamilias propuestas sin las interferencias derivadas de diferentes historias evolutivas de los hongos (Fernández-Fueyo et al., 2014a). De acuerdo con la caracterización bioquímica, las MnP de tipo corto constituyen una subfamilia verdadera con diferentes propiedades catalíticas y de estabilidad, presentando actividad independiente de Mn^{2+} sobre el ABTS y nula estabilidad a pH 2, mientras que las MnPs llamadas largas y extralargas no muestran suficientes diferencias entre sí para considerarse dos subfamilias diferentes. Ambas oxidan exclusivamente el Mn^{2+}, y lo hacen de forma mucho más eficiente que las de tipo corto, y son extremadamente estables a pH 2. Estos datos bioquímicos se

completaron con estudios estructurales y de mutagénesis dirigida, con objeto de explicar las diferencias en actividad y estabilidad observadas entre las diferentes MnPs.

Hasta la realización de esta tesis sólo se habían cristalizado MnPs de tipo largo, empezando por la de *P. chrysosporium*. Durante la presente tesis se ha cristalizado la primera MnP corta (de *P. ostreatus*), tal como se ha mencionado anteriormente, y la primera MnP extralarga (de *C. subvermipora*) para completar la caracterización de este tipo de peroxidasa. La comparación de las tres estructuras cristalográficas revela que la principal diferencia entre estos tres tipos es la longitud del extremo C-terminal y que la cola extra presente en las MnPs largas y extralargas se localiza próxima al sitio de oxidación del Mn.

Por mutagénisis dirigida se ha demostrado que la importante estabilidad al pH ácido de las MnPs largas y extralargas se debe a la presencia de la cola en el extremo C-terminal y que la ausencia de esta cola les confiere actividad independiente de Mn. Cerrando el canal con residuos voluminosos, se ha demostrado también que el ABTS se oxida en el canal del propionato del hemo de las MnP cortas o "recortadas", al igual que lo hace el Mn^{2+}, lo que representa un importante hallazgo. En este mismo sentido, la eliminación de los residuos ácidos que constituyen el sitio de unión del Mn elimina la actividad sobre el Mn^{2+} pero mejora la actividad sobre el ABTS al reducir la repulsión electrostática. Además, usando las estructuras cristalográficas obtenidas durante esta tesis se ha estudiado el acceso del ABTS hasta el cofactor, mediante el programa PELE de "docking" dinámico que predijo el posicionamiento del sustrato en el sitio de oxidación del Mn. También se han realizado otras simulaciones computacionales, cuyos resultados coincidieron con los obtenidos por mutagénesis dirigida y otros métodos experimentales.

Finalmente, la MnP extralarga cristalizada (de *C. subvermispora*), que es extremadamente estable al pH ácido, se ha usado como una base "robusta" para, mediante la introducción de un triptófano catalítico, construir una peroxidasa de interés biotecnológico capaz de actuar a pH extremadamente ácido (Fernández-Fueyo et al., 2014c). Las variantes diseñadas conservan la notable estabilidad al pH ácido de la MnP inicial pero son capaces de oxidar tanto el alcohol veratrílico, como el RB5 y el Mn^{2+}, actuando por tanto como VPs funcionales. Además, la mejora en la estabilidad al pH ácido permite incrementar el poder oxidante de estas enzimas utilizándolas a pH más ácido, lo que aumenta el potencial redox del hemo, mejorando así la actividad sobre el RB5 hasta catorce veces. De esta forma, el estudio de las diferentes MnPs del genoma de *C. subvermispora* permitió no sólo validar la existencia de dos subfamilias, cuyos diferencias catalíticas se explicaron en base a la información estructural obtenida, sino tambien identificar una MnP extremadamente estable, que fue utilizada para construir la peroxidasa de tipo VP/LiP más estable a pH ácido conocida utilizando el diseño racional.

Referencias

Bao, W. L., Y. Fukushima, K. A. Jensen, M. A. Moen, and K. E. Hammel. 1994. Oxidative degradation of non-phenolic lignin during lipid peroxidation by fungal manganese peroxidase. FEBS Lett. 354:297-300.

Camarero, S., S. Sarkar, F. J. Ruiz-Dueñas, M. J. Martínez, and A. T. Martínez. 1999. Description of a versatile peroxidase involved in natural degradation of lignin that

has both Mn-peroxidase and lignin-peroxidase substrate binding sites. J. Biol. Chem. 274:10324-10330.

Fernández-Fueyo, E., S. Acebes, F. J. Ruiz-Dueñas, M. J. Martínez, A. Romero, F. J. Medrano, V. Guallar, and A. T. Martínez. 2014a. Catalytic and stability properties of manganese peroxidase subfamilies: A structural-functional study based on the *Ceriporiopsis subvermispora* genome. Proc. Natl. Acad. Sci. USA (submitted).

Fernández-Fueyo, E., R. Castanera, F. J. Ruiz-Dueñas, M. F. López-Lucendo, L. Ramírez, A. G. Pisabarro, and A. T. Martínez. 2014b. Ligninolytic peroxidase gene expression by *Pleurotus ostreatus*: Differential regulation in lignocellulose medium and effect of temperature and pH. Fungal Genet. Biol. (in press).

Fernández-Fueyo, E., F. J. Ruiz-Dueñas, P. Ferreira, D. Floudas, D. S. Hibbett, P. Canessa, L. Larrondo, T. Y. James, D. Seelenfreund, S. Lobos, R. Polanco, M. Tello, Y. Honda, T. Watanabe, T. Watanabe, J. S. Ryu, C. P. Kubicek, M. Schmoll, J. Gaskell, K. E. Hammel, F. J. St.John, A. Vanden Wymelenberg, G. Sabat, S. S. Bondurant, K. Syed, J. Yadav, H. Doddapaneni, V. Subramanian, J. L. Lavín, J. A. Oguiza, G. Perez, A. G. Pisabarro, L. Ramírez, F. Santoyo, E. Master, P. M. Coutinho, B. Henrissat, V. Lombard, J. K. Magnuson, U. Kües, C. Hori, K. Igarashi, M. Samejima, B. W. Held, K. Barry, K. LaButti, A. Lapidus, E. Lindquist, S. Lucas, R. Riley, A. Salamov, D. Hoffmeister, D. Schwenk, Y. Hadar, O. Yarden, R. P. de Vries, A. Wiebenga, J. Stenlid, D. C. Eastwood, I. V. Grigoriev, R. Berka, R. A. Blanchette, P. Kersten, A. T. Martínez, R. Vicuña, and D. Cullen. 2012a. Comparative genomics of *Ceriporiopisis subvermispora* and *Phanerochaete chrysosporium* provide insight into selective ligninolysis. Proc. Natl. Acad. Sci. USA 109:5458-5463.

Fernández-Fueyo, E., F. J. Ruiz-Dueñas, and A. T. Martínez. 2014c. Engineering and acidic pH stable versatile peroxidase from an extralong manganese peroxidase. Biochem. J. (submitted).

Fernández-Fueyo, E., F. J. Ruiz-Dueñas, M. J. Martínez, A. Romero, K. E. Hammel, F. J. Medrano, and A. T. Martínez. 2014d. Ligninolytic peroxidase genes in the oyster mushroom genome: Heterologous expression, molecular structure, catalytic and stability properties and lignin-degrading ability. Biotechnol. Biofuels 7:2.

Fernández-Fueyo, E., F. J. Ruiz-Dueñas, Y. Miki, M. J. Martínez, K. E. Hammel, and A. T. Martínez. 2012b. Lignin-degrading peroxidases from genome of selective ligninolytic fungus Ceriporiopsis subvermispora (vol 287, pg 16903, 2012). J. Biol. Chem. 287:41744.

Floudas, D., M. Binder, R. Riley, K. Barry, R. A. Blanchette, B. Henrissat, A. T. Martínez, R. Otillar, J. W. Spatafora, J. S. Yadav, A. Aerts, I. Benoit, A. Boyd, A. Carlson, A. Copeland, P. M. Coutinho, R. P. de Vries, P. Ferreira, K. Findley, B. Foster, J. Gaskell, D. Glotzer, P. Górecki, J. Heitman, C. Hesse, C. Hori, K. Igarashi, J. A. Jurgens, N. Kallen, P. Kersten, A. Kohler, U. Kües, T. K. A. Kumar, A. Kuo, K. LaButti, L. F. Larrondo, E. Lindquist, A. Ling, V. Lombard, S. Lucas, T. Lundell, R. Martin, D. J. McLaughlin, I. Morgenstern, E. Morin, C. Murat, M. Nolan, R. A. Ohm, A. Patyshakuliyeva, A. Rokas, F. J. Ruiz-Dueñas, G. Sabat, A. Salamov, M. Samejima, J. Schmutz, J. C. Slot, F. St.John, J. Stenlid, H. Sun, S. Sun, K. Syed, A. Tsang, A. Wiebenga, D. Young, A. Pisabarro, D. C. Eastwood, F. Martin, D. Cullen, I. V. Grigoriev, and D. S. Hibbett. 2012. The Paleozoic origin of enzymatic lignin decomposition reconstructed from 31 fungal genomes. Science 336:1715-1719.

Hammel, K. E., M. Tien, B. Kalyanaraman, and T. K. Kirk. 1985. Mechanism of oxidative C_α-C_β cleavage of a lignin model dimer by *Phanerochaete chrysosporium* ligninase. J. Biol. Chem. 260:8348-8353.

Irie, T., Y. Honda, H.-C. Ha, T. Watanabe, and M. Kuwahara. 2000. Isolation of cDNA and genomic fragments encoding the major manganese peroxidase isoenzyme from the white rot basidiomycete *Pleurotus ostreatus*. J. Wood Sci. 46:230-233.

Jensen, K. A., W. Bao, S. Kawai, E. Srebotnik, and K. E. Hammel. 1996. Manganese-dependent cleavage of non-phenolic lignin structures by *Ceriporiopsis subvermispora* in the absence of lignin peroxidase. Appl. Environ. Microbiol. 62:3679-3686.

Kuwahara, M., J. K. Glenn, M. A. Morgan, and M. H. Gold. 1984. Separation and characterization of two extracellular H_2O_2-dependent oxidases from ligninolytic cultures of *Phanerochaete chrysosporium*. FEBS Lett. 169:247-250.

Martinez, D., L. F. Larrondo, N. Putnam, M. D. Gelpke, K. Huang, J. Chapman, K. G. Helfenbein, P. Ramaiya, J. C. Detter, F. Larimer, P. M. Coutinho, B. Henrissat, R. Berka, D. Cullen, and D. Rokhsar. 2004. Genome sequence of the lignocellulose degrading fungus *Phanerochaete chrysosporium* strain RP78. Nat. Biotechnol. 22:695-700.

Martínez, M. J., F. J. Ruiz-Dueñas, F. Guillén, and A. T. Martínez. 1996. Purification and catalytic properties of two manganese-peroxidase isoenzymes from *Pleurotus eryngii*. Eur. J. Biochem. 237:424-432.

Mester, T. and J. A. Field. 1998. Characterization of a novel manganese peroxidase-lignin peroxidase hybrid isozyme produced by *Bjerkandera* species strain BOS55 in the absence of manganese. J. Biol. Chem. 273:15412-15417.

Palma, C., A. T. Martínez, J. Lema, and M. J. Martínez. 2000. Different fungal manganese-oxidizing peroxidases: A comparison between *Bjerkandera* sp and *Phanerochaete chrysosporium*. J. Biotechnol. 77:235-245.

Ruiz-Dueñas, F. J., E. Fernández, M. J. Martínez, and A. T. Martínez. 2011. *Pleurotus ostreatus* heme peroxidases: An *in silico* analysis from the genome sequence to the enzyme molecular structure. C. R. Biol. 334:795-805.

Ruiz-Dueñas, F. J., T. Lundell, D. Floudas, L. G. Nagy, J. M. Barrasa, D. S. Hibbett, and A. T. Martínez. 2013. Lignin-degrading peroxidases in Polyporales: An evolutionary survey based on ten sequenced genomes. Mycologia 105:1428-1444.

Ruiz-Dueñas, F. J., M. J. Martínez, and A. T. Martínez. 1999. Molecular characterization of a novel peroxidase isolated from the ligninolytic fungus *Pleurotus eryngii*. Mol. Microbiol. 31:223-236.

Sáez-Jiménez, V., E. Fernández-Fueyo, F. J. Medrano, A. T. Martínez, and F. J. Ruiz-Dueñas. 2013. Mejora de la estabilidad de la peroxidasa versátil de *Pleurotus eryngii* mediante diseño racional. Proc. Red Lignina, Pontevedra, 25-27 Septiembre.

Salame, T. M., D. Knop, D. Levinson, S. J. Mabjeesh, O. Yarden, and Y. Hadar. 2012. Release of *Pleurotus ostreatus* versatile-peroxidase from Mn2+ repression enhances anthropogenic and natural substrate degradation. PLoS One 7, 12.

Salame, T. M., D. Knop, D. Levinson, O. Yarden, and Y. Hadar. 2013. Redundancy among manganese peroxidases in *Pleurotus ostreatus*. Appl. Environ. Microbiol. 79:2405-2415.

Tien, M. and T. K. Kirk. 1983. Lignin-degrading enzyme from the hymenomycete *Phanerochaete chrysosporium* Burds. Science 221:661-663.

Capítulo 10

Conclusiones

CONCLUSIONES

1. El análisis del genoma de *C. subvermispora* (Poliporales) ha permitido identificar 2 LiPs funcionales, que no habían podido ser detectadas en este hongo ligninolítico, junto con 13 MnPs

2. El estudio de las peroxidasas del genoma de *P. ostreatus* (Agaricales) muestra 6 MnPs y 3 VPs, siendo estas últimas capaces de degradar la lignina por lo que desempeñarían el mismo papel que la LiP en los poliporales

3. La presencia de los residuos conservados asociados a la actividad (aminoácidos de unión de Mn y triptófano superficial) no es sinónimo de la funcionalidad de los mismos (como se ha visto para las peroxidasas de *P. ostreatus* y *C. subvermispora*)

4. Las 6 MnPs y las 3 VPs de *P. ostreatus* presentan grandes diferencias en su estabilidad a la temperatura y al pH, que se han relacionado con diferencias estructurales, y su expresión se ve afectada por las condiciones ambientales

5. Las MnP de tipo corto constituyen una subfamilia verdadera con propiedades catalíticas diferentes (oxidación de ABTS) mientras que las MnP largas y extralargas no muestran suficientes diferencias para separarlas en dos subfamilias

6. El ABTS se oxida en el canal del propionato del hemo de las MnP cortas, como se ha demostrado por mutagénesis dirigida, y la eliminación de los residuos ácidos que unen el Mn mejora su oxidación

7. Se ha diseñado una peroxidasa de tipo VP a partir de una MnP extralarga extremadamente estable al pH ácido, lo que le confiere mejores propiedades catalíticas que las VP tradicionales

Material Suplementario

Capítulo 3

"**Ligninolytic peroxidase genes in the oyster mushroom genome: Heterologous expression, molecular structure, catalytic and stability properties and lignin-degrading ability"**
Fernández-Fueyo, E., F. J. Ruiz-Dueñas, M. J. Martínez, A. Romero, K. E. Hammel, F. J. Medrano, and A. T. Martínez.
Biotechnol. Biofuels 7:2. 2014.

Additional file 1

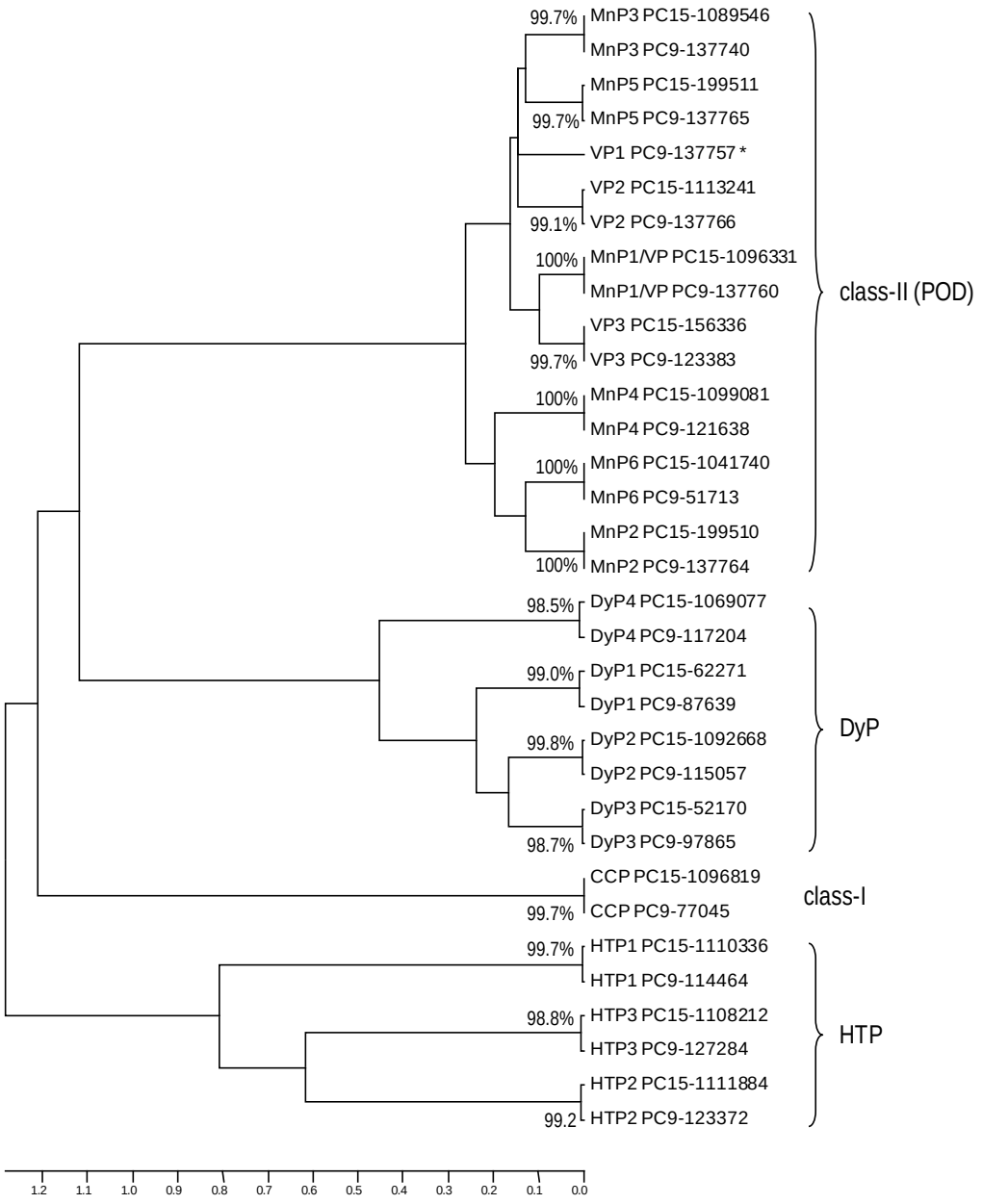

Figure S1. Phylogram of heme peroxidase sequences from the genomes of two *P. ostreatus* monokaryons. The evolutionary analysis of the deduced peroxidase sequences was performed with MEGA5 using Poisson distances and UPGMA clustering. Accession numbers correspond to the monokaryons PC9 v1.0 and PC15 v2.0 catalogs. The sequence identities between each pair of allelic models are shown (*indicates the existence of a premature termination codon in PC15 1089895, resulting in a pseudogene not included in the phylogram). Three main clusters were identified corresponding to POD (VP and MnP), DyP and HTP sequences, together with a unique class I gene (CCP). The 1096331/137760 PC15/PC9 models, initially classified as VPs [1], are reclassified as MnP1.

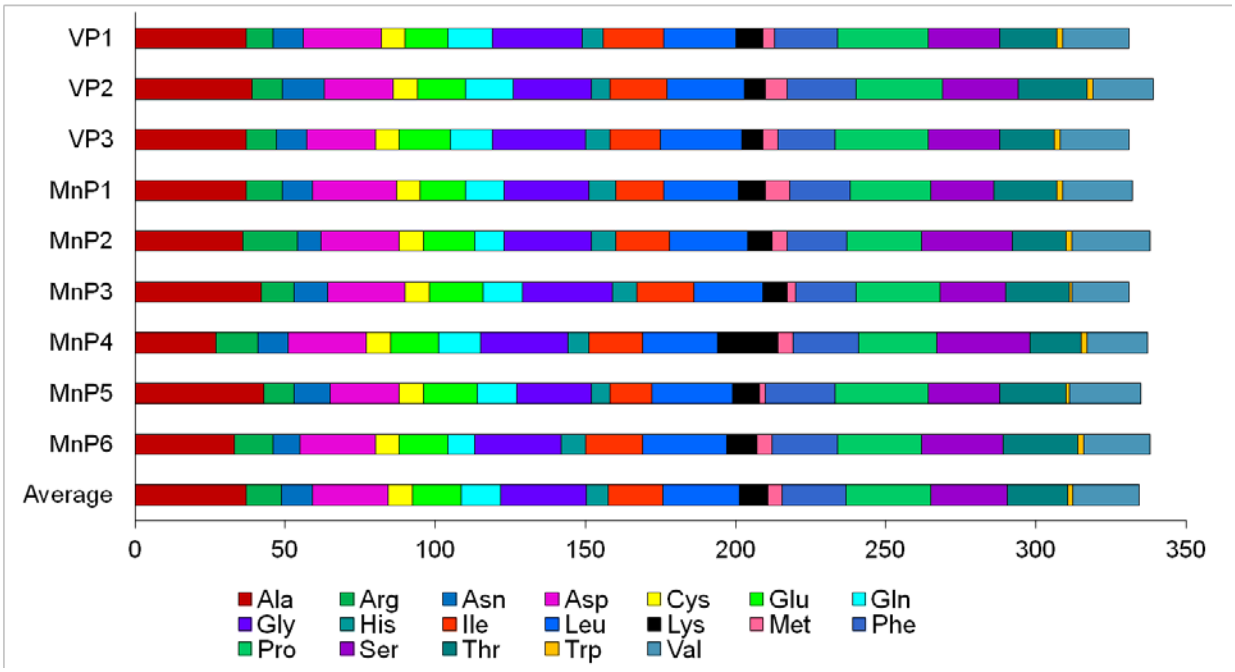

Figure S2. Amino-acid composition of the nine VP and MnP isoenzymes from the *P. ostreatus* genome (predicted mature proteins, Figure 1). The comparatively high number of lysine residues (20 compared with the 10 average) in MnP4 is among the most significant differences observed.

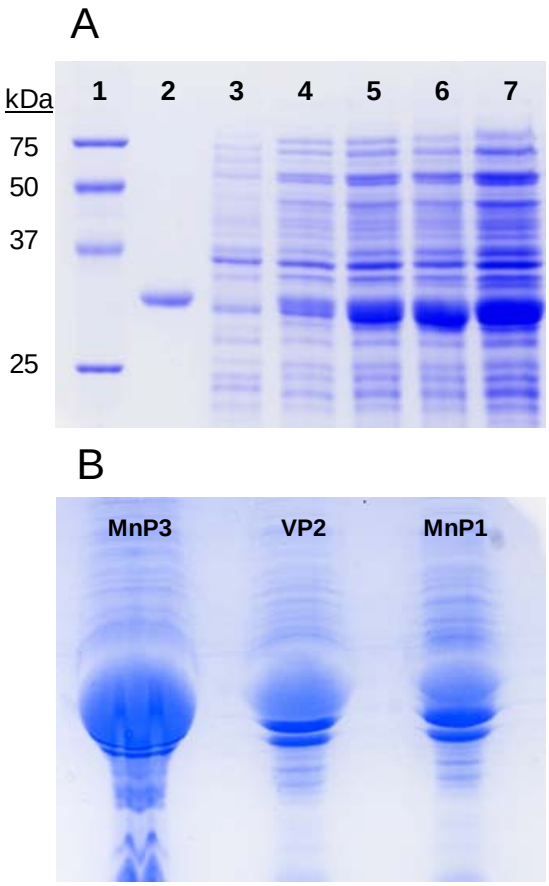

Figure S3. *E. coli* expression of *P. ostreatus* genome peroxidases (SDS-PAGE). (**A)** Time-course of MnP4 overexpression in IPTG-induced cultures (lane 1, standards; lane 2, purified MnP4; lanes 3-7, total proteins 0, 1, 2, 3 and 4 h after induction, respectively). (**B)** Inclusion bodies from MnP3, VP2 and MnP1 isoenzymes.

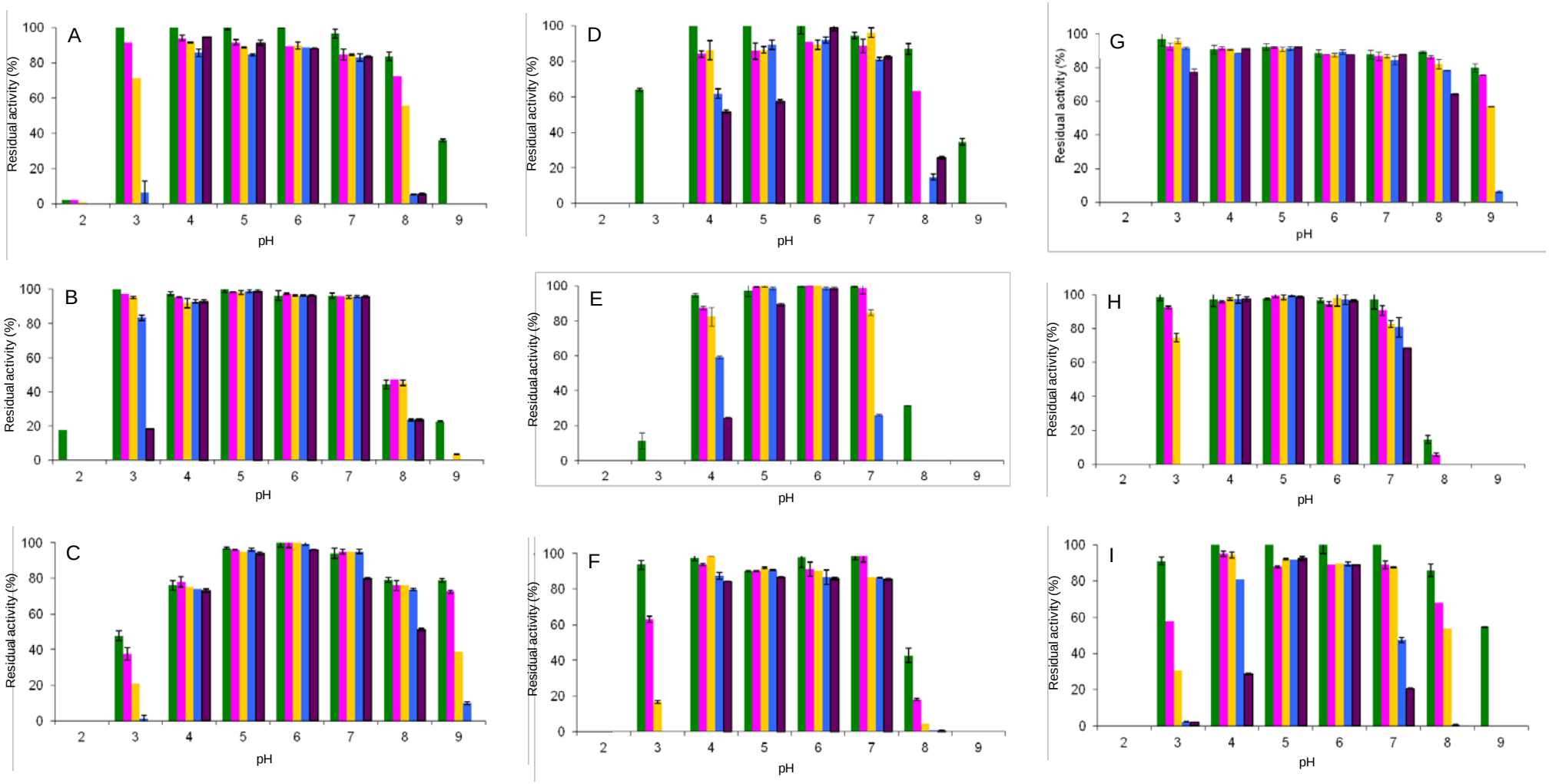

Figure S4. pH 2-9 stability of the nine PODs from the *P. ostreatus* genome at different incubation times. Residual activities after 1 min (green), 1 h (magenta), 4 h (orange) 24 h (blue) and 120 h (purple) incubation at 4 ºC in 100 mM B&R buffer (pH 2-9) were estimated for VP1 **(A)**, VP2 **(B)**, VP3 **(C)**, MnP1**(D)**, MnP2 **(E)**, MnP3 **(F)**, MnP4 **(G)**, MnP5 **(H)**, and MnP6 **(I)**. Activity was assayed as described in **Figure 2**. Means and 95% confidence limits.

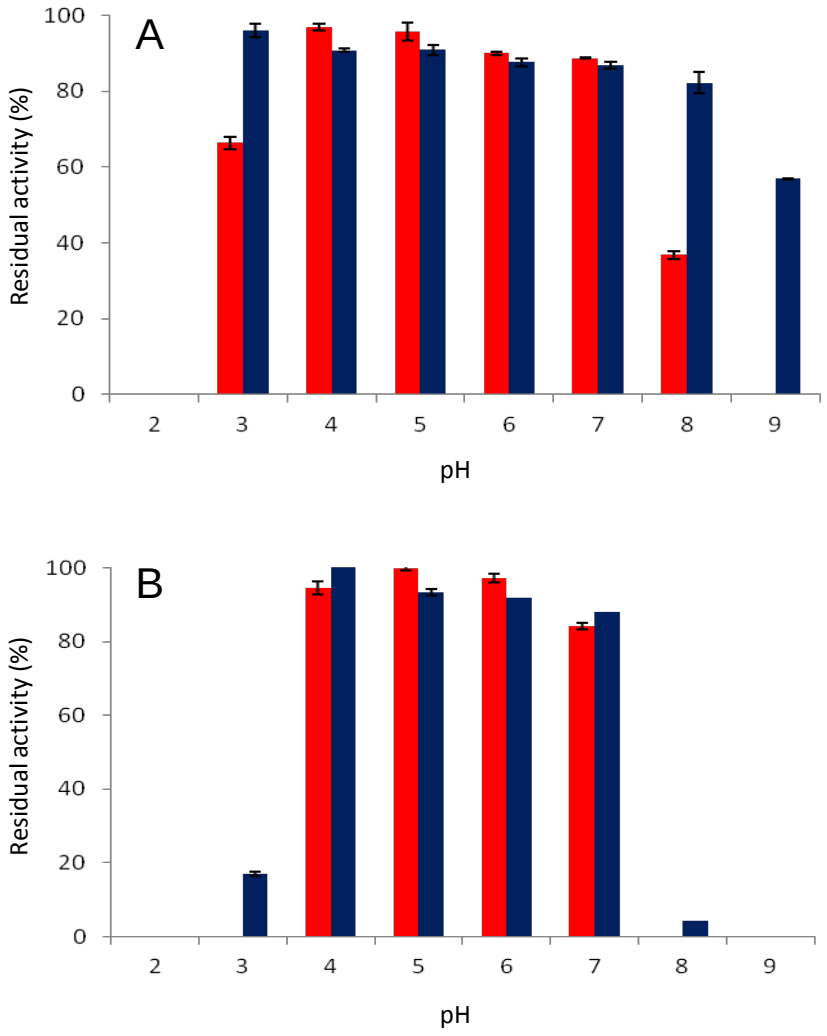

Figure S5. Influence of temperature on the pH stability of PODs from the *P. ostreatus* genome. The stable MnP4 **(A)** and the unstable MnP3 **(B)** were incubated for 4 h at 4 ºC (dark-blue bars) or 25 ºC (red bars) in 0.1 mM B&R buffer (pH 2-9) and the residual activity was estimated as described in **Figure 2**. Means and 95% confidence limits.

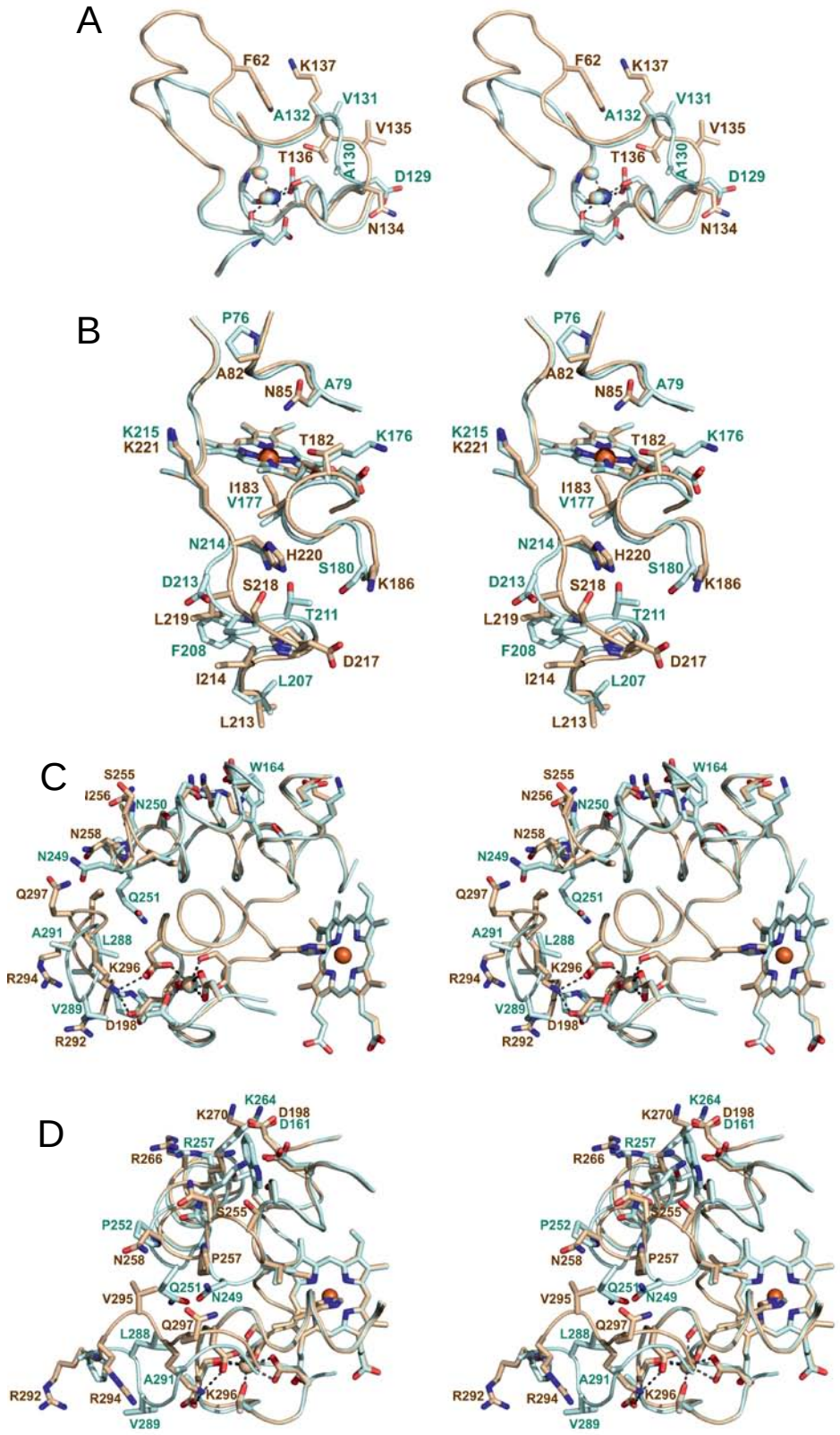

Figure S6. Stereo views of some of the main differences between VP1 (light blue**) and MnP4** (light brown) **crystal structures. (A)** Loop close to the distal Ca^{2+} ion (**Figure 5A**). **(B)** Main heme access channel region (**Figure 5C**). **(C** and **D)** Two sequence stretches (V248-P252 and P286-H293 in VP1, and I254-S259 and R292-P298 in MnP4) at the back of the protein, from two different orientations (the heme cofactor, proximal Ca^{2+} and its ligands, and VP1 W164 are also visible) (**Figure 5B**).

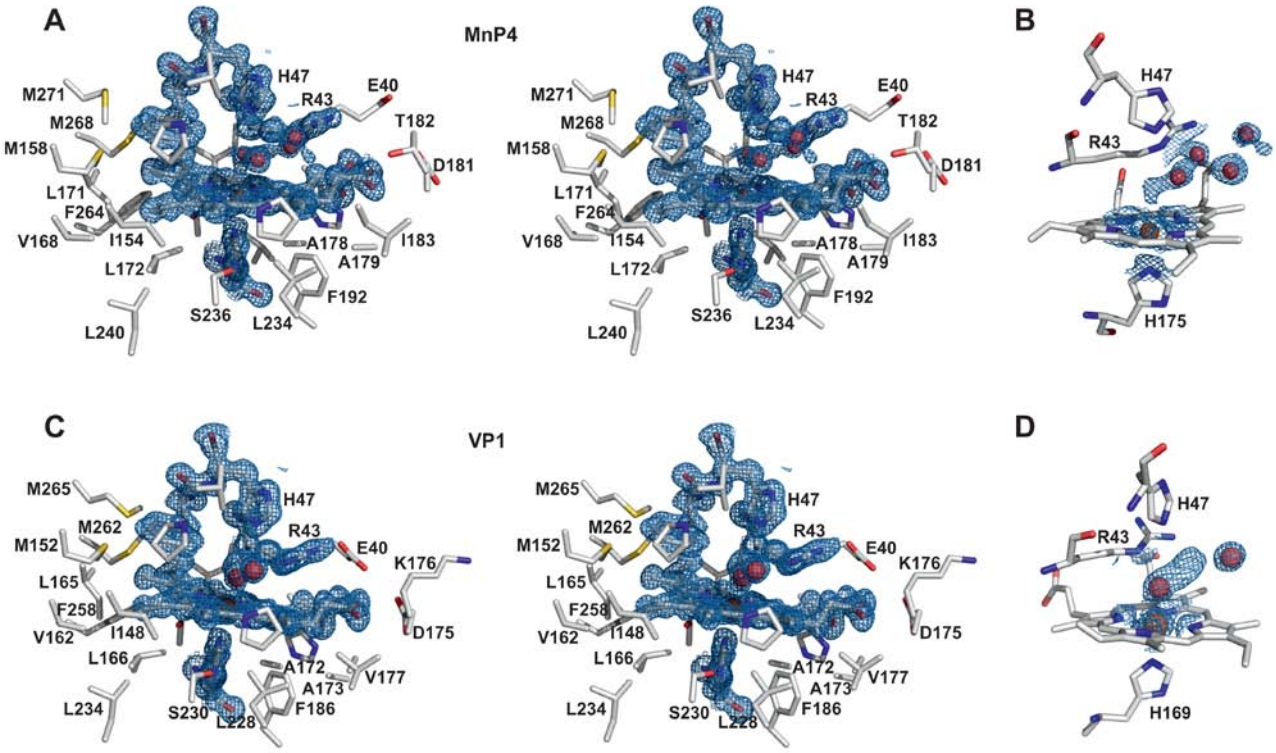

Figure S7. Partial 2*Fo-Fc* electron density map, contoured at the 1.1 σ level, of heme cofactor, some neighbor residues and several water molecules in the VP1 and MnP4 crystals. (A and **C)** Stereo views of VP1 and MnP4, respectively, from the heme δ-position side. The heme pocket is delimited by H39, E40, L42, R43, F46, H47, P139, P141, I148, M152, V162, L165, L166, S168, H169, I171, A172, A173, A174, D175, K176, V177, F186, L228, S230, L234, M262 and M265 in VP1, and H39, E40, L42, R43, F46, H47, P145, P147, I154, M158, V168, L171, L172, S174, H175, V177, A178, A179, Q180, D181, T182, I183, F192, L234, S236, L240, M268 and M271 in MnP4, some of them being shown in the stereo views. **(B** and **D)** Detail of the electron density maps of several water molecules in MnP4 and VP1, respectively, from the heme α-position side, also showing two conserved histidine and one conserved arginine residues.

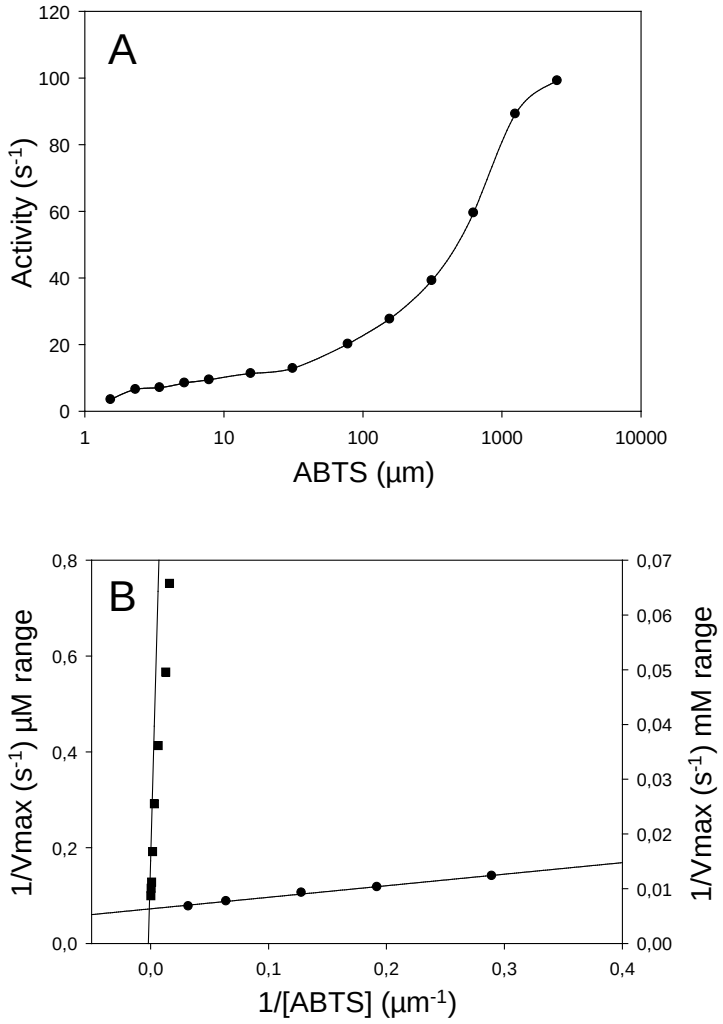

Figure S8. Sigmoidal curve for ABTS oxidation by VP isoenzyme VP1 (A) enabling calculation of two sets of kinetic constants (B) as shown in Table 1.

1. Ruiz-Dueñas FJ, Fernández E, Martínez MJ, Martínez AT: ***Pleurotus ostreatus*** **heme peroxidases: An *in silico* analysis from the genome sequence to the enzyme molecular structure.** *C R Biol* 2011, **334:**795-805.

Additional file 2

Table S1. Inventory of peroxidase genes in the genomes of *P. ostreatus* monokaryons PC9 and PC15 (type, ID, scaffold number and position) and some characteristics of the purified PODs from *E. coli* expression (yield referred to inclusion-body protein, RZ, ε_{406} and PDB entry).

	PC9 (v1.0) genome			PC15 (v2.0) genome			Purified PODs			
Type	ID #	Sc	Position	ID #	Sc	Position	Yield (%)	RZ	ε_{406} (mM^{-1})	PDB
MnP1	137760	2	3291830-3293748	1096331	4	186162-188472	3.3	4.1	149.0	-
MnP2	137764	9	32682-34394	199510	2	1135915-1137627	6.7	3.8	135.0	-
MnP3	137740	3	1767677-1769279	1089546	5	1981555-1983678	13.3	3.9	153.0	-
MnP4	121638	1	2703196-2704913	1099081	1	1827850-1829567	24.0	4.3	135.0	4BM1
MnP5	137765	3	1625766-1627664	199511	5	1840285-1842183	2.7	4.2	167.5	-
MnP6	51713	12	2544215-2545903	1041740	5	2768778-2770466	4.0	4.2	123.0	-
VP1	137757	8	536529-538627	1089895	6	1701105-1704309	28.0	4.3	137.5	4BLK
VP2	137766	8	635476-637382	199491	6	1618102-1620009	5.0	4.1	142.0	-
VP3	123383	2	3246008-3247917	156336	4	212622-214530	14.0	4.0	160.8	-
HTP1	114464	1	3116892-3118095	1110336	1	1483346-1484549	-	-	-	-
HTP2	123372	2	3213565-3214450	1111884	4	262016-262902	-	-	-	-
HTP3	127284	7	560895-561684	1108212	9	535259-536048	-	-	-	-
DyP1	87639	7	191407-193574	62271	9	213879-216064	-	-	-	-
DyP2	115057	2	2850334-2852370	1092668	4	657069-659105	-	-	-	-
DyP3	97865	6	2056440-2058411	52170	7	3196067-3198039	-	-	-	-
DyP4	117204	12	215278-217337	1069077	11	2524348-2526415	-	-	-	-
CCP	77045	3	583621-585384	1096819	5	734156-735921	-	-	-	-

Table S2. Structural properties potentially related to temperature/pH stability in the nine PODs from the *P. ostreatus* genome (JGI references included) - such as distal/proximal Ca^{2+} ligands, number of disulfide bridges, number of proline residues (at different positions), variable loop allowing (or not) the formation of an extra α-helix, and surface charge (number of exposed basic/acidic residues, and pI) - together with experimentally-determined thermal stability ($T_{50\text{-activity}}$ at short and long incubation times) and pH stability range (where enzymes retained >50% activity after 120 h at 4ºC).

	VP1 (137757)	**VP2** (1113241)	**VP3** (156336)	**MnP1**[a] (1096331)	**MnP2** (199510)	**MnP3** (1089546)	**MnP4** (1099081)	**MnP5** (199511)	**MnP6** (1041740)
Distal Ca^{2+} ligands[b]	D48(b/s)	D55(b)	D55(b)	D55(b)	D53(b)	D53(b)	D48(s/b)	D53(b)	D55(b)
	G60(b)	G73(b)	G67(b)	G68(b)	G71(b)	G65(b)	G66(b)	G65(b)	G73(b)
	D62(s)	D75(s)	D69(s)	D70(s)	D73(s)	D67(s)	D68(s)	D67(s)	D75(s)
	S64(s/b)	S77(s)	S71(s)	S72(s)	S75(s)	S69(s)	S70(s)	S69(s)	S77(s)
Proximal Ca^{2+} ligands[b]	S170(b)	T183(b)	T177(b)	S178(b)	S181(b)	S175(b)	S176(b)	T175(b)	T183(b)
	D187(s)	D200(s)	D194(s)	D195(s)	D198(s)	D192(s)	D193(s)	D192(s)	D200(s)
	T189(b/s)	T202(s)	T196(s)	T197(s)	T200(s)	T194(s)	T195(s/b)	T194(s)	T202(s)
	V192(b)	T205(b)	I199(b)	L200(b)	A203(b)	E197(b)	D198(b)	A197(b)	S205(b)
	D194(s)	D207(s)	D201(s)	D202(s)	D205(s)	D199(s)	D200(s)	D199(s)	D207(s)
S-S bridges	4	4	4	4	4	4	4	4	4
Total prolines (t/h/o)[c]	30 (12/4/14)	29 8/4/17	31 (10/5/16)	27 (8/3/16)	25 (8/2/15)	28 (10/3/15)	26 (8/6/12)	31 (12/3/16)	28 (9/3/16)
Pro_{i+1} turn-I[d]	4	3	2	3	2	2	2	4	3
Pro_{i+1} turn-II[d]	2	1	2	2	2	2	1	2	2
Pro_{i} turn-II[d]	1	1	1	1	1	1	1	1	1
Pro_{Ncap} helix[e]	0	1	0	0	1	1	2	1	1
Variable loop	normal	α-helix	normal	normal	α-helix	normal	α-helix	normal	α-helix
Surface basic (H/R/K) residues	4/8/9	4/7/7	5/8/7	5/10/9	5/16/8	5/8/8	4/10/20	3/9/8	5/11/10
Surface acidic (E/D) residues	12/23	11/18	13/21	10/24	14/22	14/23	14/22	15/20	13/21
Measured (predicted) pI	3.81 (4.25)	4.42 (4.47)	4.04 (4.28)	4.25 (4.30)	4.34 (4.56)	4.12 (4.19)	5.35 (5.43)	4.11 (4.28)	4.29 (4.47)
$T_{50\text{-activity}}$ (ºC) at 10 min/4 h	62.8/56.5	53.0/33.0	53.0/48.0	52.8/48.5	53.0/34.0	51.0/46.5	56.8/50.0	49.8/43.5	43.3/37.5
pH range	4-8	4-7	4-8	4-7	5-6	4-7	3-8	4-7	5-6

[a] Described as MnP [1], classified as VP because of the putative catalytic tryptophan [2], and reclassified now as MnP1 because of the catalytic properties in **Table 1**.
[b] (b), coordination to backbone carbonyl; and (s), coordination to side-chain oxygen.
[c] (t/h/o), prolines in β-turns/helices/other secondary structures
[d] Proline residues at i+1 position of Type-I β-turns, and at i and i+1 positions of Type-II β-turns [3].
[e] Proline residues at N-caps of α-helices.

Table S3. Crystallographic data collection and refinement statistics of *P. ostreatus* VP1 and MnP4 (data in parenthesis correspond to the last resolution layer).

	VP1 (137757)	**MnP4** (1099081)
Data collection:		
Space group	$P4_3$	P1
Cell constants	a = b = 96.5, c = 38.4 Å	a = 40.0, b = 75.4, c = 75.6 Å
		$\alpha = 69.8^{\circ}$, $\beta = 75.7^{\circ}$ $\gamma = 75.8^{\circ}$
Resolution range (Å)	50.00 - 1.02 (1.11 - 1.05)	50.00 - 1.10 (1.16 - 1.10)
Nº of total reflections	1717654	939715
Nº of unique reflections	156095	271193
Mosaicity (˚)	0.087	0.171
R_{merge} (%)	6.8 (85.9)	5.3 (54.0)
Completeness (%)	94.3 (66.9)	83.9 (43.0)
$<I/\sigma(I)>$	19.3 (1.2)	13.5 (1.9)
Multiplicity	11.0 (3.5)	3.5 (3.0)
Solvent content (%) / Matthews coef.	49.78 / 2.45	54.16 / 2.68
Subunits per asymmetric unit	1	2
Wilson B factor ($Å^2$)	12.4	12.9
Refinement:		
Resolution range	50.0 - 1.05 Å	50.0 - 1.10 Å
Working reflections	156081	271117
R_{work} / R_{free}	13.0 / 13.7 %	13.1 / 14.7 %
Protein atoms (non H)	2445	5277
Heme group	1	2
Ca^{2+}	2	4
Water molecules	452	1212
SO_4 / Citrate ions	-	21 / 2
Mean B factors ($Å^2$)		
Protein atoms (non H)	12.06	10.81
Heme group	7.47	8.24
Ca^{2+}	8.49	6.59
Water molecules	24.10	23.14
SO_4 / Citrate ions	-	25.86 / 13.51
Deviations from ideality		
rmsd bond lengths	0.008 Å	0.016 Å
rmsd angles	1.288º	1.710º
Ramachandran plot statistics		
Preferred %	98.48	98.36
Allowed %	1.52	1.64
Outliers %	0.00	0.00
PDB entry	4BLK	4BM1

Table S4. Kinetic constants (K_m, µM; k_{cat}, s^{-1}; and k_{cat}/K_m, s^{-1}·mM^{-1}) of W165, E35A, E39A, D175A and E35A/E39A variants of *P. ostreatus* VP1 oxidizing VA, RB5 and Mn^{2+}, compared with native VP1.[a]

		VP1 (137757)	W164A (137757)	E35A (137757)	E39A (137757)	D175A (137757)	E35AE39A (137757)
VA	K_m	5500±46	-[b]	5700±46	5450±61	5613±28	5325±46
	k_{cat}	12.7±0.5	0	12.5±0.9	11.9±0.8	12.8±0.6	12.9±0.5
	k_{cat}/K_m	2.3±0.2	0	2.2±0.2	2.2±0.3	2.3±0.3	2.4±0.1
RB5	K_m	5.4±0.2	-	4.9±0.1	5.3±0.2	5.6±0.3	5.4±0.2
	k_{cat}	12.9±0.3	0	12.1±0.4	13.2±0.3	12.7±0.4	12.6±0.3
	k_{cat}/K_m	2380±50	0	2469±36	2490±89	2267±44	2333±65
Mn^{2+}	K_m	98±5.6	134±14	ns[c]	ns	ns	-
	k_{cat}	185±2.6	279±15	ns	ns	ns	0
	k_{cat}/K_m	1900±90	2082±120	3.1±0	2.8±0	1±0	0

[a]Kinetic constants were estimated at 25 °C in 0.1 M tartrate, pH 3 for VA, pH 3.5 for RB5, and pH 5 for Mn^{2+} (means and 95% confidence limits).
[b]Dashes correspond to undetermined K_m values when no activity was detected (k_{cat} 0).
[c]ns, K_m and k_{cat} not determined because of non-saturation of the enzyme (but k_{cat}/K_m estimated from slope of observed activity *vs* substrate concentration).

Table S5. Kinetic constants (K_m, µM; k_{cat}, s^{-1}; and k_{cat}/K_m, s^{-1}·mM^{-1}) of E36A, E40A, D179A and E36A/E40A variants of *P. ostreatus* MnP4 oxidizing Mn^{2+}, compared with native MnP4.[a]

		MnP4 (1099081)	E36A (1099081)	E40A (1099081)	D179A (1099081)	E35A/E39A (1099081)
Mn^{2+}	K_m	88±4	-[b]	-	-	-
	k_{cat}	125±2	0	0	0	0
	k_{cat}/K_m	1410±60	0	0	0	0

[a]Kinetic constants were estimated at 25 °C in 0.1 M tartrate, pH 5 (means and 95% confidence limits).
[b]Dashes correspond to undetermined K_m values when no activity was detected (k_{cat} 0).

Table S6. Kinetic constants (K_m, µM; k_{cat}, s^{-1}; and k_{cat}/K_m, s^{-1}·mM^{-1}) of two variants in the environment of Trp165 of *P. ostreatus* MnP1, compared with the native MnP1, VP1, and a related POD from *P. pulmonarius* (GenBank AAX40734), oxidizing VA, RB5, ABTS, DMP and Mn^{2+}.[a]

		MnP1 (1096331)	**D261G** (MnP1 variant)	**I198F** (MnP1 variant)	**VP1** (137757)	**VP** *P. pulmonarius*
VA	K_m	-[b]	-	-	5500±46	-
	k_{cat}	0	0	0	12.7±0.5	0
	k_{cat}/K_m	0	0	0	2.3±0.2	0
RB5	K_m	-	-	2.3±0.4	5.4±0.2	-
	k_{cat}	0	0	10.0±0.8	12.9±0.3	-
	k_{cat}/K_m	0	0	4270±410	2380±50	0
ABTS[c]	K_m	111±18	185 ±16	496±95	4.0±0.4 (605±81)	33.1±0.4
	k_{cat}	90±8	94 ±6	85±7	14.4±0.4 (126±5)	13.4±0.4
	k_{cat}/K_m	803±7	508 ±19	172±19	3600±20 (209±21)	403±34
DMP	K_m	0	ns[d]	ns	54±4 (45100±3600)	35200±13300
	k_{cat}	0	ns	ns	6.6±0.1 (98±4)	17.4±4.0
	k_{cat}/K_m	-	<0.1	<0.1	122±7 (2.2±0.1)	0.5±0
Mn^{2+}	K_m	7±1	6.8 ±0.2	4.6 ±0.5	98±5.6	487±70
	k_{cat}	9±0	7.8±1.4	5.8±0.1	185±2.6	5.8±0.3
	k_{cat}/K_m	1200±80	1147 ±106	1261±97	1900±90	12±0

[a]Kinetic constants were estimated at 25 °C in 0.1 M tartrate, pH 3 for VA, pH 3.5 for RB5, DMP and ABTS, and pH 5 for Mn^{2+} (means and 95% confidence limits).
[b]Dashes correspond to undetermined K_m values when no activity was detected (k_{cat} 0).
[c]ABTS and DMP oxidation by VP1 showed biphasic kinetics enabling determination of a second set of constants (parenthesis) characterized by a low enzyme affinity.
[d]ns, K_m and k_{cat} not determined because of non-saturation of the enzyme (but k_{cat}/K_m estimated from slope of observed activity *vs* substrate concentration).

Table S7. Amino-acid sequence identities between the nine PODs from the *P. ostreatus* genome, *P. chrysosporium* LiP and MnP, and two *P. eryngii* VPs (the number of residue pairs considered for each comparison is shown in parenthesis).

	***P. chrysosporium* LiPH8** (Y00262)	***P. chrysosporium* MnP1** (Q02567)	***P. eryngii* VPL** (AF007224)	***P. eryngii* VPS1** (AAD54310)	**MnP6** (1041740)	**MnP5** (199511)	**MnP4** (1099081)	**MnP3** (1089546)	**MnP2** (199510)	**MnP1** (1096331)	**VP3** (156336)	**VP2** (1113241)	**VP1** (137757)
VP1 (137757)	57% (344)	52% (338)	97% (331)	71% (325)	70% (330)	77% (328)	63% (337)	77% (318)	65% (324)	65% (325)	79% (318)	71% (325)	100% (331)
VP2 (1113241)	57% (341)	53% (336)	73% (338)	98% (339)	65% (338)	73% (338)	60% (337)	70% (325)	63% (327)	62% (326)	81% (325)	100% (339)	-
VP3 (156336)	55% (340)	51% (333)	78% (331)	74% (325)	70% (330)	73% (331)	59% (337)	76% (318)	60% (324)	80% (332)	100% (331)	-	-
MnP1 (1096331)[a]	53% (341)	50% (338)	69% (330)	65% (325)	56% (325)	67% (332)	53% (335)	68% (319)	53% (324)	100 332	-	-	-
MnP2 (199510)	54% (344)	52% (334)	67% (337)	63% (327)	78% (324)	64% (337)	69% (336)	66% (324)	100% (338)	-	-	-	-
MnP3 (1089546)	61% (340)	56% (338)	77% (331)	69% (325)	64% (337)	78% (331)	63% (337)	100% (331)	-	-	-	-	-
MnP4 (1099081)	55% (339)	50% (342)	63% (337)	61% (324)	71% (325)	61% (334)	100% (337)	-	-	-	-	-	-
MnP5 (199511)	60% (341)	55% (333)	77% (328)	71% (325)	63% (325)	100 (335)	-	-	-	-	-	-	-
MnP6 (1041740)	55% (340)	48% (336)	67% (338)	62% (326)	100% (338)	-	-	-	-	-	-	-	-
***P. eryngii* VPS1** (AAD54310)	57 (341)	53% (337)	73% (338)	100% (339)	-	-	-	-	-	-	-	-	-
***P. eryngii* VPL** (AF007224)	56% (344)	53% (338)	100% (331)	-	-	-	-	-	-	-	-	-	-
***P. chrysosporium* MnP1** (Q02567)	47% (343)	100% (357)	-	-	-	-	-	-	-	-	-	-	-
***P. chrysosporium* LiPH8** (Y00262)	100% (344)	-	-	-	-	-	-	-	-	-	-	-	-

[a] Described as MnP [1], classified as VP because of the putative catalytic tryptophan [2], and reclassified now as MnP1 because of the catalytic properties in **Table 1**.

1. Asada Y, Watanabe A, Irie T, Nakayama T, Kuwahara M: **Structures of genomic and complementary DNAs coding for *Pleurotus ostreatus* manganese (II) peroxidase.** *Biochim Biophys Acta* 1995, **1251:**205-209.
2. Ruiz-Dueñas FJ, Fernández E, Martínez MJ, Martínez AT: ***Pleurotus ostreatus* heme peroxidases: An *in silico* analysis from the genome sequence to the enzyme molecular structure.** *C R Biol* 2011, **334:**795-805.
3. Fu HL, Grimsley GR, Razvi A, Scholtz JM, Pace CN: **Increasing protein stability by improving β-turns.** *Proteins* 2009, **77:**491-498.

Material Suplementario

Capítulo 4

"**Ligninolytic peroxidase gene expression by *Pleurotus ostreatus*: Differential regulation in lignocellulose medium and effect of temperature and pH"**
Fernández-Fueyo, E., R. Castanera, F. J. Ruiz-Dueñas, M. F. López-Lucendo, L. Ramírez, A. G. Pisabarro, and A. T. Martínez.
Fungal Genet. Biol. 2014.

Supplemental Information

Differential expression of ligninolytic peroxidase genes by *Pleurotus ostreatus* growing on lignocellulose medium under different environmental conditions

Elena Fernández-Fueyo[a], Raul Castanera[b], Francisco J. Ruiz-Dueñas[a], Maria F. López-Lucendo[a], Lucia Ramírez[b], Antonio G. Pisabarro[b] and Angel T. Martínez[a,]

[a]*Centro de Investigaciones Biológicas, CSIC, Ramiro de Maeztu 9, E-28006 Madrid, Spain*
[b]*Department of Agarian Production, Genetics and Microbiol Research Group, Universidad Pública de Navarra, E-31006 Pamplona, Spain*

Supplemental Information includes a section on the promoter region of the ligninolytic peroxidase genes, the peroxidase peptide sequences identified in the secretome of *P. ostreatus* (**Table S1**), a list of putative regulatory elements in the different promoters (**Table S2**), the N-terminal sequence identity of the peroxidase purified from lignocellulose cultures (**Table S3**), the crossing point distribution of ten candidate reference genes at different temperature and pH conditions (**Fig. S1**), the expression stability of these ten genes using GeNorm and Normfinder (**Fig. S2**), the complete heatmap and dendrograms of gene expression after changing the temperature and pH conditions (**Fig. S3**), and the relative expression of the nine ligninolytic peroxidase genes at different times after changing the incubation conditions (**Fig. S4**) and the same information excluding *mnp3* (**Fig. S5**).

S.1. Analysis of the promoter region of the ligninolytic peroxidase genes in the P. ostreatus *genome*

An *in silico* study of the promoter regions of the nine ligninolytic peroxidase genes in the *P. ostreatus* (PC9) genome, highlighted the presence of many regulatory elements differentially distributed between the promoters analyzed (**Table S2**). Each of the promoters consists of one unique TATA element upstream of the ATG codon. In addition, the promoter region of all the peroxidase genes contains a minimum of one direct CAAT motif (the binding site for transcriptional factors) except in the case of *mnp3, mnp4* and *vp3*, together with at least one inverted CAAT motif (ATTGG) upstream of the transcriptional initiation site. CAAT boxes occur upstream by 39-872 bases to the initial transcription site and are typically accompanied by a conserved consensus sequence.

Besides the regulatory TATA and CAAT boxes, suggested MREs, HSEs and XREs were identified in some of the promoters of the ligninolytic peroxidase genes. HSEs are the most extended elements present in all the promoters regions except in genes *vp3* and *mnp1*. In the case of MREs, genes *mnp6, vp1,* and *vp3* present only one, while the *vp2* promoter contains two of them. On the other hand, the presence of XREs is limited to genes *vp2* and *mnp3*.

The promoter region also contains putative recognition sites for the general transcription factor SP-1 in all ligninolytic peroxidase gene promoters except in *mnp2* promoter. In the majority of the peroxidase gene promoters more than one SP-1 transcription factors is present (two in *mnp1, mnp4, mnp5, vp1*, and three in *vp2*). The *mnp2* promoter lacks SP-1, but presents a putative recognition site for the activator protein AP-1 and one for AP-2, which may be involved in regulation by the availability nutrient nitrogen level. GATA factor, is also a nitrogen regulatory element, and surprisingly is only present in *vp* promoters. Moreover, the carbon regulatory element, CRE-A, is only present in gene *vp1*.

Table S1
Ligninolytic peroxidase peptide sequences identified in the extracellular and intracellular proteomes of *P. ostreatus* (PC9) growing in lignocellulose medium under standard conditions. Those peptides present in both proteomes are marked (*).

Peroxidase	Peptide sequences	Identified ions	Length (aa)
Extracellular			
VP1	IPFFLGRPDAVAASPDHLVPEPFDSVDTILAR	93	32
	DPQTAcEWQSMVNNQPK (*)	8	17
	DPQTAcEWQSmVNNQPK (*)	9	17
	MGDAGFSAVEVVWLLASHSIAAADK	13	26
	mGDAGFSAVEVVWLLASHSIAAADK	3	26
	LFPGTPDNKGEVQSPLQGEIR (*)	6	21
	GEVQSPLQGEIR	10	12
	MALLGQDK	3	8
	mALLGQDK	3	8
	Total	*148*	
VP2	SAcEWQSMVNNmPK	1	14
	SAcEWQSMVNNMPK	2	14
	LNFFLGRPDATQIPPDGLVPEPFDSVDK (*)	10	26
	FTQVMR	1	6
	Total	*14*	
MnP2	LTDcSDVIPVPQVR (*)	3	14
	LTKPVTIPAGR (*)	5	11
	LATLGQVR	2	8
	IQSDFLLAR	3	8
	Total	*15*	
MnP6	GQSLSPIPGEFR	16	12
	SLADIEAAcR (*)	6	10
	TAcEWQSFITDHASMVSK	1	18
	MSTLGQIR	2	8
	mSTLGQIR	2	8
	IPFHAGR	1	7
	ALLTDcSDVIPVPK	1	14
	Total	*29*	
VP3	GTSFPGSGGNHGEVESPLAGEIR (*)	3	23
	Total	*3*	*23*
MnP3	IQSDHDLAR	4	9
	Total	*4*	
MnP5	GTSFPGTAGNQGEVESPLR	2	19
	Total	*2*	
Intracellular			
VP1	DPQTAcEWQSMVNNQPK (*)	2	17
	DPQTAcEWQSmVNNQPK (*)	2	17
	LFPGTPDNKGEVQSPLQGEIR	6	21
	VDPSIPGTPFDSTPGVFDSQFFIETQLK	1	28
	Total	*11*	
VP2	KLSLLGHNQADLIDcSDVIPVPK	1	23
	LNFFLGRPDATQIPPDGLVPEPFDSVDK (*)	1	28
	LSLLGHNQADLIDcSDVIPVPK	1	22
	Total	*3*	
MnP2	LTDcSDVIPVPQVR (*)	1	14
	LTKPVTIPAGR (*)	1	11
	Total	*2*	
VP3	AASPIGLVPEPFDTVTDILDR	1	21
	GTSFPGSGGNHGEVESPLAGEIR (*)	2	23
	Total	*3*	
MnP3	GTAFPGVGGNQGEVESPLAGEIR	1	23
	LIDcSDVIPVPKPLQSK	1	17
	TAcEWQSFVNNQAK	1	14
	Total	*3*	
MnP6	LTSDFLLAR	2	9
	SLADIEAAcR (*)	1	10
	Total	*3*	

Table S2

Localization of putative regulatory elements in the promoter regions of the nine ligninolytic peroxidase genes in the genome of *P. ostreatus*.

gene	TATA	ATTG (CAAT)	SP-1	AP-1	AP-2	HSE	MRE	XRE	CRE-A	GATA
mnp1	-70	-581, -147 -843	-430 GGGAT -20 ACTGC-20							
mnp2	-69	-810, -872, -148		-614 TGACTCA	-84 TGGGGA	-656 CGAATTC				
mnp3	-58	-127	-440 ACTGC			-525 C-GAA-TT				
mnp4	-80	-918, -795, -374	-850 ACTGC -234 GGGAT			-512 C-GAA-TT				
mnp5	-120	-837, -39 -258, -96	-526 ACTGC -597 GGGAT			-537 C-GAA-TTC				
mnp6	-84	-343, -162 -579, -193	-763 GGGAT			-992 GAA-TTC	-44 TGCTCTC			
vp1	-59	-342, 390 -106	-114 GGGAT -662, -1 ACTGC			-879, -772 C-GAA-TT	-531 TGCACTC		-385 CCGGGG	-798, -457 TGATAA
vp2	-55	-659, -387 -81	-842 GGGAT -287, -181 ACTGC			-29 GAA-TTC	-922 TGCTCTC -113 TGCACAC	-874 TCACGG		-371 TGATAG
vp3	-69	-841, -86	-662, -1 ACTGC				-335 TGCACAC			-855 TGATAG

Table S3
Predicted N-termini of nine ligninolytic peroxidases from the *P ostreatus* (PC9) and identity with the N-terminus of the main peroxidase found in lignocellulose cultures (cysteine residues excluded).

Protein	N-terminal sequences	Identity
VP1 (137757)	ATCADGRTTANAACCVLFPILDDIQ	100%
VP2 (137766)	VTCATGQTTANEACCALFPILEDIQ	73%
VP3 (123383)	ATCAGGQVTANAACCVLFPILEDLQ	77%
MnP1 (137760)	ATCAGGQVTANAACCVLFPLMEDLQ	68%
MnP2 (137764)	VTCSGGRTTSDASCCVWFDVLDDIQ	59%
MnP3 (137740)	ATCADGRTTANAACCVLFPILDDIQ	100%
MnP4 (121638)	AKCSKGRTASNDACCVWFDVLDDIQ	64%
MnP5 (137765)	ATCADGNTVTNAACCVLFPILEDIQ	86%
MnP6 (51713)	ATCSGGRTTAHASCCIWFDVLDDIQ	73%

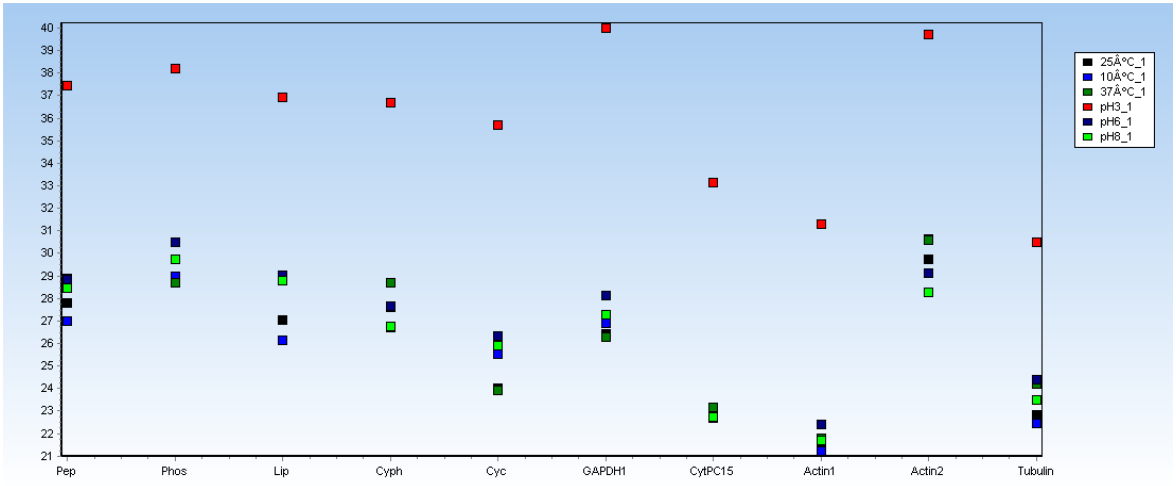

Fig. S1. Crossing point distribution of ten candidate reference genes after 1 h treatment of *P. ostreatus* cultures under different temperature (10 ºC, 25.5 ºC and 37 ºC) and pH (3, 6 and 8) conditions. Genes (IDs in PC9 V1.0): Pep (115017), Phos (49690), Lip (75430), Cyph (72928), Cyc (86026), GAPDH1 (88005), CytPC15 (112752), Actin1 (114148), Actin2 (90915) and Tubulin (117235).

A

Gene	M-value
Pep	0.4567
Actin1	0.4567
Cyph	0.5668
CytPC15	0.6308
Phos	0.7459
Lip	0.8540
Tubulin	0.9188
Cyc	1.0081
Actin2	1.0783
GAPDH1	1.2087

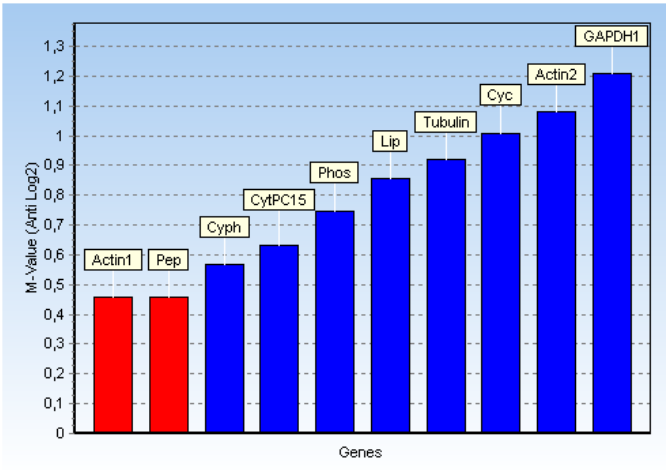

B

Gene	SD	Acc. SD
Actin1	0.2284	0.2284
Pep	0.3589	0.2127
CytPC15	0.5251	0.2253
Cyph	0.6338	0.2316
Phos	0.6933	0.2314
Cyc	0.9972	0.2546
Lip	1.0381	0.2638
Actin2	1.1405	0.2713
Tubulin	1.1627	0.2736
GAPDH1	1.6250	0.2950

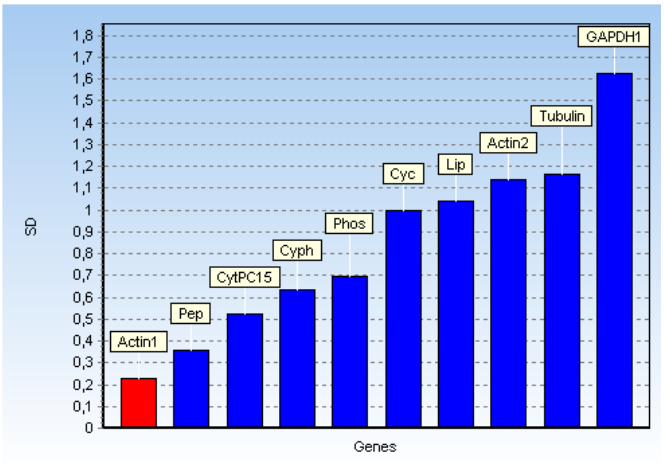

C

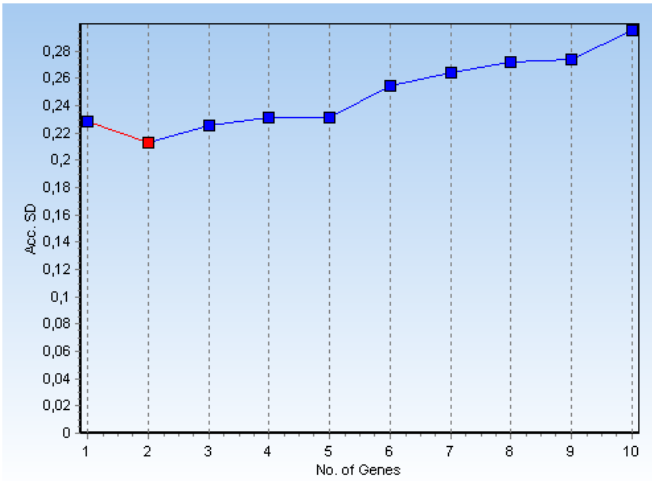

Fig. S2. Evaluation of the expression stability of ten candidate genes using GeNorm (**A**) and Normfinder (**B**) including the accumulated standard deviations (Acc. SD) at increasing number of reference genes (**C**). Red bars represent genes with better expression stability. Red square indicates the ideal number of reference genes. See **Fig. S1** legend for full gene names.

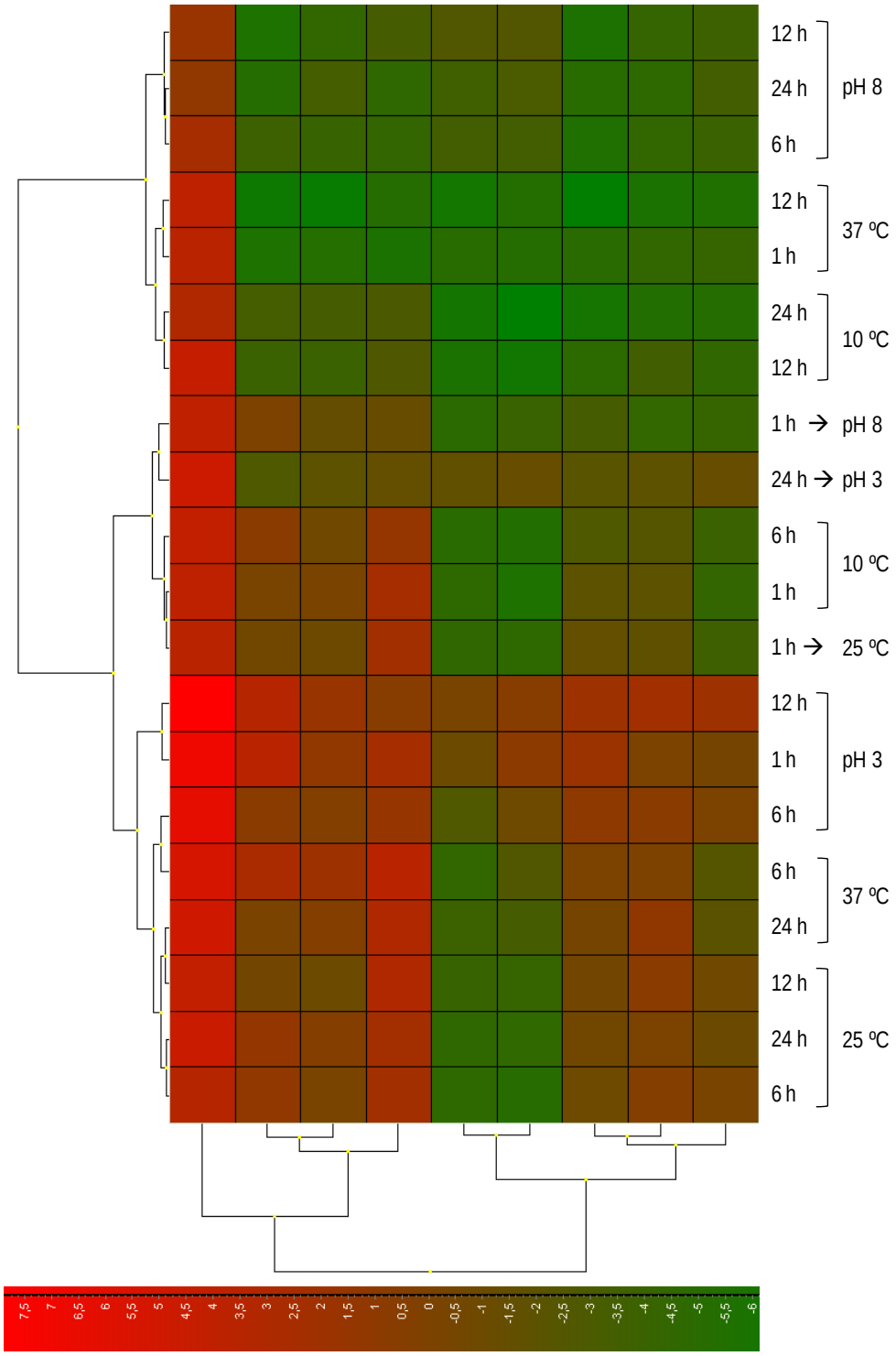

Fig. S3. Complete heatmap showing the transcriptional levels of the nine ligninolytic peroxidase genes of *P. ostreatus* at four sampling times (1, 6, 12 and 24 h) after changing the temperature (to 10 ºC and 37 ºC) and pH (3 and 8) conditions compared with the standard conditions (25 ºC and pH 5.5) and dendrograms showing gene and conditions groups according to the above expression results (**Fig. S3**).The pH 3 expression values are in a different scale.

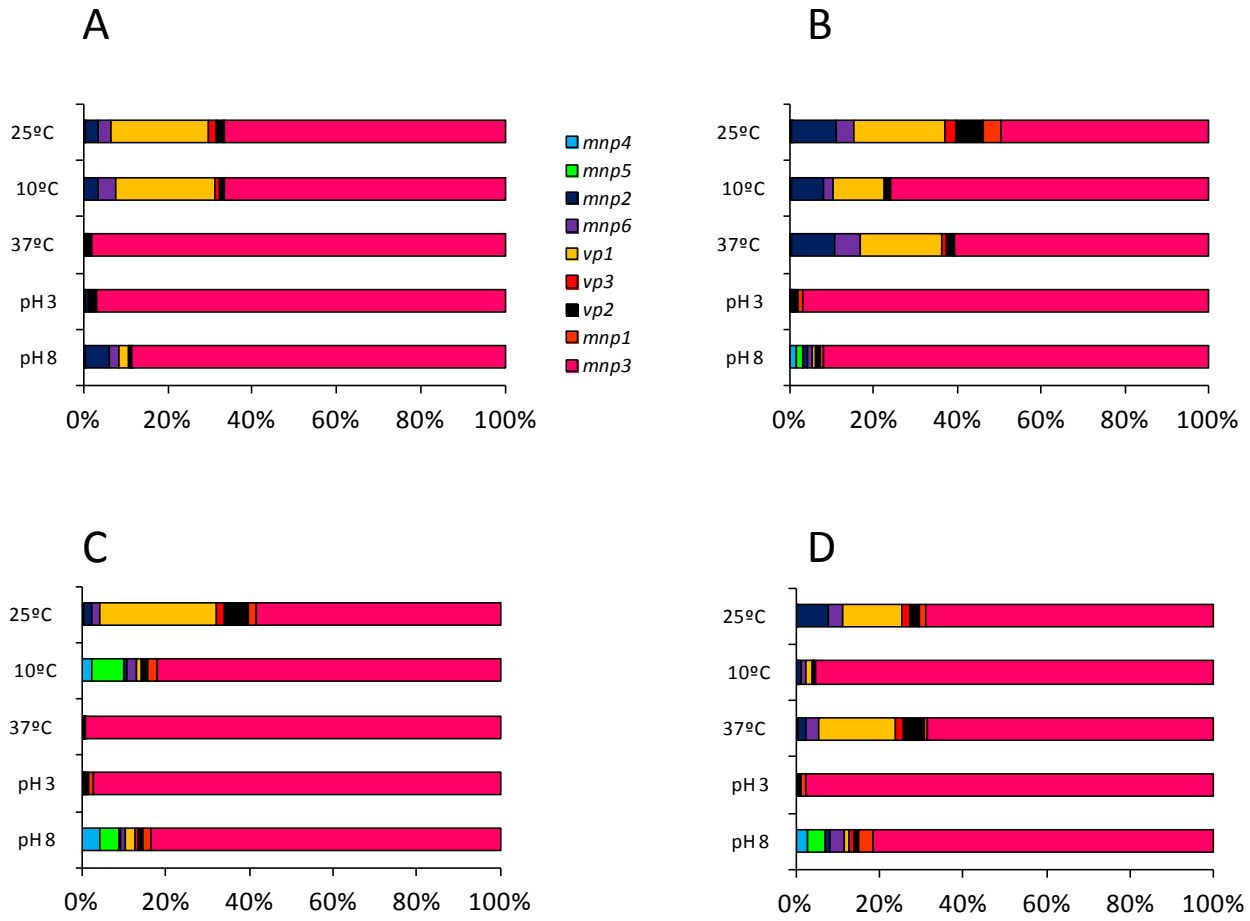

Fig. S4. Relative expression of the nine *P. ostreatus* ligninolytic peroxidase genes (as percentage of the total expression) at different times after changing the incubation (temperature and pH) conditions. **A**) 1 h. **B**) 6 h. **C)** 12 h. **D**) 24 h.

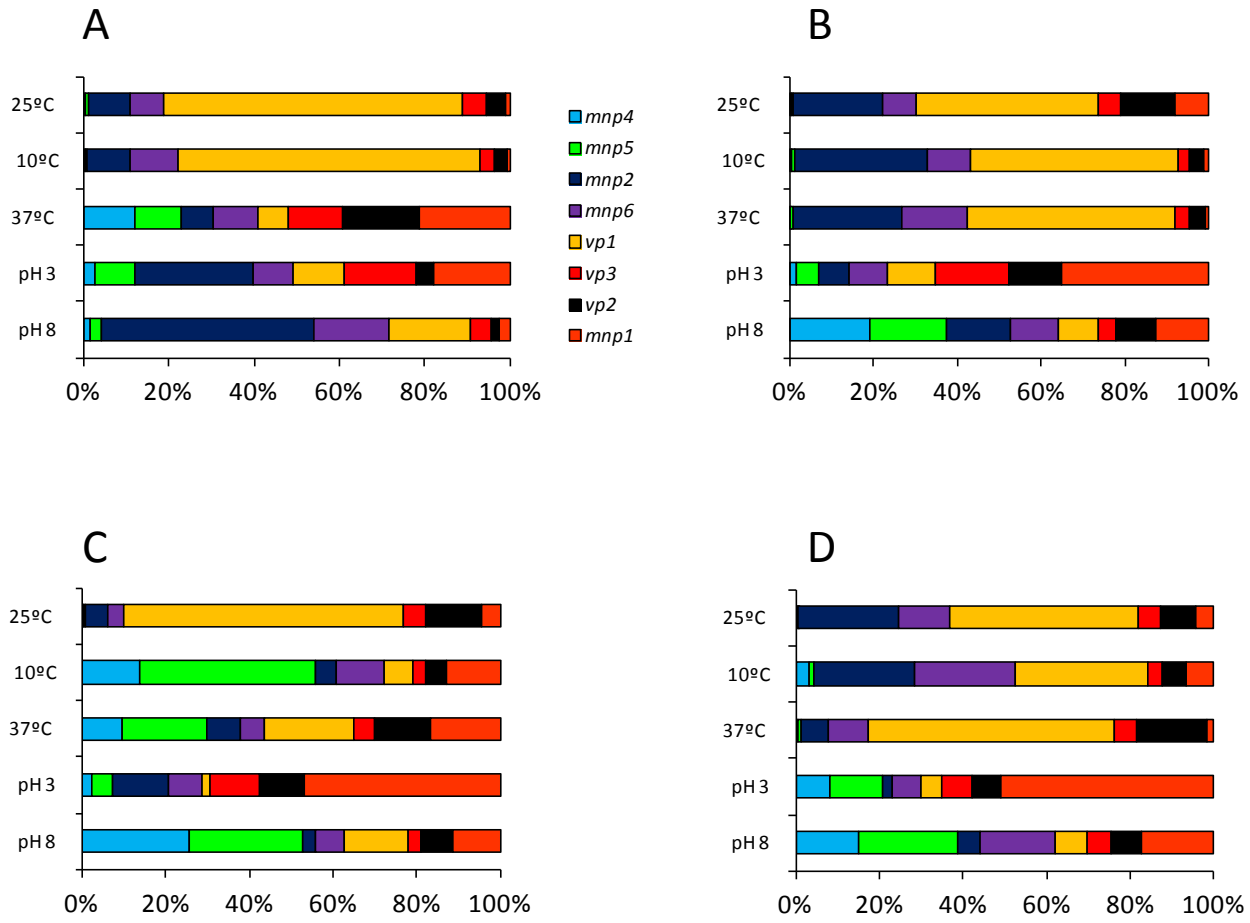

Fig. S5. Relative expression of eight *P. ostreatus* ligninolytic peroxidase genes (*mnp3* excluded) at different times after changing the incubation (temperature and pH) conditions (as percentage of the total expression). **A**) 1 h. **B**) 6 h. **C)** 12 h. **D**) 24 h.

Material Suplementario

Capítulo 5

"Comparative genomics of *Ceriporiopisis subvermispora* and *Phanerochaete chrysosporium* provide insight into selective ligninolysis"

Fernández-Fueyo, E., F. J. Ruiz-Dueñas, P. Ferreira, D. Floudas, D. S. Hibbett, P. Canessa, L. Larrondo, T. Y. James, D. Seelenfreund, S. Lobos, R. Polanco, M. Tello, Y. Honda, T. Watanabe, T. Watanabe, J. S. Ryu, C. P. Kubicek, M. Schmoll, J. Gaskell, K. E. Hammel, F. J. St.John, A. Vanden Wymelenberg, G. Sabat, S. S. Bondurant, K. Syed, J. Yadav, H. Doddapaneni, V. Subramanian, J. L. Lavín, J. A. Oguiza, G. Perez, A. G. Pisabarro, L. Ramírez, F. Santoyo, E. Master, P. M. Coutinho, B. Henrissat, V. Lombard, J. K. Magnuson, U. Kües, C. Hori, K. Igarashi, M. Samejima, B. W. Held, K. Barry, K. LaButti, A. Lapidus, E. Lindquist, S. Lucas, R. Riley, A. Salamov, D. Hoffmeister, D. Schwenk, Y. Hadar, O. Yarden, R. P. de Vries, A. Wiebenga, J. Stenlid, D. C. Eastwood, I. V. Grigoriev, R. Berka, R. A. Blanchette, P. Kersten, A. T. Martínez, R. Vicuña, and D. Cullen.

Proc. Natl. Acad. Sci. USA 109:5458-5463. 2012.

III. Oxidative systems potentially involved in lignin degradation

IIIA. Heme peroxidases in the *C. subvermispora* genome

i. Manual annotation of the different peroxidase gene models. A preliminary screening of the automatically-annotated genome of *C. subvermispora* was performed using the Advanced Search option ("peroxidase" as search term) at the JGI web-site, and forty-four gene models were initially identified. Then, a sequence-by-sequence exhaustive analysis revealed that only twenty-six of the above gene models encode heme peroxidases.

These could be classified into four different groups (after amino acid sequence alignment and detection of characteristic amino acid residues specific for each group) corresponding to classical families and recently described superfamilies, as follows: **i)** Cytochrome *c* peroxidase (CCP) (1 model, Cesubv83438); **ii)** Ligninolytic peroxidases (15 models), including twelve typical "long" manganese peroxidases (MnP) (Cesubv49863, Cesubv50297, Cesubv50686, Cesubv94398, Cesubv105539, Cesubv114036, Cesubv114076, Cesubv116608, Cesubv117436, Cesubv139965, Cesubv143390, Cesubv157986) specific for Mn^{2+} and one "short" MnP (Cesubv124076) also able to oxidize phenols and ABTS in the absence of Mn^{2+} and evolutionarily more related to lignin peroxidases (LiP) and versatile peroxidases (VP) than to the classical long MnPs (3), one putative VP (Cesubv99382) and one putative LiP (Cesubv118677); **iii)** "Low redox-potential" peroxidase (one model, Cesubv112162); and **iv)** Heme-thiolate peroxidase/ peroxygenases (chloroperoxidase/aromatic peroxygenase, CPO/APO, type enzymes) (nine models, Cesubv80799, Cesubv81391, Cesubv114787, Cesubv114799, Cesubv115079, Cesubv115379, Cesubv118102, Cesubv121474, Cesubv122198).

Classification of the 15 ligninolytic peroxidases as LiP, MnP and VP was made on the basis of amino acid residues at their respective active center and substrate oxidation sites after homology modeling, using related crystal structures as templates and programs implemented by the automated protein homology modeling server "SWISS-MODEL" (17).

ii. Comparison with other basidiomycete peroxidases. Heme peroxidase gene models in the *C. subvermispora* genome were aligned with 107 basidiomycete and 2 ascomycete heme peroxidase protein sequences, and theoretical molecular structures for selected peroxidases were examined (Figure S2**)**. This was followed by an analysis of the evolutionary relationships among all the basidiomycete heme peroxidases described to date, where the positions of the 26 gene models from the *C. subvermispora* genome were compared.

The dendrogram (Figure S3) shows: **i)** A large cluster containing all the ligninolytic peroxidases (a total of 90 including LiP, MnP, VP - most of them included in compressed sub-trees - and a few related sequences described with different names) together with five generic peroxidases (putative low redox-potential enzymes) from *Coprinopsis cinerea*, *Coprinellus disseminatus*, *P. placenta,* the so-called NOPA peroxidase identified in the genome of *P. chrysosporium* and *C. subvermispora* Cesubv112162 found in the *C. subvermispora* genome; **ii)** The dye-decolorizing peroxidases (DyP) sub-tree (formed by 14 peroxidases from *Pleurotus ostreatus*, *Marasmius scorodonius*, *Bjerkandera adusta*, *Termitomyces albuminosus* and

Polyporus sp.; **iii)** The group of APO/CPO-type heme-thiolate peroxidases including the *Agrocybe aegerita* APO and related enzymes from *P. chrysosporium* and *Agaricus bisporus*, as well as peroxidases recently reported for the first time in the genome of *Pleurotus ostreatus* (Ruiz-Dueñas et al., submitted) and now in the genome of *C. subvermispora* where nine gene models of this peroxidase superfamily were localized (unexpectedly, the related *Leptoxyphium fumago* CPO did not fit in this cluster); and **iv)** a group of evolutionarily distant peroxidases formed by CCPs, including one model from *C. subvermispora* not related with the previous ones.

A closer view of the ligninolytic peroxidase cluster is also shown in Figure S3**.** The structural-functional classification based on the presence of a Mn^{2+}-oxidation site and/or a catalytic tryptophan, previously used to classify the *C. subvermispora* ligninolytic peroxidase genes, is extended here to all the 90 basidiomycete peroxidases described to date (the presence of a catalytic tyrosine in a *Trametes cervina* LiP is also indicated).

In this expanded dendrogram, typical "long" MnPs (from *Lentinus edodes*, *Ceriporiopsis rivulosa, C. subvermispora, Dichomitus squalens, P. chrysosporium, Phanerochaete sordida, Phlebia radiata* and an unidentified basidiomycete) form a large and homogeneous cluster clearly separated from the rest of ligninolytic peroxidases, all of them exhibiting a shorter C-terminal tail. By contrast, VP, LiP and "short" MnPs seem to have divergent and recurrent evolution pathways. Peroxidases Cesubv118677 and Cesubv99382 seem to represent transition states of these evolutionary processes, not only by their position in the dendrogram but also by their catalytic properties, as discussed below.

iii. Heterologous expression and purification of *C. subvermispora* peroxidases

Following careful inspection and revision of automated annotations, three *C. subvermispora* genes were selected for *Escherichia coli* expression; putative VP (Cesubv99382), LiP (Cesubv118677) and MnP (Cesubv117436). The latter exhibited the highest induction levels in medium containing ball-milled aspen versus glucose as sole carbon source (main text Figure 1). The precise positions of introns were determined by comparison with other known ligninolytic peroxidase genes, and the corresponding cDNA sequences were synthesized (ATG-Biosynthetics). The synthesized cDNAs coding for the mature proteins were cloned into the pFLAG1 expression vector under the control of the IPTG-inducible *tac* promoter. The enzymes were overexpressed in *E. coli* W3110, and SDS-PAGE analysis of the cell extracts showed accumulation of the recombinant peroxidases in the insoluble fraction containing the inclusion bodies. The proteins were subsequently activated *in vitro* under conditions previously optimized for *P. eryngii* VP (18). Direct veratryl alcohol (VA) oxidation was measured to check the activity of peroxidases in the refolding mixtures confirming enzyme activation. Then, the enzymes were purified to homogeneity using an anion exchange column (Resource Q from GE Healthcare). Finally, their molar extinction coefficients at the absorption maximum of the Soret band (407 nm) were determined.

LiP from *P. chrysosporium* (isoenzyme LiPH8) and VP from *P. eryngii* (isoenzyme VPL) were also expressed in *E. coli* and purified for comparison with the *C. subvermispora* peroxidases, after *E. coli* expression and *in vitro* activation following the protocols of Doyle and Smith (19) and Pérez-Boada *et al*. (18) respectively.

iv. Enzyme characterization. Oxidation of three representative substrates, namely Mn^{2+}, and high redox-potential veratryl alcohol (VA) and Reactive Black 5 (RB5), by both recombinant peroxidases were investigated under steady-state conditions. The corresponding steady-state kinetic constants were compared with those of *P. eryngii* VP and *P. chrysosporium* LiP produced by this method (main text Table 1).

As described in the main text, Cesubv118677 could not oxidize Mn^{2+} as expected according to the absence of a typical manganese oxidation site in its theoretical molecular structure (Figure S2A)**.** Surprisingly, Cesubv99382, tentatively identified as a VP, was also not able to oxidize Mn^{2+}, even though a typical manganese oxidation site is predicted in its structural model (Figure S2C).

Typical VPs and MnPs oxidizing Mn^{2+} do not include an acidic residue contiguous to the aspartate forming the manganese binding site, whereas Cesubv99382 presents a glutamic acid at the corresponding position. Typical LiPs, unable to oxidize Mn^{2+}, exhibit an acidic residue at an equivalent position. Effective transformation of LiP into MnP have been obtained by removing this acidic residue, in addition to introducing the corresponding aspartic acid at the manganese binding site (20).

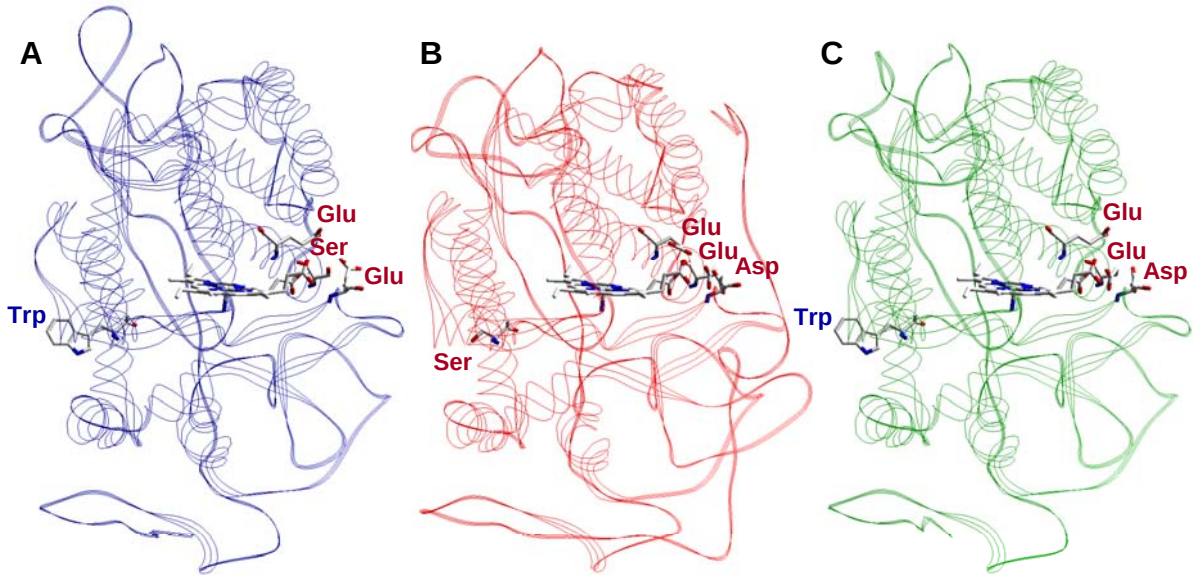
A
Glu
Ser
Glu
Trp
B
Glu
Glu
Asp
Ser
C
Glu
Glu
Asp
Trp

Figure S2. Homology-based molecular models of three *C. subvermispora* peroxidases were obtained automatically using *Pleurotus ostreatus* VP and *P. chrysosporium* MnP crystal structures (PDB entries 2BOQ and 3M5Q, respectively) as templates. **A)** LiP-type model **(**Cesubv118677) including an exposed tryptophan potentially involved in oxidation of high redox-potential substrates; **B)** MnP-type model (Cesubv 117436) including a putative Mn^{2+} oxidation site (formed by two glutamates and one aspartate); and **C)** VP-type model (Cesubv99382) including both putative catalytic sites described in **A** and **B**. Note that a serine residue in the LiP-type model occupies the position of one of the two catalytic glutamates involved in Mn^{2+} oxidation in the MnP and VP-type models. Another serine residue occupies the position of the putative catalytic tryptophan present in the LiP and VP-type models.

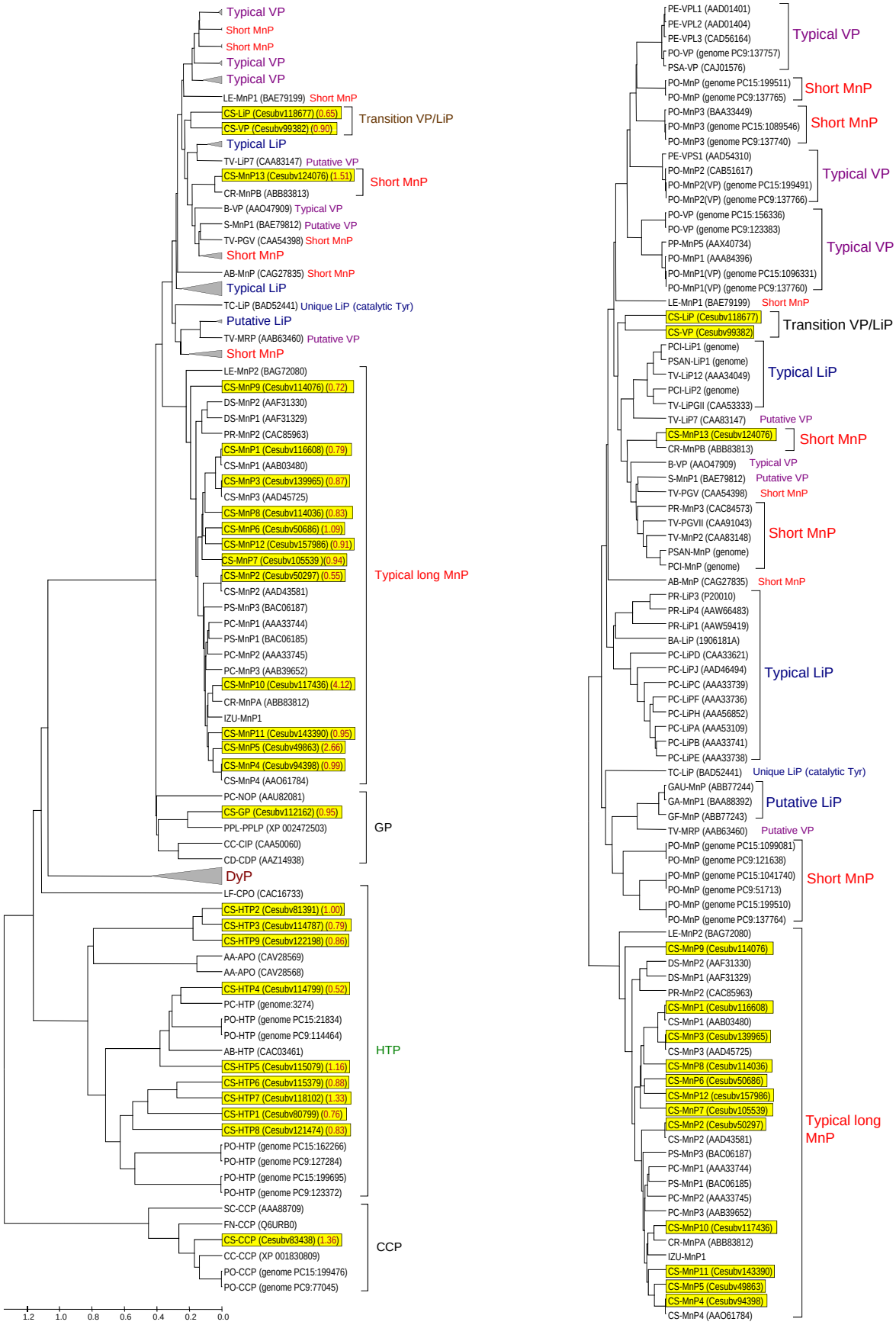
Typical VP
Short MnP
Short MnP
Typical VP
Typical VP
LE-MnP1 (BAE79199) Short MnP
CS-LiP (Cesubv118677) (0.65)
CS-VP (Cesubv99382) (0.90)
Transition VP/LiP
Typical LiP
TV-LiP7 (CAA83147) Putative VP
CS-MnP13 (Cesubv124076) (1.51)
Short MnP
CR-MnPB (ABB83813)
B-VP (AAO47909) Typical VP
S-MnP1 (BAE79812) Putative VP
TV-PGV (CAA54398) Short MnP
Short MnP
AB-MnP (CAG27835) Short MnP
Typical LiP
TC-LiP (BAD52441) Unique LiP (catalytic Tyr)
Putative LiP
TV-MRP (AAB63460) Putative VP
Short MnP
LE-MnP2 (BAG72080)
CS-MnP9 (Cesubv114076) (0.72)
DS-MnP2 (AAF31330)
DS-MnP1 (AAF31329)
PR-MnP2 (CAC85963)
CS-MnP1 (Cesubv116608) (0.79)
CS-MnP1 (AAB03480)
CS-MnP3 (Cesubv139965) (0.87)
CS-MnP3 (AAD45725)
CS-MnP8 (Cesubv114036) (0.83)
CS-MnP6 (Cesubv50686) (1.09)
CS-MnP12 (Cesubv157986) (0.91)
CS-MnP7 (Cesubv105539) (0.94)
CS-MnP2 (Cesubv50297) (0.55)
Typical long MnP
CS-MnP2 (AAD43581)
PS-MnP3 (BAC06187)
PC-MnP1 (AAA33744)
PS-MnP1 (BAC06185)
PC-MnP2 (AAA33745)
PC-MnP3 (AAB39652)
CS-MnP10 (Cesubv117436) (4.12)
CR-MnPA (ABB83812)
IZU-MnP1
CS-MnP11 (Cesubv143390) (0.95)
CS-MnP5 (Cesubv49863) (2.66)
CS-MnP4 (Cesubv94398) (0.99)
CS-MnP4 (AAO61784)
PC-NOP (AAU82081)
CS-GP (Cesubv112162) (0.95)
PPL-PPLP (XP 002472503)
CC-CIP (CAA50060)
CD-CDP (AAZ14938)
GP
DyP
LF-CPO (CAC16733)
CS-HTP2 (Cesubv81391) (1.00)
CS-HTP3 (Cesubv114787) (0.79)
CS-HTP9 (Cesubv122198) (0.86)
AA-APO (CAV28569)
AA-APO (CAV28568)
CS-HTP4 (Cesubv114799) (0.52)
PC-HTP (genome:3274)
PO-HTP (genome PC15:21834)
PO-HTP (genome PC9:114464)
AB-HTP (CAC03461)
CS-HTP5 (Cesubv115079) (1.16)
CS-HTP6 (Cesubv115379) (0.88)
CS-HTP7 (Cesubv118102) (1.33)
CS-HTP1 (Cesubv80799) (0.76)
CS-HTP8 (Cesubv121474) (0.83)
HTP
PO-HTP (genome PC15:162266)
PO-HTP (genome PC9:127284)
PO-HTP (genome PC15:199695)
PO-HTP (genome PC9:123372)
SC-CCP (AAA88709)
FN-CCP (Q6URB0)
CS-CCP (Cesubv83438) (1.36)
CC-CCP (XP 001830809)
PO-CCP (genome PC15:199476)
PO-CCP (genome PC9:77045)
CCP
1.2
1.0
0.8
0.6
0.4
0.2
0.0
PE-VPL1 (AAD01401)
PE-VPL2 (AAD01404)
PE-VPL3 (CAD56164)
PO-VP (genome PC9:137757)
PSA-VP (CAJ01576)
Typical VP
PO-MnP (genome PC15:199511)
PO-MnP (genome PC9:137765)
Short MnP
PO-MnP3 (BAA33449)
PO-MnP3 (genome PC15:1089546)
PO-MnP3 (genome PC9:137740)
Short MnP
PE-VPS1 (AAD54310)
PO-MnP2 (CAB51617)
PO-MnP2(VP) (genome PC15:199491)
PO-MnP2(VP) (genome PC9:137766)
Typical VP
PO-VP (genome PC15:156336)
PO-VP (genome PC9:123383)
PP-MnP5 (AAX40734)
PO-MnP1 (AAA84396)
PO-MnP1(VP) (genome PC15:1096331)
PO-MnP1(VP) (genome PC9:137760)
Typical VP
LE-MnP1 (BAE79199) Short MnP
CS-LiP (Cesubv118677)
CS-VP (Cesubv99382)
Transition VP/LiP
PCI-LiP1 (genome)
PSAN-LiP1 (genome)
TV-LiP12 (AAA34049)
PCI-LiP2 (genome)
TV-LiPGII (CAA53333)
Typical LiP
TV-LiP7 (CAA83147) Putative VP
CS-MnP13 (Cesubv124076)
CR-MnPB (ABB83813)
Short MnP
B-VP (AAO47909) Typical VP
S-MnP1 (BAE79812) Putative VP
TV-PGV (CAA54398) Short MnP
PR-MnP3 (CAC84573)
TV-PGVII (CAA91043)
TV-MnP2 (CAA83148)
PSAN-MnP (genome)
PCI-MnP (genome)
Short MnP
AB-MnP (CAG27835) Short MnP
PR-LiP3 (P20010)
PR-LiP4 (AAW66483)
PR-LiP1 (AAW59419)
BA-LiP (1906181A)
PC-LiPD (CAA33621)
PC-LiPJ (AAD46494)
PC-LiPC (AAA33739)
PC-LiPF (AAA33736)
PC-LiPH (AAA56852)
PC-LiPA (AAA53109)
PC-LiPB (AAA33741)
PC-LiPE (AAA33738)
Typical LiP
TC-LiP (BAD52441) Unique LiP (catalytic Tyr)
GAU-MnP (ABB77244)
GA-MnP1 (BAA88392)
GF-MnP (ABB77243)
Putative LiP
TV-MRP (AAB63460) Putative VP
PO-MnP (genome PC15:1099081)
PO-MnP (genome PC9:121638)
PO-MnP (genome PC15:1041740)
PO-MnP (genome PC9:51713)
PO-MnP (genome PC15:199510)
PO-MnP (genome PC9:137764)
Short MnP
LE-MnP2 (BAG72080)
CS-MnP9 (Cesubv114076)
DS-MnP2 (AAF31330)
DS-MnP1 (AAF31329)
PR-MnP2 (CAC85963)
CS-MnP1 (Cesubv116608)
CS-MnP1 (AAB03480)
CS-MnP3 (Cesubv139965)
CS-MnP3 (AAD45725)
CS-MnP8 (Cesubv114036)
CS-MnP6 (Cesubv50686)
CS-MnP12 (cesubv157986)
CS-MnP7 (Cesubv105539)
CS-MnP2 (Cesubv50297)
CS-MnP2 (AAD43581)
PS-MnP3 (BAC06187)
PC-MnP1 (AAA33744)
PS-MnP1 (BAC06185)
PC-MnP2 (AAA33745)
PC-MnP3 (AAB39652)
CS-MnP10 (Cesubv117436)
CR-MnPA (ABB83812)
IZU-MnP1
CS-MnP11 (Cesubv143390)
CS-MnP5 (Cesubv49863)
CS-MnP4 (Cesubv94398)
CS-MnP4 (AAO61784)
Typical long MnP

Figure S3. Comparative analysis of basidiomycete peroxidases. Left, relationships among 133 basidiomycete (and two reference ascomycetes, *Leptoxyphium fumago* and *S. cerevisiae*) peroxidases (GeneBank references in parentheses, and *C. subvermispora* protein models in yellow). Amino-acid sequence comparisons as Poisson distances and clustering based on UPGMA and "pair-wise deletion" option of MEGA4. Compressed sub-trees are shown to facilitate the *C. subvermispora* peroxidases analysis. Induction levels in ball milled aspen (BMA) *vs* glucose as sole carbon source for each peroxidase are shown in red in brackets. Abbrev: AA, *Agrocybe aegerita*; AB, *Agaricus bisporus*; B, *Bjerkandera* sp; BA, *Bjerkandera adusta*; CC, *Coprinopsis cinerea;* CD, *Coprinellus disseminatus*; CR, *Ceriporiopsis rivulosa*; CS, *C. subvermispora*; DS, *Dichomitus squalens*; FN, *Filobasidiella neoformans*; GA, *Ganoderma applanatum*; GAU, *Ganoderma australe*; GF, *Ganoderma formosanum*; IZU, basidiomycete IZU-154; LE, *Lentinula edodes*; LF, *Leptoxyphium fumago*; MS, *Marasmius scorodonius*; P, *Polyporus* sp; PC, *P. chrysosporium*; PCI, *Pycnoporus cinnabarinus*; PE, *Pleurotus eryngii*; PO, *Pleurotus ostreatus*; PP, *Pleurotus pulmonarius*; PPL, *Postia placenta*; PR, *Phlebia radiata*; PS, *Phanerochaete sordida*; PSA, *Pleurotus sapidus*; S, *Spongipellis* sp; SC, *Saccharomyces cerevisiae*; TA, *Termitomyces albuminosus*; TC, *Trametes cervina*; and TV, *Trametes versicolor*. CCP, cytochrome *c* peroxidase; CDP, *Coprinellus disseminatus* peroxidase; CIP, *Coprinopsis cinerea* peroxidase; DyP, dye-decolorizing peroxidase; HTP, heme-thiolate peroxidase; LiP, lignin peroxidase; MnP, manganese peroxidase; MRP, manganese-repressed peroxidase from *T. versicolor*; NOP, *P. chrysosporium* hypothetical (generic) peroxidase; PGV, *T. versicolor* hypothetical peroxidase; PGVII, *T. versicolor* hypothetical peroxidase; PPLP, *P. placenta* peroxidase; VP, versatile peroxidase. Right side dendrogram focuses on 90 ligninolytic peroxidases showing putative evolutionary relationships and structural-functional classification. “Short” and “long” MnPs have an experimentally confirmed or a putative Mn^{2+}-oxidation site formed by two glutamic and one aspartic residues, and differ in the length of the C-terminal tail. Typical LiPs contain an experimentally confirmed or a putative catalytic tryptophan whereas TC-LiP is a “unique” ligninolytic peroxidase with a catalytic tyrosine. Typical VPs harbor catalytic sites described above for both MnPs and Typical LiPs. Two *C. subvermispora* peroxidases initially annotated as LiP (Cesubv118677) and VP (Cesubv99382) are in fact a new type of “hybrid” peroxidase sharing catalytic properties with VP and LiP being also unable to oxidize Mn^{2+} (Main text Table 1), in spite of exhibiting (Cesubv99382) a typical Mn^{2+} oxidation site.

Material Suplementario

Capítulo 6

"**Lignin-degrading peroxidases from genome of selective ligninolytic fungus *Ceriporiopsis subvermispora*"**
Fernández-Fueyo, E., F. J. Ruiz-Dueñas, Y. Miki, M. J. Martínez, K. E. Hammel, and A. T. Martínez.
J. Biol. Chem. 287:16903-16906. 2012.

Revised version for *The Journal of Biological Chemistry*

Supplemental Data

Lignin-degrading peroxidases from the genome of the selective ligninolytic fungus *Ceriporiopsis subvermispora*

Elena Fernández-Fueyo[‡1], Francisco J. Ruiz-Dueñas[‡2], Yuta Miki[‡], María Jesús Martínez[‡], Kenneth E. Hammel[§3] and Angel T. Martínez[‡4]

From the [‡]Centro de Investigaciones Biológicas, CSIC, Ramiro de Maeztu 9, E-28040 Madrid, Spain; and the [§]USDA Forest Service, Forest Products Laboratory, 1 Gifford Pinchot Dr, Madison, WI 53726, USA

SUPPLEMENTAL TABLE AND FIGURES

One supplemental table summarizing all the heme peroxidase genes found in the *C. subvermispora* genome and their initial structural-functional classification (**Table S1**) and two supplemental figures providing the nucleotide and amino-acid sequences of the five *C. subvermispora* genes (and a mutated variant) expressed in *E. coli* (**Fig. S1**) and their electronic absorption spectra, compared with *Phanerochaete* LiP and *Pleurotus* VP (**Fig. S2**) are included below.

TABLE S1

Summary of heme peroxidase genes (a total of 26) **in the *C. subvermispora* genome, including members of the Classes I** (model 17) **and II** (models 1-16) **of the plant-fungal-prokaryotic peroxidase superfamily, and the HTP superfamily** (models 18-26)**.**

Reference (ID #), scaffold number (Sc.), position of the manually curated/annotated sequences, best hit protein after species abbreviation (protein identity in parenthesis), catalytic residues in Class II peroxidases (C-II Wc, Ea, Eb and Dc), and peroxidase type and name, based on the structural-functional classification (1).

					C-II catalytic residues				
	ID #	Sc.	Position	Best hit	Wc	Ea	Eb	Dc	Type/Name
1.	116608	11	869417-870990	CS-MnP[4] (98%)	-	+	+	+	MnP1 (long)*
2.	50297	6	1533603-1535152	CS-MnP[2] (94%)	-	+	+	+	MnP2 (long)*
3.	139965	11	865873-867462	CS-MnP[3] (100%)	-	+	+	+	MnP3 (long)*
4.	94398	6	474703-476192	CS-MnP[1] (99%)	-	+	+	+	MnP4 (long)
5.	49863	6	424184-425664	CS-MnP[1] (90%)	-	+	+	+	MnP5 (long)
6.	50686	6	141012-142559	CS-MnP[3] (79%)	-	+	+	+	MnP6 (long)*
7.	105539	6	1237989-1239477	CS-MnP[3] (80%)	-	+	+	+	MnP7 (long)
8.	114036	6	401273-402765	CS-MnP[3] (83%)	-	+	+	+	MnP8 (long)
9.	114076	6	549832-551335	CS-MnP[3] (70%)	-	+	+	+	MnP9 (long)
10.	117436	14	183695-185226	CR-MnP[5] (89%)	-	+	+	+	MnP10 (long)
11.	143390	19	448324-449814	CR-MnP[5] (89%)	-	+	+	+	MnP11 (long)
12.	157986	11	948929-950605	CS-MnP[3] (83%)	-	+	+	+	MnP12 (long)*
13.	124076	7	1607900-1609371	CR-MnP[6] (91%)	-	+	+	+	MnP13 (short)
14.	99382	20	496211-498070	TV-MnP[7] (69%)	+	+	+	+	LiP1**
15.	118677	20	490596-492455	BA-VP[8] (67%)	+	-	-	-	LiP2**
16.	112162	3	1562281-1563961	TC-LiP[9] (42%)	-	-	-	-	GP
17.	83438	6	1560404-1561943	FN-CCP [10] (65%)	n/a	n/a	n/a	n/a	CCP
18.	80799	2	2721162-2722070	LB-POX[11] (38%)	n/a	n/a	n/a	n/a	HTP1
19.	81391	3	2160792-2162116	PT-HP[12] (44%)	n/a	n/a	n/a	n/a	HTP2
20.	114787	7	815278-816708	BF- POD[13] (25%)	n/a	n/a	n/a	n/a	HTP3
21.	114799	7	847603-846537	LB-POD[14] (47%)	n/a	n/a	n/a	n/a	HTP4
22.	115079	7	1856409-1857503	CC-POD[15] (42%)	n/a	n/a	n/a	n/a	HTP5
23.	115379	8	810181-810427	LB-POD[11] (35%)	n/a	n/a	n/a	n/a	HTP6
24.	118102	16	872151-873482	LB-POD[11] (37%)	n/a	n/a	n/a	n/a	HTP7
25.	121474	2	1700699-1701478	LB-POD[16] (16%)	n/a	n/a	n/a	n/a	HTP8
26.	122198	3	2164152-2165004	PN-POD[17] (22%)	n/a	n/a	n/a	n/a	HTP9

Protein abbreviations: CCP, cytochrome *c* peroxidase; GP, generic peroxidase; HP, hypothetical protein; HTP, heme-thiolate peroxidase; LiP, lignin peroxidase; MnP, manganese peroxidase; MnP-long, typical long MnP; MnP-short, short MnP; POD, putative peroxidase; VP, versatile peroxidase; *Five MnP-long enzymes that could be classified as "extralong" MnPs (2); **LiP-type enzymes representing LiP/VP transition stages. Fungal abbreviations: BA, *Bjerkandera adusta*; BF, *Botryotinia fuckeliana*; CC, *C. cinerea*; CR, *Ceriporiopsis rivulosa*; CS, *C. subvermispora*; FN, *Filobasidiella neoformans*; LB, *Laccaria bicolor*; PN, *Phaeosphaeria nodorum*; PT, *Pyrenophora tritici-repentis*; TC, *Trametes cervina*; TV, *Trametes versicolor*. Catalytic residues (Class II peroxidases): Wc, catalytic tryptophan; Ea, Eb and Dc, three acidic catalytic residues (2 glutamates and 1 aspartate) forming the manganese oxidation-site; n/a, not applicable (3). Best hit references: [1]AAO61784, CS MnP4; [2]AAB92247, CS MnP2; [3]AAD45725, CS MnP3; [4]AAB03480, CS MnP1; [5]ABB83812, CR MnPA; [6]ABB83813, CR MnPB; [7]CAA54398, TV MnP-PGV; [8]AAY89586, BA VP; [9]BAE46585, TC LiP; [10]Q6URB0, FN CCP; [11]XP_001887896, LB POX; [12]XP_001934218, PT HP; [13]XP_001551585, BF POX; [14]XP_001879054, LB POX; [15]XP_001837979, CC POX; [16]XP_001879928, LB POX; and [17]XP_001796167, PN POX

FIGURE S1. **DNA and predicted amino acid sequences of four *C. subvermispora* Class II peroxidases (and one mutated variant) expressed in *E. coli*.** Signal sequences are in italic uppercase, and exon/intron sequences in uppercase/lowercase. A start codon (asterisk) was included before the sequences encoding the mature proteins that were optimized for *E. coli* (optimized codons underlined). Protein numbering starts at the first residue of the mature protein. The three residues involved in Mn^{2+} oxidation and the catalytic tryptophan are bold underlined. Genomic coordinates are included (see **Table S1** for more details).

A) ID# 99382 (LiP1*). The **E183K** variant was obtained by mutation of codon 183 (GAG → AAG)

```
498070 ATGGTTTTCCAGGTCCTTGCGTCCTTCATCACCGTACTTGCCGTTCTCCAAGTCAACAGAGgtccgtcta 498001
        M  V  F  Q  V  L  A  S  F  I  T  V  L  A  V  L  Q  V  N  R

498000 cgttatcctttaccatctatcatccacggaaatccactcacgtccctgatcacagCTGCCGTCACCAAGC 497931
                                                              A  A  V  T  K

497930 GCGTTACCTGCCCGGACGGTAGCATGACCGCGAATGAGGCTTGTTGTGTGCTTTTCCCTGTCCTTGAGGA 497861
       R *V  T  C  P  D  G  S  M  T  A  N  E  A  C  C  V  L  F  P  V  L  E  D     23

497860 CATTCAGCAGAACCTCTTCGACGGCGGTCTGTGCGGCGAGGAAGCACATGAGTCCCTCAGACTCACGTTC 497791
         I  Q  Q  N  L  F  D  G  G  L  C  G  E  E  A  H  E  S  L  R  L  T  F     46

497790 CACGACGCTTTTGGCTTCTCGCCAGCCCTCCAGGCTCAGGGACAATTTGGGtacgtgcactcattccgct 497721
        H  D  A  F  G  F  S  P  A  L  Q  A  Q  G  Q  F  G                       63

497720 agtgattatacatctctgatcgagtatcagTGGCGGAGGTGCAGATGGCTCCGTCATCGTCTTCGAAGAA 497651
                                    G  G  G  A  D  G  S  V  I  V  F  E  E        76

497650 ACAGAGGCAAACTTCGCCGCCAATATCGgtgtgttcacataggtcctcagctggaaaatcctggttaatc 497581
        T  E  A  N  F  A  A  N  I                                                85

497580 ctcgtcctgtagGCATCGACGAGATCATAAACGCCCAGAAGCCCTTCATTGCCAGACACAACATCACCCC 497511
                  G  I  D  E  I  I  N  A  Q  K  P  F  I  A  R  H  N  I  T  P    105

497510 TGGTGACTTgtaagtctgtacatgcatgttcttggactagtgctcacgcatacgctatcgtgtcatagCG 497441
          G  D  F                                                               108

497440 TCCAATTTGCCGGCGCTGTCGGCGCCGCCAATTGTCCGGGAGCTCCCCAACTGCAATTCATGCTTGgtaa 497371
       V  Q  F  A  G  A  V  G  A  A  N  C  P  G  A  P  Q  L  Q  F  M  L         130

497370 gctctgctgcgagtctttggattagacgttgattcaatgctcttgtagGCCGCCCGATGCgtaagtctcg 497301
                                                     G  R  P  M                 134

497300 gcatgctatacgaatcaaatactatctgactggatttcaccccagCTGTCGCTTCATCCCCCGATGGTCT 497231
                                                   P  V  A  S  S  P  D  G  L    143

497230 TATTCCCGAGCCCTTCGgtacggtgtaatgtatgaactagatgactgccgttgctgagcattccaaactt 497161
          I  P  E  P  F                                                         148

497160 ttagACACTGTCGATTCGATCATTGAGCGCTTCGCTGATGCTGGCAATTTCACTGAAACAGAAATTATTT 497091
             D  T  V  D  S  I  I  E  R  F  A  D  A  G  N  F  T  E  T  E  I  I     170

497090 GGCTGCTCACAGCgtgagtagagttttattccagtgaaccgaaaggtataacccaagttgcattagCCAC 497021
       W  L  L  T  A                                                        H     176

497020 TCGATCGCGGCTGCCGACGAGGTCGATCCTACCATCCCGGGCACACCGTTCGACTCTACACCAGGCATTT 496951
         S  I  A  A  A  D  E  V  D  P  T  I  P  G  T  P  F  D  S  T  P  G  I     199

496950 TCGACAGTCAAATCTTCATCGAGGTTCAGCTGAGAGGCACCAGCTTCCCAGGgtcagttgtcaacattgt 496881
       F  D  S  Q  I  F  I  E  V  Q  L  R  G  T  S  F  P  G                     217

496880 gtacactaaatgtatctgacatccgtccgcagAACTGGCGGCAACCAGGGCGAGGTTGAATCTCCGCTCA 496811
                                      T  G  G  N  Q  G  E  V  E  S  P  L        229

496810 GGGGAGAACTGCGCCTGCAATCCGACTCTGAGgtttgtgtcgtatacctgtcatcatctgcaactggctg 496741
       R  G  E  L  R  L  Q  S  D  S  E                                          240

496740 acggggcctcacagCTCGCTCGTGACTCGCGTACTGCCTGCGAGTGGCAGGCGTTTGTCGgtgggcatca 496671
                     L  A  R  D  S  R  T  A  C  E  W  Q  A  F  V                255

496670 ttaacacgcatctcacatattagaaggctcatggtttctccaaaacagATAACGTGCCGAGGATGCAGAC 496601
                                                     D  N  V  P  R  M  Q  T    263

496600 TTTGTTTAGTGCTGCTATGTCGACGCTCGCCGTGATTGGACAGGACACCTCCCAGATGGTCGACTGTTCC 496531
         L  F  S  A  A  M  S  T  L  A  V  I  G  Q  D  T  S  Q  M  V  D  C  S     286

496530 GATGTGgtccgtgctgcttgcttcgaatactatgcatgtgcatgatgcttgtccgcagATCCCGGTCCCA 496461
        D  V                                                   I  P  V  P      292

496460 CCCCCGCCTCAGGGAACCGCTCACATCCCTGCTGGCCTGAGCAACGCTGACATAGAGCAGGCTgtgcgtc 496391
        P  P  P  Q  G  T  A  H  I  P  A  G  L  S  N  A  D  I  E  Q  A            313

496390 atttctctttcgtttcgtgaaaaccatatgctcattgcactacccagTGCGCTACTGCTGCGTTCCCGAG 496321
                                                     C  A  T  A  A  F  P  S    321

496320 TCTCCCGGTTGACCCCGGTCCGGCTACTTCTGTTGCCCCCGTgtaagtgtgaccacaatgtggagtgcgc 496251
         L  P  V  D  P  G  P  A  T  S  V  A  P  V                             335

496250 ataatgctaatcggattcgtgtcgcagTCCGCCAGCTTAA                                 496211
                                P  P  A End                                     338
```

B) ID# 117436 (MnP10)

```
185226 ATGGCTTTCACTTCCTTCGTTGCCCTCGCTGCCCTTGTCGGCATTGCTAGTGCAGCGCCGACTACCATTT 185157
        M  A  F  T  S  F  V  A  L  A  A  L  V  G  I  A  S  A *A  P  T  T  I       5

185156 GCCCGGACGGTACTCGCGTGAGCAACCATGCCTGCTGCGCTTTTATCCCGgtatgtgcgataccaccgga 185087
       C  P  D  G  T  R  V  S  N  H  A  C  C  A  F  I  P                        22

185086 tgcccgttgagaatgatagggttctaaactttacgtgaatagCTTGCTGAGGATCTGCAGAAGACCATCT 185017
                                               L  A  E  D  L  Q  K  T  I        31

185016 TCATGAACGATTGTGGCGAAGATGgtaagtgcattcctagtatcttgtatctaactcaactaagaatatc 184947
       F  M  N  D  C  G  E  D                                                   39

184946 atcagCGCACGAGGTCATCCGTCTCACTTTCCgtcagtagtcaatttgcactcaatggtgtttcggtgat 184877
            A  H  E  V  I  R  L  T  F                                           48

184876 tgatttgccactgcagATGATGCCGTCGCAATTTCTCGCAAGCTCGGCCCCAAAGCgtacgttatgaacg 184807
                       H  D  A  V  A  I  S  R  K  L  G  P  K  A                 62

184806 tcttcggtgtttcgattagacattgattctgagaaccatcagTGGTGGCGGAGCTGACGGTTCGATGCTG 184737
                                                  G  G  G  A  D  G  S  M  L     71

184736 CTCTTCCCTACCGTGGAGCCAAATTTCTCTGCCAACAACGGTATCGACGACAGCGTGAATAACTTGATTC 184667
        L  F  P  T  V  E  P  N  F  S  A  N  N  G  I  D  D  S  V  N  N  L  I     94

184666 CCTTCATGGCCAGGCATCCTACTGTCAGTGCTGGTGATCTGGTCCAGTTTGCTGGTGCTGTGGCACTGAG 184597
       P  F  M  A  R  H  P  T  V  S  A  G  D  L  V  Q  F  A  G  A  V  A  L  S   118

184596 CAACTGCCCAgtgagttaatcgtctcgtactttcattatcctgagattaagcacagtttgacattcacag 184527
         N  C  P                                                                121

184526 GGTGCTCCTCGTCTTGAATTTCTTGCAGGCCGCCCTAATCACACCATCGCTGCCATTGACGGTCTGATTC 184457
        G  A  P  R  L  E  F  L  A  G  R  P  N  H  T  I  A  A  I  D  G  L  I     144

184456 CGGAGCCACAAGATGACGTGACCAAGATTCTCGAGCGTTTCGACGACGCGGGCGGATTCACGCCATTCGA 184387
       P  E  P  Q  D  D  V  T  K  I  L  E  R  F  D  D  A  G  G  F  T  P  F  E   168

184386 GGTTGTGTCTCTTCTTGCCTCCCATACTGTCGCTCGTGCGGACAAGGTCGACGAGACCATTGATGCTGCA 184317
         V  V  S  L  L  A  S  H  T  V  A  R  A  D  K  V  D  E  T  I  D  A  A    191

184316 CCATTCGATTCCgtaagttacgcttgcatcttgatccgagtcatgccctgaccatttctgtaccagACTC 184247
        P  F  D  S                                                        T     196

184246 CCTTCACGTTCGACACTCAGGTCTTCCTCGAAGTATTGCTGAAGGGCGTCGGATTTCCAGGAACGGACAA 184177
       P  F  T  F  D  T  Q  V  F  L  E  V  L  L  K  G  V  G  F  P  G  T  D  N   220

184176 CAACACCGGCGAGGTCGCGTCCCCGCTTCCGAAGGGCAGTGGCAACGACACCGGCGAGATGCGTCTGCAG 184107
         N  T  G  E  V  A  S  P  L  P  K  G  S  G  N  D  T  G  E  M  R  L  Q    243

184106 TCCGATTTTGCGCTCGCCCGCGACCCGCGCACGGCTTGCTTCTGGCAAGGTTTCGTCGATGAGCAGGAAT 184037
        S  D  F  A  L  A  R  D  P  R  T  A  C  F  W  Q  G  F  V  D  E  Q  E     266

184036 TTATGGCAGAGAGCTTCAAGGCCGCAATGGCTAAACTTGCGATCCTCGGCCACAATCGCGCAAGCCTGAC 183967
       F  M  A  E  S  F  K  A  A  M  A  K  L  A  I  L  G  H  N  R  A  S  L  T   290

183966 CGACTGCTCCGACGTCGTGCCCATTCCAAGGCCCGCTGTTAAAAAGCCTGCGTCCTTCCCTGCCACTACC 183897
         D  C  S  D  V  V  P  I  P  R  P  A  V  K  K  P  A  S  F  P  A  T  T    313

183896 GGTCCAAAGGACCTCGAGCTGACTTGTAGGGCTGAGAGGTTCCCTACCCTTACCGTCGACCgtacgtcat 183827
        G  P  K  D  L  E  L  T  C  R  A  E  R  F  P  T  L  T  V  D              333

183826 tctcaacttgaaataaaacgtttctcctgactttattttggtggtatagGTGGTGCTGTCCAAGCTCTCA 183757
                                                     R  G  A  V  Q  A  L     340

183756 TTCCCCATTGCTCCAACGGCGGCCAAGACTGCCCTTCTGTCCAGTTCGATGGACCAGCTTAA         183695
       I  P  H  C  S  N  G  G  Q  D  C  P  S  V  Q  F  D  G  P  A End          360
```

C) ID# 112162 (GP)

```
1563961 ATGCGGGAGTCATCAAAGTTGCAATACACGACGCTCATTATTTGCGTCATTCGCCTATGTAGCACTTTTT 1563892
         M  R  E  S  S  K  L  Q  Y  T  T  L  I  I  C  V  I  R  L  C  S  T  F

1563891 GCTCAGgtacggatacccatctcggagtaaaagtgtacactgcagtgtgttgaccagccgtatagCGTTC 1563822
        C  S                                                           A *F       1

1563821 GTGATCTCCAACTCCTTGAACGCAACCgtgagtttgttgcgctcggtttctgtcacgtgaatatctgaac 1563752
         V  I  S  N  S  L  N  A  T                                              10

1563751 catgcatgcgcagTGCCTAAGCTGGTTTGGTgtaaggtcgttctcgttttcaaaaggtgttctgaggaaa 1563682
                    C  L  S  W  F  G                                            16

1563681 gttcgcagGTGCTGGACGACATACAAACCAATATgtgagtgtttgcatcaacctacaccacgagcctcga 1563612
              V  L  D  D  I  Q  T  N  M                                        25

1563611 aataagaacgcagatgaagGTTTGGTGGAGGAACCTGCAATGACCTGGCGCGGGCCGCCATAAGATTGAC 1563542
                           F  G  G  G  T  C  N  D  L  A  R  A  A  I  R  L  T    42

1563541 CTTTCACGATGGTATAGGCCGATCTATGGCGCTGAGCAATTCCGGAGAGTTCGGgtgattatttcattgg 1563472
         F  H  D  G  I  G  R  S  M  A  L  S  N  S  G  E  F  G                  60

1563471 gttagtggctaccgcctggatgttctgacaaaatcggtggatgtatagCGGCGAAGGCGCAGgtacgttc 1563402
                                                      G  E  G  A               64

1563401 atttcaggccgttggatagtccggtgaaacgtatcgtgagtgcctcctttagATGGCAGTATCATCACAT 1563332
                                                        D  G  S  I  I  T       70

1563331 TTTCCAGGACTGAGTTGTCATACCgtgagacatgacgtgcacctgacacctatattgagtctgacatctt 1563262
        F  S  R  T  E  L  S  Y                                                 78

1563261 cgtacagCCGCCAACAAAGGCTTGGAACTGATTGTAGACGCTCTGGGACATTTCGCAGACGCCCATGGTG 1563192
              P  A  N  K  G  L  E  L  I  V  D  A  L  G  H  F  A  D  A  H  G    99

1563191 TCAGTTACGGCGATATgtaagccggattcatccgtcgggacgtcgctgactggctgaggtccttcagTAT 1563122
        V  S  Y  G  D  I                                                   I    106

1563121 ACAGTTTGCAGGCGCGGTAGCTACTTCGAATTGCCCTGGTGCCCCACGACTTCCTTTCCACGCTGGACGT 1563052
         Q  F  A  G  A  V  A  T  S  N  C  P  G  A  P  R  L  P  F  H  A  G  R   129

1563051 CCGAACGCCATCGCACCATCGCCGCCCGATCTCGTTCCGTCTCCTTCGGATTCTGTCGAGATGATTCTAG 1562982
         P  N  A  I  A  P  S  P  P  D  L  V  P  S  P  S  D  S  V  E  M  I  L   152

1562981 CTCGCATGTCTGACGCTGGTCTCACAACAGAAGACACTATTGCCCTTCTCGCGGCACATTCCGTTGGCAA 1562912
        A  R  M  S  D  A  G  L  T  T  E  D  T  I  A  L  L  A  A  H  S  V  G  K   176

1562911 GCAGAGAACGCTGGATCTCAACATCACCGGCATGCCATTCGATACCACTCCAGATGCTTTTGACACACAA 1562842
         Q  R  T  L  D  L  N  I  T  G  M  P  F  D  T  T  P  D  A  F  D  T  Q   199

1562841 TTTTACCTTGACgtgagcgtctctgtctcaacttctatgccgatgctcacagtaaatatagACGTCATTA 1562772
         F  Y  L  D                                                   T  S  L   206

1562771 CGTGGCACGGTCATGCCCGGTCCTGGCAGAAGTGATTTTGAAGTTAAATCTCCTTCGAAAGACGAATTTC 1562702
         R  G  T  V  M  P  G  P  G  R  S  D  F  E  V  K  S  P  S  K  D  E  F   229

1562701 GAATCGCTTCAGATGCCGCATTCGCACGACATCCCTTGACCGCATGTGTATGGCAGTCATTCGTTGgtag 1562632
        R  I  A  S  D  A  A  F  A  R  H  P  L  T  A  C  V  W  Q  S  F  V       251

1562631 gccgtccactagatggcatagaccttcgttactcaagcatgacctggctcagTGAACCAAAGCAGGCTAC 1562562
                                                          V  N  Q  S  R  L     257

1562561 AAGGCTCATTCTCACAAGCCATGATCAAATTGGCTAATGCGGGTCATTCGAACTTAATTGATTGCTCTAT 1562492
        Q  G  S  F  S  Q  A  M  I  K  L  A  N  A  G  H  S  N  L  I  D  C  S  I   281

1562491 TGCCATACCGCCCTCGCGCTCATGGTCCCGGCTGCCCGTGTATCCTCCCGGAAAGAGCCGATCGGATATC 1562422
         A  I  P  P  S  R  S  W  S  R  L  P  V  Y  P  P  G  K  S  R  S  D  I   304

1562421 GATCACTCGgtccgtgctcctgacccgcttgactgtgctcaaagcttatgtagagcttagTGTTCCACGA 1562352
         D  H  S                                                   C  S  T     310

1562351 CAGCCTTCCCAGATATTCCATCGGATTGGGTGCCTGTCGCACACCACATACCATTCTCACGCCTAATGTAA1562281
        T  A  F  P  D  I  P  S  D  W  V  P  V  A  H  H  I  P  F  S  R  L  M End   333
```

D) ID# 118677 (LiP2*)

```
492455 ATGGCCTTCTCAATCCTCGCATCCCTTGTCTCTGTGCTCGTGGTTCTCCAGGCTGCCAGTGgtactgaat 492386
       M  A  F  S  I  L  A  S  L  V  S  V  L  V  V  L  Q  A  A  S

492385 tctgctcatacactgtatggacggacactgaataactattattcagGTGCTATTACCCGCAAGGCGACCT 492316
                                                    G  A  I  T  R  K  *A  T      2

492315 GTCCTGACGGTAACACGGTCACTAATGAGGCCTGCTGCTTCCTCTTCCCAATTCTCGAGGATATTCAGGC 492246
       C  P  D  G  N  T  V  T  N  E  A  C  C  F  L  F  P  I  L  E  D  I  Q  A     26

492245 GAACCTGTTCAATGGTGGCGAGTGCGGCTCGGAGGCGCACGAGTCTCTCAGACTCACCTTCCACGATGCC 492176
         N  L  F  N  G  G  E  C  G  S  E  A  H  E  S  L  R  L  T  F  H  D  A     49

492175 ATCGGCTTTTCCCCTGCACTCACTGCCCAGGGACAATTTGGgtatgcttcgatgttcttcgttacgttcg 492106
       I  G  F  S  P  A  L  T  A  Q  G  Q  F  V                                 63

492105 cgtttagtgacgctttaacctcagTGGCGGAGGTGCTGATGGCTCCGTTATTACATTCGCGTCGATCGAG 492036
                              G  G  G  A  D  G  S  V  I  T  F  A  S  I  E     78

492035 ACTGCCTATGCAGCGAACGCTGgtatgcattcaatcgcgaacatctgcttctcattctaatatcgaatat 491966
       T  A  Y  A  A  N  A                                                     85

491965 tctagGCATCGAGGATATTGTGGCAGAGCAGGCACAATTTGTTGCGAAATACAATGTTTCCGCCGGAGAC 491896
           G  I  E  D  I  V  A  E  Q  A  Q  F  V  A  K  Y  N  V  S  A  G  D    107

491895 TTgtgagcccattaatcgactcgatcttgagaattcactgatagtgggatatcagCGTTCAATTTGCGGG 491826
       F                                                        V  Q  F  A  G    113

491825 CGCTGTCGGACTGAGCAACTGCCCGGGTGCGCCTCAGCTTGACTTCGTGATCGgtcagtaaacggcaatg 491756
         A  V  G  L  S  N  C  P  G  A  P  Q  L  D  F  V  I                     130

491755 atttaaccaagaatcacgtgctgacgctggcaccgcagGTCGTCCTGCAGgtacacgatcaattctagat 491686
                                          G  R  P  A                           134

491685 taacgaaagtatagtatctaagcatcgatctagCTACCGCGGCCTCTCCTGACGGTCTCGTACCGGAGCC 491616
                                    A  T  A  A  S  P  D  G  L  V  P  E  P    147

491615 TTTCGgtatgtcgttcacgttcgctgtatgaataaatccactaacgcgacacaaccacagATAACGTGAC 491546
         F                                                        D  N  V  T    152

491545 AAGCATTCTTGCGCGCTTCAACGATGCGGGCGGTTTTGATCCTCAGCACGTTGTCTGGCTGCTGTCTTCg 491476
         S  I  L  A  R  F  N  D  A  G  G  F  D  P  Q  H  V  V  W  L  L  S  S    175

491475 tgagttctctctggcgttgataaagagacggggattctaagtgggcgaaagGCATTCGGTTGCCGCCGCG 491406
                                                      H  S  V  A  A  A     181

491405 GAGCTTGTTGACCCCTCGATCCCCGGCGCACCATTTGACTCAACTCCCGGTCTGTTCGACACGCAGTTTT 491336
         E  L  V  D  P  S  I  P  G  A  P  F  D  S  T  P  G  L  F  D  T  Q  F     204

491335 TCATTGAGACCCAACTCACTGGCACTCTCTGGCCCGGgtacgctgattctgttatctgtattcaggccat 491266
       F  I  E  T  Q  L  T  G  T  L  W  P  G                                   217

491265 atctaaataccgcttcctgctcattagTACTGCTAACAACCAGGGCGAGGTCGAGTCTCCCCTCCTGGGA 491196
                                  T  A  N  N  Q  G  E  V  E  S  P  L  L  G     231

491195 GAGATCCGTCTCCAGTCCGACTTCTTGgttcgtatgctcgtcagtcatcctctgccgagattctaacgca 491126
         E  I  R  L  Q  S  D  F  L                                             240

491125 ttcgcgcagCTCGCCCGCGATAACAGAACTGCATGCGAATGGCAGTCCTTCGCTAgtgagtgcaagttcc 491056
                  L  A  R  D  N  R  T  A  C  E  W  Q  S  F  A                 255

491055 gactttccaatatgaccatatgctcaccgggattctacccagACGACTTGAGCAGGCAGCAGACCCTGTT 490986
                                                N  D  L  S  R  Q  Q  T  L  F    265

490985 CAAGGCCGCGATGAGCACCCTCGCTACGATCGGCCAGGATACTAGCACCCTTACGGACTGCTCTGACGTC 490916
         K  A  A  M  S  T  L  A  T  I  G  Q  D  T  S  T  L  T  D  C  S  D  V    288

490915 gtacgtctcatcatgttctcgtatttctgccgtctgcttgactctttgcagATCCCGGTACCGGCTGCGC 490846
                                                      I  P  V  P  A  A     294

490845 CCGTGGGCACGCCTCACTTCCCCGCTGGCCTGACAAATGCTGATGTCGACCAAGCGgtgcgtttcagttg 490776
       P  V  G  T  P  H  F  P  A  G  L  T  N  A  D  V  D  Q  A                 313

490775 tgcgctgtcgtagattacgctcttatgttgatatcgtcacacagTGCACTACCGCCGCATTCCCGACTCT 490706
                                                C  T  T  A  A  F  P  T  L    322

490705 CTCAACAGATCCTGGTCCGGCGACCTCCGTTGCTCCTGTgtaagtcagcgtccgagcttctctatggaat 490636
         S  T  D  P  G  P  A  T  S  V  A  P  V                                 335

490635 acattgatgacggtctctttcctttagACCCACTGCTTAA                                 490596
                              P  T  A  End                                     338
```

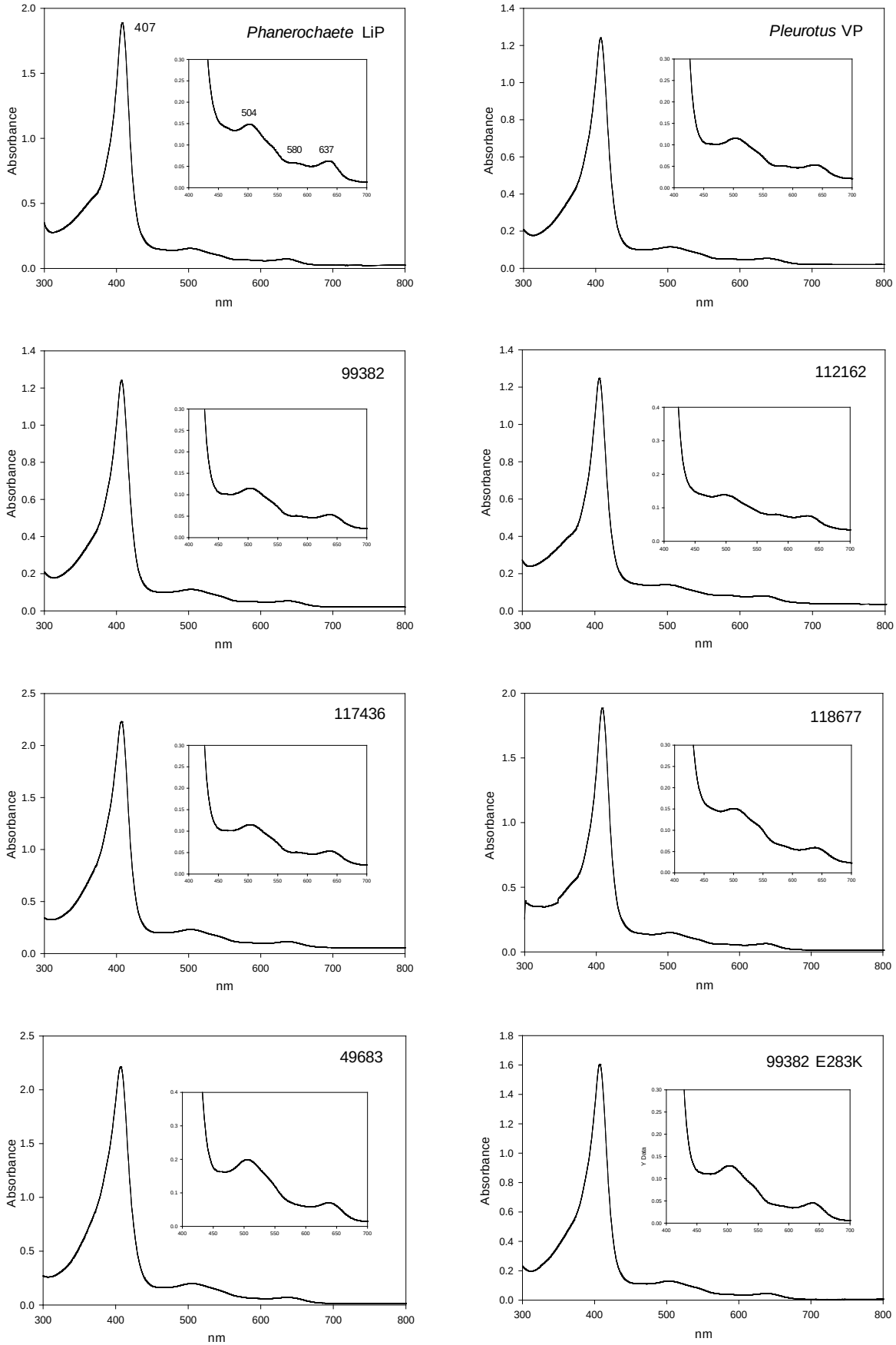

FIGURE S2. **Electronic absorption spectra five *C. subvermispora* peroxidases expressed in *E. coli*** (and the E283K variant of 99382) **after their *in vitro* activation** (compared with *Phanerochaete* LiP and *Pleurotus* VP).

REFERENCES

1. Ruiz-Dueñas, F. J. and Martínez, A. T. (2010) In *Biocatalysts based on heme peroxidases* (Torres, E. and Ayala, M., eds) pp. 37-59, Springer-Verlag, Berlin
2. Li, D. M., Li, N., Ma, B., Mayfield, M. B., and Gold, M. H. (1999) *BBA Protein Struct. Mol. Enzym.* **1434,** 356-364
3. Ruiz-Dueñas, F. J., Morales, M., García, E., Miki, Y., Martínez, M. J., and Martínez, A. T. (2009) *J. Exp. Bot.* **60,** 441-452

Material Suplementario

Capítulo 7

"Catalytic and stability properties of manganese peroxidase subfamilies: A study based on the *Ceriporiopsis subvermispora* genome"
Fernández-Fueyo, E., S. Acebes, F. J. Ruiz-Dueñas, , M. J. Martínez, A. Romero, F. J. Medrano, V Guallar and A. T. Martínez.
(enviado)

Supporting Information

Catalytic and stability properties of manganese peroxidase subfamilies: A study based on the *Ceriporiopsis subvermispora* genome

Elena Fernández-Fueyo, Sandra Acebes, Francisco J. Ruiz-Dueñas, María Jesús Martínez, Antonio Romero, Francisco Javier Medrano, Victor Guallar, and Angel T. Martínez

Supporting Information includes H-bond involving the C-terminal tail of extralong MnP6 (100 ns MD) (**Table S1**), sequence identities between MnPs from *C. subvermispora* and other fungi (**Table S2**), crystallographic data of *C. subvermispora* MnP6 (**Table S3**), multiple alignment of extralong, long and short MnPs sequences from *C. subvermispora* and other basidiomycetes (**Fig. S1**), molecular structures of *C. subvermispora* extralong, long and short MnPs (**Fig. S2**), ABTS binding on extralong MnP6 as shown by PELE (**Fig. S3**), closure of the propionate channel in the MnP6 short-variant by the double G82L/D85L mutation (**Fig. S4**), effect of pH on ABTS oxidation by single and multiple variants of the MnP6 short-variant (**Fig. S5**), and phylogram of *C. subvermispora* and other basidiomycete peroxidases (**Fig. S6**).

Table S1. H-bonds involving the C-terminal tail residues of *C. subvermispora* extralong MnP6 during a 100 ns MD (300 K)

C-tail residue	Second residue	H-bond
Phe357-backbone	Gln356-side chain	18.27%
Phe357-backbone	Asn89-side chain	**23.97%**
Phe357-backbone	Ash85-side chain*	1.82%
Ala361-backbone	Asn88-side chain	**22.09%**
Ala361-backbone	Asn88-side chain	10.81%
Thr362-side chain	Asp363-backbone	1.23%
Asp363-side chain	Ash84-side chain*	**36.55%**
Asp363-side chain	Lys180-side chain	19.35%
Asp363-side chain	Ser364-side chain	**21.86%**
Ser364-side chain	Asn81-side chain	**26.99%**
Ser364-side chain	Asn81-side chain	4.66%
Ser364-side chain	Lys180-side chain	2.71%
Ser364-backbone	Asn81-side chain	9.57%
Ser364-backbone	Lys180-side chain	4.51%
Pro365-side chain	Lys180-side chain	0.56%
Pro365-backbone	Lys180-side chain	0.90%

*Ash, protonated aspartate

Table S2. Sequence identities between representative MnPs from *C. subvermispora, D. squalens, P. chrysosporium, P. radiata* and *P. ostreatus*, LiP from *P. chrysosporium*, and VP from *P. ostreatus* (all references are from the corresponding genomes, except those of *P. radiata* MnPs that are from GenBank; the number of residue pairs included in each comparison is shown in parenthesis)

	D. squalens short MnP3 (169524)	*D. squalens* extralong MnP3 (169843)	*P. chrysosporium* long MnP1 (66512)	*P. chrysosporium* LiPH8 (131707)	*P. ostreatus* short MnP4 (1099081)	*P. ostreatus* VP1 (137757)	*P. radiata* short MnP3 (Q96TS6)	*P. radiata* extralong MnP2 (CAC85963)	*C. subvermispora* extralong MnP12 (157986)	*C. subvermispora* extralong MnP6 (50686)	*C. subvermispora* long MnP10 (1117436)	*C. subvermispora* long MnP5 (49863)	*C. subvermispora* short MnP13 (1124076)
C. subvermispora short MnP13 (124076)	68% (342)	52% (343)	52% (341)	59% (344)	62% (336)	66% (337)	71% (339)	52% (343)	49% (346)	48% (346)	51% (342)	54% (341)	100% (338)
C. subvermispora long MnP5 (49863)	53% (346)	75% (356)	83% (357)	47% (337)	51% (342)	52% (339)	50% (341)	74% (355)	77% (361)	78% (361)	87% (356)	100% (356)	-
C. subvermispora long MnP10 (117436)	50% (345)	73% (357)	83% (356)	44% (346)	49% (341)	51% (338)	47% (342)	72% (357)	77% (360)	79% (360)	100% (357)	-	-
C. subvermispora extralong MnP6 (50686)	47% (351)	75% (344)	76% (361)	43% (347)	49% (347)	48% (344)	45% (346)	73% (361)	84% (362)	100% (365)	-	-	-
C. subvermispora extra-long MnP12 (157986)	50% (351)	72% (363)	73% (361)	44% (342)	48% (347)	49% (344)	48% (346)	74% (366)	100% (368)	-	-	-	-
P. radiata extralong MnP2 (CAC85963)	49% (346)	78% (366)	73% (355)	47% (342)	47% (341)	48% (339)	49% (342)	100% (366)	-	-	-	-	-
P. radiata short MnP3 (Q96TS6)	79% (341)	49% (342)	50% (340)	58% (339)	58% (337)	68% (337)	100% (339)	-	-	-	-	-	-
P. ostreatus VP1 (137757)	65% (342)	47% (337)	52% (338)	57% (344)	63% (337)	100% (331)	-	-	-	-	-	-	-
P. ostreatus short MnP4 (1099081)	59% (342)	47% (341)	50% (342)	55% (339)	100% (337)	-	-	-	-	-	-	-	-
P. chrysosporium LiPH8 (131707)	59% (344)	43% (332)	47% (343)	100% (344)	-	-	-	-	-	-	-	-	-
P. chrysosporium long MnP1 (66512)	54% (345)	72% (356)	100% (357)	-	-	-	-	-	-	-	-	-	-
D. squalens extralong MnP3 (169843)	43% (331)	100% (366)	-	-	-	-	-	-	-	-	-	-	-
D. squalens short MnP6 (169524)	100% (342)	-	-	-	-	-	-	-	-	-	-	-	-

Table S3. Crystallographic data collection and refinement statistics of *C. subvermispora* extralong MnP6, and MnP6 with Mn^{2+} and Cd^{2+} (normal and anomalous). Data in parenthesis correspond to the last resolution layer.

	MnP6	**MnP6+Mn^{2+}**	**MnP6+Mn^{2+}** (anomalous)	**MnP6+Cd^{2+}**	**MnP6+Cd^{2+}** (anomalous)
Data collection					
Space group	$P4_32_12$	$P4_32_12$	$P4_32_12$	$P4_32_12$	$P4_32_12$
Cell constants (Å)	a =b= 108.6, c= 68.8	a=b= 108.5, c= 68.5	a=b= 108.7, c= 68.2	a=b= 108.8, c= 68	a=b= 108.8, c= 68.4
Wavelength (Å)	0.933400	0.980110	1.741350	0.980110	1.922240
Resolution range (Å)	50.00-1.20 (1.27-1.20)	50.00-1.20 (1.27-1.20)	50.00-1.90 (2.01-1.90)	50.00-1.20 (1.27-1.20)	50.00-1.90 (2.10-1.98)
Nº of total reflections	1124979	1410599	576129	1055455	311398
Nº of unique reflections	128076	127081	60358	128714	47444
R_{merge} (%)	8.2 (119.6)	8.3 (174.2)	5.5 (34.5)	4.7 (128.9)	2.9 (6.4)
Completeness (%)	99.9 (99.3)	99.5 (97.2)	97.9 (87.4)	99.8 (98.9)	87.4 (33.4)
$\langle I/\sigma(I)\rangle$	18.7 (1.8)	14.2 (1.0)	25.2 (2.9)	19.2 (1.1)	42.6 (7.3)
Multiplicity	8.8 (8.6)	11.1 (7.1)	9.5 (3.5)	8.2 (4.9)	6.6 (1.4)
Solvent (%)/Matthews	50.77/2.50	50.77/2.50	50.77/2.50	50.77/2.50	50.77/2.50
Subunits/asymmetric unit	1	1	1	1	1
Wilson B factor ($Å^2$)	10.5	13.7	26.1	15.1	21.8
Refinement					
Resolution range (Å)	50.0-1.20	50.0-1.20	50.0-1.90	50.0-1.20	50.0-1.98
Working reflections	127105	126815	60357	127474	47437
R_{work}/R_{free} (%)	13.4/15.1	13.9/15.4	16.7/19.1	15.1/16.2	15.9/19.1
Protein atoms (non H)	2701	2713	2701	2715	2701
Heme group	1	1	1	1	1
Ca^{2+}	1	2	2	2	2
Water molecules	595	491	296	445	333
Na/Mn/Cd ions	1/0/0	0/2/0	0/2/0	0/0/3	0/0/3
Mean B factors ($Å^2$):					
- Protein atoms (non H)	12.56	18.86	28.17	18.86	22.53
- Heme group	8.89	11.49	23.42	14.75	18.76
- Ca^{2+}	7.90	10.99	21.96	13.06	15.65
- Water molecules	25.78	28.24	33.04	30.42	31.46
- Na/Mn/Cd ions	12.28/-/-	-/20.51/-	-/39.05/-	-/-/20.42	-/-/45.60
Deviations from ideality:					
- rmsd bond lengths (Å)	0.008	0.009	0.007	0.008	0.007
- rmsd angles (º)	1.244	1.371	1.079	1.366	1.231
Ramachandran plot (%):					
- Preferred	98.08	98.08	97.53	97.26	96.70
- Allowed	1.65	1.92	2.47	2.74	3.30
- Outliers	0.27	0.00	0.00	0.00	0.00
PDB code					

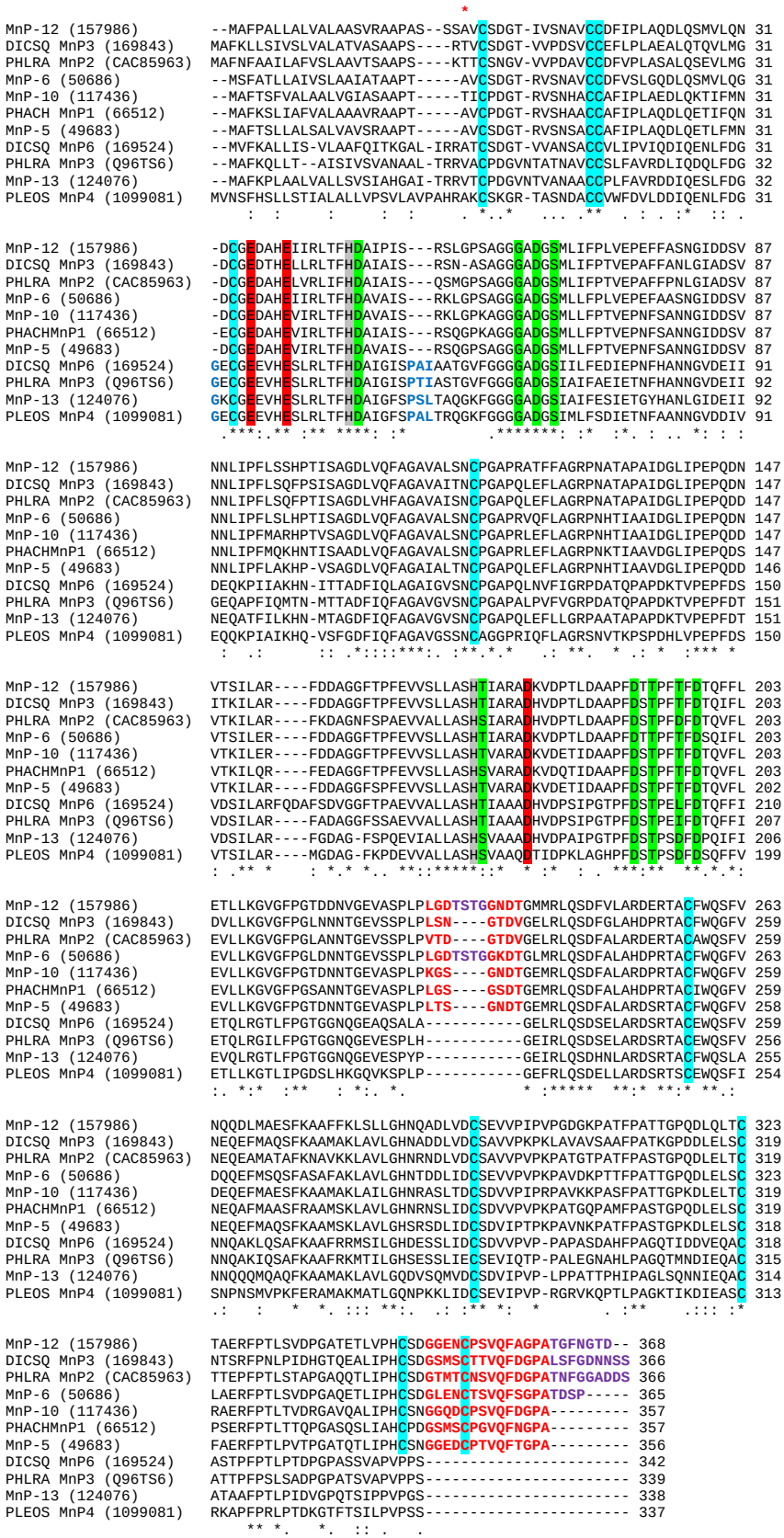

Fig. S1. Multiple alignment of extralong, long and short MnPs sequences. *C. subvermispora* extralong (MnP6 and MnP12), long (MnP5 and MnP10) and short (MnP13) MnPs are included, together with extralong MnPs from *P. radiata* (GenBank CAC85963) and *D. squalens* (JGI model 169843), long MnP from *P. chrysosporium* (JGI model 66512), and short MnPs from *P. radiata* (GenBank Q96TS6), *D. squalens* (JGI model 169526) and *P. ostreatus* (JGI model 1099081). Extra residues in long and extralong MnPs

are in magenta and red, respectively. Conserved residues include: **i)** eight cysteines (cyan); **ii)** nine Ca^{2+} ligands (green); **iii)** two active site histidines (dark gray); and **iv)** three acidic residues (red) forming the Mn^{2+}-oxidation site. Numbering starts at the first residue of the mature protein (red asterisk). Symbols below indicate full conservation of the same (*) or equivalent residues (:) and partial residue conservation (.).

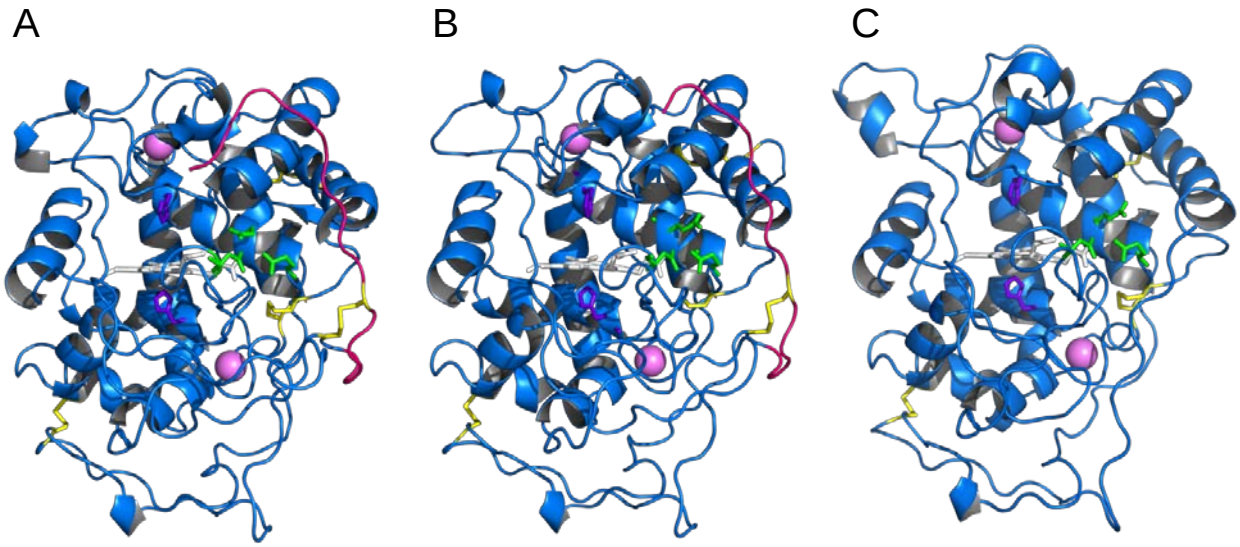

Fig. S2. Comparison of molecular structures of extralong MnP6 (**A**), long MnP10 (**B**) and short MnP13 (**C**) from the *C. subvermispora* genome showing different extension C-terminal tails. In addition to the variable C-terminal tail (magenta), two Ca^{2+} ions (pink van der Waals spheres), the heme cofactor (white sticks), 4-5 disulfide bonds, and the Mn^{2+}-oxidation site (green sticks) are shown. From extralong MnP6 crystal structure (PDB XXX), and MnP10 and MnP13 homology models based on other long (*P. chrysosporium*) and short (*P. ostreatus*) MnP crystal structures (PDB entries 1YYD and 4BM1, respectively).

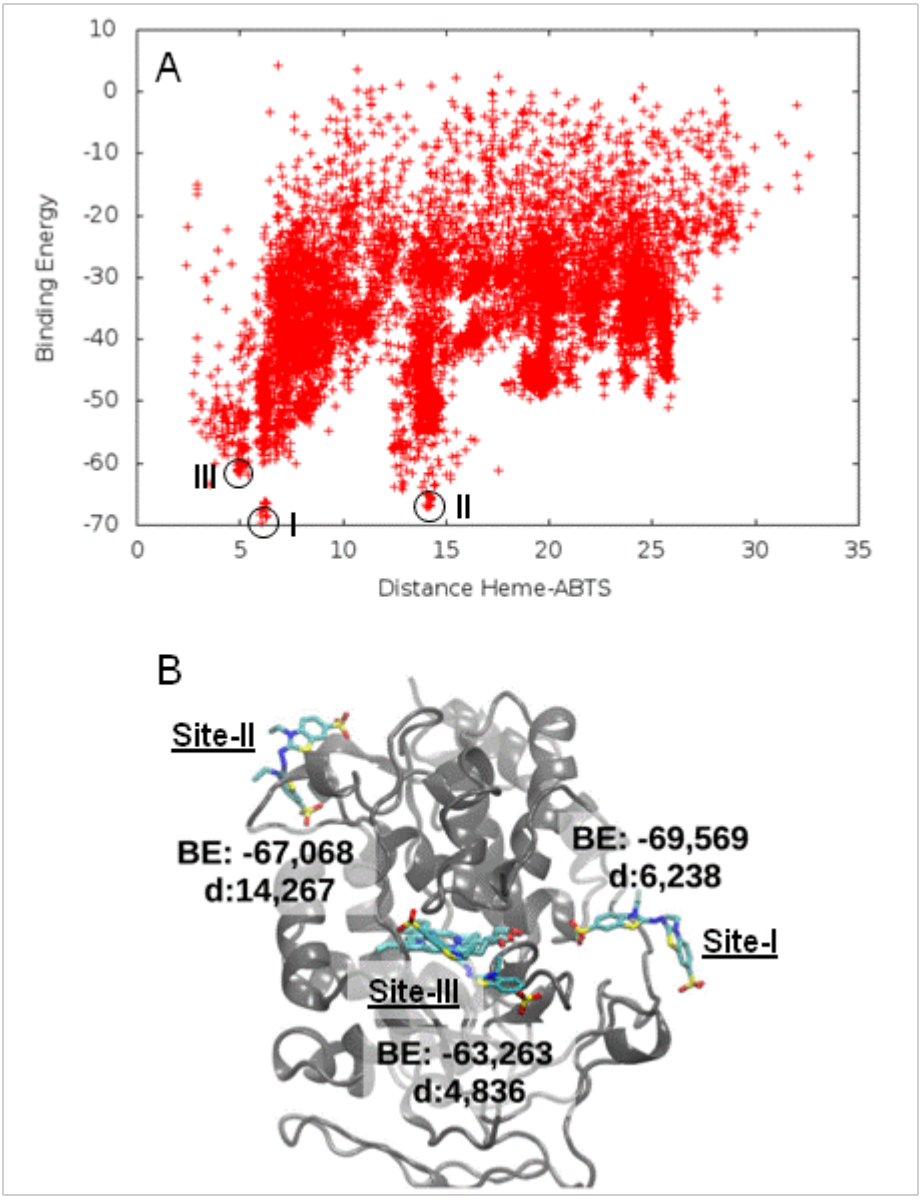

Fig. S3. Preliminary exploration on ABTS diffusion with PELE on extralong MnP6 to identify the regions where the ligand would bind preferentially. **(A)** Heme-ABTS distance *vs* binding energy showing thee (I-III) minima. **(B)** Location of three sites on the MnP6 crystal structure: (I) entrance of the propionate channel at 14.3 Å from the heme; (II) near the distal Ca^{2+} binding site at 14.3 Å from the heme; and (III) main heme access channel at only 4.8 Å but with the worst binding energy.

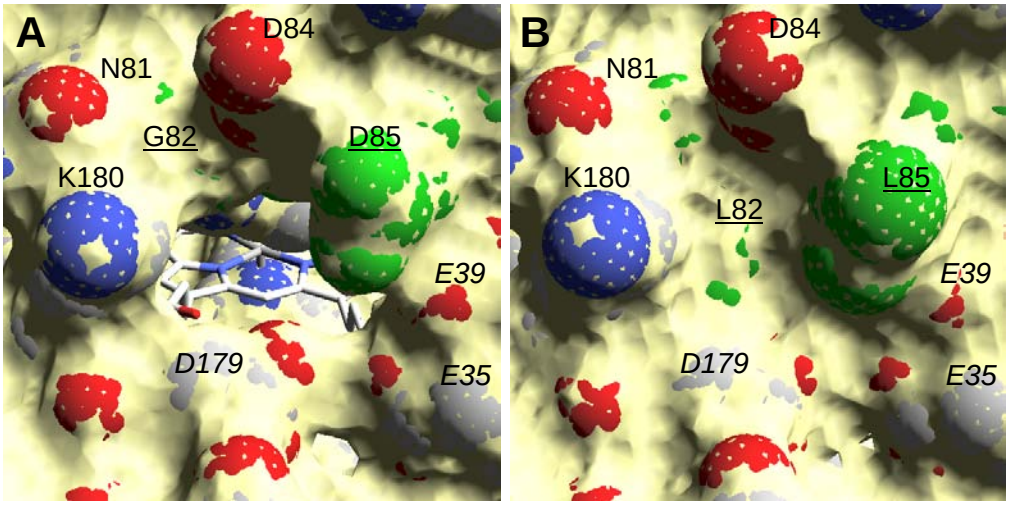

Fig. S4. Heme propionate channel in the MnP6 short-variant (**left**) and after the double G82L/D85L mutation closing the channel (**right**).

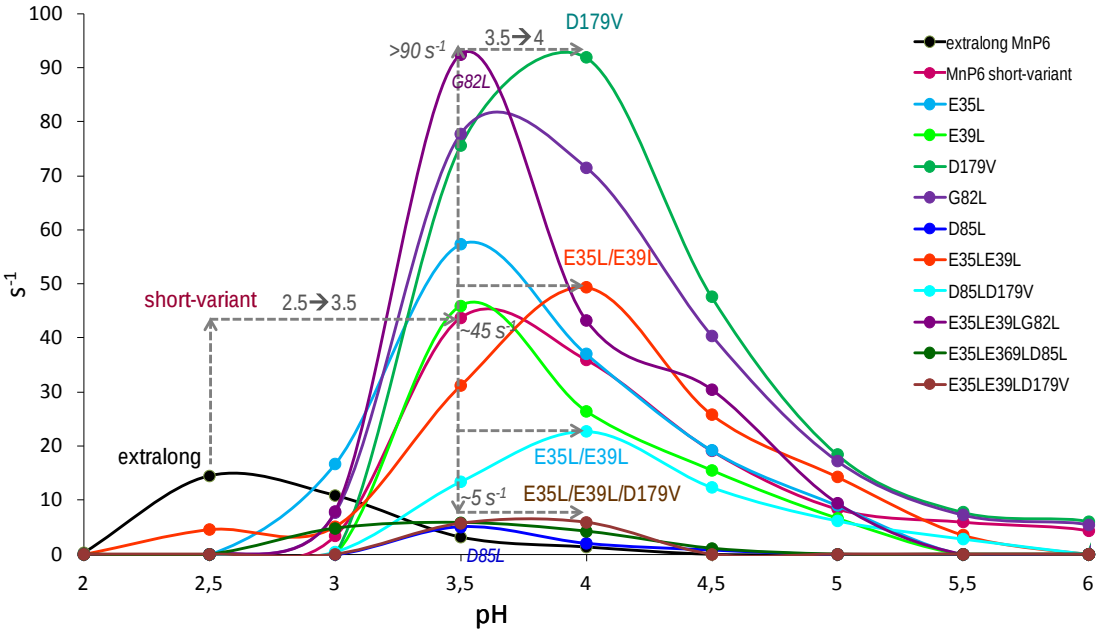

Fig. S5. Effect of pH (2-6 range) on ABTS oxidation (s^{-1}) by the short-variant of the extralong MnP6 of *C. subvermispora*, and different single and multiple variants at the heme propionate channel of this short-variant, compared with the native MnP6.

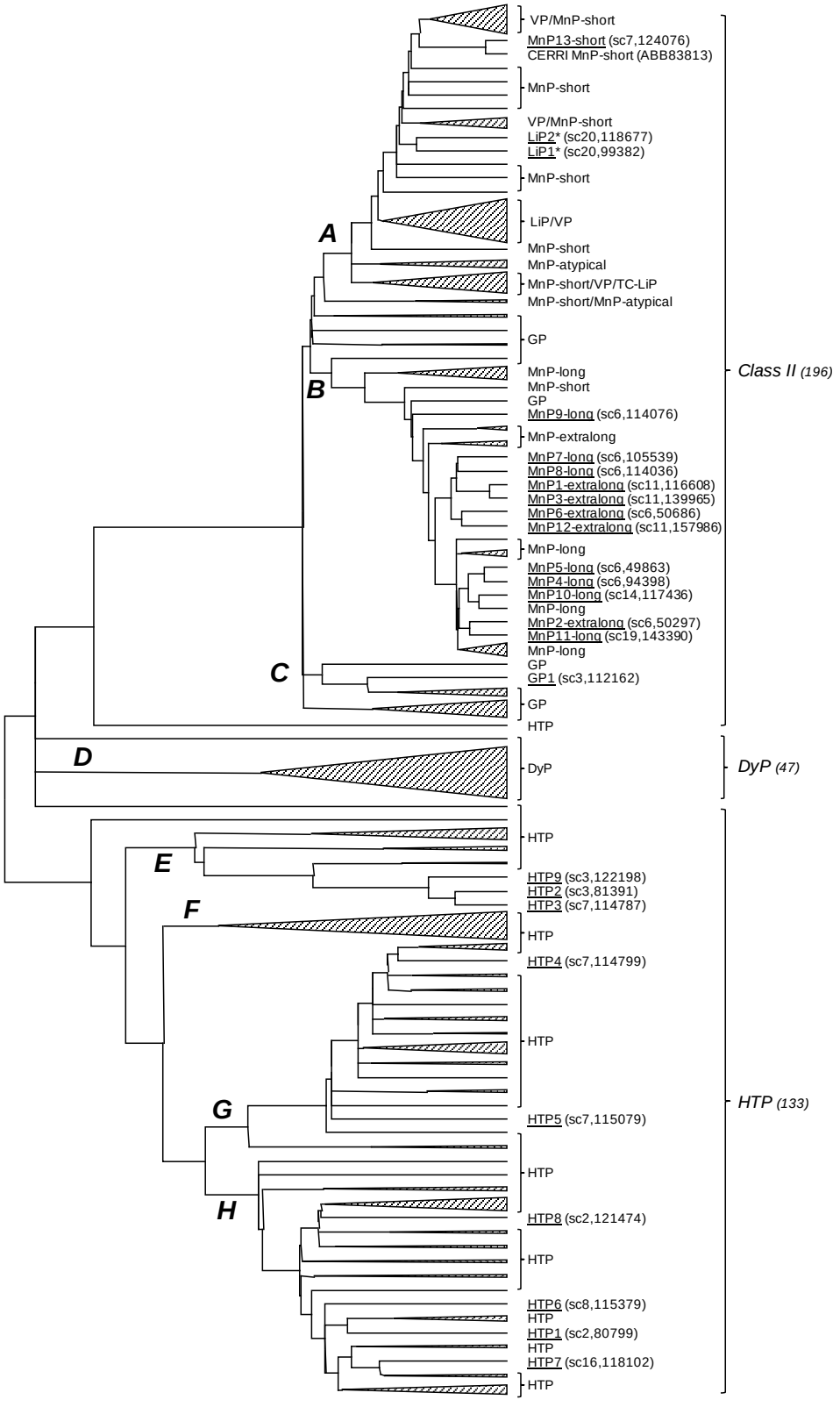

Fig. S6. Phylogram of basidiomycete peroxidases (GenBank and genomes) showing 25 sequences from the *C. subvermispora* genome (underlined) including one short, seven long and five extralong MnPs, two LiP/VP transition forms (*) and one GP (all of them in Class II of the plant-fungal-prokaryotic peroxidase superfamily), and nine members of the heme-thiolate peroxidase (HTP) superfamily. Those clusters where *C. subvermispora* sequences are not included were collapsed, and prokaryotic Class I peroxidases are not included. The three main peroxidase groups, Class II, HTP and dye-decolorizing peroxidases (DyP), and the number of sequences in each of them (parentheses) are indicated, together with the scaffold and JGI references of the *C.*

*subvermispor*a gene models (parentheses). Additionally, MnP-atypical corresponds to a MnP type with only two acidic residues at the oxidation site; TC-LiP corresponds to the unique LiP from *T. cervina*; and CERRI MnP-short corresponds to a *Ceriporiopsis rivulosa* MnP (GenBank BBB83813) clustering together with *C. subvermispora* short MnP13. Adapted from (22).

Material Suplementario

Capítulo 8

Engineering a lignin-degrading peroxidase acting at very acidic pH
Fernández-Fueyo, E., F. J. Ruiz-Dueñas and A. T. Martínez.
(enviado)

SUPPLEMENTARY ONLINE DATA

Engineering a lignin-degrading peroxidase acting at very acidic pH

Elena FERNÁNDEZ-FUEYO, Francisco J. RUIZ-DUEÑAS and Angel T. MARTÍNEZ[1]

Centro de Investigaciones Biológicas, CSIC, Ramiro de Maeztu 9, E-28040 Madrid, Spain

Supplementary data include the catalytic tryptophan surface environment in *P. ostreatus* VP1, *P. chrysosporium* LiP-H8 and the S168W-environment variant of *C. subvermispora* MnP6, compared with the same region in *C. subvermispora* MnP6 (**Figure S1**).

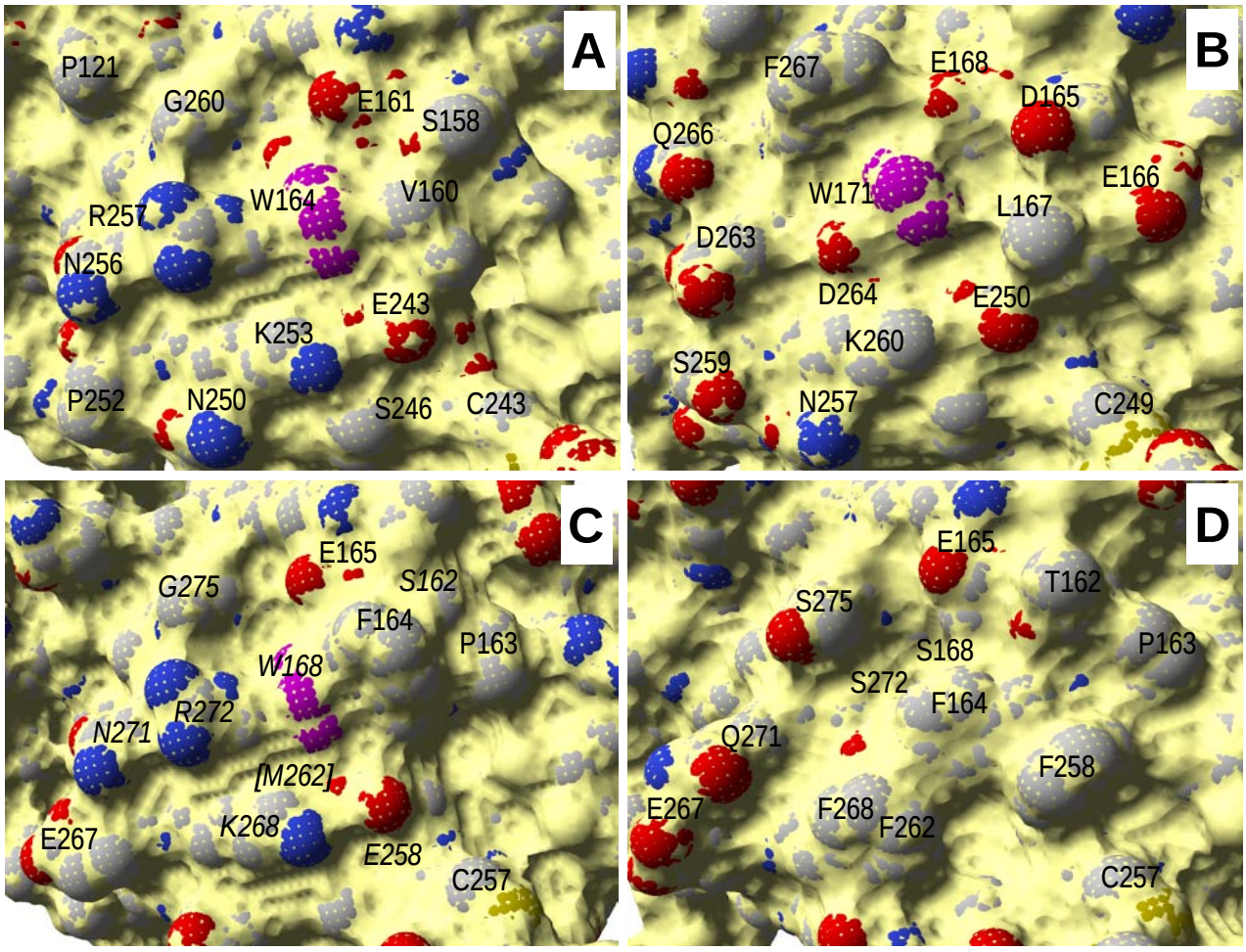

Figure S1 Detail of the catalytic tryptophan surface environment in *P. ostreatus* VP1 (A) *P. chrysosporium* LiP-H8 (B) and the S168W-environment variant of *C. subvermispora* MnP6 (C) compared with the same region in the native *C. subvermispora* MnP6 (D)
Solvent access surface (yellow) and amino acids as magenta (VP1, LiP-H8 and S168W-environment catalytic tryptophan residues) and CPK colored (other residues) van der Waals spheres. The mutated residues in C are in italics. From PDB entries 4BLK (A), 1LGA (B) and XXX (D),and homology model of the SW168-environment variant based on 4BLK (C).

[1] To whom correspondence should be addressed (email ATMartinez@cib.csic.es)